CHEMICAL REVIEWS

Review

pubs.acs.org/CR

Molecular-Scale Electronics: From Concept to Function

Dong Xiang,[†,‡,⊥] Xiaolong Wang,[†,⊥] Chuancheng Jia,[†] Takhee Lee,[*,§] and Xuefeng Guo[*,†,∥]

[†]Beijing National Laboratory for Molecular Sciences, State Key Laboratory for Structural Chemistry of Unstable and Stable Species, College of Chemistry and Molecular Engineering, Peking University, Beijing 100871, China

[‡]Key Laboratory of Optical Information Science and Technology, Institute of Modern Optics, College of Electronic Information and Optical Engineering, Nankai University, Tianjin 300071, China

[§]Department of Physics and Astronomy, and Institute of Applied Physics, Seoul National University, Seoul 08826, Korea

[∥]Department of Materials Science and Engineering, College of Engineering, Peking University, Beijing 100871, China

ABSTRACT: Creating functional electrical circuits using individual or ensemble molecules, often termed as "molecular-scale electronics", not only meets the increasing technical demands of the miniaturization of traditional Si-based electronic devices, but also provides an ideal window of exploring the intrinsic properties of materials at the molecular level. This Review covers the major advances with the most general applicability and emphasizes new insights into the development of efficient platform methodologies for building reliable molecular electronic devices with desired functionalities through the combination of programmed bottom-up self-assembly and sophisticated top-down device fabrication. First, we summarize a number of different approaches of forming molecular-scale junctions and discuss various experimental techniques for examining these nanoscale circuits in details. We then give a full introduction of characterization techniques and theoretical simulations for molecular electronics. Third, we highlight the major contributions and new concepts of integrating molecular functionalities into electrical circuits. Finally, we provide a critical discussion of limitations and main challenges that still exist for the development of molecular electronics. These analyses should be valuable for deeply understanding charge transport through molecular junctions, the device fabrication process, and the roadmap for future practical molecular electronics.

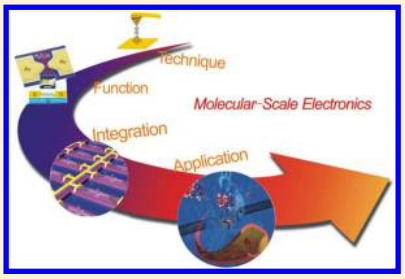

CONTENTS

Received: November 20, 2015
Published: March 16, 2016

DOI: 10.1021/acs.chemrev.5b00680
Chem. Rev. 2016, 116, 4318−4440

1. INTRODUCTION

What does the future hold for electronic devices? To what extent can their dimensions be reduced in the future? Forty years ago, the gate length of a transistor was approximately 10 μm; however, over the past few decades, traditional transistors have shrunk dramatically and now reach dimensions of less than 10 nm in research devices.[1,2] The further miniaturization of electronic devices remains extremely challenging, which is primarily due to either technique limitations or lack of fundamental understanding of transport mechanisms.[3] In this sense, it is remarkable that chemically identical molecules, with sizes on the order of 1 nm, can be synthesized in bulk while accomplishing a variety of electronic tasks, including conducting wire, rectification, memory, and switching; thus, they have the potential to partly replace traditional solid-state device counterparts in the future. Comprehensive experimental findings in electron transport through individual molecules introduce the idea that beyond traditional complementary metal oxide semiconductor (CMOS) technology, the ultimate goal for shrinking electrical circuits is the realization of molecular-scale/single-molecule electronics because single molecules constitute the smallest stable structures imaginable.[4−7] Molecular-scale electronics, which is the concept of creating functional electrical circuits on the basis of properties inherent in individual or ensemble molecules, have several unparalleled advantages as compared to silicon-based electronic devices. First, the extremely reduced size of the molecules in order of 1 nm may enable heightened capacities and faster performance. Moreover, such small size of the molecule provides the ability to surpass the limit of conventional silicon circuit integration. Second, the abundant diversity in the molecular structures, which can be changed via flexible chemical designs, may lead to a direct observation of novel effects as well as the fundamental discovery of physical phenomena that are not accessible using traditional materials or approaches. Third, another attractive feature of this approach is the universal availability of molecules due to the ease of bulk synthesis, thus potentially leading to low-cost manufacturing.

In fact, molecular-scale electronics is currently a research area of focus because it not only meets the increasing technical demands of the miniaturization of traditional silicon-based electronic devices but also provides an ideal window of exploring the intrinsic properties of materials at the molecular level. Generally, molecular-scale electronics refers to the use of single molecules or nanoscale collections of single molecules as electronic components.[2,8−10] The primary theme in this field is the construction, measurement, and understanding of the current−voltage responses of electrical circuits, in which molecular systems play an important role as pivotal elements.[11] Indeed, over the past decade, we observed significant developments achieved in both experiments and theory to reveal the electronic and photonic responses of these conceptually simple molecular junctions.[5−12]

The history of molecular-scale electronics is surging forward with great momentum, and outstanding scientists have provided significant contributions to the development of molecular-sale electronics. Briefly, several pioneering studies were performed in the 1970s at the laboratory of Hans Kuhn along with Mann, Polymeropoulos, and Sagiv.[10,13−15] They

DOI: 10.1021/acs.chemrev.5b00680
Chem. Rev. 2016, 116, 4318−4440

developed the first effective self-assembly techniques (via molecular bond formation) to prepare molecular structures in which organic molecules adhered to solid substrate surfaces without using simple dispersion forces. Additionally, these groups reported a few of the earliest reproducible electrical transport measurements through molecules. Following Mann and Kuhn's study, there were a number of important follow-up experiments and measurements.[10] During the same period, a visionary concept of exploiting the intrinsic functionalities of molecules for electronics (i.e., a single molecule could function as a rectifier) was sketched out by Aviram and Ratner.[16] The desire of using molecules as functional units in electronic circuits then motivated many researchers over the next few decades. A significant development occurred in 1982 with the development of scanning probe microscopy (SPM).[17] The SPM is a powerful technique regarded as a milestone in the history of molecular electronics, by which both the surface topography and its transport information can be addressed.[18] Using SPM, Weiss and his colleagues performed the first experiment resembling transport through single molecules, thus launching a promising approach to realizing the goal.[19] Nonetheless, the SPM technique is limited to lab experiments and cannot be directly applied to realistic device fabrication. In addition to the development of SPM, various techniques based on either metal or carbon nanoelectrodes have been introduced for single-molecule studies in the following years, including mechanically controllable break junctions, electromigration breakdowns, electrical chemical depositions, and surface diffusion-mediated depositions, etc.[20−23]

The success of these techniques led to an explosion of interest in using individual molecules in molecular-scale electronics and significantly promoted the development of the field. With improved measurement capability, a number of new effects beyond electronic transport, including electromechanics, thermoelectrics, optoelectronics, quantum interferences, and spin transports, were discovered at the single-molecule level.[6,24−27] In contrast to metal electrodes, nonmetal materials, such as conducting polymers and carbon-based materials, can be regarded as molecules themselves, and they possess a natural compatibility with the traditional silicon-based technique and excellent mechanical flexibility.[28,29] Hence, the past decade was an exciting developmental period for nonmetal-based molecular electronics. For example, nanotubes and graphene have been used as point contacts for creating robust single-molecule junctions with desired functions, thus paving the way for practical applications.[30,31]

The theory developed for interpreting the current−voltage characteristics in molecular junctions began to appear in the 1990s. The early approach was to use the Landauer formulation to explain the electron transport behavior.[32,33] In this simple picture, the charge transport through the molecular junctions was interpreted in terms of elastic scattering with a key parameter, known as the "transmission coefficient", which described how effective a molecule was in scattering the incoming electron from the right lead into the left lead. Additionally, more powerful formulations, including the nonequilibrium Green's function (NEGF) approach, Breit−Wigner formula, and Simmons model, have been used to interpret the electron transport behaviors through a molecule.[34−37] Particularly, the NEGF approach demonstrated the capability of combining both the elastic and the inelastic effects with the metal−electrode coupling and gating effects.[38] However, practical molecular junctions are really complex, and the development of advanced theories that consider all of the factors, including real molecules, electrodes, molecule−electrode interfaces, electron−phonon interactions, spin−orbit interactions, and electron−solvent couplings, is of significant importance to the comprehensive advancement in the field.[34] The motivation for the theory development is far from saturated, and significant efforts are needed to reduce the gap between the theoretical calculations and the experimental data.

Nonetheless, numerous challenges need to be addressed before single-molecule devices can be used as commercial products. The basic challenge involves determining the structure−function relationships for the electronic transport (intra- or intermolecular) through a junction containing one or a few molecules. It is a complicated engineer because the behaviors of the molecular devices are strongly dependent on the electrode fabrication process, selection of electrode materials, contact chemistry, and number of molecules to be tested. Unlike traditional semiconductors that use a standard product line, there are no standard processes for molecular device fabrication thus far. A small variation in each process may result in a large change in the molecular devices. The resulting challenge is the reproducibility. Generally, the passing current detected is small (∼nA) when the target unit scales down to the single-molecule scale, and thus the current is sensitive to the environmental changes, for example, contamination, radiation, humidity, temperature variation, and other external vibrations. Furthermore, molecular aging is another factor that leads to the reproducibility problem. Another primary challenge involves developing a technology for the mass production of single-molecule devices at low cost. Although the molecules can be synthesized in large quantities, most widely used techniques, such as electron beam lithography (EBL) for nanoelectrode fabrication, are expensive for mass production. Decreasing the unit size and increasing the integration level without sacrificing cost remains a difficult task in the future.

Although it is a long way to achieve commercially available molecular electronics, basic research in this area has advanced significantly. Specifically, the drive to create functional molecular devices has pushed the frontiers of both measurement capabilities and our fundamental understanding of varied physical phenomena at the single-molecule level. The field of molecular electronics has become a fascinating playground for scientists to explore new fundamental concepts and new applications. Several recent articles focused on specific experimental aspects of molecular electronics.[11,39−51] In this comprehensive Review, we offer a broad overview of this field, with a particular focus on several vital issues, such as developing fabrication techniques for molecular junctions, discovering novel physical phenomena, using characterization techniques, and developing strategies for integrating molecular functionalities into electronic device configurations. We address the primary advances with the most general applicability and emphasize new insights into the development of efficient platform methodologies for building reliable molecular electronic devices with desired functionalities using a combination of programmed bottom-up self-assembly and sophisticated top-down device fabrication. To do so, we first summarize a number of different efficient approaches for forming molecular-scale junctions and discuss various experimental techniques for examining these nanoscale circuits in detail. We then highlight the major contributions and new concepts of integrating molecular functionalities into the

DOI: 10.1021/acs.chemrev.5b00680
Chem. Rev. 2016, 116, 4318−4440

Table 1. Comparison of Molecular Junctions Fabricated by Different Approaches

methods for molecular junctions	number of molecules	gating control	addressability	fabrication	yield[a]	ref
scanning probe microscopy	single	electrochemical	difficult	sophisticated	H	17
mechanically controllable break junction	single	electrostatic	no	sophisticated	H	20
electromigration nanogap	single	electrostatic	yes	sophisticated	L	21
electrochemical deposition	single	electrostatic	yes	sophisticated	H	22
surface-diffusion-mediated deposition	single	no	no	sophisticated	H	23
lift-and-float approach	ensemble	no	difficult	straightforward	H	232
liquid metal	ensemble	electrochemical	difficult	straightforward	H	239
nanopore or nanowell	ensemble	no	yes	straightforward	M	129
nanoimprint lithography	ensemble	no	yes	sophisticated	H	285
self-aligned lithography	ensemble	electrostatic	difficult	straightforward	M	275
on-wire lithography	ensemble	no	difficult	sophisticated	M	269
buffer interlayer-based junction	ensemble	no	possible	straightforward	H	28
crosswire or crossbar	ensemble	no	possible	sophisticated	M	308
on-edge molecular junction	ensemble	no	difficult	straightforward	H	338
CNT-based junction	single	electrostatic	yes	sophisticated	M	31
graphene-based junction	single	electrostatic	yes	sophisticated	H	30
silicon-based junction	ensemble	no	difficult	sophisticated	M	384
polymer-based junction	ensemble	no	difficult	sophisticated	M	386

[a]H, M, and L indicate the high, middle, and low yield, respectively.

electrical circuits, which have been neglected in most previous reviews. Furthermore, the perspectives and key issues that are critical to the success of the next-generation single-molecule devices toward practical applications are discussed, such as device reproducibility, system integration, and theoretical simulation. These analyses are valuable for thoroughly understanding how device fabrication processes, such as the testbed architectures used, molecule number and defect density tested, as well as the nature of the electrode−molecule interface, influence the intrinsic properties of the molecules, which is of crucial importance to the development of future practical molecular electronic devices.

2. METAL ELECTRODES FOR MOLECULAR ELECTRONICS

In molecular electronic junctions, where molecules are used as electronic device components, the electrical signal comes in and out of the molecules via contact-coupled electrodes. The electrodes can be classified as metal or nonmetal electrodes. The development of molecular electronics initially started from the use of metal electrodes. Hence, we first summarize the development of molecular devices based on metal electrodes and then move to those based on nonmetal electrodes, particularly carbon-based electrodes. The typical methods for the different electrodes are listed in Table 1. It can be observed that each method has its own unique advantage as well as disadvantage.

2.1. Single-Molecule Junctions

The initial idea of using individual molecules as active electronic elements provided the impetus to develop a variety of experimental platforms to probe their electronic transport properties. Among these platforms, single-molecule junctions based on a metal−molecule−metal architecture have received considerable attention and contributed significantly to the fundamental understanding of the physical phenomena required to develop molecular-scale electronic devices.[39] As mentioned above, the SPM technique is regarded as a milestone in the history of molecular electronics because it has made a great contribution to the development of molecular electronics and continues to promote the advancement of molecular electronics in the future.

2.1.1. Scanning Probe Microscopy Break Junction. Scanning probe microscopy typically includes both scanning tunneling microscopy (STM) and atomic force microscopy (AFM). STM plays a unique role in the field of molecular electronics via STM break junctions. The most commonly used method is the in situ molecular break junction technique, as skillfully demonstrated by Tao and collaborators.[52,53] This in situ method can rapidly create thousands of molecular junctions by repeatedly moving a tip in and out of contact with the substrate electrode adsorbed with the sample molecules. The tip movement can be precisely controlled by a piezoelectric transducer, which is constructed with lead zirconate titanate. Typically, the molecules in the study have two end groups that bind to the tip and the substrate electrodes. The molecules have an opportunity to bridge both the tip and the substrate electrode when the tip is brought close enough to the substrate, as indicated in Figure 1. The tip is then pulled away from the substrate to break the metal−molecule−metal junction. By accurately controlling the movement of the tip, that is, changing the distance between the tip and the substrate, the number of bridged molecules can be changed.[53]

The conductance can be measured as a function of the relative tip displacement to yield conductance traces. Xu et al. reported a simple and unambiguous measurement of a single-molecule conductance, achieved by repeatedly forming thousands of gold−molecule−gold junctions.[52] The conductance histograms were constructed from thousands of conductance traces and revealed well-defined peaks at integer multiples of a fundamental conductance value. This observation provides a method to identify the conductance of a single molecule. Using the conductance histograms, Cheng et al. demonstrated that the formation of a direct Au−C bond was likely and determined that the conductance of these molecular junctions is ∼100 times larger than that of the other binding groups.[54] By comparing the Au−N, Au−S, Au−P, and donor−acceptor bonds, Venkataraman et al. discovered that the binding strength and the conductivity gradually increased from Au−NH_2R and Au−SMeR to Au−PMe_2R.[55,56] The

DOI: 10.1021/acs.chemrev.5b00680
Chem. Rev. 2016, 116, 4318−4440

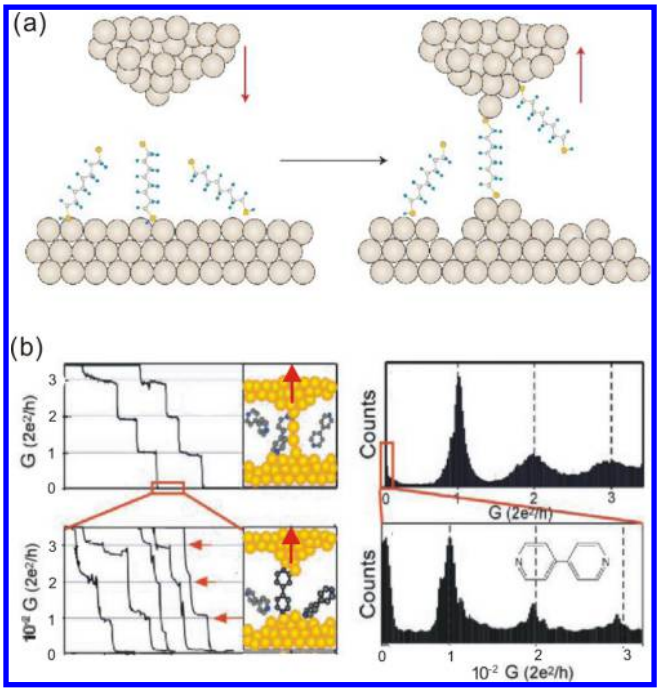

Figure 1. (a) STM-based technique used to form single Au−molecule−Au junctions. When the Au tip moves near the Au substrates, which are covered with target molecules, Au−molecule−Au junctions are formed. When the Au tip is pulled away, the molecular bridges then lose contact with either the tip or the Au substrate. Reproduced with permission from ref 41. Copyright 2006 Nature Publishing Group. (b) Single-molecule conductance measurement. The conductance of a gold−gold contact decreases in quantum steps as the tip is gradually pulled away from the substrate. The corresponding conductance histogram illustrates well-defined peaks near 1 G_0, 2 G_0, and 3 G_0 due to the conductance quantization. After the gold−gold contact is completely broken, a new series of conductance steps appear due to the formation of the molecular junctions. A conductance histogram shows peaks near 0.01 G_0, 0.02 G_0, and 0.03 G_0, which can be ascribed to one, two, and three molecules, respectively. Reproduced with permission from ref 52. Copyright 2003 AAAS.

detailed discussion related to the electrode−molecule contact interface can be found in a review article by the Guo group.[57] These findings offer a new method for creating reproducible and highly conducting metal−organic contacts.

A technique closely related to STM is atomic force microscopy (AFM), in which a force is used to control the tip-positioning.[58] The difference between AFM and STM should be noted. In STM, current instead of force is used to control the tip-positioning. Because the conductance properties of the molecules are generally unknown, the position of the probe with respect to the molecules is ambiguous, which may result in the penetration of the tip into the monolayer in the STM experiments. Conversely, with independent feedback signals, AFM allows the probe to be controllable in either the contact or the noncontact mode, thus effectively avoiding the tip penetration. However, one disadvantage of AFM is that the electrical properties of the target molecules are unavailable. To solve this problem, a significant improvement was demonstrated by Wold et al., who described a new approach for the formation of metal−molecule−metal junctions by placing a conducting AFM tip in contact with a metal-supported molecular film, which is known as the conducting probe atomic force microscopy (CP-AFM) technique.[59] Although the conducting probe tip of the CP-AFM coated with a metallic layer is larger than an atomically sharp STM tip, the CP-AFM method measures both the mechanical and the electrical properties of the molecules simultaneously.[53,60] Using the CP-AFM method, Aradhya et al. measured the conductance of pyridine derivatives and simultaneously acquired consistent force traces during the junction elongation, thus providing a quantitative characterization of the van der Waals' interactions at the metal/organic interfaces, as indicated in Figure 2.[61,62]

In the STM or CP-AFM experiments, once the molecular junctions are formed, the tip (top electrode) can be fixed, and the characterization of the electron transport through the molecule junction can be performed.[63,64] To date, STM and AFM have revealed many interesting phenomena in single-molecule junctions, such as large magnetoresistance,[65,66] spin-split molecular orbitals,[67] Kondo resonance,[68] Coulomb

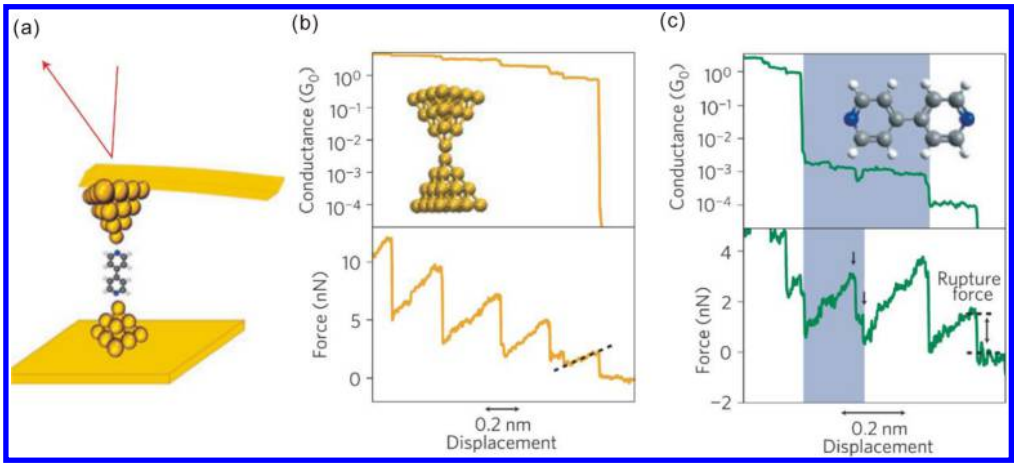

Figure 2. Working principle of AFM: (a) Schematic of a 4,4′-bipyridine junction formed between a gold-coated AFM tip and a gold substrate. Using a laser beam, the deflection of the cantilever can be monitored, and the corresponding mechanical force between the tip and the sample can be obtained. (b,c) Experimentally measured conductance (upper panel) and corresponding simultaneously acquired force (lower panel) traces during the junction elongation of bare gold junctions (b) and molecular junctions (c). The shaded areas in the upper panel represent high-conductance molecular regimes. The shaded areas in the low panel represent structural rearrangements within the high-conductance regime. The dashed lines indicate a complete rupture of the molecular junctions. Reproduced with permission from ref 61. Copyright 2012 Nature Publishing Group.

DOI: 10.1021/acs.chemrev.5b00680
Chem. Rev. 2016, 116, 4318−4440

blockade effect,[69] negative differential resistance behavior,[70,71] strain-induced binding configuration,[72] and redox switch,[73,74] significantly accelerating the development of molecular electronics. Additionally, over the past few decades, the electron transport pathway through the molecular junctions[75,76] and the charge transport mechanisms[54,77,78] have been further understood. Correspondingly, these single-molecule junctions represent the possibility of achieving the ultimate goal of miniaturizing the electrical circuits and providing ideal platforms for probing the quantum transport phenomena.

Particularly, experiments on individual molecules using scanning probe microscopies have led to further insights into the quantum electronics of the molecular systems.[25,79,80] The conductance properties of solid-state mesoscopic structures are primarily dominated by quantum effects at low temperatures. For example, if partial electron waves propagating through the two branches of a ring-shaped mesoscopic structure interfere destructively with each other, the conductance will be suppressed. Conversely, if they interfere constructively, the conductance will be enhanced. For certain classes of molecular junctions, a similar quantum interference is expected to occur as the electron waves propagate through the molecular orbitals (or quasi-degenerate electronic states) that are separated in both space and energy.[81,82] Guédon et al. reported the observation of a destructive quantum interference in the charge transport through the molecular junctions.[79] They synthesized a few rigid-conjugated molecular wires. Two exemplary molecular structures (AQ-DT and AC-DT) are illustrated in Figure 3. The two-dimensional conductance histograms indicated that the conductance of the AQ-DT was nearly 2 orders of magnitude lower than that of the AC-DT, as seen in Figure 3. This result is remarkable because the energy difference between the highest occupied molecular orbital (HOMO) and the lowest unoccupied molecular orbital (LUMO) levels is extremely similar for these molecules, and the two types of molecules possess the same end-groups and a similar molecular length. Combined with the density functional theory (DFT) calculations, they demonstrated that there were three unaligned localized molecular orbitals (LMOs) for the AQ-DT. Thus, the electron can be transported through two different pathways via the LMO_S, thereby yielding the phase difference within the HOMO−LUMO gap; that is, the partial waves interfere destructively, which results in a poor conductance of the AQ-DT. Their investigation revealed that it is possible to control the degree of interference and change the value of the molecule conductance through chemical modifications of the molecular structure.

The occurrence of the destructive quantum interference strongly depends on the molecular structure as well as the temperature. In an experiment, the vibrations are inherent to any molecular junction, particularly at room temperature. At a high temperature, the vibrations coupled to the electronic states may provide a strong decoherence mechanism in the molecular junctions, where the electron transport is governed by destructive interference effects. Consequently, the destructive interference between the involved pathways can be quenched.[82] With an appropriate molecular structure design, it is possible to observe the constructive quantum interference phenomenon. Vazquez et al. provided direct evidence for constructive quantum interference in molecular junctions at room temperature.[25] As indicated in Figure 3b (inset), they synthesized a series of molecular systems that contained either one backbone or two backbones in parallel that were bonded together

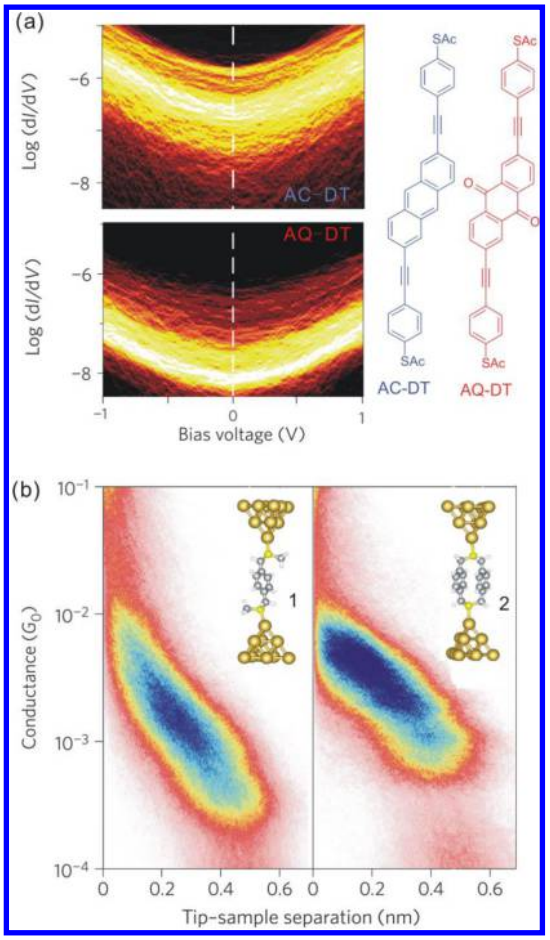

Figure 3. Quantum interference. (a) Logarithmically binned two-dimensional histograms for dI/dV values versus a bias voltage V. The color scale indicates the number of counts. Right panel: Similar chemical structures of the investigated molecules AQ-DT and AQ-DT. Because of the destructive interference, the conductance of the AQ-DT is 2 orders of magnitude lower than that of the AC-DT. Reproduced with permission from ref 79. Copyright 2012 Nature Publishing Group. (b) Two-dimensional conductance−displacement histograms for junctions with molecules 1 and 2. Inset: Chemical structures of the investigated molecules with single- (1) and double- (2) backbone molecules. Because of the constructive interference, the conductance of a double-backbone molecular junction is 2 times higher than that of a single-backbone junction. Reproduced with permission from ref 25. Copyright 2012 Nature Publishing Group.

cofacially by a common linker on each end. The conductance measurements indicated that the conductance of a double-backbone molecular junction could be 2 times higher than that of a single-backbone junction, thus providing clear evidence for constructive interference as electrons were transported through the parallel molecular wire components under ambient conditions at room temperature.

2.1.1.1. Beyond Traditional SPM Break Junctions. In the STM or AFM methods, a challenge is that even though molecules are adsorbed onto the substrate and form a well-defined molecule−substrate bottom contact, the tip−molecule contact is typically less well-defined.[53] Moreover, due to the relatively large size of the tip, it will be difficult to directly address the individual molecules if the tip attempts to contact the molecular layer, and the number of sandwiched molecules will be uncertain, which prevents the absolute conductance and electrical properties of the target molecule to be determined.

DOI: 10.1021/acs.chemrev.5b00680
Chem. Rev. 2016, 116, 4318−4440

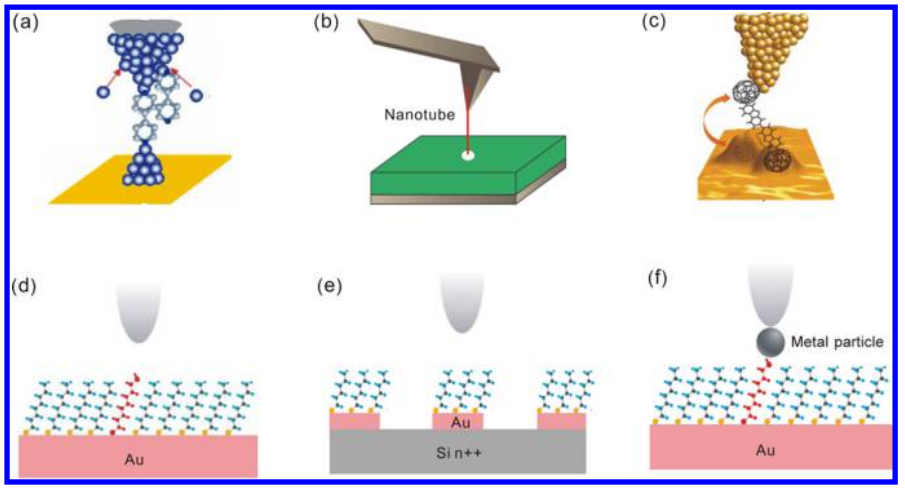

Figure 4. SPM-based molecular junctions. (a) Electrochemical jump-to-contact scanning tunneling microscopy break junction (EC-STM). Reprinted with permission from ref 83. Copyright 2013 American Institute of Physics. (b) Attaching nanotubes to a metal-coated AFM tip. Reprinted with permission from ref 84. Copyright 2009 Nature Publishing Group. (c) C_{60}-terminated SPM break junction. Reprinted with permission from ref 85. Copyright 2011 American Chemical Society. (d) Inserted target molecules into an ordered array of reference molecules. Reprinted with permission from ref 19. Copyright 1996 AAAS. (e) Substrate-modified SPM junction. Reprinted with permission from ref 86. Copyright 2012 American Chemical Society. (f) Nanoparticle-based SPM junction. Reprinted with permission from ref 87. Copyright 2001 AAAS.

Fortunately, different research groups have presented novel strategies to reduce the number of addressed molecules and create well-defined (strong) top contacts over the past few years, as indicated in Figure 4. These strategies can be classified as tip modification and substrate modification.

(1) EC-STM break junction: Zhou et al. developed an electrochemical strategy for STM break junctions by establishing a chemically well-defined metallic contact through a jump-to-contact mechanism between the tip and the substrate, as indicated in Figure 4a.[83,88] The gold tip is fixed above the substrate, and the tip is electrochemically deposited in situ with a foreign metal of interest until a bridge between the tip and the substrate is formed. Different foreign metals, such as Cu, Pd, and Fe, were successfully used to form a thin nanowire to bridge the tip and the substrate.[83,89] When the tip was pulled away from the substrate, the elongation of the bridged nanowires generated two atomic-scale sharp electrodes, which made it feasible to form single-molecule junctions. The strategy presented in their study not only extends the capability of STM break junctions to create a variety of metal nanowires for further investigations but also provides opportunities to generate well-defined metal−molecule−metal junctions with a variety of choices of metals in the junctions.

(2) Nanotube-tip-based SPM break junction: In addition to producing smaller tips, the AFM researchers made great efforts to develop tips that were long enough, provided faithful representations of the surface topographies with high resolution, and were mechanically noninvasive. Carbon nanotubes have demonstrated considerable potential to be used as AFM tips.[84] The main features of the carbon nanotubes are their nanometer-scale diameters, high aspect ratio, and remarkable mechanical and electrical properties. The carbon nanotubes were first used as AFM tips five years after their discovery.[90] It should be noted that to electrically probe molecules using this method, it should be ensured that the nanotubes are metallic; otherwise the electrical interpretation would be complicated. There are two key aspects to the fabrication of the nanotube AFM tips: attachment[91,92] (the nanotube must be fixed to the AFM probe) and modification.[93] The fabrication, modification, and application of the nanotube-based SPM can be found in the article.[84] It is expected that with a proper modification to the end of the nanotube, it is feasible to form nanotube−molecule−metal junctions and characterize the properties of these molecular junctions, as shown in Figure 4b. To improve AFM to even higher resolutions, Gross et al. replaced the metal tip of conventional AFMs with a single molecule of carbon monoxide (CO),[94,95] which is extremely stable as well as subject to significantly smaller van der Waals forces when in close proximity to a sample. To demonstrate their new tool, the researchers applied their AFM tips to several types of molecules, and the observed spacing between individual atoms was as small as 0.14 nm, thus dramatically improving the resolution of AFM.

(3) C_{60}-terminated SPM break junction: One of the challenging goals in molecular electronics is to wire exactly one molecule between two electrodes due to the different coordination modes of the anchor group, especially under ambient conditions. To solve this problem, Leary et al. described a new and straightforward method for unambiguously addressing a single C_{60}-Fl_2-C_{60} molecule on a metal surface,[85] as indicated in Figure 4c. Their strategy used C_{60}-terminal groups as molecular beacons to make molecules to be visualized, which allowed the single molecule to be accurately targeted using STM. The C_{60} groups not only provide a clear visual signature for the molecule but also serve as the effective anchoring groups. Once the tip and the surface are wired, the manner in which the conductance of a purely one-molecule junction evolves with time can be monitored by stretching the molecule in the junction, observing the characteristic current plateaus upon elongation, and performing a direct I/V spectroscopy. Thanks to C_{60} spherical geometry and the multi-interaction configurations of its carbon atoms with metal electrodes, it has been widely used as molecular bridges between two electrodes in break junctions, and different experiments had been performed to reveal this new class of molecules, which allows incorporation of many linkers between the two C_{60} termini. For example, Moreno-García et al. investigated charge transport in C_{60}-based dumbbell-type molecules recently.[96] Two distinct single-molecule conductance states were observed, depending on the pressure exerted by the probe on the junction, thus

DOI: 10.1021/acs.chemrev.5b00680
Chem. Rev. 2016, 116, 4318−4440

allowing the molecule to function as a mechanically driven molecular switch.

(4) Molecule layer-modified SPM junction: One advantage of the SPM technology is that the gap size between the tip and the substrate can be continuously and accurately changed. Using a tip-withdrawing strategy, the number of wired molecules can change, and the single-molecule junctions can be addressed. However, it will be a significant challenge to address the individual molecules when the molecule only possesses one bonding group, for which the tip-withdrawing strategy did not work efficiently. One way to solve this problem is to embed target molecules into the matrix of another, which is often the less conducting molecule, as shown in Figure 4d. Bumm et al. presented an approach to study the current through high-conductance molecular wire candidates inserted into a nonconducting alkanethiol monolayer.[19] In this approach, the target molecules were taller (higher) than the surrounding poor conducting molecules, thus ensuring that only the target molecules were contacted. This strategy provides a method to study single-molecule electrical properties when the in situ break junction technology is unavailable.

(5) Substrate-modified SPM junction: Clement et al. reported a new approach that allows the conductance of up to a million junctions to be measured within a single CP-AFM image,[97] as indicated in Figure 4e. They first fabricated a large array of single-crystal Au nanodots on a highly doped silicon substrate. A molecular layer then was formed at the nanodot surface. Finally, a conducting AFM tip was driven to contact the molecules, and a metal−molecule−metal−silicon junction was subsequently formed. Because the diameter of the nanodots is less than 10 nm, the number of adsorbed molecules can be less than one hundred.[86] Because the Au nanodots are fabricated using electron beam lithography (EBL) and an annealing process, which have high geometrical, positional, and crystal uniformity, this approach is useful for studying electron transport through molecular junctions.

(6) Nanoparticle-based SPM junction: The nanoparticles have a smaller size as compared to the traditional SPM tip and can be easily visualized using the SPM technology, thus suggesting a potential application for molecular break junctions. Cui et al.[87] presented an approach using a conducting atomic force microscope to contact gold nanoparticles capped by alkanedithiol molecules, which were embedded in a matrix of alkanethiols molecules. The octanethiol monolayer acts as a molecular insulator, which isolates the dithiol molecules from one another. The thiol groups at the top of the film are attached to the nanoparticles by incubating the monolayer with a gold nanoparticle solution. A gold-coated conducting AFM probe was used to locate and contact individual particles bonded to the monolayer, as indicated in Figure 4f. The measured I/V characteristics can be categorized into several distinct sets of curves that are integer multiples of a fundamental curve, and the fundamental curve presents the single-molecule I/V response. In addition to measuring the molecular conductivity, this approach can avoid the effects of variations in the contact force and other problems encountered with the nonbonded contacts. One drawback of this strategy is that, because the Au nanoparticles are typically coated with an organic surfactant layer, the tip and the nanoparticle may form an additional tunneling junction (Coulomb island). Consequently, the electron transport between the tip and the substrate via the nanoparticle may exhibit Coulomb blockade effects.[69]

2.1.1.2. Applications of SPM beyond Electron Transport. The application of SPM in molecular electronics is not only limited to measuring the properties of the electron transport through the molecular junctions; that is, SPM has been extended to vast regimes. We tentatively classify these additional SPM applications into five groups, which are presented in the following paragraphs.

(1) Imaging: SPM allows the single-molecule structure, bond structure,[98,99] and charge distribution with submolecular resolution to be imaged.[100] In this attractive field, several pioneer groups provided significant contributions.[94,95,98,101,102] Here, we just provide one of the pioneering studies. Oteyza et al. used a noncontact atomic force microscopy to investigate the reaction-induced changes in the detailed internal bond structure of individual molecules on the silver surface.[101] Both the reactant and the final products were probed at the single-molecule level. Their bond-resolved images revealed how the thermally induced complex bond rearrangement resulted in unexpected products. Combined with the density functional theory calculation, they proposed a detailed reaction pathway.

(2) Optoelectronics and stereoelectronics: Addressing the optical properties and understanding their influence on the electronic transport in individual molecular-scale devices, known as "molecular optoelectronics", is an area with potentially important applications. However, the mismatch between the optical (approximately at the micrometer scale) and the molecular-length scales (approximately at the nanometer scale) became an obstacle to the experimental investigations. The SPM technique reduces this obstacle and plays an important role in the single-molecule optoelectronic studies in two aspects: optical spectroscopies and optical control.[39] Raman is a typical optical spectroscopy method. Recently, Liu et al. used the STM-based break junction technique combined with the Raman spectroscopy to perform simultaneous conductance and Raman measurements on single-molecule junctions, thus providing detailed structural information.[103] Experiments that probe electroluminescence, which is photon emission induced by a tunneling current, also offer insight into the structure−conductance correlations. For example, Qiu et al. demonstrated the simultaneous measurement of differential conductance and photon emissions from individual molecules using STM.[104] Instead of depositing molecules directly on a metal surface, they used an ultrathin alumina insulating film to decouple the molecule from the metal. This critical improvement prevents the metal electrodes from quenching the radiated photons, and the emitted photons carry additional molecular fingerprint information. For an advanced technical overview from a different perspective, readers can refer to two recent comprehensive reviews on molecular optoelectronics.[44,105]

Over the past few decades, chemists have made considerable efforts to develop a fundamental understanding of stereoelectronics to establish how the electronic properties of molecules relate to their conformation; the recent developments of the single-molecule STM technique provide the tools to change the conformation with a level of control previously unimagined. For example, using the STM technology, Venkataraman et al. performed a systematical conductance measurement of biphenyl junctions as a function of the molecular twist angles, thus building a comprehensive mapping of how the junction conductance changes with the molecular conformation.[106] In another example, Su et al. demonstrated the dependence of single-molecule conductance on a stereo-

DOI: 10.1021/acs.chemrev.5b00680
Chem. Rev. 2016, 116, 4318−4440

electronic effect in permethyloligosilanes with methylthiomethyl electrode linkers.[107] This result occurs because the strong σ conjugation in the oligosilane backbone couples the stereoelectronic properties of the sulfur−methylene σ bonds that terminate the molecule. Additional discussion regarding the conformation-induced switching is provided in section 7.4.

(3) Heating: Local heating is known to be an important factor in the design of conventional silicon-based microelectronics. It is natural to question how important this effect is in the electrode−molecule−electrode structures. Huang et al. investigated the current-induced local heating effects in single molecules covalently bound to two electrodes by measuring the force required to break the molecule−electrode bonds.[108] Because the breakdown process is thermally activated, the breaking force can be used to extract the effective temperature of the molecular junction. They demonstrated that the local temperature of a 1,4-benzenedithiol-based (BDT) molecular junction could be raised to 463 K by applying a bias voltage of up to 1 V. The heat dissipation and transport in the molecular devices remain poorly characterized due to experimental challenges. Lee et al. used custom-fabricated scanning probes with integrated nanoscale thermocouples to investigate the heat dissipation in the electrodes of single-molecule junctions.[109] Their results clearly related the electronic transmission characteristics of the atomic-scale junctions to their heat dissipation properties, thus enabling the study of heat transport in atomic and molecular junctions, which is an important and challenging scientific and technological goal. From an opposing perspective, another interesting and challenging issue is how to use the environmental heat, such as converting heat energy to electricity at the molecular level. We highlight the recent significant advances in thermoelectricity using different molecular junction platforms in sections 5.5 and 7.5.

(4) Mechanics: Mechanical forces can be used to manipulate the molecular junction geometries[110,111] and the molecular orbital alignments by pulling and compressing a single-molecule junction.[112] Tao and colleagues performed a pioneering study to determine the change in the electromechanical properties of a molecular junction as the junction was stretched and compressed.[112] It was found that the conductance increased by more than an order of magnitude during stretching and then decreased as the junction was compressed. This finding was attributed to a strain-induced shift in the molecular orbital toward the Fermi level of the electrodes, thus leading to a resonant enhancement of the conductance. Using the CP-AFM technology, Xu et al. performed simultaneous force and conductance measurements on Au metal−molecule−metal junctions. In their experiment, the spring constant of the molecular junction and the dependence of the conductance on the stretching force were determined.[113] By controlling the stretching force and the stretching rates, the breakdown mechanism of the molecule junctions[111] as well as the breaking mechanism of the nanotubes were revealed,[114] which possessed extremely high tensile strengths.

(5) Nanolithography: In addition to its well-known capabilities discussed above, SPM recently demonstrated significant potential for patterning material structures at the nanometer scale. It has received attention from not only the scientific community but also the industry. Using STM, the single atoms can be directly manipulated to form a nanostructure.[115] The AFM equipped with a gold-coated tip can be used to provide a localized electron source for exposing ultrathin poly(methyl methacrylate) (PMMA) resists to make a pattern.[116] Furthermore, SPM can be used to make nanostructures by material deposition in which the STM tip acts as an emission source.[117,118] Recently, Pires et al. presented a new method to pattern molecular resists with a half pitch down to 15 nm using the local desorption of a glassy organic resist with a heatable SPM probe.[119] He et al. presented the well-patterned nanogap electrodes fabricated by mechanically scratching the graphene-based substrate with an AFM tip.[120] A detailed discussion on the SPM-based nanolithography can be found in the review paper.[121−123]

2.1.2. Mechanically Controllable Break Junction. *2.1.2.1. Work Principle and Advantages.* The idea of mechanically controllable break junctions (MCBJ) was initially introduced by Moreland and Ekin to investigate the tunneling characteristics of superconductors in 1985.[124,125] Muller and van Ruitenbeek further developed this idea to investigate the atomic point contacts from 1989−1998.[126−128] This MCBJ method was first used by Reed et al. to measure the properties of single molecules in 1997.[20,129] The work principle of the MCBJ is relatively simple with unique advantages, and it has been widely used in the field of molecular electronics. A detailed study with respect to the fabrication progress, application, and outlook of the MCBJ techniques can be found in a recently published report.[130]

As shown in Figure 5a, an MCBJ setup typically consists of three parts: a flexible substrate containing a macro-fabricated

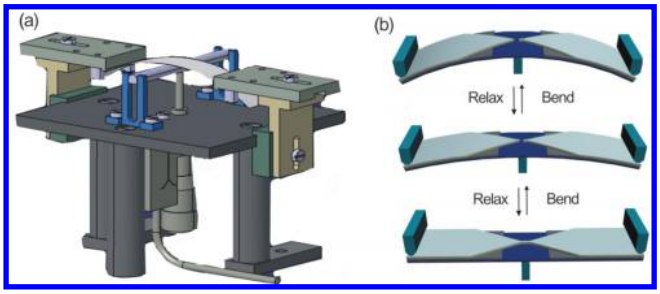

Figure 5. MCBJ setup and work principle. (a) Side-view schematic of the MCBJ setup. A MCBJ setup mainly consists of three parts: a flexible substrate containing a patterned nanostructure, a push rod for breaking the nanostructure, and a counter support. (b) Working principle of the MCBJ setup. A suspended metal bridge with a constriction is microfabricated onto the substrate. When the push rod exerts a bending force on the substrate, the movement (ΔZ) in the Z direction causes an elongation of the constriction until a break occurs in the metal bridge, resulting in the formation of two separated nanoscale electrodes. The gap size (ΔX) between the two electrodes can be precisely controlled by bending or relaxing the substrate. Reproduced with permission from ref 130. Copyright 2013 American Chemical Society.

metal wire or patterned nanostructure, a push rod to break the nanostructure, and a counter support to bend the substrate. In the early stages of the MCBJ setup, a small piece of a metallic wire with a notch in the middle is fixed onto a flexible substrate.[124] The substrate can be bent due to the three-point counter support configuration. A vertical (Z direction) movement of the push rod, which can be accurately controlled by an operator, can exert a force on the flexible substrate. When the substrate is bent, the metal wire starts to elongate, resulting in a decrease in the cross section at the notch. A further elongation will eventually lead to a complete fracture of the metal wire at the notch point. After breaking the metal wire, two clean facing electrodes are automatically generated. The

DOI: 10.1021/acs.chemrev.5b00680
Chem. Rev. 2016, 116, 4318−4440

distance between the electrodes can be accurately controlled by bending or relaxing the substrate. After integrating the molecules with anchoring groups at both ends into the tunable gap, the opposite electrodes can be bridged, and the electronic properties of the molecules can be addressed.

Because of the mechanical configuration of the three-point bend apparatus, as indicated in Figure 5b, a long vertical movement (ΔZ) of the push rod will result in only a short horizontal gap size change (ΔX) between the two electrodes. The attenuation factor, r, is defined as $r = \Delta X/\Delta Z$. Here, ΔX is the gap size change between the two nanoelectrodes, and ΔZ is the displacement of the push rod. The attenuation factor can be estimated by a geometrical configuration of the setup.[131] In a typical nanofabricated chip, the attenuation factor can be estimated as $r = \Delta X/\Delta Z = 6ut/L^2$, where u is the length of the suspended metal bridge, t is the thickness of the substrate, and L is the distance between the outer supports above the spring steel substrate.[131,132] For instance, u is approximately 1×10^{-3} mm in an EBL-defined sample, t is approximately 0.3 mm with a spring steel substrate, and L is approximately 30 mm in our homemade MCBJ setup. Using these parameters, we can determine that $r = \Delta X/\Delta Z = 6ut/L^2 = 6 \times 10^{-3} \times 0.3/30 \times 30 = 2 \times 10^{-6}$, which indicates that the gap size can be controlled with subangstrom precision and that the mechanical stress can be accurately changed. Also, the attenuation factor can be accurately calculated from the data obtained in the experiment (tunneling current vs displacement of the push rod).[133] Briefly, the gap size change (ΔX) can be deduced from the measured tunneling current, and the corresponding displacement of the push rod (ΔZ) can be recorded by the driven software of the push rod. The value of r can then be calculated on the basis of the formula $r = \Delta X/\Delta Z$.

Typically, there are three types of driving approaches for the push rod: piezoelectric actuator,[134] motor via gear-coupling,[135,136] and motor via differential-screw.[137] For the first type, a piezoelectric actuator generally comprises a longitudinal effect-type laminated piezoelectric element. When a voltage is applied to the piezoelectric element, it will expand in the horizontal direction, and a push force will be generated to bend the substrate, as illustrated in Figure 6a. The advantage of this strategy is that the movement of the push rod can be precisely controlled with nanometer accuracy in a sensitive feedback system. The disadvantages of this strategy are that (1) it is relatively expensive for a piezo actuator push rod, especially when a long distance movement of the push rod is required; and (2) typically, only a weak force can be generated in the cryogenic environment, for example, 4 K, and the weak force makes it hard to bend the substrate. For the second type, a motor via gear coupling is used to drive the push rod, in which the movement speed of the push rod can be rapidly reduced, as shown in Figure 6b. Using gear-coupling combined with a smart motor, the movement of the push rod can be accurately controlled. The flaw in this strategy is that a tiny discrete movement of the push rod always exists due to the mechanical gear-coupling, resulting in a discontinuous change in the gap size. For the third type, a differential-screw push uses two screws with different pitches, as indicated in Figure 6c. The slight pitch difference between screw 1 and screw 2 enables operators to accurately control the movement of the push rod with high resolution while simultaneously guaranteeing a continuous gap change.

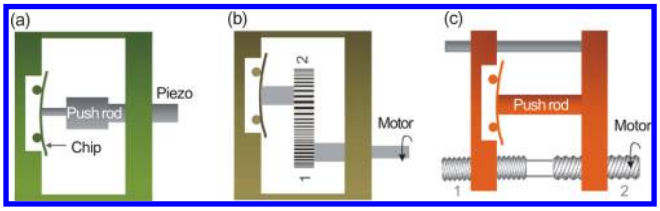

Figure 6. Schematic of three typical types of MCBJ setups. (a) Piezoelectric actuator, in which the displacement of the push rod is driven by the piezo actuator. (b) Motor drive via gear-coupling, the small gear (1) coupled to the large gear (2), reducing the movement speed of the push rod. (c) Motor drive via differential-screw, where the tiny pitch difference between screw 1 and screw 2 guarantees a precise control of the push rod.

The MCBJ technique has several advantages. (1) The MCBJ setup can be easily integrated with other systems, such as a Raman spectrometer or high vacuum TEM system, due to its small size and flexible configuration.[138,139] (2) The influence of contaminants is decreased because a fresh break cross section of the gold bridge is mechanically created in the MCBJ experiment without additional chemical treatments.[140] (3) With advanced lithographic techniques, the electrodes can be scaled down to molecular dimensions, which makes it well suitable for single-molecule measurements.[141] Moreover, the number of bridged molecules can be changed by accurately controlling the gap size; for example, a few molecules will break from one of the electrodes due to a further increase in the gap size. (4) The most impressive feature of the MCBJ technique is its high mechanical stability of the system as compared to other techniques, such as the STM technique.[130] Because the electrodes are rigidly fixed to the same substrate at a short distance (less than 1 μm by the advanced lithographic fabrication), the length of the freestanding parts is significantly shorter than the tip in a typical STM setup, which results in an extremely stable electrode with a high resonant frequency. Furthermore, as discussed above, the amazing attenuation factor spontaneously leads to the fact that the motion of the push rod (ΔZ) causes a reduced horizontal displacement (ΔX) in the electrodes by several magnitudes. This attenuation indicates that any disturbing effect from the push rod, for example, mechanical vibration, thermal expansion, or voltage instability with piezoelectric component, can be strongly suspended.

In addition to the important advantages of the MCBJ technique, the main disadvantages can be described. (1) The MCBJs cannot be operated in a manner similar to the crossbars to address a specific cross-section, which limits the potential applications in information processing. (2) Unlike the STM technique, the MCBJs cannot obtain the surface topography of the sample. Nevertheless, as a fundamental research technique with considerable mechanical stability, MCBJs are powerful and practical for investigating single-molecule properties.

2.1.2.2. MCBJ Chip Fabrication. The fabrication of the MCBJ chip is summarized in Figure 7. According to the fabrication methods, there are three main types of MCBJ chips: mechanically cut-based, electrochemically deposition-based,[142] and nanofabricated.[131,143] On the basis of the structure of the chip, it can be classified as a two-terminal chip[144] or a three-terminal chip.[145] In the three-terminal chip, one of the electrodes generally operates as the gate electrode by which the electron transport can be modulated, and the other two electrodes are used as the source and the drain electrodes.

DOI: 10.1021/acs.chemrev.5b00680
Chem. Rev. 2016, 116, 4318−4440

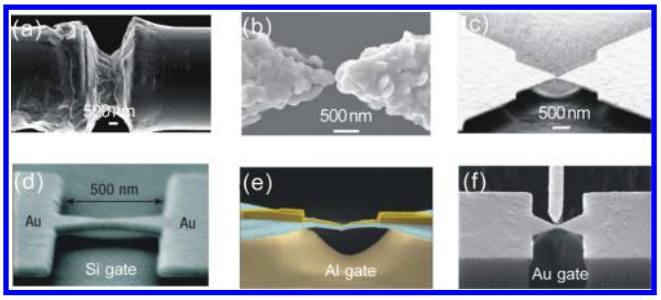

Figure 7. Typical MCBJ chips. (a) Mechanical cut to create a notch on the gold wire. (b) Electrochemically deposition-based electrodes. Reproduced with permission from ref 147. Copyright 2006 Wiley-VCH. (c) EBL-defined electrodes on flexible metal substrates. Reproduced with permission from ref 144. Copyright 2006 Wiley-VCH. (d) Suspended gating (indirectly contacted) above a doped silicon substrate. Reproduced with permission from ref 154. Copyright 2010 AAAS. (e) Back gate in direct contact with the source and drain electrodes. Reproduced with permission from ref 152. Copyright 2013 Nature Publishing Group. (f) Side gating with a nanometal electrode. Reproduced with permission from ref 150. Copyright 2013 American Chemical Society.

An early low-cost macrofabricated chip for an MCBJ experiment is presented in Figure 7a. A thin metal wire, normally less than a few millimeters in diameter, was fixed onto an insulated flexible substrate using two drops of glue. A notch was created using a knife through a mechanical cut in the middle of the metal wire to allow it to easily break when subjected to a bend force. These types of chips are cheap and simple to fabricate. The disadvantages of this macrofabricated chip can be described as follows. (1) The large size and the rough surface of the electrode are not quite suitable for single-molecule investigations. (2) Contamination may occur because the mechanical cutting is typically performed in an ambient environment. (3) There is a limited attenuation factor, which indicates that the mechanical stability of the macrofabricated chips is not as good as that of the microfabricated chip.

The chips for the MCBJ experiments can also be fabricated using electrodeposition on template electrodes that were predefined on the substrate (Figure 7b).[146−148] The initial electrodes, which have a relatively large gap, are generally fabricated using optical lithographic techniques on the substrates. The gap is then narrowed and fused by depositing specific atoms onto the electrodes. The fused nanobridge can be reopened by controlling the substrate bend configuration. This strategy, which combines the electrochemical deposition advantages with the MCBJ advantages, for example, the use of optical lithography instead of EBL, is facile for the fabrication, and the gap size can be changed in situ.[149] The disadvantage of this strategy is that the fabrication process is time-consuming, and contamination is likely due to the electrochemical process.

Recently, advanced EBL and reactive ion etching (RIE) techniques were used to fabricate the MCBJ chip based on a flexible substrate.[144,150] Figure 7c illustrates a typical EBL fabricated MCBJ chip.[144] The chip fabrication process consists of several key steps: (1) an isolating layer (polyimide or silicon dioxide several micrometers thick) is spun onto the substrate, such as thin silicon wafer, spring steel sheet, or bronze sheet; (2) a standard EBL process is performed to define the metal wire with a constriction in the middle; and (3) the isolating layer is partly removed by an RIE to obtain a suspended metal bridge.

A significant development of the MCBJ is the introduction of gating control. Ralph et al. initially reported the implementation of both electrostatic gating and mechanical adjustability within the same single-molecule device by adding a bottom gate electrode to a mechanically controlled break junction.[151] To fabricate the bottom-gated chip, a thick silicon dioxide film was first grown on top of a doped silicon wafer. An EBL process then was performed to pattern the gold electrode structure. Finally, hydrofluoric acid was used to remove the SiO_2 under the gold electrode, thus suspending it above the silicon substrate. In this chip, the doped conductive silicon was used as the gate electrode, as shown in Figure 7d. This newly designed chip combines both the ability to mechanically adjust the spacing between the electrodes and the ability to shift the energy levels of the molecules.

Zant et al. further developed the bottom gate architecture for the independent mechanical and electrostatic tuning of the charge transport,[152,153] as shown in Figure 7e, in contrast to previous gated mechanical break junctions, in which the source−drain electrodes are suspended above the gate electrode, and the fabricated source−drain electrodes are in contact with the gate electrode via a thin Al_2O_3 insulator. It was demonstrated that the electrical continuity of the gate electrode was maintained upon the bending of the substrate and successfully achieved mechanical and electrical control of the charge transport through the nanoscale island using such bottom gating. The technique was further applied to the molecular electronics investigation, which clarified the dominant role of the image-charge effects in the single-molecule junctions. A minor fault in this design is that the available gap size range was limited to avoid the partial breakage of the gate dielectric.

Inspired by the bottom gating, Xiang et al. proposed a new design for the MCBJ chips by adding a side-gate electrode near the source−drain electrode,[150] as shown in Figure 7f. Using the advanced EBL and RIE methods, a suspended metal bridge and a gate electrode in plane were fabricated simultaneously. The Au gate electrode was located a few nanometers away from the suspended metal bridge. Using this noncontact side-gate electrode, the position of the molecular energy level was shifted, and the electron transport characteristics were modulated. The advantage of this design is that the gate electrode can remain unchanged during the operation; that is, the fracture of the gate electrode can be avoided when one tries to break the metal wire or to obtain a large gap by deeply bending the substrate. The shortcoming in this design is that the gate efficiency is average and strongly depends on the distance between the gate electrode and the molecular junctions.

2.1.2.3. MCBJ Applications. Because of their advantages, for example, excellent mechanical stability, continuously precise tunable gap size, atomic scale electrodes, and minimum contamination, MCBJs have been extensively used for investigating molecular electronics.[80,155,156] Here, we highlight several significant reports detailing the applications of the MCBJs. Additional information on the MCBJ-based functional devices is presented in section 7. A review of the overall applications of the MCBJ can be found elsewhere.[130]

(1) Surface-enhanced Raman scattering: Surface-enhanced Raman scattering (SERS), which provides fingerprint information on the molecules, has been a subject of renewed interest since the late 1990s, primarily motivated by the observation of SERS from single molecules. Detailed information on the SERS

DOI: 10.1021/acs.chemrev.5b00680
Chem. Rev. 2016, 116, 4318−4440

technique is addressed later in section 5.6. Here, we just show the novel idea to combine the MCBJs with the SERS technique. Tian et al. reported a combined SERS and MCBJ method to measure the SERS signals of molecules located inside the nanogap between two electrodes.[138] The enhancement of the SERS intensity with decreasing gap sizes was observed, indicating that the signals were obtained from the molecules inside the gap. These experiments provide us with a better understanding of the mechanism of the SERS and lead to detecting and studying single molecules. Later, simultaneous measurements of the conductance and the SERS were performed in a solution using nanofabricated MCBJ electrodes, and the geometrical and electronic structural dynamics of a single-molecule junction was revealed.[157] The dynamics of the 4,4′-bipyridine motion were observed between the vertical and the tilting configurations in the Au nanogap; that is, a slight increase in the tilting angle of the molecule could lead to an increase in the energies of the Raman modes and a decrease in the conductance of the molecular junctions.

(2) Electron transport: Because of the feature of continuous precise control of the gap size, the size of the between electrodes can be reduced to be as small as that of a single atom, assisting the formation of metal−molecules−metal junctions and the investigation of electron transport. For example, the conductance of single organic molecules wired by chains of metal atoms was recently addressed, revealing that hybrid junctions can exhibit a metallic-like conductance, and the conductance is insensitive to further elongation of the junction.[158] Liu et al. determined that single naphthalene and anthracene molecular junctions could exhibit well-defined high-conductance values (~0.3 G_0), which are close to the values of the metal atomic contacts.[159] The high conductance was attributed to a direct π-binding of the molecules to the Au electrodes. This study demonstrated that the direct π-binding method is one of the promising approaches to fabricate highly conductive and structurally well-defined molecular junctions. Zant et al. studied the effects of electrode separation on the molecular orbital levels in porphyrin metal complex-bridged molecular junctions based on the MCBJs.[152] They found that both the occupied and the unoccupied energy levels moved significantly toward the Fermi level upon reduction of the electrode spacing; for example, increasing the electrode separation by a few angstroms could lead to a substantial increase in the transport gap and level shifts as high as hundreds of meV. Supported by the DFT calculations, the dominant role of the image-charge effects was clarified in the single-molecule junctions. The conductance and electron transport characterization of different metal complexes were also extensively studied using the MCBJ method.[149,160,161]

(3) Control of the spin state: Single-molecule spintronics investigate the electron transport through magnetic molecules (such as transition-metal complexes) that have an internal spin degree of freedom. A detailed introduction of molecular spintronics can be found elsewhere.[162] To understand and control individual molecules, it is important to read and further control their spin state. Ralph et al. performed experiments in which they controllably stretched individual cobalt complexes while simultaneously measuring the current flow through the molecules. It was demonstrated that the molecule's spin states and the magnetic anisotropy can be manipulated in the absence of a magnetic field by modifying the molecular symmetry through stretching the molecular junction, revealing a new mechanism of spin control in single-molecule devices.[154] Weber et al. measured the electronic transport through a single-molecule junction containing two coupled spin centers that were confined on two Co^{2+} ions using the MCBJ method.[163] It was demonstrated that the electronic states of the coupled spin system could be repeatedly switched between the pseudosinglet state and the pseudotriplet state by applying a finite bias. More details are presented in section 7.4.

(4) Vibrational states: The changes in the molecular conformation, contact geometry, and molecular vibration in the electron transport can be revealed by inelastic electron tunneling spectroscopic (IETS) and noise spectroscopic measurements.[164,165] By combining the IETS with mechanical control and electrode material variation, Kim et al. successfully separated the effects of the contact geometry and the molecular conformation.[164] This experiment demonstrated that the mechanical strain of different electrode materials could be imposed onto the molecules, thus opening a new route for controlling the charge transport through individual molecules. Tsutsui et al. reported the observation of inelastic contributions to the electrical conductance and current fluctuations in single-organic molecule junctions.[166] They analyzed the conductance fluctuations in molecular junctions under a high field and found stepwise increases in the current oscillation amplitudes at distinct voltages, indicating that the field-induced current noises originated from inelastic excitations of vibration modes inherent to the target molecules. Recently, a combination of the real-time conductance fluctuations and the noise spectroscopy measurements on a series of single-molecule junctions employing the MCBJ technique demonstrated that the telegraph-like current fluctuations at room temperature should not originate from either the electron trapping or detrapping processes or the molecule reconformation, thus putting light on the fundamental understanding of the current fluctuation mechanism.[140,167]

One limitation of the MCBJ applications, especially the application in the production of highly integrated molecular commercial devices, is the out-plane push rod components. In other words, the movement of the push rod is out of the source−drain plane, which blocks the on-chip mass-fabrication and hinders the further reduction in the device dimension. Also, it is difficult to use this MCBJ method to control the number of junctions simultaneously, which limits its commercial application. To overcome the problem mentioned above, the following strategies can be potentially used: (1) A novel push rod is required. It has been reported that a micrometer-scale motor has been put into use, which may be utilized as a potential push rod to reduce the device size in the future. (2) Discovering a new architecture that is not limited to a three-point apparatus may lead from fundamental research to application-related research. For example, Chao et al. introduced an idea to fabricate a completely on-chip structure using a thermal actuator that generated rectilinear displacements and forces by leveraging deformations.[168] Although this idea remains in the theory simulation stage, the experimental realization of this idea will be helpful in mass production. (3) As an additional option, one can use a terahertz wave (optical wave) to replace the traditional push rod. For example, a structure can be designed that is similar to a bimaterial microcantilever.[169] This biomaterial cantilever will be deformed and deflected when it is exposed to the terahertz radiation. With a suitable on-chip design, this cantilever deflection can be used to form a junction within one plane. Thus, multijunction controllability and highly integrated molecular electronic devices may be available.

DOI: 10.1021/acs.chemrev.5b00680
Chem. Rev. 2016, 116, 4318−4440

2.1.3. Electromigration Breakdown Junction. The phenomenon of electromigration has been well-known for over a hundred years. In an applied electric field, the momentum of the moving electrons can be transferred to the metal atom, which results in the gradual movement of the atoms. Electromigration has been considered as the primary failure mode in microelectronic circuitry for a long time. Recently, it has been well suited to fabricate nanogapped electrodes and molecular-based devices.[170] Generally, a constriction is fabricated in the metal (e.g., gold) wire for nanogap formation. The current density is largest at the constriction part, which favors electromigration. A local reduction in the constriction width increases the local current density, thus leading to the eventual breakage of the nanowire into two distinct (source and drain) electrodes. To incorporate the molecules into the EBJs, two different approaches were developed. One approach is to deposit the molecules onto the electrode surface, after which the breaking process is performed.[171] The other approach first breaks the nanowire and then assembles the molecules into the separated electrodes.[172]

In contrast to the MCBJs, the nanogapped junctions formed by electromigration cannot make substantial repeatable measurements with the same junction. Thus, a large number of devices need to be fabricated to examine the statistical behaviors of the molecular junctions.[173] Additionally, two primary issues need to be carefully handled when processing the electromigration procedures. The first is heating in the breakage of a nanowire. The second is the gap size control. When the gap distance is comparable to the molecular length, only then it is possible to bridge the two electrodes using molecules. To control the gap size, several strategies have been introduced, which are addressed below in detail.

Although electromigration is a thermally assisted process that requires Joule heating to start gap formation, excessive heating should be avoided because it can result in undesired melting of the metal, destruction of the molecules, and formation of gold debris (islands) inside the gap.[174] Unintentional metal debris in the gap interferes with the insertion of the molecules of interest and may mask the intrinsic molecular signals.[174,175] This metal debris can exhibit the same behavior as the molecules, for example, similar current−voltage characterization, Coulomb blockade, and Kondo effect.[175−177] To distinguish the molecular transport from the transport through small gold grains or other imperfections, three strategies are typically used: (1) the lead−molecule coupling in three-terminal devices can be used to realize this distinction because metal grains and molecules exhibit completely different behaviors on the gating voltage;[174,175] (2) using specific characterization techniques, for example, inelastic-tunneling spectroscopy, to address the molecular vibration modes to realize the distinction;[171,178] and (3) using functional molecules; that is, the molecules with magnetic properties or light-sensitive molecules will behave differently from that expected for gold grains.[179] To reduce the metal debris in the nanogap, one relatively simple method is to reduce the resistance in series with the junction. By minimizing the total series resistance of the system, the temperature can be kept low during the electromigration process.[180]

2.1.3.1. Device Fabrication. The wire with a constriction was typically defined using optical lithography or the EBL. Employing the lithographic technique, different types of metal wires were prepared. Following the electromigration process, different types of nanogaps, such as gold nanogaps,[180] zinc nanogaps,[181] nickel nanogaps,[182] silver nanogaps,[183] platinum nanogaps,[184] and palladium nanogaps,[185] were fabricated. In addition to the standard lithographic method used to fabricate the metal wire, several novel methods were recently reported. (1) Optical lithography combined with focused ion beam (FIB) lithography: Asghar et al. reported the use of a FIB to "scratch" and remove a thin layer of gold wires predefined by optical lithography. The scratch results in thinning of the metal wire at the designated point, which is unavailable using the standard optical lithography. Combining FIB scratching with electromigration provides an elegant approach to create nanoscale break junctions at an exact location with an extremely narrow distribution of the nanogap sizes.[186] (2) Electrochemical deposition combined with electromigration: Valladares et al. reported a method to repeatedly generate a nanogap.[182] Briefly, an electrochemical deposition technique was used to bridge two electrodes. During the deposition process, a metal atom was deposited at the predefined electrodes, and the gap width decreased exponentially with time until the electrode gaps were eventually bridged. Once the bridge was formed, the ex situ electromigration technique was used to reopen the nanogap. (3) Evaporation synchronized with electromigration: Naitoh et al. developed a procedure for the fabrication of Au electrodes using evaporation synchronized with electromigration.[187] The key point is that the electromigration process was performed simultaneously with the metal evaporation process. It was demonstrated that the application of this method can form nanogaps with a gap size as small as 1 nm, and the gap size can be simply controlled by changing the magnitude of the applied voltage.

In addition to metal materials, nonmetal materials, such as graphene[188,189] and SWNTs,[190] can use the electromigration technique to fabricate the nanogap. For example, Zhang et al. reported visualizing the electrical breakdown of suspended graphene sheets.[189] Using a pulsed electrical breakdown technique, narrow gaps were formed in suspended single to few-layer graphene devices. It was observed that the broken region started from the center of the graphene sheet and expanded. Upon a further increase in the amplitude of the pulse voltage, the graphene sheet was completely broken but remained freestanding. This observation underscores the potential of all-carbon devices to be integrated with graphene electronics. An additional discussion on molecular devices based on carbon-based electrodes is provided in section 3.2.

Because a gate electrode can be easily fabricated on the substrate using the standard lithographic technique before the electromigration process, the EBJ is especially advantageous in creating three-terminal device configurations, in which the molecule energy level can be changed on the basis of the applied gate voltage.[176,179] The gate coupling efficiency factor (α), which describes the effectiveness of the molecular orbital gating, is of key importance to a three-terminal device. For example, if α = 0.1 eV V^{-1}, then the molecular orbital energy changes by 0.1 eV when 1 V is applied to the gate electrode. To obtain a large gate coupling efficiency, two conditions need to be satisfied: (1) a large local electrostatic field is generated upon the gate voltage;[175] and (2) the molecule resides near the gate metal−dielectric interface to reduce screening by the electrodes.[171]

Typically, two types of gate geometries were used. The first type, noted as bottom gating, is commonly used.[175,176] In this geometry, a gate electrode is fabricated beneath source−drain electrodes that are separated by an insulation layer. Currently,

DOI: 10.1021/acs.chemrev.5b00680
Chem. Rev. 2016, 116, 4318−4440

two materials are frequently used for bottom gating: highly doped Si substrates with a thermally grown SiO_2 layer on the surface and Al strips with a native oxide Al_2O_3 layer on the surface. An example of the Al gate electrodes is provided in Figure 8a. Two factors, which are (1) a higher relative dielectric

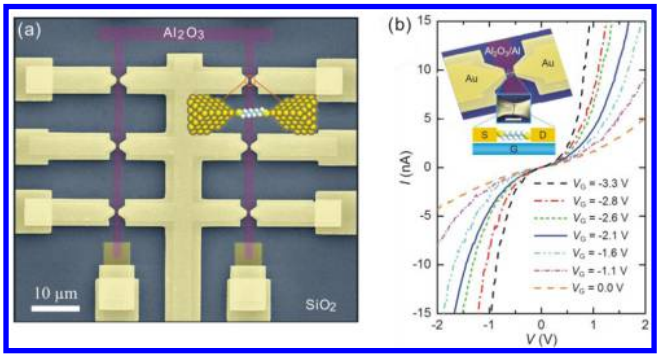

Figure 8. Electromigration breakdown molecular junctions. A nanogap was obtained by breaking Au wires using the electromigration technique. (a) SEM image of the device pattern. The entire structure was fabricated on an oxidized silicon wafer. The yellow regions represent the Au electrodes, and the purple region represents the oxidized Allium gate electrode. (b) Gate-controlled $I-V$ curves measured at 4.2 K of an Au−octanedithiol−Au junction. Inset: Device structure and schematic. Reproduced with permission from ref 171. Copyright 2009 Nature Publishing Group.

constant of the Al gating and (2) a thinner insulation layer (Al_2O_3), result in the gating efficiency of aluminum-based devices to be higher than that of silicon-based devices.[175]

The second geometry is an in-plane side-gate electrode, in which the gate electrode and the source−drain electrodes are located in the same plane.[174] In this geometry, the electrical field is enhanced by the thickness of the gate electrodes, especially on the gate side as compared to a typical back gate configuration. Generally, to directly visualize the electromigration process and discriminate the trapped molecules/metal clusters from dusts inside the gap, transmission electron microscopy (TEM) requires the use of electron transparent substrates, which are noncompatible with the most common three-terminal devices that have a back gate electrode. This side gate geometry is relatively compatible with the transmission electron microscopy inspection and can overcome this problem. Besides these advantages, the side gate geometry also faces the challenge; that is, the gating potential could be screened by the source−drain electrodes, which means that only the molecules facing the gate electrodes can be influenced by the gate electrodes.

2.1.3.2. Gap Size Control. As mentioned above, controlling the gap size is of key importance to the electromigration method. The earlier electromigration approaches that used a single voltage ramp normally yielded a thermal runaway and a random distribution of the gap sizes. Most of the gap sizes are larger than hundreds of nanometers, resulting in them being unsuitable for the single-molecule investigation. There are two typical strategies, that is, self-breaking and feedback-control, used to control the gap size between the eventually formed electrodes.

Self-breaking: The self-breaking method has recently proven to be an efficient technique for reducing the gap size and avoiding the nanodebris formation.[191] In this method, a nanosized metal junction is gradually shrunk using a typical electromigration procedure where bias ramps are applied repetitively. When the metal junction was narrowed to the atomic size, the active breaking process was stopped, and the junction was held under a very low field conditions. The atom-sized contact then ruptures spontaneously due to the thermal fluctuations, efficiently avoiding excessive heating. Employing this self-break method, O'Neill et al. demonstrated that there were no signs of metal clusters or metal islands inside the gap, a problem that is often observed in the traditional electromigration techniques.[191] Tsutsui et al. demonstrated that 0.5 nm electrode gaps could be achieved using the self-breaking technique assisted by the MCBJ technique.[192]

The self-breaking process is relatively easy for gold (Au) electrodes at room temperature due to the high mobility of the Au atoms and the residual stress on the wire after electromigration. However, for other metals, such as Pt, self-breaking is not possible at room temperature due to the higher activation barrier. Fortunately, Prins et al. found that self-breaking did occur at a temperature approximately 100 °C or higher. On the basis of these results, they developed a method by which they performed electromigration and self-breaking of Pt nanowires at lifted temperatures. The sample then was cooled to room temperature to freeze the atomic mobility. This process results in nanogaps that are free of metallic clusters and relatively stable at room temperature for months.[184]

Feedback-control: A feedback-controlled electromigration (FCE) technique was recently developed, which actively adjusted the applied voltage in response to the changing conductance of the weak link to controllably create the nanoscale junctions.[177,193] The distinctive advantage of the FCE is that the feedback is used to ensure that the nanogap formation occurs through electromigration at a regulated onset temperature in the constriction region, and a small gap size can thus be obtained. Unlike earlier electromigration approaches that used a single voltage ramp, the FCE typically uses a programmed algorithm to govern the electromigration process.[194,195] For example, Xiang et al. used a LabVIEW-programmed voltage algorithm to control the electromigration process.[194] The process for their method involved four steps. (1) An initial voltage bias was applied to the metal wire, and the initial wire resistance was measured. (2) A bias voltage was then increased gently in a ramp, and the wire resistance was measured simultaneously. (3) When the resistance change ratio exceeded a predefined threshold, the applied voltage was reduced by 5%. (4) A new reference resistance value was measured again, and the cycle was repeated.

In addition to the resistance as well as the effective conductance, noise can also be used as a feedback signal. Dong et al. observed that the measured relative current noise immediately before the nanogap formation increased 2 orders of magnitude higher than the resistance in the first stage of the electromigration process.[196] The considerable change in the current noise during the electromigration process makes it an attractive candidate to be used as a parameter in the control feedback loop to break the wires. They also presented initial results for using noise to control the disassembly process. In a typical two-terminal system, a fixed bias voltage U_0 is applied to the junction resistance as well as the series lead resistance. Consequently, as electromigration begins to shrink the junction, the junction resistance increases, and the voltage falls to the junction increase. The power dissipated in the junction increases proportionally to the junction resistance, which may cause a thermal runaway and destroy the junctions.

DOI: 10.1021/acs.chemrev.5b00680
Chem. Rev. 2016, 116, 4318−4440

To overcome this problem, Schönenberger et al. developed a highly reproducible method to fabricate metallic electrodes with a nanometer separation using four terminal devices.[197] The four terminals comprise two symmetric pairs of contacts. In one pair, the bias voltage U_0 is supplied, and in the other pair, the voltage drop U_J over the junction is simultaneously measured. Regardless of the actual value of the junction resistance, the source maintains a constant U_J value. This novel design effectively avoids the thermal instability because the power over the junction will decrease with a fixed U_J and an increased junction resistance.

The limitation of the FCE is that it is time-consuming to fabricate a complex circuitry because the formation of multiple nanogaps requires each junction to undergo the FCE process individually. To overcome this problem, Johnston et al. developed a technique using the FCE that permits the simultaneous fabrication of dozens of nanogaps at room temperature in a single processing step.[198] In their experiments, the formation of parallel nanogaps is achieved by a balanced simultaneous process that uses a novel arrangement of nanoscale shorts between the parallel constrictions where the nanogaps are formed. This technique can be potentially used for constructing complex circuits of molecular-scale electronic devices.

2.1.3.3. Electromigration Applications. Imaging the electromigration process: Several research groups found that the gaps formed during electromigration may contain metal nanoparticles that might produce artifacts for the molecular signals.[177,199,200] Taychatanapat et al. addressed this issue by observing the electromigration process in real time within a scanning electron microscope (SEM).[201] It was found that the amount of series resistance in the electromigration circuit is a critical parameter in controlling the overall morphology of the junction after electromigration. This study provides a direct confirmation that the simple voltage ramp with no added series resistance in the circuit gradually changes the wire morphology without the formation of any visible nanoparticles.

Unfortunately, scanning electron microscope images of the nanogaps do not have the subnanometer resolution required to view the detailed structure of the nanogap; thus, it is a big challenge to view the electromigration process at atom-scale resolution. To address this critical issue, Strachan et al. prepared electromigrated nanogaps on free-standing SiNx membranes that are transparent to the high-energy electrons and are thus compatible with the transmission electron microscopy (TEM) at a subnanometer resolution.[202] It was determined that the junction pinched away from the edges of the original leads for the samples prepared using the FCE technique. They pointed out that the electrodes were clear of residual debris left from the evaporation procedures, and it was possible to avoid potential parasitic conductance channels through spurious metallic particles using the electromigration samples.

Moreover, Strachan et al. used real-time TEM imaging to monitor the dynamics of the FCE process at the subnanometer scale, which was not accessible to the earlier electromigration investigations.[195] It was determined that well-defined crystal facets appeared during the nanogap formation, indicating a layer-by-layer electromigration process. Furthermore, it was observed that the electromigration process is reversible; for example, the void can be refilled with gold atoms when the applied voltage is reversed. This finding is clear evidence that the nanogap does not melt during the FCE process, which is contrary to what occurs during the single voltage ramp procedure.

Although several attempts have been made to develop electron transparent substrates and perform two-terminal transport measurements in addition to the TEM inspection,[195,203,204] it is a considerable challenge to perform these measurements with bottom-gated devices. Gao et al. first demonstrated a technique to perform three-terminal transport measurements that were compatible with the ex situ TEM inspection.[205] An electron-transparent Si_3N_4 membrane was used as the substrate, and A Cr/Au layer was deposited on the backside of the membrane, which served as the back gate. The nanogaps were formed on the membrane using electromigration. The three-terminal electron transport measurements were performed without molecules at cryogenic temperatures, and the Coulomb blockade features were observed. After the transport measurements, the Cr/Au back gate was removed to make the substrate transparent, and the TEM inspection was conducted ex situ again on these samples. The TEM inspection revealed the presence of a few nanoparticles in agreement with the transport measurements. In other words, the sample topology deduced from the differential conductance (dI/dV) plots agreed with the one used for the TEM. This technique can be used to reduce the ambiguous interpretation by providing more information on the sample topology and the structure.

Inelastic electron tunneling spectroscopy (IETS): With the $I-V$ characterization, it is difficult to distinguish the molecular transport from the transport through small gold debris or other imperfections.[175] Molecule-specific features (such as vibrational modes or gate coupling) can distinguish the presence of single molecules in the gap from spurious gold dots.[172] The inelastic electron tunneling spectroscopy (IETS) provides not only a characterization technique to identify the molecules in the junctions but also important insights into how the interaction of tunneling charge carriers with molecular vibrational modes influences the overall charge transport characteristics. Most of the IETS studies have been performed on the basis of the enormous number of molecules in the monolayer junctions. At the single-molecule level, Song et al. measured the vibrational signatures of the molecular junctions using the IETS, which was confirmed by the estimated conductance.[206] The Au−S stretch mode was clearly observed in the measurement, and the IETS was extremely sensitive to the chemical structures of the target molecules, suggesting that a reliable metal−molecule contact was formed. The IETS provided unambiguous experimental evidence of the existence of molecules in the nanogap electrodes fabricated using the electromigration technology.

Surface-enhanced Raman spectroscopy: Surface-enhanced Raman spectroscopy (SERS) is a useful tool for accessing vibrational and chemical information down to the single-molecule level. The SERS typically relies on plasmon excitations in metal nanostructures to concentrate the incident radiation. Generally, the SERS platforms involve metal nanoparticles to generate the required electromagnetic enhancements. The electromigration technique provides a true nanoscale gap between the extended electrodes instead of discrete subwavelength nanoparticles. The ability to fabricate precise gaps on demand combined with the simultaneous electronic transport measurements of the nanogap provides the fingerprint information on the molecules.[45] Ward et al. used the nanoscale gap structures prepared using the electromigration technology to perform simultaneous measurements of the

DOI: 10.1021/acs.chemrev.5b00680
Chem. Rev. 2016, 116, 4318−4440

electronic transport and the SERS.[207] It was observed that the conductance changes often correlated with sudden changes in the intensity of different sets of Raman modes. These correlated fluctuations in the tunneling conductance and the SERS intensity could not be explained by the changes in the gap configuration due to the fact that the tunneling conductance depended exponentially on the gap geometry (e.g., conductance could change by a factor of 10 for a 0.1 nm change in the gap separation); however, the electromagnetic enhancement was not as strongly affected by the gap size. The experiments suggested that both the SERS and the conductance changes were most likely due to changes in the conformation and the binding of the individual molecules, indicating a single- or few-molecule SERS sensitivity.

Typically, incident light with an electric field polarized across the gap (along the nanowire) is well-known to induce the strongest SERS enhancements.[138] Surprisingly, Herzog et al. observed that for a nanogap located within a nanowire, the greatest enhancement and resulting SERS signal occurred when the electric field of the incident light was polarized along the gap (transverse to the nanowire).[208] This polarization dependence was interpreted by the striking asymmetries in the nanogap fabricated using the electromigration technique. Because of the intrinsic asymmetries of the nanogap, the dipolar plasmon mode that resonated transversely across the nanowire coupled with dark multipolar modes, thus causing the intense hybrid plasmon modes to be significantly stronger than that of the longitudinal modes in the structures. These results put light on the understanding of the nature of plasmons in the asymmetric structures and open the possibility of further geometric optimization of the near field-far field. In a further study, the same group developed the Raman technology to address vibrational and electronic heating in situ in nanoscale junctions fabricated using the electromigration technology.[209] When the current flowed through the molecules, the inelastic processes transferred energy from the electrons to the local molecular vibrational modes. In the presence of optical radiation, direct optical absorption and the decay of plasmon excitations produced hot electrons and holes in the metal. These hot electrons and a hot substrate can excite the molecular vibrational modes during the Raman scattering processes. It was demonstrated that the SERS could be used to determine the effective temperature in the molecular junction regime. By measuring the Stokes spectrum, anti-Stokes spectrum, and electrical transport characterization, it was revealed that the mode-specific vibrations could be pumped by both optical excitation and direct current with effective temperatures exceeding several hundred degrees kelvin. These experiments open a new window to investigate local heating in the molecular junctions.[209]

Kondo effect: When a quantum dot (e.g., nanocrystal and nanotube) is attached to the metallic electrodes via the tunneling barriers, the electron transport is dominated by single-electron charging and energy-level quantization.[210] As the coupling to the electrodes increases, higher-order tunneling and correlated electron motion will lead to new phenomena, including the Kondo effect, which results from the exchange interaction between an unpaired localized spin and the conduction electrons in the metallic electrodes. Most of the studies on the Kondo phenomena in quantum dots were typically performed on systems where precise control over the spin degrees of freedom was difficult. Using a chemical design, the spin and the orbital degrees of freedom can be controlled for those molecules (e.g., metal ion complex), thus providing a new system for the Kondo phenomena investigations. Liang et al. first reported the observation of the Kondo effect in single-molecule junctions, where an individual divanadium molecule was trapped in the nanogap by the electromigration method and served as a spin impurity.[210] In the differential conductance maps (dI/dV as a function of the gate voltage V_G and the source−drain voltage V_{SD}), a diamond-shape pattern was observed, indicating the achievement of a single electron transistor. More significantly, the Kondo resonance (i.e., a sharp zero-bias conductance peak) was clearly observed, and it was demonstrated that this Kondo resonance could be tuned reversibly by using the gate voltage to alter the charge and the spin state of the molecules.

In another example, the Kondo effect in C_{60} single-molecule junctions was investigated.[211] Yu et al. used the electromigration technique to fabricate C_{60}-based single-molecule transistors, and demonstrated that each of them could act as a single-electron device in the Coulomb blockade regime at low temperatures. Interestingly, sidebands parallel to the zero-bias peak were observed, thus indicating the conduction processes that involved both multibody correlations and inelastic coupling to the vibrational modes. In the same year, Pasupathy et al. measured Kondo-assisted tunneling using C_{60} molecules in contact with ferromagnetic nickel electrodes fabricated by the electromigration method.[24] It was demonstrated that the C_{60} molecules could be strongly coupled to nickel (Ni) electrodes to exhibit the Kondo effect. More importantly, it was revealed that ferromagnetism could suppress Kondo-assisted tunneling; however, Kondo correlations were still present within the ferromagnetic electrodes. They found that a Kondo peak split was strongly affected by the magnetic moment alignment in the two electrodes under an applied magnetic field, hence proving a new window was needed to modulate the Kondo resonance.

2.1.4. Electrochemical Deposition Junction. As mentioned above, it is difficult to use the MCBJ method to fabricate an integrated microchip due to the drive apparatus.[130] The electromigration method is unlikely to reproducibly fabricate nanogaps with a precise tunable width.[206] Unlike the electromigration and the MCBJ methods, the electrochemical method, for example, electrodeposition or electrodissolution, is reversible and device-compatible.[212−214] By electrodepositing metal atoms onto a specific face of the electrodes, the gap between two facing electrodes can be sequentially narrowed. The electrochemical process can be reversed in an electrodissolution mode for controlled etching/dissolution of the metal atoms from a wire/electrode; thus, the gap can be widened.

The working principle of the electrochemical deposition method is sophisticated.[213] Briefly, an array of original metal electrode pairs were fabricated using the EBL[214,215] or optical lithography[216] techniques on a chip (such as thermally oxidized Si wafer). The separation between two facing electrodes in each pair was normally larger than dozen of nanometers. It should be noted that the electrodes were typically covered with Si_3N_4,[215] SiO_2,[216] or photoresists,[147] except for a window exposing the gap region of the electrodes to the electrolyte for electrochemical deposition and etching. This insulating layer reduced the leakage current due to ionic conduction. When a voltage was applied between the counter electrode (CE) and the working electrode (WE) in the electrolytes, the metal ions were reduced to metal atoms at the surface of the WE. The gap was then reduced due to the electrodeposition of the Au atoms

DOI: 10.1021/acs.chemrev.5b00680
Chem. Rev. 2016, 116, 4318−4440

onto the electrodes layer by layer. Using the electrochemical deposition, different metals can be deposited to form junctions of heterogeneous compositions, for example, the deposition of Cu on Au leads.[217]

A key issue of the electrochemical method is the use of a feedback system to precisely control the gap width. There are several strategies using different experimental parameters as feedback signals to control the gap size. (1) The first is using the electrochemical current and the electrolyte conductance as a feedback indicator to critically monitor the gap width, especially when the gap is narrowed below the submicrometer scale.[212,218] The electrodeposition process was stopped by switching off the potentiostat when the conductance reached a preset value. This provides an accurate and reproducible way to control the gap width below a couple of nanometers. (2) Next is using the tunneling current as a feedback indicator to accurately monitor the electrochemical deposition or etching.[213,219] During the electrodeposition process, the current flow between the two work electrodes was monitored throughout the experiment. Initially, the current was small due to the ionic leakage current; however, it increased rapidly when the gap was small enough to detect a tunneling current across the gap. The tunneling current served as a feedback signal to control the deposition process. This method provides the possibility of achieving a suitable gap fitting different molecules. However, this promising method has a limitation: the gap width range is small; typically, the gap is less than 1 nm because it is based on the detection and the feedback of the tunneling current. (3) Third is using the electrode potential (V_{gap}) as the feedback indicator.[22,216] In the previous report, both of the facing electrodes served as the working electrodes (WE), and the metal layer was deposited on both of them simultaneously. Tian et al. introduced a new design in which the pair of facing electrodes served as the WE and the reference electrode (RE).[22,216] Experiments were performed on this new electrode arrangement by applying a controlled current between the WE and the CE, as shown in Figure 9a. Metal atoms were deposited layer by layer only on the WE, and the gap width between the WE and the RE was reduced. The value of V_{gap} (between the WE and the RE) decreased and eventually reached zero, thus indicating that the WE and RE electrodes were fully connected. In this way, the monitored V_{gap} can be used as a feedback signal to control the gap width. The disadvantage of this strategy is that the asymmetric deposition will result in asymmetric electrodes, as illustrated in Figure 9b–e. (4) Next is utilizing high-frequency impedance in the feedbacks system.[220,221] Liu et al. reported a new system that demonstrated an interesting frequency dependency on the final gap size. In their design, both electrodes of the gap were used as cathodes to symmetrically deposit the metal. The symmetric design guaranteed that the current signal traveled only in the symmetric circuit loop, and the faradic current was recorded independently on the electrochemical workstation. The amplitude of the ac voltage (V_m) recorded at one electrode decreased as the gap distance was close enough. The time evolution of V_m in a complete deposition process was strongly dependent on the frequencies, thus making it a promising tool to control the gap size.[220] (5) The final strategy is using a self-termination reaction to control the gap size. Majima et al. demonstrated a self-termination reaction during electroless gold plating (EGP), which provided a uniform gap separation with different initial separations.[222,223] They designed and implemented a chemical reaction in which the growth of the plating

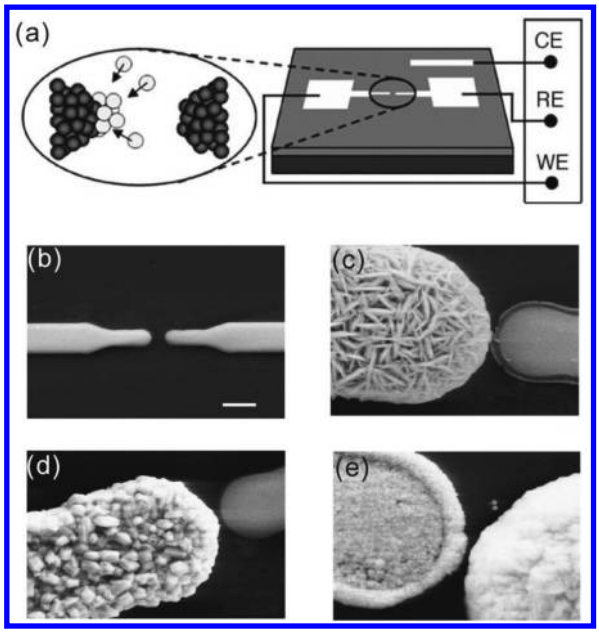

Figure 9. Electrochemical deposition. (a) Schematic drawing of the experimental setup. A pair of original facing gold electrodes were fabricated on silicon wafers. Three electrodes were used: counter electrode (CE), work electrode (WE), and reference electrode (RE). The gap was reduced by electrochemically depositing metal atoms on the WE. (b) The original electrodes were separated by two micrometers. (c–e) Layer-by-layer metal atom deposition using different constant current densities: 1.0 mA cm^{-2} (c), 0.4 mA cm^{-2} (d), and 0.1 mA cm^{-2} (e). Reproduced with permission from ref 216. Copyright 2005 Elsevier.

layer in the space between the electrodes was self-terminated. Briefly, the probability of the ions and the reducing agent accessing the nanogap decreased as the gap narrowed in opposition to other areas. Therefore, the electroless plating rate between the electrodes decreased as the gap separation decreased, even becoming zero when no plating ions were transported into the nanogap. Using this method, nanogap electrodes for nanodevices with a separation of 3.0 nm were simultaneously mass-produced at a yield of 90%.[223]

The structure of the electrochemically deposited material can be tuned by the deposition current,[216] electrode potential,[147] electrolyte concentration,[216] and plating mode (pulse or DC).[224] After systematic studies, Liu et al. pointed out that it was essential to select a suitable constant current (I_{dep}) to ensure the deposited layers were smooth and compact rather than rough or loose.[216] They found that a relatively small deposition current led to a more uniform and compact electrode, as shown in Figure 9b. Yi et al. reported that the morphology of the electrode surface could be modified by the applied electrochemical potential,[147] which created nanoelectrodes with rounded surfaces at high over potentials and needle-like surfaces at low over potentials.

Although the electrode shape and the gap size can be accurately controlled by the electrochemical deposition method, this deposition method cannot offer a gap size change in situ; for example, the gap size cannot be changed to match the length of the target molecules after the molecule is integrated into the gap. To overcome this problem, two strategies were introduced, that is, deposition combined with the MCBJ[142,146,148] and deposition combined with STM.[89,148,225] Three groups did the main contributions to

DOI: 10.1021/acs.chemrev.5b00680
Chem. Rev. 2016, 116, 4318–4440

the combined deposition method with MCBJ method, that is, Tian's group, Tao's group, and Mayer's group. It was demonstrated by Tian et al. that the chip fabricated by the deposition method can be further etched to obtain a suspended metal bridge.[142] Using an MCBJ setup, the substrate of the chip can be bent to break the metal bridge mechanically, offering a tunable gap size in situ. In this way, a series of molecule junctions can be fabricated with a high yield, and the properties of the single molecules can be correspondingly investigated.[138,146] Tian et al. also presented an electrochemical strategy to extend the capability of the STM break junctions to create nanowires as well as nanogaps using various metals.[89,226] The principle of the approach was based on the electrochemical atom on an STM tip. The tip was driven toward the surface to a sufficiently close distance within an extremely short period of time to allow a jump-to-contact occurrence, which led to the transfer of the deposited atoms from the tip to the substrate surface to create a nanoconstriction. Subsequently, the nanoconstriction was gradually stretched and eventually broken to create two sharp nanoelectrodes. This strategy has been successfully proven to measure the conductance of Cu, Pd, Fe, and various single molecules.

2.1.5. Surface-Diffusion-Mediated Deposition Junction. The introduction of molecular devices into integrated circuits will most likely use the metal evaporation and deposition technique to form top contacts; however, this approach often results in the metal atoms penetrating or damaging the molecular layer. McCreery et al. reported a method of forming "soft" metallic contacts on the molecular layers using surface-diffusion-mediated deposition (SDMD), in which the metal atoms were deposited remotely and then diffused onto the molecular layer.[23,227] Employing the SDMD method, one can eliminate the problems of penetration and damage.

The SDMD fabrication process is illustrated schematically in Figure 10. In brief, pyrolyzed photoresist films (PPF) or carbon films were fabricated on thermally oxidized silicon wafers. PPF/carbon provides the necessary surface chemistry to allow the formation of a C−C bond between the conducting PPF and the molecular layer. A patterned SiO_2 mask was fabricated on top of the PPF surface using optical lithography. A reactive ion etch (RIE) process was used to etch the unprotected PPF and optimized to create a nearly vertical sidewall beneath the etching mask. The undercutting caused the etching mask to overhang the underlying PPF sidewall, as shown in Figure 10b. The molecular layers then were electrochemically grafted to the PPF/carbon sidewall, resulting in a covalently bonded molecular layer. Last, metallic contacts (Au) were deposited using electron beam evaporation in a vacuum chamber followed by a diffusion process to complete the formation of the molecular junctions. It should be noted that for direct electron-beam evaporation on the molecular layers, metal deposition occurred in a direction normal to the molecular surface, without shielding the molecular layer from radiation from the evaporation source. However, for the SDMD process, the deposition angle can be varied with respect to the surface, and the overhang of the etching mask shadowed the molecular layer from direct impingement of both incident metal atoms and radiation from the evaporation source. The key step in the SDMD process is that electronic contact with the molecular layer was achieved via surface diffusion of the deposited metal atoms toward the molecular layer, as indicated in Figure 10e.

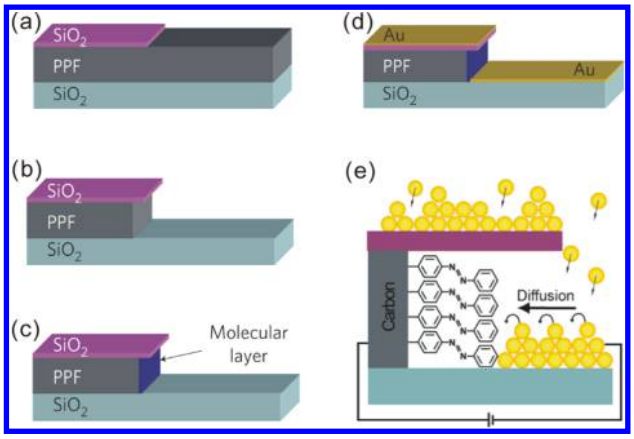

Figure 10. In situ surface-diffusion-mediated deposition technique. (a−d) Schematic of the SDMD process (a) SiO_2 etching mask was patterned on a PPF layer using optical lithography. (b) Sidewall was formed via reactive ion etching. (c) Molecular layer was adsorbed on the surface of the PPF layer. (d) Au surface diffusion during metal deposition mediates second contact formation. Reprinted with permission from ref 23. Copyright 2010 Nature Publishing Group. (e) Schematic of the atom-diffusion process to complete the molecular junctions. One terminal of molecules was attached to the conductive carbon sidewall, and another terminal of molecules was attached to the diffusion gold atom. The overhanging SiO_2 mask prevented the depositing Au atoms from directly landing on the molecular layer. Reprinted with permission from ref 227. Copyright 2011 American Chemical Society.

The remote deposition and diffusion method reduces the metal atom momentum and allows the kinetic energy and the heat of the depositing metals to be dissipated away from the molecular layer. Thus, the SDMD method can eliminate the molecular damage caused by heating and metal penetration. In the experiment, the conductance steps were clearly observed during the process when the metal atoms contacted individual molecules one at a time within a monolayer. The conductance histogram extracted from the real-time conductance curves indicated clear multiple peaks, which were dependent on the types of target molecules. Hence, the ability to fabricate molecular junctions containing single to tens of molecules "one molecule at a time" was really demonstrated. The molecular junctions fabricated using this method exhibited excellent yield (typically >90%) and reproducibility and allowed the effects of the molecular-layer structure, thickness, and work function of the contact materials on the conductance to be examined.

2.2. Ensemble Molecular Junctions

In addition to the single-molecule junctions, ensemble molecular junctions, which are formed from more than a few or self-assembled monolayers (SAMs) of molecules, are another important branch of molecular-scale electronics. Currently, there are mainly three universal strategies for forming ensemble molecular junctions for large-area electrical measurements: (1) direct formation of metal electrodes using either electron beam/thermal evaporation or electrochemical deposition, (2) incorporation of electrically conducting polymers/nanomaterials as an electrode, and (3) utilization of liquid metals as electrodes. The following section details the fabrication of ensemble molecular junctions using different state-of-art methods, including lift-and-float, liquid metal contact, nanopore and nanowell, on-wire lithography, nanoimprint lithography, crossbar or crosswire, self-aligned lithog-

DOI: 10.1021/acs.chemrev.5b00680
Chem. Rev. 2016, 116, 4318−4440

raphy, buffer interlayer-based junctions, and on-edge molecular junctions.

2.2.1. Lift-and-Float Approach. The flotation of metals on target substrate provides an efficient way to overcome the physical damage that is involved in most vacuum deposition procedures for top contacting. This method relies on capillary interactions, induced by the liquid−solid interfaces between two solids, and a common liquid for transferring thin solid metal films onto solid substrates modified by molecules. The idea, termed as a lift-off float-on (LOFO) approach, was inspired by the sample preparation in transmission electron microscopy experiments to deposit GaAs on foreign substrates[228] and primarily developed by Cahen et al.[229−231]

Briefly, the general procedure for the LOFO approach includes four steps, as shown in Figure 11: (1) evaporating the metal film, denoted as a leaf, onto a solid support, such as a glass slide, (2) detaching the metal leaf from the solid substrate and floating it at the liquid surface, (3) adsorbing a molecular layer onto the substrate or the metal film or both to add molecular functionality, and (4) attaching the metal film to the target substrate using a liquid-mediated process to complete the metal−molecule−substrate junction.

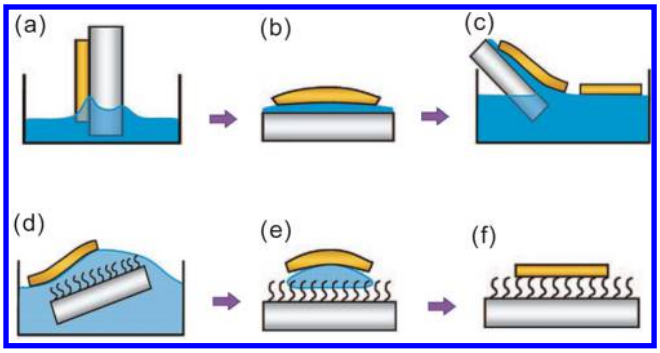

Figure 11. Schematic description of the lift-off, float-on (LOFO) procedure. (a−c) Lift-off of the evaporated leaf (metal layer) from a glass slide. (a) The glass slide is partly inserted into a detaching agent to induce the peeling process. (b) The disjoining pressure detaches the leaf from the glass substrate. (c) The metal leaf floats on solvent due to the capillary interaction. (d,e) Float-on of the leaf on the solid substrate. (d) The metal pad floats on the substrate adsorbed with molecules. (e) The solvent is rapidly removed to prevent the wrinkling of the leaf. (f) The metal/monolayer/substrate is completed. Reprinted with permission from ref 232. Copyright 2008 American Chemical Society.

Using the LOFO method, several different types of molecular junctions, such as Au−molecule−GaAs, Au−molecule−Si, and Au−molecule−ZnO, were created and deeply investigated by Cahen et al.[229,233,234] Vilan et al. first reported the fabrication of the Au−molecule−GaAs junction using the LOFO approach.[229] By adsorbing a series of functional molecules, whose dipoles varied systematically, onto single crystals of n-type GaAs semiconductors, diodes were produced with an effective barrier height that could be tuned using the molecule's dipole moment. These barrier heights correlated with the change in the work function of the GaAs surface after molecular modification. Remarkably, it was demonstrated that the molecules could control the electrical characteristics of the metal−semiconductor junctions without the need for electrons to be transferred onto and through the molecules. These results suggest that the properties of electronic devices can be tuned using molecular dipoles instead of actual electrons being transported through the molecules.[229]

Later, Salomon et al. replaced GaAs with ZnO to form Au−molecule−ZnO junctions and demonstrated that the molecular control over the effective barrier height was more effective with ZnO (ionic semiconductor) than with GaAs (covalent semiconductor).[234] Their results further proved that the molecular dipoles could control the electrical characteristics of semiconductor−metal junctions, without needing electrons to pass through the molecules due to the electrostatic interactions between the substituent groups of the adsorbed molecules and the top metal contact. These systematical experiments performed by Cahen et al. demonstrated that the free semiconductor surface, for example, surface state density, could dominate the junction behavior instead of direct metal−semiconductor interactions.[235]

Normally, Au is used to fabricate the top electrode (metal leaf). To lift off contacts between the gold and the substrate, the LOFO method requires a detaching agent, such as HF or acetic acid solutions. For gold, this may be an easy treatment, but it is too harsh for other metals, such as Ag, Al, and Cu (used for low cost fabrication of molecular junctions). Because these metals react vigorously with alkalis and acids to form metal−hydroxides and halides, such contamination hinders the stable electronic contact to the molecules. Recently, Ikram et al. put forward a relatively simple method for forming Ag and Al electrical contacts on the soft surfaces of monolayer molecules without using chemical etching treatments.[236] In their experiment, the glass substrates were first spin-coated with a thin layer of the starch solution as a sacrificial layer. Ag contacts then were formed by screen printing conductive silver pastes onto the glass substrate, and similar contacts of aluminum were also deposited onto the glass substrates using thermal evaporation. With this method, metal contacts can be easily lifted off by dissoluting the sacrificial layer in water.

The primary advantage of the LOFO method is that the pinholes involved in the atom deposition, physical damage due to the overload force, and chemical damage expected from the electrochemical deposition can be relatively avoided. Another advantage of the LOFO method is that it is relatively suitable for studying biological molecules. This LOFO method does not rely on the actual chemical binding of the molecules to the top metal layer, and the surfaces that are to be bound are kept wet until the establishment of the electrical contact at (or very close to) room temperature, which makes it suitable for electronic devices incorporating biological molecules. Beside these advantages, challenges in the LOFO method remain, even though several improvements had been introduced to overcome these challenges.[230,236] For example, it is a considerable challenge to accurately control the force between the floating electrodes and the substrates, so it is hard to behave like an AFM to make a defined contact between the top electrodes and the molecules. In fact, the repulsion between the floating film and the substrate is often observed, which may generate an additional air gap between the top electrode and the molecular layer. Additionally, it is difficult to completely prevent wrinkling of the thin metal film (float film) during contacting process.

Shimizu et al. further developed a polymer-assisted lift-off (PALO) process to overcome the wrinkling problem and made a big step toward actual integrated molecular devices.[231] This method allowed for the transfer of the top parallel electrodes onto molecular films without experiencing macroscopic distortion or damage. The key component is a hydrophobic

DOI: 10.1021/acs.chemrev.5b00680
Chem. Rev. 2016, 116, 4318−4440

polymer, that is, a backing layer on the top electrodes, thus guaranteeing the mechanical stability and a thermodynamic driving force to eliminate wrinkling. Using this technique, high-quality metal-electrode devices can be fabricated in parallel over a wide range with lithographically defined geometry. Furthermore, the floating parallel electrodes were transferred to the substrates to create a cross bar structure. No shorted molecular junctions were observed for over 90% of the examined devices. The PALO method combined several advantages of the nanotransfer-print (denoted as nTP, which will be introduced later) and the LOFO methods, parallel electrodes fabrication, small electrode sizes, high-quality metal films, and nondamaging deposition.

2.2.2. Liquid Metal Contact. The liquid metal contact is relatively stable and can effectively prevent problems that are encountered with the direct evaporation of metal top-contacts, such as metal atom penetration into the junction and mechanical damage. Reynolds et al. first introduced a method to use liquid metal electrodes to form the molecular junctions.[237,238] Using a clean mercury (Hg) drop electrode as the top electrode, electrical measurements were performed on multilayer molecular films. In their experiment, a number of different bottom contacts based on barium, cadmium, calcium, copper, and lead were used.[237] They found that a mercury drop was the only satisfactory material at the time to form a contact with low resistance and without physical damage.

The principle used to form the Hg—molecule—Ag is relatively simple, as illustrated in Figure 12.[239] The junction

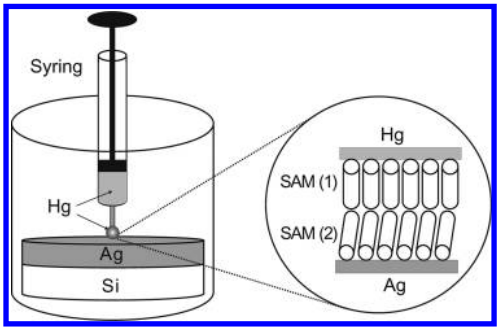

Figure 12. Schematic illustration of the fabrication of the Hg—molecule—Ag junction. The electrical junction was formed by the mechanical contact of the two SAMs. SAM (1) indicates the SAM on the solid Hg electrode, and SAM (2) indicates the SAM on the Ag electrode. The Hg drop was suspended from a syringe and assembled molecules in situ. Reprinted with permission from ref 239. Copyright 2002 American Chemical Society.

can be formed by a mechanical contact between an SAM on a mercury drop and an SAM on the silver film supported by a silicon wafer. A SAM-coated silver film was placed in a beaker and covered with a hexadecanethiol-containing solution used to form the SAM on the Hg drop. The SAM on the Hg drop was formed in situ on the drop surface suspended from a syringe. A micromanipulator allowed mechanical contact between the SAM on the Hg drop and the SAM on the Ag film. The diameter of the Hg drop was ~1 mm, and the contact area was $\sim 5 \times 10^{-3}$ cm^2. A related junction in which the organic film was sandwiched between two mercury drops was also possible.[240,241] Similarly, the Hg—molecules—Si junction can be generated by placing an Hg drop on the monolayer above the silicon wafer using the hanging mercury drop electrode apparatus.[242]

Using an Hg drop as an electrode has several advantages.[241] First, the Hg surface, as a liquid, is free of structural features, for example, edges, terraces, and pits, which normally result in defects in the adsorbed monolayer. Second, the formed junctions are stable and reproducible; that is, less than 20% of the junctions form short circuits. Third, Hg forms well-ordered SAMs after coming into contact with the target molecules for a short time, and Hg can host a large variety of molecules.[243] Finally, the Hg drop can conform to the topography of the solid surfaces, thus forming a good conformal contact with the molecular layers on a solid surface. However, Hg may have harmful effects on the health of the user, which is a disadvantage of this method.

The method using liquid metal alloy electrodes was developed by Whiteside et al.[244−249] They initially introduced an idea where eutectic gallium—indium (EGaIn) could replace Hg and be used as one of the electrodes.[245,248,249] The work function of EGaIn (~4.2 eV) is close to that of Hg (~4.5 eV); however, EGaIn does not flow until it experiences a critical surface stress. In their experiment, an EGaIn drop suspended from the needle of a syringe was brought into contact with the bare Ag surface, and the syringe was then raised until the EGaIn separated into a conical tip. The top EGaIn tip protruding from the needle did not typically retract into a semispherical droplet. Thus, the contact area can be dramatically reduced.[249] The thin Ga_2O_3 layer (~1 nm) on the surface of the EGaIn electrode due to oxidation may play an important role in the system. This film of Ga_2O_3, which is similar to a protective layer, helps prevent the formation of metal filaments, leading to high yields of the molecular junctions. The effects of the Ga_2O_3 thin films were extensively investigated, and it was demonstrated that the molecular structure of the SAM, and not the characteristics of the Ga_2O_3 film, dominated the observed electron transport behavior.[246] This method also has disadvantages: it suffers from user-dependent variations in the details of the formation of tips and the SAM//GaO_x/EGaIn contacts, and the mechanical stability of the junctions is limited by the details of the micromanipulator on which the top-electrode is mounted.[250]

Combined with optical lithography, Whitesides et al. further presented a method for fabricating small arrays of tunneling junctions based on liquid metal alloy electrodes. These junctions had EGaIn top-electrodes stabilized in microchannels and ultraflat silver bottom-electrodes.[248,250] These junctions using the EGaIn did not require a clean room, ultrahigh vacuum, toxic substances, such as the previously used Hg, or a second SAM. Using this method, several significant results on the electron transport through molecules were achieved, such as (1) the role of the binding group and the purity of the thiols in the performance of the molecular diodes were revealed;[251] (2) the dependency of the tunneling decay coefficient on the topography of the bottom electrodes as well as the rate of charge transport on the molecule structure were studied;[252−254] and (3) the effects of the molecule structure and the molecular interaction on the electron transport were extensively addressed.[245,255,256]

Nevertheless, the optical lithography process is time consuming and relatively high-cost for production. Wan et al. put forward a low-cost strategy to form the molecular junctions sandwiched between the tin/indium electrodes, known as capillary tunnel junctions.[257,258] The capillary tunnel junctions are formed within a commercially available capillary fiber with a ~0.1 mm diameter. As illustrated in Figure 13, there are three primary steps used to prepare this type of capillary tunnel

DOI: 10.1021/acs.chemrev.5b00680
Chem. Rev. 2016, 116, 4318−4440

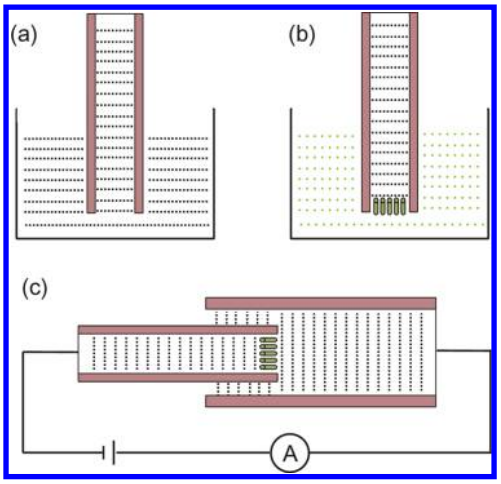

Figure 13. Schematic of the preparation procedure for a capillary junction. (a) The fiber is filled with liquid tin or indium via the capillary effect at high temperatures. (b) The end-point of the fiber is immersed into solution to form an SAM on the solid metal (tin or indium) surface at room temperature. (c) The SAM-modified fiber is inserted into another fiber with a larger diameter filled with tin to complete the molecule junction. Reprinted with permission from ref 258. Copyright 2004 American Chemical Society.

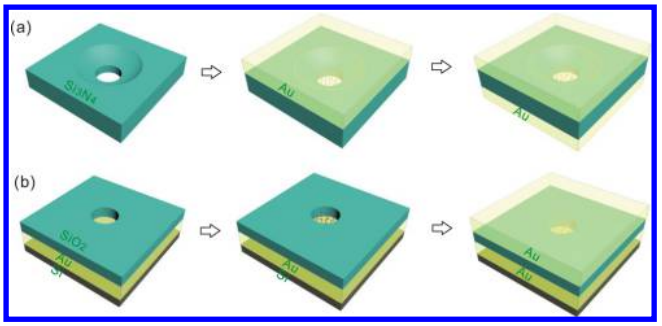

Figure 14. Schematic of the molecular device structure based on a hole: nanopore versus nanowell. (a) Nanopore-based molecular junctions. A pore was made through the Si_3N_4 membrane via etching. The top Au electrode was obtained by evaporating Au onto the top side of the membrane, which filled the top end of the pore. After self-assembling the molecules on the top electrode, the pore was filled to complete the molecular junction by evaporating Au onto the bottom side of the membrane. (b) Nanowell-based molecule junctions. A hole was drilled through the SiO_2 layer to the bottom Au layer. After self-assembling the molecules on this bottom electrode, the hole was filled with Au to complete the Au−molecule−Au junction.

junction. (1) The melted tin or indium is filled into the fiber to a target height due to the capillary effect, which is when the temperature is slightly higher than the melting point of tin or indium. The fiber will be filled with solid tin or indium when it is cooled to room temperature. (2) The end-point of the fiber is then immersed into the molecule-containing solution to obtain an SAM at the metal surface. (3) The SAM modified fiber is subsequently inserted into another fiber with a larger diameter filled with tin or indium to seal the SAM inside the capillary fiber. Finally, the molecule junction will be completed as the temperature is again cooled to room temperature.

The molecular junctions based on the capillary fibers were stable and could be used permanently. Tin or indium was selected as the electrode materials because of their relatively low melting points and wide applications in optoelectrical devices. Both tin and indium are the main constituents of transparent conductive glasses. Moreover, the naturally existing hydroxyl groups at the tin oxide or indium oxide surfaces provide a potential for functionalization via molecular self-assembly approaches. The primary limitation of this method is that the contact area as well as the distance between the two electrodes is fixed as the junction is formed. Another disadvantage of this method is that physical damage to the molecular layer may appear when the small fiber is inserted into the large fiber to complete the molecular junction.

2.2.3. Nanopore and Nanowell. The molecular junctions fabricated via a hole, such as a nanopore or a nanowell, to our knowledge, were first introduced by Reed et al.[129,259,260] The starting substrate for the nanopore device fabrication was a double-sided polished silicon wafer, on which a thin Si_3N_4 layer was deposited. Using optical lithography, reactive ion etching (RIE), and wet etching techniques, a window of the silicon nitride membrane suspended over the silicon wafer was obtained. All of the following processes were performed on the basis of this silicon nitride membrane.[260] (1) A hole with a bowl-shaped geometry (~50 nm in diameter) was created through the membrane using the EBL and RIE methods, as shown in Figure 14a. (2) An Au layer (~200 nm thickness) was evaporated onto the top side of the membrane, which filled the pore with Au and worked as the top electrodes. (3) The sample was then immediately transferred into a solution to assemble a molecular layer on the top electrode surface. (4) The sample then was loaded into a vacuum chamber to thermally deposit the bottom Au electrode to complete the Au−molecule−Au junction. Because several delicate processes were involved during the sample fabrication, the electrical behavior typically varied from sample to sample. Song et al. presented a statistical method to determine the intrinsic electronic transport properties of these SAM-based devices.[261] Another disadvantage of this nanopore strategy is that the fabrication yield of the molecular junctions is relatively low (~2%) due to the metal atom penetration into the molecular layer, which creates a short device during the period of evaporating the bottom Au electrode.[261] Several improved processes had been introduced to reduce the short phenomenon, such as using a packed assembled monolayer, low temperature evaporation metal atom, and precisely controlling the atom evaporation rate.[260]

Nanowell-based molecular junctions were first presented by Tour et al.[259] The nanowell is a planar device as opposed to the nanopore, in which a hole is created through the wafer. As illustrated in Figure 14b, the nanowell devices were fabricated on silicon wafers that had prepatterned gold electrodes covered with silicon dioxide. Using the FIB technique instead of the EBL technique, a small hole (10−40 nm in diameter) was drilled in the silicon dioxide layer.[259] A hole with a diameter as small as 1 nm was also reported employing the FIB technique.[262] Because of the small size of the hole, the yield of the short devices was reduced. Furthermore, in comparison with the nanopore, the fabrication process was simplified in three aspects: evaporating at a faster deposition rate, performing the evaporation on an uncooled substrate, and eliminating the step of bottom electrode evaporation.[262] However, the formation of the metal filaments that short the junctions cannot be completely eliminated by directly evaporating the metal atoms above the molecular layer, especially for those holes with a large diameter. To overcome this shorting problem and increase the yield of the molecular junctions, a conducting buffer layer can be inserted between the metal layer and the

DOI: 10.1021/acs.chemrev.5b00680
Chem. Rev. 2016, 116, 4318−4440

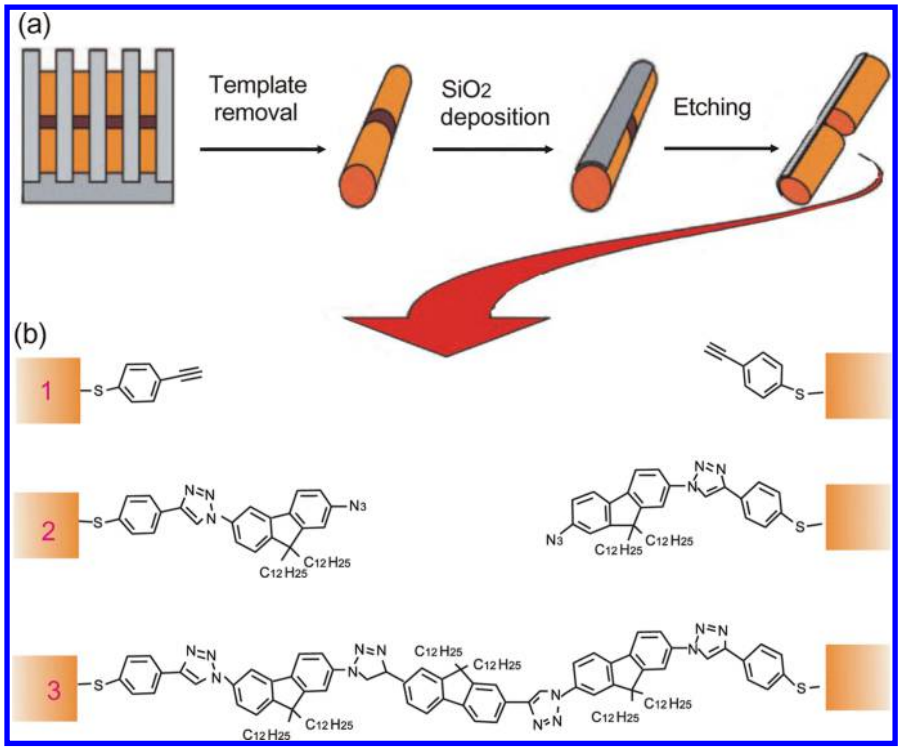

Figure 15. On-wire lithography. (a) Schematic of the OWL for fabricating metal electrodes. (b) Schematic illustration of the click chemistry within the nanogaps prepared by the OWL. The junction was closed by a stepwise in-gap oligomer assembly. Reprinted with permission from ref 269. Copyright 2008 American Chemical Society.

molecular layer, thus preventing damage to the molecular layer. The conducting interlayer can be a highly conductive hybrid polymer PEDOT:PSS,[28] multilayer graphene,[263] or single-walled carbon nanotube (SWNT) layer.[264] The strategy of inserting a conducting interlayer to create large-area molecular junctions will be addressed in detail in section 2.2.7.

2.2.4. On-Wire Lithography. This procedure, which is known as on-wire lithography (OWL), combines advances in the template-directed synthesis of nanowires with the electrochemical deposition. OWL was initially introduced by Mbindyo et al.[265] The initial idea for on-wire lithography is similar to the method discussed in the above section, that is, nanopore-based junctions. A primary difference between them is that the pore in the OWL is fabricated on the basis of the polycarbonate membrane instead of silicon wafers, and the polycarbonate membrane is completely dissolved in dichloromethane. After the membrane was removed, nanowire segments with a sandwiched molecular layer can be obtained, thus forming the metal−molecule−metal junction. Later, this idea was further developed and popularized by Mirkin et al., in which a precisely controlled gap was initially obtained.[266−268]

As shown in Figure 15, the OWL procedure can be briefly described as follows:[266] (1) typical electrochemical growth of pillars consisting of multiple layers of at least two different metals in a porous alumina template, in which one of the metal layers is used as a sacrificial segment; (2) removal of the template, thus producing nanowires with different segments; (3) formation of a layer of silica (thickness is approximately one-half of the nanowire diameter) on the nanowire-coated substrate using plasma-enhanced chemical vapor deposition; the nanowire with a silica supporting layer was released from the substrate by the ultrasonic cleaner; and (4) removal of the sacrificial segment from the wire using wet etching to generate nanowire structures with gaps accurately controlled by the length of the original sacrificial segments. It is anticipated that on-wire lithography could dramatically boost the development of molecular electronics.

The last critical step is to bridge the nanogaps with the molecules, and two different strategies have been presented to bridge the gap with the molecules. (1) "Dip-pen nanolithography" so-called DPN strategy:[270] In this strategy, an atomic force microcopy is used, and the molecules are delivered from the AFM tip to the gap area of the nanowire via a capillary transport in a manner similar to that of a dip pen. Thus, the molecules are immobilized onto the microelectrodes and fill the gap. This strategy is suitable for a larger gap size. Qin et al. successfully deposited conducting polymers into a 13 nm gap using the DPN method and studied the transport properties with and without the conducting polymer.[266] (2) Self-assembly: In this strategy, the molecules are self-assembled onto the electrode surface. The molecule will bridge the two opposite electrodes when the molecular length is comparable to the gap size between the electrodes.[269] However, there is a mismatch in the length because the molecule length is typically a few nanometers, whereas the gap size is generally dozens of nanometers. Fortunately, the nanowire, which is dozens of nanometers in diameter, and sub-3 nm gaps were obtained using fine control and optimization of the conditions in each fabrication step.[267,271,272]

As discussed above, the previous study on the molecular junction fabrication primarily relies on the ex situ syntheses of molecular wires followed by the subsequent insertion of the molecules into the gap separated by the nanorods. In this ex situ approach, the molecular length should be similar to the gap size, which limits the yield of the molecular junction. To circumvent the problems, Mirkin et al. used click chemistry for

DOI: 10.1021/acs.chemrev.5b00680
Chem. Rev. 2016, 116, 4318−4440

the in situ modular synthesis of molecular wires to bridge OWL-fabricated nanogaps.[273] Click chemistry is a synthetic approach popularized by Sharpless et al. that involves controlling reactions step by step.[274] The general scheme for bridging the nanogaps using click chemistry for molecular junction fabrication is illustrated in Figure 15b. First, 4-ethynyl-1-thioacetylbenzene was assembled into a monolayer on the surfaces of the electrodes, which are located at opposite ends of an OWL-fabricated nanogap (step 1). The device then was immersed in a solution containing 2,7-diazidofluorene. One of the azide groups in 2,7-diazidofluorene reacted with the alkyne group from step 1 to form a 1,2,3-triazole unit at one end, and the azide group at the other end was left unchanged (step 2). This structure can be further extended through a reaction with 2,7-diethynyl-fluorene (step 3), which, in turn, can react again with the azide groups. Following the appropriate number of reaction cycles, the molecular wires grow from the opposing electrodes and eventually bridge the nanogap. One advantage of forming molecular wires using the click methodology within the OWL-fabricated nanogaps is that in situ fabrication is challenging for other existing testbeds due to the limited gap space or solution-processable problems. By monitoring the process using Raman spectroscopy or X-ray photoelectron spectroscopy, one can watch and confirm the gap closes process.[275,276]

The advantages of using the OWL method to form nanoelectrodes include (1) the ability to fabricate sub-5 nm gaps in high yield with precise dimensional control (the diameter of the wire is controlled by the template-pore diameter, and the length of the wire and the size of the gap are controlled electrochemically);[272] (2) the remarkable simplicity, stability, and reproducibility of the OWL method to offer a transport testbed; and (3) the flexible selection of the source and drain electrode materials by thermally depositing different types of metals.[271] Recently, the applications of the OWL technology have dramatically increased beyond molecular junctions, such as the fabrication of nanotube-bridged nanorods,[277,278] graphene ribbons using OWL-based nanomasks,[279] free-standing nanorings,[280] and resettable electronic logic gates,[281] enhancement of the electric field/Raman spectroscopy,[282−284] and biological applications.[267]

2.2.5. Transfer Printing Techniques. In an attempt to reduce electrical shorts between the contacts, mercury droplets, lift-off float-ons, nanowells, and on-wire lithography were introduced, and successfully demonstrated the ability to increase the yield of the molecular junctions. Although these approaches are able to produce laboratory test structures, they are not easily scaled up for the fabrication of circuits and systems containing molecular devices. In this sense, the nanotransfer imprinting lithographic (NIL) approach is rapid, simple, and occurs readily under ambient conditions, offering a promising approach to fabricate integrated molecular devices.

Melosh et al. first introduced this novel approach to fabricate top-contact electrodes in Au/1,8-octanedithiol/GaAs junctions.[285] As illustrated in Figure 16, their nanotransfer printing procedure can be briefly stated as follows: (1) the GaAs substrate is first etched to remove the native oxide layer and then immediately exposed to 1,8-octanedithiol to form an SAM on the GaAs surface; (2) a gold-coated elastomeric PDMS stamp is brought into contact with the substrate, and the GaAs−molecule−Au junctions are formed; and (3) removing the stamp from the substrate completes the printing process. The elasticity and the mechanical conformability of the PDMS

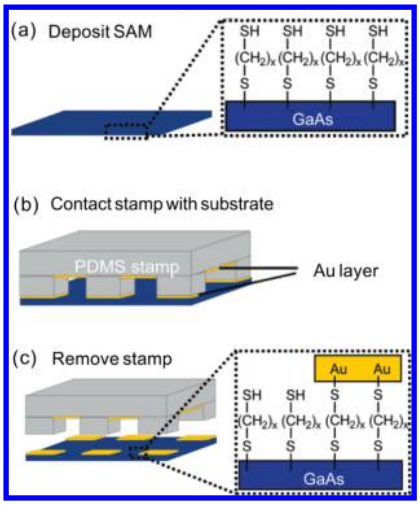

Figure 16. Schematic of the nanotransfer printing procedure. (a) The GaAs substrate is first etched in concentrated NH_4OH or HCl and then immediately exposed to a 1,8-octanedithiol vapor or solution for self-assembly. (b) The gold-coated elastomeric PDMS stamp is brought into contact with the treated substrate. (c) Removing the stamp from the substrate completes the nanoimprinting process. The Au on the PDMS stamp is bonded by the molecules and transferred to the molecule-coated GaAs substrate. Reprinted with permission from ref 285. Copyright 2003 American Chemical Society.

stamp ensure a good contact at the stamp/substrate interface. Because the adhesion of the Au to the PDMS is poor as compared to the Au−S bonding, the stamp can be easily removed from the substrate to complete the pattern-transfer process. Subsequently, current−voltage and photoresponse experiments were performed. It was determined that the current densities were independent of the contact area for the NIL-fabricated devices, thus confirming that the current distribution is uniform in the NIL-fabricated junctions.

In the NIL approach, direct Au/GaAs contact can be successfully avoided, and we move a big step forward to fabricate integrated molecular devices. However, challenges for reliable interfaces remain. One challenge is that the top electrode roughness may generate small gaps between the metal and the organic monolayer, leading to unreliable electrical responses. In other words, it is difficult to obtain an ultrasmooth surface when a metal layer is evaporated on the PDMS mold, which may generate an additional air gap and obstruct the analysis of the actual molecular properties. Hacker et al. demonstrated a novel fabrication route for high-quality molecular junctions bonded to ultrasmooth silicon and ultrasmooth gold using a flip-chip lamination approach.[286] Generally, it is easy to obtain large-area ultrasmooth silicon bottom electrodes; however, obtaining the ultrasmooth top gold electrodes is quite difficult. To generate an ultrasmooth gold layer, Hacker et al. directly evaporated a gold layer onto an ultrasmooth Si substrate previously treated with a fluorinated releasing layer. This ultrasmooth gold layer can be attached using the stamp (similar to PDMS). After it is peeled off from the silicon substrate, the ultrasmooth gold layer attached to the stamp can be obtained. The functional molecules then were self-assembled on this gold layer. Last, the gold electrodes as well as another silicon electrode were laminated together to form a high-quality molecular junction.

Another challenge for the NIL is the resolution limitation. Generally, the potential minimum dimension of the NIL has

DOI: 10.1021/acs.chemrev.5b00680
Chem. Rev. 2016, 116, 4318−4440

been limited to approximately 50 nm due to the deformation, collapse, and merging of the molds during transfer printing, resulting from the low modulus of the elastomeric molds. Although a relatively improved resolution of 20 nm was reported by adjusting the modulus and the surface energy of the elastomers,[287] the partial deformation and degraded quality of the elastomeric molds still remain significant issues. The resolution of the NIL can be enhanced using hard molds with a block copolymer (BCP) self-assembly.[288] Jeong et al. reported an NIL method to create a pattern with sub-10 nm resolution using the BCP self-assembly.[289] The microphase separation of two mutually incompatible blocks in a BCP led to the formation of ordered arrays with sub-30 nm structures. After the transfer of the BCP films onto the substrate, they could be converted easily into sub-10 nm SiO_x nanostructures employing plasma oxidation treatments. It was further demonstrated that the BCP patterns with a line width of 8−16 nm could be successfully transferred onto a wide range of materials. The resolution of the NIL can also be enhanced by employing soluble polymer. Sanetra et al. reported that junctions with half-pitches down to 50 nm could be fabricated in a parallel process. In their experiment, the transfer of the top electrode was facilitated by a water-soluble polymer film, which supported the lifting process of the nanometer-sized electrode and enhanced the yield of the transfer process.[290] The primary disadvantage of the NIL is that it requires a molecular layer that adheres to the top contact, usually with a thiol group, which restricts the materials that can be used.[231] Here, we only present a brief introduction and discussion to the NIL technique. The detailed technique development, wide application, and limitation of the NIL technique can be found elsewhere.[47,291,292]

One promising device architecture to achieve next-generation memory and logic devices based on metal−molecule−metal junctions may be the crossbar/crosswire latch.[290,293,294] Because it can be fabricated in parallel, it has the potential for achieving high-throughput production with low cost.[295] In the crossbar and crosswire methods, electrodes are placed on top of each other with a sandwiched molecular layer. A crossbar is a set of rectangular block wires with microscopic dimensions that cross each other with a functional layer in the crosspoints. The critical step in the fabrication of the molecular junctions is to apply the metal top electrode array above the bottom electrode array. In principle, the top electrode can be fabricated by metal deposition through a shadow mask consisting of parallel lines.[296] However, vapor-deposited metals normally create shorts in the SAMs due to the filamentary growth, even though several novel techniques have been introduced to reduce this problem.[297−299] Alternatively, the nanotransfer printing (stamp printing)[285,300,301] and the direct metal-transfer[302,303] techniques were used to fabricate the high-yield crossbar structures, in which shorting was eliminated.

In reality, the SAMs typically have defects due to several reasons: (1) step edges due to the roughness of the electrode surface; (2) pin holes or filaments formed during the top electrode evaporation; and (3) impurities or residuals on the electrode surface introduced in the lithography process. To reduce defects in the SAMs, Nijhuis et al. presented a method to create a crossbar array based on Ga_2O_3/EGaIn stabilized in the microchannels in a transparent polymer (PDMS).[210,212] The primary fabrication process is schematically depicted in Figure 17a. In their experiments, an ultraflat template-stripped silver (Ag^{TS}) electrode embedded in a cured optical adhesive (OA) was used as the bottom substrate. The pattern of Ag

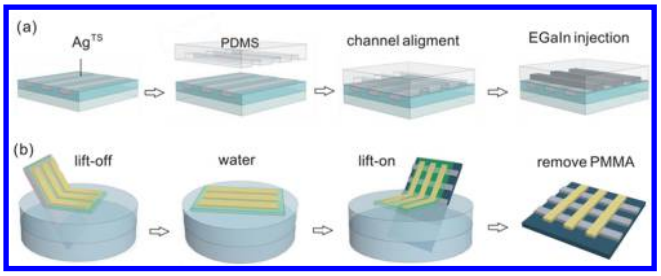

Figure 17. Schematic of the two types of crossbar fabrication. (a) Processes for microchannel-assisted crossbar formation. An ultraflat, template-stripped silver (Ag^{TS}) electrode embedded in a cured optical adhesive (OA) was used as the bottom electrode. A microchannel in a transparent PDMS then was brought perpendicular to the bottom electrode. Last, the microchannels were filled with Ga_2O_3/EGaIn to complete the crossbar devices. Reprinted with permission from ref 248. Copyright 2010 American Chemical Society. (b) Processes for producing PALO crossbars. The PMMA was spin-cast as a hydrophobic backing layer onto the electrode-patterned substrates. Subsequently, the metal−polymer layer was lifted off onto the water surface upon immersion of the substrate. The crossbar device was assembled by floating the metal−polymer film onto a bottom substrate followed by the removal of the PMMA to complete the crossbar device. Reprinted with permission from ref 231. Copyright 2006 Wiley-VCH.

electrodes was fabricated using a standard lithography technique. A glass substrate then was affixed to the silver electrode pattern using a cured UV-curable adhesive. The optical adhesive interacts strongly with the Ag and the glass support but not the wafer. After the Ag/adhesive/glass composite was cleaved from the wafer, the bottom substrate was obtained. Subsequently, a microchannel in the PDMS was aligned perpendicularly to the bottom electrodes after the SAMs were formed. Last, the microchannels were filled with Ga_2O_3/EGaIn to complete the crossbar device. The crossbar devices fabricated using this method have a few clear advantages. (i) They are mechanically stable, and it is possible to perform $J-V$ measurements over a broad range of temperatures. (ii) They do not require metal deposition, either by electron-beam evaporation or by sputtering directly onto the SAMs, to form a top electrode. (iii) They do not suffer from alloying between the metal electrodes or require intermediate layers of the conducting polymer's processing steps.

Recently, Shimizu et al. presented a process known as polymer-assisted lift-off (PALO), which is a promising printing technique that rapidly forms crossbar junctions.[231,304] The fabrication process is shown in Figure 17b. (i) The PMMA was spin-cast as a hydrophobic backing layer onto the metal electrodes, which was previously patterned on a sacrificial substrate. (ii) The Si substrate was then slowly dipped into a buffer solution of acetic acid, where the polymer−Au layer was detached from the substrate and floated on top of the aqueous solution without wrinkling due to the surface tension of the water. (iii) The crossbar device was assembled by floating the metal−polymer film onto a bottom substrate, which was patterned with the bottom electrodes and adsorbed with the molecules. Because of the hydrophobicity of the polymer and the molecular film, the polymer was drawn into contact with the substrate once an initial point of contact was made. (iv) Last, the crossbar device was completed after the polymer layer was removed via etching. This PALO method allows for the transfer of a top metal contact onto molecular films without macroscopic distortion or damage. The key component is a

DOI: 10.1021/acs.chemrev.5b00680
Chem. Rev. 2016, 116, 4318−4440

hydrophobic polymer backing layer on the preformed top electrodes that provides mechanical stability and a thermodynamic driving force to eliminate wrinkling. Originally, this technique was developed to generate and transfer electrodes in the large micrometer range. Sanetra et al. presented a modified PALO-based process that combined soft lithography and nanoimprint lithography.[290] It was demonstrated that not only was it a low-cost technique, but highly integrated crossbar junctions with half-pitches of 50 nm could be also fabricated in a parallel process.

In addition to the crossbar architecture, another similar and popular used architecture to form molecular junction is crosswire architecture.[47] As early as decades ago, Lieber et al. selected different types of nanowires to produce the crossed wire junctions.[305] They demonstrated that an electric-field-directed assembly could be used to create highly integrated nanowire arrays. The crossed nanowire junctions were obtained using layer-by-layer alignments with the electric field applied in orthogonal directions in the two assembly steps.[305] Later, Yoon et al. reported a versatile and highly scalable crossed-nanowire molecular junction device that enabled the direct measurement of current−voltage−temperature characteristics simultaneously with inelastic electron tunneling and Raman vibrational spectra on the same junction.[306] In their experiment, the bottom electrode was fabricated via a lithographical process. A separately synthesized nanowire with a flat surface was used as a top contact. To accurately position the top wire perpendicular to the bottom wire preassembled with an SAM, a dielectrophoretic method was used. This highly flexible nanofabrication process allows wide variations in the wire diameters and the types of nanowires, with expansion to diverse materials, including semiconductors, superconductors, and nanotubes.[306]

A primary challenge in fabricating the crossbar/crosswire-based molecular junctions is to form an intimate contact between the molecular layer and the second electrode; that is, it is not easy to form a tight molecule/electrode contact in each cross-point, especially when it is fabricated via the transfer printing method without an external compression force. Kushmerick et al. proposed a new type of crosswire-based tunnel junction, in which a molecular monolayer was sandwiched between two macroscopic gold wires under a controllable force.[307,308] As shown in Figure 18a, the wires were mounted in a custom-built test stage so that they were crossed and the wire spacing was controlled by the Lorentz force; the DC current in one wire deflected it in a magnetic field.[308] The deflection current was slowly increased to bring the wires gently together to form a junction at the point contact. The $I-V$ characteristics of the junctions were obtained by ramping the bias voltage (V) while monitoring the current flow (I) across the junction (Figure 18a, inset). In this crosswire testbed, the features of these types of junctions were analyzed, and the characterization of the different types of molecules was studied.[307,308] Additionally, the vibronic contributions to the charge transport as well as the selection rules in the inelastic electron tunneling spectroscopy were revealed.[178,309] Kushmerick et al. further applied this Lorentz force-assisted crosswire method to different materials, providing a primary contribution to this testbed.[310] However, the number of contacted molecules and their orientation on the wire were not well-defined because of the surface curvature of the wires in the device architecture.[311]

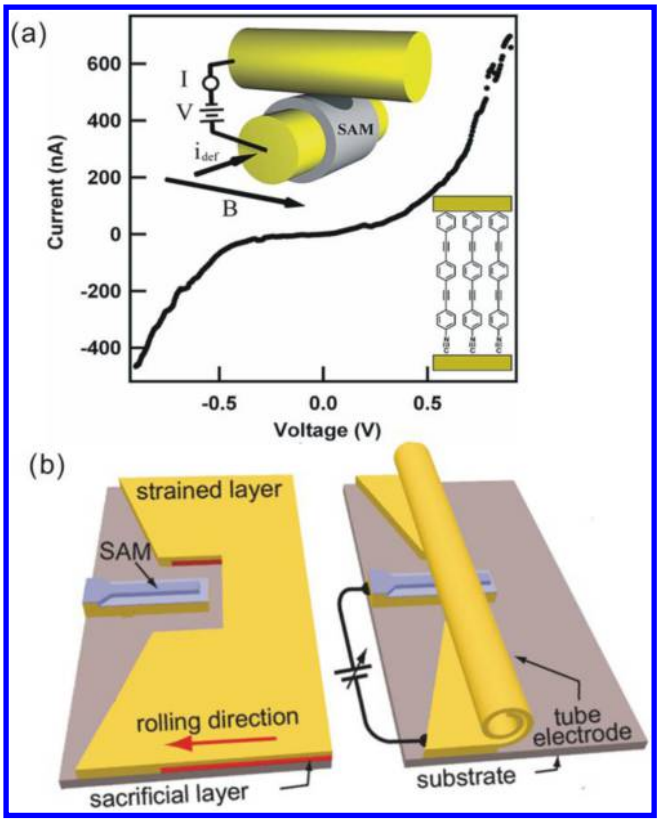

Figure 18. Schematic of the crosswire-based tunnel junctions. (a) Schematic of the crossed wire tunnel junction controlled by the Lorentz force. The crossed wires were mounted in a custom-built test, and the wire spacing was controlled by the Lorentz force; the DC current in one wire deflected it in a magnetic field to bring the wires gently together to form a junction at the contact point. Inset: $I-V$ characteristics of the metal−molecule−metal junction. Reprinted with permission from ref 308. Copyright 2003 American Chemical Society. (b) Molecular heterojunctions based on the strained nanomembranes. The left image depicts the device structure before the membrane rolling, and the right image depicts the device structure after rolling. The strained layer consists of a metallic nanomembrane patterned on top of a sacrificial layer. Once the sacrificial layer is selectively removed, the strained layer curls toward the Au finger structure, which was previously adsorbed with the molecular layer. After the rolling process, the tube-shaped electrode rests on top of the Au finger, thus establishing a molecular junction. Reprinted with permission from ref 312. Copyright 2011 American Chemical Society.

Another strategy used to form a tight contact between the top wire and the bottom wire is illustrated in Figure 18b, in which metal−molecule−metal heterojunctions were fabricated on the basis of rolled-up metallic nanomembranes.[312] The strained layer consists of a metallic nanomembrane patterned on top of a sacrificial layer. Once the sacrificial layer is selectively removed, the strained layer rolls toward the Au finger structure, where the alkanethiol SAM that has chain lengths considerably larger than the roughness of the finger surface was preassembled on the surface. After the rolling process, the tube-shaped electrode is placed on top of the Au finger, establishing an electrical connection through the SAM. The strained nanomembrane-based electrodes provide a soft yet robust contact on top of the SAM, where short circuits via pinholes are largely prevented. Because of the nature of this fabrication approach, the devices can be patterned in parallel on-chip and even be integrated with preexisting structures on a

DOI: 10.1021/acs.chemrev.5b00680
Chem. Rev. 2016, 116, 4318−4440

wafer. The primary challenge for fabricating this type of structures lies in the ability to accurately control/adjust the force between the tube electrode and the SAM, even though the metal electrode can intimately contact with the molecular layer.

2.2.6. Self-Aligned Lithography. When using the click chemistry strategy, extra attention should be given to the "bridge" molecules. These "bridge" molecules may be randomly attached to arbitrary points on the electrodes or even bind both of their surface-active groups to the same electrode, reducing the yield of the molecular junctions. To mitigate this problem, one potential approach is to select a bifunctional molecule such that only one end of the molecule reacts with the electrode; the second functional group has no affinity for the electrode. A second molecule then is used to bridge the gap between the termini of the first molecule. The second molecule is selected to have a double affinity for the second functional group of the first molecule but no affinity at all for the electrode surface, for example, cobalt ions.[42] To test this strategy within molecular electronic devices, a new technique, known as self-aligned lithography, has been created to fabricate molecular-scale electrical testbeds.[275] With this self-aligned electrodes, they demonstrated that reaction chemistry offers molecular materials an overwhelming amount of diversity and functionality and could provide a method for nanoscale electronics to be synthesized rather than fabricated.

The primary steps to produce nanoscale electrodes via the self-aligned lithographic approach is depicted in Figure 19.

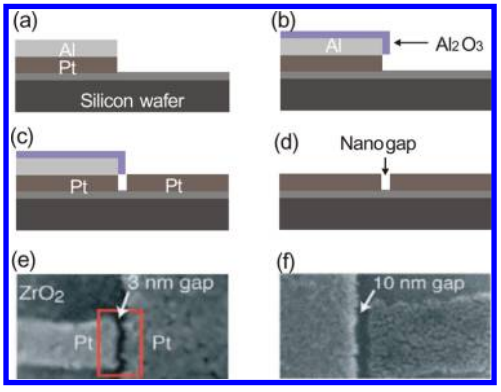

Figure 19. Fabrication process of nanoscale electrodes based on self-aligned lithography. (a) Al on Pt was patterned by the EBL on a silicon wafer coated with ZrO_2. (b) Al was oxidized in the ambient aluminum to produce an overhanging aluminum oxide layer. (c) The counter electrode was produced via platinum evaporation separated by the amount of Al_2O_3 overhang. (d) Closely spaced platinum electrodes were obtained by dissolving the aluminum/aluminum oxide layer. Scanning electron micrograph (SEM) images illustrate a 3 nm gap (e) and a 10 nm gap (f). Reprinted with permission from ref 275. Copyright 2007 Wiley-VCH.

First, a thin layer of ZrO_2 was deposited onto a clean silicon wafer using atomic layer deposition. The first Al/Pt electrode (~200 nm wide, ~3 nm thick) was defined by the EBL. To obtain the narrowest gaps, a thin SiO_2 was added between the Pt and the Al films to aid the subsequent removal of the thin Al film. After being exposed to ambient oxygen, a native oxide layer was formed on the Al surface; the oxide on the edge of the Al film produced an overhanging structure over the Pt electrode, as shown in Figure 19b. The second electrode (~30 nm wide), which consisted of 2.5 nm Pt defined by electron-beam evaporation/lithography, then overlapped with the first electrode, as indicated in Figure 19c. The overlapping part and the oxidized aluminum were removed using a tetramethylammonium hydroxide solution to complete the nanosized gaps (Figure 19d). The key advantage of this technique is that it is a self-aligned lithographic process capable of producing large numbers of molecular-scale gaps with a remarkably high yield.

Kim et al. presented another simple semiconductor process to fabricate nanogap arrays for potential application in molecular electronics, as shown in Figure 20.[313] The basic

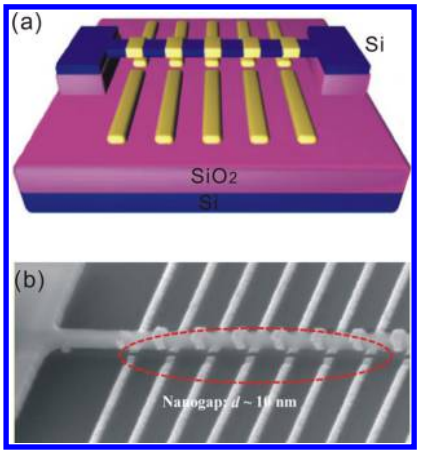

Figure 20. Nanogap array fabrication. (a) A schematic diagram of the nanogap arrays fabricated via a suspended silicon nanowire mask. A SOI with a 100 nm top silicon layer and 200 nm buried oxide was used as the substrate. (b) Side-view SEM image of the metal nanogap arrays. The gap size between the opposing metal electrodes is 1–10 nm. Reprinted with permission from ref 313. Copyright 2009 Korea Electronics and Telecommunications Research Institute.

idea behind the fabrication is using suspended silicon nanowires as a mask for the metal evaporation.[314] The gap size is controlled by the height of the suspended Si nanowire, width of the Si nanowires, and evaporation angle. It was demonstrated that sub-10 nm gap arrays could be achieved using this method. To verify the practical viability of the nanogap array, the fabricated nanogap devices were applied to DNA-mediated single-charge tunneling devices, and revealed the electrical properties of the DNA-linked gold nanoparticles.[313]

2.2.7. Buffer Interlayer-Based Junction. Self-assembled monolayers (SAMs) may offer a promising route leading to the fabrication of reliable devices using the nanopore or nanowell techniques. Unfortunately, electrical shorts in SAMs are often formed during the vapor deposition of metal thin films for the top electrode, which cause electrical shorts in the molecular junctions and low device yield of the junctions. An efficient way to prevent the penetration of the metal atom into the SAM and avoid shorting is to insert a buffer interlayer between the top electrode and the SAM. The material for the buffer interlayer can be nanoparticles,[265] aluminum oxide,[315] conducting polymers,[28,316] and graphene.[263,317]

Akkerman et al. first reported a method for manufacturing high-yield molecular junctions with diameters up to 100 μm.[28] The reported method involves processing the molecular junctions in the holes of a lithographically patterned photoresist and then inserting a conducting polymer buffer layer between the metal top electrode and the SAM. The detailed fabrication process is illustrated in Figure 21. (1) A thin chromium

DOI: 10.1021/acs.chemrev.5b00680
Chem. Rev. 2016, 116, 4318–4440

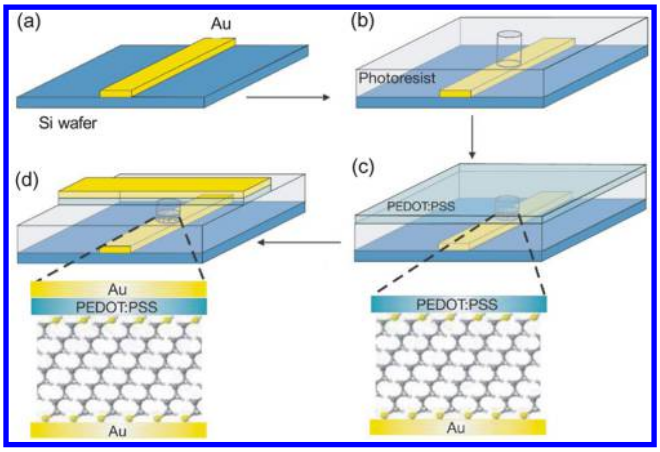

Figure 21. Processing steps of large-area molecular junctions. (a) The bottom gold electrodes were deposited on a silicon wafer. (b) The photoresist was spin-coated onto the wafer, and holes were photolithographically defined in the photoresist layer. (c) A highly conductive polymer PEDOT:PSS was spin-coated above the photoresist layer as a top electrode. A self-assembled molecule layer was sandwiched between a gold bottom electrode and the conducting polymer. (d) The junction was completed by the deposition of gold on top of the polymer through a shadow mask, and the redundant PEDOT:PSS was removed by reactive ion etching. Reprinted with permission from ref 28. Copyright 2006 Nature Publishing Group.

adhesion layer and a 40 nm gold bottom electrode were vapor-deposited onto silicon wafers with a thermally grown oxide. (2) A photoresist was spin-coated onto the wafer, and holes were produced using a standard photolithography technique. (3) The substrate was submerged in a freshly prepared ethanol solution containing alkane dithiol. After the self-assembly of the alkane dithiolate on the bottom gold electrode, a water-based suspension of poly(3,4-ethylenedioxythiophene) stabilized with poly(4-styrenesulfonic acid) (PEDOT:PSS) was spin-coated on top of the SAM with a thickness of a hundred nanometers. (4) The top gold electrode was vapor-deposited through a shadow mask. Last, the exposed PEDOT:PSS was removed by reactive ion etching, in which the top electrode acted as a self-aligned etching mask. The junctions fabricated using this method demonstrated excellent stability and reproducibility, and the obtained conductance per unit area was similar to those achieved using other methods. This simple fabrication process is potentially low-cost and could lead to practical molecular device fabrication.

Later, Boer et al. gave further contribution to systematically utilize this type of technology (e.g., the image potential, barrier height, and tunneling decay coefficient (β) in this large-area junction were determined;[318,319] the effects of molecular concentration and the fabrication parameters to the electrical characterization were investigated;[320,321] and the bias window as well as the application regime were expanded[322,323]). Moreover, the stability of this type of large-area molecular junction was analyzed by the same group.[324] It was demonstrated that this molecular junction was quite stable under ambient conditions for more than 2 years. Additionally, a transition temperature of 50 °C was observed, above which the resistance decreased exponentially with temperature. They also observed that the contact resistance and the transition voltage of the PEDOT:PSS−interlayer molecular junctions decreased as the temperature increased, which was attributed to the increased grain size of the PEDOT-rich cores and the removal of the residual water from the PEDOT:PSS−molecules interface.[325] Using the conducting polymer interlayer technique, the functional molecular electronic devices on both the rigid and the flexible substrates were further investigated by Lee et al. The stability of the molecular junctions on the flexible substrates was tested under mechanical stress configurations,[326] and the electrical properties of the redox molecules[327] as well as photoswitching molecules were thoroughly investigated.[328]

Although the fabrication of the PEDOT:PSS-based molecular electronic devices is very useful for producing high-yield molecular devices, the use of a conductive polymer has a few limitations and presents a few uncertainties to be used as a platform for molecular electronics. (1) The electrical properties of these molecular junctions may be influenced by the thermal treatment. The low transition temperature (50 °C) limits the process window during the fabrication and the temperature window during operation.[324] (2) The contact between the PEDOT:PSS and the molecules is not fully understood. The resistance of the devices fabricated using this technique is sensitive to the temperature and is different from those of the molecular junctions that do not have the polymer interlayer due to the poor contact between the PEDOT:PSS and molecules. (3) The electrical characterization of the junctions depends on the type of the isolating layer (photoresist or SiO_2) and the molecular contact groups (hydrophilic or hydrophobic),[329] which may limit its further application. Thus, groups were eager to develop alternative solid-state molecular device structures beyond the PEDOT:PSS-based molecular structure.

Graphene, with its outstanding electronic properties, chemical stability, and mechanical properties, is considered to be a good electrode candidate for molecular junctions.[330] Wang et al. first reported a new approach for fabricating reliable solid-state molecular devices using multilayer graphene as the buffer interlayer.[263] Instead of spin-coating the conducting polymer above the SAM, they transferred a multilayer graphene film onto the SAM surface as the buffer interlayer using chemical vapor deposition, as shown in Figure 22. The properties of the interface between the graphene and the molecules were statistically investigated. It was demonstrated that these graphene-based devices had a low resistance comparable to those of pure metal−molecule−metal devices, and the yield of these molecular devices was found to be approximately 90%, regardless of the properties of the contact groups (hydrophobic or hydrophilic). Particularly, this new method produced excellent durability, thermal stability, and long lifetimes for the devices.

An additional branch of graphene research, which is chemically exfoliating graphite oxides into individual graphene oxide (GO) sheets and subsequently converting them into chemically derived graphene (CDG), provides a low-cost solution-processing route that can be incorporated into large-area molecular junctions. Recently, Li et al. reported the use of solution-processed ultrathin CDG films for nondestructive fabrication of the molecular electronic junctions.[317] Molecular features, such as nonlinear charge transport properties and molecular length dependence of the junction resistance, have been confirmed in this CDG-based junction. Because of the tunable optoelectronic properties of the GO, it was predicted that the GO would be an attractive material for the optoelectrical applications.[317] One year later, they further employed ultrathin graphene oxide films as transparent top contacts for light switchable solid-state molecular junctions.[331] The flexible, conductive, and transparent GO films permitted

DOI: 10.1021/acs.chemrev.5b00680
Chem. Rev. 2016, 116, 4318−4440

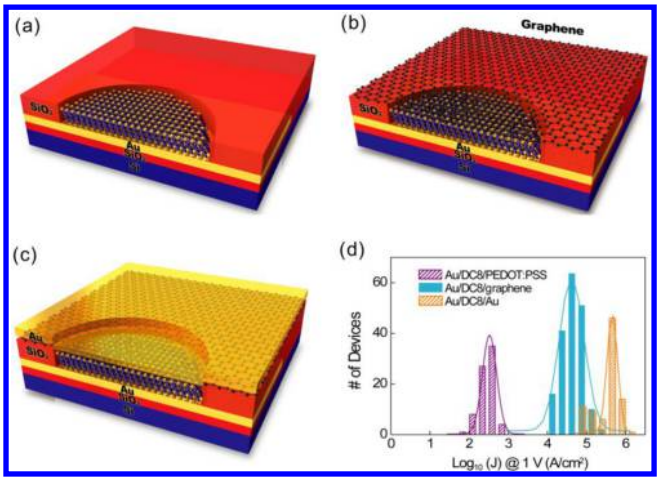

Figure 22. Graphene-based large-area molecular junctions. (a–c) Junction fabrication process: (a) SAM of alkanethiol on the exposed Au bottom electrode. (b) Alkanethiol molecular layer sandwiched between the Au bottom electrode and the graphene top electrode. (c) The junction was completed using Au vapor deposition above the graphene film. (d) Histogram of the logarithmic current densities at 1 V with different types of top electrodes (PEDOT:PSS, graphene, and Au, respectively). Reprinted with permission from ref 263. Copyright 2011 Wiley-VCH.

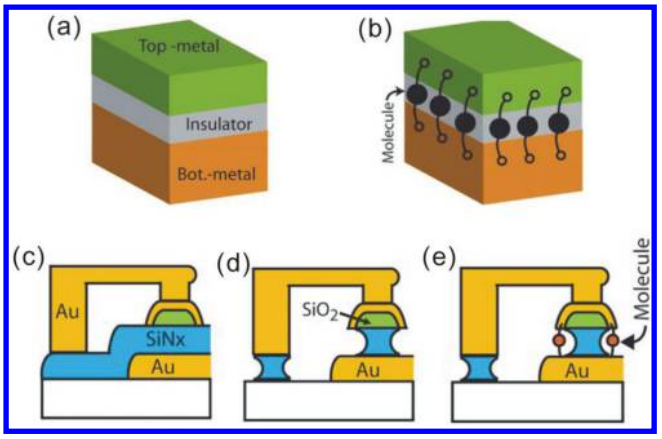

Figure 23. Schematic of OEMJ devices. (a,b) Molecular junction designs before (a) and after (b) attaching molecules. Reprinted with permission from ref 338. Copyright 2005 American Institute of Physics. (c–e) Fabrication process for molecular junctions. (c) Using SiN_x as an insulator layer. (d) Etching SiN_x to obtain the exposed electrodes. (e) Bridging the molecular channels across the gap between the top and the bottom electrodes. Reprinted with permission from ref 332. Copyright 2007 Royal Society of Chemistry.

the molecular monolayers to be photoswitched in situ while simultaneously enabling the charge transport measurements across the molecules, thus resulting in a significant development for the application of large-area molecular junctions.

2.2.8. On-Edge Molecular Junction. On-edge molecular junctions (OEMJs) were independently and nearly contemporarily developed by several groups.[332−335] Unlike planar metal break junctions, the OEMJs are out-of-plane (perpendicular) to the junction plane. It is a prerequisite to fabricate an inorganic tunnel junction with exposed vertical side edges for the OEMJ approach. On the exposed side edges, the molecular channels are covalently bridged over the insulator gap. The primary strength of the OEMJs lies in its enabling larger numbers of control experiments, in which the actual effects arising from the bridged molecules can be addressed because molecules are able to be curtailed to retrieve the characteristics of the original bare junctions.[332,334]

A popular method for producing an OEMJ is chemical etching. Chemical SiO_2 etching was used in pioneer OEMJ experiments (Figure 23a,b). After the etching process, the yielded gap size between two conducting silicon electrodes (~7 nm) was larger than the typical physical length of the molecules.[335] Correspondingly, a multistep chemistry approach was used to tether the molecules with nanoparticles to increase the effective length of the conducting channels.[335] The use of metallic electrodes enables a simple and more stable metal-molecular binding. To connect the molecules to the metal electrodes instead of the semiconducting surface, Tornow et al. produced molecular electrodes with an altered design in which the vertical gap on the exposed edges was produced by the selective etching of a gallium arsenide (GaAs) spacer between two aluminum gallium arsenide (AlGaAs) electrodes.[336] Subsequently, the gold metallization of the exposed AlGaAs edges was performed to produce highly conducting electrodes for molecular bonding. The average gap (~8 nm) between the electrodes was suitable for the selective long molecular junctions. Ashwell et al. made an improvement to reduce the gap size by introducing a thin layer of silicon nitride (SiN_x) between the gold electrodes, as shown in Figure 23c–e.[332] Hence, a minimum vertical separation of ~3.5 nm between two gold electrodes on both sides was produced. After the molecular channels were bridged over the silicon nitride gap, a >3 order increase in the effective device current with respect to the background current was observed. The device current reverted to the background level after breaking down the molecular channels in their experiment, thus substantiating the fact that the increased current originated from the molecular channels.

In OEMJs, an important issue is that the background current, that is, the leakage current passing through the insulator layer,[337] should be engineered to be considerably smaller than that through the molecular channels. To reduce the leakage current, one can increase the thickness of the insulator layer; however, this method is limited by the fact that one should keep the insulator thickness smaller than the physical length of the molecules to form a junction. The leakage current of a tunnel junction can be reduced using an additional three methods: (i) Shrinking the junction area to reduce the leakage current. For example, Chen et al. constructed a Pt–AlO_x–Pt junction using a chemical etching protocol and achieved a typical junction area of ~200 × 200 nm^2 with a leakage current as small as ~0.04 pA.[333] (ii) Growing high-quality ultrathin insulators. The leakage is strongly affected by the morphology, materials, and quality of the insulator layers. (iii) Creating atomically smooth bottom electrodes. An atomically smooth bottom electrode enables the use of thinner insulators and simultaneously yields a low leakage current.

Recently, Pang et al. developed a method to acquire both the electrical and the chemical information by combining the on-edge strategy with the nanopore approach.[339] For these devices, the tunnel gap was defined as a dielectric layer (Al_2O_3) with a thickness of ~2 nm, deposited by atomic layer deposition. Reactive ion etching was used to drill a nanopore through the layers so that the tunnel junction can be exposed to the molecules in the solution. After the metal electrodes were functionalized with recognition molecules, which can capture

DOI: 10.1021/acs.chemrev.5b00680
Chem. Rev. 2016, 116, 4318–4440

the DNA nucleotides, the identities of the individual nucleotides were revealed by the fluctuating tunnel current associated with the single-molecule binding events. Because of the small size of the nanopore (few micrometers in diameter), the experiment can be performed in an analyte solution with a relatively small leakage current. Therefore, the chemical information can be obtained. It was clearly demonstrated that the junctions produced signals that changed with the DNA nucleotide in solution. Furthermore, the devices provided clear signals of the nanomolar concentrations of the analyte and operated reliably for several hours.[339]

The OEMJ design possesses the following merits. First, the molecules are only attached onto a prefabricated tunnel junction via surface chemistry; hence, no damage is caused to the molecular channels. In other approaches, for example, the direct deposition of the top metal electrode on to the molecular monolayer, the molecules' properties are likely to be changed due to the penetration of the metal atoms; the application of an intense electric field during the electromigration step for generating a nanometer gap may alter the molecule's property. Second, different types of metals, including a single molecular magnet and complex molecular clusters, can be used for the electrodes, as even the bottom and top electrodes can be fabricated with different types of metals, respectively. Conversely, other approaches are limited to a few types of metals. Third, the OEMJs can be produced in an extremely large-scale integrated circuit layout using conventional microfabrication techniques, thus offering a low-cost approach.

The challenging issue of the OEMJs is the extreme difficulty of exploring the charge transport properties through individual molecules. The effective number of attached molecular channels is governed by the width of the bottom electrode. To host only single molecules, the width of the bottom electrode needs to be decreased to a few nanometers in width, and its mechanical stability needs to be maintained, which is an intractable task. The additional limitation of the OEMJ method is that the introduction of a third electrode or a gate electrode to control the electron transport is not straightforward. Thus far, only chemical gating is available for the OEMJ method. Potential strategy for adding a solid gating electrode can be described as follows: (1) burying an inner conducting core inside the insulation layer, in which the conducting core can be used as the gating electrode; and (2) using the FIB technique to cut the wire (contains three layers, metal−insulation−metal), which will result in a gap a few nanometers in width to appear around the cutting point. One side of the gap can be used as the source−drain electrode, while the other side can be used as the gate electrode. In this way, new functional devices with electrical gating may be available.

3. CARBON ELECTRODES FOR MOLECULAR ELECTRONICS

While ordinary metal electrode-based molecular junctions remain operational, different experimental platforms based on nonmetal materials have been constructed, thus leading to new possibilities for molecular-scale electronics. Among these new testing systems, carbon electrode−molecule junctions, where carbon nanomaterials, including single-walled carbon nanotubes (SWNTs) and graphene, are used as point contacts, are particularly promising because of their unique advantages. First, both the SWNTs and the graphene are molecular chemicals made entirely of sp^2-hybridized carbon atoms arranged in a honeycomb lattice,[340,341] thus offering a natural compatibility with organic/biological molecules. Second, these crystalline carbon nanomaterials exhibit extraordinary electronic properties with high stability and chemical flexibility due to their π-conjugated skeletons. Unlike mobile metal electrodes, they are atomically stiff and naturally functional at their ends. When lithographically patterned as point contacts, they are end-functionalized by carboxylic acid groups. These functional groups could be used to form robust covalent bonds at the molecule/electrode interface through amide linkages that can endure chemical treatments and external stimuli, thus significantly improving the device stability. Third, they are easily available in large areas through bottom-up chemical approaches and can be easily micro-/nanofabricated onto a large range of substrates with high accuracy. Finally, another unique feature of these nanocarbons results from the fact that the low-dimensional nature is molecular in size, ensuring the number of bridged molecules down to the single-molecule level. Because of all of these features, carbon nanomaterials, such as SWNTs and graphene, are most likely better suited as nanoscale electrode materials for molecular electronics, as commented in the special issue of *Nature Nanotechnology* in June, 2013.[342] In this section, we detail the methodologies used to develop robust molecular electronics platforms based on SWNTs and graphene.

3.1. Carbon Nanotube-Based Electrodes

Since their discovery in the 1990s,[343] carbon nanotubes have led to a significant amount of research due to their tremendous potential applications in the chemical, physical, and electrical fields.[344] Although they have the simplest chemical composition and atomic bonding configuration, their electronic properties are highly dependent on chirality and diameter. This structural dependence leads to infinite electrical diversity and richness, thus offering unlimited opportunities to tune the energy alignments between the tubes and the molecules of interest. Another important distinction between the SWNTs and the metal contacts is that the SWNTs are molecularly sized in their diameter, centimeter-scale long, and functional on their ends (not their sides). Therefore, in conjunction with the remarkable properties mentioned above, the SWNTs are good contacts for modular single-molecule devices. To form the SWNT electrodes, there are several efficient ways to cut the SWNTs and obtain nanogaps, such as focused-ion-beam etching (FIB), electrical breakdown, and lithography-defined oxidative cutting. The FIB etching method uses high-energy ion beams to etch the SWNTs as well as the substrates.[345] After FIB etching, the tube edges were treated with nitric acid to introduce the carboxylic acid end groups. These functional groups then were used to bridge the individual DNA molecules, allowing direct electrical measurements of the DNAs using the SWNT electrodes. The key step is that the interelectrode spacing was controlled by adjusting the ion beam current and the exposure time, which is challenging due to the use of the high-energy ion beams. In the following discussions, we primarily introduce two reliable methodologies with more universality to build molecular devices based on the SWNT point contacts, including electrical breakdown and lithography-defined oxidative cutting.

3.1.1. Electrical Breakdown. Similar to the formation of the metal electrodes using electromigration previously discussed, the electrical breakdown of the SWNTs will occur when a high-density current passes through them, eventually resulting in a gap by truncating a complete tube.[346] It was determined

DOI: 10.1021/acs.chemrev.5b00680
Chem. Rev. 2016, 116, 4318−4440

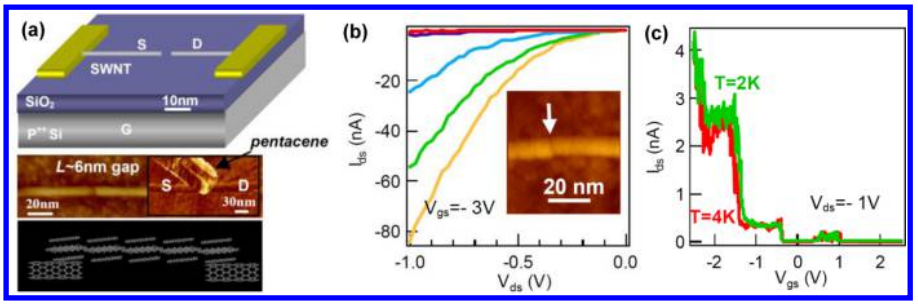

Figure 24. SWNT electrodes for ultrasmall OFETs. (a) Top: Schematic demonstration of a cut SWNT with a nanoscale gap used as the source and drain electrodes of an OFET. The doped Si serves as a back gate. Middle-left: AFM image of a cut SWNT (diameter ≈ 2 nm, and gap size measured to be ~6 nm after correction of the tip size effect). Middle-right: AFM image of a vapor-deposited pentacene crystallite bridging a cut SWNT. Bottom: Drawing of a pentacene crystallite bridging two SWNT electrodes. (b) I_{ds}−V_{ds} curves for a device recorded at V_{gs} = −3, −2, −1, 0, and 1 V at room temperature. Inset: An AFM image of the SWNT after electrical cutting and before pentacene deposition. (c) I_{ds}−V_{gs} curves (at V_{ds} = 1 V) for the same device at T = 4 and 2 K. Reproduced with permission from ref 190. Copyright 2004 American Chemical Society.

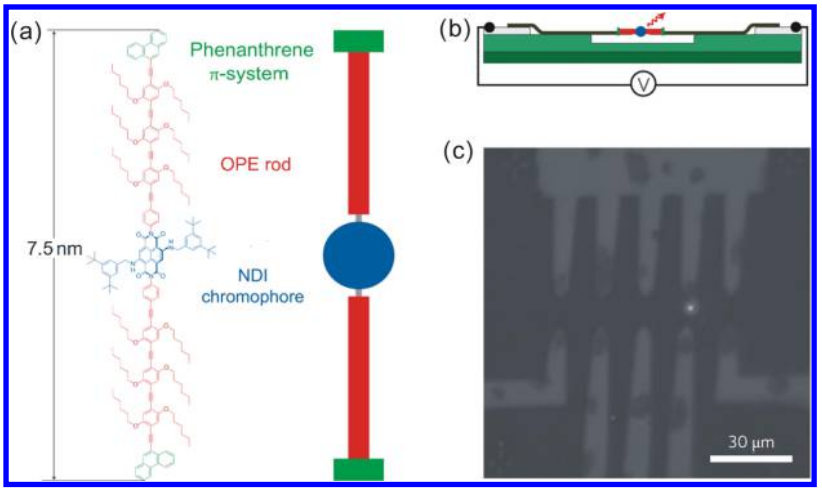

Figure 25. Single-molecule electroluminescence. (a) Chemical structure of the molecule, which consists of a central 2,6-dibenzylamino core-substituted NDI chromophore (blue), two OPE rods (red), and phenanthrene anchor units (green). (b) Schematic drawing of the device geometry. (c) Optical micrograph of an image acquired for 20 min with one device under a bias of V = 4 V and without external illumination. A bright electroluminescent spot is visible at the location of the biased carbon nanotube−molecule junction. Reproduced with permission from ref 354. Copyright 2010 Nature Publishing Group.

that the size of these gaps was extremely sensitive to the air exposure because this electrical breakdown was initiated by oxidation at a particular power in air.[347] This result implies that nanogaps with different sizes could be achieved in the middle region of a nanotube by varying the proportion of the oxidative gas in the cutting environment, potentially providing a way to fabricate the SWNT electrodes.

In 2004, two independent studies on miniaturized organic transistors based on carbon nanotube electrodes were reported by Qi et al.[190] and Tsukagoshi et al.[348] In the former study, molecular-thickness pentacene was deposited into the gap on a single SWNT fabricated by the electrical breakdown (Figure 24a). The reported size of the nanogaps could be reproducibly controlled in the range of 1−3 nm by varying the lengths of the SWNTs with a ~2 nm diameter. The scale of this channel is only able to accommodate several organic molecules of interests, which could circumvent the low carrier mobility problem to afford ballistic organic field-effect transistors (OFETs) with high performances. It was demonstrated that the smallest OFETs based on the SWNT electrodes with a channel length of L ≈ 1−3 nm and a width of ~2 nm indicated a strong capability of effective conductance modulation (Figure 24b). However, in ultrashort OFETs with bulky metal source/drain (S/D) electrodes that were lithographically patterned as the control, the electrostatic gating was ineffective due to the screening of the gate electric fields by the S/D electrodes. In addition to the measurements at room temperature, this study also tested the properties of the devices with different-size nanogaps at low temperatures (e.g., 2 and 4 K). When the size (1−3 nm) of the nanogaps approached that of the pentacene, step-like features were observed in the I−V spectra (Figure 24c), which could be related to the tunneling currents through the discrete molecular orbitals of the pentacene, while the devices with larger gaps became insulated in the entire gate-voltage range. In the latter study conducted by Tsukagoshi et al.,[349] the device structure was fabricated similarly. They revealed that the electrode leads are composed of six-membered carbon rings, common for the compositing unit of pentacene, which will facilitate local epitaxial adhesion due to the commensurate absorption of the van der Waals force connection, thus resulting in an effective electron injection. Additionally, the carbon nanomaterial electrodes have a smaller difference in the organic molecules regarding the thermal expansion coefficient as compared to that of the metal electrodes. This difference ensures the stiffness of the molecule−electrode interface, thus providing additional possi-

DOI: 10.1021/acs.chemrev.5b00680
Chem. Rev. 2016, 116, 4318−4440

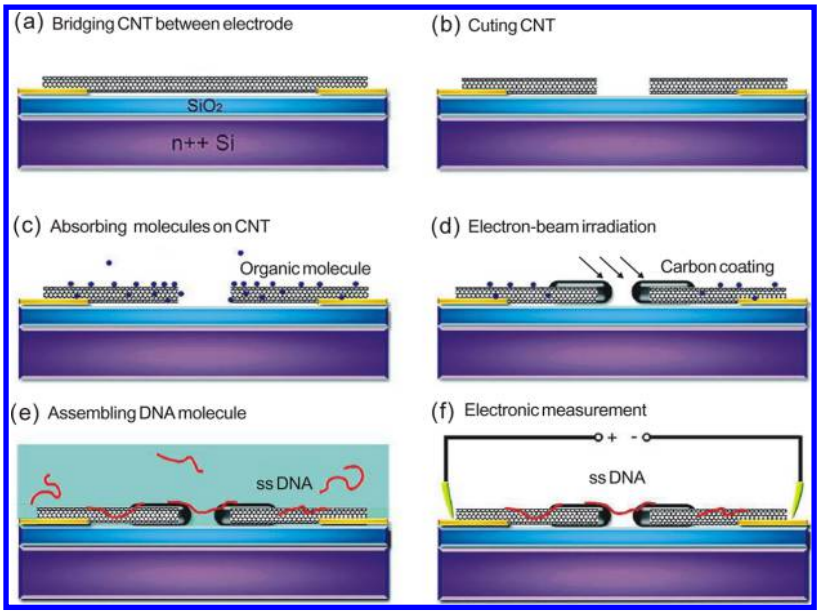

Figure 26. Schematic diagram of fabricating nanotube electrodes by the EBID. (a) Building a nanotube transistor. (b) Cutting the nanotubes using the electrical breakdown. (c) Adsorbing organic molecules on or in the CNT. (d) Irradiating the gap of the CNT with an electron beam for in situ observation in the SEM. (e) Assembling DNA molecules between the CNT electrodes by being immerged in a DNA buffer solution. (f) Measuring the electronic properties of the bridged DNA molecules. Reproduced with permission from ref 355. Copyright 2008 American Chemical Society.

bilities for temperature-dependent measurements. For example, the carbon nanotube-based device was still conductive when cooled to 4.2 K, whereas several organic transistors with metal electrodes exhibited no conduction below the liquid-nitrogen temperature because the connection interface was damaged due to different degrees of expansion. The advantages of using carbon nanotubes as electrodes promise new opportunities for forming new types of molecular FETs and exploring the intrinsic transport properties of few and even single molecules.[350−353]

Following the impressive studies mentioned above, Marquardt et al.[354] conducted single-molecule electroluminescence measurements on the basis of molecular devices using free-standing SWNTs as electrodes. Similarly, these SWNT electrodes with a nanogap <10 nm were fabricated controllably through the electrical breakdown in combination with the regulation of the oxygen partial pressure. The organic molecules of interest with special designs were incorporated into the nanogap using two types of interactions: electrostatic attraction between the polarizable π-systems (oligo(phenylene ethynylene), OP) on both sides of the molecules and the nanotube electrodes and $\pi-\pi$ stacking between the terminal phenanthrene units and the nanotubes, both of which could produce a strong connection, thus ensuring the execution of the systematical experiments (Figure 25a). Generally, for use as efficient electrodes, an SWNT with an excellent metallic transport property is required; however, the amount of delocalized electrons should be limited to avoid the quenching of the excited state of the molecule because the low level orbital in the excited state is necessary for luminescence (Figure 25b). Fortunately, the metallic carbon nanotubes have perfect ballistic transport properties with a simultaneous suppressed degree of electron delocalization, thus ensuring the successful observation of electroluminescence (Figure 25c). This finding is remarkable because it provides visible evidence for the current flow through rigidly mounted carbon nanotube-molecule junctions and the likelihood of obtaining molecular light-emitting devices with different emission chromophores.

In another study, Wei et al.[355] developed a new process through a combination of the electrical breakdown and the electron beam-induced decomposition (EBID) to fabricate nanotube nanogaps with a controllable size. In the process, wide nanogaps of approximately 10−60 nm were initially formed on the nanotubes using a high-density current (Figure 26a,b) followed by exposure to organic vapors (such as ethanol or toluene) to absorb the organic molecules in the cavity or on the surfaces of the nanotubes (Figure 26c). The SEM then provided an electron beam with an appropriate energy to induce the EBID to regulate the gap size of the nanotube electrode while avoiding the destruction of the carbon nanotubes (Figure 26d). Because this process allowed an in situ and real time characterization during the nanotube diameter broadening and nanogap narrowing process, it is relatively feasible and facile to control the nanogap size in a relatively accurate manner. Importantly, after the EBID process, a π-conjugated surface stemming from the deposition of sp^2-rich amorphous carbon was formed, thus offering the option to develop molecular electronics by bridging the circuits with similar π-conjugated molecules, such as DNA, through π-stacking interaction (Figure 26e and f).

As described above, the electrical breakdown methodology is useful for achieving nanoscale gaps within carbon nanotubes with relative controllability and efficiency. Although the electrical breakdown method has achieved remarkable progress, several considerable challenges remain, such as the lack of precise control of the gap size and electrode geometry, weak interfacial connection due to π-stacking or the van der Waals forces caused by physical absorption, and complex extra treatment to obtain different degrees of vacuum. Therefore, there is a significant need to develop new techniques to readily fabricate nanogaps in a fully controllable manner, which is of particular importance to advance molecular-scale electronics for

DOI: 10.1021/acs.chemrev.5b00680
Chem. Rev. 2016, 116, 4318−4440

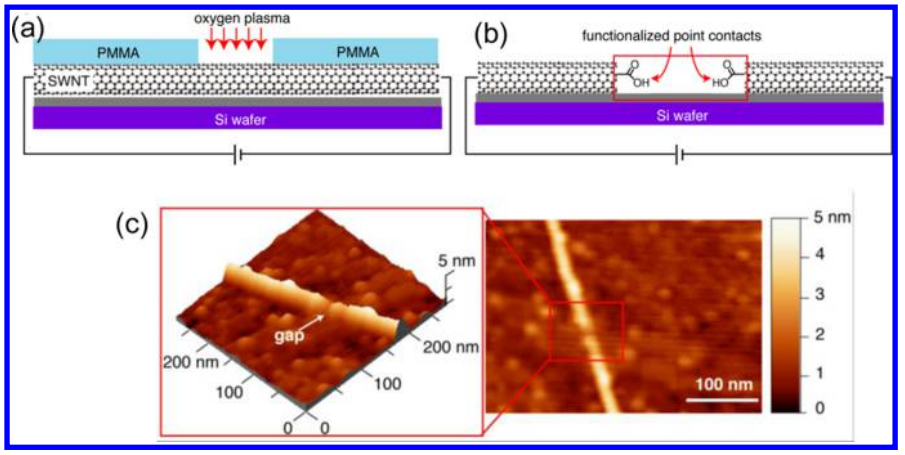

Figure 27. Lithography-defined oxidative cutting process for fabricating SWNT point contacts. (a) Precise cutting of SWNTs with oxygen plasma introduced through an opening in a window of PMMA defined with e-beam lithography. (b) Oxidative opening of a tube produces two point contacts functionalized on their ends with carboxylic acids and separated by as little as 2 nm. (c) AFM image of the gap cut into the SWNT. Inset is the height profile of the isolated tubes. The diameter of the SWNT is 1.6 nm, which is estimated from the height profile. Reproduced with permission from ref 31. Copyright 2006 AAAS.

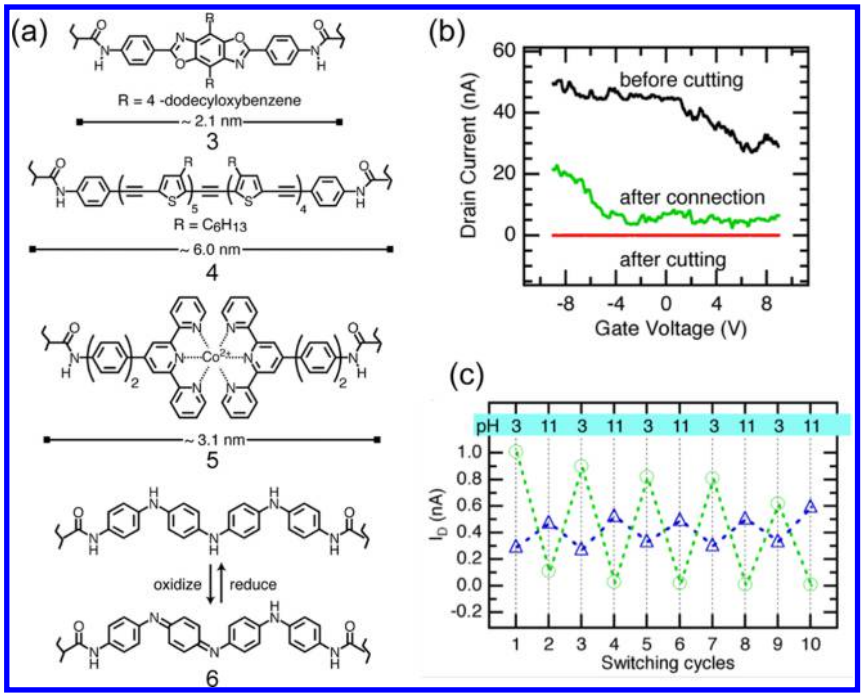

Figure 28. Reconnecting SWNT electrodes using molecules. (a) Molecular bridges (3–6) spanning the SWNT leads. Oligoaniline 6 provides a redox- and pH-sensitive molecular bridge. (b) Drain current (I) as a function of the gate voltage (V_G) at a bias voltage of 50 mV for a metallic tube reconnected with 3. Electrical measurements were made before cutting (black curve), after cutting with an oxygen plasma (red curve), and after connecting (green curve). (c) Green circles demonstrate the ON-state resistance for oligoaniline 6, of which the conductance can be altered through protonation or deprotonation when alternately immersed in solutions of low and high pH. The blue triangles depict small changes in the ON-state resistance for 4 when alternately immersed in solutions of low and high pH. Reproduced with permission from ref 31. Copyright 2006 AAAS.

either rigorous scientific research or large-scale potential industrial applications.

3.1.2. Lithography-Defined Oxidative Cutting. Chemically, carbon nanotubes are composited by sp^2-hybridized carbons, which can be easily activated using programmable techniques, thus providing several opportunities to establish new connections with the outside world, such as the carboxylic group. Driven by this proposal, Guo et al. successfully developed a reliable method in 2006 to fabricate nanoscale gaps in SWNTs on the basis of a combination of high-resolution EBL and precise oxidation by oxygen plasma.[31] At the cutting position, the SWNT leads with the carboxylic groups will be terminated, making it possible to form a robust connection between the SWNTs and the molecules using a chemically covalent bond, such as the amide linkage. This result is remarkable because the covalent linkages significantly improve the device stability. This fact is of crucial importance to develop functional SWNT-molecule single-molecule junctions that function as sensors and switches, thus leading to practical molecular devices.

The lithography-defined oxidative cutting process for fabricating SWNT point contacts is described below. Briefly,

DOI: 10.1021/acs.chemrev.5b00680
Chem. Rev. 2016, 116, 4318–4440

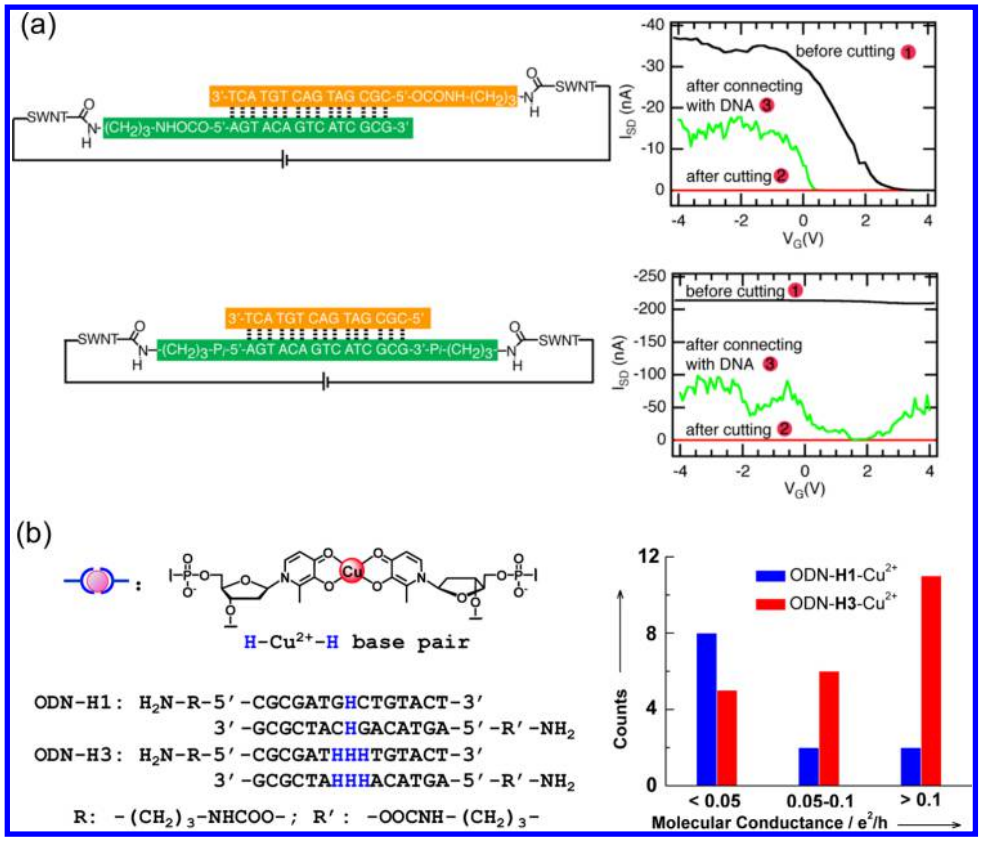

Figure 29. DNA conductivity. (a) I_{SD} versus V_G at a constant V_{SD} (50 mV) for a semiconducting SWNT device (top) and a metallic SWNT device (bottom) (black curve: 1), after cutting (red curve: 2), and after connecting with the DNA sequence shown (green curve: 3). Reproduced with permission from ref 356. Copyright 2008 Nature Publishing Group. (b) Left: Molecular structure of the Cu^{2+}-mediated base pair based on hydroxypyridone nucleobases (**H**) and the DNA sequences. Right: Statistical conductance comparison between ODN-**H1**-Cu^{2+} and ODN-**H3**-Cu^{2+} duplexes. Reproduced with permission from ref 357. Copyright 2011 Wiley-VCH.

arrays of SWNT-based transistors fabricated using photolithography are spin-coated by a blanket layer of PMMA, where an ultrasmall window is open to expose individual SWNTs through high-resolution e-beam lithography. Oxygen plasma then is injected through the lithography-defined window to produce two-faced electrodes capped with carboxylic groups by precise local oxidation, which offers access to linking with molecules containing amine terminations through amidation (Figure 27). It should be noted here that the size of these nanogaps could be controlled through different degrees of oxidation, that is, varying the time of exposure to oxygen. Under optimal conditions, such carboxylic group-functionalized SWNT electrodes, separated by a molecular-length gap, can be produced with 20−25% yield. This type of molecular electronic device can be used to explore the intrinsic properties of individual molecules or achieve special functions, which are determined by the designation of corresponding molecules, that is, the core component of the devices.

This lithographic method has three remarkable advantages, as listed below. First, the end points of the SWNT electrodes are oxidized to produce carboxylic groups, which enable the system to form covalent bonds between the electrodes and the bridging molecules terminated by the diamines. Because of the robustness of the interfacial connection, this type of molecular device can tolerate extra stimuli and chemical treatments, thus significantly improving the device stability. Second, due to their naturally quasi-1D geometric scale, these SWNT electrodes provide only limited sites for molecular connection. When combined with a special designation for the molecules, such as introducing long side chains, the purity of the single-molecule measurements can be ensured, which has the potential for uncovering a wealth of intrinsic information at the single-molecule level. Third, the entire fabrication process is implemented under ambient environment conditions, which can largely decrease the difficulty and complexity to achieve such sophisticated devices. Additionally, this fabrication process can be easily extended to industrial mass production in the future because all of the operations in the process as well as the three-terminal device architecture are compatible with conventional micro- and nanofabrication techniques, which have been completely developed in modern industry.

In the initial study, four molecules with different lengths and structures were incorporated into the nanogaps between the SWNT electrodes for two purposes: to demonstrate the capacity and universality of this platform for various molecule bridges and calibrate the etching process on the basis of the molecular rulers (Figure 28a). For the former, electrical measurements were sequentially performed on devices before cutting, after cutting, and after connecting with the molecular bridges. As indicated in Figure 28b, using molecule 3 as a representative, the black curve indicated the source−drain current (I_{ds}) plotted against the gate voltage (V_{gs}) at a constant S−D bias voltage (V_{ds} = 50 mV) before cutting. The device before cutting demonstrated a metallic behavior. The red trace, taken after cutting, indicated no conductance down to the noise limit of the measurement (≤~2.0 pA). The green trace

DOI: 10.1021/acs.chemrev.5b00680
Chem. Rev. 2016, 116, 4318−4440

depicted the devices after molecular connection of the SWNT leads. These measurements clearly proved that this platform of building single-molecule junctions could be generalized for different molecular wires. Regarding the latter, different reconnection yields for molecular bridges with different sizes could provide useful guidance for controlling specific etching degrees to achieve gaps with the appropriate scales for reconnection. Briefly, these experimental efforts offer a promising way to fabricate true single-molecule devices with high stability and reproducibility, thus setting the foundation for probing the intrinsic properties of the molecular materials. For example, after introducing target molecule 6 into the molecular circuits based on the SWNT electrodes, functional devices that were sensitive to the pH at the single-molecule level were achieved (Figure 28c).

Another important example is to explore the electrical conductivity of individual DNA molecules.[356,357] For a long time, the question of whether DNAs are conductive was controversial.[358] To prove DNA conductivity, Guo et al. developed a general method to integrate DNA strands between the SWNT electrodes and measure their electrical properties (Figure 29a).[356] In this experiment, the DNA sequences were modified with amines on either the 5′ terminus or both the 3′ and 5′ termini and coupled to the SWNT electrodes through amide linkages, thus allowing the electrical properties of the double-stranded DNAs to be measured. It was determined that the well-matched duplex DNA in the gap exhibited an average resistance of approximately 1 MΩ, which resembled the electrical characteristics of the aromatic stacked planes of graphite. In combination with other reports based on metal electrodes,[345,359−361] which described the charge transport in single DNA molecules as coherent tunneling, incoherent hopping, or both, these results provided direct evidence that clarified the DNA conductivity. However, the conductivity of wild DNAs was found to be limited, thus hampering the development of DNA-based nanoelectronics. To improve the DNA conductivity, Guo et al. further demonstrated the direct charge transport measurement of individual metallo-DNA duplexes using single-molecule break junctions (Figure 29b).[357] By comparing the conductance between ODN-**H1**-Cu^{2+} and ODN-**H3**-Cu^{2+}, it was demonstrated that the ODN-**H3**-Cu^{2+} devices tended to exhibit a higher conductance than the ODN-**H1**-Cu^{2+} devices. This result may be attributed to the synergistic effect of increased rigidity of the π-stacking and the electronic coupling for hole transfer induced by the metal ions. This study is the first direct experimental support for the hypothesis that the precise arrangement of the metal-mediated base pairs into the DNA scaffolds may improve the insufficient electrical conductance of the DNA duplexes. These findings provide a foundation for DNA-based hybrid materials as conductive biocompatible bridges that may interface electronic circuits with biological systems.

As demonstrated above, the SWNT electrode-molecule single-molecule junctions provide a promising device platform for building truly single-molecule devices with high stability. On the basis of this approach, functional molecular devices have been created to detect molecular conformation transformation, protein/substrate binding, and DNA hybridization at the single-molecule level. More information about its further applications toward functional single-molecule biosensors and switches is provided in sections 7.4 and 7.5, respectively. However, this approach has challenges stemming primarily from two aspects: the connection yield is relatively low (generally ∼5%), and the device-to-device properties vary primarily due to the variability in the properties of the SWNTs that depend on their chirality and diameter. To solve these issues, it is urgent to develop another efficient strategy to build high-throughput molecular junctions with high reproducibility.

3.2. Graphene-Based Electrodes

Graphene, another typical allotropy of carbon, is a two-dimensional zero-bandgap semimetal carbon material with extraordinary electronic properties that has received worldwide attention since its discovery by Geim and Novoselov et al. in 2004.[341] Its high mobility and the ease with which it can be doped with either holes or electrons make it suitable as a platform for sensors, electrodes in field-effect transistors, and as transparent contacts for photovoltaic devices.[362−370] Particularly, graphene does not have the inherent variability of the SWNTs and can circumvent the problems that concern the SWNTs as discussed above. Therefore, two-dimensional graphene, as compared to one-dimensional SWNTs, has the capability of largely simplifying the device fabrication process and creating stable molecular devices in high yield, thus potentially providing complementary contacts to test the intrinsic properties of different molecular devices with molecular sizes in all dimensions. In the following section, we focus on the methodologies developed for fabricating the second class of carbon electrode-molecule single-molecule junction: graphene electrode-molecule single-molecule junctions.

3.2.1. Electroburning. One early example that used graphene electrodes in molecular-scale electronics was reported by Prins et al.[371] In this study, they used feedback-controlled electroburning to slice a few-layer graphene sheet (Figure 30).

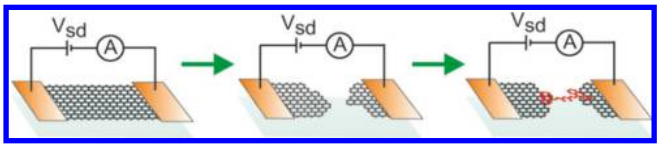

Figure 30. Schematic of the feedback-controlled electroburning process and the ideal device configuration. The device was created by assembling molecules terminated with anthracene groups using $\pi-\pi$ stacking. Reproduced with permission from ref 371. Copyright 2011 American Chemical Society.

The gaps have separations of approximately 1−2 nm, as estimated from a Simmons model for tunneling. The devices then were created by assembling molecules of interest inside the graphene nanogaps using $\pi-\pi$ stacking (Figure 30). It was determined that the molecular junctions displayed gateable $I-V$ characteristics at room temperature. However, it is difficult to control the electrode geometry and the resulting gap size due to the use of the electroburning process and the few-layer graphene sheets. Therefore, the development of a reliable approach to fabricate graphene point contacts for creating single-molecule junctions with high stability remains a considerable challenge. Recently, Ullmann et al. not only present a fabrication scheme based on epitaxial graphene nanoelectrodes employing electrical breakdown protocol, but also identified a suitable molecule (a molecular wire with fullerene anchor groups) to make a reliable graphene point contacts.[372] With these two components, stable electrical characteristics were recorded. Interestingly, electrical measurements show that single-molecule junctions with graphene and with gold electrodes display a striking agreement, which

DOI: 10.1021/acs.chemrev.5b00680
Chem. Rev. 2016, 116, 4318−4440

motivated a hypothesis that the differential conductance spectra are rather insensitive to the electrode material.

3.2.2. Dash-Line Lithography. To solve these issues, Cao et al. recently developed a new method, known as dash-line lithography (DLL), to create a robust single-molecule electronic device based on indented graphene point electrodes.[30] The key feature of this technique is the ability to produce carboxylic acid-terminated graphene point contact arrays with gaps that are ≤10 nm. Briefly, a design CAD file with a 5 nm-width dash line (A, 150 nm) exposed to an electron beam (e-beam) and separated by B (40 nm) (Figure 31a) was designed

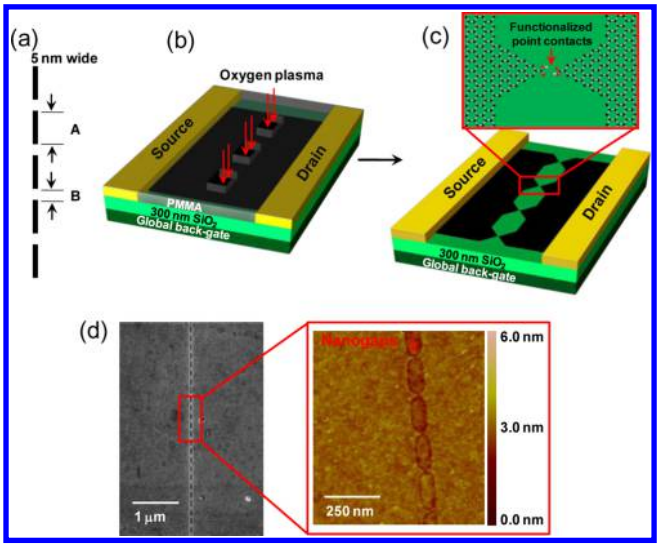

Figure 31. Fabrication of indented graphene point contact arrays. (a) A design CAD file with a 5 nm-width dash line (A, 150 nm; B, 40 nm) used for the cutting process. (b) Precise cutting of the graphene sheets using oxygen plasma through an indented PMMA window defined by the EBL. (c) Indented graphene point contacts formed by oxidative cutting were functionalized by carboxylic acid end groups and separated by as little as a few nanometers. (d) SEM and AFM images of a representative indented graphene point contact array. Reproduced with permission from ref 30. Copyright 2012 Wiley-VCH.

to open an indented window in a spin-cast layer of PMMA using ultrahigh-resolution EBL (Figure 31b). The single-layer graphene sheet with high quality was then locally cut through the open window via oxygen plasma ion etching (Figure 31c). By exploiting the gradual etching and undercutting of the PMMA, narrow gaps between the indented graphene point contacts arrays were achieved (Figure 31d). These point contacts reacted with the conductive molecules derivatized with amines to form stable molecular devices through amide linkages.

Similar to the SWNT case, the size of these nanogaps can be controlled through the regulation of the etching process. Three different-length molecules (Figure 32a) were selected as molecular rulers to characterize the relationship between the cutting yield and the reconnection yield by electrical measurements, as indicated in Figure 32b. This characterization helped optimize the device fabrication conditions. On the basis of the statistical data presented in Figure 32b, under optimized conditions, the maximum connection yield for these molecules was determined to be ∼50%, which corresponded to the cutting yield of ∼28%. This connection value significantly exceeds those of previous studies,[50] in which the connection yield was considerably lower when using metal or SWNT leads. On the basis of these data, the analysis of the number of junctions that contribute to the charge transport using the binomial distribution demonstrated that, in most cases, only one or two junctions contributed to the charge transport of the devices.[30,350]

One apparent advantage of this methodology is that the DLL technique largely simplifies the device fabrication process and creates stable molecular devices in high yield. The ease of device fabrication and device stability denote the graphene-molecule single-molecule junctions as a new-generation testbed for molecular electronics. However, most of the previous studies rely primarily on the ex situ synthesis of the molecular wires (e.g., dithiolated molecules) followed by their subsequent insertion into the nanogapped electrodes, thus complicating the systems because of the strong tendency for oxidative oligomerization and aggregation of the molecules. To solve these problems, based on the above-developed method, Cao et al. demonstrated the capability of the in situ construction of complex molecular wires through the implementation of a multiple-step reaction sequence (amide formation and coordination reaction) between the molecular-scale graphene point contacts.[373] For example, a three-step strategy is presented in Figure 33. First, the graphene point contacts were primed with a terpyridyl ligand 10 (Figure 33a), which only has a single amine group to react with the graphene electrodes; however, it has a tridentate aromatic pocket available for the subsequent coordination chemistry (Figure 33b). There was essentially no detectable current (≤100 fA) (red curve in Figure 33c). The primed devices then were immersed in a diluted methanol solution of cobalt acetate (∼10^{-5} M). After the second step of cobalt ion treatment, each of the $I-V$ characteristics of the devices were carefully screened and determined as either reconnected or open. The circuits that were open indicated zero conductance up to the noise limit of the measurement (≤100 fA) (red curve in Figure 33c). Each of these devices should contain two cobalt ions, one on each facing end of the nanogap, and each cobalt ion should be available for further coordination. In the third step of this sequence, hexapyridyl 11 (Figure 33a) was added (∼10^{-5} M in chloroform), and the conductivity of the devices was measured (blue curve in Figure 33c). The inset in Figure 33c indicates the I_{SD} as a function of the V_{SD} for the same device after sequential reactions with 10 and cobalt ions during cutting (red) and after the further addition of 11 (blue). The connection yield for this three-step strategy was ∼9%. In addition to the in situ construction of the molecular junctions, the researchers also achieved reversible switching between distinct conductance states when an azobenzene molecule (molecule 8 in Figure 32) was either illuminated by lights with different wavelengths or exposed to different pH values, thus providing the possibility of integrating multiple functionalities into a single molecular device.[373] Collectively, these results demonstrated the capability of installing molecular functionalities into electronic devices in a new platform of DLL-generated graphene-molecule junctions. Additional details on this topic can be found in section 7.4.

3.3. Other Carbon-Based Electrodes

As discussed in detail in section 2, molecular junctions based on the metal−molecule−metal architectures provide useful insights into the charge transport at the molecular level, thus leading to a better understanding of the underlying fundamental principles of molecular-scale electronics. However, nanoscale metal electrodes are mechanically unstable due to the

DOI: 10.1021/acs.chemrev.5b00680
Chem. Rev. 2016, 116, 4318−4440

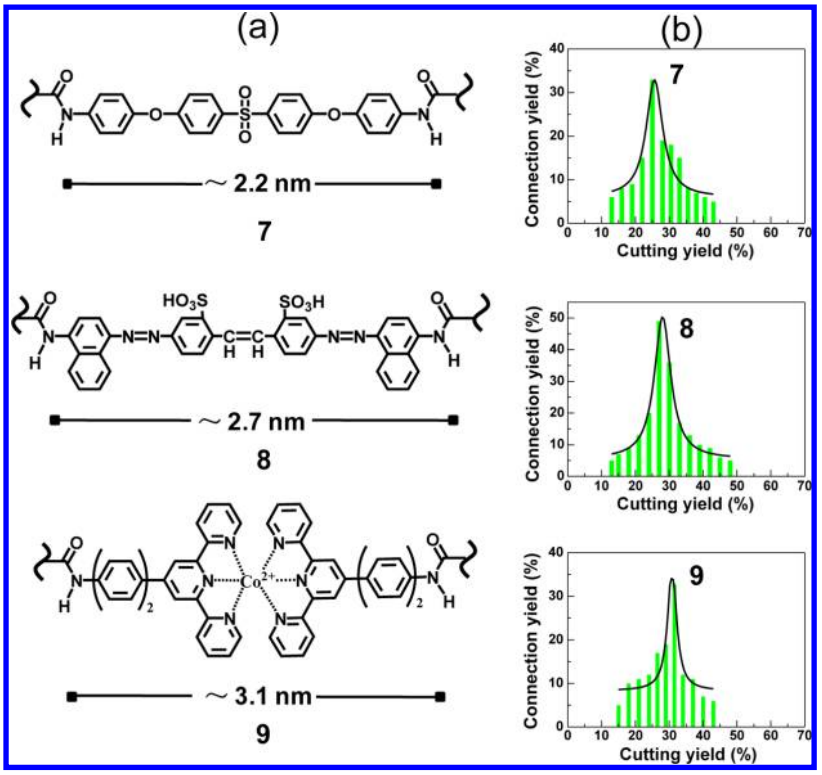

Figure 32. Improvement in the device fabrication. (a) Molecular bridges (7−9) spanning the graphene point electrodes. (b) Statistical data of the connection yields as a function of the cutting yields for each corresponding molecule. The simulated curves are depicted in black. Reproduced with permission from ref 30. Copyright 2012 Wiley-VCH.

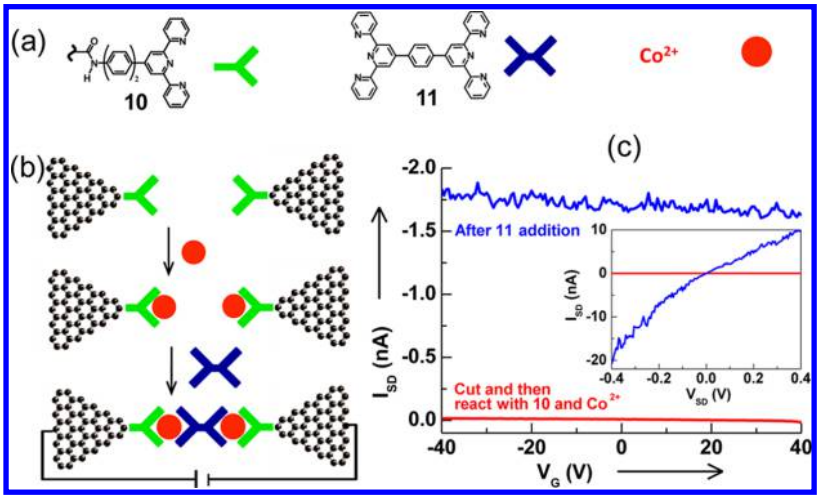

Figure 33. In situ construction of complex molecular wires. (a) Molecular structures used for device reconnection and specific recognition for Co^{2+}. (b) Schematic strategies for bridging graphene point contacts through a three-step strategy. (c) Device characteristics for the reconnected device through a three-step sequence, V_{SD} = −50 mV. Inset depicts I_{SD} versus V_{SD} data for the same device after the reactions with **8** and cobalt ions (red) as well as after the addition of **9** (blue) at the zero gate bias. Reproduced with permission from ref 373. Copyright 2013 Wiley-VCH.

high atomic mobility of the metal atoms. Furthermore, most of the metal electrodes (except Au) can be oxidized easily under atmosphere conditions. Additionally, the typical electrode density of the states near the Fermi energy is nearly energy independent, which will hamper their further applications because metal-based molecular junctions generally have smooth and featureless transmission probabilities near the Fermi energy. Carbon-based electrodes, such as graphite, have a remarkable mechanical strength as well as a variable highly dispersive density of states near its Fermi energy[374] and strong noncovalent interactions through the van der Waals-based $\pi-\pi$ stacking.[330,354,371] This result implies that these materials can be used to create molecular junctions by combining metal with the carbon electrodes. Recently, Kim et al.[375] demonstrated the formation of molecular junctions using the STM technique, where an Au metal tip and a microfabricated graphite substrate were used as the two electrodes (Figure 34a). One remarkable feature of this junction is that the mechanical strength of the graphite and the single-crystal properties of their substrates allowed measurements to be taken over a few thousand junctions without any change in the surface properties. The conductance of a series of graphite/amine-terminated oligo-

DOI: 10.1021/acs.chemrev.5b00680
Chem. Rev. 2016, 116, 4318−4440

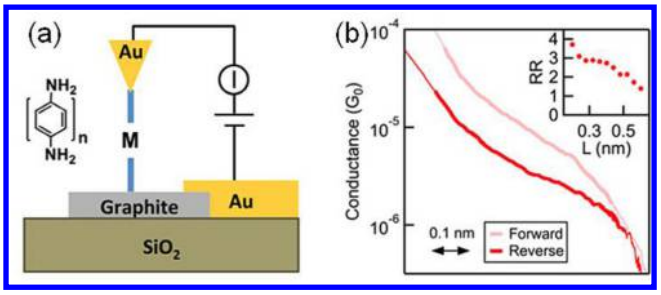

Figure 34. Schematic and rectification data for graphite/molecule/Au junctions. (a) Schematic of the junctions and the molecular structure. (b) Conductance profiles determined from 2D conductance−displacement histograms for the junctions measured under forward- and reverse-bias conditions. The inset depicts the rectification ratio as a function of displacement for these junctions. Reproduced with permission from ref 375. Copyright 2014 American National Academy of Sciences.

phenyl/Au molecular junctions was measured, and it was determined that the conductance decayed exponentially with the molecular backbone length, which is consistent with a decay constant observed in the same measurements with two Au electrodes. Interestingly, despite the inherent symmetry of the oligophenylamines, rectification was observed in these junctions (Figure 34b). This observation occurred because the highly energy-dependent graphite density of the states contributes variations in the transmission that, when coupled with an asymmetric voltage drop across the junction, lead to the rectifying effect. These results indicate the possibility of creating hybrid molecular-scale devices with purposefully designed functionalities using layered 2D materials.

4. OTHER ELECTRODES FOR MOLECULAR ELECTRONICS

Generally, materials used as electrodes in molecular junctions should have superior properties in four aspects. (1) The first premise is good electrical conductivity, which can maintain its high value with dimension scale-down. (2) The second is the stability of the material composition and configuration, which is of great importance for resisting external perturbation/oxidation and ensuring the success of forming molecular junctions. (3) The third is the abundant availability using either bottom-up or top-down approaches. (4) Last, the fourth is the ease of material processing, which should be compatible with industrial micro/nanofabrication techniques. On the basis of these considerations, the past two decades have witnessed a large variety of materials being used in molecular electronics, ranging from conventional noble metals to novel carbon allotropies, which continuously and creatively update the paradigms for device architecture and operation. In addition to the materials mentioned above, there were also other attempts to expand the research regimes of molecular electronics, including silicon and polymer-based nanoelectrode systems, as discussed in the following section.

4.1. Silicon-Based Electrodes

It is well-known that silicon materials led to the prosperity of the modern microelectronics industry because of their nearly perfect fitness for complementary metal oxide semiconductor

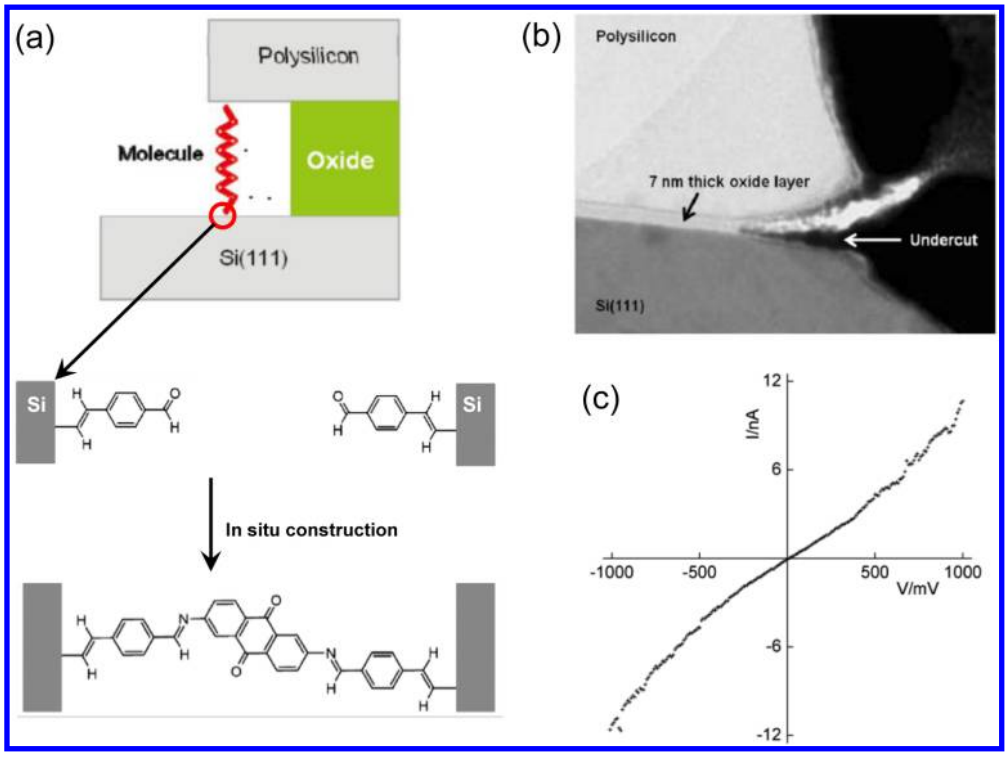

Figure 35. Molecular devices based on silicon electrodes. (a) Schematic representation of single-molecule junctions between the silicon electrodes. Inset: Chemical method for in situ construction of the interfacial connection by grafting 4-ethynylbenzaldehyde, Si−CH═CH−C_6H_4−CHO to activate the surfaces and then coupling with molecules with amine end groups. (b) TEM cross-section of the V-shape electrode gap obtained by undercutting the gate oxide layer. (c) *I*−*V* characteristics of the silicon nanogap-bridged devices achieved following the grafting reaction for 5 min in a solution of the amino-terminated linker, which may ensure the linkage of few or even single molecules. Reproduced with permission from ref 384. Copyright 2010 American Chemical Society.

DOI: 10.1021/acs.chemrev.5b00680
Chem. Rev. 2016, 116, 4318−4440

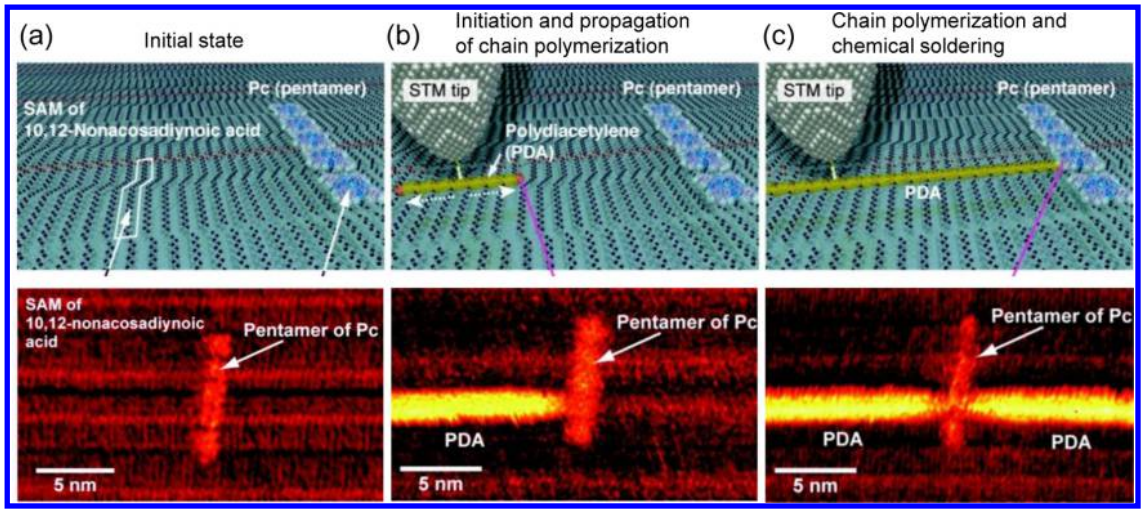

Figure 36. Schematic images of chemical soldering. (a) Top: Illustration of a Pc pentamer adsorbed to an SAM of 10,12-nonacosadiynoic acid. Bottom: Corresponding STM image. (b) Top: Chain polymerization initiated by an STM tip. Bottom: STM image obtained after initiating chain polymerization. The fabricated PDA chain, which is seen as a bright line, is connected to a Pc molecule. (c) Top: Polymer chain reached the adsorbed molecule and a spontaneous chemical bond formation occurred. Bottom: STM image depicting two PDA chains connected to a single Pc molecule. Reproduced with permission from ref 386. Copyright 2011 American Chemical Society.

(CMOS) technology, such as controllable conductivity and tunable Fermi level by doping.[376] Physically, the work function of silicon can be varied by changing the doping, type, and density without changing the interface structure and chemical binding, which will facilitate the interfacial energy level alignment.[377] Chemically, the incorporation of the organic molecule onto silicon is directional and stable, which is different from the case of thiols incorporated on Au. In the case of the Au−S bonds, the thiolates can move easily from one Au site to another at room temperature, even without applying a voltage, because the energy barrier between the two chemisorbed modes on Au (the corrugation energy) is approximately 2.5 kcal/mol (~0.11 eV mol^{-1}). Conversely, the corrugation energy is ~4 eV for Si−C and ~4.7 eV for Si−O−C in the downside of the stable binding to Si, whereas the upside is more robust against substrate oxidation to withstand heating and other harsh conditions. In fact, among the other binding chemistries, only the C−C bonding to graphite is comparable to the Si−C or Si−O−C binding modes.[378] Additionally, the currently developed micro-/nano-processing techniques are established for silicon materials. Collectively, silicon materials have clear advantages when used as efficient electrodes for molecular junctions.

Currently, molecular devices based on silicon electrodes use a fabrication process that first completes the construction of the contact structure and then the molecular connection. This approach is designed for avoiding two troublesome issues: (1) perturbations stemming from high temperatures and solvents used during conventional silicon processing after molecule deposition; and (2) short-circuit effects resulting from the process of depositing metal electrodes on the SAMs of molecules previously grafted on the silicon surface.[379] On the basis of these considerations, the combination of classical photolithographic techniques and selective etching methods, including wet and dry etching, is used to fabricate silicon-based electrodes.[380] For molecular bridging, the ever-developing silicon-related chemistry provides a large abundance of approaches to form the relatively robust electrode−molecule interface, which can be exemplified by the developed photoassisted reactions to construct the Si−O−C[381] or direct Si−C[382] linkages. Using these methods, several prototypes of molecular devices based on silicon electrodes have been developed. Berg et al.[383] manufactured a series of silicon nanogaps with a gap size ranging from 3 to 7 nm by partly removing the silicon dioxide insulator from a silicon−oxide−silicon material stack using a selective oxide etchant. Dirk et al.[380] detailed a simple four-step procedure to create a one-dimensional nanogap on a buried oxide substrate that relied on conventional photolithography and metal evaporation. The feasibility of forming molecular circuits using these nanogaps was further verified by electrical measurements of the 1,8-octanedithiol and 5 nm Au nanoparticles after attachment. This approach was further extended by Howell et al.[335] through a self-assembling approach based on the reaction of silicon with a diazonium salt.

A challenging issue in molecular electronics is the difficulty in identifying the number of molecules spanning the junction due to the naturally bulky dimension of the electrodes. To solve this problem, a study established in 2010 by Ashwell et al. appeared to introduce this particular consideration.[384] The construction of molecular silicon electrodes with a vertical architecture was reported (Figure 35a). Briefly, a highly doped n-type Si(111) bottom electrode and a polycrystalline Si top, which were separated with a V-shape gap of ~7 nm (Figure 35b), were fabricated using programmable CMOS processing and chemical etching. The molecular bridge then was achieved by the in situ synthesis of conjugated wires within the nanogaps. In this study, 4-ethynylbenzaldehyde, which has been covalently grafted to the Si electrodes by a simple thermally activated addition reaction, was used as a molecular bridge to connect the targeted molecules terminated with amines, thus forming the sandwich structure (Figure 35a). Therefore, the molecule−electrode interface is robust due to the Si−C covalent bond connection, consequently ensuring the charge transport (Figure 35c). In the following study,[385] the authors further reduced the scale of the molecular junctions to a span of ~2.8 nm with the featured device characteristics. It should be noted that the nanogaps between the silicon electrodes are likely to reconnect a large number of molecules. Importantly, a deliberate mismatch between the molecule length and the nanogap

DOI: 10.1021/acs.chemrev.5b00680
Chem. Rev. 2016, 116, 4318−4440

scale, combined with different in situ assembling times, was introduced to limit the number of bridges, thus constructing few- or single-molecule devices. Using this testbed, the transport properties of two types of molecular wires (oligofluorenes and anthraquinone) were measured.

For the initial exploration of silicon materials used in molecular electronics, this approach is significant for scaling the mature silicon system to a molecular scale. However, to generalize this method, certain challenges remain. First, although the CMOS processing techniques have a high degree of professional proficiency, the construction of these types of molecular electronics platforms is still complex, especially for commercial applications. Second, the chemical stability and the electrical conductance of the silicon electrodes are not suitable to provide molecular devices with high performance and stiffness against harsh environments. Third, it is difficult to determine the number of molecular bridges in the molecular junctions. Therefore, there are numerous issues in the system that need to be further studied.

4.2. Polymer-Based Electrodes

Despite the significant achievements mentioned above, it is still difficult to fabricate a practical single-molecule integrated circuit. One of the reasons is the lack of viable methods for wiring each functional molecule: how to create conductive nanowires at the designated positions, and how to ensure chemical bonding between the nanowires and the functional molecules. One possible solution is to integrate each molecule into the electrical circuits with atomic precision. Recently, a novel method known as "chemical soldering" was reported in 2011 by Yuji Okawa et al.,[386] in which they connected a single functional molecule with a single conductive polymer nanowire via covalent bonds. Briefly, functional phthalocyanine (Pc) molecules were placed on an SAM of diacetylene compounds (Figure 36a). An STM probe tip was then positioned on the molecular row of the diacetylene compound and then stimulated its chain polymerization to form conductive polydiacetylene (PDA) nanowires (Figure 36b and c). Because the front edge of the chain polymerization had a reactive chemical species, the resulted polymer nanowire reacted with an encountered phthalocyanine molecule and formed a connection through chemical bonding. Using this approach, a resonant tunneling diode stemming from a single phthalocyanine molecule bridging two conductive polymer nanowires (Figure 36c, bottom) was demonstrated.

The integration of using new materials as efficient electrodes in molecular electrical circuits remains an active and challenging area of research because it can offer a wealth of opportunities to construct robust interfacial connections, tune energy level alignments, and establish novel device architectures. It is of crucial importance to solve the critical issue of the electrode–molecule contact interface and develop true single-molecule circuits for the next generation of electronics with higher efficiencies and lower power dissipations. Specifically, the introduction of using semiconductors, such as silicon and low-dimensional nanomaterials, as nanoscale electrodes presents significant physical, chemical, and technological advantages, and the development of conductive polymer-based electrodes holds great potential for all synthesized molecular electronic circuits, thus leading to new branches in molecular electronics.

5. CHARACTERIZATION TECHNIQUES FOR MOLECULAR ELECTRONICS

The typical methods for characterizing molecular electronic devices are presented in Table 2. Each method has its own unique advantages and falls into five primary categories: microscopic, electrochemical, electrical, optical, and optoelectronic. The microscopic methods for molecular electronics have been discussed in previous sections, and the electrochemical technique is regarded as a classic method, thus falling beyond our primary interest. Here, we mainly address the electrical techniques characterizing the intrinsic optoelectronic properties of individual molecules, including inelastic electron tunneling spectroscopy (IETS), temperature-length-variable transport measurement, noise spectroscopy, transition voltage spectroscopy (TVS), thermoelectricity, and optoelectronic spectroscopy.

Table 2. Typical Methods for Characterizing Molecular Electronic Devices

techniques	methods	primary functions	ref
microscopy	scanning tunneling microscopy	image, carrier transport properties	39
	atomic force microscopy	conductance, nanolithography	387
	scanning electron microscopy	surface topography, component properties	388
electrochemistry	cyclic voltammetry	redox potential, electrochemical reaction	389
	AC impedance spectroscopy	density and resistance of molecule layer	390
	chronocoulometry	electrode surface area, concentration	391
electrical	IET spectroscopy (IETS)	fingerprint information on molecules	171
	length–temperature variation	electron transport mechanism	392
	noise spectroscopy	localized states, transmitting channels	393
	transition voltage spectroscopy	energy level alignments	394
	thermoelectricity	type of charge carriers	27
optical	enhanced Raman spectroscopy	structural, vibrational, and polarization	395
	infrared spectroscopy	vibrational modes, chemical structure	396
	ultraviolet–visible spectroscopy	energy gap, rate constant of reaction	397
optoelectronics	X-ray photoelectron spectroscopy	elemental composition, chemical state	398
	ultraviolet photoelectron spectroscopy	molecular orbital energies	399
	photoemission spectroscopy	interface electronic structure, orientation	400

5.1. Inelastic Electron Tunneling Spectroscopy

In molecular junctions, the optical spectroscopy has not yet been used as a standard tool for several reasons. (1) In a conventional vertical metal–molecule–metal device structure, it is difficult for light to penetrate through a metal electrode to probe the molecular layer. (2) The sample is as small as a single molecule, implying a small signal-to-noise ratio.[43] Inelastic electron tunneling spectroscopy (IETS), which is associated with the interaction between the transporting electrons and the molecular vibrations, is relatively suitable for a small gap,

DOI: 10.1021/acs.chemrev.5b00680
Chem. Rev. 2016, 116, 4318–4440

making it a primary characterization technique to identify the chemical species and supply the fingerprint information on the molecular junctions.[311,401,402] The IETS can make an unambiguous determination of the molecular species in the junction because the impurities (such as nanoparticles) present completely different IETS features as compared to the target molecules. Furthermore, it has an ultrahigh sensitivity to the molecular conformation and the contact geometry of the molecular junctions. Using sophisticated comparisons between the experiments and the theoretical computations, the IETS can be more useful for characterizing numerous aspects of the molecular junctions, such as the conformation of molecules, orientation of molecules, and electronic pathways.[311] Additionally, the IETS is not subject to the selection rules as infrared or Raman spectroscopy. Both infrared- and Raman-active vibrational modes can appear in the IETS. These advantages prove that the IETS is a powerful and informative spectroscopic tool that can be used for probing molecular junctions and devices.[403,404]

5.1.1. History and Background. The IETS was initially measured by Jaklevic and Lambe in 1966.[405] This pioneering study demonstrated that it was possible to obtain the vibrational spectra sandwiched in the Al−Al_2O_3−Pb tunnel junctions and clearly showed that the anomalous peaks in the d^2I/dV^2 versus V traces were due to the presence of organic adsorbates in the junctions. Over the next several decades, metal−insulator−adsorbate−metal (MIAM) junctions were typically used to study the surface effects on the vibrational modes as well as the electron−phonon interactions in the molecular systems. Another important advance was made in 1998 by Stipe et al. when IETS at a single-molecule level was demonstrated employing STM.[406] This technology, known as STM-IETS, is capable of mapping the phonon activation within a molecule adsorbed on a solid surface to perform a type of phonon imaging. It was demonstrated that the vibrational microscopy from the spatial imaging of the inelastic tunneling channels could be further used to distinguish the two isotopes.[406,407] Recently, it was reported that the IETS could be directly modulated by an external gate voltage. It was found that the IETS was resonantly enhanced in the Au−molecule−Au junctions due to the fact that the transport orbital strongly coupled with the internal vibrational modes upon a gating voltage.[171]

Figure 37 presents the expected IETS behavior as the applied voltage V_{SD} is increased. When a small negative bias is applied to the left metal electrode, the Fermi level of the left electrode is lifted. When an electron with an occupied state on the left side tunnels into an empty state on the right side with a conserved energy, it is known as an elastic tunneling process.[311] However, if there is a vibrational mode with a frequency of ω localized inside this barrier, and the applied bias is large enough such that $eV \geq \hbar\omega$, then the electron can lose a quantum of energy $\hbar\omega$ to excite the vibrational mode, where $\hbar$ is Planck's constant divided by 2π.[401] In the case of molecular junctions, the transporting electron can deposit $\hbar\omega$ onto the molecule to excite the molecular vibrational mode. This inelastic tunneling process opens an additional transmission channel for the electron, resulting in an increased current. Thus, the total tunneling current shows a nonlinearity characteristic and has a kink at the point ($V_{\hbar\omega} = \hbar\omega/e$). Typically, only a small fraction of electrons inelastically tunnel through the junction due to the small cross-section for such an excitation, and thus the nonlinearity in the current only manifests as a small change

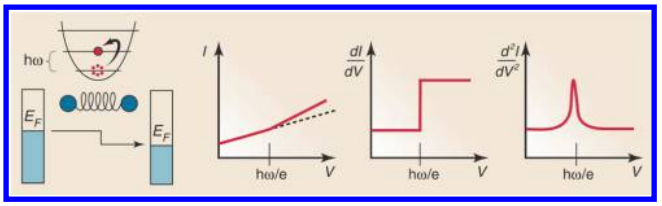

Figure 37. Expected inelastic electron tunneling spectroscopy behavior as the applied voltage increases via a vibrational resonance. For a bias energy (eV) larger than the vibrational energy ($\hbar\omega$), the transporting electron can deposit $\hbar\omega$ onto the molecule to excite the molecular vibration mode. An additional transmission channel then is open, resulting in a current increase. The change caused by opening the vibrational resonance channel at $eV_{sd} = \hbar\omega$ becomes a step in the differential conductance (dI/dV) plot and a peak in the d^2I/dV^2 plot. A plot of d^2I/dV^2 versus V is typically referred to as the IETS spectrum. Reprinted with permission from ref 43. Copyright 2008 AAAS.

in the slope of the $I-V$ characteristics. It is more common to plot the differential conductance (dI/dV vs V) curve, allowing the steps at $V_{\hbar\omega}$ to be observed, where each phonon mode is activated. A popular way to display the data is to plot the trace as d^2I/dV^2 versus V, in which the peaks at $V_{\hbar\omega}$ can be clearly observed.

5.1.2. IETS Measurement. The IETS signal can be obtained by a mathematical differential approach that computes the numerical derivatives of the directly measured $I-V$ curves.[166,408] However, this method is generally not easily achieved in practice due to insufficient signal-to-noise ratios or limited resolutions of the instrumentation used to acquire the data. In practice, the IETS signal, which is proportional to the second derivative of the $I-V$ curve, can be directly measured by an AC modulation method employing a lock-in amplifier.[409,410] In this strategy, a small AC voltage with a certain frequency ω is superimposed on the main DC bias so that the current can be written as follows:

$$I(V) = I(V_0 + V_{ac}\cos(\omega t)) \tag{1}$$

Using the Taylor series expansion about V_{DC}, the expression can be obtained as follows:

$$I(V) = I\left(V_0 + \left.\frac{dI}{dV}\right|_{V_0} V_{ac}\cos(\omega t) + \frac{1}{2}\left.\frac{d^2I}{dV^2}\right|_{V_0} [V_{ac}\cos(\omega t)]^2 + \ldots\right) \tag{2}$$

This equation can be rewritten using a trigonometric double angle formula as follows:

$$I(V) = I\left(V_0 + \left.\frac{dI}{dV}\right|_{V_0} V_{ac}\cos(\omega t) + \frac{1}{4}\left.\frac{d^2I}{dV^2}\right|_{V_0} [V_{ac}^2\cos(2\omega t)] + \ldots\right) \tag{3}$$

Thus, by measuring the output of the system at the frequency ω as the DC bias is slowly swept, a signal that is directly proportional to dI/dV can be obtained, that is, the differential conductance. Moreover, by measuring the output at 2ω, it is possible to directly obtain the IETS spectrum.[401,410] So far, the AC modulation technique using a lock-in amplifier is very popular for the IETS measurement.[171,406]

To verify that the observed spectra are indeed valid IETS data, the line width broadening can be examined as a function of modulation voltage and temperature.[406,411] The full width at

DOI: 10.1021/acs.chemrev.5b00680
Chem. Rev. 2016, 116, 4318−4440

the half-maximum (fwhm) of the d^2I/dV^2 vibrational peak can be written as follows:

$$V = [(1.7V_m)^2 + (5.4kT/e)^2 + W^2]^2 \quad (4)$$

where V_m is the AC modulation voltage; k is the Boltzmann constant; T is the temperature; and W is the intrinsic line width, which can be determined from a fit to the modulation broadening data.[406] On the basis of this formula, it can be determined that the line width will increase as the temperature and the modulation voltage increase.

The IETS has been measured on different test platforms, and each platform demonstrates its own unique features and limitations. The first focused IETS experimental study on adsorbed molecules was performed on the basis of Al−Al_2O_3−Pb tunnel junctions.[405,410] The fabrication of this metal−insulator−adsorbate−metal tunnel junction is summarized elsewhere.[410] On the basis of this type of junction, the relationships between the IETS, IR, and Raman spectroscopies were revealed, noting that the IETS is a new vibrational spectroscopy complementary to the IR and Raman spectroscopies but governed by different selection rules that allow optically forbidden transitions to be easily observed.[410,412,413] However, the tunnel current was relatively small in this type of junctions due to the effects of the insulation layer, which decrease the sensitivity of the IETS. To overcome this problem, the IETS measurements were directly performed in the metal−molecule−metal junctions.[178,411,414] For example, Wang et al. reported the IETS measurements for metal−molecule−metal junctions fabricated using the nanopore strategy, in which the effects arising from the insulation layer were avoided.[411] However, the yield of forming the nanopore junctions was relatively low due to the penetration of metal atoms into the molecular layer, which may short the junctions. One of the most fruitful techniques for the IETS measurement arose from the pioneering work of Gregory, in which a metal junction between two crossed wires was delicately made, and the distance between the two wires could be adjusted via a deflecting Lorentz force.[415] One main feature of this crosswire platform is that the distance between the two wires is adjustable, and the filament can be completely avoided. Kushmerick et al. demonstrated that the reproducible molecular junctions could be formed using this method with a sufficient stability for clear IETS measurements and selection rule investigation.[178,308,309] Yoon et al. further demonstrated that the crossed nanowire molecular junction was a versatile and highly scalable device platform, which allowed a direct correlation between the junction conduction properties and the molecular structure using both the IETS and the SERS on the same junction.[306] However, in practice, it is not easy to obtain the IETS signal of exact single molecules due to the large surface area of the crossed wires. The first definite observation of the IETS for a single molecule was obtained in the STM platform.[316,326] In the STM implementation of the IETS, the junction was formed using a sharp metallic tip, a vacuum gap, and a surface with the adsorbed molecules. Using this STM-IETS approach, elegant imaging and vibrational spectroscopic studies on a single molecule can be performed simultaneously.[317,327] Another advantage of the STM-IETS method is that the changes in the conductance and the vibrational modes of a single molecule can be simultaneously recorded when the junction is stretched.[416] Despite this great achievement, the vibrational spectroscopy using STM has met challenge because extreme mechanical stability is needed to suspend the small changes in the tunneling currents. For example, the tunneling physics requires a tunneling gap stability of 0.01 Å to maintain a stable conductance within 2%, which is a difficult target for STM due to the piezo drift.[406] To obtain a reproducible IETS signal at the single-molecule level, the IETS of single molecules was performed in the molecular junctions fabricated by the electromigration method,[137,176,329] in which the mechanical stability was guaranteed by sacrificing the adjustable gap size. Recently, the IETS signals were obtained on the basis of the MCBJs by several groups,[330−332] in which both the mechanical stability and the adjustable gap size were available. However, it is impossible to obtain a photographic image via the MCBJ platform as compared to that achieved by STM. Therefore, each platform for the IETS has its own unique advantages and disadvantages, and several intrinsic and interesting molecular properties were revealed, as discussed in the next section.

It is relatively easy to obtain the IETS with certain molecular junctions. However, it is difficult to directly determine which vibrations occur in the IETS, that is, which part of the molecules primarily contributes to the IETS signal. One point of view is that the IETS signal originates mainly from the molecular parts closest to the electrodes.[309] To accurately investigate which vibrational modes are active in the IETS, Okabayashi et al. introduced the isotope labeling of alkanethiols with specifically synthesized isotopically substituted molecule.[315,333,334] They systematically deuterated different parts of the alkanethiol ($CD_3(CH_2)_7S$, $CH_3(CH_2)_6CD_2S$, and $CD_3(CD_2)_7S$). Subsequently, the IETS was systematically measured with these partially and fully deuterated self-assembled monolayers. It was revealed that the IETS weights of the peaks [F (ν(C−C)), K (CH_2 wagging), and L (CH_2 scissoring)] did not change appreciably with the deuteration of the CH_2 closest to the sulfur atom ($CH_3(CH_2)_6CD_2S$). Supported by the first principle calculations, they provided unambiguous assignments of the IETS peaks and demonstrated the minimal site-selectivity for the IETS measurement; that is, the terminal groups provided almost the same contribution to the IETS signals as the middle part of the molecules, thus providing new insights into the electron transport through molecules.[417]

It should be noted that the IETS features may be reversed; that is, the peaks could be transited to the dips within the same type of molecular junctions. The IETS measurement is extremely sensitive to the electrode−molecule coupling, and the IETS contribution to the current is strongly dependent on the transmission of the junction.[418] It is known that the transmission of the junction is influenced by the strength of the electrode−molecule coupling, which is dependent on both the tilted angle of the molecule and the binding site of the end group. In the low transmission regime, the possibility of inelastic charge transport can result in an enhanced probability of forward scattering, which leads to a positive contribution to the current. However, in the range of higher transmissions, the electron back scattering increases due to a momentum transfer to the excited mode, leading to a negative contribution to the current.[335,336] Hence, in the low conductance tunneling regime, the inelastic excitations appear as peaks in the IETS feature. Conversely, the excitation of the vibrational modes results in the dips in the IETS when the transmission exceeds the threshold transmission value. This varied IETS contribution to the current in the different conductance regimes (high or low conductance) was revealed by Kim et al.[419] In their experiments, the electrode−molecule coupling was changed

DOI: 10.1021/acs.chemrev.5b00680
Chem. Rev. 2016, 116, 4318−4440

by mechanically stretching or pushing the molecular junctions using a low-temperature MCBJ technique. By tuning the transmission probability via stretching the BDT molecular junctions, they observed reversed contributions of vibronic excitations on the charge transport, that is, an antisymmetry IETS feature in the low-conductance and high-conductance regimes.[419] This transition from a peak to a dip was also carefully observed in single octanedithiol molecular junctions by Hihath et al. using the STM technique.[420] Their experiments and analysis provided a considerably contribution to the development of the IETS measurement as well as the theory interpretation.

5.1.3. IETS Applications. An ongoing challenge for single-molecule electronics is to understand the molecular conformation and the local geometry at the molecule−surface interface. Typically, it is an extreme challenge to acquire such information inside the junction by most of the characterization techniques.[311] The IETS probes the electron−phonon interactions in the molecular junctions, which are in turn extremely sensitive to the changes in the molecular geometry and the molecular conformation. Therefore, the IETS can be a powerful tool for studying the molecular and metal contact geometries in molecular electronic devices,[206,421] such as the orientation of the adsorbed molecules[422,423] and the tilted angle at the interface.[411] By comparing the calculated spectra with the experimental results, the most likely conformations of the molecule under different experimental conditions can be successfully determined.[424] With the help of the theoretical calculations, it becomes possible to fully understand and assign the complicated experimental IETS and, more importantly, provide the structural information on molecular electronic devices.[404,425]

Single-molecule inelastic tunneling investigations not only provide the molecular structure as well the interfacial information but can also be used to generate real-space imaging of the molecular structure and the chemical bonding. Ho's group, who first performed the single-molecule IETS measurement,[406] recently demonstrated an approach based on the STM technique to image the skeletal structure and bonding in an adsorbed molecule using a single-molecule inelastic tunneling probe.[99] They constructed a novel inelastic tunneling probe based on STM to sense the local potential energy landscape of an adsorbed molecule with a carbon monoxide CO-terminated tip. As the CO-terminated tip scanned over the molecule during imaging, changes in the energy and intensity of the hindered translational vibration of CO were measured by inelastic electron tunneling spectroscopy (IETS). This low-energy CO vibration sensed the spatially varying potential energy landscape of the molecule and its surroundings. The capability of STM to image the molecular structure and chemical bonds broadens its previous applications to determine the electronic and vibrational properties of single molecules.

The switching mechanism in molecular junctions can be identified by the IETS. To date, various possible mechanisms for conductance switching behavior have been proposed, including oxidation/reduction of molecules,[426] rotation of functional groups,[427] interactions with neighbor molecules,[428] fluctuation of bonds,[429] and effects of molecule−metal hybridization.[430] However, the lack of a proper characterization tool to determine the exact structure of the molecular junctions makes it difficult to distinguish the different switching mechanisms. Fortunately, the IETS has proven to be extremely useful in distinguishing the mechanisms by comparing the theoretical and experimental IETS.[431−434] For example, Cao et al. conducted hybrid density functional theory calculations for the IETS of an oligoaniline dimer dithiolate junction. Both the conjugation changes and the oxidation effects on the IETS have been demonstrated. The comparison between the calculated IETS and the experimental spectra confirmed that the observed conductance switching was most likely induced by the conjugation change rather than the oxidation.[433] Hihath et al. observed that the conductance switching occurring in a single octanedithiol molecular junction was approximately a factor of 2.[420] More interestingly, it was determined that, although the general features of the IET spectrum in this junction were the same before and after switching, the energies of certain peaks for this single-molecule junction could be either blue- or red-shifted after the conductance change, thus implying a small reorganization of the entire junction structure.[420] This finding revealed that conductance switching could result from a change in geometry. The IETS was further used to reveal the detailed switching information under light irradiation. Azobenzene-derivative molecules can change their conformation due to a cis−trans transition when exposed to ultraviolet or visible light irradiation. Kim et al. demonstrated that the cis−trans isomers possessed unambiguously different IETS fingerprints, which enabled an alternative technique for identifying the state of the azobenzene-based molecular switches.[435] Additionally, the IETS was used to reveal the switching mechanism due to the effects of hydration on the molecular junctions. In a pioneering study, Long et al. used magnetically assembled microsphere junctions incorporating thiol monolayers to reveal the current change mechanism when the junction was exposed to air.[434] A prominent S−H stretching vibration mode was observed, and the Au−S mode was missing in the IETS after the device was exposed to air. These results indicate that upon exposure to air, the water molecules are rapidly associated with the electronegative thiolate moiety, thus disrupting the Au−S bond to the electrode and decreasing the current. These detrimental effects on molecular conduction revealed by the IETS are important for understanding the electron transport through gold−thiol molecular junctions once exposed to atmospheric conditions.

The IETS was further used to elucidate the transport mechanisms in the molecular junctions. Hihath et al. performed $I-V$ measurements as well as IETS measurements on the diode molecule.[436] They found that the current rectification occurred at relatively low biases, indicating a significant change in the elastic transport pathway. Interestingly, the peaks in the IETS were symmetric around the zero bias and depicted no significant changes in shape or intensity in the forward or reverse bias directions. This result indicated that despite the change in the elastic transmission probability, there is little impact on the inelastic pathway in a diode molecule. In another example, Tao et al. observed simultaneous changes in the conductance and vibrational modes of a single molecule as the junctions were stretched.[112,416] Using the STM technique, the vibrational modes in a single-molecule junction were measured, and the differential conductance was recorded as the strain in the junction was changed by separating the two electrodes. This unique approach allowed the changes in the conductance to be correlated with the changes in the configuration of a single-molecule junction. This approach opened a new door of better understanding of the relationship between the molecular conductance, electron−phonon interactions, and the configuration. This approach was later employed in the MCBJ experiments for revealing the molecule−electrode contact as

DOI: 10.1021/acs.chemrev.5b00680
Chem. Rev. 2016, 116, 4318−4440

Table 3. Type and Mechanisms of Conduction

conduction mechanism[446,447]	current density (J)	temperature dependence	voltage dependence
direct tunneling (low bias)	$J \approx V \exp(-)\frac{2d}{\hbar}\sqrt{2m\Phi}$	none	$J \approx V$
Fowler–Nordheim tunneling	$J \approx V^2 \exp\left(-\frac{4d\sqrt{2m}\,\Phi^{3/2}}{3q\hbar V}\right)$	none	$\ln\left(\frac{J}{V^2}\right) \approx \frac{1}{V}$
thermionic emission	$J \approx T^2 \exp\left(-\frac{\Phi - q\sqrt{qV/4\pi\varepsilon d}}{kT}\right)$	$\ln\left(\frac{J}{T^2}\right) \approx \frac{1}{T}$	$\ln(J) \approx V^{1/2}$
hopping conduction	$J \approx Vd \exp\left(-\frac{\Phi}{kT}\right)$	$\ln\left(\frac{J}{V}\right) \approx \frac{1}{T}$	$J \approx V$
space-charge-limited conduction	$J \approx V^2/d^3$	none	$J \approx V^n$

well as the information on the molecular conformation change.[435,437−439] A case in point is that the different behavior of the thiol-ended and amine-ended molecular junctions was systemically examined by Kim et al.[438] The vibrational modes ν(Au−S) and ν(Au−N) in the IETS while increasing the electrode separation were compared. The comparison indicated that the ν(Au−S) mode was extremely stable, and no significant changes in the vibrational energy were observed during the stretching of the Au−ODT−Au junction. Conversely, the energy of the ν(Au−N) mode in the Au−ODA−Au junction was red-shifted while increasing the electrode separation. This behavior was consistent with an increase in the Au−N bond length due to its weak bond strength going along with the reduction of the force constant. The IETS measurements provided unambiguous evidence that the Au−N bind was weaker than the Au−S bond. Combined with the conductance trace measurement during stretching (the conductance plateau of the thiol-ended octane junctions was significantly longer than that of the amine-ended octane junctions), it was demonstrated that for amine-ended molecular junctions, no atomic chains were pulled under stretching, whereas the Au electrodes were strongly deformed for the thiol-ended molecular junctions. By characterizing the molecular vibrational modes and the metal−phonon modes in alkanedithiol molecular junctions with mechanically controlled nanogaps and an electrode material variation strategy, Kim et al. further demonstrated that the effects of the contact geometry and the molecular conformation on the IETS could be distinguished.[164]

Using the IETS technique, the quantum interference as the electron transports through molecular junctions can be investigated.[440] In most theoretical studies, only the elastic contributions to the current are considered. For molecules with a destructive quantum interference, the elastic current is effectively blocked, leading to a suppressed level of the elastic current. This allows the inelastic contributions to the current carried by vibrations to become important. Lykkebo et al. calculated the IETS of cross-conjugated molecules, which exhibited a destructive quantum interference. They found that the inelastic contribution to the current was larger than that for molecules without interference, and the overall behavior of the molecule was dominated by the quantum interference feature.[440] Furthermore, they predicted that the overtone modes (several small peaks besides the typical vibration modes) should be present in the IETS of the cross-conjugated molecules, although the overtone modes were generally thought to not exist. They studied the origin of the overtones and revealed that the interference features in these molecules were the key ingredient.

Although the IETS technique possesses many merits and becomes a powerful method for characterizing molecular junctions, there are still several obstacles that limit its further applications. First, the IETS requires cryogenic temperatures (typically liquid He) for an experimental investigation to suppress the thermal effect, which is unavailable in most laboratories. Second, only certain specific vibrational modes can be detected in a given molecule, partly due to the low signal-to-noise ratio in the IETS measurements.[309,441] Additionally, certain modes arising from the backbone may be masked by modes arising from the large anchoring groups.[442] Third, the analysis of the IETS is not always unambiguous, especially for systems with a large number of nuclei and numerous bonds; that is, there are a large number of possible modes that can result in the peaks for molecules containing many atoms.[443] Finally, discrepancies and device-to-device variations may occur in the IETS data, which can originate from defects in the molecular junctions and other elements, such as insulating walls introduced during the device fabrication process and from the junction particular structure.[444]

5.2. Temperature-Length-Variable Transport Measurement

The temperature-length-variable transport measurement in molecular junctions, that is, performing the electrical measurement with a variable molecular length or under different temperatures, is a useful technique for revealing the transport mechanism as electrons transport through the molecular junctions.[392,445] The conduction mechanisms listed in Table 3 indicate their characteristic relationships between the current density (J), temperature, and voltage. On the basis of whether thermal activation is involved, the conduction mechanisms can generally be classified in two distinct categories: (1) direct tunneling or Fowler−Nordheim tunneling, which does not have temperature-dependent electrical behavior; and (2) thermionic or hopping conduction, in which the electrical responses are strongly dependent on the temperature.[446]

The tunneling mechanism is often refer as "non-resonant", in which the tunneling electron energies do not exactly match with the molecular orbital energies.[447] For the sufficiently short conjugated molecules, the electrons can pass through the molecular junctions via a tunneling process; that is, an electron crosses the molecular junctions in a single step without an appreciable residence time on the molecules. In this case, the junction resistance can increase exponentially with the molecular length as follows:[392]

$$R = R_0 \exp(\beta d) \quad (5)$$

DOI: 10.1021/acs.chemrev.5b00680
Chem. Rev. 2016, 116, 4318−4440

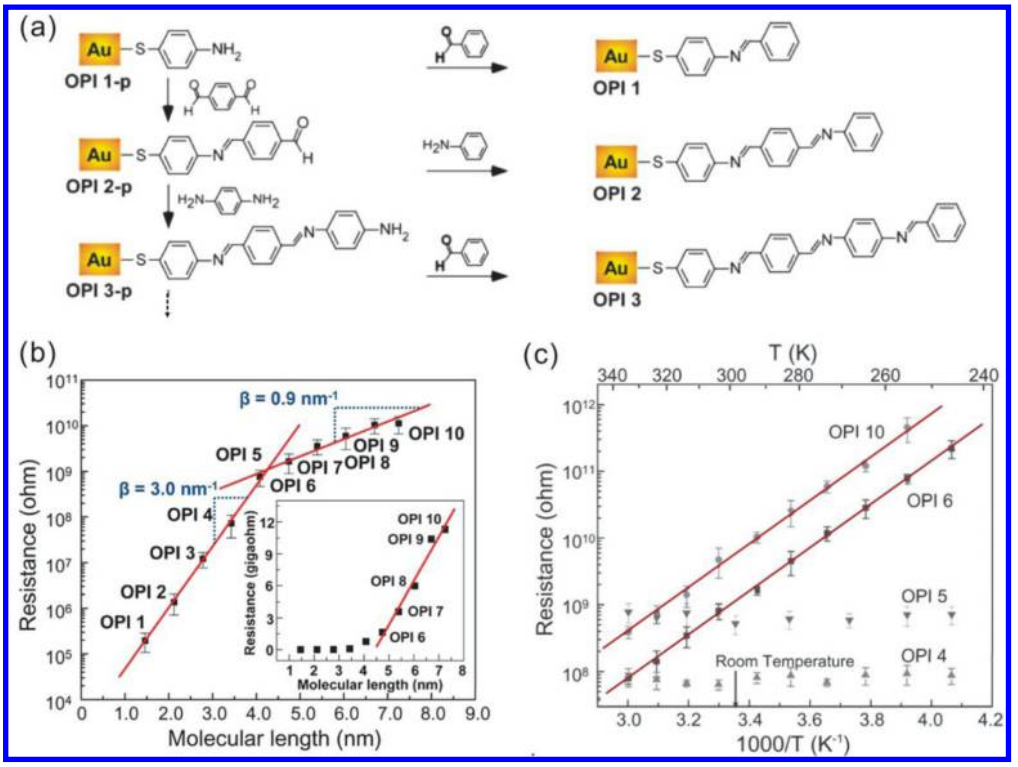

Figure 38. Measurements of the molecular wire resistance with CP-AFM. (a) Molecular structure and synthetic route to OPI-p and OPI monolayers on the gold substrates. (b) Semilog plots of R versus L for the gold/wire/gold junctions. Straight lines are linear fits based on eq 5. Inset: A linear plot of R versus L, demonstrating that the resistance is linearly dependent on the molecular length for long OPI wires. (c) Arrhenius plots for OPI 4, OPI 5, OPI 6, and OPI 10. Straight lines are linear fits to the data, demonstrating that the resistance is strongly dependent on temperature for long OPI wires. Reprinted with permission from ref 392. Copyright 2008 AAAS.

where R_0 is the effective contact resistance; d is the molecular length; and β is a structure-dependent tunneling attenuation factor depending on the effective tunneling barrier height. The tunneling barrier height is often approximated as the energy difference between the Fermi level of the electrodes (E_F) and the closest molecular frontier orbital (e.g., E_{HOMO} or E_{LUMO}).

Conversely, the hopping construction mechanism is a "resonant" process, in which charges can be injected into the frontier orbitals of the wired molecules and transported by an incoherent hopping mechanism. In other words, the electron first enters into the molecular orbitals from the source electrode and then drifts through a series of discrete steps to reach the drain electrode.[448] For longer conjugated molecular wires at moderate temperatures, the tunneling process is strongly suppressed, and the thermally activated hopping transport is often dominated.[449] The activation energy (E_a) corresponds to the energy required to reach the transition state for the electron transfer within the molecule. The resistance can be predicted to be linearly dependent on the molecular length as follows:[447]

$$R = R_0 + \alpha d = \alpha_\infty d \exp(-E_a/kT) \quad (6)$$

where R_0 is the contact resistance; d is the molecule length; k is the Boltzmann constant; and T is the temperature. In this equation, $\exp(-E_a/kT)$ can be regarded as a molecular specific parameter presenting a unit resistance per unit length. On the basis of eqs 5 and 6, the R versus d data can be used to determine the transport mechanism; that is, if the dependence on d is exponential, then the mechanism is likely tunneling, and if it is linear, then it is likely hopping. Additionally, the temperature dependence of R can be used to confirm the transport mechanism.

Frisbie et al. first provided direct evidence for a change in the transport mechanism from tunneling to hopping in oligophenyleneimine (OPI) molecular junctions.[392] They used a conducting AFM to contact the OPI molecular wires, which grew from a substrate-controlled aryl imine addition chemistry. It was demonstrated that near 4 nm in length, the mechanism of transport in the wires changed from tunneling to hopping, as evidenced by the striking changes in the length, temperature, and electric field dependence of the current−voltage (I−V) characteristics. As shown in Figure 38, the resistance was exponentially dependent on the molecular length ($\beta \approx 3.0$ nm^{-1}) for short molecular wires (OPI 1−4). However, there was a much flatter resistance versus molecular length relation ($\beta \approx 0.9$ nm^{-1}) for long molecule wires (OPI 5−10). Furthermore, from a plot of R versus d, as depicted in the inset of Figure 38b, it was determined that the resistance was linearly dependent on length for long wires, indicating a hopping transport mechanism. This change in the transport mechanism was confirmed by measuring the resistance versus temperature; that is, the resistance is independent of temperature for short wires and strongly affected by temperature for long wires.

Frisbie et al. further performed length-dependent conduction measurements and temperature-dependent conduction measurements for oligonaphthalenefluoreneimine (ONI) wires,[450] oligophenylenetriazole (OPT) wires,[451] and oligotetrathiafulvalene-pyromelliticdiimide-imine (OTPI) wires[452] to better understand the change in the transport mechanisms. They observed the transition from tunneling to hopping at approximately 4−5 nm for ONI, OPT, and OTPI, which was a distance similar to that of the OPI molecules.[450,451] Inspired

DOI: 10.1021/acs.chemrev.5b00680
Chem. Rev. 2016, 116, 4318−4440

by Frisbie and co-workers' research, the length-temperature-variable transport measurement has become a popular technique for distinguishing the transition of the transport mechanisms.[449,453−455] It should be noted that the critical point for the transport mechanism transition strongly depends on the molecular structure; for example, Tada et al. observed a transition in the direct current transport from tunneling to hopping at approximately 4.5 nm in single oligothiophene molecular wires.[448] Wang et al. revealed that a transition occurred at approximately 2.75 nm for the oligo(*p*-phenylene ethynylene) (OPE) molecular wires.[456] Wandlowski et al. determined that a transition from coherent transport via tunneling to a hopping mechanism occurs when the oligo(aryleneethynylene) (OAE) wires are longer than 3 nm.[454] Ferreira et al. examined the conductance of well-defined porphyrin self-assembled molecular wires up to 14 nm in length, thus determining a transition in the conduction regime at 6.5 nm.[457]

It should be mentioned that, although a pronounced temperature dependence and a small decay factor are commonly characteristics of hopping, it is reported that coherent tunneling can also lead to the apparent temperature dependence of the conductance in the case of resonance tunneling.[458] In far off-resonance, where the energy dependence of the transmission coefficient is not pronounced, the molecular conductance is nearly temperature-independent. However, in the case of resonant tunneling, the temperature dependence of the Fermi distribution function of the leads can lead to the conductance dependence on temperature.[458] On the basis of the electrical measurements of single-molecule junctions using STM, Nichols et al. presented that the conductance of oligoporphyrin wires as long as 5−10 nm had a strong dependence on the temperature and a weak dependence on the length of the wires. Although it is widely accepted that such behavior indicates a thermally assisted hopping mechanism, they successfully proved that the observed temperature and length dependences were consistent with coherent tunneling via the density functional theory calculations and an accompanying analytical model.[459]

The mechanism of rectification can also be clarified via temperature-length-variable transport measurements. For example, Nijhuis et al. examined the SAMs of alkanethiolates with ferrocene termini using liquid-metal top-electrodes and found that these junctions rectified currents with large rectification ratios.[248] One might assume that this observation was due to the space asymmetry of the junction. However, the temperature-variable transport measurements indicated that the values of the current density (J) were dependent on T at the negative biases but independent of T at the positive biases. This observation indicated that tunneling was the dominant mechanism of the charge transport at the positive biases whereas hopping was the dominant mechanism of the charge transport at the negative biases. A model was successfully developed to clarify the rectification mechanisms; that is, the rectification of the Fc-terminated SAMs was due to the charge transport processes that changed with the polarity of the bias: from tunneling (at positive biases) to hopping (at negative biases).[248] The rectification properties of the ferrocene-alkanethiolate SAMs were also investigated by Jeong et al. using a conductive polymer interlayer between the top electrode and the SAM.[288] Interestingly, it was found that the current density (J) was dependent on the temperature at both the positive and the negative biases. Particularly, a decrease in J as the temperature increased was observed at a high positive bias (V_g > 0.6 V), which was never observed at the negative bias. This unique feature could not be explained by the change in the transport mechanism (i.e., the change between tunneling and hopping). This observation was attributed to the redox-induced conformational changes in the ferrocene-alkanethiolates.[327]

In addition to tunneling and hopping, several classical mechanisms in the molecular junctions, including thermionic emission, field ionization (i.e., Fowler−Nordheim tunneling), and space-charge-limited conduction, were distinguished via temperature-length-variable transport measurements combined with the I/V measurements. Among these mechanism, the Fowler−Nordheim tunneling is independent of temperature and is predicted to yield a linear plot of $\ln(J/V^2)$ versus $1/V$, where V is the bias voltage. Yan et al. investigated the charge transport in molecular electronic junctions from 4.5 to 22 nm, one of the longest distances reported thus far.[460] They found that hopping is important for thicker films at low electric fields (low bias), whereas field ionization becomes dominant at high electric fields (high bias). This mechanism was consistent with the field-induced ionization of the molecular orbital or the interface states to generate charge carriers. Following the ionization, the empty state could be rapidly refilled from the biased electrode or reorganized to form a new conducting channel.

Generally, it is necessary to perform length-dependence, temperature-dependence, and I/V characteristics measurements to fully determine the transport mechanism.[445] If only length-dependence measurements can be performed, it is still useful for revealing the junction properties because the effective contact resistance R_0 and the tunneling attenuation factor β can be extrapolated from the plots of resistance versus molecular length. On the basis of the equation, $R = R_0 \exp(\beta d)$, the plots of log R versus d yield estimates of β from the slope and R_0 from the zero length intercept. A comparison of the R_0 values for different junctions will clearly indicate the relative roles of the contact resistance. Searching for a robust molecular wire that could transport a charge over a long distance (i.e., small β) became one of the major important goals of molecular electronics. Several innovative groups revealed numerous types of molecular wires among the smallest β values, which were able to transport the charge efficiently over long distances.[457,461−463] Frisbie et al. systemically investigated the effects of the linking groups and the metal work function to the factor β.[464] They determined that β was not simply characteristic of the molecular backbone but strongly affected by the number of chemical contacts, that is, thiol contact or dithiol contact; however, β was independent of the metal work function Φ because of the weak Fermi level pinning ($(E_F - E_{HOMO})$ varied only weakly with Φ).

5.3. Noise Spectroscopy

The noise measurements in mesoscopic tunneling junctions have been studied for a long time, for example, in semiconductor double barriers, quantum point contacts, and Coulomb blockaded Josephson junctions.[465] Recently, significant results obtained from the measurements in molecular tunneling junctions were reported.[165,393,466−468] Noise spectroscopy allows the special features of a single-molecule charge transport to be studied, which are not accessible by standard current−voltage measurements. In addition to the $I-V$ behavior, noise characteristics can provide useful fundamental

DOI: 10.1021/acs.chemrev.5b00680
Chem. Rev. 2016, 116, 4318−4440

information on molecular junctions, such as the local environment and metal−molecule interfaces of the molecule junctions,[140,393,469] electron−phonon interactions,[165,465,470] transmission probability of the conduction channel,[393,466,467] and stability of the junctions.[140,167] Understanding the conductance fluctuations and the corresponding noise characteristics is of great significance for developing molecular-scale devices because it influences the performance and the reliability of the devices, especially for molecular switches and memories. The mechanisms of noise generation can be distinguished by two different phenomena: whether the spectral density $S_{II}(f)$ depends on the frequency or not. There are two types of noises in which the spectral density is independent of the frequency. One is the thermal noise, also known as the Johnson−Nyquist noise, and the other is the shot noise. In contrast to these frequency-independent noises, the flick noise and the generation-recombination noise are frequency-dependent.

5.3.1. Thermal Noise and Shot Noise. Thermal noise is generated by the thermal agitation of the charge carriers (generally the electrons) inside an electrical conductor at equilibrium, which occurs regardless of any applied voltage. This noise results from fluctuations in the quantum occupation of the electronic states and, consequently, the temperature-dependent statistical distribution of the kinetic energy of the electrons. It leads to a variation in the current despite the mean value of the current being zero, that is, no current flow.[471] The thermal noise is also known as the Johnson−Nyquist noise and can be expressed as follows:[471] $S_{II}(f) = 4k_BT/R$, or $S_{II}(f) = 4k_BTG$, where k_B is the Boltzmann constant; T is the ambient temperature; R is the equivalent resistance; and G is the conductance.

In contrast to the thermal noise, the shot noise is the result of the current fluctuations induced by the discrete charges and is highly dependent on the correlations between the tunneling charges. The shot noise is due to the nonequilibrium electron distribution and occurs only when a net current flows a defined barrier (the current pass through the system fluctuates around the average value).[471] For $k_BT \ll$ eV, the shot noise power can be expressed as $S_{II}(f) = 2eIF$, where I is the average current; and F is the Fano factor, which characterizes the correlations of the tunneling charge.[393] The Fano factor can be extracted from the dependence of noise on the applied bias current based on this equation. For a system that has N conductance channels, each of which has a transmission probability (τ), F can be given by the equation as follows:[466]

$$F = \frac{\sum_{n=1}^{N} \tau_n(1 - \tau_n)}{\sum_{n=1}^{N} \tau_n} \tag{7}$$

Thus, the shot noise and the conductance measurements can be used to analytically determine the transmission probabilities for at least the two-channel case. In the case where one may have a single perfect transmitting channel ($\tau \approx 1$) for which the electrons are in a coherent state across the entire structure, the shot noise vanishes ($F = 0$). This result is possible when a mesoscopic system is comparable to a few typical lengths that determine the level of correlation between the electrons. Therefore, by measuring the level of the shot noise, one can gain insights into the mesoscopic electronic properties that are not accessible using standard conductance measurements.[466] In the absence of a correlation between the tunneling charges, the Fano factor would indicate a full shot noise (Poissonian shot noise), that is, $F = 1$. For a transmission probability between 0 (high-barrier tunneling junction) and 1 (perfect transmitting channel) ($0 < F < 1$), the noise level is determined by the partition noise: the degree of freedom for the electron to choose between being transmitted or reflected.[466] In the case of $F > 1$, the shot noise, also known as the super-Poissonian shot noise, is associated with a correlation between the tunneling charges resulting from the Coulomb repulsion and scattering.[393,472]

5.3.2. Generation-Recombination and Flicker Noise. The generation-recombination noise and the flicker noise are two typical noises that are frequency-dependent. To explain the frequency-dependent noise behavior, the Lorentz oscillator model can be used. Let us imagine that the fluctuations arise from the elementary processes, and each process has its own time-constant τ_0. A single process leads to an autocorrelation function proportional to e^{-t/τ_0}. Hence, the Fourier transform of its noise density spectroscopy represents a Lorentz curve and can be expressed as follows:

$$S_{II}(f) \propto \frac{1/\pi\tau_0}{4\pi f^2 + (1/\tau_0)^2} \tag{8}$$

$$\tau_0 = 1/2\pi f_0 \tag{9}$$

where f_0 is the characteristic frequency, which can be obtained from the inflection position of the noise spectra. Equations 8 and 9 depict the noise spectroscopy of a single fluctuator, $S_{II}(f) \propto f^{-2}$ in the case $f \gg f_0$. For a finite number of fluctuators, the time constant τ_0 will have a broadened distribution. For an adequate number of fluctuators, the summation will approximately lead to $S_{II}(f) \propto f^{-1}$.[471]

One example of a single Lorentz fluctuation is the generation-recombination noise, which typically appears in semiconducting materials. In the solid-state physics of semiconductors, the carrier generation and the recombination process, for example, the charge carrier transition between the impurity levels and the conduction band, leads to a random fluctuation of the mobile charge carrier (electrons and holes) number. Furthermore, the generation-recombination noise has been found in the metal−insulator−metal tunneling junction. For example, Rogers et al. studied the conductance fluctuation of metal−insulator−metal tunneling junctions with a small amplitude.[473] They found that the measured voltage noise spectrum could be resolved into a limited number of distinct Lorentzian conductance noise spectra. The generation-recombination noise was attributed to the filling and emptying processes of the localized electron states in the tunneling barrier. Changes in the occupation of such states resulted in the changes of the local tunneling barrier and thus the fluctuations in the conductance. In addition to the generation-recombination process, the trapping/detrapping processes in the molecular junctions as well as the molecular structural changes can also lead to a Lorentz fluctuation.[167,393]

Another frequency-dependent noise is the flicker noise, also known as the $1/f$ noise. In contrast to the frequency-independent noise, there is no global theory to describe the flicker noise, even though it occurs in all electronic devices, resistances, semiconductor devices, and molecular devices. There are several processes that may be responsible for this noise: generation-recombination processes, varying mobility of charge carriers, fluctuating impurities, movement of defects, and so on.[468,471] Although the source of the $1/f$ noise is a complicated issue, the $1/f$ noise has been widely used to

DOI: 10.1021/acs.chemrev.5b00680
Chem. Rev. 2016, 116, 4318−4440

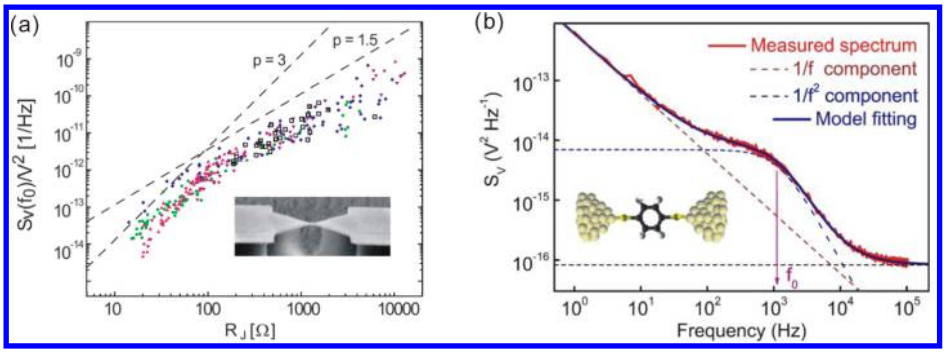

Figure 39. Noise feature for bare gold and molecule junction. (a) Magnitude of the $1/f$ noise as a function of the junction resistance R_J, shown as a log–log scattering plot of $S_V(f_0)/V^2$ for four MCBJ samples obtained in the process of stretching the samples. Here, f_0 = 100 kHz. An SEM image of the MCBJ sample was shown in the inseted figure. Dashed lines are guide lines for the expected power-law dependencies of $S_V(f_0)/V^2$ in the diffusive (p = 3) and ballistic transport regimes (p = 1.5). Reprinted with permission from ref 468. Copyright 2008 American Physical Society. (b) The voltage noise power spectral density of single BDT molecules, which bridge two gold electrodes, as depicted in the inseted figure. The solid red curve is the measured total noise density, and the solid blue curve is a fit to the experimental data, which takes $1/f$, $1/f^2$, and the thermal noise components into consideration. The noise components are depicted by the different colored dashed lines. Reprinted with permission from ref 475. Copyright 2015 American Institute of Physics.

characterize the electron transport properties,[165,393,468] which will be discussed later in detail.

5.3.3. Noise Spectroscopy Measurements. The noise signal characterization can be analyzed on the basis of the real-time current curves. However, this current temporal measurement only depicts limited time fragments. To understand the mechanism of the conductance fluctuation thoroughly, a statistical measurement is needed. Noise spectroscopy is a powerful tool that is used to investigate the statistical features of the current fluctuation. Using this method, each noise spectrum is automatically obtained by averaging hundreds of individual spectra with a spectrum analyzer. In any measurement of the electrical conductance, the current is not constant in time but exhibits fluctuations around a mean value. If we use the $K_I(t)$ to denote the autocorrelation function of the current, then $K_I(t) = \langle \Delta I(t')\Delta I(t' + t)\rangle$. Its Fourier transform is the spectral density $S_I(f)$: $S_I(f) = 2\int K_I(t)\ \exp(-i2\pi ft)\ dt$.

Generally, the shunt resistance R_S is inserted into the circuit for the current measurement, converting the current into a voltage signal. The voltage signal then is detected by a spectrum analyzer. The measured voltage fluctuations are accumulated and fast Fourier transformed by the spectrum analyzer, resulting in a voltage noise power spectrum $S_V(f)$ over the bandwidth of interest. This is also known as the spectral power distribution. The expected noise level is very small, especially at 4 K. To measure such small signals, a battery is used as the voltage source, and the signal is first amplified several times by two wide band preamplifiers. To suppress the noise of the preamplifiers, two sets of preamplifiers in parallel feed the signals into a spectrum analyzer. The spectrum analyzer can be operated in the cross spectrum mode and determines the Fourier transform of the cross-correlation signal from the two amplifiers.[468,474] The correlation techniques can eliminate the additional voltage noises originating from the two amplifiers. The detailed information concerning the measurement system of both the monolayer and the single-molecule junctions can be found elsewhere, which were reported by several research groups.[165,393,466−468]

5.3.4. Application of Noise Spectroscopy. Each type of noise spectroscopy, for example, flick noise, shot noise, and random noise, has been used to study the properties of bare metallic nanocontacts as well as molecular junctions.[467,468,475] Schönenberger et al. were the first to focus on the flick noise investigation of bare metallic nanocontacts at single atom level. Using electromigration and mechanically controllable break junctions, they measured the magnitude of the $1/f$ noise in tunable metallic nanoconstrictions. It was demonstrated that as a function of R, the normalized noise S_V/V^2 showed a pronounced crossover from $\propto R^3$ in low-ohmic junctions to $\propto R^{1.5}$ in high-ohmic junctions, as illustrated in Figure 39a,[468] where S_V is the voltage noise power spectral density, V is the applied voltage, and R is the resistance of the nanocontacts. The measured power changed from 3 to 1.5, indicating that the $1/f$ noise was generated in the bulk, and reflected the transition from diffusive to ballistic transport. According to Hooge's law, $S_V/V^2 \propto 1/N$, where N denotes the number of statistically independent fluctuators in the volume.[468] If a characteristic length of the junction is denoted by l, then the junction volume is $\sim l^3$. In a diffusive transport through a wire of length L and cross section A, the resistance R can be given by $R = \rho L/A$. Hence, $R \approx l^{-1}$. Because $S_V/V^2 \propto 1/N \approx l^{-3}$, it is reasonable to obtain $S_V/V^2 \propto R^3$. However, in the ballistic transport regime, where the characteristic length of the junction becomes shorter than that of the scattering mean-free path, the conductance is determined by the number of transport channels that are proportional to the junction area. So, $R \approx A^{-1} \approx l^{-2}$. Consequently, $S_V/V^2 \propto R^{1.5}$. Therefore, their research opened a window for the electron transport mechanism investigation using the $1/f$ noise characterization.

Shot noise measurements have proven to be a powerful method for evaluating the Fano factor as well as the number and transparency of channels for the charge transmission.[43] Van Ruitenbeek et al. first studied the shot noise in bare atom-size metallic contacts.[474] In their study, the MCBJ technique was used to obtain a stable point metallic contact at cryogenic temperatures. They were interested in the amount of noise above the thermal noise, which they called the excess noise. To measure the excess noise, white noise was sent from a calibration source through a 1 V series resistance to measure the frequency responses of the setup. After a concise data analysis, the excess noise was obtained. They demonstrated that they indeed achieved the shot noise by plotting the excess noise values as a function of the bias current.[474] By applying a fitting to this plot, a nearly linear dependence of the excess noise on

DOI: 10.1021/acs.chemrev.5b00680
Chem. Rev. 2016, 116, 4318−4440

the bias current was clearly observed, which agreed well with the shot noise feature, that is, $S_{II}(f) = 2eIF$. The Fano factor can be derived from the slope of the linear fitting curve. Interestingly, the smallest value of (0.02 ± 0.005) $2eI$ was observed for a contact with a conductance $\sim G_0$. This finding, $F \approx 0$, indicated that the conductance was due to the mostly fully transmitted modes ($T_n \approx 1$) based on eq 7. Furthermore, a small value of the Fano factor F was obtained for G near integer conductance values, which indicated the quantum suppression of the shot noise as $G = nG_0$. Similar experiments were also performed on aluminum, which indicated a much weaker suppression of the shot noise, revealing that the conductance at $G = G_0$ was not carried by a fully transmitted mode for the aluminum nano wire.[474]

Recently, Ruitenbeek et al. further used the shot noise to infer the transmission coefficients in the dominant channels of the carrier transport through single deuterium molecules.[466] The shot noise measurement process was optimized to remove the effects from other types of noises. Once a stable contact was identified, they first took a dI/dV curve using the lock-in technique. The zero-bias noise spectrum then was recorded, which showed the thermal (Johnson−Nyquist) noise. Subsequently, the total noise was measured at the finite biases, which consisted of a white shot noise, thermal noise, and $1/f$ noise (dominant at low frequencies). After dropping the $1/f$ noise, compensating for the roll-off, and subtracting the thermal noise for a series of bias currents on a given contact, the dependence of the excess noise was obtained as a function of the bias current. It was determined that the shot noise was strongly suppressed when the currents passed through the Pt−D2−Pt junctions; a similar phenomenon was presented in the bare gold junctions at $G = G_0$. Therefore, this study indicated that the transport in the Pt−D2−Pt bridges was carried dominantly by one nearly fully transparent channel.[466] Hence, these results, in return, verified that the junction was indeed formed by only a single molecule.

In contrast to the previous noise measurements at low temperatures, Natelson et al. presented the measurements of the shot noise in the Au break junctions acquired under room temperature and ambient conditions.[467,476] Using the MCBJ technique and a high-frequency technique, the noise data and the conductance histograms for the Au junctions were acquired simultaneously at room temperature. The measured shot noise showed a strong suppression at precisely the same conductance values as the peaks in the conductance histograms. This result demonstrated that the quantum suppression of the noise due to fully transmitting contacts survived even at room temperature. It should be noted that the inelastic processes were much stronger as compared to those at low-temperature experiments. One interpretation for this observation was provided: the inelastic processes can operate on length scales longer than the single nanometer junction size, and inelastic processes, such as electron−phonon scattering, can remove energy from the "hot" electron system and redistribute electrons between the different quantum channels, leading to the suppression of the shot noise at room temperature. Although their experiments were performed without molecules, these results indicated that the noise characterizations could be used as a tool to study the inelastic transport process in the molecular junctions.

Although the effects of the electron−vibration interactions in the atomic-scale junctions with a single conduction channel received considerable attention,[419,467,477,478] the more general case of junctions with several conduction channels has received very little attention. Recently, Ben-Zvi et al. studied the electron−vibration interaction in multichannel molecular junctions, that is, the benzene junctions and carbon dioxide junctions sandwiched by the Pt electrodes.[479] It is well-known that the activation of the electron−vibration interactions can either enhance or suppress the conductance. However, the relationship between the electron−vibration interaction contribution to the conductance and the transmission distribution in the conduction channel is unclear (e.g., the exact number of channels is unclear). Ben-Zvi et al. overcame the difficulties and extracted the transmission probabilities of the main conductor channels by the shot noise measurements.[479] They found (1) for all of the junctions that yielded the conductance suppression due to the vibration activation, one dominant channel (high transmission properties) was clearly observed; and (2) for those junctions that yielded conductance suppression, the conduction channels were more equally distributed; that is, all of the channels had transmission probabilities less than 0.5. The analysis of the vibration activation effects on the conductance in view of the distribution of conduction channels confirmed the theory that a high-conductance junction (with a dominant conduction channel) typically demonstrated conductance suppression due to the inelastic tunnel process.[479,480]

The theoretical shot noise studies in the molecular junctions also received extensive attention.[465,481,482] By combining the Monte Carlo methods with the Langevin approach, Koch et al. successfully calculated the shot noise of tunneling currents with a model: transport through the molecule was to be dominated by a single, spin degenerate electronic level in the presence of one vibrational mode with a frequency ω_0.[481] They reported that Franck−Condon physics, which is a characteristic of molecules, could lead to a low-bias current suppression (Franck−Condon blockade) and large Fano factors (10^2−10^3) in single-molecule devices, which originated from the coupling of the electronic and vibrational degrees of freedom. The Fano factor enhancement has been explained by the avalanche-like transport of electrons interrupted by long times without a charge transfer. One year later, Galperin et al. thoroughly investigated the inelastic tunneling effects on the noise properties of the molecular junctions.[465] The inelastic tunneling and its influence on the zero frequency noise based on a simple one-level molecular junction model were investigated, which arbitrarily selected one molecular orbital to support the resonance transmission beyond a certain voltage bias threshold. This molecular orbital was coupled to a local oscillator representing the molecular nuclear subsystem. By employing this one-level model within the nonequilibrium Green function (NEGF) methodology, they investigated inelastic effects on the noise spectrum in molecular junctions in both the weak and the strong electron phonon coupling regimes. In the weak coupling regime, it was found that the noise amplitude could increase or decrease due to an inelastic channel opening and based on the distance of the resonance as well as the junction asymmetry. Particularly, it was determined that the relative Fano factor decreased when the molecule was far from the resonance. Their calculation and analysis suggested the usefulness of the "noise spectroscopy" for measuring the values of the electron−vibration coupling on the bridging molecules.[465] Haupt et al. employed the extended NEGF technique to determine the cumulant generating function, from which the current I and the noise S can be easily calculated.[483] The key idea for this approach is to modify the Hamiltonian by adding a time-dependent phase to the tunneling matrix

DOI: 10.1021/acs.chemrev.5b00680
Chem. Rev. 2016, 116, 4318−4440

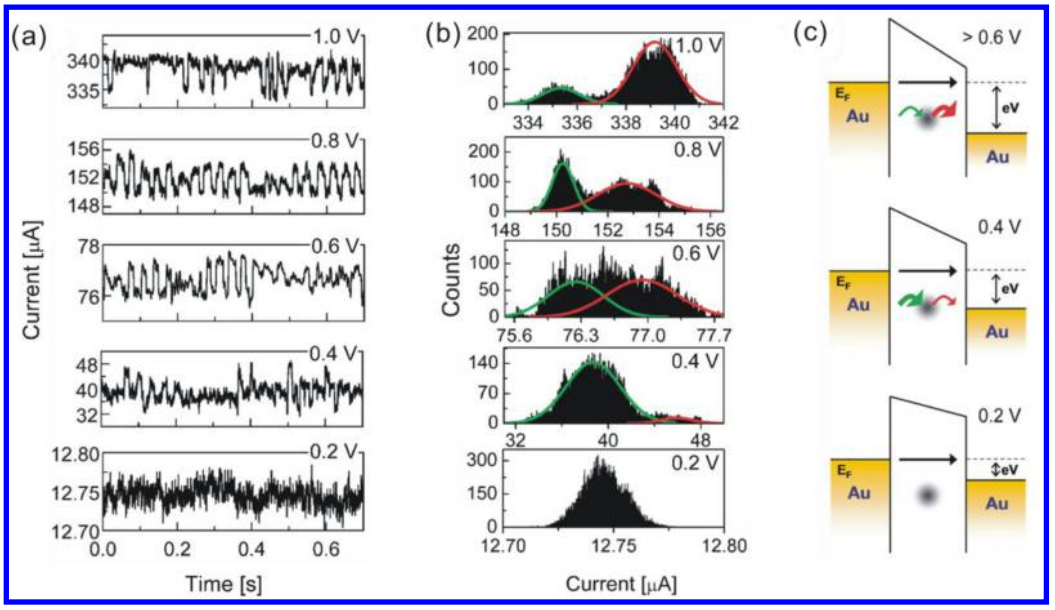

Figure 40. Random telegraph noise. (a) Time-dependent two-level random telegram noises of Au−HDT−Au junctions under different biases. The random telegram noise was recorded at room temperature for 0.7 s. (b) Corresponding current histograms for the random telegram noise. Two peaks in the histograms were observed when the applied bias was above 0.4 V. The histograms are fitted with the Gaussian peaks, where the green and red lines indicate the trapping and detrapping events, respectively. (c) Schematic trapping and detrapping processes in the molecular junction with a single localized trap. Reprinted with permission from ref 393. Copyright 2010 American Chemical Society.

elements. An analytical expression was successfully derived for the inelastic noise at an arbitrary temperature and distinguished the terms that corresponded to the simple renormalization of the transmission coefficients. By applying the theory to the experimentally relevant case of a deuterium molecular junction,[466] they predicted a significant positive contribution to the total noise due to the inelastic processes.[483] Kumar et al. further pointed out that the inelastic signal, that is, the signal due to the vibration excitations, could become negative as the transmission probability decreased below a certain transmission value.[470] They argued that the negative contribution to the noise arose from the coherent two-electron processes mediated by the electron−phonon scattering and the Pauli exclusion principle.[470] Let us assume that two electrons are injected from the left lead with a high energy E and a low energy $E - \hbar\omega_0$, respectively. If the higher energy electron emits a phonon, it would lose an energy $\hbar\omega_0$ and tend to occupy the same outgoing state as the low energy electron. This inelastic process tends to reduce the noise and make a negative contribution by narrowing the energy distribution of the outgoing electrons. However, this process would be blocked at the perfect transmission, that is, with a high transmission probability. Thus, the inelastic process can make either a positive or a negative contribution to the total noise. Therefore, the theatrical calculations performed by different groups indicate that the shot noise can be used as a powerful tool to address the particular characterization as the charges transport through the molecular junctions, which is unavailable using the $I-V$ characteristics.

Recently, several groups used random telegram noise to study the electron transport properties and the stability of the molecular junctions.[140,167,471,484] Kim et al. studied the noise characteristics of the charge transport through alkyl-based monolayer Au−molecule−Au junctions.[393] Specifically, the random telegraph noise (RTN) was examined. First, it was determined that all of the spectra followed a $1/f$ (at a low frequency regime) and a $1/f^2$ (at a high frequency regime) power law depending on the frequency. This result indicated a superposition of the $1/f$ and the generation-recombination noise (the Lorentzian distribution) in the measured spectroscopy. The Lorentzian distribution noise spectra may result from the trapping/detrapping processes of the charge carriers to/from the localized states in the molecular junctions. They pointed out that the localized states could be formed by defects that may unintentionally be introduced into the molecular layer in the junction fabrication process. To verify this trapping/detrapping interpretation, they further measured the time-dependent current fluctuations, referred to as the random telegraph noise as shown in Figure 40. In this figure, a discrete temporal fluctuation was observed under the different bias voltages. Interestingly, it was observed that the low current events prevailed at a low bias (below 0.6 V), which indicated that the trapping process resulting from the charging effect on a localized state occurred in the molecular barrier. Conversely, the high current events became predominant with an increasing bias (above 0.6 V), which agreed with the fact that a large potential difference could lead to the re-emission of the trapped charge carriers (detrapping process). Their study demonstrates that noise characterization is useful for evaluating the influences of the localized states on the charge transport in molecular or other electronic junctions.[393]

In contrast to the experiment mentioned above, several groups studied the telegram noise in single-molecule junctions under small bias voltages (below 0.2 V).[140,167,471,484] The total measured noise spectroscopy showed a transition from $S_V \propto f^{-1}$ at a low frequency to $S_V \propto f^{-2}$ at a high frequency by independent groups.[167,471,475,484] One noise spectroscopy for benzene−dithiol junctions is illustrated in Figure 40b. The total noise spectroscopy in this figure can be described as follows:

$$S_V(f) = \frac{A}{f} + \frac{B}{1 + (f/f_0)^2} + 4kTR \tag{10}$$

DOI: 10.1021/acs.chemrev.5b00680
Chem. Rev. 2016, 116, 4318−4440

were A and B represent the amplitudes of the $1/f$ and $1/f^2$ noise components, respectively; f_0 is the characteristic frequency, which can be derived from the inflection position of the total noise spectra; R is the junction resistance; and T is the ambient temperature. Equation 10 provides a good fit of the experimental data. The measured noise spectroscopy indicated that the telegram-like noise still existed in this single-molecule junction, which was later confirmed by the real-time dependent conductance measurements.[475,484] It should be noted that such a small bias voltage (below 0.2 V) is not enough to cause both the trapping and the detrapping events. Additionally, single-molecule junctions contain much less defects (e.g., particles and impurities) as compared to monolayer junctions. So, where does the telegram-like noise come from? In the case of single-molecule junctions, the stability of the junction becomes a dominant factor, which strongly affects the current characterization. Thereby, the stability should be considered for the interpretation of the telegram-like noise. To explain the telegram-like fluctuations in view of the junction stability, several mechanisms have been proposed and can be primarily classified into three groups: (1) dynamic reconfigurations of the molecular backbone structure;[167,471,485] (2) movement of the surface metal atoms tethered to the molecules;[140,486] and (3) bond breakage and reconnection for the metal−molecule contacts.[429] The reconfiguration changes can occur without the complete bond breakage and involve the near-configuration states with similar electric properties, leading to a small amplitude telegram-like current fluctuation. A direct evidence supporting this mechanism is that the telegram-like current fluctuation was enhanced as the pass current increased.[140] If the telegram noise originates from the current induced by the dynamic reconfigurations of the molecules, then an enhanced telegram fluctuation was expected as the current increased. Please note, the local junction temperature also increased as the pass current increased, promoting the movement of the metal atoms tethered to the molecule. Hence, the telegram-like noise may originate from the atom moving at the electrode surface, especially for those junctions with a fresh electrode surface after physical breakage. One clear evidence of this type of interpretation is that the telegram-like fluctuation was suppressed in a densely molecular packed environment.[140] Thus, the telegraph-like current fluctuation in fresh molecular junctions is more likely associated with the rearrangement of the metal atoms tethered with a molecule. In contrast to the small amplitude current fluctuation discussed above, Brunner et al. observed a larger fluctuation in the solution environment, which was reasonably attributed to the formation and the thermally driven breakage of bonds between a molecule and a metal electrode.[484]

The noise analyses can provide valuable insights into single-molecule science but are not limited to electron transport properties and junction stability. Tsutsui et al. extended the application of the current noise to identify single-molecule junctions.[166] They found stepwise increases in the current oscillation amplitudes at distinct voltages, synchronous to the voltages in which the vibration modes were activated due to the inelastic tunneling. The specific change in the noise amplitudes was attributed to the electron−vibration interaction. The vibration interactions in the molecular junctions are known to cause local heating and increase the junction temperature above the bath temperature, which may lead to an increase in the noise amplitude, as noted by the authors. These results suggest that the field-induced current noise can be used as a complementary tool for the IETS in single-molecule identification.[166] Noise spectroscopy can also be extended to study biomolecules; for instance, several groups used random telegraph noises for sequencing biomolecules such as DNA and amino acids.[487,488] They demonstrated that single amino acids could be identified using electron tunneling currents measured as individual molecules passing through a nanoscale gap between the electrodes.

5.4. Transition Voltage Spectroscopy

Measuring the energy level alignment in the molecular junctions, especially the position of frontier molecular levels with respect to the Fermi levels (E_F) of the electrodes, is of crucial importance to study the mechanisms of the charge transport and realize the functions of the molecular junctions. One approach to obtain the molecular energy level alignments of the molecular junctions is to measure the peak position in the dI/dV curve, which requires the use of a bias voltage that forces the E_F of the electrodes to reach the position of the molecular levels where the electrons can resonantly transport. However, in most cases, such as alkane-based molecular junctions, a high applied voltage leads to a high electronic field, which could break the junctions before the dI/dV peak is reached. On the basis of the mechanism of the field emission, Beebe et al. found that the position of the nearest molecular energy level with respect to the E_F of the electrodes in the molecular junctions can be determined from the current−voltage ($I-V$) measurements, also known as "transition voltage spectroscopy" (TVS).[394] With this TVS technique, an inflection point (V_{trans}) can be obtained, which is equal to the effective barrier height (Φ) and corresponds to the energy offset between the E_F of the electrode and the closest frontier molecular orbital, either HOMO or LUMO.

To demonstrate the effectiveness of the TVS, Beebe et al. simplified the molecular charge transport as electron tunneling through a rectangular barrier using the Simmons model (Figure 41a).[394] In the zero-bias limit, for electron tunneling through the rectangular barrier, the relationship between the current and the voltage can be described as follows:

$$I \propto V \exp\left[-\frac{2d\sqrt{m_e \Phi}}{\hbar}\right] \tag{11}$$

where m_e is the electron effective mass; and d is the width of the barrier, which is typically equal to the length of the connected molecules. Therefore, $\ln(I/V^2)$ is proportional to $\ln(1/V)$. At the opposite limit, for the applied bias voltage exceeding the barrier height, the tunneling barrier changes from trapezoidal to triangular, and the $I-V$ dependence can be described as follows:

$$I \propto V^2 \exp\left[-\frac{4d\sqrt{2m_e \Phi^3}}{3\hbar q V}\right] \tag{12}$$

where q is the electronic charge. From the above equation, it can be deduced that $\ln(I/V^2)$ against $1/V$ has a linear relationship in the high-voltage regime with the triangular barrier. Therefore, electron tunneling through the triangular barrier has the characteristics of Fowler−Nordheim (F−N) tunneling or field emission. From the plot of $\ln(I/V^2)$ versus $1/V$ (the F−N curve), a well-defined minimum voltage point, that is, an inflection point (V_{trans}), can be obtained, which results from the fact that the mechanism of the charge transport

DOI: 10.1021/acs.chemrev.5b00680
Chem. Rev. 2016, 116, 4318−4440

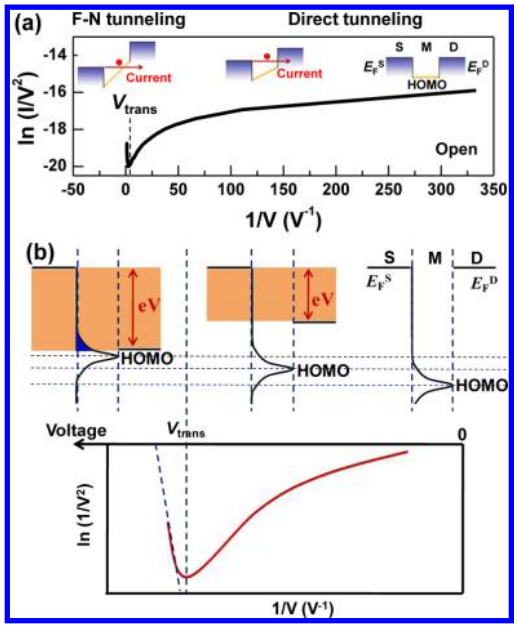

Figure 41. Schematic models for qualitatively explaining the transition of the F−N plots. (a) An F−N plot for a typical molecular junction. The insets depict the Simmons tunneling barrier model to explain the inflection of the F−N curve. (b) The corresponding resonant model for explaining the inflection of the F−N curve. Reproduced with permission from ref 490. Copyright 2013 Wiley-VCH Verlag GmbH & Co. KGaA.

transits from direct tunneling with a trapezoidal barrier to F−N tunneling with a triangular barrier. This fact demonstrates that the value of V_{trans} is equal to the barrier height (Φ) and the energy offset between E_F and the closest molecular energy level. For a hole-dominated molecular transport, the nearest molecular energy level is the HOMO of the molecules, that is, $\Phi = E_F - E_{HOMO}$, whereas for LUMO-dominated electron transport, $\Phi = E_{LUMO} - E_F$.

Remarkably, by measuring the Au−molecule−Au junctions formed from the π-conjugated thiols, Beebe et al. discovered that V_{trans} changed linearly with the energy offset between the E_F of the Au electrodes and the HOMO, which was determined using ultraviolet photoelectron spectroscopy.[394] Additionally, for a series of alkanethiol-based junctions with various molecular lengths, it was determined that V_{trans} was constant across the alkane series, which was consistent with the fact that the HOMO−LUMO energy alignment of these molecules is independent of the molecular length.[489] All of these important observations demonstrate that the TVS can be used as a promising technique to determine the energy level of the dominant charge transport orbital in a given molecular junction.

However, due to the simplicity of the Simmons model, the presented experimental data were far from being fully understood. To improve the understanding, Huisman et al.[491] introduced a coherent resonant molecular transport model. In this model, the molecular levels are Lorentz-broadened by coupling with the electrodes at both electrode−molecule interfaces, thus leading to a better consistency with the experiments. Furthermore, on the basis of the resonant tunneling model, Araidai et al.[492] theoretically calculated the transition behavior of the F−N curve using the transmission function of the resonant peaks, where either the Lorentzian or the Gaussian functions were used to describe the shape of the resonant peaks. By analyzing the relationship between the behavior of the F−N plot and the transmission function, the inflection (V_{trans}) in the F−N curve occurs when the resonant peak responsible for the charge carrier transport has a certain amount of its tail entering the bias window (Figure 41b). Because the resonant peak typically corresponds to the nearest molecular energy level of the molecular junctions, the V_{trans} in the F−N curve is proportional to the energy offset between E_F and the closest molecular orbital.

Because the $I-V$ curves for the charge transport in the molecular junctions can be approximated to a generic parabolic shape for either the resonant or the off-resonant tunneling, Vilan et al.[493] studied the TVS using a Taylor expansion view (TyEx). Other than the original view of the TVS, where the TVS indicates the tunneling transition between the different charge transport regimes, the interpretation of the TVS in the TyEx view is established as a genuine characteristic over the full bias range of the charge tunneling. In this TyEx view, V_{trans} is closely related to a bias-dependent perturbation of V_0, a bias scaling factor, which can be deduced from the third coefficient of the TyEx expression of the conductance. In other words, the TVS reflects the conductance nonlinearity of the junctions, which partially originates from the energy level alignment. During resonant tunneling, V_0 is proportional to the height of the tunneling barrier in most metal−molecule−metal junctions, whereas for off-resonant or deep tunneling, V_0 is proportion to the ratio between the barrier height and the barrier width. For a specific case, a highly nonlinear charge transport and nonphysical TVS values could be observed in the semiconducting electrode-based molecular junctions due to the small bias-dependent density of the states for the semiconducting electrode. Therefore, the TVS measurements for when the current becomes "superquadratic" with the bias voltage is a promising tool for studying the respective energy level alignment in most molecular junctions.

5.4.1. Applications of TVS. Because the asymmetry of the molecular junctions has a significant effect on the inflection behavior of the F−N plot, the TVS has been used to investigate the asymmetry and the energy level alignment of several asymmetric molecular junctions. Intuitively, the asymmetric voltage drops on both sides of the metal−molecule interfaces will lead to different barrier heights for carrier tunneling. Correspondingly, the polarity-dependent different values of V_{trans} can be observed to confirm the asymmetric interfacial contacts in the molecular junctions.[394] This polarity-dependent V_{trans} was also confirmed by Bâldea et al., who calculated the ambipolar TVS using asymmetric molecule−electrode couplings.[494] Furthermore, on the basis of extensive ab initio calculations using an analytical model of a Lorentzian-shaped transmission function, Chen et al.[495] found that asymmetry coupling at the two molecule−electrode interfaces had a significant effect on the ratio between V_{trans} and the energy offset of the nearest molecular orbital (ε_0) to E_F. The ratio $|\varepsilon_0 - E_F|/V_{trans}$ increased from 0.86 for a symmetric junction to 2.0 for a completely asymmetric junction. On the basis of experimental investigations of the asymmetric coupling effect of the molecule junctions using the TVS, Wang et al.[496] observed a similar tendency: by increasing the asymmetric coupling degree, the energy offset ($|\varepsilon_0 - E_F|$) was decreased, and V_{trans} became smaller.

The length of the molecules has a clear effect on the energy level alignment and the charge transport process in the molecular junctions. Using the TVS, the length-dependent

DOI: 10.1021/acs.chemrev.5b00680
Chem. Rev. 2016, 116, 4318−4440

properties of the molecular junctions with conjugated and nonconjugated molecules have been widely studied. For most molecular junctions formed from conjugated molecules, where the voltage drop is expected to span the entire molecule, the ratio between V_{trans} and the frontier conducting orbital with respect to E_F is approximately constant.[489] For example, in HOMO-dominated molecular junctions with aromatic series, V_{trans} decreased with an increase in the molecular lengths because the conjugating effect and the coupling effect lifted the HOMO level of the molecules with an increased length.[497] However, for molecular junctions with nonconjugated alkyl molecules, V_{trans} is relatively length-independent. This result is partially due to the unchanged molecular energy level for the alkyl molecules with different molecular lengths.[498] Furthermore, for nonconjugated systems, the frontier orbitals are expected to be strongly localized at the end groups of the molecules, which leads to a voltage drop at the interfaces and thus the length-independent V_{trans}.[499] Additionally, it was determined that the voltage drop in the molecular junctions was affected by the temperature.[500] Using the TVS investigations of 2-[4-(2-mercaptoethyl)-phenyl] ethanethiol (MePET)-based molecular junctions with either Au or Al electrodes, the voltage drop at low temperatures occurred at the contact interfaces using the injection barrier dominated transport, whereas at high temperatures, the voltage drop occurred along the entire molecule using the molecular barrier dominated transport. Because V_{trans} in the TVS is deduced from the tunneling model, when the connected molecules are long enough for transferring the charge transport from tunneling to hopping, the inflection behavior of the F−N plot changes.[450] For the conjugated junctions with a hopping transport, it was determined that the F−N plot had three distinct transport regimes, corresponding to ohmic conduction, field emission, and a space charge-limited conduction regime between them.

The electrode properties, especially the contact interfaces, generally affect the charge transport in the molecular junctions. The TVS is widely used to study the interface-related properties of the molecular junctions. For molecular junctions with various electrodes having different work functions, such as Ag, Au, and Pt, it was determined that for HOMO-dominated molecular junctions with thiol linkages, V_{trans} decreased with an increase in the work functions of the electrodes. However, for LUMO-dominated molecular junctions with isocyanide linkages, V_{trans} changed in the opposite direction, which corresponded to the energy offset between the dominated molecular orbital and the electrode E_F.[464,489] Furthermore, it was determined that the degree of V_{trans} variation is considerably slower than that of the changes of the work functions. This result can be ascribed to the specific bonding site for the S atom end group in different electrodes, where S atoms are most likely bound to the hollow-bridge site of the Ag/Au surface and the adatom site of the Pt electrode.[501] For nonmetal electrodes, such as carbon nanotubes, theoretical calculations demonstrated that V_{trans} corresponds to the voltages that exhibit a negative differential resistance (NDR), which only occur during the coherent transport in molecular junctions when the tail of the resonant peak comes into the bias window.[502] For a fixed molecular junction, the fluctuations of the Coulomb interaction at the contacts have a minimal effect on V_{trans}.[503] However, from the statistical TVS studies of the alkanedithiol- and biphenyldithiol-based single-molecule junctions, Guo et al.[504] determined that the molecule−electrode contact geometry had a slight effect on V_{trans} because different V_{trans} values were obtained for molecular junctions with different conductance values. Furthermore, from individual thiol-tethered porphyrin molecular junctions with Au electrodes, Bennett et al.[505] determined a multipeaked distribution of the V_{trans} values, which is due to the existence of a small number of distinct configurations at the interfacial contacts. For molecular junctions made from the tip−substrate technique, the distance between the molecule and the electrodes at the interfacial contacts was determined to have an effect on V_{trans}, which is because different molecular orbitals participate in the charge transport with varying distances.[506] Additionally, the chemical states of the electrodes in the molecular junction can be monitored using the TVS. For example, for molecular junctions made from Hg, GaIn, or Si electrodes, the oxidization of the electrode surface was observed at a lower value of V_{trans} for the junctions.[507] Although the contact geometry, molecular conformation, and the electrode local density of states have apparent effects on V_{trans}, the fluctuations of V_{trans} are extremely small in most cases, which distinguishes the TVS as an effective tool for studying the charge transport in molecular junctions.[508]

Because the TVS is able to qualitatively measure the energy offset between the nearest molecular energy level and E_F, it was used to monitor the gating effect for the molecular junctions. One good example is that by using single-molecule transistors with ∼3 nm thick Al_2O_3 films as a back gate dielectric layer, Song et al.[171] used the TVS to quantitatively monitor the energy level shift process of the molecular orbital gating. For both the Au-1,8-octanedithiol (ODT)-Au and the Au-1,4-benzenedithiol (BDT)-Au junctions, the value of V_{trans} was observed to shift toward the lower bias with an increasingly negative applied gate voltage (V_G). This effectiveness of the molecular orbital gating can be estimated using $\alpha = \Delta V_{trans}/\Delta V_G$ as the gate efficiency factor. The positive large values of α = +0.25 for the ODT junctions and α = +0.22 for the BDT junctions indicated a strong gate coupling efficiency for the HOMO-mediated charge transport. For the Au−benzodifuran (BDF)−Au junctions with similar gate structure, Xiang et al.[509] determined that the gate efficiency factor is as small as ∼0.035, again proving the effectiveness of the TVS. In addition to electrostatic gating, the chemical gating effect in the molecular junctions can be analyzed using the TVS. With different substituents attached to the pyridinoparacyclophane (PC) moiety as the edge-on chemical gate, the energy offsets obtained from the statistical V_{trans} indicated that the orbital energy level could be tuned by changing the attached gating substituents from strong electron acceptors to strong electron donors.[510] In graphene−molecule junctions with photochromic diarylethene derivatives as the key elements, Jia et al.[490] demonstrated a photogated transition (V_{trans}) using TVS measurements, which originated from the optically controlled open/closed isomerization as well as the distinct electronic structures of the functional diarylethene center.

Last, the TVS is a potential tool for distinguishing molecular junctions from vacuum tunneling junctions. For example, Trouwborst et al.[511] measured the TVS of Au−vacuum−Au junctions, where voltages up to 3 V were applied over small vacuum gaps of clean electrodes at cryogenic temperatures. They determined that V_{trans} was sensitive to the local configuration of the Au electrodes, which can be ascribed to the local density of states (LDOS) of Au. Furthermore, V_{trans} decreased with an increase in the tunneling distance. A similar relation between V_{trans} and the vacuum gap width was also found in the W−vacuum−Au junctions and the W−vacuum−

DOI: 10.1021/acs.chemrev.5b00680
Chem. Rev. 2016, 116, 4318−4440

Pt junctions at room temperature, where V_{trans} decreased linearly with an increase of the gap width.[512] However, this relation between V_{trans} and the gap width is considerably weaker than the prediction from standard vacuum tunneling models, which is partially due to the image charge effect. Because this variation of V_{trans} with the gap width is comparable to that in molecular junctions, it is difficult to use only this distance-dependent relation to differentiate the molecular junctions from the vacuum junctions. In certain cases, the absolute values of V_{trans} for vacuum junctions could reach >1.4 V, which is significantly larger than that of the molecular junctions, particularly those formed from conjugated molecules. For the origin of V_{trans} in the vacuum junctions, using the theoretical calculation, Bâldea et al. proposed that it may be due to the electron states (or resonances) at the surface of the electrodes.[513] This result has been proven by Wu et al.,[501,514] who used metal−vacuum−metal junctions with atomically sharp electrodes to determine that V_{trans} was determined by the LDOS resulting from the 6p atomic orbitals of the apex metal atoms. A higher energy position of the metal 6p atomic orbitals led to a larger V_{trans} value of the metal−vacuum−metal junctions.

5.5. Thermoelectricity

The thermoelectricity of the molecular junctions, which measures the induced voltage drop or the induced current across the junctions between two electrodes with a temperature difference, is important to understand the basic scientific mechanism of the thermoelectronic effect at the single-molecule level and improve the technologies for converting wasted heat into useful electrical energy.[39] Furthermore, thermoelectronic characterizations, especially the Seebeck coefficient ($S_{junction} = \Delta V/\Delta T$), of the molecular junctions can determine the type of charge carriers (either p- or n-type) and the relative energy position of the Fermi level of the electrodes with respect to the HOMO or LUMO levels of the connected molecules.[27] In the off-resonance limit, the $S_{junction}$ of the molecular junctions at zero applied voltage can be related to the transmission function ($T(E)$) at the Fermi level using the Landauer formula as follows:

$$S(E_F) = -\frac{\pi^2 k_B^2 T}{3e} \frac{\partial \ln(T(E))}{\partial E}\bigg|_{E=E_F} \quad (13)$$

where k_B is the Boltzmann constant; e is the charge of the electron; T is the average temperature of the junctions; and E_F is the Fermi level. In other words, the $S_{junction}$ is related to the slope of $T(E)$ at the Fermi level of the systems. With the Fermi level in the middle of the HOMO and LUMO levels in most molecular junctions (Figure 42), when the HOMO level is closer to E_F for a p-type transport, a negative slope of the $T(E)$ and a positive value of $S_{junction}$ are obtained. However, for an n-type transport with a LUMO level closer to E_F, a positive slope of the $T(E)$ and a negative value of $S_{junction}$ are achieved. Therefore, using the $S_{junction}$ value, the type of charge carriers and the relative position between E_F and the HOMO or LUMO levels can be determined using the thermoelectronic investigations of the molecular junctions.

On the basis of the Landauer formula of the $S_{junction}$, it is reasonable to conclude that the slope of the transmission function ($T(E)$) determines the thermoelectronic characteristics of the molecular junctions. When the transmission function is simplified to a single Lorentzian shape peak form, $T(E)$ can be written as follows:

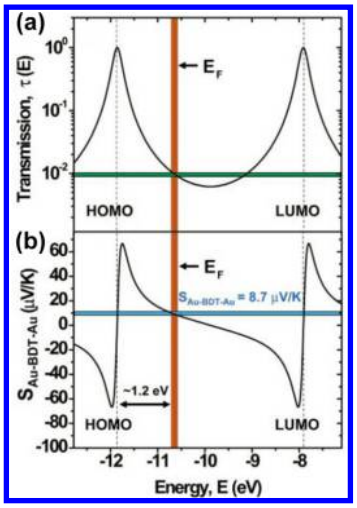

Figure 42. Theory of thermoelectricity in representative Au−1,4-benzenedithiol (BDT)−Au molecular junctions. (a) Theoretical prediction of the transmission function of a Au−BDT−Au junction plotted as a function of the position of the Fermi level of the Au electrodes with respect to the HOMO and LUMO levels. (b) Predicted Seebeck coefficient of the Au−BDT−Au junction plotted as a function of the position of the Fermi level with respect to the HOMO and LUMO levels. Reproduced with permission from ref 27. Copyright 2007 AAAS.

$$T(E) = \sum_{i=1}^{N} \frac{4\Gamma_{i,L}\Gamma_{i,R}}{(\Gamma_{i,L} + \Gamma_{i,R})^2 + 4(E - E_i)^2} \quad (14)$$

where i indicates the molecular orbital (HOMO or LUMO); E_i is the molecular energy level from E_F; and $\Gamma_{i,L}$ and $\Gamma_{i,R}$ are the broadening of the ith orbitals due to the coupling with the left and right electrodes, respectively. In other words, in addition to the relative energy position between E_F and the ith orbitals, the broadening of the molecular orbitals can also be investigated using the thermoelectronic measurements of the molecular junctions. Thus far, the experimental characterization of thermoelectricity for molecular junctions is limited. However, a few key results have emerged, such as the Seebeck coefficient determination and its modulation, thus offering a promising research branch of molecular electronics. Detailed information and discussions are provided in section 7.5.

5.6. Optical and Optoelectronic Spectroscopy

Electronic characterization methods, such as the $I-V$ curve and the TVS, are critical for analyzing the device behavior but do not provide direct information on the molecular energy and structure. To obtain more detailed information on the molecular structure, location of the relevant molecular orbitals, density of the adsorbed molecules, and thickness of the monolayer, numerous optical spectroscopic tools have been applied. When these approaches are combined with the photoelectron spectroscopic methods, correlations between the chemical features and the electronic performance can be assessed. Photoelectron spectroscopies have a high surface sensitivity, which makes them attractive for characterizing thin molecular layers as well as single-molecule junctions.[515] Furthermore, there are various operation modes that can provide useful information on different aspects of a molecular device.[516]

5.6.1. Raman Spectroscopy. Raman spectroscopy (named after one of its discoverers, the Indian scientist Sir C. V. Raman,

DOI: 10.1021/acs.chemrev.5b00680
Chem. Rev. 2016, 116, 4318−4440

who received the Nobel Prize in 1930) is a spectroscopic technique used to observe vibrational, rotational, and other low-frequency modes in a system.[517] Raman spectroscopy is now commonly used in chemistry to provide fingerprint information by which molecules can be identified and quantitatively analyzed.[517] The technique involves shining a monochromatic light source (such as laser light) on a sample and detecting the scattered light. The majority of the scattered light is of the same frequency as the excitation source, which is known as Rayleigh or elastic scattering. A very small amount of the scattered light is shifted up or down in energy from the incident laser due to interactions between the incident electromagnetic waves and the vibrational energy levels of the molecules in the sample. For a spontaneous Raman effect, a photon excites the molecule from an original vibrational energy state to a virtual energy state for a short period of time, and then the molecule returns to a new vibrational energy state accompanied by a photon emission process. The difference in the energy between the original rovibronic state and this resulting rovibronic state leads to a shift in the emitted photon's frequency away from the incident laser wavelength. Plotting the intensity of this shifted light versus frequency results in a Raman spectrum of the sample. The energy shift and the corresponding wavenumber shift provide information on the vibrational modes in the system.

Raman scattering is an example of inelastic scattering because of the energy and momentum transfer between the photons and the molecules during the interaction, and it should not be confused with emission (such as fluorescence), where a molecule in an excited electronic state instead of a virtual energy state emits a photon of energy and returns to a ground electronic state.[518] The intensity of the Raman scattering is proportional to the electric dipole−electric dipole polarizability derivative, which differs from infrared spectroscopy, where the interaction between the molecule and the light is determined by the electric dipole moment derivative; thus, this contrasting feature allows one to analyze vibrational modes that might not be IR active via Raman spectroscopy.[519]

Currently, the Raman spectroscopy is extensively used to identify unknown molecules, especially biomolecules,[520,521] because the Raman scattering directly exhibits the fingerprint vibrational modes of the target Raman-active molecule. In accordance with the need for identifying an unknown molecule at the single-molecule level, researchers have sought methods capable of achieving this goal, that is, surface-enhanced Raman scattering (SERS) and tip-enhanced Raman scattering (TERS), in which an enormously enhanced Raman signal was detected when molecules were adsorbed onto the surface of a roughened metal surface. Briefly, the enhancements of the SERS are classified into two categories: electromagnetic and chemical. The former is believed to be the predominant enhancement because it largely amplifies both the incident and the scattered electromagnetic fields. The latter is related to an increase in the polarizability of the adsorbed molecule. Detailed information on the enhanced mechanism, platform for the Raman spectroscopy investigation, and new strategy for implementing the SERS can be found in several impressive reports.[522−525]

Recently, the Raman spectroscopy was used to probe the structural change in single molecules during time-dependent dynamic processes, and several significant important results were reported.[522] As was mentioned in section 2.1.3, Ward et al. reported simultaneous measurements of electronic conduction and real-time Raman responses in molecular junctions formed using the electromigration technique.[207] These conductance/Raman observations demonstrated that the electromigrated nanogaps between the extended electrodes could achieve enhancements sufficient for single-molecule SERS sensitivity, thus leading to an investigation of single-molecule structural changes. Following this study, Konishi et al. further reported the SERS of a single molecule under conditions of an in situ current flow in MCBJ-based molecular junctions.[157] Significant changes in the SERS intensity and the selectivity of the Raman vibrational bands that are coincident with current fluctuations provide information related to the electronic structural dynamics of a single molecule in their experiments. Another recent advance is that Jiang et al. reported a method, which combined molecule-resolution scanning tunneling microscopy and tip-enhanced Raman spectroscopy.[526] This method provides a powerful tool for the real-time study of vibrational, rotational, and other low-frequency modes of molecules, which not only chemically identifies the molecules adsorbed on a surface but also yields information on the adsorption configuration and the chemical bonding between molecules. Generally, direct probing of the dynamic structure and chemical changes in the nanoscale molecular junctions upon application of an electric field remains a major challenge. Using in situ gap-mode Raman spectra, Cui et al. established a relationship between the applied electrochemical gate field and the conformational changes in sandwiched molecular junctions, such as the torsion angle of the molecules.[527]

Furthermore, Raman spectroscopy was employed to investigate vibrational and electronic heating in the nanoscale junctions. Until now, understanding and controlling the flow of heat is a major challenge in nanoelectronics. When a junction is driven out of equilibrium by light or the electric charge flow, the vibrational and electronic degrees of freedom cannot be described by a single temperature. In a pioneering study, Ward et al. demonstrated that surface-enhanced Raman spectroscopy can be used to determine the effective temperatures in a biased metallic nanoscale junction covered with molecules (the junction was fabricated using the electromigration method).[209] Using an anti-Stokes electronic Raman emission followed by a delicate calibration, they demonstrated that the effective electronic temperature at small bias voltages can reach values up to several times that of the values measured when there is no current; that is, molecular vibrations show mode-specific pumping by both optical excitation and current with effective temperatures exceeding several hundred degrees kelvin.

During the past four decades, considerable efforts and ingenuity have been made, thus leading to the continuous development of theoretical and experimental progress regarding the Raman spectroscopy. However, a few challenges in performing Raman spectroscopy still remain, which include the reproducible generation of hot spots providing sufficient signal amplification to sensitively detect single molecules, compatibility under various conditions, and establishment of robust statistical strategies.[522] The strength of the SERS is its high content of molecular information combined with sensitivity, quantification, and multiplexing. Other vibrational spectroscopy techniques (such as fluorescence microscopy, ultraviolet−visible spectroscopy, and inelastic electron tunneling spectroscopy) also have their own unique advantages.[516] Comparing and combining the performance of the SERS with other existing techniques will supply and confirm comprehensive information on the studied molecular junctions.

DOI: 10.1021/acs.chemrev.5b00680
Chem. Rev. 2016, 116, 4318−4440

5.6.2. Ultraviolet−Visible Spectroscopy. Ultraviolet−visible spectroscopy (UV−vis) refers to the absorption spectroscopy or reflectance spectroscopy in the ultraviolet−visible spectral region. UV−vis uses light in the visible and adjacent regions, that is, the regime between the near-ultraviolet and the near-infrared ranges, and measures the molecule transitions from the ground state to the excited state. This technique is a technique complementary to fluorescence spectroscopy, which addresses the molecular transitions from the excited state to the ground state.[528] The instrument used in ultraviolet−visible spectroscopy is called a UV−vis spectrophotometer. It measures the intensity of light (I) passing through the sample and compares it to the intensity of incident light (I_0) before passing through the sample. The ratio $T = I/I_0$ is known as the transmittance. The UV−vis spectrophotometer can also be configured to measure the reflectance. In this case, the spectrophotometer measures the intensity of the reflected light from the sample and compares it to the intensity of light reflected from a reference material. This ratio is known as the reflectance.

The UV−vis spectroscopy can be used to address the molecular energy structure.[529] For example, for those molecules containing π-electrons or nonbonding electrons, they can absorb the energy of the ultraviolet or visible lights to excite these electrons to higher antibonding molecular orbitals. When the energy gap between the HOMO and the LUMO is low, electrons will be easily excited, leading to an absorption of longer wavelength. Therefore, the peak's position in spectroscopy indicates the energy structure of the interested molecules. The wavelengths of the absorption peaks and the amplitude of the peaks also correlated with the types of bonds in a given molecule; thus, the UV−vis spectroscopy is valuable in determining the functional groups within a molecule.[530] According to the Beer−Lambert law, the absorbance of a solution is directly proportional to the concentration of the absorbing species in the solution. Thus, for a fixed path length, the UV−vis spectroscopy can be used to determine the concentration of the absorber in a solution.[531] Furthermore, the UV−vis can be applied to determine the rate constant of a chemical reaction based on the concentration measurement.[532] The rate constant of a particular reaction can be determined by measuring the UV−vis absorbance spectrum at specific time intervals to observe the changes in the levels of absorbed wavelength over time in accordance with the solution color changes (energy state change). From these measurements, the concentration as well as the reaction rate can be calculated.

5.6.3. X-ray Photoelectron Spectroscopy. X-ray photoelectron spectroscopy (XPS) is a widely used technique for analyzing the surface chemistry of a material. In the 1950s, Kai Siegbahn et al. developed the X-ray photoelectron spectroscopy (XPS) for surface chemical analysis and received the Nobel prize for this pioneering and outstanding work.[533] The XPS can measure the elemental composition, empirical formula, chemical state, and electronic state of the elements within a material. In principle, the XPS spectra are typically obtained by irradiating a solid surface with a beam of X-rays in high vacuum and simultaneously measuring the kinetic energy as well as the number of electrons that are emitted from the top of the material being analyzed. When an atom or molecule absorbs an X-ray photon, an electron can be ejected. The kinetic energy of the ejected electron depends on the photon energy ($h\nu$) and the binding energy of the electron based on the equation $E_{binding} = E_{photon} - (E_{kinetic} + \text{Ø})$, where $E_{binding}$ is the binding energy of the electron and can be regarded as the energy required to remove the electron from the material surface, E_{photon} is the energy of the X-ray photons, $E_{kinetic}$ is the kinetic energy of the electron that can be measured by the instrument, and Ø is the work function of the material detected. For an electron ejection, the excitation energy must be large enough for the electrons to overcome the work function of the solid. Because the energy of an X-ray with a particular wavelength is known, and the emitted electrons' kinetic energies can be measured, the electron binding energy of each of the emitted electrons can be determined using this equation.

A typical XPS spectrum is a plot of the number of electrons detected (Y-axis) versus the binding energy of the electrons detected (X-axis). Because the inner shell electrons for each element have a different binding energy, the XPS peaks at the characteristic binding energy values can be used to identify each element that exists in the surface of the material being analyzed. The number of detected electrons in each of the characteristic peaks is directly related to the number of elements within the XPS sampling volume. Thus, the XPS can be used to identify the elements as well as the amount in the targeted material. Please note, the binding energy depends not only on the element from which the electron is emitted but also on the orbitals from which the electron is ejected as well as the chemical environment of the atom from which the electron was emitted. Thus, by measuring the kinetic energy of the emitted electrons, it is possible to determine which elements are near a material's surface and their "chemical states", which refers to the local bonding environment of the studied species. The local bonding environment of a species in a study is affected by its formal oxidation state, identity of its nearest-neighbor atom, and bonding hybridization to the nearest-neighbor atom. Thus, the so-called chemical shift (peak shift), which is dependent on the chemical environment, can be observed. In return, the chemical shift provides the chemical state information, such as the molecular structural information.

The XPS has been widely applied in the field of molecular electronics.[534] For example, the XPS can be used as a tool to check the thin film thickness of the molecular layer due to the finite mean free path length, which is a function of the kinetic energy of the photoelectron. Using the XPS, the thickness of the molecular layer on the substrate (such as Au) can be calculated by the relative intensities of the specific peaks and a standard length SAM on Au as a reference.[452,535] By analyzing the XPS, one can obtain insight into the molecule-adsorbed state and the configuration at the interface;[536] furthermore, the XPS was used to reveal the interaction information between the molecular layer and the top contacts and verify that the intended functional groups remained intact after the fabrication of the junction.[537,538] With the development of third generation synchrotron light sources and promoted resolution, the XPS was developed to become an outstanding tool to study surface properties, even surface reactions, at an unprecedented level.[539]

5.6.4. Ultraviolet Photoelectron Spectroscopy. The ultraviolet photoelectron spectroscopy, denoted as UPS, refers to the measurement of the kinetic energy spectra of the photoelectrons emitted by molecules that have absorbed ultraviolet photons. The UPS method was developed by David W. Turner et al. during the 1960s.[540] Similar to the X-ray photoelectron spectroscopy, it is also based on the photoelectric effect discovered by Albert Einstein in 1905. In comparison to the XPS, which is based on high energy X-ray sources to study the energy levels of the atomic core electrons,

DOI: 10.1021/acs.chemrev.5b00680
Chem. Rev. 2016, 116, 4318−4440

the UPS uses a helium discharge lamp (with wavelengths in the ultraviolet region) to study the valence electrons with more accuracy. As Einstein's photoelectric law is applied to a free molecule, the kinetic energy of an emitted photoelectron is based on the equation $E_K = h\nu - I$, where h is Planck's constant, ν is the frequency of the ionizing light, and I is the ionization energy for the formation of a singly charged ion.[541] On the basis of Koopmans' theory, each ionization energy may be identified by the energy of a molecular orbital.[542] The ultraviolet photoelectron spectrum of a molecule contains a series of peaks, and each corresponds to one valence-region molecular orbital energy level.[515]

In the UPS technique, the valence-level instead of the core-level orbitals was probed, which yield insights into the alignment of the contact energy levels and the molecular orbitals.[543] Combining the UPS measurement with the $I-V$ measurement (showing negative differential resistance), Yaffe et al. demonstrated that the energy difference between the Fermi level and the LUMO was considerably smaller than that between the Fermi level and the HOMO, indicating that the lowest unoccupied molecular orbital primarily controlled the charge transport.[544] Hill et al. used the photoemission spectroscopy to investigate the interfacial energy formed by the deposition of different molecular thin films on various metals.[545] They found that the interface electron and the hole barriers were not simply defined by the difference between the work functions of the metals and the organic solids, demonstrating the breakdown of the vacuum level alignment rule at interfaces between the organic molecular solids and metals.[545] Additionally, the high resolution of the UPS allows the observation of the fine structures due to the vibrational levels of the molecules, which facilitate the assignment of the peaks to bonding, nonbonding, or antibonding molecular orbitals.[539,546] The ultraviolet photoelectron spectroscopy method was later extended to the study of the solid surfaces, where it was generally known as photoemission spectroscopy (PES).[547]

6. THEORETICAL ASPECT FOR ELECTRON TRANSPORT THROUGH MOLECULAR JUNCTIONS

6.1. Theoretical Descriptions of the Tunneling Process

The current flowing through a molecular junction consisting of two electrodes separated by a molecule/molecules is realized dominantly through tunneling.[548,549] There are a number of approaches used to derive the characteristics of the tunneling current: the well-known Wentzel–Kramers–Brillouin (WKB) approximation, Fowler–Nordheim equation, Simmons equation, Borden formalism, and Landauer equation.[12,550] The simplest and most fundamental 1-D model is a free electron with energy E separated by a rectangular barrier of height (Φ) and thickness (d). The time-independent Schrödinger in this scenario can be written as follows:

$$\left[-\frac{\hbar^2}{2m}\frac{\partial^2}{\partial x^2} + V(r)\right]\psi = E\psi \tag{15}$$

where m and E are the mass and the energy of the electron, respectively; and $V(r)$ describes the potential barrier. The exact solutions of eq 11 can be obtained corresponding to the wave functions outside and inside the barrier (Figure 43).

$$\psi_I = e^{ikz} + A\cdot e^{-ikz} \tag{16}$$

$$\psi_{II} = \alpha\cdot e^{\kappa z} + \beta\cdot e^{-\kappa z} \tag{17}$$

$$\psi_{III} = B\cdot e^{ikz} \tag{18}$$

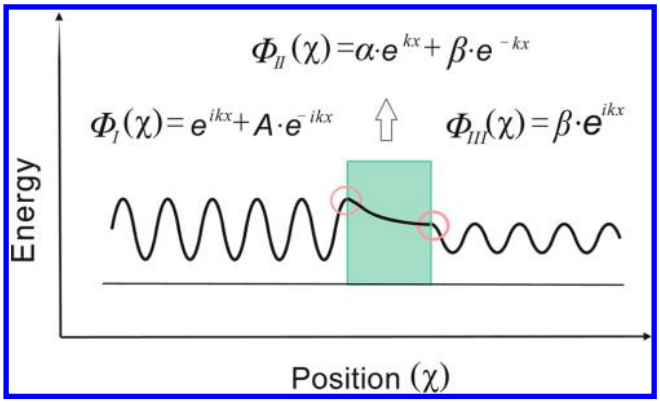

Figure 43. Schematic drawing of electron tunneling through a rectangular barrier. Reproduced with permission from ref 551. Copyright 2012 Forschungszentrum Jülich.

with

$$k = \frac{\sqrt{2mE}}{\hbar} \quad \text{and} \quad \kappa = \frac{\sqrt{2m\phi - E}}{\hbar} \tag{19}$$

The relative probability of an incident electron transmitting the barrier, that is, the transmission coefficient, is $T = |B|^2/|A|^2$. By matching the continuities of the wave functions and their first derivatives at the boundaries, the transmission coefficient can be expressed by the formula as follows:

$$T = \frac{1}{\left[(k^2 + \kappa^2/2k\kappa)^2 \sinh(\kappa d)\right]} \tag{20}$$

For a high potential, where $\Phi \gg E$ or $\kappa d \gg 1$, T can be simplified as follows:

$$T \approx \frac{16k^2\kappa^2}{(k^2 + \kappa^2)^2}\cdot e^{-2\kappa d} \tag{21}$$

The tunneling current is proportional to the transmission coefficient; thus, it will reduce its magnitude exponentially with an increase in the molecular length in a molecular junction. The potential barrier in the molecular junctions is approximated to be the HOMO or the LUMO when either of them is close enough to the Fermi level of the metal electrodes. The barrier shape is not always a standard rectangle due to the applied voltage, which elevates the Fermi level of, for instance, the left electrode while lowering the right one. The Simmons model[548] assuming a trapezoidal barrier is an excellent approximation.[552] The tunneling current density in the $eV < \Phi$ regime can be described as follows:

$$J = \frac{e}{4\pi^2\hbar d^2}\left\{\left(\Phi - \frac{eV}{2}\right)\exp\left[-\frac{2(2m)^{1/2}}{\hbar}\alpha\left(\Phi - \frac{eV}{2}\right)^2 d\right] - \left(\Phi + \frac{eV}{2}\right)\exp\left[-\frac{2(2m)^{1/2}}{\hbar}\alpha\left(\Phi + \frac{eV}{2}\right)^2 d\right]\right\} \tag{22}$$

where Φ, d, and V are the barrier height, thickness, and applied voltage, respectively; and α is a parameter that accounts for either adjusting the effective mass of the tunneling electrons,[446]

DOI: 10.1021/acs.chemrev.5b00680
Chem. Rev. 2016, 116, 4318–4440

providing a way of applying a rectangular tunneling to a nonrectangular case, or both.[553] The bare electron tunneling through a rectangular potential barrier corresponds to $\alpha = 1$. Equation 22 can be simplified in two limits based on the relative difference between the bias V and the barrier height Φ. In a low bias range, the simplified form can be expressed as follows:

$$J = \left(\frac{(2m\Phi)^{1/2}e^2\alpha}{\hbar d^2}\right)V \exp\left[-\frac{2(2m)^{1/2}}{\hbar}\alpha(\Phi)^{1/2}d\right] \quad (23)$$

In a high bias regime, the tunneling current density becomes

$$J = \left(\frac{e}{4\pi^2\hbar d^2}\right)\left(\Phi - \frac{eV}{2}\right)\exp\left[-\frac{2(2m)^{1/2}}{\hbar}\alpha\left(\Phi - \frac{eV}{2}\right)^{1/2}d\right] \quad (24)$$

Equations 23 and 24 illustrate that as the barrier thickness increases, often corresponding to the larger molecular length in the molecular junctions, the tunneling current shows an exponential decrease. This length-dependence regulation is widely used in the experimental analysis[255,554] and commonly adopted in a further more simplified form expressed as follows:[555]

$$J = J_0\, e^{-\beta d} \quad (25)$$

where $\beta = 2(2m\varphi/\hbar^2)^{1/2}$ is defined as the tunneling decay coefficient; and J_0 is the hypothetical zero-length current. The Simmons model for molecule junction is established on the assumptions that the molecular energy level (HUMO or LUMO) is constant throughout the entire tunneling distance and the uniform dielectric constant of the medium seldom affects the shape of the tunneling barrier. Additionally, the effects from an image potential are neglected in the tunneling process. However, in actual molecular junctions, due to the coupling between the molecules and the electrodes, the energy levels are shifted from the positions inherent to the isolated molecules, and the discrete energy levels are broadened to the bands, for which the density states, in a simplest way, are represented using the Lorentz function as follows:

$$D(E) = \frac{1}{2\pi}\frac{\Gamma}{(E - E_0)^2 + (\Gamma/2)^2} \quad (26)$$

where E_0 is the discrete energy level inherent to the single molecule; and Γ is a parameter with an energy dimension describing the coupling strength of the molecule to electrodes. The energy level distributions along the tunneling distance are not uniform, resulting from varied bond formations. The average energy level may be a compromised way to adopt the Simmons model; however, it is unsuitable when the nonuniform levels are close to the electrode Fermi levels.[255] Introducing a tunneling matrix, as inspired from the tunneling mechanisms in the scanning tunneling spectroscopy,[556] would shed light on dealing with the tunneling process through molecular junctions with the energy levels far from uniform.

6.2. Electron Transport Mechanism

6.2.1. Coherent Electron Transport through Molecular Junctions. The charge transport through a macroscopic conductor obeys Ohm's law, and the resistance is proportional to the length of the conductor. However, these laws are not valid for a conductor downscaling to the nanometer regime, in which the conductance is quantized. When the length is reduced to less than that of the mean free path of electrons, the transport mechanism changes from diffusive to ballistic. The quantum confinement arising from width narrowing results in not all transverse modes that come from the electron reservoir transmitting through the conductor. Electrons with an energy E (mass m) contributing to the conductance must satisfy $p_z^2 = 2mE - (p_x^2 + p_y^2) > 0$, where p_z is the momentum parallel to the length of the conductor, and both p_x and p_y are the transverse momentums, which are discretely constrained as $p_x, p_y = hn/2w$, with w representing the width of the conductor. The nonequality constrains the electrons to exceed the Fermi wavelength λ_F or the Fermi energy $E_F = h^2/2m\lambda_F^2$. The potential difference (V) between the two electrodes creates a transmission window $E_F \approx E_F + eV$. Each transverse mode in the transmission widow opens a conductance channel. In a ballistic transport scenario, this contributes a quantum unity conductance $G_0 = 2e^2/h$; thus, the total conductance of a nanowire can be given as follows:

$$G = N(2e^2/h) \quad (27)$$

where N is the total number of the conductance channels determined from the transmission window and the nonequality mentioned above. Increasing the applied voltage will allow more modes to be included, and because of the quantization of the wavelength, the current will rise stepwise.[35] The number of channels depends on the width of the conductor; thus narrowing the width will lead to a stepwise decrease in the conductance.[557] The transport in practical molecular junctions is generally nonidealistic, and it can take a more general form as follows:

$$G = 2e^2/h \sum T_i \quad (28)$$

where T_i is the transmission coefficient of the conductance channels associated with the molecular orbitals. By applying a gate that modulates the molecular orbitals, Topinka et al. clearly demonstrated a quantized conductance in the molecular junctions,[558] as shown in Figure 44.

A metal−molecule−metal junction is hypothesized as a phase coherence conductor connected to two electron reservoirs. Considering that the net current flow occurs only between the energy levels of μ_L and μ_R, the tunneling current can be expressed in a form of the Landauer formula as follows:[550]

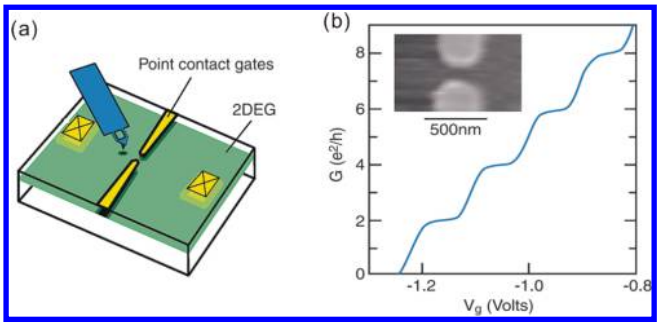

Figure 44. Quantized conductance effect. (a) Schematic diagram of the experimental setup. The quantum point contact (QPC) conductance was measured as a function of the AFM tip position. (b) Point contact conductance G versus gate voltage V_g with no tip present. The point contact conductance as a function of the gate voltage clearly depicts a quantized conductance effect. Reprinted with permission from ref 558. Copyright 2000 AAAS.

DOI: 10.1021/acs.chemrev.5b00680
Chem. Rev. 2016, 116, 4318−4440

$$I = \frac{2e}{h}\int T(E)[f_L(E) - f_R(E)]\,dE \tag{29}$$

where

$$f_\beta = \frac{1}{1 + \exp[(E - \mu_\beta)/kT]}\ (\beta = L, R) \tag{30}$$

is the Fermi distribution function for the left (β = L) and right (β = R) electrodes with an electrochemical potential μ_β; and $T(E)$ is the transmission function.

The coupling of the molecule to the electrode affects both the transmission coefficient associated with each energy level and the molecular orbitals. Taking a simple model where a single spin-degenerated molecular orbital with an energy E_0 is regarded as the channel for the charge transport, the coupling of the leads characterized by Γ_β ($\beta \in$ L, R) results in a level broadening, and the transmission coefficient changes into a Lorentz function as follows:[419,559,560]

$$T(E) = \frac{\Gamma_L\Gamma_R}{[E - E_0]^2 + [\Gamma_L - \Gamma_R]^2} \tag{31}$$

Addition energy (U_{add}) is the energy needed to release one electron from the HOMO minus the energy gained to add one electron onto the LUMO. $\Gamma_\beta \ll U_{add}$ corresponds to a weak coupling. In this scenario, electrons coming from the left electrode first hop to the molecule and then to the right electrode. Conversely, the strong coupling $\Gamma_\beta \gg U_{add}$ results in a significant broadening of the molecular levels. Therefore, the electrons in the left lead transport directly to the right, thus eliminating the middle procedure of stopping at the molecular bridge. In the intermediate regime, the molecular orbitals are partially broadened, and the phenomena due to the electron−electron correlation effects, such as the Kondo effect and cotunneling, are observed.[561]

6.2.2. Electron−Phonon Interaction Effects on Transport Mechanism. The electron transport mechanism illustrated by the Landauer formula corresponds to the electrons traveling through a conductor in which ions are frozen in their equilibrium position. In practical molecular junctions, because of the thermal motion of the ions, the Landauer equation is treated as a limited case.[562] The traversal time is defined as the time it takes for an electron to finish one tunneling process, and it is proportional to the number of sites in the molecular linker.[563] For a molecular junction with a length of ∼1 nm and an energy level of ∼1 eV above the tunneling electrons, the value is approximately 0.2 fs.[550] For a short molecular linker at low temperatures, the traversal time is considerably smaller than that of the ionic motion periods; thus the coherent tunneling dominates.[564] The decoherence effects are important when the energy of the tunneling electron resonates with a molecular orbital, which causes a substantially long traversal time.[565,566] This electron−phonon coupling enhances itself as the molecular length and the temperature increase.[392,564] In an extremely strong coupling case, the localization effects of the electron wave functions change the transport mechanism from tunneling to thermally activated hopping, where the conductance increases as the temperature increases[311] and, in contrast, the conductance decreases when the temperature increases in the tunneling transmission.

The strong electron−phonon coupling means the breakdown of the coherent tunneling transmission depicted by the Landauer formulizm, and the standard electron transfer theories are applicable, which describe the electrons hopping from an initial localization state (donor) to a final localization state (acceptor). When the electronic coupling between the donor and the acceptor is weak, the electron transfer rate k_{ET} can be expressed using the Fermi golden rule as follows:[550,567,568]

$$k_{ET} = \frac{4\pi^2}{h}|H_{DA}|^2\left(\frac{1}{4\pi\lambda k_B T}\exp\left[-\frac{(\lambda + \Delta G^0)^2}{4\pi\lambda k_B T}\right]\right) \tag{32}$$

where h, k_B, and T are the Planck constant, Boltzmann constant, and temperature, respectively; $|H_{DA}|$ is the electronic coupling matrix of the donor to the acceptor; ΔG^0 is the free energy difference between the acceptor and the donor; and λ is the reorganization energy representing the energy difference between the donor and the acceptor if the system makes an instantaneous vertical transition from the donor state to the acceptor state.

For a strong electronic coupling between the donor and the acceptor, the charge transfer is essentially realized through a way of redistributing the electrons of the mixed states attached to the donor and the acceptor because of the stochastic fluctuations. The electron transfer rate in this situation follows an Arrhenius relation given by

$$k_{ET} \propto \exp\left(-\frac{E^*}{k_B T}\right) \tag{33}$$

where E^* is the effective potential barrier between the donor and the acceptor, which is also known as the hopping activation energy.[311,569]

6.3. First-Principles Modeling

6.3.1. Introduction to Density Functional Theory. Using the first-principles modeling as a supplementary tool for the experimental studies in molecular electronics allows researchers to construct a quantitative picture of the mechanisms on the electron transport in the molecular junctions and form predictions to guide further experimental studies. The key task in the theoretical studies for molecular electronics is to calculate the electronic structures of the molecular linker under the electrode environments. By employing the transport mechanism, such as the Landauer formula, the Berit−Winger formula, and others, the characteristics of electron transport can be unraveled.[570−573] Depending on the coupling to the leads, the electronic structure of the molecules is generally different from that in the isolated gas phase. One effective approach to tackle this problem is to extract an "extended molecule" with several electrode atoms attached to its two terminals.[574,575] This is based on the assumption that the effects from the molecule−electrodes coupling are always localized to the small regimes on the contact surfaces where only small amounts of atoms are involved.

The electron behavior in the molecular linkers is essentially a multibody problem. The density functional theory (DFT) reduces the complex electron−electron and electron nuclei interactions to a single electron moving in an effective potential field that is the functional of the electron density. The Hamiltonian for an electron can be given by

$$\mathcal{H}[\rho(\mathbf{r})] = T[\rho(\mathbf{r})] + V_{eff}[\rho(\mathbf{r})] \tag{34}$$

where T is the free-electron kinetic energy; and V_{eff} is the effective potential energy. In the Born−Oppenheimer approx-

DOI: 10.1021/acs.chemrev.5b00680
Chem. Rev. 2016, 116, 4318−4440

imation,[576] when the electron−phone interaction is neglected, it can be expressed as follows:

$$V_{\text{eff}} = \frac{e^2}{2}\int \frac{\rho(\mathbf{r}')}{|\mathbf{r}-\mathbf{r}'|}\,\mathrm{d}\mathbf{r}' + U_{\text{e-nuc}}[\rho(\mathbf{r})] + v_{\text{xc}}[\rho(\mathbf{r})] \tag{35}$$

where the first term in the right side of the equation is the Hartree mean potential representing the average potential caused by the electron−electron Coulomb repulsions; $U_{\text{e-nuc}}$ describes the electron−nuclei electrostatic interactions; and v_{xc} is the exchange-correlation energy, which is the only term of the three that needs to be reasonably approximated. The local density approximation (LDA) assumes that the exchange-correlation energy for an infinitesimal $\rho(\mathbf{r})$ d$\mathbf{r}$ in a system is equal to that of a homogeneous electron gas of a density $\rho = \rho(\mathbf{r})$.[577] The local spin density approximation develops the LDA by taking the electron spin as the parameters.[578] A further improvement in the exchange-correlation function assumes a gradient (GGA) or a second-derivative dependency.[579,580] The Hamiltonian of the electron-nuclei system is the spatial integral of the single electron Hamiltonian, which can be given as follows:

$$H = \int \mathcal{H}\rho(\mathbf{r})\,\mathrm{d}\mathbf{r} \tag{36}$$

The ground state of the system has the electron density function that minimizes the system energy. By applying the variational principle, we obtain

$$\frac{\delta H}{\delta \rho} = \mu \tag{37}$$

where μ is the Lagrange multiplier corresponding to the conservation of the total electron number of the system. In the self-consistent calculation method, the solution to eq 37 can be found by solving a set of one-particle Schrödinger equations as follows:

$$\left(-\frac{\hbar^2}{2m_{\text{e}}}\nabla^2 + V_{\text{eff}}\right)\psi_i = \int_i \psi_i \tag{38}$$

and the electron density function can be expressed as follows:

$$\rho(r) = \sum \psi_i^* \psi_i \tag{39}$$

In the actual calculations, the plane wave basis is a simple and often effective way to represent the wave function[577,581] for the ith electron; thus, we can obtain

$$\psi_i = \sum_n C_n^i \exp(i\mathbf{k}_n \cdot \mathbf{r}) \tag{40}$$

The work then becomes to vary the coefficients C_n^i rather than the wave function values at each spatial point to obtain the minimized system energy. To represent the wave functions for the system explicitly, the infinite wave basis should be collected. However, there generally are finite plane waves (labeled by $\mathbf{k}_n$) that have a predominant position on determining the characteristics of the system; thus only countable numbers of the wave bases are adopted in the actual calculations, and this work is called k-point sampling. Clearly, for a more massive k-point sampling, a more accurate result is obtained. In addition to the plane wave basis, several other wave bases, such as augmented plane waves, linearized muffin-tin orbitals, the Gaussian orbitals, and others, are widely used.[575,582,583] Once the electron density of the optimized system is derived from iteration, other properties, especially the electronic structures, can be calculated in terms of the corresponding specific approaches.

The model based on the self-consistent field approach mentioned above works fairly well in describing the electron behaviors in the molecular junctions, except in a so-called "Coulomb blockade" regime, which is briefly elaborated here. For a system containing N electrons, the gross electron−electron interaction potential U can be given as follows:

$$U = U_0 C_N^2 \tag{41}$$

where U_0 describes the average potential between any two electrons. By adding one electron to the system, the system energy increment can be given as follows:

$$\Delta U = U_0(C_{N+1}^2 - C_N^2) = NU_0 \tag{42}$$

where NU_0 is the charging energy for an N-electron system; and U_0 is regarded as the single electron charging energy. The effects of the electron−electron interactions will be predominant if the single electron charging energy exceeds the thermal energy $k_{\text{B}}T$ and the level broadening resulting from the coupling to the electrodes. Under this condition, the tunneling current at a low bias value is significantly suppressed, and this phenomenon is known as the Coulomb blockade. The single charging effect plays a dominant role in the Coulomb blockade regime, which is not well described by the self-consistent field approach, even at equilibrium. The self-consistent field models also do not work well when dealing with the systems associated with the nonequilibrium electron−electron interactions.[584]

A further improvement in minimizing the gross energy of the system to determine the ground state considers the atomic coordinates as variables in the DFT energy functional. The optimized molecular geometric structures are those at the mechanical equilibrium states where the forces defined as the partial derivatives of the system energy with respect to the atomic coordinates reduce to zeros. The DFT approach was also developed for describing the excited electronic states of the molecular systems. For further information, interested readers can review the studies of Perdew et al.[585] and Barauh et al.[586]

6.3.2. Current−Voltage Characteristics Calculations. The current−voltage characterization is a conventional approach used to investigate the properties of the electrical structures. The simplest structure is a metal wire, where we have Ohm's law or junctions in the mesoscopic regime. The theoretical model and its calculations provide a detailed understanding of the charge transport mechanisms, which are essentially important for the design of electronic devices with novel properties. Molecular junctions are often seen as a molecular linker connecting two infinite electron reservoirs. There is a coupling between the molecules and the leads where the fixed point boundary condition or the periodic boundary condition can no longer be used in the electronic structure calculation. Molecular junctions are open systems in which the molecules, or the extended molecules in metal contacts, have a continuous density of state rather than discrete energy levels owned by their isolated gas counterparts. The exchange of electrons occurs between the electrodes and the molecular linker; thus, the number of electrons in the spacer is generally not conservative. What makes the calculation more sophisticated is that the system formed by the molecular junctions is of nonequilibrium, and the effects, such as chemisorptions,

DOI: 10.1021/acs.chemrev.5b00680
Chem. Rev. 2016, 116, 4318−4440

bonding types, molecular tilted angles, and molecular interactions in the self-assembled monolayer junctions, are expected to play a nontrivial role in the charge transport.

For a junction at the equilibrium state, where the chemical potential for both leads is the same, the electron density function in the linker regime can be written as follows:

$$n(\mathbf{r}) = \sum_i |\psi_i^2| f(\varepsilon_\alpha - \mu) \tag{43}$$

where μ is the chemical potential, and ψ_i can be obtained by solving the Kohn−Sham equations as follows:

$$\left[-\frac{\hbar^2}{2m}\nabla^2 + V_{\text{eff}} + U\right]\psi_i = \varepsilon_\alpha \psi_i \tag{44}$$

where V_{eff} is the DFT effective potential field, which, in its simplest case, can be approximated simply in the Hartree form as follows:

$$V_{\text{eff}} = \frac{e^2}{2}\int \frac{n(r')}{|r - r'|}\,\mathrm{d}r' \tag{45}$$

where U is the extra potential, which arises due to the electron transfer between the linker and the electrodes and needs to be calculated self-consistently. U satisfies the Poisson equation as follows:

$$\nabla^2 U = e^2(n_0 - n)/\varepsilon \tag{46}$$

where n_0 is the electron density of an isolated linker device without connecting to any electrodes.

By iterating between the Poisson equation and the equilibrium statistical mechanics, the charging potential profile and the electron density of the system can be solved self-consistently; furthermore, so long as the electron density of the system is known, all qualities of interest, such as energy and current, can be calculated. However, for a nonequilibrium system, the electron density function can no longer be expressed by eq 46 because there are different chemical potentials at the two contacts, and the correlated occupations between the different states cannot be neglected. In this case, the density function can be characterized by a density matrix ρ_{ij} and expressed as follows:

$$n(\mathbf{r}) = \sum_{ij} \rho_{ij}\psi_j^*\psi_i \tag{47}$$

The nonequilibrium Green function (NEGF) then is introduced to deal with problems in open systems. The system is generally partitioned into three parts, that is, the device and the two contact parts, which correspond to the molecular linker and the electrodes in the molecular junctions, respectively. The molecular junction electrodes are often seen as semi-infinite entities; thus, the matrix representing the contact effects is regularly semi-infinite, which results in intractable calculations. The Green formulism replaces the effects arising out of contacts with a self-energy matrix that is the same size as the device's Hamiltonian, thus making the problem tractable. The Hamiltonian of the system can be expressed using a blocked matrix as follows:

$$H = \begin{pmatrix} H_{\text{L}} & H_{\text{ML}}^\dagger & 0 \\ H_{\text{ML}} & H_{\text{M}} & H_{\text{MR}} \\ 0 & H_{\text{MR}}^\dagger & H_{\text{R}} \end{pmatrix} \tag{48}$$

where subscripts M, L, and R represent the molecule, left electrode, and right electrode, respectively; and subscript ML (MR) describes the coupling between the molecule and the left (right) electrode. Here, the coupling between the two electrodes is neglected. The Green function of the system can be written as follows:

$$G(\varepsilon) = \begin{pmatrix} G_{\text{L}} & \cdots & \\ & G_{\text{M}} & \\ \cdots & & G_{\text{R}} \end{pmatrix} = \begin{pmatrix} (\varepsilon + i\delta)S_{\text{L}} - H_{\text{L}} & \tau_{\text{L}}^\dagger & 0 \\ \tau_{\text{R}} & (\varepsilon + i\delta)S_{\text{M}} - H_{\text{M}} & \tau_{\text{R}} \\ 0 & \tau_{\text{L}}^\dagger & (\varepsilon + i\delta)S_{\text{R}} - H_{\text{R}} \end{pmatrix}^{-1} \tag{49}$$

where $\delta \to 0^+$; S_β (β = L,M,R) is the overlap matrix; and τ_β (β = L,R) is the contact matrix. For the device part, S_{M} can be expressed in terms of the wave basis employed for solving the Kohn−Sham equation:[587]

$$(S_{\text{M}})_{ij} = \int \phi_i\phi_j\,\mathrm{d}\mathbf{r} \tag{50}$$

It is straightforward that the Green function for the device parts goes

$$G_{\text{M}}(\varepsilon) = \frac{1}{\varepsilon S_{\text{M}} - H_{\text{M}} - \Sigma_{\text{L}} - \Sigma_{\text{R}}} \tag{51}$$

where $\sum_{\text{L}}$ and $\sum_{\text{R}}$ are the non-Hermitian self-energy matrixes:

$$\Sigma_\beta = \tau_\beta G_\beta \tau_\beta^\dagger \ (\beta = \text{L, R}) \tag{52}$$

The Hermitian part of the self-energy matrix describes the shift of the molecular energy levels and its anti-Hermitian part.

$$\Gamma_\beta = i(\Sigma_\beta - \Sigma_\beta^\dagger) \ (\beta = \text{L, R}) \tag{53}$$

represents the level broadening. If the molecular junction is at an equilibrium state where there is no applied bias, then the density matrix ρ_{ij} can be expressed as follows:

$$\rho_{ij} = \frac{1}{\pi}\int \text{Im}[G_{ij}(\varepsilon)] f(\varepsilon - \mu)\,\mathrm{d}\varepsilon \tag{54}$$

where μ is the equilibrium chemical potential of the system; and G_{ij} is the elementary of the retarded Green function for the device part, for which the self-energy is zero. This equation is essentially the same as eq 45. If a bias V is applied to the molecular junction, and $eV = \mu_{\text{L}} - \mu_{\text{R}}$, then the density matrix can be described using the NEGF as follows:

$$\rho = \frac{1}{\pi}\int G_{\text{M}}(\varepsilon)\,\text{Im}[\Sigma_{\text{L}}] G_{\text{M}}^\dagger f_{\text{L}}\,\mathrm{d}\varepsilon + \frac{1}{\pi}\int G_{\text{M}}(\varepsilon)\,\text{Im}[\Sigma_{\text{R}}] G_{\text{M}}^\dagger f_{\text{R}}\,\mathrm{d}\varepsilon \tag{55}$$

where f_β (β = L,R) is the Fermi function with an electron potential μ_β.

$$f_\beta = \left[1 + \exp\left(\varepsilon - \frac{\mu_\beta}{k_{\text{B}}T}\right)\right]^{-1} \tag{56}$$

Using the density matrix, the electron density can be derived as follows:

DOI: 10.1021/acs.chemrev.5b00680
Chem. Rev. 2016, 116, 4318−4440

$$n(\mathbf{r}) = \sum_{ij} \rho_{ij}\phi_i\phi_j \tag{57}$$

It should be noted that there is an extra potential in the molecular junctions arising from the electron exchange between the electrodes and the molecular linker. By performing a transform for the right side of eq 46, $e^2(n_0 - n) \rightarrow eTr(\rho S_M)$, we can obtain the Poisson equation for the nonequilibrium system. To achieve a full description of the electronic behaviors in molecular junctions, we need to self-consistently calculate the Schrödinger equation and the Poisson equation simultaneously, which is similar to the work done for the equilibrium system. Once G_M and Γ_β (β = L,R) are available, the transmission for coherent transport can be calculated as follows:[565,575]

$$T(\varepsilon) = Tr(\Gamma_L G \Gamma_R G^\dagger) \tag{58}$$

which is valid for being used in the Landauer formula to calculate the current flow, that is

$$I = \frac{2e}{h}\int Tr(\Gamma_L G \Gamma_R G^\dagger)[f_L(\varepsilon) - f_R(\varepsilon)]\, d\varepsilon \tag{59}$$

We have presented an overview on how to calculate the charger transport characteristics of molecular junctions using the NEGF formalism. The next task is to implement them into actual systems. The key work is to calculate the transmission coefficient, which relates to the number of propagating waves and corresponding conduction channels. To derive the transmission coefficient function, reasonable schemes should be constructed for calculating the self-energy matrix, which includes the calculations of the contact matrixes τ_β (β = L,R) and the Green functions of the electrode. The "extended molecule" is artificially constructed to reduce the molecule−electrode interactions τ_β from semi-infinite dimensions to tractable finite dimensions. The electrodes are treated as semi-infinite entities, and the properties of interest are calculated using the standard DFT techniques for the 3D bulk systems.[575,587] Once the contact matrix and the Green functions of the electrodes are available, the transmission spectrum can be obtained to calculate the current flow in the molecular junctions and perform a further analysis of the detailed mechanisms for the electron transport.

On the basis of the assumption that the electrodes induce an external potential localized in the scattering region, the NEGF in combination with the density functional theory works well on figuring out the details of how the electrodes affect the electron transport in molecular junctions. Xu et al. successfully demonstrated the relationship between the gate-modulated molecular levels and the current−voltage characteristics under varied gate voltages.[573] However, it should be noticed that the approximation of the electrodes with its 3D bulk form is not always adoptable. In break junction experiments, the atomic structures exist on both contact surfaces. Similar cases can be found in the STM experiments, where the atomic structures lie on the STM apex. For additional information, interested readers can review the studies listed in the references.[35]

To date, the advances in the theoretical development are substantial but are beyond the primary goal of this Review. As an outlook for this theoretical section, we want to point out that the gap between the theoretical calculations and the experimental data is decreasing for numerous relatively molecular systems. To further develop the electron transport theory, it is of critical importance to include a realistic treatment of molecules, electrodes, and atomic-scale details of the molecule−electrode interface.[588] Because of the lack of the atomic-scale detail in most experiments, the recent treatment of a range of different molecule−electrode contact geometries is an important step for a fair comparison between the theories and the experiments.[41] Furthermore, significant effort is still needed for the development of a computationally accurate theory of transport that involves a charge localization on the molecules (i.e., reduction and oxidation).[34] A key important parameter in electron transport is the transmission coefficient, which is strongly affected by the quantum interference and yields the electrical conductance, current−voltage relations, and thermopower of single-molecule devices. The symbiotic relationship between the quantum interference and the electronic structure, which is sensitive to environmental factors and can be manipulated through conformational control, polarization, or redox processes, leads to new opportunities for controlling the electrical properties of single molecules.[37] The room-temperature quantum interference in single molecules was experimentally demonstrated recently, and it is opportune to develop new strategies for exploiting the quantum interference in both the technological and the theoretical aspects. It should be noted that the goal of this theoretical tutorial is to gather a few basic concepts and mathematical tools, which emphasize the fundamentals of electron transport through molecules. We apologize to all colleagues whose work is not described in detail or cited here. Please consult the numerous excellent review articles,[35,37,38] as well as the original research articles for a complete overview of the extensive literature on the theoretical progress.

7. INTEGRATING MOLECULAR FUNCTIONALITIES INTO ELECTRICAL CIRCUITS

Undoubtedly, the substantial experimental and theoretical progress detailed above lays the foundation for both the measurement capabilities and a fundamental understanding of the various physical phenomena of molecular junctions. Despite these considerable achievements, there are still no commercially available molecular electronic devices. To satisfy the requirements for actual applications, the development of practical molecular devices with specific functions is a prerequisite. In fact, recent experimental developments have demonstrated conductance switching/modulation and rectification as well as how quantum interference effects play a critical role in the electronic properties of molecular junctions. The focus of these experiments illustrates the engineering of functionalities that are beyond conventional electronic transport properties using a rational chemical design in single-molecule junctions. In this section, we focus on reviewing the ever-developing trends of integrating molecular functionalities into electrical circuits based on single molecules (Figure 45), which were neglected in most previous reviews, including (1) wiring toward nanocircuits; (2) rectification toward diodes; (3) modulation toward transistors; (4) switching toward memory devices; and (5) transduction toward sensors. For different functions resulted from individual molecules, both molecular "cores" and molecular "tails" are equally important due to the fact that the proposed functions could be affected not only by molecular electrical characteristics but also by the electrode−molecule bonding. Therefore, in each part of this section, we will pay specific attention to the design of the molecular structures and their influence on the device functions.

DOI: 10.1021/acs.chemrev.5b00680
Chem. Rev. 2016, 116, 4318−4440

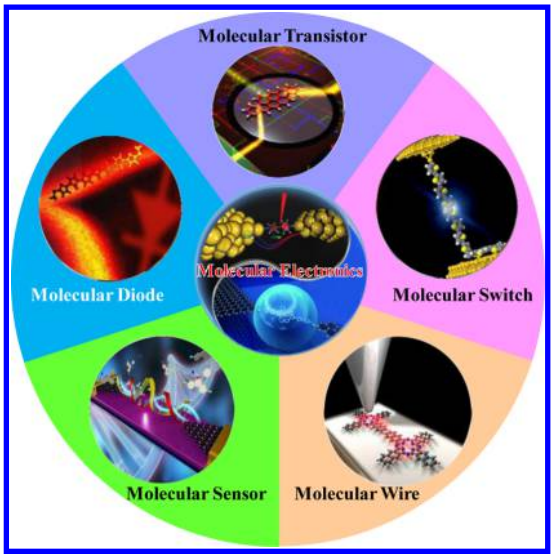

Figure 45. Schematic description of current trends in developing different types of functional molecular electronic devices.

7.1. Wiring toward Nanocircuits

Nanocircuits comprised of individual functional molecular electronic components are the ultimate goal of molecular electronics. Therefore, it is fundamentally necessary and critical to understand the role of molecular wires, which connect the electronic components to one another or to the macroscopic world, thus ensuring the efficient transport of the charge.[592] Meanwhile, molecular wires are the simplest of electrical devices and are particularly suited for the development of certain fundamental understandings and techniques required for the realization of molecule-scale electronics.[593] Thus, several studies have been established centering on the design, synthesis, and conductance measurements of molecular wires. Generally, the molecular wires used in the nanocircuits can be structurally divided into two parts: anchoring groups that connect external electrodes and molecular backbones that function as charge transport pathways.[594] The superiority of the wire can be evaluated partly by its electrical conductivity, which can be determined from the conductance measurements. However, as generally accepted, both the structure of the molecules and the nature of the electrode−molecule contact interface can affect the conductance measurement; thus, the backbones and the anchoring groups of the molecular wires are designed on the basis of the device architecture, and the electrode materials hold the same importance. It should be noted here that the term "molecular wires" has a relatively strict scope: discrete molecules rather than crystals, films, or chains of metal atoms formed through octahedral μ-bridging or flat-molecule stacking.[595]

7.1.1. Backbones as Charge Transport Pathways. Several types of molecules with different backbones have been suggested as molecular wires: (1) hydrocarbon chains, including saturated and conjugated species; (2) metal-containing compounds; (3) porphyrin arrays; (4) carbon nanotubes; and (5) biological molecules, such as DNAs. The most important requirement that these wire-shaped molecules share is electron or hole conductiveness to provide a more efficient pathway other than space for charge transport from one reservoir to the other.[593]

7.1.1.1. Hydrocarbon Chains. The continuous development of organic synthetic methodologies forms various types of molecular scaffolds with specific construction, configuration, and conformation as well as precise length to be accessible, thus providing a large wealth of probabilities to promote molecular electronics. Particularly, hydrocarbon molecules, including the saturated and conjugated species, have been prepared and explored systematically.

Saturated chains: Saturated hydrocarbon chains generally refer to the system of alkanes consisting of sp^3 C−C backbones and their terminated groups. Although these molecules are thought to possess poor conductivity due to the large gaps between their highest occupied molecular orbitals (HOMO) and lowest unoccupied molecular orbitals (LUMO), they calibrate the development of both experimental techniques and theoretical calculations.[41] As indicated by the theoretical prediction, alkane backbones have a limited degree of electron delocalization, resulting in poor conductance that decreases exponentially with the molecular length. In 2002, Wold et al.[596] measured the conductance of alkanes with different lengths and determined a quantitative result of $R = R_0 \exp(\beta L)$, where R_0 is a constant, L is the molecular length, and β is a decay constant with a value of 0.94 ± 0.06 $Å^{-1}$. In light of this formula, Solomon et al.[597] systematically compiled, compared, and discussed the conductance of such saturated chains with different lengths established in different testbeds, further verifying the general relationship of the molecular length and the conductance. Recently, various protocols and efforts were presented to improve the conductance of saturated backbones by introducing active centers into the molecular chains. For example, Wierzbinski et al. prepared dithiolated oligoethers by inserting oxygen heteroatoms into chains of alkanedithiols.[598] Although the conductance of the oligoethers was lower than that of the alkanes with the same length, the idea showed a positive inspiration. Sun et al. successfully enhanced the electrical conductivity of saturated wires by inserting ferrocene centers, which were postulated to reduce the tunneling barrier and the HOMO−LUMO gaps.[599] The conduction mechanism for these saturated molecules is considered to be electron tunneling, which can be supported by the exponential decay, characteristic current−voltage (I−V) curves, and temperature independence.[41] It can be assumed that molecules with saturated hydrocarbon backbones have limited applications as molecular wires. However, the system of saturated alkanes also provides a significant contribution to the progress of the molecular components for their initial role in establishing the theoretical and experimental models.

Conjugated chains: As compared to saturated chains, conjugated hydrocarbon chains can ensure superior charge transport by providing π-conjugated systems formed primarily by unsaturated bonds, such as double/triple carbon−carbon bonds or aromatic rings. Because of the excellent electrical conductivity and the ease of preparation, conjugated molecules have been and still are viewed as candidates for molecular wires with the most potential. By further developing the molecular electronics and synthetic methodologies, the research focus has evolved from obtaining insights into the structure−property relationship to controlling the conductance and installing multiple functions, such as switching and sensing (which are detailed elsewhere in this section), by elaborately changing the construction, configuration, and conformation of the molecular backbones. Generally, two primary types of molecular wires with conjugated hydrocarbon backbones attract the most attention: double/triple bond-dominated chains and aromatic ring-dominated chains, both of which can be achieved using

DOI: 10.1021/acs.chemrev.5b00680
Chem. Rev. 2016, 116, 4318−4440

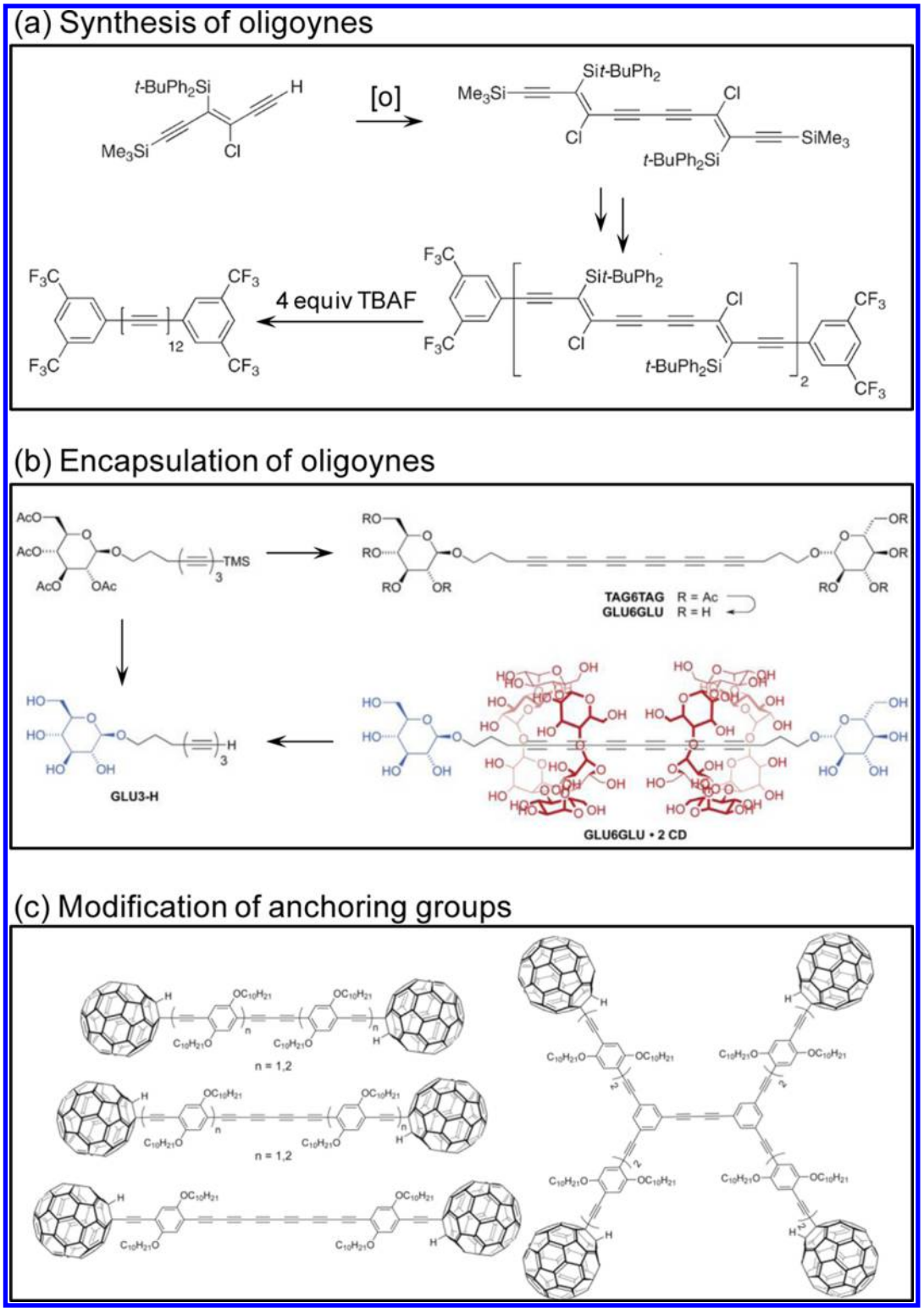

Figure 46. Examples for synthesis: (a) encapsulation (to ensure charge transport); (b) termination (to connect to electrodes); and (c) modification of oligoynes. Reproduced with permission from refs 589−591. Copyright 2008, 2015, and 2010 American Chemical Society, Royal Society of Chemistry.

mature organic and/or organometallic synthetic methods. The former includes limited types of variants, while the latter contains numerous types of derivatives due to several types of aromatic rings. In this section, only the commonly used molecules with the most general importance are covered.

Double/triple bond-dominated chains: Molecules with double/triple bond-dominated backbones are commonly known as acetylene oligomers or oligoynes, which comprise an array of sp-hybridized carbon atoms with approximately cylindrical electron delocalization along a one-dimensional, rigid-rod, length-persistent backbone.[600] Several methods have

DOI: 10.1021/acs.chemrev.5b00680
Chem. Rev. 2016, 116, 4318−4440

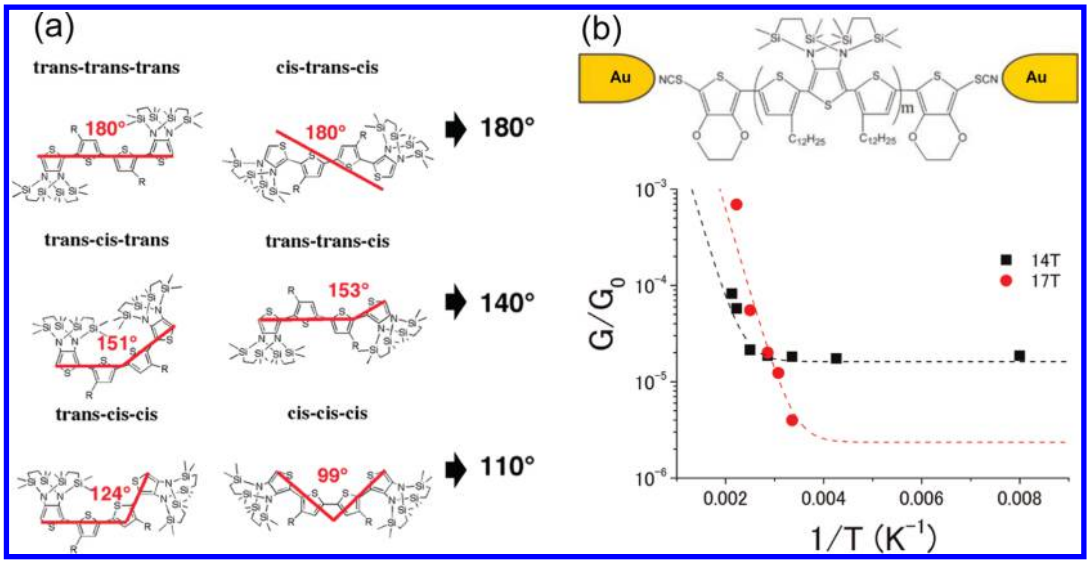

Figure 47. Conformation and conductance of OTs. (a) Six possible conformations of an *N*-silyl-substituted quaterthiophene, which were characterized by rotational variations in the thiophene rings at three thiophene−thiophene bonds. In these conformations, solid lines indicate bending angles of the quarter thiophene when coplanar conformations are assumed. These angles can reproduce the experimentally obtained angles (180°, 140°, and 110°) measured between two *N*-silyl groups. Reproduced with permission from ref 608. Copyright 2008 American Chemical Society. (b) Device structure and scaling analyses of the experimental results for the 14T-di-SCN and 17T-di-SCN oligothiophene molecules. Reproduced with permission from ref 609. Copyright 2012 American Chemical Society.

been developed to prepare the π-conjugated backbones[589,601] (Figure 46a); furthermore, to enhance the conductivity, additional synthetic protocols are being introduced to encapsulate and insulate the backbones[590] (Figure 46b) as well as techniques to modify various anchoring groups to connect with the electrodes of the molecular testbed[591,602,603] (Figure 46c).

On the basis of these efforts, Wang et al.[600] reported the electrical conductance of oligoyne-based molecular wires at the single-molecule level using STM break junctions, in which it was determined that the conductance was independent of the molecular length for the low decay constant, β, and dependent on the contact geometries between the pyridyl head groups and the gold electrodes, as detailed below. An extensive study was conducted by Moreno-Garcia et al.,[135] who conducted more experimental and theoretical efforts to obtain insights into the length and anchoring group dependence of the electrical conductance at the single-molecule level for a series of oligoyne molecular wires. These systematic studies demonstrated that the oligoynes or the acetylene oligomers are indeed an appealing type of linear molecular wire because their extensive conjugations have nearly cylindrical electron delocalization within a one-dimensional space.[600] This result may produce a higher efficiency of electron transport as compared to that of molecular wires possessing aromatic ring-dominated chains (as discussed below) because there is no rotation barrier between the adjacent conjugation units as compared to the aromatic systems.[604,605] The disadvantage of these wires, if any, is that it is contradictory to introduce other moieties with the linear configuration into the backbones, thus reducing the possibility to enrich the system.

Aromatic ring-dominated chains: Another mature conjugated molecular backbone used in the nanowiring is aromatic ring-dominated molecules, known as "oligoarylenes", which are broadly defined as a chain of aromatic rings linked by acetylene, ethylene, or other π-system units. The widely used aromatic rings include thiophene and benzene. On the basis of the types of inter-ring linkages, the thiophene-dominated chains can be classified as oligothiophene (OT) and oligo(thiophene ethylene), while the benzene-dominated chains can be classified as oligophenylene, oligo(phenylene ethylene), and oligo(phenylenevinylene).

Thiophene-dominated chains: Previous studies have demonstrated that the effective conjugation length of the oligothiophenes is ~20 thiophene units in the neutral state and ~30 units in the oxidized state.[593] This fact, along with their thermal stability and superior electronic properties, inspired many interests in the synthesis, characterization, and optimization of the oligothiophenes because of their potential application in molecular electronics. A large number of synthetic methods have been developed for precisely controlling the molecular length,[606,607] which is fundamentally required by electronic circuits. In addition to length control, the structural and conformational determination of the α-connected thiophene oligomers at the single-molecule level are of significant importance for distinguishing two conformations induced by the rotational flexibility: *s-trans* and *s-cis*. The latter, with a torsional angle of approximately 145° between adjacent thiophenes and an approximately 0.5 kcal/mol energy barrier, is more stable as compared to the former form with an angle of approximately 47° and a barrier of 2 kcal/mol. However, it proved to be challenging to characterize the conformation using conventional methods, such as NMR and X-ray scattering. To solve the problem, in 2008 Nishiyama et al. directly identified straight and all-*s-trans* chains using the STM imaging technique (Figure 47a).[608] This research laid the foundation for constructing molecular junctions on the basis of individual oligothiophenes, thus paving the way to systematically studying their electronic properties. For example, Lee et al. observed a universal temperature crossover behavior of the electrical conductance in a single oligothiophene wire in 2012.[609] They proposed that the competition between the two transport mechanisms (superexchange and TIH processes, which are detailed below) depends not only on the wire length but also

DOI: 10.1021/acs.chemrev.5b00680
Chem. Rev. 2016, 116, 4318−4440

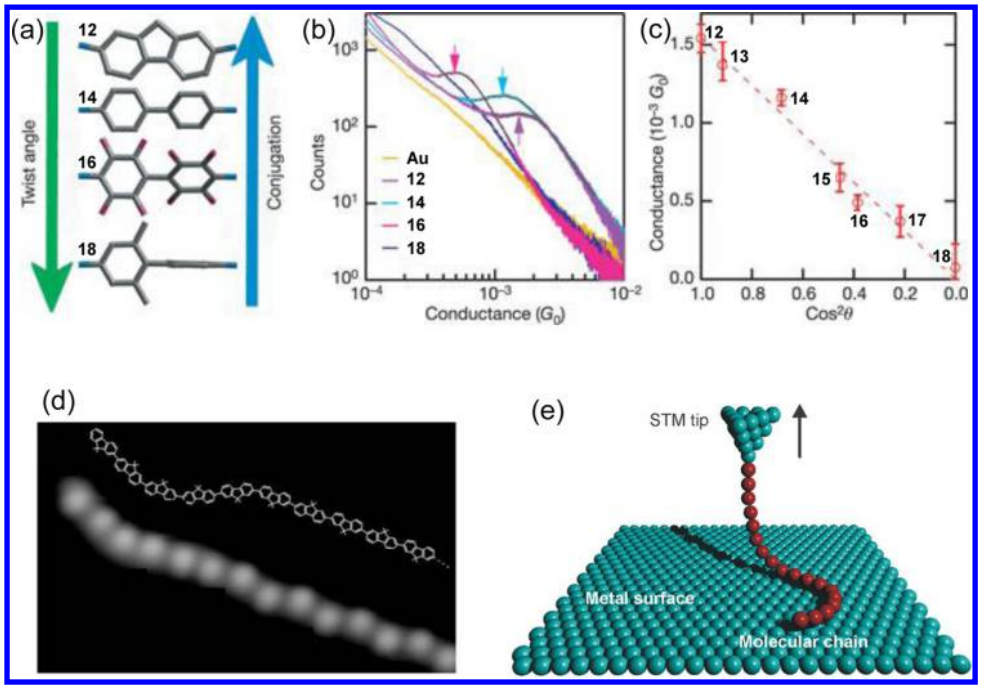

Figure 48. Structure−conductance relationship. (a) Structures of a subset of the biphenyl series studied, which are shown in order of increasing twist angle or decreasing conjugation. (b) Conductance histograms obtained from measurements using molecule 12 (purple), 14 (cyan), 16 (pink), and 18 (blue). Additionally, the control histogram obtained from the measurements is depicted without molecules between the contacts (yellow). The arrows denote the peak conductance values obtained from the Lorentzian fits (solid black curves). (c) Position of the peaks for all of the molecules studied plotted against $\cos^2\theta$, where θ is the calculated twist angle for each molecule. Reproduced with permission from ref 106. Copyright 2006 Nature Publishing Group. (d) STM image of a single oligofluorene chain. (e) Conductance measurement of single oligofluorene molecules in the STM setup, which can explore the relationship between the molecular length and the conductance. Reproduced with permission from ref 613. Copyright 2009 AAAS.

on the temperature (Figure 47b). To enhance the electronic transport property of the oligothiophenes, Endou et al. reported a strategy to completely encapsulate the oligothiophenes to prevent intermolecular electronic communication.[610] Using the STM technique, they determined the decay constant β of electronically neutral oligothiophene chains to have an estimated value of 1.9 nm^{-1}. As compared to oligothiophenes, oligo(thiophene ethynylene) (OTE) and oligo(thiophene vinylene) (OTV) can be viewed as their derivatives, where the thiophene units are connected by acetylene and vinylene instead of single C−C bonds. Both of the oligomers hold features similar to oligothiophenes: long effective conjugation and high stability in various oxidation states. Recently, additional methods have been developed to introduce heterostructures into the oligomer's backbones to realize specific functions beyond the electronic transport, which is discussed later.

Benzene-dominated chains: Benzene-dominated oligomers, including oligophenylene (OP), oligo(phenylene ethylene) (OPE), and oligo(phenylenevinylene) (OPV), all, similar to the thiophene-dominated ones, possess a large degree of electron delocalization to function as molecular wires. Furthermore, due to the structural symmetry, there are less conformational issues to be considered in the synthesis or characterization process, thus leading to additional development in this field.

On the basis of mature synthetic methods,[611,612] oligophenylene molecules consisting of a chain of benzenes linked by C−C bonds can be synthesized and diversified by introducing special moieties. Because of their easy preparation, oligophenylenes were thoroughly investigated as molecular wires. As early as the year 2002,[596] individual oligophenylene molecules with different lengths have been integrated into the nanogap in the CP-AFM setup to explore the length−conductance relationship. In the following year, another study achieved the systematical conductance values of these molecules.[597] Benefiting from the convenience of side group substitution on the benzene ring, a relationship can be established between the conductance and the molecular conformation, which has been demonstrated by Venkataraman et al. in 2006 (Figure 48a).[106] This study demonstrates that to reduce the twist angle between the two benzene rings to zero, two respective but adjacent α-sites were fixed, which was equal to introducing a fluorene unit. They determined that the conductance for the series decreases with an increasing twist angle, which is consistent with the cosine-squared relationship predicted for the transport through p-conjugated biphenyl systems (Figure 48b,c). Maximizing the ratio of the fluorene units in the oligophenylene chains formed the molecular basis of two studies performed in 2009 and 2011 (Figure 48d). The former used single oligofluorene molecules to explore the relationship between the conductance and the molecular length by changing the tip−substrate height in the STM setup (Figure 48e),[613] while the latter appended C_{60} terminal groups to the oligofluorene molecules, thus leading to the unambiguous formation of STM-based single-molecule junctions.[85]

Oligo(phenylene ethylene)s (OPEs) are another benzene-dominated oligomer, whose backbones are formed by linking acetylene with benzene. These molecules have been systematically explored by Tour et al. on the basis of the iterative divergent/convergent methods developed at the beginning of this century.[614] Because of the ease of self-assembly, it is

DOI: 10.1021/acs.chemrev.5b00680
Chem. Rev. 2016, 116, 4318−4440

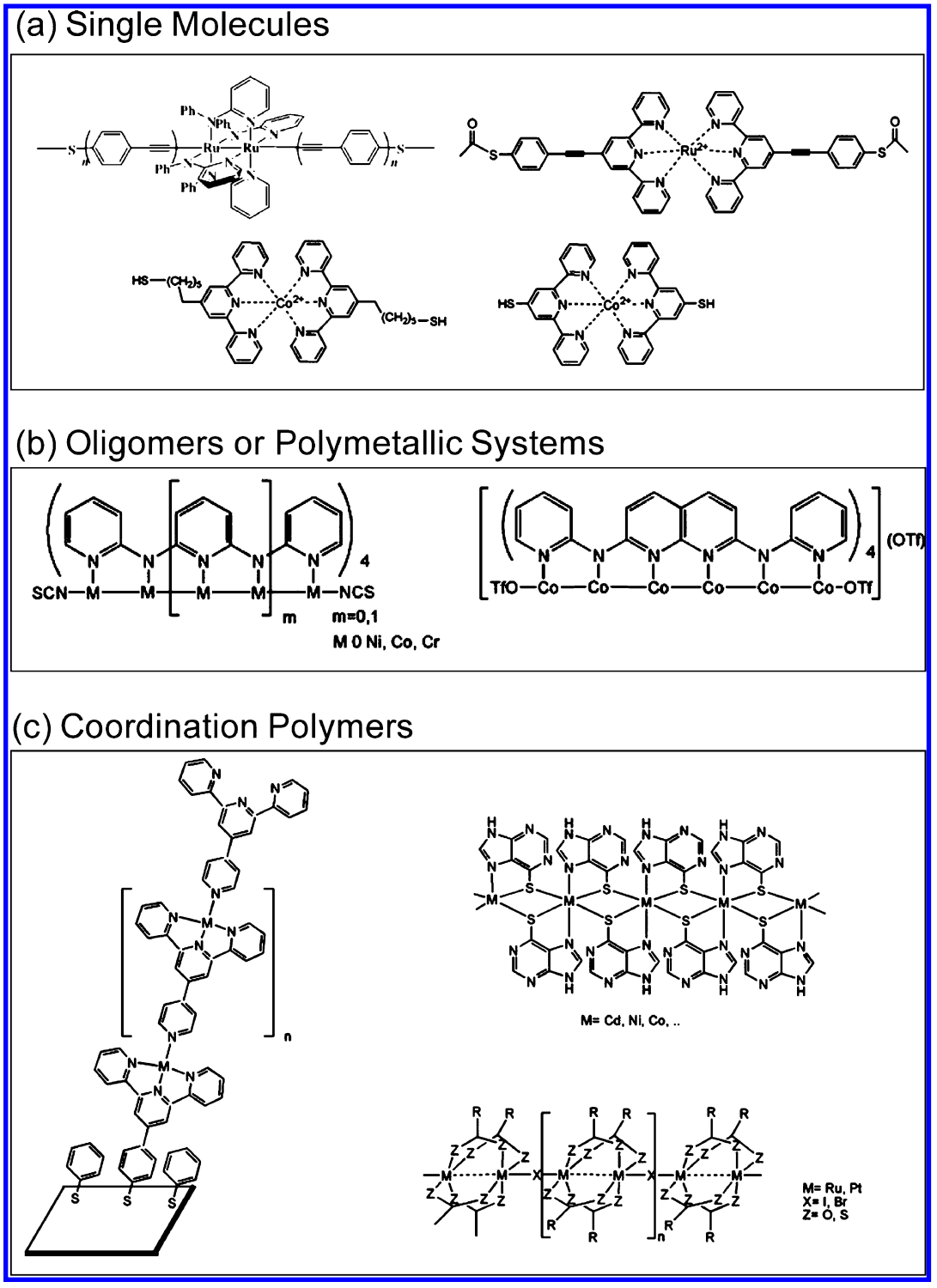

Figure 49. Representative organometallic compounds as prototypes of molecular electronic wires. Reproduced with permission from ref 632. Copyright 2009 Wiley-VCH.

feasible to measure the conductance of these wire-shape molecules, which was performed using an STM in 2003[615] and a CP-AFM in 2004.[616] Interestingly, Donhauser et al. determined the conductance switching behavior of single OPE molecules isolated in matrixes of alkanethiolate monolayers, which may result from conformational changes in the molecules.[485] In another systematical study,[617−619] the relationship between the molecular conformation and the conductance was established, where the authors carefully introduced specially designed moieties with different dihedral angles into the oligomer chains to vary the conformation of the molecules. Both the experimental and the theoretical results suggested that the conductance of the OPE molecular junctions could be tuned by controlling their intramolecular conformation, which was consistent with a cosine-squared relationship, as reported by Venkataraman et al.[106] Remarkably, Kaliginedi et al.[618] determined that the introduction of a cross-conjugated anthraquinone central unit resulted in lower conductance

DOI: 10.1021/acs.chemrev.5b00680
Chem. Rev. 2016, 116, 4318−4440

values. This observation may be attributed to a destructive quantum interference phenomenon. To enhance the one-dimensional conductivity of the OPE molecules, the oligomer's backbones could be isolated using a polyrotaxane protective sheath[620] or encapsulated by dendrimer shells.[621,622] To install new functionalities, other moieties can also be inserted into the backbones of the OPE molecules, for example, the rectification effect caused by the 9-[di(4-pyridyl)methylene]fluorene insertion[87] and switching caused by the tetrathiafulvalene insertion.[623,624]

Replacing ethylene with vinylene in the OPE backbones leads to oligophenylenevinylene (OPV) molecules.[625,626] It is predicted that the conductance of the OPV and its derivatives is higher than that of the OPE. Because the degree of disrupting the conjugation of the backbone using a longer vinyl bond (C═C length ca. 1.35 Å) in the OPV is less as compared to using a shorter ethynyl linkage (C≡C length ca. 1.22 Å) in the OPE, there is less bond alternation and a smaller HOMO−LUMO gap in the OPV than that in the OPE.[600] The exact conductance value was measured and estimated in two studies in 2003,[597,615] whereas the charge transport mechanisms were discussed in detail in another two studies.[627,628] It is evident that there are different configurations for the existence of the vinyl bond. In fact, Martin et al. elucidated the effects of *E*/*Z* isomerizations on the conductance of such molecules at the single-molecule level using the STM technique.[629] They demonstrated that the isomerization led to significant changes in the electrical conductance of these molecules, with the *Z* isomer exhibiting a higher conductance than that of the *E* isomer. Using the method of controlled aryl imine addition chemistry, Choi et al.[392] prepared oligophenyleneimine (OPI) wires with different lengths (Figure 38) and studied the role of molecular length and bond architecture on the molecular conductivity. The theoretically predicted change in the direct-current (DC) transport from tunneling to hopping was observed as a function of the systematically controlled wire length (Figure 38). The transition occurred near 4 nm. As a systematic extension, in 2010, oligonaphthalenefluoreneimine (ONI) molecular wires were developed by assembling larger conjugated molecular building blocks based on naphthalene dialdehydes and fluorene diamines into the OPI backbones.[451] A consistent transition in the DC transport from tunneling to hopping was observed near 4 nm. These nanoscale transport measurements elucidated the role of the molecular length and the bond architecture on the molecular conductivity and led to opportunities for a greater understanding of the electrical transport in conjugated polymer films.

As indicated above, we discussed several types of conjugated hydrocarbon molecules in the context of molecular wires. The accessibility of various types of molecular scaffolds makes it possible for wire-shaped molecules to be synthesized and modified with a large degree of precise controllability of construction, configuration, and conformation. Furthermore, due to the development of efficient strategies to introduce heteromoieties, for example, anchoring groups and functional centers, in specific positions of the chains, additional individual molecules could be connected into the nanogaps between the external electrodes to conduct current and/or function as, for example, switches or rectifiers. We believe that the conjugated hydrocarbon molecules will have additional contributions to the improvements in the molecular wires.

7.1.1.2. Metal-Containing Compounds. Recently, significant progress has been made in using tailored carbon-rich organometallic compounds as prototypes for molecular electrical wires because these molecules may have the potential to be more conductive than their all-carbon counterparts.[630] Furthermore, an optimal match in orbital energies can be achieved more readily to yield compounds with smaller HOMO−LUMO gaps by structurally engineering the metal unit together with carbon-rich bridges. This molecular engineering will endow a superior conductivity to the prototype wires.[631] In this section, we review the development and progress of organometallic compound-based molecular wires, which can be classified into three types: small molecules, coordination oligomers, and polymetallic systems (Figure 49).[632] It should be noted that in literature surveys, a large number of studies focus on systems of unsaturated carbons capped with two metal moieties. These systems are not in the scope of this Review, although they also contain metal, because they were initially developed for charge transfer rate studies instead of direct conductance measurements.

Single molecules or oligomers: Although the study performed by Mayor et al.[633] in 2002 appeared to decrease the conductivity of wire-shaped molecules, which was contrary to the trend of increasing the conductivity, it deserved to be highlighted for its pioneering exploration in the process of direct conductance measurements using the MCBJ technique. In this study, the authors designed a molecular insulator based on *trans*-acetylene-platinum(II) complexes, for which the platinum−acetylene bond had hardly any π character and separated the molecular rod into two independent conjugated systems to increase its resistance. The key progress in the chemical synthesis provided access for the preparation of the σ-alkynyl compounds of $Ru_2(LL)_4(C_{2n}Y)_2$ (LL is an *N*,*N*′-bidentate bridging ligand and Y is an anchoring group), which were wire-shaped molecules containing double ruthenium centers used as building blocks in molecular electronics.[631] The development of the corresponding optical and electrochemical characterizations provided the possibility of clarifying the electronic structure and the redox characteristics of such molecules. All of these studies led to their application as molecular wires as well as more sophisticated molecular switches that are described below in detail.

Using the STM break junctions, the potential of the metal−alkynyl compounds as molecular wires was first discovered using $Ru_2(ap)_4$(σ-OPE) (ap: 2-anilinopyridinate) molecules as a representative.[631] The same results were also observed by Wen et al.,[149] who established conductance measurements of different organometallic wires with two ruthenium(II) centers bridged by 1,3-butadiyne based on an electrochemically assisted-mechanically controllable break junction approach. It was determined that the single-molecular conductance of these diruthenium(II) incorporated systems was significantly higher than that of the OPEs with comparable lengths. This result may be ascribed to a better energy match of the Fermi level of gold electrodes with a molecular HOMO. In 2008, another series of compounds belonging to the metal−alkynyl molecular set, *trans*-$Ru_2(ap)_4((C{\equiv}CC_6H_4)_2S-)_n$ (n = 1 or 2), were integrated into the molecular junctions, and the hysteresis effects that occurred during voltage sweeping in different directions were discovered.[634]

From 2007 to 2011, Rigaut and Frisbie et al. systematically developed and extended a series of redox-active conjugated organometallic wires, which consisted of covalently coupled ruthenium(II) bis(σ-arylacetylide) complexes.[445,635,636] The most important feature of this type of organometallic molecule

DOI: 10.1021/acs.chemrev.5b00680
Chem. Rev. 2016, 116, 4318−4440

is its precise length controllability during the synthetic process, leading to the production of Ru1−Ru3 compounds with a length ranging from 2.4−4.9 nm. The authors used this advantage to thoroughly investigate the length dependence of the molecular conductance under different temperatures, which facilitated the clarification of two general electron transport mechanisms: direct tunneling and thermally activated hopping.

One common characteristic of the above-discussed molecules is that they all contain ruthenium, which forms an important branch of the organometallic molecular wires. Additionally, Albrecht and Chen et al. developed another class of Os(II)/(III)- and Co(II)/(III)-complexes (Figure 49a,b),[637,638] which were robust and conductive for functioning as molecular wires. The former, Os-complexes $[Os(bpy)_2(p2p)_2]^{2+/3+}$ and $[Os(bpy)_2(p0p)Cl]^{+/2+}$, are still new to being used in molecular electronics, while the latter, Co-complexes, have been explored in several studies. For example, Guo et al. connected terpyridyl-containing molecules to both sides of either the SWNT or the graphene electrodes using amide bonds and then added Co^{2+} into the system to form Co-complexes.[30,31] It should be noted that the covalent connection provided enough robustness to the interfacial linkage, leading to a good reliability for investigating the electrical conductance of the organometallic molecules as well as the corresponding coordination reaction at the single-molecule level. In two additional studies,[21,275] Park and Tang incorporated the Co-complexes into nanogapped metal electrodes to study how electrons were transported through the well-defined charge states of a single atom. It was determined that changing the length of the insulating linkages altered the coupling of the metal ion to the electrodes so that interesting single-electron phenomena, such as the Coulomb blockade and the Kondo effect, were observed.

Coordination polymers: The combination of Co ions and terpyridyl-related ligands inspires the idea that through the suitable selection of molecular building blocks, organometallic polymer architectures, which are defined as coordination polymers in Figure 49c, can be prepared. In fact, the coordination polymers are infinite aggregates of metal ions or fragments bridged by ligands. These aggregates can self-assemble by coordinate bonding into one, two, or three dimensions, thus producing a wide variety of supramolecular structures.[639] The study conducted by Cao et al.[373] involved the ideology of constructing prototypes of coordination polymers, in which the terpyridyl-related ligands were initially linked to both sides of the graphene electrodes followed by the addition of cobalt ions and hexapyridyl sequentially (Figure 33). The apparent current flowing through the metallic molecules reflected both the conductivity of such molecular wires and the feasibility of molecular self-incorporation. Additionally, this strategy also allows the in situ construction of complex molecular wires through the implementation of programmable reactions, as discussed previously. In 2009, Tuccitto et al. prepared a coordination polymer as long as 40 nm by incorporating a large number of cobalt centers into rigid molecular backbones comprising terpyridyl-based ligands via a sequential stepwise coordination.[640] The remarkable mechanical robustness, length-independent conductance, and easy-to-assemble characteristics led to a new generation of molecular wires.

7.1.1.3. Porphyrin Arrays. Porphyrin, a square planar 18π aromatic macrocycle that possesses four pyrroles and four methine carbons, has been extensively studied in a wide range of research disciplines due to its tremendously advantageous properties, such as structural robustness, attractive optical properties, strong aromaticity, and rich metal coordination chemistry.[593,641−643] Particularly, the HOMO and the LUMO of the conjugated porphyrin arrays are generally only separated by 2 eV. If this gap is slightly narrowed, the molecules would have useful electrical properties required for molecular wires.[644] Another important advantage in using porphyrin arrays as molecular wires is the large size of the monomeric unit, which is ∼16 Å. Therefore, the linear tetramers have a span of ∼56 Å. This size is large enough to bridge the nanogap in a molecular junction. In addition to these features, the porphyrin electronic system is susceptible to a conjugative perturbation at the periphery and metal chelation, thus allowing a rational electronic modulation that can build systems displaying tunable optical and electronic properties. Consequently, the conjugated porphyrin arrays can be considered as promising candidates for molecular wires in future molecular electronics applications.

In the last two decades, a wide variety of conjugated porphyrin arrays have been synthesized and explored. Their synthetic chemistry can be found in detail in several previous reviews.[645−648] There are two methods used for linking large individual porphyrin rings together (Figure 50). The first

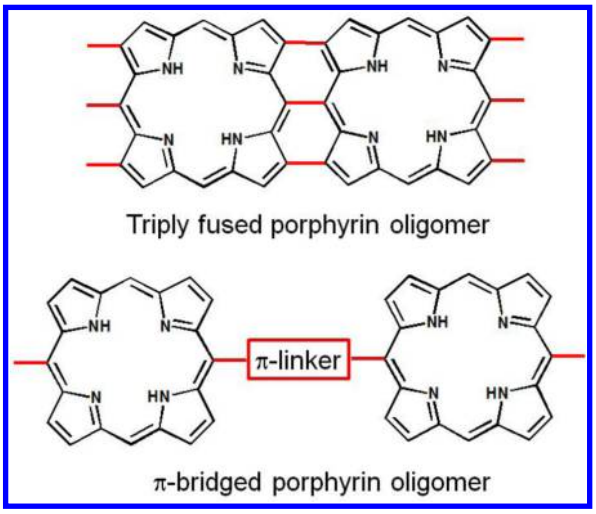

Figure 50. Two representative types of conjugated porphyrin wires. Reproduced with permission from ref 645. Copyright 2015 Royal Society of Chemistry.

method is to fuse porphyrins with multiple direct bonds; that is, each porphyrin structure is directly linked to the next. Generally, the fused porphyrins were synthesized through the oxidation of metallo-porphyrins with tris(4-bromophenyl) aluminum hexachloroantimonate, where the two porphyrin units are doubly or triply linked through the ring carbon atoms. This forces a coplanar geometry that should be favorable for the electronic π conjugation, thus displaying remarkable photophysical properties, such as extremely red-shifted absorption profiles that reach the IR region, large two-photon-absorption cross-section values, and drastically reduced charge-transport attenuation factors. As compared to the doubly fused diporphyrins, the triply linked diporphyrin structures indicated greater conjugation, which is likely due to more planar geometries, thus leading to a better π-overlap (Figure 50). Furthermore, stronger electronic interactions and smaller optical HOMO−LUMO gaps (1.14−1.33 eV) were demonstrated. In addition to the doubly/triply fused porphyrins, new

DOI: 10.1021/acs.chemrev.5b00680
Chem. Rev. 2016, 116, 4318−4440

conjugated arrays of porphyrinoids have been developed, including directly linked corrole oligomers, hybrid tapes of porphyrin and rectangular hexaphyrins, and subporphyrin dimers. The second method is to bridge the porphyrins with a π-linker, such as ethyne and ethene, which has been conducted in a controlled manner using classical organic reactions or transition metal-catalyzed reactions. The electronic interaction depends highly on the nature of the linker, bridging position, and geometric relationship of the functionalized porphyrins. For example, it was determined that porphyrin oligomers could behave similar to photonic molecular wires, which absorbed light at one end of an array of porphyrins and then emitted a different photon at the other end. These results strongly highlight the necessity for the further exploration of the conjugated porphyrinoids.

Most of the reported studies are based on large areas of the SAMs for porphyrinoids, where minimal molecular or nanoscale level measurements have been performed. Recently, single-molecule conductance measurements of porphyrin-based molecular wires were demonstrated using an STM break-junction technique.[459,462,649] In this system, the molecular conductance, σ_M, generally decreased exponentially with the molecular length, as quantified by the attenuation factor, β, which is a useful measure of the ability to mediate long-range charge transportation. It was determined that the β value of butadiyne-bridged porphyrin wires with terminal thioacetate anchors was 0.04, which is significantly lower than those of typical organic molecules (0.1−0.6). As compared to the butadiyne-bridged arrays (β = 0.04) and the *meso*−*meso* linked arrays (β = 0.11), the fused porphyrin arrays indicated an exceptionally weak attenuation nature (β = 0.02). Similar to the butadiyne-bridged arrays, the ethyne-bridged porphyrin wires bearing terminal thiophenol anchor groups indicated β values of 0.03. Although current practical and technological limitations confine the fabrication of molecular junctions formed from these conjugated porphyrin arrays, the remarkable features of the conjugated porphyrin arrays, as detailed above, receive considerable attention and can lead to significant scientific breakthroughs in the near future.

7.1.1.4. Carbon Nanotubes. In section 4.2, we demonstrated the potential of carbon nanotubes (CNTs) to be used as point contacts for forming molecular electronic devices. In fact, CNTs themselves are macromolecular systems with unique physical and chemical properties. A CNT can be defined as being formed by rolling a piece of graphene to create a seamless cylinder. Depending on their chirality and diameter, they can be metallic or semiconducting.[340,463,650] Another key feature of the CNTs is that all chemical bonds are satisfied and strong, leading to extremely high mechanical, thermal, and chemical stability. Furthermore, the small diameter and the long length of single-walled carbon nanotubes (SWNTs) lead to large aspect ratios and suggest the possibility of ballistic devices with drastically reduced carrier scattering, thus making them nearly ideal one-dimensional molecular wire systems.

There are four primary approaches to produce carbon nanotubes: (1) arc discharge; (2) chemical vapor deposition (CVD) over metal catalysts; (3) laser ablation; and (4) electrolysis using graphite electrodes immersed in molten ionic salts.[651] The ample availability, unique electrical properties, and mechanical rigidity associated with the carbon nanotubes lead to the construction of a device that indicates one possible method in which integrated molecular electronics can operate.[652,653] In 2000, Rueckes et al. developed a concept for molecular electronics using carbon nanotubes as both molecular device elements and molecular wires for information reading and writing (Figure 51a).[654] Each point on the array

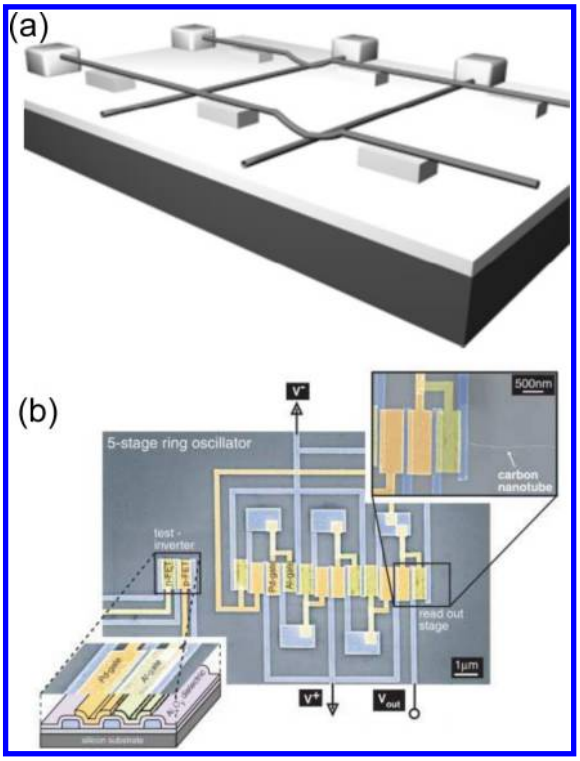

Figure 51. Carbon nanotube device architectures. (a) 3D view of a suspended cross bar array of carbon nanotubes, which indicates four junctions with two elements in the ON (contact) state and two elements in the OFF (separated) state. Reproduced with permission from ref 654. Copyright 2000 AAAS. (b) SEM image of a SWCNT ring oscillator consisting of five CMOS inverter stages. A test inverter was added to determine the parameter set for the actual measurement. Reproduced with permission from ref 655. Copyright 2006 AAAS.

where two nanotubes cross represents a device element that can be switched between two positions. The OFF state is used when the two SWNTs are separated by the gap created by the supports, and the resistance between the two separated wires is high. The transient charging of the nanotubes produces an attractive force, which causes them to move so that they are touching, leading to a higher conductivity between the wires and an ON state. The advantage of this approach is that the device elements are naturally addressable by the carbon nanotube molecular wires in large arrays. These reversible, bistable device elements can be used to construct nonvolatile random access memory and logic function tables at an integration level approaching 10^{12} elements per square centimeter and an element operation frequency in excess of 100 gigahertz. This concept is important because it identified a method where a few of the requirements concerning the integration of wires into addressable devices could be achieved.

For practical applications, an important next step would be the construction of integrated circuits along a single SWNT. This has been demonstrated by the study performed by Chen et al. in 2006,[655] where a CMOS-type 5-stage ring oscillator was built entirely on one 18 mm-long SWNT (Figure 51b). The polarities of the FETs were controlled using metals with different work functions as the gates, and Pd was selected as the

DOI: 10.1021/acs.chemrev.5b00680
Chem. Rev. 2016, 116, 4318−4440

metal gate for the p-FET while Al was selected for the n-FET. The key feature of this design is that the distinct difference in the work functions of these two metals effectively shifts the SWNT FET characteristics to form a p/n-FET pair. By arranging five pairs (10 FETs) side-by-side on one SWNT, a ring oscillator circuit with a frequency reaching 52 MHz could be achieved. Another breakthrough study performed by Shulaker et al. demonstrated the first computer built entirely using CNT array-based transistors.[656] The CNT computer was able to run an operating system that was capable of multitasking. To demonstrate the generality of the CNT computer, they implemented 20 different instructions from the commercial MIPS instruction set. This is a significant development because it confirms that CNT FET-based circuits are a feasible and plausible emerging technology. However, the significant challenges are clearly the current inability to selectively and cleanly synthesize particular nanotubes with a specific diameter and chirality as well as the lack of sites for further functionalization. This result makes constructing electronics from nanotubes difficult because there is no control over the electrical properties. Fortunately, recent remarkable developments have been achieved to realize the controllable growth of chirality-specific individual SWNTs using solid alloy catalysts,[657] temperature control and cloning,[658] or high-density SWNT arrays using Trojan catalysts,[659] thus promising a bright future for CNT-based nano-/molecular electronics.

7.1.1.5. Biological Wires. Although synthetic methodologies are steadily being used for realizing various types of artificial molecular scaffolds, which accommodate the specific requirements that are necessary for molecular electronics, considerable attention is being given to nature, that is, producing numerous unbelievable structures through time accumulation and survival of the fittest to determine the best candidates for the most convenient accessibility and low-cost applications. In the following section, we discuss the feasibility and superiority of using biological molecules, such as DNA and carotene, as molecular wires.

DNA is the carrier of genetic information and is of crucial importance in the continuation of life and of great interest as a functional nanosized material due to its unique features, which possesses the ability of self-assembling base pairs, that is, adenine with thymine and guanine with cytosine, using hydrogen bonds with extreme complementarity and veracity. Importantly, the hydrogen-bonded base pairs parallel stack with the face-to-face mode, which implies that the DNA should be electrically conductive over significant distances. In fact, the use of DNA as molecular wires has been explored for decades, and the answer to the question whether single DNA can conduct an electrical current remains uncertain.[660] However, it should be noted that the controversy may stem from the differences in the measured samples (e.g., base sequences, structure of DNA) or the measurement environments and methods. By developing advanced testing methods and systems along with an improved controllability for subtle and uniform testing conditions to study the DNA conductivity, it is imperative to evaluate the conductance of such one-dimensional biopolymers.

On the basis of previous studies, the intrinsic conductivity of DNAs can be affected by their length, base-pair related sequence, and conformation types, including Z, A, and B forms. In addition to these factors, single DNA conductance measurements are also influenced by the contact nature, temperature, and testing medium. Several early studies on the length dependence of the DNA conductivity consistently concluded that electrical transport was feasible in short DNA molecules and blocked in long single molecules.[661−663] The sequence-dependent conductance is also a hot point in the field. Generally, DNA can be classified as homogeneous-sequence and complex-sequence. The former refers to DNAs with poly(G)-poly(C) or poly(A)-poly(T) base pairs, among which G−C-based sequences have been demonstrated to be more conductive.[664,665] The latter can be defined as arbitrary base pair-based DNAs, where considerable attention has been given to the phenomenon of single-nucleotide polymorphisms (SNPs). Tao et al. in 2005[666] and Guo et al. in 2008[356] promoted the fundamental understanding of the relationship between the conductance and the SNP, both of which observed that well-matched DNAs were more conductive than those with mismatched base pairs. In addition to length and sequence, DNA configurations or DNA structure types also have important effects on its conductance, which have been comprehensively discussed by Kawai et al. in 2006.[660] In addition to the common types (Z, A, and B forms), G-quadruplex structures formed by single-strand DNAs with certain guanine-rich bases were also investigated, thus providing higher conductance.

As mentioned previously, the DNA conductance acquired by different methods varies in the insulator, semiconductor, or conductor regimes primarily due to the differences in the samples. However, testing conditions may result in discrepancies in various measurement systems, such as temperature and medium, which may be an important aspect in inducing the inconsistency. For example, Zalinge et al. systematically explored the effects of temperature on the conductance of different homogeneous-sequence DNAs, in which the $I-V$ curve did not indicate (within experimental error) any dependence of the DNA conductance on the temperature. This result is contrary to the observation of long homogeneous-base sequence DNAs in a vacuum.[667] The authors analyzed that such differences indicated that the medium had a significant influence on the temperature dependence of the DNA conductance. In fact, the importance of the medium, such as the concentration of the countercation and the relative humidity, could affect the structure types of the DNA as well as the conductance measurement.

The possibility of transporting charge carriers along short single DNA molecules has been verified by further evidence from direct electrical transport measurements,[358] but the conductivity is relatively poor. The transport through long single DNA molecules (>40 nm) is evidently blocked. Therefore, suitable strategies are needed to enhance the conductivity of the DNA if they are going to be used as molecular wires in electrical circuits or as a model system for studying electrical transport in a single one-dimensional molecular wire. Generally, there are two primary approaches for improving the DNA conductivity. The first is to use more exotic structures, such as DNA quadruple helices, instead of double-stranded structures, which may offer an improved stiffness and electronic overlap to potentially enhance the conductivity of these molecules. This proposal has been demonstrated by Erbe et al. in 2010[361] and Guo et al. in 2011.[668] The second approach is to dope DNAs through the addition of intercalators or metal ions. To verify this technique, in 2012, Liu et al.[357] provided direct evidence that it was possible to enhance the electrical conductance of DNA using a rational arrangement of multiple metal ions inside the core of the DNA base-pair stack. These results demonstrated that DNA

DOI: 10.1021/acs.chemrev.5b00680
Chem. Rev. 2016, 116, 4318−4440

molecules bridging nanodevices could serve as an effective mediator for charge transport, thus introducing a new scientific research field that interfaces molecular nanodevices with biological systems.

Carotene is a prototypical natural molecular conductor with a large delocalized π-electron system produced from electronic states that are delocalized over a chain of approximately 20 carbon atoms connected by alternative single/double bonds. The efficiency of this natural molecule in photoinduced electron transfer as donors as well as the importance of its role in photosynthesis as electron shuttles reflect its considerable potential to be used as molecular wires.[669] In fact, there have been several direct conductance measurements demonstrating the high conductivity of carotene and its derivatives. As early as 1999, Leatherman et al. embedded carotenoid molecules in insulating *n*-alkanethiol SAMs and measured the single-molecule electrical properties using the CP-AFM. It was determined that the conductance of these natural molecules was over a million times higher than that of an alkane chain of similar length.[670] An improvement for forming through-bond electrical contacts, Lindsay et al. tethered an Au nanoparticle to each molecule via the protruding thiol group and observed a more recognizable single-molecule conductance of carotene in the matrix of the docosanethiol monolayer, which again stressed the possibility of using carotene as nanowires.[671] However, one of the most important issues in the carotene conductance measurements at the single-molecule level is to distinguish whether the current is through one or more molecule. To solve this problem, Tao et al. introduced a new method for single-molecule measurements based on repeated STM break junctions, which was easier to use for various molecule lengths and yielded better data in comparison with the CP-AFM approach.[52] On the basis of this method, Lindsay et al. tested a series of homologous carotenoid molecules with different lengths and obtained a corresponding electronic decay constant, $\beta = 0.22 \pm 0.04$ Å^{-1}, in close agreement with the value obtained from the first-principles simulations ($\beta = 0.22 \pm 0.01$ Å^{-1}).[672] By incorporating different polar aromatic substituents, Koo and Lindsay et al. demonstrated the capability of modulating the conductance of various carotenoid wires.[673,674]

Recently, Lindsay et al. determined that the conductance of carotenoid molecules could be enhanced by oxidization through direct measurements at the single-molecule level under the potential control of a membrane-mimicking environment.[675] In view of the requirements for molecular wires, the stability in the electrical conduction is necessary to operate the molecular device. However, the antioxidant activities of the carotenoid molecules in quenching singlet oxygen and scavenging reactive radical species lead to apparent instability. Inspired by the natural prevention of free radical-mediated carotenoid degradation or the repair of semioxidized carotenoid molecules via vitamin E, Koo et al.[674] devised novel carotenoid wires to provide a labile conjugated polyene chain with stability as well as a range of conductance by attaching aromatic phenyl groups containing the *para*-substituent X (OMe, Me, H, and Br) of diverse electronic natures to the polyene chain at C-13 and C-13′. The origin of this stability can be expected from the repulsive steric interactions between the phenyl substituents with attacking nucleophiles and/or the reversible trapping of incoming radicals (e.g., reactive oxygen species) that would cause fragmentations of the conjugate polyene chain.

7.1.2. Conductance of Single Molecules. To function as conductive wires, a material should have the ability to transport electrical current with minimal resistance. However, unlike bulk materials, the conductance of single molecules is a complicated issue because it is highly related not only to the intrinsic molecular structures but also to the details of connecting and communicating with the external world.[53] Generally, conductance can be defined as $G = I/V$, and it is an important property describing the efficiency of electron transport in bulk materials. Similarly, in addition to this definition, the conductance of single molecules is proportional to the transmission probability of electrons from one electrode (L) to another (R) and can be described as follows (also see eq 27):[676]

$$G = \frac{2e^2}{h}T \tag{60}$$

where e is the electron charge; h is Planck's constant; and T is the total transmission probability over all possible transmission channels. It should be noted that T is related to the coupling strengths (Γ^L and Γ^R) of the molecule to the two electrodes as well as the transmission probability through the molecule as follows:

$$T = \Gamma^L\Gamma^R|G_{1N}| \tag{61}$$

where G_{1N} is the Green function.[550,677] Therefore, the single-molecule conductance can be defined as follows:

$$G = \frac{2e^2}{h}\Gamma^L\Gamma^R|G_{1N}| \tag{62}$$

Clearly, the measured conductance has relationships with both the molecule and the coupling strengths between the electrodes and the molecules.

Formula 62 indicates the mathematical relationship between the interfacial coupling strength and the conductance. This formula can also be written as follows:

$$G = \frac{2e^2}{h}T_R T_L T_{mol} \tag{63}$$

where T_R, T_L, and T_{mol} are the transmission coefficients of the left interface, right interface, and molecule, respectively. This definition form expresses that single-molecule conductance can also be affected by the alignment of the molecular energy levels, especially the HOMO and the LUMO, relative to the Fermi levels of the electrodes for the tunneling transport mode,[53,57] in which the Fermi levels of the electrodes lie in the gap between the HOMO and the LUMO of the molecules. Following the molecular conductance discussion above, we systematically clarify the critical aspects that have considerable effects on the single-molecule conductance and the conductance measurements.

7.1.2.1. Interfacial Coupling. The occurrence of both the charge injection and the collection across the molecule–electrode interfaces underlines the significance of the interfacial properties. A clear recognition of the interfacial coupling strength can lead to obtaining insights into distinct transport mechanisms, thus facilitating the improvement in the molecular conductance. Generally, the interfacial properties depend considerably on the coupling between the molecules and the electrodes, which has a relationship with both the intramolecular coupling of the molecules and the coupling between the terminal of the molecules and the electrodes.[678] For the

DOI: 10.1021/acs.chemrev.5b00680
Chem. Rev. 2016, 116, 4318–4440

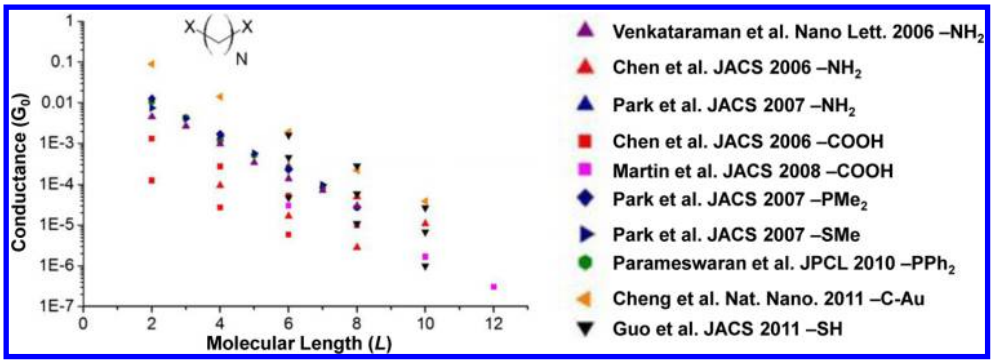

Figure 52. Conductance values for alkane chains of several different lengths with different end groups, as indicated in the legend. Although the conductance for each different linker group is different, the β value does not appear to change significantly with the contact resistance. Reprinted with permission from ref 681. Copyright 2014 IOP Publishing Ltd.

former, the saturated carbon providing weak coupling and the direct π-conjugated bond offering strong coupling can affect the intramolecular coupling, whereas for the latter, both the interaction types and the contact geometries at the molecule−electrode interface are significant.[57]

Interaction types: The types of interfacial linkages between the molecules and the electrodes are primarily determined by the materials and the corresponding physical or chemical interactions. Generally, noncovalent interfacial linkages, such as donor−acceptor coordination,[678] van der Waals binding,[671,672,679] and aromatic stacking,[354] are thought of as weak coupling, while covalent interactions, due to the formation of robust chemical bonds, are viewed as strong coupling. Venkataraman and her colleagues systematically studied the interaction of amines and gold as a noncovalent interfacial linkage.[61,678] Initially, they determined that molecules with amines as anchoring groups could couple with gold electrodes through the interaction of electron lone pairs from the amine nitrogen to coordinatively unsaturated surface Au atoms.[678] This bonding mode possesses sufficient angular flexibility for easy junction formation and a well-defined electronic coupling of the N lone pair to the Au, thus facilitating conductance measurements of single-molecule junctions in a statistical manner. Furthermore, using single-molecule mechanics measurements, it was discovered that anchoring groups of pyridine can bind to nanostructured Au electrodes through a van der Waals interaction beyond the chemically specific Au−N donor−acceptor bond.[61] Although the reproducibility of the interfacial linkage in these studies is sufficient to obtain statistical information on conductance, the contact resistance is higher than that of the covalent bonding, such as the Au−S interaction, which is contradictory to the efficient electrical conductance. In fact, metal-based noncovalent interaction is rarely used for constructing a reliable molecule−electrode interface due to its weakness. However, aromatic stacking, which is another type of noncovalent interaction, is widely used to create molecular junctions, especially in systems currently containing carbon electrodes.[354,355,371] Detailed discussions can be found in section 3. In terms of conductance, the aromatic stacking is considered to be a weak coupling, which results in a large contact resistance, thus discounting the efficiency of the charge transport. Furthermore, it is difficult to use these interaction types to provide robust linkages against external perturbations, which is of crucial importance to the ultimate goal of developing molecular electronics.

Conversely, covalent bonding is superior in creating the interfacial linkages in molecular devices, which can provide robustness and reliability. For the charge transport, there is a vast majority of criteria when selecting electrodes and anchoring groups; however, the concern of whether the interfacial linkage is covalent or not is often considered first. The detailed discussions have been provided in sections 2−4.2. It should be noted that the metal-containing covalent bonds could potentially be affected by both the σ and the π characters due to the distinct orbital characteristics of the electrode atoms. For example, because Pd and Pt are group 10 elements with significant d-orbital characteristics, π contributions are expected at the contact, especially for −NCS headgroups with a strong π character, which may generate an additional channel for electron transport.[57,680]

Although there were a few reports clarifying the insensitivity of the molecular junctions on the interfacial contacts,[253,254] additional studies consistently prove that different interfacial interactions result in different coupling strengths. Figure 52 displays the conductance of several single-alkane chains of different lengths and linker groups by plotting $\log(G)$ versus L (molecular length).[681] A similar slope for each molecular set with distinct anchoring groups could be viewed as a representation that the alignment between the molecular energy levels and the Fermi energy of the electrodes does not change significantly in the case of the alkanes, and that the difference in conductance for different molecular sets is due to the contact resistance resulting from the linker groups. The implication of these results is that the best possible interface for the molecular electronic system should have strong covalent bonding, thus underlining the importance of selecting electrodes and anchoring groups as well as developing interfacial chemistry and characterization methods (such as the IETS,[438] as detailed in section 5), especially at the single-molecule level. If the molecules are charged, other potential interactions, such as the rearrangement of electron density, partial charge transfer, and attraction through image forces, could be further involved in the interface formation.[676] Therefore, due to the complexity of the interface formation, it is crucial to determine the exact way in which the interface is formed.

Contact geometries: In certain cases, the same molecular junction can display different conductance values due to the different headgroup−substrate binding geometries, which generally play a significant role in the molecular conductance. Different structures of electrodes at the binding points could result in various contact geometries with different coupling strengths, which are evident in the systems using break junction techniques, such as STM and AFM.[680,682] The molecular junctions are formed by pulling the gold atoms out of the

DOI: 10.1021/acs.chemrev.5b00680
Chem. Rev. 2016, 116, 4318−4440

electrodes, resulting in the possibility of top and hollow geometries at the two ends of the molecular junctions (Figure 53). For the Au−S contacts created using these techniques,

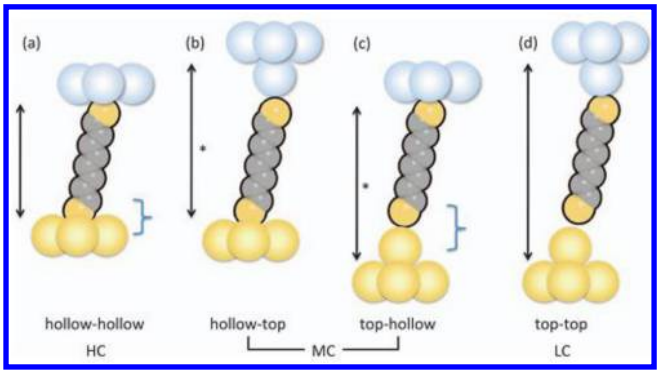

Figure 53. Different contact configurations. The distance between the electrodes affects the binding force, and the number of involved electrons for the charge transport can determine the conductance of the metal−molecule−metal system. The double arrows indicate the transport lengths for (a) hollow−hollow, (b,c) hollow−top/top−hollow, and (d) top−top. Reprinted with permission from ref 682. Copyright 2013 American Institute of Physics.

when one headgroup is connected to the 3-fold hollow sites of the substrate and the other is connected to the top sites (denoted top−hollow), a high conductance can be obtained; molecular termini sitting on the two top sites (top−top) result in a low conductance. Although its existence is relatively rare, the hollow−hollow configuration is the ideal contact geometry.

In addition to the geometry of the contact points, the electrode orientations have a clear effect on the interfacial coupling because different electrode orientations have different band structures. Sen and Kaun obtained the results of high/low conductance values for Au−alkanedithiol−Au single-molecule junctions with two distinct electrode orientations.[683] On the basis of the theoretical calculations, they attributed the observed binary conductance of the junctions to the distinct electrode orientations and determined that the interfacial coupling is stronger for Au electrodes with the (100) direction than that with the (111) direction. In fact, the contact structures in the single-molecule junctions play a significant role in affecting the conductance, as discovered by Venkataraman et al. experimentally and theoretically.[684] A modified conducting AFM was used to simultaneously probe the conductance of a single-molecule junction and the force required to rupture the junction, which accommodated the possibilities of obtaining various molecule−electrode contact structures (Figure 54). The experimental data verified that the broadly distributed conductance values resulted from substantial variations in the Au−S linking structure, which was also supported by the DFT calculation. The fact that the interfacial contact strength could be characterized by the value of the bond rapture force and that the corresponding conductance could be confirmed simultaneously in this study led to obtaining insights into the relationship between the interfacial coupling and the conductance.[685] However, the factors affecting the contact details and the molecular conductance are considerably more complicated than those previously described. Generally, the contact geometry has been accepted as a determining value in the absolute conductance of a molecule, for which any perturbance may change the interfacial coupling as well as the contact resistance without a significant change in the orbital

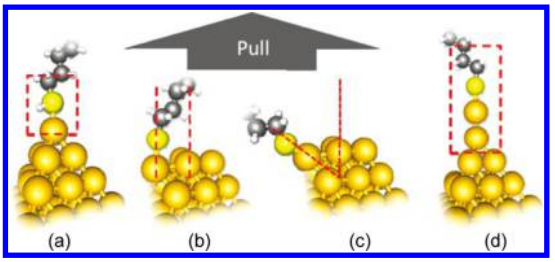

Figure 54. Possible Au−S contact structures in AFM-based single-molecule junctions. Scenarios: (a) H atom remains on S; (b) Au atom is not at the apex of the electrode; (c) junction is formed at an angle; and (d) Au atom coordination is different. Reprinted with permission from ref 684. Copyright 2012 American Chemical Society.

alignment.[681] The lack of corresponding methods of characterization and recognition signifies that the ability to understand and control the charge transport precisely is far from realized.

Coupling strength and transport mechanism: The coupling strength between the electrons in the molecules and those in the electrodes, which can be physically depicted as an energy barrier between the molecules and the electrodes, is one of the most important properties of the molecule−electrode interface. On the basis of the results of comparing the strength of the interfacial coupling (Γ) with the addition energy (U), three different coupling regimes are classified: weak coupling ($\Gamma \ll U$), strong coupling ($\Gamma \gg U$), and intermediate coupling, where the addition energy is the difference between the energy needed to take one electron from the HOMO of the system ($U^{N-1} - U^N$) and the energy obtained by injecting one electron to the LUMO of the system ($U^{N+1} - U^N$). Intrinsically, different coupling regimes indicate different degrees of mixing of the wave functions of the molecules and the electronic states of electrodes, thus leading to different transporting mechanisms and electrical conductances.[57]

In the weak coupling regime, no charge transfer or an integer charge transfer occurs between the molecules and the electrodes so that the electron transport in this case may be accomplished through a two-step process in which the electrons first hop from one electrode to the molecule, which has matching energy levels at a proper position, and then hop to the other electrode (Figure 55a). At low temperatures, the absence of matching energy levels will lead to the electron transport being blocked unless the bias voltages are high enough to bring the Fermi energy of the electrodes to the molecular energy levels or the external tuning, such as the gate voltage, gives rise to such an energy-level alignment. This phenomenon is also known as the Coulomb-blockade, which forms classic Coulomb diamonds in differential conductance maps.[21] In the intermediate coupling regime, due to the partial broadening of the molecular energy levels, the transferred electrons can be affected by the electrons on the molecules (Figure 55b). In the presence of an unpaired electron on the molecules, its spin state can be reversed by electrons passing through the molecules, thus leading to a spin screening that could result in new transport channels. A zero-bias Kondo resonance below a certain temperature is the result of the spin screening. Additionally, a cotunneling process can occur in this regime, in which one electron tunnels into the LUMO of the molecule with another electron simultaneously tunneling out of the HOMO, thus leaving the molecule in the excited state. In the strong coupling regime, the energy levels of the molecules are considerably broadened for the significant overlapping of

DOI: 10.1021/acs.chemrev.5b00680
Chem. Rev. 2016, 116, 4318−4440

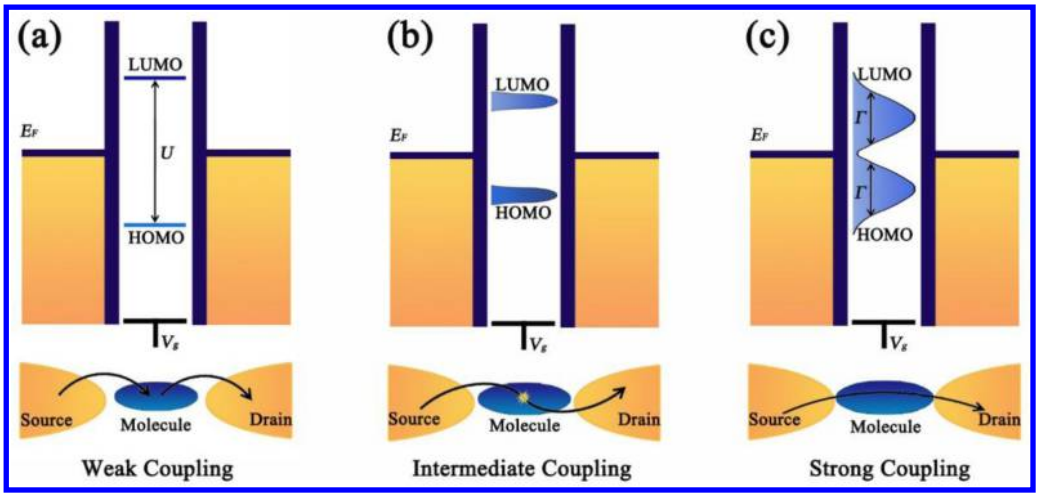

Figure 55. Schematic representation of the energy levels and the charger transport processes of the molecular junctions with different coupling strengths between the molecules and the electrodes. (a) In the weak coupling regime, the HOMO and the LUMO of the molecules are well-defined, and the electron transport occurs in a two-step process. (b) In the intermediate coupling regime, the HOMO and the LUMO become broader and closer to the Fermi energy of electrodes (E_F), and the electron transport occurs through the molecules interacting with the electrons on the molecules. (c) In the strong coupling regime, a large broadening of the molecular energy levels occurs, and electrons move from the source to the drain through a one-step process. Reprinted with permission from ref 57. Copyright 2013 Royal Society of Chemistry.

the molecule−electrode electronic states as well as the feasibility of the partial charger transfer between the molecules and the electrodes (Figure 55c). Therefore, the electrons could efficiently transport from one electrode to another through a one-step coherent process without stopping on the molecules. On the basis of these general transport mechanisms, it can be predicted that strong interfacial coupling with low contact resistance would facilitate acquiring a high conductance. Therefore, the proper selection of the electrodes and anchoring groups, precise control of the interfacial interactions and contact geometries, and extensive understanding of the corresponding transport mechanisms are necessary for improving the molecular conductance.

7.1.2.2. Energy Level Alignment. Another important factor that significantly affects the molecular conductance is the alignment of the molecular energy levels, especially the HOMO and the LUMO, relative to the Fermi levels of the electrodes.[53] Generally, when the energy level of the frontier molecular orbitals is sufficiently close to the Fermi level of the electrodes, resonant transport occurs, and the conductance depends only on the contact resistance due to the different coupling strengths, as detailed above. Conversely, for the tunneling transport, where the Fermi level of the electrodes lies in the gap between the HOMO and the LUMO of the molecules, the energy level alignment between the Fermi level of the electrodes and the molecular energy level responsible for the charge transport can play a dominant role.

The energy level alignment is primarily determined by the intrinsic properties of the molecule and the electrodes and the molecule−electrode interactions, which are often difficult to determine in both theory and experiment. It is evident that different molecules hold distinct HOMO and LUMO energies, which can be tailored using molecular engineering. For example, Jia et al. intended to modify the diarylethene backbones by substituting hydrogenated cyclopentene with rationally designed fluorinated side groups to tune the energy level alignments at the molecule−electrode interface, leading to a decrease in both the HOMO and the LUMO and a reduction in the HOMO−LUMO gap by 0.5 eV at the open state and 0.1 eV at the closed state.[490] For the electrodes, as described elsewhere in this report, various types of materials with identified but distinct work functions can be selected to adjust the interfacial energy level alignment as well as the coupling strength. For example, when Ag, Au, Pd, and Pt are used as the electrodes,[489] which have work functions of 4.26, 5.10, 5.12, and 5.65 eV, respectively, the Fermi energy of the electrodes reduces with an increase in the work function. Correspondingly, the energy offsets between the Fermi energy of the electrodes and the HOMO of the molecules decrease for the hole tunneling systems, in which the HOMO dominates the conduction of the molecular junctions, but increase for the LUMO-mediated tunneling systems. Additionally, the different anchoring groups used to create interfacial linkages can adjust the energy levels of the frontier molecular orbitals for the charge transport, which can be exemplified by the Au−N D−A bonds. Specifically, electron-donating amine[686] groups can bring the HOMO of the molecules closer to the Fermi level, thus favoring the hole transport by lifting the frontier orbital energies, while electron-withdrawing pyridine[687] and nitrile (−C≡RN)[688] groups can reduce the energy barrier between the LUMO of the molecules and the Fermi level of the electrodes to promote electron transport by decreasing the frontier orbital energies.

Although there are numerous difficulties in characterizing the alignment between the Fermi level of the electrodes and the molecular energy level related to the charge transport at the single-molecule level, the TVS-related techniques possess a strong hold on this field. As elaborated in section 5, the TVS exploits the nonlinear current−voltage characteristics of the molecular junctions to investigate the energy offset between the Fermi energy of the electrodes and the closest molecular energy levels. On the basis of this technique, Guo et al. systematically studied the transport features of single-alkanedithiol junctions to determine whether different binding geometries could cause the differences in the energy barrier of the molecules.[504] Recently, Bruot et al. performed a study on single-molecule junctions based on benzenedithiol (BDT), in which the anionic state is predicted to possess a HOMO level energy similar to

DOI: 10.1021/acs.chemrev.5b00680
Chem. Rev. 2016, 116, 4318−4440

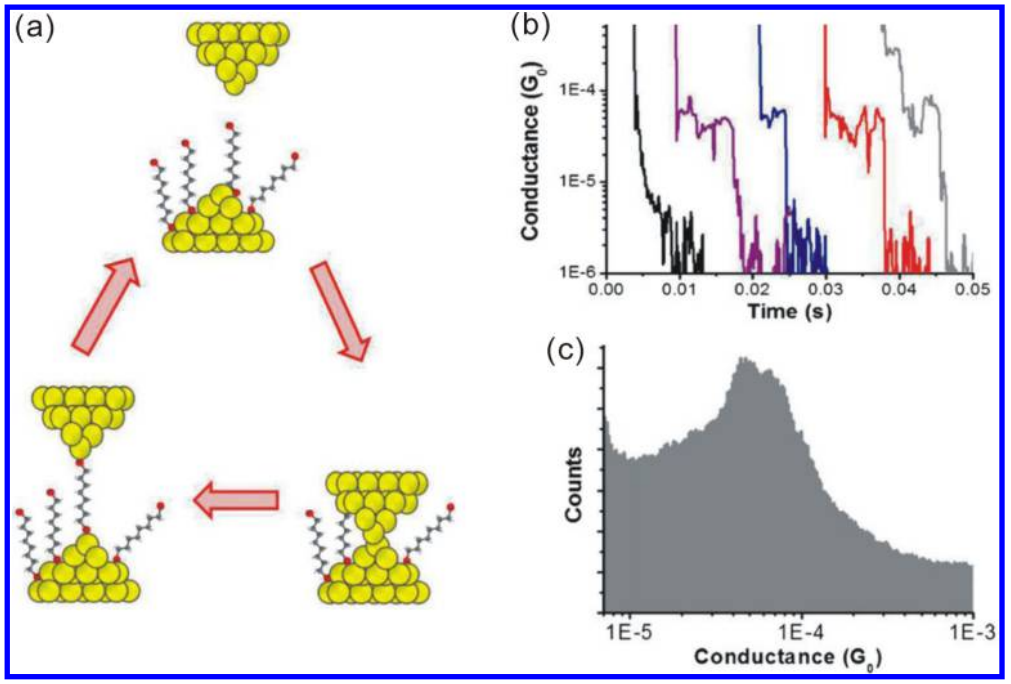

Figure 56. Break junction-based measurements for obtaining single-molecule conductance values. (a) Schematic depiction of break junction system used for measuring conductance. The distance between the two electrodes is cycled repeatedly while a bias is applied between them and the measured current. (b) Several sample conductance versus time traces used to construct a conductance histogram. (c) Conductance histogram with a peak at the most probable conductance value for a single-molecule junction. Reprinted with permission from ref 681. Copyright 2014 IOP Publishing Ltd.

the Fermi energy of the gold electrodes, using the TVS to directly explore the possibility of the conductance increase and the energy offset decrease while weakening the interfacial linkage by straining.[112] For graphene-based single-molecule systems, the TVS was also used by Jia et al. to explain the observation of the photogated transport mechanism transition from direct tunneling to field emission due to the photoinduced conformation transformation.[490]

In addition to the interfacial coupling and energy level alignment, the local environment of a molecule can influence its conductance, which has been demonstrated by studies established for obtaining the relationship between the conductance and the external stimuli, such as the solvent, pH, ion, and dopant. In fact, this relationship underlies the operational principle for developing various molecular sensors, as discussed later.

7.1.2.3. Molecular Conductance Measurements. The research on molecular conductance and its measurements was initiated from bulk electrode approaches, in which mono- or multilayer molecular films prepared by either self-assembly or Langmuir−Blodgett methods were sandwiched between two bulk and flat electrodes.[53] Because of the introduction of several novel micro-/nano-systems created using the crude-tip AFM,[59,689] cross-bar techniques,[690−692] or nanopore fabrication,[265] the area of the molecular films investigated decreased, and the conductance measurement was closer to the molecular level. Clearly, it is difficult to accurately determine the number of molecules successfully connecting both electrodes, thus making the averaging calculation impossible. In fact, even if the averaging process is possible, the calculated value cannot exactly represent single-molecule conductance because there is no way to ensure each connection possesses identical types and geometries, both of which have a significant effect on the single-molecule conductance. Furthermore, the conformational changes in the molecules could be suppressed by the interaction with neighboring molecules in a close-packed film, which may affect their electron-transport properties.[626]

To determine the conductance of a molecule, it must be first brought into contact with at least two external electrodes. The contact must be robust, reproducible, and able to provide sufficient electronic coupling between the molecule and the electrodes, which is one of the most significant aspects needed to reduce the discrepancies between the groups measuring the same molecules. In fact, the development of various methods to control, tailor, and characterize the interfacial interactions as well as the contact details is leading to the realization of this goal. Additionally, the electronic signature indicating the current not only through molecules but also through one molecule between a pair of electrodes should be identified, which was challenging before the introduction of techniques using nanoscale moveable electrodes that could be mechanically controlled with sub-angstrom precision. Furthermore, the capability of efficiently measuring thousands of individual junctions accommodates the feasibility for establishing statistical investigations, which can provide the most likely conductance of a single-molecule junction by analyzing the resulting current versus distance traces (Figure 56). In sections 2−4.2, we comprehensively reviewed state-of-art methodologies to obtain the measurements of single-molecule conductance. Among these approaches, the AFM and STM break-junction techniques are primarily known for the advantages listed above.

In this section, we systematically reviewed various types of molecular candidates to be potentially used as conductive wires. The combination of enriched molecular scaffolds with ever-improving molecular engineering offers the possibility of creating novel molecular wires with superior conductance. Additionally, the interfacial issues between the molecules and

DOI: 10.1021/acs.chemrev.5b00680
Chem. Rev. 2016, 116, 4318−4440

the electrodes, including interaction types, contact geometries, and energy level alignments, have a significant impact on the conductance of molecular junctions. Therefore, beyond the development of synthesizing wire-type molecules, the exploration of efficient methods to accurately tailor the interfacial properties is of the same significance. In fact, controllability on the electrode−molecule interface is not just needed in the molecular wires but is also necessary for realizing other functionalities in molecular electronics. Because of the maturity of the molecular conductance measurements, in the following sections, we summarize the primary contributions and new concepts of integrating molecular functionalities into electrical circuits toward practical applications using the holistic consideration of device fabrication and measurements, including the testbed architectures, molecule number, and defect density, and nature of the molecule−electrode interface.

7.2. Rectification toward Diodes

The diode or rectifier, which facilitates the current flow in one (forward) bias direction and suppresses under the opposite (reverse) direction, is an important two-terminal electronic component. Conventionally, rectifiers can be integrated as p−n junctions by two types of materials with different electronic states using crystal doping, one of the most mature semiconductor techniques in the silicon industry.[693] Briefly, a crystal of group IV, such as Ge or Si, can be doped with dilute concentrations of interstitial or substitutional electron-rich elements (group V, such as N, P, and As) to achieve an "n-doped" material, whereas a "p-doped" crystal can be formed by doping with group III elements (such as Al, Ga, and In). Benefiting from the development of the semiconductor industry, diodes, similar to any other digital and computational electronic components, evolve extremely but experience the same problems in the size miniaturization and performance enhancement processes. The idea of using single molecules to fabricate a new generation of rectifiers was proposed theoretically by Aviram and Ratner[16] and received significant attention since the 1970s. In this initial prototype, an organic molecule containing an electron-donating moiety (donor) and an electron-withdrawing moiety (acceptor) bridged by the σ linkage that serves as an insulating barrier for electrically separating the two segments was proposed. After bridging a pair of electrodes to construct a D−σ−A junction, it would be ideal to energetically use a simple acceptor-to-donor electron transfer for the current rectification. Similar to the conventional rectifying systems, "D" corresponds to "n" and "A" corresponds to "p", as indicated in Figure 57.[370] Single-molecule diodes are of crucial importance because, for example, they enable the electrical addressing of an individual molecular node in an ultimately scaled crossbar-type architecture, where the node consists of an ensemble or of a single functional molecule with both current-rectifying and switching/storing moieties.[694]

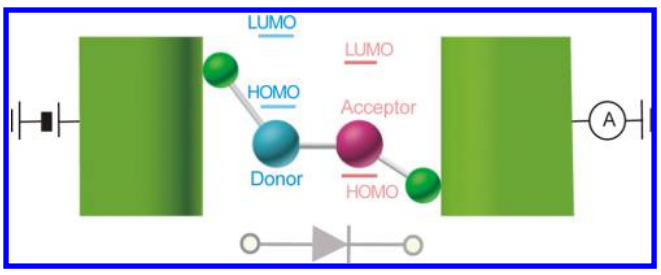

Figure 57. Schematic description of rectifiers based on single molecules and the corresponding simplified potential profile for rectifying mechanisms. Reprinted with permission from ref 370. Copyright 2012 MDPI Switzerland.

The past 40 years have witnessed a tremendous improvement in molecular electronics in both experimental and theoretical aspects, which includes progress in the development of molecular rectifiers. In fact, in addition to the Aviram−Ratner model, several other models have been proposed[694] that not only enrich the explanation for molecular rectification but also incite several ideas for the design and preparation of novel molecular diodes. In this section, we review the studies on different types of diodes using a single molecule as a core component starting with three fundamental mechanisms responsible for molecular rectification behaviors. It should be noted that the major realization of the current single-molecule rectification still depends on monolayer-based techniques that are beyond the scope of this Review. However, to present a thorough development of the molecular rectifiers, we provide a succinct but systematic introduction to these contributions. For additional detail, interested readers are recommended to reference other studies.[12,693,695,696]

7.2.1. General Mechanisms for Molecular Rectification. As mentioned above, the D region (electron-rich) of the molecular rectifiers resembles the n-doped region of the inorganic counterparts, and the A region (electron-poor) resembles the p region. However, the underlying mechanisms related to rectification for the two types of diodes are reversed. For example, in the case of the D−σ−A molecular rectifiers, the preferred direction of electron flow under a forward bias is from the metal electrode to A to D to the other metal electrode, whereas in a p−n junction rectifier, the preferred direction is from n to p. Furthermore, due to the complexity arising from the significant influence of the electrode−molecule interface on the charge transport, the explanation used for understanding the conventional p−n junction diodes is insufficient for the molecular diodes. On the basis of the theological development as well as the experimental discovery, three mechanisms, that is, the Aviram−Ratner[16] model (AR model), Kornilovitch−Bratkovsky−Williams[697] model (KBW model), and Datta−Paulsson[698] model (DP model), were proposed to explain the rectification behaviors based on single molecules,[694] which are described schematically in Figure 58.

7.2.1.1. Aviram−Ratner Model. In the millstone-like study contributed by Aviram and Ratner, the molecule with an electron-poor moiety of tetracyanoquinodimethane (TCNQ) and an electron-rich moiety of tetrathiofulvalene (TTF) linked by a covalent triple-methylene bond was assumed to be attached to a pair of electrodes (Figure 59a), thus creating a molecular diode in which the molecule functionalizes as a core component for electrical current rectification. Afterward, the specific molecule was generalized as a D−σ−A model consisting of a donor region, insulator region, and acceptor region. In fact, the corresponding mechanism underlying this proposal was the earliest approach that acquired wide agreement. In the AR model, the two electrodes are connected through three tunneling barriers, linking one electrode to the acceptor unit, the acceptor unit to the donor unit, and the donor unit to the other electrode. At a zero applied voltage bias, the HOMO of the donor is slightly below the electrode's Fermi energy and the LUMO of the acceptor is slightly above, whereas upon application of a voltage bias across the junction, the LUMO (or the HOMO) can be aligned to the Fermi energy of the leads or separated depending on the bias

DOI: 10.1021/acs.chemrev.5b00680
Chem. Rev. 2016, 116, 4318−4440

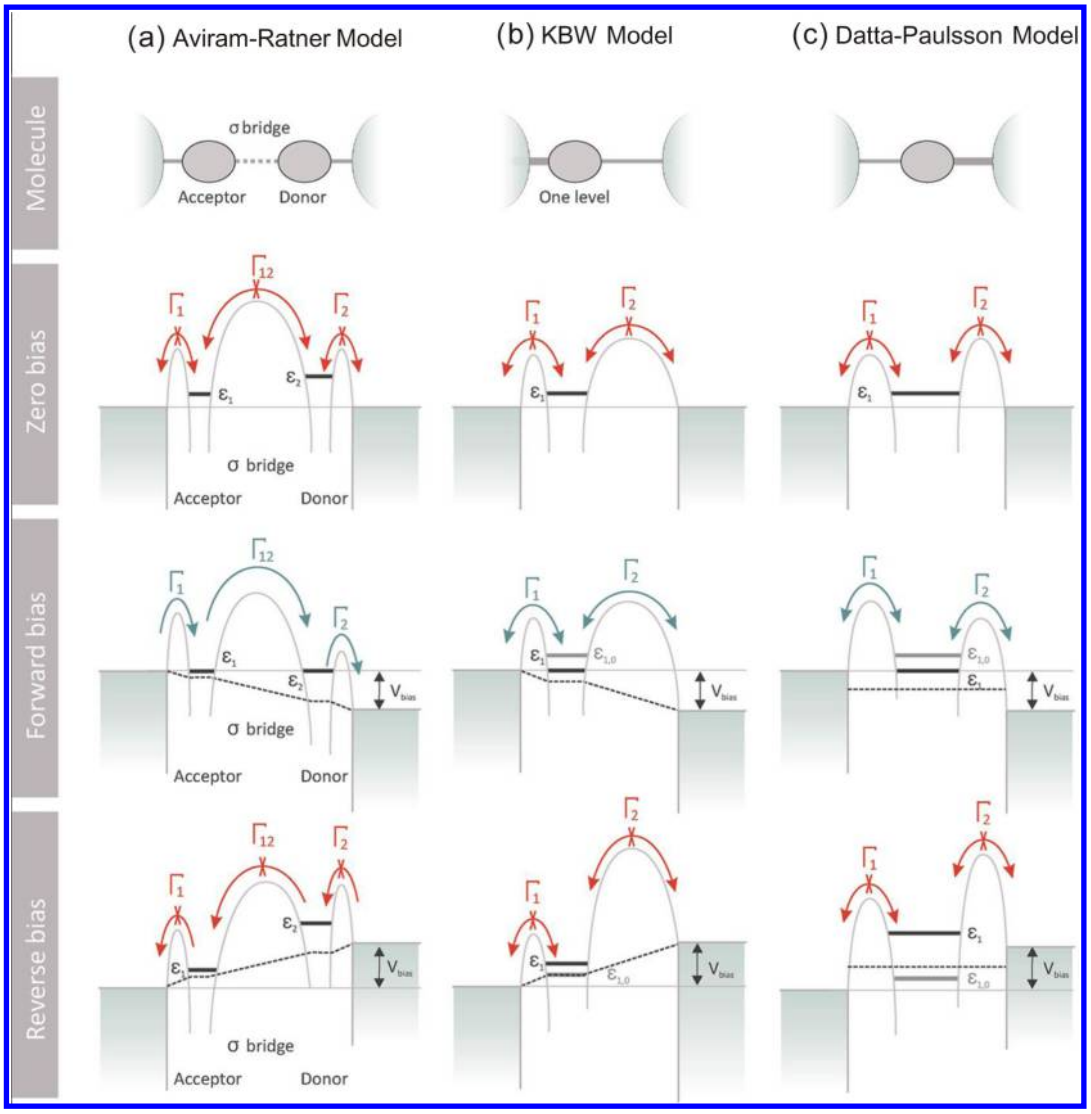

Figure 58. Comparison of three models for molecular diodes (Γ_i represents the rates of tunneling steps). (a) Aviram–Ratner proposal with molecule levels shifting through the applied electric field. The subtle energy-level alignment for the donor and acceptor moieties, in combination with the large electrical spacer separating the two moieties, eventually leads to a difference in the current onset. (b) Simplified model, as proposed by Kornilovitch, Bratkovsky, and Williams (KBW), with one level. The level is shifted with respect to the applied electric field. (c) Considering the charging of the energy levels (proposed by Datta and Paulsson) can lead to diode behavior, even without level shifting by an electric field. Reprinted with permission from ref 694. Copyright 2012 American Chemical Society.

direction. Thus, the rectification behavior that was expected to occur due to the different thresholds at the positive and negative bias voltages and shifts of the energy levels of the molecular orbitals according to their energetic positions in the gap was dominated by the electric field between the electrodes, which is depicted schematically in Figure 58a. The two separate energy levels, ε_1 and ε_2 (with respect to the Fermi energy of the electrodes, E_F), which belong to the donor and acceptor, respectively, respond differently to the electric field between the electrodes upon application of a bias voltage, thus leading to the energy-level alignment or misalignment responsible for the asymmetric charge transport. In summary, the rectification of an Aviram–Ratner diode could be viewed as a different onset of resonant tunneling for the two bias directions.[694]

7.2.1.2. Kornilovitch–Bratkovsky–Williams Model. Later, Kornilovitch, Bratkovsky, and Williams generalized the AR mechanism to a simpler system (referred to as the KBW model) with only one molecular orbital, in which asymmetric tunneling barriers led to the current rectification (Figure 58b).[697] Specifically, in this approach, the position of the orbital is not located symmetrically between the electrodes, but is closer to one of them due to the terminated tails with different lengths. Because most of the applied voltage drops on the longer insulating barrier, the conditions required for resonant tunneling through the level are achieved at different voltages for the two opposite polarities. In fact, the molecular orbital can be aligned or separated with the Fermi energy of the electrodes depending on the bias direction, which will result in the rectification behavior. In a similar study, Mahmoud et al. noted that the rectification of a molecular device could be controlled by inserting a resistive molecular path near the metallic electrodes, thus enforcing the potential drop profile along the molecule through calculations.[699] More importantly, the KBW model led to enhancing the development of molecular diodes with ease because molecules with different-length tails providing tunneling barriers were more accessible than complex

DOI: 10.1021/acs.chemrev.5b00680
Chem. Rev. 2016, 116, 4318–4440

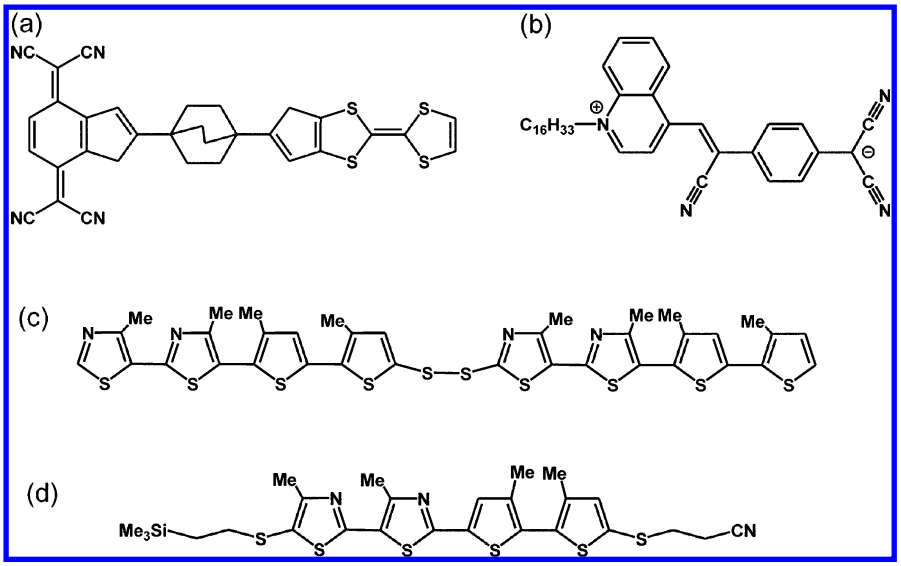

Figure 59. Molecular structures proposed for current rectification. (a) Initial model D−σ−A proposed by Aviram and Ratner. (b) D−π−A molecules used for rectification based on the Langmuir−Blodgett monolayer. (c) Conjugated diblock oligomers used for rectification through the formation of the SAMs. (d) p−n junction types of molecules used for rectification through the directed formation of SAMs with a specific orientation.

structures needed in the AR model. Furthermore, by changing the lengths of these insulating tails, the rectification ratio can be systematically changed.

7.2.1.3. Datta−Paulsson Model. For spatially symmetric molecules, the current rectification could be also achieved through unequal coupling with the electrodes at the two ends, which was stated by Datta and his colleague based on experimental and theoretical studies.[698] In the charge transport measurements of these molecules (Figure 58c), the *I*−*V* curves were initially symmetric but picked up a weak and reversible asymmetry as the contacts were manipulated. Specifically, for resonant conduction, this asymmetry is indicated by conductance peaks of different heights occurring at symmetrically disposed voltage values. Clearly, the conduction in these molecules at opposite voltages occurs essentially through the same molecular levels with similar wave functions, which is different from the two previous models mentioned above. The authors verified that the origin of the observed contact-induced asymmetry was nontrivial and involved self-consistent shifts in the energy levels due to the charging effects that typically exist in single-molecular devices with tunneling barriers to the electrodes. The asymmetric charging energies will lead to different tunneling rates between the orbital and the two electrodes, which implies that the average population of the orbital with electrons depends on the bias direction in the resonant tunneling condition, thus realizing the rectification. Although this mechanism cannot be easily separated from the asymmetric coupling to the electric field described above, it can be considered as a distinct mechanism of the rectification. In principle, molecules can be designed that allow for better coupling to either of the electrodes while maintaining the position of the resonant orbital in the center.

It should be noted that for experimental verification, it is difficult to distinguish between the three above-discussed mechanisms for several reasons. (1) A pure Aviram−Ratner diode is difficult to chemically synthesize, and a complete decoupling of the donor and acceptor orbitals is not always guaranteed.[700] (2) Experimental transport measurements suffer from uncontrolled coupling between the electrodes and the terminated groups of molecules for various interfacial interactions and random contact geometries previously detailed.[701] Recently, Zhang et al.[702] conducted a study to identify whether molecular rectification is caused by asymmetric electrode couplings or a molecular bias drop. The result that the bias drop is responsible for rectification whereas the asymmetric couplings do not directly lead to rectification indicates a discrepancy with other results, which demonstrates the complexity of differentiating specific mechanisms. In fact, in most of the studies experimentally pursuing molecular diode prototypes, the phenomenon of rectification is always a combined effect of different mechanisms. Molecular rectifiers based on pure operating principles are relatively rare.[696]

7.2.2. Rectification Stemming from Molecules. *7.2.2.1. D−σ−A and D−π−A Systems.* Encouraged by the visionary Aviram−Ratner proposal, several groups pursued building diodes with single molecules. Because of the limitations of current organic synthesis methodologies and the capability of tuning inter-/intramolecular energy-level alignment with controllability, a standard diode using single molecules with D−σ−A architecture has not been reported. However, in certain efforts based on multi-/monolayer Langmuir−Blodgett films or block copolymers,[703] the D−σ−A model was demonstrated to be successful and thoroughly confirmed.[704−709] Furthermore, considerable attention has been given to molecules with D−π−A structures because of their synthetic feasibility to rectify the electrical current at the molecule-film level.[707,710,711] For the rectifying process using this type of molecule, there are a few ambiguous issues related to the rectification mechanism. For example, it should be considered whether the ground state is exactly $D^{+1.0}-\pi-A^{-1.0}$ and the excited state $D^{0.0}-\pi-A^{0.0}$ or whether their corresponding intermediate ionicities are $D^{+\rho}-\pi-A^{-\rho}$ ($\rho \geq 0.8$ for the ground state and $\rho \leq 0.2$ for the excited state).[712] However, the D−π−A model, which is the derivative of the D−σ−A model, promotes the development of the molecular rectifiers and increases the access for realizing actual single-molecule diodes.

Several exceptional studies based on the SAM system have been reported to realize single-molecule rectifiers. In 1997,

DOI: 10.1021/acs.chemrev.5b00680
Chem. Rev. 2016, 116, 4318−4440

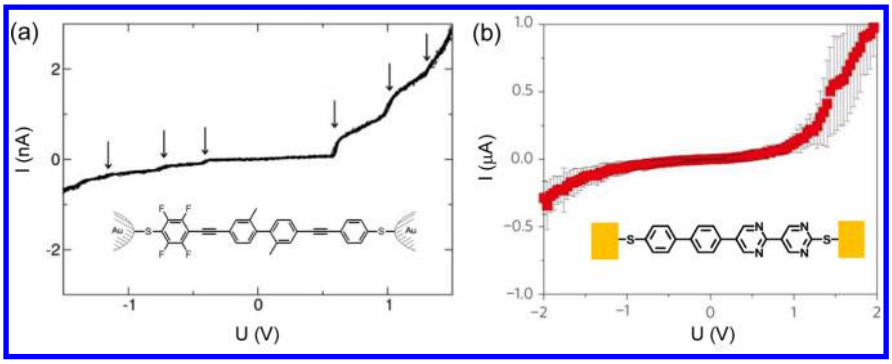

Figure 60. *I*−*V* characteristics of rectifiers based on single-diblock molecules. (a) Rectification of phenyl−ethynyl−phenyl molecules immobilized between two Au electrodes in an MCBJ setup. The arrows point to step-like features of the *I*−*V* curves. Reprinted with permission from ref 718. Copyright 2005 American National Academy of Sciences. (b) Rectification of the dipyrimidinyldiphenyl molecules integrated in an STM setup at *T* = 30 K. Reprinted with permission from ref 717. Copyright 2009 Nature Publishing Group.

Metzger et al. demonstrated a unimolecular rectification behavior with a rectification ratio (defined as the ratio of the highest conductance at the forward bias and that at the reverse bias) of up to ∼13 using a Langmuir−Blodgett monolayer of zwitterionic hexadecylquinolinium tricyanoquinodimethanide ($C_{16}H_{33}$Q-3CNQ) molecules sandwiched between two Au electrodes (Figure 59b).[695,696] By probing the SAMs with the STM techniques,[713,714] Ng and Jiang et al. achieved molecular rectifiers based on diblock molecules at the single-molecule level with a rectification of ∼7 (Figure 59c). It is evident that the orientation of molecules in the junction will have a significant impact on the direction of rectifying regardless of being in the SAM system or in the single-molecule system, which has been well described elsewhere.[715] Therefore, the controllability of the molecular orientation is of tremendous significance, which has been fundamentally acquired through a rational utilization of chemical reactions. The molecules terminated with a thiol at each end, both of which are protected with different groups, could be localized in a direct manner by removing the protection groups sequentially, which has been used successfully in both the SAM[714,716] and the single-molecule[717] systems (Figure 59d).

7.2.2.2. D−A Diblock Molecular System. The lack of synthetic methods and controllability for the energy-level alignment in the D−σ−A structures and the inferior performance of the rectifiers based on D−π−A molecules drive the focus back to the semiconductor counterparts for a breakthrough in single-molecule diodes. In this context, p−n junction molecules (known as diblock molecules) containing donor and acceptor moieties, which connect to each other through direct C−C covalent bonds rather than a σ- or π-bridge, were prepared by taking advantage of the mature polysynthetic method. Specifically, in 2002, Ng et al.[703] first synthesized a regioregular, head-to-tail coupled diblock co-oligomer comprising an electron-rich oligo(3-alkylthiophene) as the donor block and an electron-poor oligo(4-alkylthiazole) as the acceptor block and demonstrated its rectification effect using the STM technique. The synthetic approach was generally used for coupling heterocycles and thus promised sizable access for the introduction of other p−n junction diblock molecules, which has been recognized as the primary impetus for the progress in this field.

For example, in 2005, Elbing et al.[718] designed and synthesized a series of D−A diblock molecules and integrated them into electrical nanocircuits using the MCBJ technique to study their rectification behaviors (Figure 60a). These molecules consisted of two phenyl−ethynyl−phenyl π-systems, which were fused by a biphenylic C−C bond. To achieve electronic asymmetry, the parent unit of one segment was functionalized with four electron-deficient fluorine atoms, while that of the other was kept pristine at hydrogen-substituted. Furthermore, the steric repulsion of two methyl groups in an *ortho* position to the biphenylic C−C link induces a torsion angle between the segments, reducing the overlap of their π-orbitals and hence their electronic coupling. Combined with rigorous and systematic control experiments, the single-molecule rectification was confirmed with a current ratio of 1:4.5 ± 1.5 V, which is explained qualitatively below. The structurally asymmetric molecule could be viewed as two quantum dots coupled in series, termed F-dot (fluorized) and H-dot (not fluorized), for which the electronic orbitals were localized to avoid overlapping. When sweeping the bias voltage, the electronic levels of both dots are shifted with respect to one another, and at certain voltages, the two levels will cross. When an unoccupied level passes an occupied one, an additional transport channel opens for inelastic transmission from the H-dot into the F-dot. For each additional transport channel, the current grows by a certain amount, implying a stepwise increase in the *I*−*V* curves (or peaks in the differential conductance (d*I*/d*V*)).

In 2009, Tao et al.[717] used STM break junctions to probe a structurally similar but parent-unit-distinct molecule with specific bound orientation using selective deprotection strategy for its diode-like property. These nonsymmetric diblock dipyrimidinyldiphenyl molecules exhibited a pronounced rectification behavior (rectifying ratio of 5) as compared to its homologous symmetric block, with current flowing from the dipyrimidinyl to the diphenyl moieties (Figure 60b). In a further study, the same group utilized the same system as well as the same molecules along with an IETS analysis to explore the mechanism responsible for the rectification behavior at cryogenic temperatures.[436] The results of the rectification onset beginning near the zero bias and clear asymmetric currents at biases below 200 mV demonstrated that the transport mechanism was dominated by tunneling. More importantly, this study demonstrated that the bias-dependent asymmetry in the electronic coupling was important for both the elastic and the inelastic processes in the diblock diode molecule. This result was deduced from the fact that the IET spectra, with similar phonon energies and intensities, were antisymmetric in the forward and reverse bias directions, despite the asymmetry in the *I*−*V* and *G*−*V* characteristics at low biases. For further

DOI: 10.1021/acs.chemrev.5b00680
Chem. Rev. 2016, 116, 4318−4440

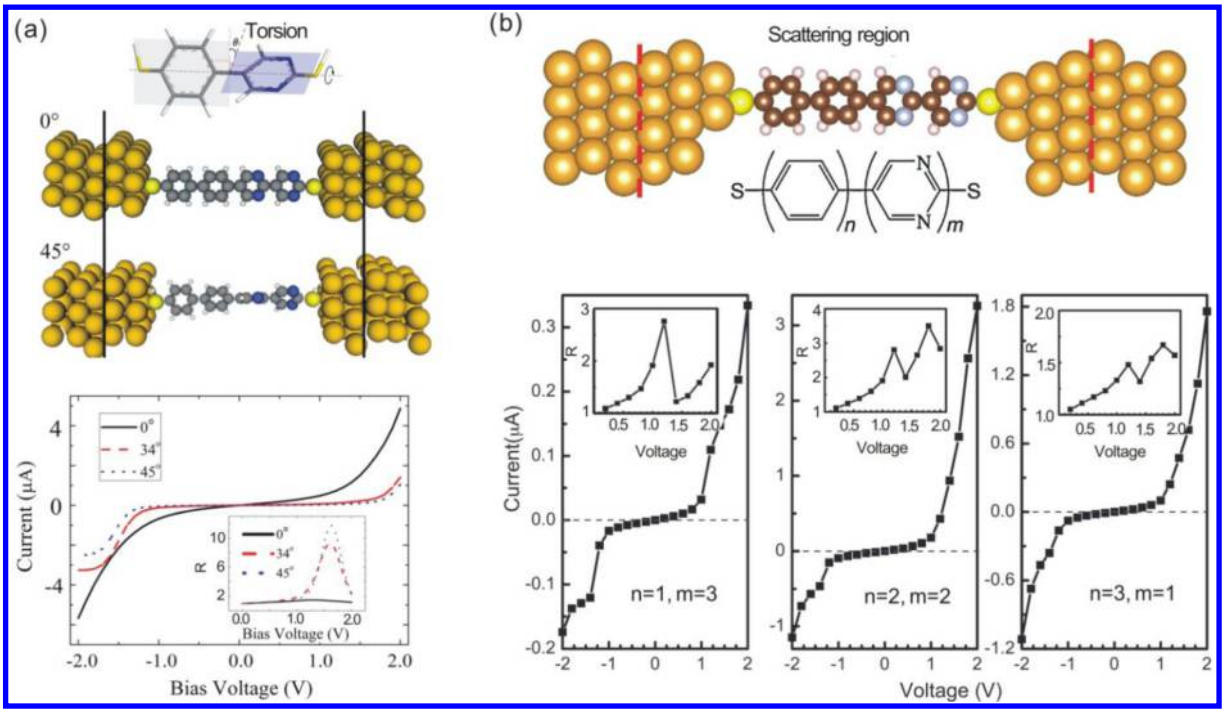

Figure 61. Torsion/proportion dependence of the rectification effect. (a) The influence of torsion between the donor part (phenyl segment) and the acceptor part (pyrimidinyl part) on the rectification. The corresponding rectification ratios are depicted in the inset. Reprinted with permission from ref 719. Copyright 2014 AIP Publishing. (b) The influence of proportion of the donor part (phenyl segment) and the acceptor part (pyrimidinyl part) on the rectification. Reprinted with permission from ref 721. Copyright 2014 Elsevier.

exploration of the mechanism for rectification based on the diblock dipyrimidinyldiphenyl molecule, Lörtscher et al.[694] used the MCBJ technique to study its charge transport in the low-bias regime and as a function of bias at different temperatures, where the *I*−*V* characteristics could be semi-empirically explained by the combination of the KBW and DP models, which indicates that the rectification originates from an asymmetric Coulomb blockade (charging effect) in combination with an electric-field-induced level shift.

It should be noted that the electronic decoupling between the donor unit and the acceptor unit is necessary for the rectification in these types of D−A diblock molecules, which could be achieved by controlling the torsion of one segment of the molecule relative to another. In fact, in one recent study established by Cui et al.,[719] further insight was obtained into the correlation between the rectification effect (the ratio) and the degree of molecular twist based on the density functional theory (DFT) combined with the nonequilibrium Green's function (NEGF) method (Figure 61a). The authors claimed that the rectification could be enhanced by the geometrical torsion-induced reduction in the conjugation length of the organic molecules. Furthermore, this significance of reducing the overlap between the orbitals of part D part and part A was stressed experimentally by Luo et al.,[720] who developed a series of long D−A diblock molecular wires with lengths ranging from 3 to 10 nm and studied their charge transport using the CP-AFM technique in the hopping regime. It was determined that when an insulating cyclohexane bridge was inserted between the 4,4′(5′)-diformyltetrathiafulvalene electron donors (D) and the *N*,*N*′-di(4-anilino)-1,2,4,5- benzenebis(dicarboximide) electron acceptors (A), an electrical rectification was achieved with ratios as high as 30 ± 1.0 V, whereas the absence of an insulating bridge led to current flow without rectification due to a large degree of conjugation in the D and A regions. When considering the initial D−σ−A model, both the intramolecular twist and the insulating barrier insertion have the function of reducing the electronic coupling between the donor part and the acceptor part, which is essential for the design of molecular diodes.

In addition to considering various methods to decouple the electronic overlap between the two distinct parts of the D−A molecules, the proportion effect on the rectification in diblock co-oligomer diodes also played an important role, which was recently proven by Hu and his colleagues using theoretical calculations (Figure 61b).[721] For rectifiers based on pyrimidinyl-phenyl diblock co-oligomers, it was determined that the 1:1 proportion of the two moieties favored a large rectification ratio for a short co-oligomer diode. However, for a long co-oligomer diode, the optimal proportion for the largest rectification ratio was not 1:1; however, an interesting proportion-dependent variation of the rectifying direction was observed. Furthermore, the perturbation from the external environment could impose an interference on the rectification behavior, as noted by Zhang et al. in the study where the protonation effects on the electron transport were investigated using a conjugated dipyrimidinyl−diphenyl diblock oligomer diode.[722] Their calculation indicated that the protonation in the outer pyrimidinyl was favorable for enhancing the rectification ratio, whereas the protonation in the inner pyrimidinyl played a dominative role in inverting the rectifying direction, which is the first time the experimental findings of the diblock molecular diodes have been clearly explained in the case of protonation in 2005.[716]

7.2.3. Rectification Stemming from Different Interfacial Coupling. The presence of the donor and the acceptor groups introduces nonsymmetry into the molecular junctions. Generally, one may expect rectification to occur from nonsymmetric molecular junctions that do not necessarily

DOI: 10.1021/acs.chemrev.5b00680
Chem. Rev. 2016, 116, 4318−4440

contain a pair of donor and acceptor groups or symmetric systems but have an unequal physical process in the forward and reverse bias. In fact, different couplings between the electrodes and the molecules on the two ends could lead to rectification, which has been predicted by the DP model. This prediction becomes common in nearly all of the single-molecule systems based on the published data. Although this rectification is not sufficient to achieve a larger diode effect if the bias voltage drop at the molecule−electrode interfaces cannot be controlled with subtlety, it still leads to new ideas for the design and implementation of molecular diodes. In section 7.1.2, we discuss the factors that influence the interfacial coupling, which coincidentally frames the outline of this section. In fact, a pair of different electrodes with distinct work functions, molecules with asymmetric terminated moieties, or both, which could lead to unequal interfacial coupling, were used to construct molecular diodes, among which several studies were based on monolayers or films instead of single-molecule junctions.

7.2.3.1. Different Electrodes. In the early 1990s, Ashwell et al.[704,723−725] developed suitable techniques for sandwiching LB multilayers or monolayers between two electrodes of different work functions to study molecular rectification. Generally, metals with different work functions provide different charge injection barriers, which may result in molecular rectification. For example, for HOMO-dominated molecules, that is, molecules whose HOMO is closer to the Fermi level than that of the LUMO, metals with a high work function provide a lower charge (hole) injection barrier as compared to metals with a low work function. Although molecules of interest in these asymmetric systems contain both donor and acceptor parts, the presence of a high-work function noble metal (Ag or Pt) on one side and a low-work function metal (Mg) on the other side lays the foundation for the molecular diodes. In these studies, metal electrodes, especially noble ones, such as Au, Pt, or Ag, possess an approximately constant density of electronic states within a narrow energy window relevant to the charge transport, which results in molecular junctions with relatively smooth and featureless transmission probabilities near the Fermi energy, thus limiting their applications including rectification. Fortunately, on the basis of the developments in material science as well as nanofabrication technology, various types of electrodes are being introduced into molecular electronics. Vuillaume et al. demonstrated a molecular rectifying junction constructed from a sequential self-assembly on silicon using Al on the other side of the electrode, which widened the selection of electrodes for molecular rectification.[726] Recently, Kim et al. introduced a hybrid device structure with a molecule trapped across a gold/graphite gap in the STM break junction system (Figure 34).[375] On the basis of this system, the charge transport characteristics of oligophenylamines were investigated, where the authors discovered a relatively high rectification ratio despite the inherent symmetry in the molecules, which could be due to the asymmetry in the voltage drop across the junction caused by the different interfacial coupling.

7.2.3.2. Anchoring Groups. As discussed previously, molecules with different anchoring groups or different tail lengths can result in asymmetric interfacial coupling, thus suggesting the considerable potential for achieving molecular rectification. Moreover, single-molecule systems with movable electrodes, such as STM, CP-AFM, and MCBJ, make it possible to tune the molecule−electrode distance with an atomic resolution, therefore modulating the interfacial coupling strength. In this context, in 2004, Kushmerick et al.[727] experimentally demonstrated the ability to achieve and tune the current rectification in metal−molecule−metal junctions through the control of the interaction strength of one metal−molecule contact by changing the anchoring groups. In 2014, this effect was further confirmed both experimentally and theoretically by Wang et al.[728] A molecule terminated by the thiol group and the amine group was attached at two ends between the Au surface and an STM tip. Similarly, Batra et al.[729] designed a molecular rectifier based on a symmetric, conjugated molecular backbone with a single methylsulfide group linking one end to a gold electrode and the other end to a covalent gold−carbon bond (Figure 62). The nonequilibrium

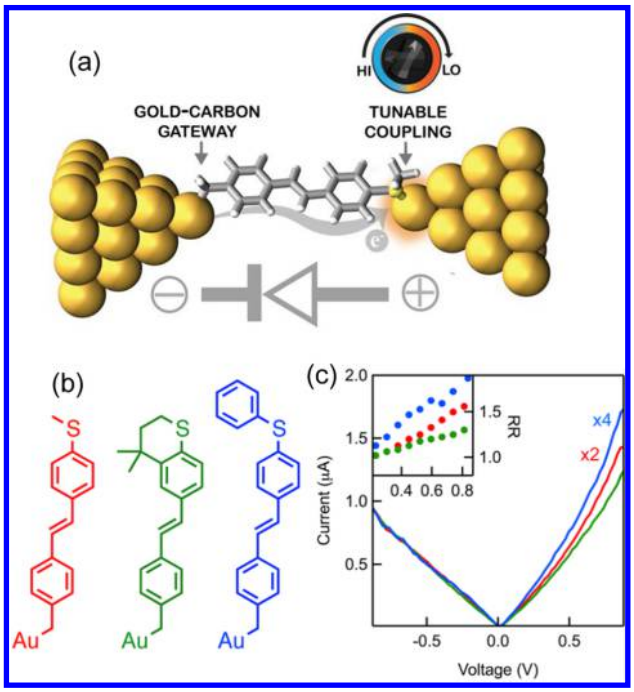

Figure 62. Molecular rectifiers with different anchoring groups. (a) Schematic for molecular circuits with a carbon−gold bond and a methylsulfide−gold bond. (b) Chemical structures for the three molecular rectifiers used. (c) Corresponding $I-V$ curves for the three molecules. Inset: Rectification ratio as a function of the bias. Reprinted with permission from ref 729. Copyright 2013 American Chemical Society.

transport calculations indicated that a hybrid gold-molecule "gateway" state was pinned close to the Fermi level of one electrode due to the formation of the gold−carbon bond, which could shift drastically with an applied bias, thus resulting in rectification at surprisingly low voltages. This study constituted the experimental demonstration of a predictably and efficiently tunable system of single-molecule rectifiers through a rational design of the anchoring groups. Recently, a theoretical study noted that the rectifying behavior of the dipyrimidinyl-diphenyl co-oligomer diode could even be reversed or largely enhanced by adjusting the asymmetric anchoring groups.[722] These studies set the foundation for a new generation of molecular rectifiers with high rectifying ratios and high tunability through interface engineering.[730]

7.2.3.3. Contact Geometry. As previously discussed in this report, the contact geometry in the electrode−molecule interface has a significant influence on the charge transport

DOI: 10.1021/acs.chemrev.5b00680
Chem. Rev. 2016, 116, 4318−4440

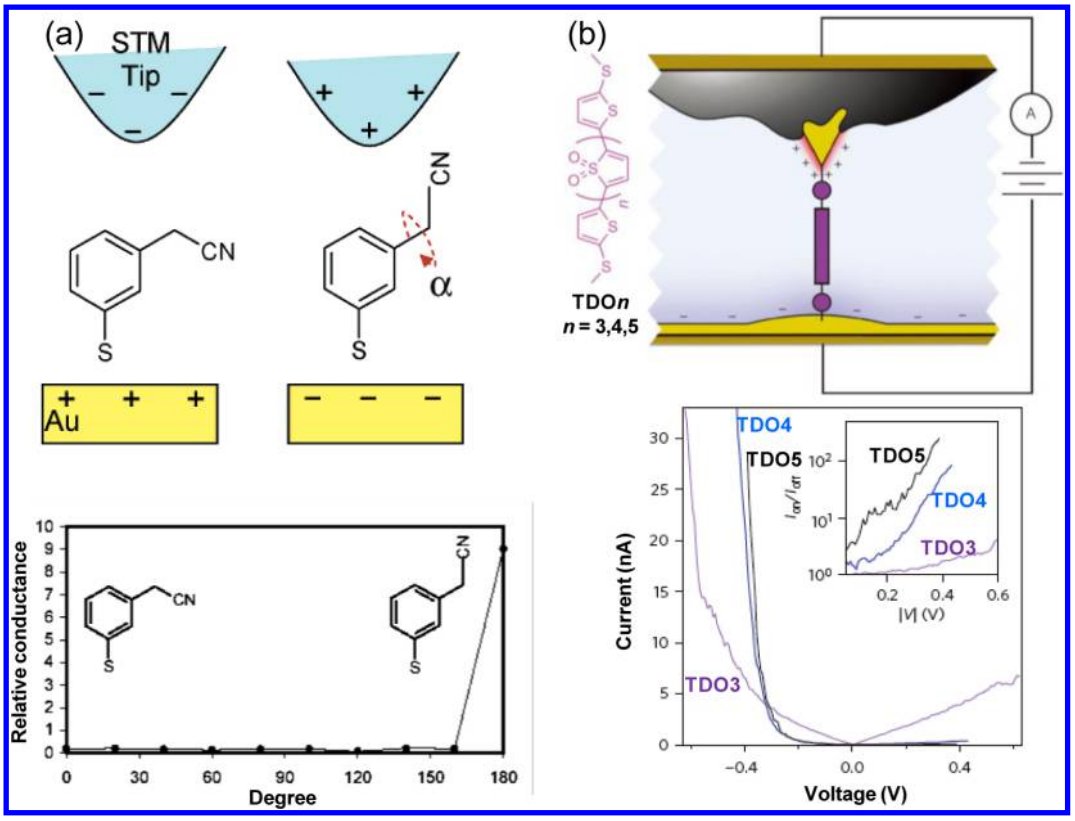

Figure 63. Other types of molecular rectifiers. (a) Top: Schematic representation of current rectification based on molecular conformational change. Bottom: Corresponding conductance as a function of a dihedral angle. Reprinted with permission from ref 735. Copyright 2002 American Chemical Society. (b) Top: TDO molecular structure used and schematic of molecular junctions created using asymmetric area electrodes through environmental control. Bottom: Average $I-V$ curves for TDOs (with n = 3–5). Inset: Rectification ratio (I_{on}/I_{off}) versus magnitude of applied voltages, which depict ratios of ~200 at 0.37 V for TDO5. Reprinted with permission from ref 737. Copyright 2015 Nature Publishing Group.

properties of the molecular junctions. Clearly, this effect is also embodied in the molecular rectification. In the task of building a diblock co-oligomer rectifier by adjusting the anchoring groups,[722] the authors determined that the asymmetric contact geometries playing a positive or negative role in improving the rectifying behavior is closely related to each molecular diode. In fact, one recent theoretical study precisely and systematically calculated the effects of different interfacial contact geometries, especially the absorption sites of an S atom in the headgroups of molecules on the surface of Au electrodes, on the rectifying behaviors of the molecular diodes.[701] These studies provide direct evidence highlighting the significance of the contact-geometry asymmetry to the rectification behavior, which serves as an aid to interpret future single-molecule electronic behavior.

7.2.3.4. Interfacial Distance. Additionally, the coupling strength could be tuned by the length of the insulating terminated tails used to connect to the electrodes. As noted by Kornilovitch, Bratkovsky, and Williams in their KBW model,[697] different tails on each side indicate different tunneling barriers, consequently leading to molecular rectification. For example, a single electroactive unit positioned asymmetrically with respect to the electrodes, and the corresponding HOMO and LUMO being distributed asymmetrically with respect to the Fermi level, could rectify electrical current. It should be noted that the construction of this model was an interesting accident, where the long insulating tail of $C_{16}H_{33}$ added to the molecule core not only leads to asymmetry but also helps form suitable LB films.[731] Afterward, additional studies, combined with other considerations for designing molecular diodes, were conducted on the basis of this general mechanism. Recently, Liu et al.[732] studied the rectification of current through a single molecule with an intrinsic spatial asymmetry. In this study, a rectifier with a large voltage range, high current, and low threshold was predicted by taking advantage of the relatively localized and high-energy d states of the cobaltocene moiety in the molecule. Combined with the calculations based on a self-consistent nonequilibrium Green function, the plausibility of forming excellent molecular diodes using metallocenes was demonstrated, resulting in a productive class of molecules.

In addition to terminated tails with unequal lengths, the spatially asymmetric molecule–electrode distance could also result in different interfacial coupling. In 2002, Taylor et al.[733] calculated the change in the current–voltage characteristics by securing one of the molecule–electrode interfaces while increasing the distance of the other, thus weakening the molecule–tip coupling. They stated that the operation range and rectification in the strongly chemisorbed molecules were limited by the width of the transmission resonances and their proximity to the Fermi level, both of which were strongly related to the interfacial coupling strength. Recently, using the theoretical calculation, the effects of the interfacial stretch or contraction on the rectification in diblock co-oligomer molecular diodes were investigated by Zhang et al.,[734] who determined that different mechanical treatments could inverse the rectification direction. Additionally, two competitive mechanisms, deduced from the asymmetric molecular level shift and the asymmetric evolution of orbital wave functions under biases, were proposed to be responsible for the

DOI: 10.1021/acs.chemrev.5b00680
Chem. Rev. 2016, 116, 4318–4440

rectification inversion due to their different sensitivities to the electrode−molecule distance. Furthermore, these results clarified that the rectification performance in the molecular diodes could be manipulated using the mechanically controllable method.

7.2.4. Additional Molecular Rectifiers. The improvements in the theory of electrical conduction through molecules allowed for a relatively good understanding of the rectification observed in the above-mentioned cases. The principle of molecular rectifiers can be summarized briefly as being that the electronic resonance between the Fermi level and the molecular energy level related to the charge transport occurs at different voltages in the forward and reverse bias directions, and that the barriers inhibiting the electron conduction are asymmetric at the two electrode−molecule interfaces. As further insight is obtained into the essence of rectification based on experimental and theoretical progress, additional molecular rectifiers depending on novel operation principles are being proposed, as reviewed briefly in this section.

Although the development of the molecular diodes based on rigid-structure molecules flourishes, investigations focusing on molecules with flexible nuclear degrees of freedom, that is, conformational changes, used to achieve current rectification increase. Ratner et al.[735,736] studied unimolecular rectification based on voltage-controlled intramolecular stereochemical modification (Figure 63a). Briefly, it was predicted that different conformations induced by an external electrical field could dominate the charge transport and result in rectification because of the inherently unequal capability to conduct electrons, which, to the best of our knowledge, has not been demonstrated experimentally. To achieve a transition between configurations driven by the external field, a strong dipole, potentially provided by one or more C−F or C−CN bonds, is necessary, and the simplest model is the system with a single flexible degree of freedom, in which the asymmetry of the junction can be preserved through a chemical bond between the molecule and at least one electrode.

A gate-controlled single-molecule diode was proposed theoretically by Zhang in 2004, where a clear modulation by the gate was obtained. Furthermore, when the positive voltage was high enough, the rectification could be reversed.[738] This prediction is valuable for designing and building future molecular logic devices and integrated circuits. Recently, Capozzi et al. provided another remarkable study on single-molecule diodes, where an approach was demonstrated to induce current rectification through environmental control.[737,739] The symmetry of a symmetric single-molecule junction with two electrodes of the same metal was broken by exposing considerably different electrode areas to an ionic solution (Figure 63b). This technique allowed them to control the junction's electrostatic environment in an asymmetric manner by simply changing the bias polarity. Using this approach, they achieved rectification ratios in excess of 200 at voltages as low as 370 mV based on a symmetric oligomer of thiophene-1,1-dioxide (TDO). This result is reproducible because they observed a similar rectification using other molecules/solvent systems. This method of environmental control provides a general route for tuning nonlinear nanoscale device phenomena that is beyond single-molecule junctions.

In summary, because they are the origin of molecular electronics, molecular rectifiers have received academic and commercial attention for more than 40 years. Benefiting from both the theoretical and the experimental efforts engaged in this field, this digital component critical for logic devices has evolved from an initial D−σ−A model to a derived D−π−A model to a simplified D−A model, in which the precise energy level alignment as well as the subtle electronic coupling between the donor region and the acceptor region in the molecule are significant for the rectification behavior. By enhancing the feasibility and the ease of construction of the single-molecule system, current−voltage curves with diode-like characteristics are common, even for molecules without donor or acceptor units, which could be ascribed to asymmetric interfacial coupling, as discussed above. Driven by this phenomenon, various methodologies have been injected into the design of single-molecule rectifiers. Furthermore, due to a thorough understanding of the charge transport through single molecules, additional models are being proposed for current rectification with novel operating principles. Clearly, a long process remains to realize commercially feasible rectifiers related to single molecules; however, a positive scenario can be imagined for the continuous attention and effort.

7.3. Modulation toward Molecular Transistors

Transistors, which are typically three-terminal electrical devices that constitute the heart of the electrical circuits, control the current flow between two electrodes (source and drain electrodes) by modifying the voltage applied at a third electrode (gate electrode). Because the microelectronics industry is enthusiastically developing highly integrated circuits that require devices with smaller dimensions, a logical limit to device miniaturization is transistors, whose channels are defined by a single molecule (Figure 64). Therefore, the construction

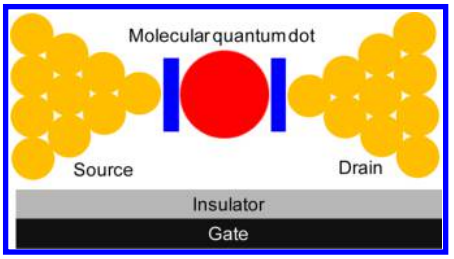

Figure 64. Schematic representation of single-molecule transistors with back gating architecture.

and understanding of such a device has been a long-standing goal of nanoelectronics. Thus, as detailed in sections 2−4.2, discrete approaches have been developed for creating nanometer-spaced electrodes. Among these approaches, carbon electrode−molecule junctions and electromigration break junctions are particularly attractive because of their intrinsic three-terminal device architectures.[740] One important feature of the former is the improved device stability due to the use of covalent chemistry for forming molecular junctions, which is of considerable importance to build molecular devices with desired functions toward practical applications. This topic has been briefly discussed in section 3 and is provided in more detail in section 7.5. In this section, we focus on the primary progress of single-molecule transistors with back gating, side gating, and chemical gating configurations.

7.3.1. Back Gating for Novel Physical Phenomena Investigation. One of the most generalized gate configurations, the back gate, is commonly found in solid-state device architecture, in which the entire nanocircuit is supported by heavily doped Si, Al, or polymer substrates and insulated from

DOI: 10.1021/acs.chemrev.5b00680
Chem. Rev. 2016, 116, 4318−4440

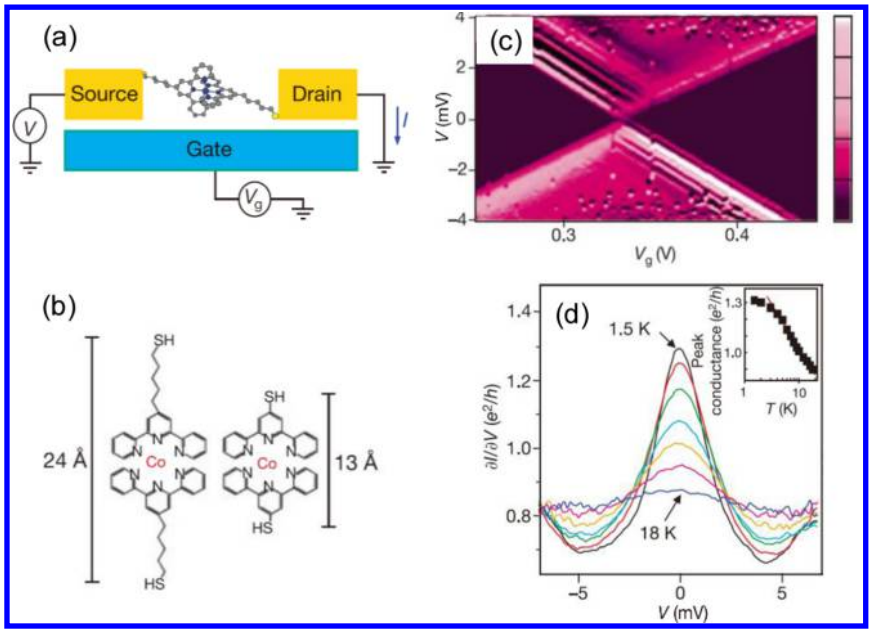

Figure 65. Solid-state single-molecule transistors. (a) Schematic diagram of the single-molecule transistors. (b) Molecular structures of the Co complexes. (c) Coulomb blockade observed in devices formed from longer molecules. (d) Kondo peaks as a function of the voltage. The inset depicts the conductance as a function of the temperature at $V = 0$. Reprinted with permission from ref 21. Copyright 2002 Nature Publishing Group.

the gate electrodes in the bottom by an insulating layer to ensure that only molecules in the nanogaps between the source and the drain electrodes would be electrostatically modulated. The insulating layer above could be produced by oxidizing the substrate to achieve the corresponding oxide insulator, such as SiO_2, Al_2O_3, etc., or a tens-of-nanometer vacuum gap,[41] for which the thickness and dielectric constant are the two most critical parameters for determining the scale that the gate modulation could reach without incurring gate−drain leakage or gate breakdown. Therefore, selecting the gate and insulator materials is important for the total level shift, and an insulator with a high breakdown voltage, reduced thickness, and easy fabrication is required to obtain high-performance single-molecule devices.

The electromigration technique is one of the most important techniques used to fabricate source−drain electrodes with a functional back-gating configuration. In fact, solid-state single-molecule transistors with back gating were reported by two separate groups as early as 10 years ago.[21,210] To achieve the strong effects of the gate voltage on the molecules, both groups used electromigration-induced break junctions to fabricate their device on silicon wafers with extremely thin dielectrics (30 nm silicon oxide or 3 nm aluminum oxide) (Figure 65a). This approach is difficult because with the gate dielectric scaling down, parasitic currents generally caused by various mechanisms (e.g., quantum tunneling, electron hopping) can lead to a current between the gate and the drain, thus overshadowing the molecular signature. Therefore, the primary challenge in device fabrication is to design a junction geometry, in combination with the proper material selection, which can reduce the gate leakage as much as possible and maximize the electric field reaching the molecule. The need for such precise control may partly explain why so few of the devices prepared by the authors functioned properly as transistors. In their studies, they observed novel physical phenomena based on two mechanisms: Coulomb blockade, in which the flow of electrons is controlled by the sequential charging of a molecule; and the Kondo effect, in which conducting electrons interact with a local spin (intrinsic angular momentum) in a molecular junction. Interestingly, changing the length of the insulating tether alters the coupling of the molecules to the electrodes, enabling the fabrication of devices that exhibit either of the single-electron phenomena mentioned previously. For example, Park et al.[21] examined two related molecules containing a Co ion bonded to polypyridyl ligands and attached to insulating tethers of different lengths (Figure 65b). It was determined that devices formed using the longer molecules indicated a blocking of the current due to the presence of the Co ion island (Coulomb blockade) (Figure 65c), whereas devices created using the shorter molecules indicated the Kondo effect (Figure 65d). This Kondo effect is indicative of the formation of a bound state between a local spin on an island and the conduction electrons in the electrodes that enhance the conductance at low biases. In another example of single-electron-transistor measurements,[741] Kubatkin et al. observed that the molecular electronic levels were strongly perturbed as compared to those of the molecules in the solution, leading to a significant reduction in the gap between the HOMO and the LOMO. This surprising observation could be caused by image charges generated in the source and drain electrodes, thus resulting in a strong localization of the charges on the molecule.

In addition to the two single-electron phenomena discussed above, Ghosh et al.[742] predicted a third phenomenon based purely on the electrostatic modulation of the molecular-orbital energy of a single molecule. Remarkably, this result was realized by Song et al.,[171] where unprecedented insight was provided into the underlying physics of the charge transport in their molecular transistors created using the electromigration technique. In this study, they performed an IETS measurement on a gate voltage with two prototype molecules, a 1,8-octanedithiol (ODT) with an alkyl backbone and a 1,4-benzenedithiol (BDT) with a delocalized aromatic ring, to examine the interactions between the tunneling electrons and the vibrational modes of the molecules. Because each dithiol

DOI: 10.1021/acs.chemrev.5b00680
Chem. Rev. 2016, 116, 4318−4440

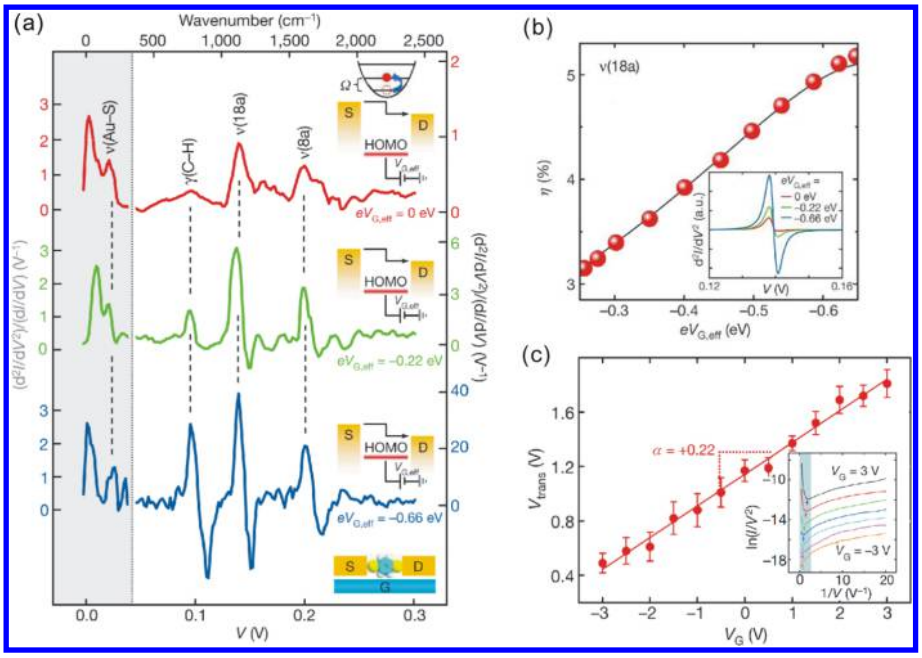

Figure 66. Gate modulation of molecular orbitals in single-molecule transistors. (a) IETS measured at 4.2 K for different values of the effective molecular orbital gating energy ($eV_{G,eff}$), with the vibration modes assigned. The left-hand *y*-axis corresponds to the gray shaded region of the spectra, and the various right-hand *y*-axes (with different scales) correspond to the related (color-coded) spectra in the nonshaded region. (b) The relative change, η, in the normalized conductance for the ν(18a) mode as a function of $eV_{G,eff}$. The circles depict the experimental data, and the solid curve represents the theoretical fit. The inset is the gate-variable IETS for the ν(18a) mode. (c) Plot of V_{trans} versus V_G. The inset is the corresponding TVS spectra. Reprinted with permission from ref 171. Copyright 2009 Nature Publishing Group.

had its own vibrational "fingerprint", this technique provided definitive proof that the measured currents actually passed through the molecules in single-molecule transistors (Figure 68a). More importantly, it was determined that the spectra of the ODT junction remained essentially unchanged at different values of the gate voltages, which is because the HOMO level for the ODT is energetically considerably farther away from the Fermi level (E_F). However, the IET spectra of the BDT junction were drastically modified by the gate voltages, thus exhibiting an enhanced spectral intensity. This observation was attributed to the dominant transport orbital (the HOMO) being strongly coupled to the internal vibrational modes of the BDT, resulting in a resonantly enhanced IETS (Figure 66b). Additionally, the TVS technique was used to reveal the energy offset (V_{trans}) between the gating orbital of the molecular junction (the orbital that modulates electron tunneling) and the Fermi levels of the source and drain electrodes. By measuring V_{trans} using the TVS at different applied gate voltages, a linear relationship was determined to exist between the gate voltage and the molecular-orbital energy in their devices, as expected for single-molecule transistors (Figure 66c). These findings demonstrated the direct gate modulation of the molecular orbitals, thus enhancing the prospects for true molecularly engineered electronic devices.

Furthermore, the three-terminal electrostatic back gate can be achieved via a mechanically controllable break junction (MCBJ). Champagne et al. first reported a device in which a gold wire was lithographically patterned on top of a silicon/silicon−oxide substrate.[151] The silicon was heavily doped, thus acting as a back-gate electrode. After the oxide layer was etched, a suspended gold wire was obtained above the substrate using a vacuum as an insulator. Their gated MCBJs provided the capability to simultaneous adjust the spacing between the electrodes and the molecule energy levels. It was determined that the mechanical motion could change a molecule's capacitance, conductance, and gate voltage value for the Coulomb blockade degeneracy. It is anticipated that this new experimental tool will enable systematic studies of how changes in molecular conformation affect the electrical conduction and how transport varies between the weak-coupling Coulomb blockade and the strong-coupling Kondo regimes. A few years later, using the same device, further experiments were reported in which the spin states in the Spin-1 molecules could be mechanically controlled in the absence of a magnetic field by stretching the individual cobalt complexes.[154] This control enabled quantitative studies of the underscreened Kondo effect and could serve as model systems for performing precise tests on correlated-electron theories.

A similar back-gate approach was introduced by Martin et al.[743] In contrast to Champagne et al., the greatest difference is that the flexibility of the substrate was used instead of that of the rigid silicon substrate; thus, the junctions could be easily broken by mechanical means. However, upon application of a gate voltage, the freshly broken electrodes were pulled toward the substrate due to the electric field. To prevent the drift of the source−drain electrodes under electrostatic gating, Martin et al. created an improved design in which the gate and the source−drain electrode were suspended (i.e., the source−drain electrode, insulation layer, and gate electrode were sandwiched and suspended above the substrate together).[153] To test the gate action of this device, the C_{60} molecules were studied, and it was determined that the total shift in the molecular levels for the devices was approximately 40 meV. Recently, the same group further investigated the image-charge effects in single-molecule junctions using this MCBJ with a back gate.[152] It was determined that a substantial increase in the transport gap and level shifts as high as several hundreds of millielectronvolt appeared when the electrode separation increased by a few

DOI: 10.1021/acs.chemrev.5b00680
Chem. Rev. 2016, 116, 4318−4440

angstroms. An analysis of this large and tunable gap renormalization based on atomic charges revealed the dominant role of image-charge effects in the single-molecule junctions.

Carbon-based electrodes (i.e., graphene sheets and carbon nanotubes) are interesting candidates to replace noble metals because they provide a higher structural stability, even under ambient conditions, and reduce the size mismatch between the electrodes and the molecule. Another advantage of carbon-based electrodes is that they allow the molecular junctions to be brought closer to the gate as compared to bulky gold, and they typically do not have electrostatic shielding properties, thus enhancing the gating efficiency. There are several significant reports in which different strategies were used to link the molecules to the carbon electrodes, and the gating of the current was observed.[740,744] Here, we only focus on the novel physical phenomenon investigation using back gating with carbon electrodes. For example, Marquardt et al. first reported an example of a single molecular junction at room temperature displaying electroluminescence.[354] The selected molecules have fluorescent cores extended with organic spacers, which not only increase the molecule length but also allow for easy electrostatical trapping of the molecules in the gap using dielectrophoresis. These results suggested a new characterization and functional possibilities as well as demonstrated a significant potential of carbon nanotubes for use in molecular electronics. One disadvantage to back gating with carbon nanotube electrodes is that, for example, an SWNT with a p-type semiconductor behavior may completely mask the gate response of the molecule. This problem could be solved using the MWNT or thicker few-layer graphene flakes. The versatility of graphene may allow the production of electrodes with intrinsic functional devices. For example, it was predicted that graphene electrodes terminated in zigzag edges may act as Fano-like resonances and spin filters, which allow the injection of spin-polarized currents into the bridged molecules.[745] However, the fabrication of the reliable, nanometer-sized, and adjustable gaps between the source and the drain electrodes in the graphene sheets remains a considerable challenge. Particularly, improving the control of the edge chemistry is crucial.

7.3.2. Side Gating for Electron Transport Control. The creation of a single-molecule field-effect transistor (FET) has been considered a critical step in molecular electronics. A nanoscale gap junction formed by "electromigration" is a highly efficient method for creating a highly integrated single-molecule FET. However, this method is limited in practice by its extremely low device yield.[171] Conversely, the MCBJ technique is advantageous because it can easily form single-molecule junctions several times mechanically, and it does not suffer from low yield.[130] In the MCBJ, the primary challenge is the method that is used to form reliable three-terminal FET junctions from single molecules. The three-terminal MCBJ with back gating geometry may suffer from the gating electrode breaking because it bears a large strain to separate the source−drain electrodes by bending the substrate. Xiang et al. demonstrated a completely different single-molecule FET junction with the MCBJ using a nanometer scale noncontact side gate to the molecular junctions (Figure 67).[150] In this geometry, the gate electrode and source−drain electrodes were located in the same plane (thus the deformation of the gate electrode was extremely reduced during bending of the substrate), and the electrical field was enhanced in the thickness of the gate electrodes, especially on the gate side as compared to that of a typical back gate configuration.[174] Using this side-gating MCBJ, the ability to form a stable single-molecule junction via the MCBJ technique and shift the energy levels of the molecule by side gating was successfully demonstrated.

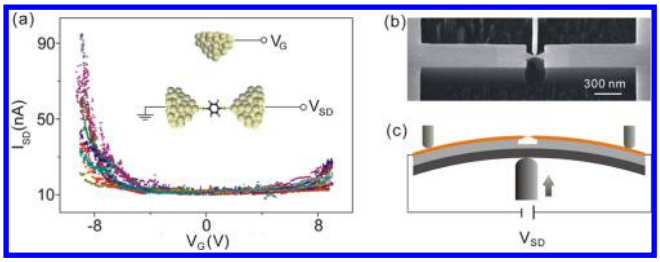

Figure 67. Molecular transistors with side gating. An external electric field generated by a side-gate electrode was applied to single-molecule junctions formed by the MCBJ. (a) Source drain current (I_{SD}) versus gate voltage (V_G) curves for the Au−BDT−Au molecule. The current was modulated by the gate voltage in 12 different molecular junctions. The inset illustrates a three-terminal junction with the BDT bridged between the source and drain electrodes. (b) Top view of a scanning electron microscopy (SEM) image of a microfabricated MCBJ chip consisting of a freestanding metal bridge with a gate electrode. (c) Schematic of the MCBJ setup. The distance between the electrodes for opening and closing the operation modes can be tuned by bending or relaxing the substrate, respectively. Reprinted with permission from ref 150. Copyright 2013 American Chemical Society.

Generally, to directly visualize the electromigration process and discriminate trapped molecules/metal clusters from dusts inside the gap or visualize a source−drain breaking process, a transmission electron microscopy (TEM) requires the use of electron transparent substrates, which are noncompatible with the most common three-terminal devices with a back gate electrode. The side gate geometry is relatively compatible with the transmission electron microscopy inspection and can overcome this problem.[174] In addition to this advantage, the gate potential could be screened by the source−drain electrodes, which indicates that only those molecules facing the gate electrodes can be easily influenced by the gate electrodes. Nevertheless, the in-plane three-terminal molecular junction presents a new platform for fabricating highly stable single-molecule transistor junctions.

7.3.3. Electrochemical Gating for Efficient Gate Coupling. Electrochemical gating is a promising method for efficient gate coupling that provides a unique opportunity to manipulate the energy alignment and the molecular redox processes for a single-molecule junction.[746] Because the gate voltage falls across the double layers at the electrode−electrolyte interfaces, which are only a few ions thick, a field of approximately 1 V/Å can be reached. Hence, a large gate field and a high gating efficient can be achieved using an electrochemical gate.[747] One advantage of an electrified solid/liquid interface is that the two potential differences can be controlled simultaneously: (1) the bias voltage between the source and the drain electrodes; and (2) the potential drop between the working electrodes and the reference electrode. Generally, the electrochemical gating effect is realized via tuning the Fermi level of the junction electrodes, thus changing the redox state of the molecular functional unit. The STM break junction (EC-STM-BJ) is the most widely used technique in electrochemical gating studies thus far, and numerous significant results, such as current enhancement mechanisms, electrolyte gating models, and molecule structure changes via electrochemical gating, have been reported.[527,747−750] It should

DOI: 10.1021/acs.chemrev.5b00680
Chem. Rev. 2016, 116, 4318−4440

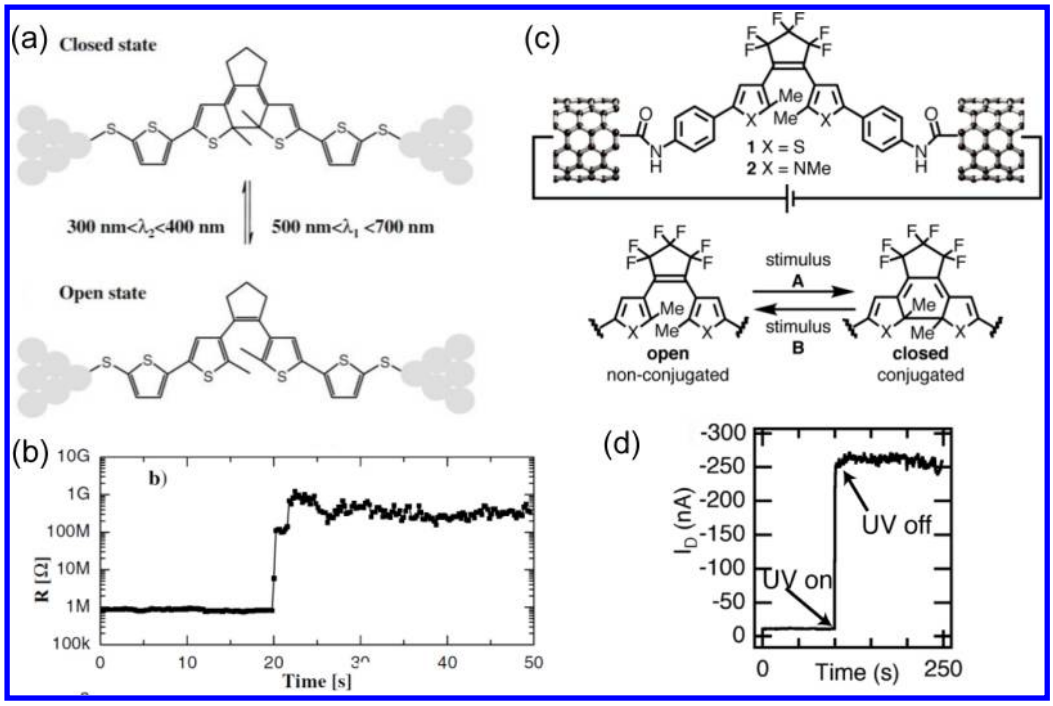

Figure 68. One-way photoswitching in single-molecule junctions. (a) Photochromic molecular switch between two Au contacts in the closed state (top) and the open state (bottom). (b) Resistance versus time, which depicts the switching of the junctions from the conducting to the insulating state. Reprinted with permission from ref 765. Copyright 2003 American Physical Society. (c) Molecular bridges between the ends of an individual SWNT electrode. (d) Drain current as a function of time, which depicts the switching of the junctions from the low to the high state. Reprinted with permission from ref 766. Copyright 2007 American Chemical Society.

be noted that to reduce the electrochemical leakage currents, it is necessary to insulate the STM tip by a nonconductive material, except for the very end of the tip. The tip insulation is a simple procedure and can be performed in any laboratory in the EC-STM-BJ configuration. However, the insulation process is challenging for fixed nanospaced electrodes in the MCBJ configuration.[146,751]

It should be noted that the control of the charge transport in a single-molecule junction using electrolytic gating based on one nonredox active molecular system is also possible.[74,752,753] For example, Capozzi et al. reported modulation of the conductance of electrochemically inactive molecules in single-molecule junctions using an electrolytic gate.[753] This experimental study combined with the density functional theory calculations indicated that electrochemical gating can directly modulate the alignment of the conducting orbital relative to the metal Fermi energy, thus changing the junction transport properties. More recently, Baghernejad et al. demonstrated that the single-molecule conductance could be controlled via both the Fermi level tuning and the redox switching.[74] In the small potential region (redox-inactive), the effect of the gating is to shift the Fermi level relative to the molecular energy level, thus leading to a modest change in the conductance. A further shift in the electrode potential led to large and reversible jumps in the conductance due to the change in the molecular redox state and the molecular conjugation switching. The study indicated that the electrochemical gating of single-molecule junctions could be modeled using computational models via conversion of the potential to the energy scale.

In summary, different approaches, including carbon electrode−molecule junctions, electromigration-induced molecular junctions, and three-terminal MCBJ-based break junctions, have been successfully developed to realize single-molecule transistors and demonstrated a direct gate modulation of molecular orbitals through the multispectroscopy approaches.[740] These studies set the benchmark for the validation of future studies in the charge transport for molecular systems. However, additional work must be performed before molecular electronic devices can effectively compete with their larger silicon-based equivalents. One of the most urgent issues is to develop an efficient fabrication method that allows high yields of densely packed single-molecule devices. It is expected that the electron transport through the molecule may be controlled by a universal gate electrode, including electrical gates, electrochemical gates, magnetic gates, optical gates, terahertz wave gates, and mechanical gates. Additional new designs and device architectures are needed to transition from laboratory research to practical applications.

7.4. Switching toward Memory Devices

The important next step in molecular electronics toward actual applications is the construction of a reliable molecular switch, that is, a particularly attractive molecular electronic device. It is improbable to build a circuit without a switch. The reason for this is that transistors, a core component of current computer circuits, are ultimately operated as switches, where the conductance is efficiently and controllably turned on and off by a gate electrode. Therefore, single-molecule switches could be the prototypical device used to complement silicon in the logic and memory elements because of its clear advantage for ultralarge density integration.

In principle, a molecular switch can alter the conductance, which occurs from changes in its physical properties (such as the electronic structure of the molecule and correspondingly its density of states) upon exposure to external stimuli (e.g., light, heat, ion, magnetic, or electric field). This requires the

DOI: 10.1021/acs.chemrev.5b00680
Chem. Rev. 2016, 116, 4318−4440

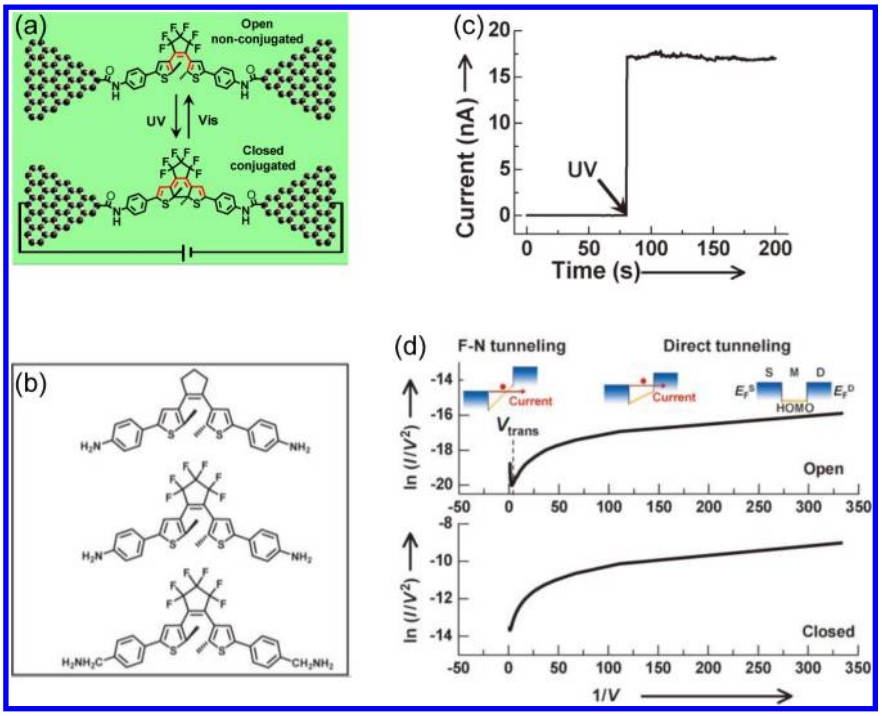

Figure 69. Switching properties of graphene−diarylethene single-molecule junctions. (a) Switching of graphene−diarylethene junctions. (b) Molecular structures. (c) Current-versus-time curve of a graphene−diarylethene junction. (d) F−N plots of the *I*−*V* characteristics for the same junction. The insets indicate the conventional barrier model. Reprinted with permission from ref 490. Copyright 2013 Wiley-VCH.

molecules to have several (at least two) stable isomers and transition between the isomers. From an engineering point of view, the challenge is to build single-molecule switches whose conductance changes are detectable, ideally from zero (OFF state) to infinity (ON state). Early studies on molecular switches were performed on the basis of self-assembled monolayers,[331,754−757] particularly using the STM or AFM setups, which have been surveyed in a recent review.[758] In the following section, we focus on summarizing the design, construction, and electrical properties of recent single-molecule switches, including conformation-induced switches, electrochemically triggered switches, and spintronics-based switches.

7.4.1. Conformation-Induced Switch. To create memory effects in a molecular switch, an external stimulus is required to generate independently stable states so that the information can be encoded as "0" and "1" in the same device. To achieve electrical bistability, a promising approach recently developed relies on the use of molecular photochromics because they undergo reversible photoisomerization between two isomers upon irradiation with light of different wavelengths.[759,760] These conformational changes result in remarkable differences in their electronic structures and their distinct photophysical properties, which has been well observed in solution, thus forming the basis for new types of optoelectronic devices and molecular switches.[761] However, in practice, a significant challenge is to maintain the photophysical properties existing in solution when sandwiched between two solid-state electrodes at the single-molecule level. This is because the operational parameters, switching voltages, and bistability are sensitive to the environment. The strong coupling with the electrodes and/or electrostatic interaction with the substrate could be detrimental for realizing the single-molecule switches. For example, Lara-Avila et al.[762−764] demonstrated an environmental effect on the electronic structure of a bianthrone molecule that was connected to silver electrodes on aluminum oxide substrates. In addition to the observation of persistent switching of the electric conductance at low temperatures, it was determined that the measured activation energy of the photoisomerization process was on the order of 35−90 meV, which is an order of magnitude lower than that measured for free bianthrone (ΔE_{act} = ∼0.9 eV). The reason for this is that when positioned in intimate contact with silver and on an aluminum oxide dielectric with high permittivity, one bianthrone isomer acquired a negative charge that shifted the molecular geometry (due to image forces in the substrate), which in turn decreased the transition barrier.

Another series of examples that highlight the importance of the electrode−molecule contact interface are single-molecule photoswitches based on photochromic diarylethenes (DAEs).[490,560,765,766] In 2003, Dulić et al.[765] first fabricated dithiolated photochromic molecular switches using a mechanically controllable break-junction technique (Figure 68a). They observed the molecules switching from the conducting to the insulating state when illuminated with visible light (λ = 546 nm) but failed to observe the reverse process, even when illuminated with UV light (λ = 313 nm) (Figure 68b). They attributed this to quenching of the molecule's excited state in the open form due to the presence of the gold surface plasmon through the Au−S bonds. To decouple the strong interaction between the DAE molecules and the electrodes, innovative molecular design and device architectures are required to preserve the molecular functions. In an attempt to solve this problem, Whalley et al.[766] built different types of single-molecule switches using the SWNTs as point contacts, where they used covalent amide linkages to form a robust contact interface (Figure 68c). It was observed that these SWNT-diarylethene single-molecule junctions could switch from the low conductance state (open form) to the high-conductance state (closed form) but not back again (Figure 68d). Interestingly, this phenomenon is contrary to the situation

DOI: 10.1021/acs.chemrev.5b00680
Chem. Rev. 2016, 116, 4318−4440

occurring in the devices made from gold electrode break junctions with dithiolated molecules, as discussed above. In the case of SWNT-diarylethene single-molecule junctions, the reason is most likely due to the energy dissipation of the excited state of the closed form by the electrodes. This result is consistent with the fact that the length of the π-conjugation on the termini of the DAE switches decreases the quantum yield for opening.[767] The nanotube is the ultimate extension of this conjugation. These results imply that the electrode−molecule contact interface is one of the most challenging issues in realizing functional molecular electronic devices.

In another attempt, Jia et al.[490] developed a series of single-molecule photoswitches based on a new device platform of graphene-molecule single-molecule junctions (Figure 69a). In this study, to tailor the energy level alignments at the molecule−electrode interface, the diarylethene backbones were modified with rationally designed side and anchoring groups. As indicated in Figure 69b, the second molecule was achieved by substituting the hydrogenated cyclopentene of the first molecule with the fluorinated unit, while the third was based on the second by further introducing a methylene group (CH_2) between the terminal amine group and the functional center on each side. Demonstrated by the theoretical calculations, molecular engineering can be an efficient tool for tuning the molecule−electrode coupling strength. A reproducible optoelectronic switching from the off state to the on state (Figure 69c) was achieved. Unfortunately, continuous reversible switching was not realized, which indicated that the presence of the strong coupling between the molecules and the electrodes remained, hence consistent with the case of the SWNT-based molecular junctions. In addition to the observation of one-way photoswitching, detailed spectroscopic analyses based on both barrier and resonant tunneling models were performed, which supported the experimental observation of the photogated tunneling transition in the molecular junctions from direct to Fowler−Nordheim (F−N) tunneling (Figure 69d). This approach of molecular engineering was also reported by Kim et al.,[560] where four sulfur-free diarylethene molecules were developed to reduce the possibility of unintended binding. Furthermore, the charge transport of the open and closed isomers of the photoswitching molecules in the MBCJ-based single-molecule junctions was studied at low temperatures (Figure 70a). The single-molecule conductance was examined by breaking and forming the atomic contacts repeatedly, which revealed that both the conduction properties and the conductance switching ratios were significantly influenced by the end groups as well as the side chains of the molecules (Figure 70b). By analyzing the $I-V$ curves within the framework of the single-level transport model, an unexpected behavior of the current-dominating molecular orbital was found upon isomerization. These investigations provide new insight into designing novel types of functional molecule-based devices toward practical applications. The realization of in situ continuous reversible switching of the single-molecule photoswitches between two measurable conductance levels remains a formidable challenge, thus leaving an interesting opportunity for future studies to address.

Another possibility for controlling electronics at the single-molecule level by directing molecular conformation is stereoelectronic effects because they determine how the properties and reactivities of the molecules depend on the relative spatial orientations of their electron orbitals. Recently, this idea was first demonstrated by Su et al.,[107] who developed a single-molecule switch that operated through the stereoelectronic effect. Using permethyloligosilanes with methylthiomethyl electrode linkers, it was determined that the strong σ conjugation in the oligosilane backbone coupled the stereoelectronic properties of the sulfur−methylene σ bonds at the contact interface. As predicted by theory, this strong coupling led to three distinct dihedral conformations that had extremely different electronic characteristics (Figure 71a). Remarkably, by simply lengthening or compressing the molecular junction, the transition between the three species could be controlled, thus realizing conductance switching between the two states (Figure

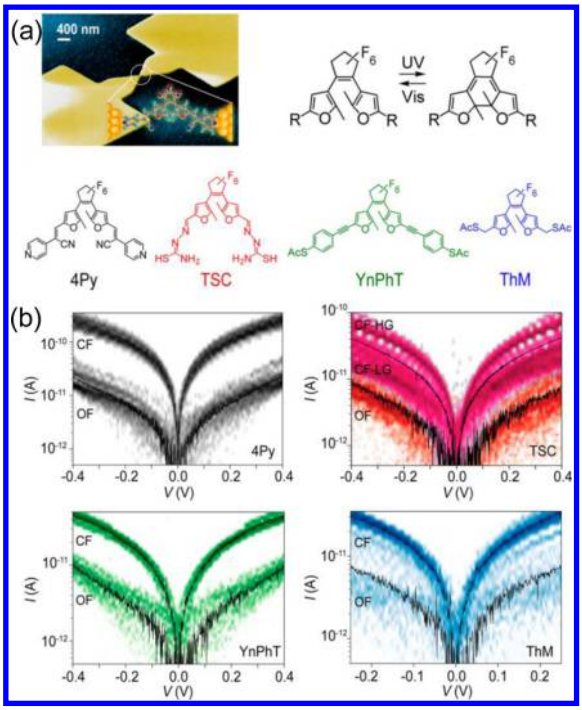

Figure 70. Switching properties of sulfur-free diarylethene molecules. (a) SEM image of an MCBJ device and the structure of four photochromic molecules: 4Py (black), TSC (red), YnPhT (green), and ThM (blue). (b) Density plots of approximately 20 $I-V$ curves of the open form (OF) and the closed form (CF). Reprinted with permission from ref 560. Copyright 2012 American Chemical Society.

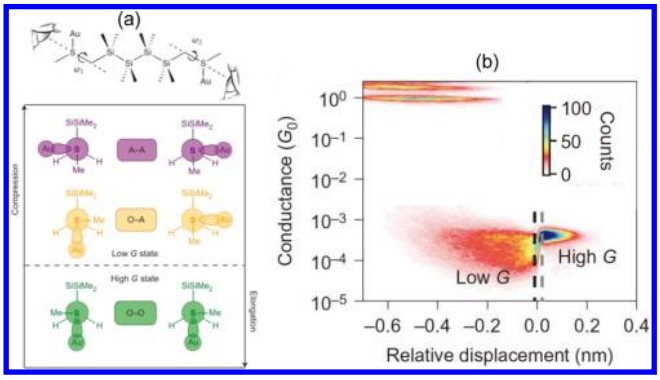

Figure 71. Directing molecular conformation by stereoelectronic effects. (a) Three dihedral configurations: A−A (purple), O−A (yellow), and O−O (green) from the perspective of the sulfur−methylene σ bond in the Au−Si4−Au system. (b) 2D conductance−displacement histogram for Si4 compiled from traces that demonstrate switching. Reprinted with permission from ref 107. Copyright 2015 Nature Publishing Group.

DOI: 10.1021/acs.chemrev.5b00680
Chem. Rev. 2016, 116, 4318−4440

71b). This study leads to a unique technique for incorporating reaction chemistry into the design of a new generation of functional molecular electronic devices. Using MCBJ-based two-terminal junctions, Schirm et al.[768] demonstrated that a metallic atomic-scale contact could be operated as a reliable switch driven by the controlled current. They also provided evidence that the switching process was caused by the reversible rearrangement of single atoms in the MCBJs. By employing MCBJ junctions, Lörtscher et al. demonstrated that a single molecule in a two-terminal configuration could be reversibly and controllably switched between two stable states in response to an external voltage stimulus. With the same measurement protocol but different molecules, they concluded that the observed switching had truly a molecular origin and the possible reason for switching was the conformational change.[144] Because of the hysteretic behavior of conductance with two distinct states, these two-terminal switches can be potentially used as a nonvolatile information storage element.

7.4.2. Electrochemically Triggered Switch. As discussed in section 7.3, three-terminal molecular junctions have the capability of tuning wave functions and, particularly, the redox energy states of the molecular bridges due to the consequent control over the junction conductance. However, placing three electrodes in intimate proximity of a molecule is extremely challenging. This result has been demonstrated in solid-state planar device architectures, where a metal gate electrode is separated from the source–drain contacts by a thin dielectric film. One disadvantage of these approaches is the lack of precisely controlling the degree of molecule–gate electrode coupling, which is crucial to modulating the molecular energy levels of the molecule necessary for sufficient electrical coupling with both leads. Additionally, another possible challenge is to avoid the evaporation of metal grains in the electrode gap during metal evaporation in the junction fabrication, which is detrimental to the electrical characterization of the molecular junctions. To solve these issues, an alternative approach to realizing strong gating effects is an electrochemical gate. The measurement of the electrochemical gating of a single molecule is performed in an electrolyte, as schematically illustrated in Figure 72. In this setup, the bridge energies are controlled

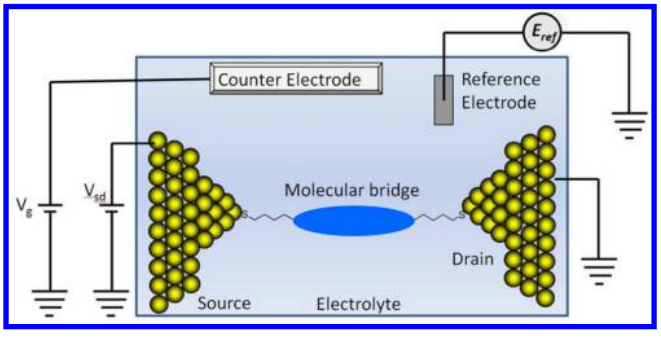

Figure 72. Schematic illustration of the electrochemical gating in a single molecule in an electrolyte. Reprinted with permission from ref 769. Copyright 2012 American Chemical Society.

through the electrochemical potential for molecular devices immersed in an electrolyte solution relative to a reference electrode. This is typically achieved in a four-electrode electrochemical setup with counter and reference electrodes serving alongside the source and drain electrodes (both of which are the working electrodes of the electrochemical cell). In strong electrolytes, a remarkable feature of the electrochemical setup is that the Debye screening length can be extremely short, that is, approximately a few angstroms. Although the counter and reference electrodes are physically far from the molecular bridge, any charge on the molecular bridge can be detected by the charge in the solution at a distance significantly shorter than what can be generally achieved in the solid-state planar device architectures (see section 7.3). For example, if a 0.5 V potential difference exists across an electrochemical double layer with a thickness of 0.5 nm, a mean electric field strength of 10^9 V m^{-1} can be achieved across this double layer region. Therefore, this strong and reproducible gate field is sufficient to significantly modulate the current across single molecules. It should be noted that to minimize the electrochemical leakage currents and the capacitive current components, the source–drain electrodes should be insulated by a nonconductive material, except at the very end of the electrode. However, in the case of nanogapped electrodes in the break junction configuration, the insulation process is relatively challenging.

To obtain the switching property using electrochemical gating, redox-active molecules represent a particularly attractive class of switches because they can be reduced or oxidized upon an applied electrochemical gate field. In this context, the primary challenge is to achieve a high ratio between the ON and OFF states of the nanojunction conductance. For example, Kay et al.[769] assembled a redox active pyrrolo-tetrathiafulvalene (pTTF) derivative (Figure 73) to gold contacts at both ends

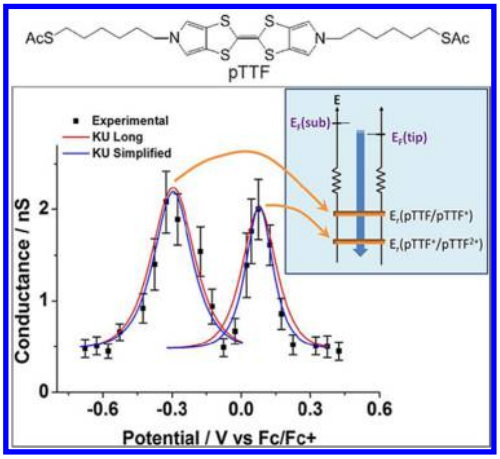

Figure 73. Conductance–sample potential relationship of pTTF. The red lines depict the long KU model, and the blue lines depict the simplified KU model. For both redox transitions, the KU model versions fit the experimental data well. The inset depicts a schematic energy level representation of the KU model for the two redox transitions. When the electrode potential is scanned positive, the pTTF/pTTF$^+$ redox transition is first brought into "resonance", and then at more positive potentials, the second redox transition (pTTF^{2+}/pTTF$^+$) comes into resonance. Reprinted with permission from ref 769. Copyright 2012 American Chemical Society.

using $-(CH_2)_6S-$ groups. By using an in situ STM break junction configuration (Figure 73), they observed a multiple OFF–ON–OFF–ON–OFF conductance switching behavior with a conductance ratio of ~4 when the electrode potentials matched the redox peak positions (Figure 73). These redox peaks can be ascribed to two reversible redox processes of the pTTF moiety: the formation of a radical cation and a dication. This molecular conductance versus electrochemical potential

DOI: 10.1021/acs.chemrev.5b00680
Chem. Rev. 2016, 116, 4318–4440

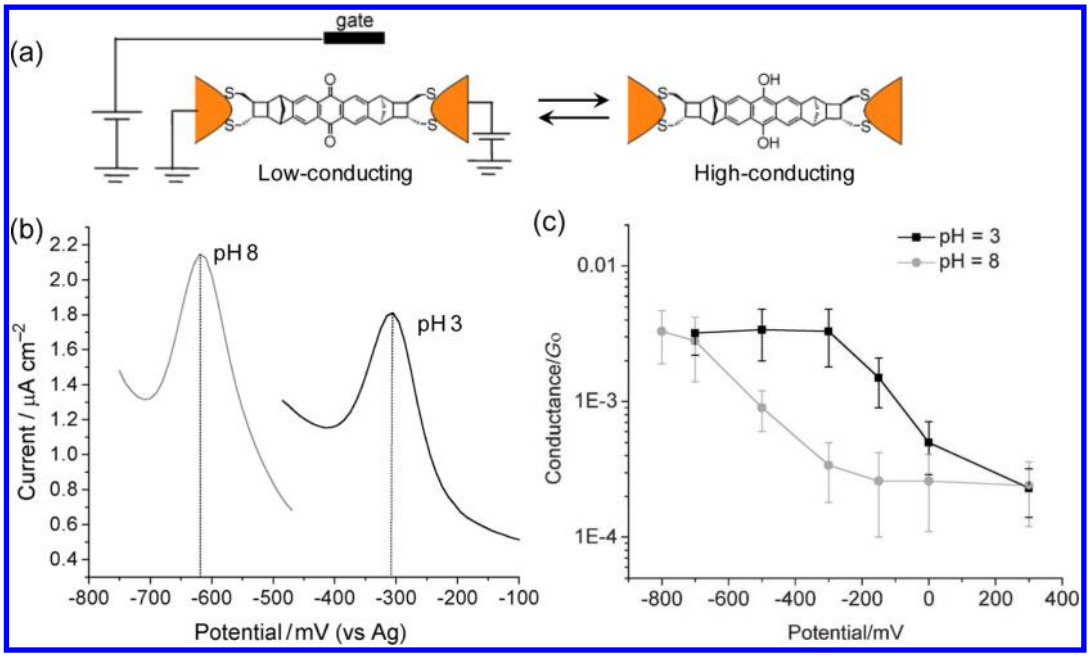

Figure 74. Electrochemical gating of an anthraquinone/hydroanthraquinone redox couple. (a) Redox reaction of the AQ moiety to an H_2AQ moiety. (b) Alternating current voltammograms at pH 3 (black line) and pH 8 (gray line). (c) Evolution of the conductance of the AQ molecule with a gate potential at pH 3 (black line) and pH 8 (gray line). Reprinted with permission from ref 771. Copyright 2012 Wiley-VCH.

relation could be modeled well as a sequential two-step charge transfer process with full or partial vibrational relaxation (Kuznetsov–Ulstrup (KU) model).[770] Using this view, the reorganization energies of ~1.2 eV were estimated for both the first and the second redox transitions for the pTTF bridge in the 1-butyl-3-methylimidazolium trifluoromethanesulfonate ionic liquid environment. This value is significantly larger as compared to that obtained for the same molecular bridge in aqueous environments (~0.4 eV). These differences should be attributed to the large, outer-sphere reorganization energy for the charge transfer across the molecular junction in the ionic liquid environment. To improve the electrochemical switching behavior of the molecular junctions, Li et al. chose redox-active benzodifuran-based molecules with optimal anchoring groups ($-CS_2^-$ anchoring group) instead of thiolate, thus resulting in a significant increase in both the junction conductance and the switching efficiency (ON/OFF ratio: ~8).[73]

Another example of a single-molecule switch was developed by Darwish et al.,[771] where a redox couple of anthraquinone/hydroanthraquinone (AQ/H_2AQ) was selected as the functional element (Figure 74a). A key feature of this design is the cementing of the AQ group into a rigid, structurally well-defined norbornylogous unit bearing two pairs of thiol groups at each end, thereby conferring additional stability to the SAMs. Using in situ STM break junctions, they were able to electrochemically and reversibly switch the molecules between the high-conducting H_2AQ system and the low-conducting AQ system with a conductance on/off ratio of an order of magnitude (Figure 74b and c). This high magnitude is attributed to destructive quantum interference effects operating in the AQ form, which is consistent with both the theoretical prediction and the bulk conductance results across the SAMs. Additionally, the possibility of modulating the potential range of the conductance enhancement was demonstrated by different pH values. Recently, a similar result was also reported by Baghernejad et al.,[74] where a conductance ratio of over >1 order of magnitude was achieved on the basis of organic molecules containing an anthraquinone (AQ) center. In comparison with the study discussed above, one important distinction observed in this study was that in the redox-inactive potential region, the effect of the gating is to shift the Fermi level relative to the molecular resonances, thus leading to a modest change in the conductance.

It should be noted that in addition to redox active molecules, nonredox active molecular systems, such as 1,2-bis(4,4-dimethylthiochroman-6-yl)ethylene and 4,4-bipyridine, also indicated a tunable charge transport, as demonstrated experimentally and theoretically by Capozzi[753] and Baghernejad et al.[752] The working principle is that the electrochemical gate potential could suitably tune the energy level alignment between the LUMO or the HOMO in the molecular orbitals with the Fermi level of the electrode, thus resulting in the modulation of the charge transport in the single-molecule junctions.

7.4.3. Spintronics-Based Switch. Recent years have witnessed the emergence and rapid growth of a new field, known as "molecular spintronics", which combines the ideas and the advantages of spintronics and molecular electronics.[772] The key is to use one or a few molecules, which respond to a magnetic field, to create molecular devices. Because of their apparent advantages, such as fine-tunability of their rich properties (for example, spin–orbit and hyperfine interaction), high degree of purity, and ease of synthesis, these molecular materials appear as an incredibly versatile and unique playground for exploring new spintronics concepts and/or implementing existing ones. Among these molecules, single-molecule magnet (SMM) compounds appear to be particularly attractive because their magnetization relaxation time is extremely long at low temperatures, reaching years below 2 K. In conjunction with the advantages of the molecular scale using the properties of bulk magnetic materials, these systems are promising for high-density information storage as well as quantum computing due to their long coherence times.[773] Furthermore, their molecular nature may lead to several

DOI: 10.1021/acs.chemrev.5b00680
Chem. Rev. 2016, 116, 4318–4440

appealing quantum effects of the static and dynamic magnetic properties.[774,775] The rich physics behind the magnetic behaviors present interesting effects, such as a negative differential conductance and a complete current suppression, which are useful for molecular electronics. More importantly, specific functions (for example, switching ability with light and electric field) can be directly integrated into the molecule. In this section, we are going to briefly review the primary developments in exploring the switching behaviors in single-molecule spintronics. For additional fundamental information on the different aspects of molecular spintronics, interested readers are recommended to refer to several comprehensive reviews.[162,772,776−783]

Currently, there are two techniques to attach a magnetic molecule between two electrodes. One possibility is to use an STM tip as the first electrode and the conducting substrate as the second electrode. Because this method has been detailed in refs 162 and 784, and is irrelevant to the topic in this section, we omit this approach. Although STM is a powerful tool for understanding the basic mechanism of the magnetic interaction between a molecule and a substrate, such as Kondo effects[785] and single-atom magnetic anisotropies,[786] it is not a device fabrication platform. Another possibility is based on the three- (or two-) terminal break junctions, which have an additional gate electrode in addition to the source and drain electrodes. This three-terminal transport device, known as a molecular spin-transistor, is a single-electron transistor with nonmagnetic electrodes and a single magnetic molecule as the island. The current passes through the magnetic molecule through the source and drain electrodes, and the electronic transport properties are tuned using a gate voltage V_G (Figure 64). It is worthwhile to point out that Schwarz et al. recently demonstrated that the oxidation and reduction of Mo compounds could be solely triggered by the electric field applied to a two-terminal molecular junction presenting voltage-induced conductance switching.[787]

For reliable molecular spin-transistors, a fundamental issue to be solved is the fact that, despite numerous classes of magnetic molecules that can be chemically synthesized, most of them are extremely fragile away from the solution and often sensitive to a metallic surface. In a few cases, certain molecules will lose their magnetic moment entirely due to coupling with electrodes. This disadvantage leads to a substantial difficulty in constructing robust magnetic single-molecule devices. By assuming that these three-terminal devices incorporating magnetic molecules, which preserve their SMM properties, can be achieved, the next important question is how should these devices operate? Particularly, how do these devices function as a switch or sensor to read, write, and process information upon exposure to an external stimulus? In the case of the SMMs, two key ingredients useful for making the devices function are the ability of the electrodes to produce a spin-polarized current and the possibility of altering the mutual orientation of the electrodes' magnetization vectors. The first property depends on the ability of manipulating the exchange interaction in a controllable way, thus converting spin information to molecular orbital information. The second property relies on the magneto-crystalline anisotropy, that is, spin−orbit coupling.

In fact, recent experimental and theoretical developments demonstrated the possibilities for switching the magnetic molecules as well as the effects that the switch produces on the electron transport[162,784] using two classes of magnetic molecules: spin-crossover compounds and molecules presenting valence tautomerism.[788] These two broad classes of molecules are particularly appealing for a number of reasons. First, they have an extremely long-living magnetization relaxation time, which signifies that such molecules have an intrinsic nonvolatile nature. Second, because the crossover generally depicts an internal charge rearrangement and an atomic relaxation, the two different molecular states display distinct electronic structures. The different electronic structures are expected to indicate different $I-V$ curves for different spin-states; that is, the spin-state is likely to be electrically readable. Finally, the crossover transition is sensitive to the local electrostatic environment such that an electric field may be used to induce the transition, which indicates that a potential device may be electrically switchable.

For example, in 2005 Rocha et al.[789] theoretically predicted a type of organic spin valve, which was obtained by sandwiching an organic molecule between magnetic contacts. Using a combination of state-of-the-art nonequilibrium transport methods and the density functional theory, they demonstrated that these spin valves could display a large bias-dependent magnetoresistance and that it could be engineered by an appropriate selection of molecules and anchoring groups. Four years later,[776] the same group proposed another general route, that is, the possibility of switching the sign of the exchange coupling between two magnetic centers using an electric potential. This general effect, which they named the electrostatic spin crossover, occurs in insulating molecules with superexchange magnetic interaction and inversion symmetry breaking. To prove its efficiency, a family of dicobaltocene-based molecules was selected to demonstrate that these molecules had critical fields for switching of approximately 1 V nm^{-1}, as calculated from the first principles. More importantly, the critical fields could be engineered by incorporating appropriate substituents into the basic dicobaltocene unit. Consistently, this possibility of controlling the molecular spin state by an electric field is also proved by Diefenbach et al.[790] They used $Ba_2(C_6H_6)$ to obtain the distinct difference in response to the molecular electronic states upon perturbation with an external electric field. These results may inspire future experimental studies toward the synthesis and spectroscopic characterization of molecular magnetic switches to prove this switching concept.

In fact, these theoretical predictions inspired a series of remarkable experimental studies. For example, in 2011 Prins et al.[791] demonstrated that nanoparticles consisting of spin crossover molecules presented a temperature hysteresis in their conductivity, which was attributed to the spin crossover transition. Intriguingly, although this activity used nanoparticles or crystals, not single molecules, this experiment demonstrated that the crossover could be induced by a static electric field, thus paving the way for electrically controlled spin devices at the molecular level. In fact, these functional single-molecule spin devices were realized recently by Osorio[792] and Wagner et al.[163] In the former study, they used electromigration to create a three-terminal device incorporating a single Mn^{2+} ion coordinated by two terpyridine ligands and demonstrated an electrically controlled high-spin ($S = 5/2$) to low-spin ($S = 1/2$) transition by adjusting the gate voltage. Using low-temperature inelastic cotunneling spectroscopy, they also uncovered a strongly gate-dependent singlet−triplet splitting on the low-spin side, which was consistent with an exact diagonalization of the Mn-complex. In the latter study, they used the MCBJ

DOI: 10.1021/acs.chemrev.5b00680
Chem. Rev. 2016, 116, 4318−4440

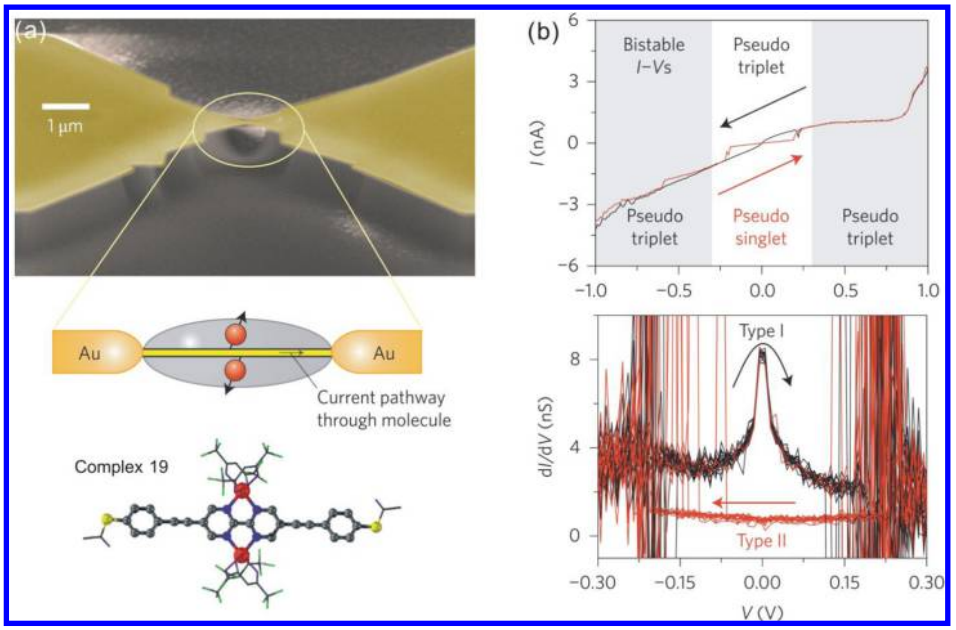

Figure 75. Switchable single-molecule spin devices created using the MCBJ technique. (a) Schematic of the experiment and molecular structure of complex 19. A molecule with a pair of spin centers is contacted in a single-molecule junction. The magnetic ion pair is attached orthogonally to the current pathway. (b) Bistable $I-V$ characteristics due to the hysteresis of the coupled spin pair. Type I is a Kondo-like zero-bias anomaly; this is identified as the electrical fingerprint of the pseudotriplet state. Type II is not a Kondo-like anomaly; this is assigned as the pseudo singlet. Reprinted with permission from ref 163. Copyright 2013 Nature Publishing Group.

technique to measure the electron transport through a single-molecule junction containing two coupled spin centers that were confined to two Co^{2+} ions (Figure 75a). They claimed that this method could detect a coupled spin pair in a single magnetic molecule and that a bias voltage could be used to switch between two states of the molecule. This claim was proven experimentally and theoretically. In theory, spin−orbit configuration interaction methods were used to calculate the combined spin system, which indicated that the ground state was determined to be a pseudosinglet whereas the first excitation behaved as a pseudotriplet. In the experiments, these states could be assigned to the absence and the occurrence of a Kondo-like zero-bias anomaly in the low-temperature conductance data (Figure 75b). This result is remarkable because one can repeatedly switch the molecules between the pseudosinglet state and the pseudotriplet state by simply applying a finite bias.

Last, another idea to be noted is to build molecular multidot devices, where a controlled number of molecules or multiple centers inside the same molecule are attached to two electrodes. This approach may lead to more interesting phenomena. For example, negative differential conductance effects were discovered in a double-metallocene molecule as a multidot system with molecular-level crossings.[793] In another study, Ouyang et al. executed the chemical self-assembly approach to form multidot devices[794] containing a programmed sequence of CdSe QDs connected by *p*-benzenedithiol molecular bridges. Using a femtosecond time-resolved Faraday rotation spectroscopy, the authors probed the spin transfer process through the π-conjugated molecular bridge, which proved that the process was coherent and that the bridging molecule functioned as a quantum-information bus. The primary advantage of these multidot devices is that the intrinsic properties of the SMMs can be preserved because the coupling between the SMMs and the quantum conductor is weak, potentially enabling a nondestructive readout of the spin states.

7.5. Transduction toward Molecular Sensors

A sensor can be generally defined as a transductor that is able to reflect the specific presence of an invisible event or substance using certain types of signals with clear resolution. On the basis of this definition, electrical sensors imply that the detection of targets can be read through the electrical current. In fact, various types of electrical sensors have been created by taking advantage of the relationship between the conductance of the sensing centers and their interaction with external targets over the years, which provides a convenience and improvement for several fields, including disease diagnosis, food security, and environment monitoring. As compared to conventional sensors that are based on optical, chemical, or physical methods, such as fluorescence/Raman spectroscopies, polymerase chain reactions (PCR), and enzyme-linked immunosorbent assays (ELISA), electrical sensors are complementary but still offer unique advantages, such as simplicity, low-cost, portability, ultrahigh sensitivity, excellent selectivity, and label-free real-time electrical detection, in a nondestructive manner.[364,795−802]

Driven by the digitalization and informalization of contemporary society, electrical sensors are leading toward structural minimization, functional intelligentialization, and highly detecting resolution, which constitutes an important branch of molecular electronics, that is, molecular sensors. Instead of the average properties of large numbers of molecules being detected by conventional electrical sensors based on nanomaterials, such as carbon nanotubes, nanowires, nanopores, nanoclusters, or graphene, the molecular sensors discussed here have the capability of probing the complex behaviors of targets at the molecular level and consequently providing new opportunities to uncover the wealth of molecular information that is typically hidden in conventional ensemble experiments. It should be noted that probing the interaction of individual molecules could address the "unanswerable" questions in the physical, chemical, and

DOI: 10.1021/acs.chemrev.5b00680
Chem. Rev. 2016, 116, 4318−4440

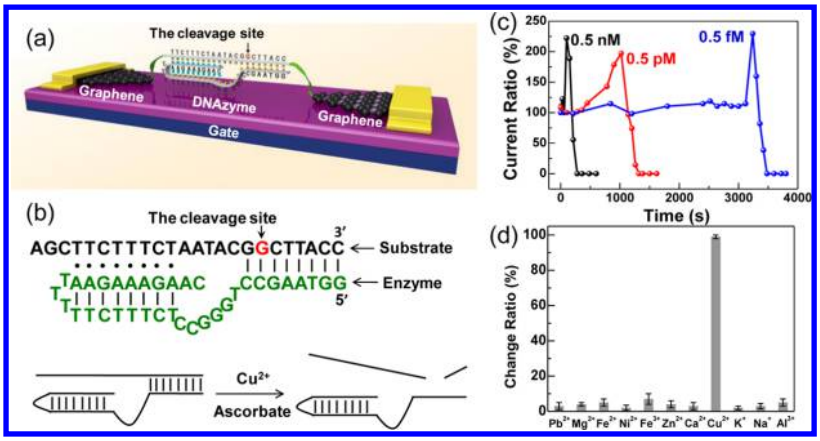

Figure 76. DNAzyme-based Cu^{2+} sensors. (a) Schematic representation of graphene−DNAzyme junctions. (b) The structure of the Cu^{2+}-sensitive DNAzyme and corresponding catalytic activity. The DNA substrate has been functionalized by amines on both ends for molecular connection. (c) Concentration-dependent dynamics of the Cu^{2+} catalytic reactions, which depict the femtomolar sensitivity. (d) Statistical comparisons of conductance changes under the same conditions in the presence of different ions (0.5 nM of Pb^{2+}, Mg^{2+}, Fe^{2+}, Ni^{2+}, Fe^{3+}, Zn^{2+}, Ca^{2+}, and Cu^{2+}; and 5 mM of K^{+}; 135 mM of Na^{+}; 60 nM of Al^{3+}). Reprinted with permission from ref 805. Copyright 2015 Royal Society of Chemistry.

biological sciences, which is meaningful for understanding the fundamental scientific essence and developing accurate molecular diagnosis in the biological regime.[803] Promoted by the significance of molecular detection as well as the continuous and diligent efforts, various electrical sensors have been developed for capturing the minimum events, thus displaying a great potential to excavate the "elementary information". In fact, the burgeoning development of standard wafer-scale semiconductor processing techniques, especially the construction of molecular devices, provides the feasibility of molecular sensing, which is driving the field to move from fundamental problems toward practical biosensors. In this section, we review the primary advances of single-molecule sensors in three regimes: chemical reaction, biological interaction, and thermoelectricity, focusing on studies that use single molecules as the core component. Here, the principles of operation for electrical sensing as well as the primary strategies for enhancing their performance are discussed in addition to key challenges and opportunities in current stages and further development.

7.5.1. Sensing Based on Chemical Reactions. Generally, chemical reactions are responsible for most of the changes in nature. The establishment of understanding and controllability for these chemical reactions, which are embodied in mature methods based on kinetic and thermodynamic investigations, is of crucial importance in both basic science and industry communities. Particularly, incorporating the paradigms of reaction chemistry into the design of molecular electronic components can provide a tremendous impetus to advance the field of molecular electronics. In fact, the development of deeper insight into chemical reactions, especially for the interaction between two reactants at the single-molecule level essential in chemical reactions, leads to creating various sensors with high selectivity and extreme sensitivity and clarifies previously indecipherable intrinsic reaction mechanisms. As detailed in section 7.4, chemical principles such as photocyclization, tautomerization, and redox reaction have inspired the genesis of several new types of molecular electronic switches. In the following section, we highlight the chemical principles and strategies used to develop functional single-molecule chemical sensors.

In 2004, Tao et al.[804] demonstrated that the binding of a guest species onto a single host molecule could be studied electrically by wiring the host molecule to two electrodes. In this study, peptides were selected as the host molecules because of the unlimited number of different sequences that could be tuned to obtain an optimal binding strength and specificity for the selected guest, that is, transition-metal ions, such as Cu^{2+} and Ni^{2+}. The specific binding of peptides with the metal ions was expected using deprotonated peptide bonds, which could change the molecular configuration and alter the charge transport pathway. Therefore, the difference in the molecular conductances before and after binding can be used to reflect the chemical reaction, which also laid the foundation for metal−ion sensors with molecular sensitivity.

Despite the demonstration of detecting metal ion binding in this study, the application for actual single-molecule sensors is inhibited because the research was established on the basis of an STM setup, whose two-terminal architecture is so sophisticated that it is more commonly used for fundamental science rather than actual applications. Furthermore, this limitation originates from the instability of the Au−S contact interface. To solve these problems, an improved approach was introduced by Guo et al., who successfully developed novel molecular devices using carbon electrodes based on SWNTs[31] in 2006 and graphene[30] in 2012 (as discussed in section 3). On the basis of this reliable approach, another system was constructed to demonstrate host−guest binding at the single-molecule level. First, a molecule containing two terpyridyl ligands linked by a Co^{2+} was integrated to a pair of carbon electrodes using covalent amide bonds. Interestingly, the conductance of the host−guest junctions could disappear and appear repeatedly to form cycles through alternate treatments of EDTA and Co^{2+}. This strategy is reliable because it was proven by another study from the same group, where the capability of controlling the conductivity of individual DNAs was demonstrated using coordination chemistry.[357] Briefly, the carbon nanoelectrodes were bridged by single ODN-**H1** (Figure 29) using amide linkages to form single DNA molecular devices. Similarly, it was determined that the electrical properties of these devices can be efficiently switched on-and-off by sequentially alternating treatments with the EDTA and the Cu^{2+} ions. This is because sequential treatments with the EDTA and Cu^{2+} formed metal-free or metallo DAN structures, respectively, which have different electronic

DOI: 10.1021/acs.chemrev.5b00680
Chem. Rev. 2016, 116, 4318−4440

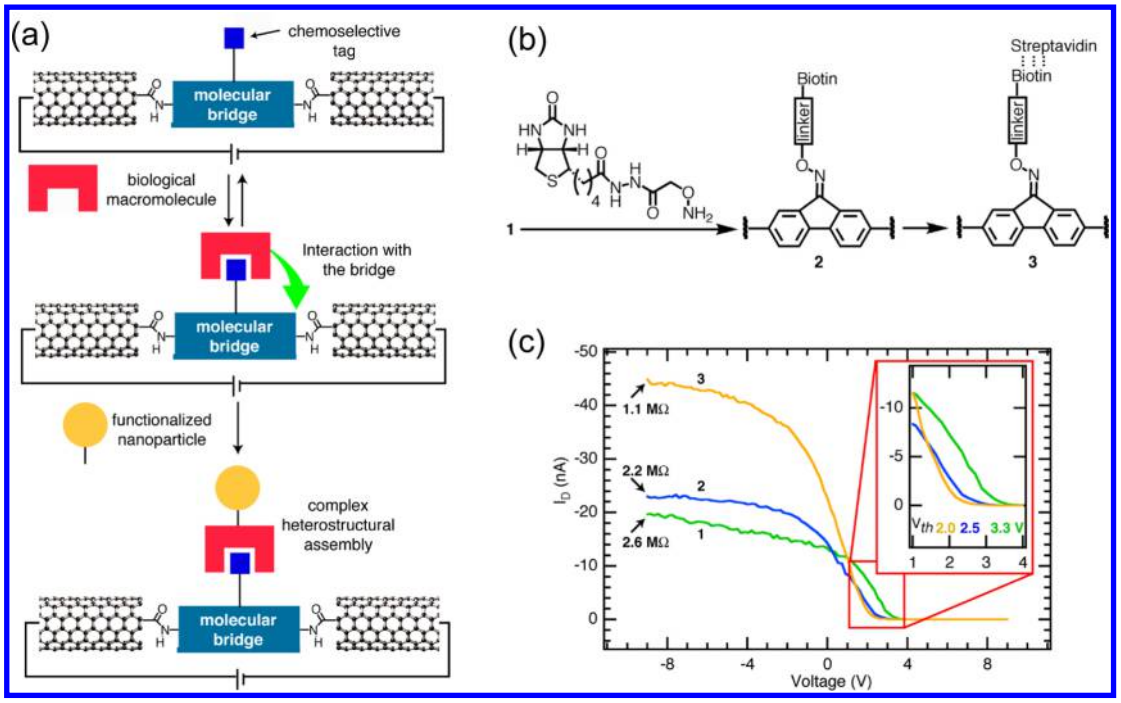

Figure 77. Proof-of-principle strategy for single-molecule biodetection. (a) Schematic depicting the use of single-molecule electronic devices as scaffolding for the assembly of biological macromolecules and complex, multimeric assemblies. (b) Reaction sequence, where a fluorenone (1) is condensed with a biotin derivative that bears an alkoxyamine to form an oxime (2) on the molecular bridge. The derivatized bridge is then able to bind streptavidin to form noncovalent complex (3). (c) Current–voltage characteristics, which depict the gate voltage versus the drain current at a constant source–drain voltage for each step in the reaction sequence. Reprinted with permission from ref 812. Copyright 2007 American Chemical Society.

structures and different conductances. The sensing property of these devices is reproducible because a similar phenomena was observed using different metal ions, such as Ni^{2+} and Fe^{3+}. Among these metal ions, Fe^{3+} had the best reversibility. The proven switching reproducibility and reversibility of the single-molecule devices bridged by metallo-DNAs form the basis for new types of molecular switches and chemical sensors.

Recently, the same group[805] took a further step toward molecular chemical sensors by constructing a platform that integrated a Cu^{2+}-dependent DNAzyme into graphene–molecule junctions, which was capable of directly detecting paramagnetic Cu^{2+} with femtomolar sensitivity and high selectivity (Figure 75a). DNAzymes belong to a type of DNA-based biocatalysts with the ability to perform chemical and biological reactions in the presence of specific metal ions. In this study, they designed a Cu^{2+} electrical sensor consisting of a DNA substrate strand with amines on both ends for connecting to the graphene–molecule junctions as well as an enzyme strand that could hybridize to the substrate strand through two base-pairing regions (Figure 76a). The sensing principle is that Cu^{2+} could recognize and then bind with the specific site in the DNAzyme sequence, followed by the cleavage reaction that thus destroyed the conducting pathway (Figure 76b). The contribution of this study could be summarized from three aspects: (1) ultralow sensitivity with the femtomolar level due to the single-molecule sensing component (Figure 76c); (2) high selectivity resulting from the specific biological catalysts, as demonstrated by a series of control experiments using different metals (Figure 76d); and (3) potential universality for other metal–ion sensors because various types of DNAzymes specific for different ions are available. This universality has been strengthened by another study,[806] where a similar approach was described for directly revealing the stepwise effect of individual intercalations on DNA conductance based on DNA-functionalized molecular junctions using ethidium bromide and SYBR Green I as representatives. Generally, the ability to detect chemical and biological species at ultralow concentrations is important in several areas, ranging from the diagnosis of life-threatening diseases to the detection of biological agents in warfare or terrorist attacks. These results demonstrate that these device-like architectures are promising for actual sensors with extreme sensitivity and high selectivity, thus leading to commercial applications.

7.5.2. Sensing Based on Biological Interactions. A key goal of modern bioscience is to monitor biomolecular interactions with high sensitivity and high selectivity in real time, with the ultimate aim of detecting single-molecule events in natural samples. Directly probing the in situ activities of biological species at the single-molecule level can provide access to uncovering the incredible wealth of molecular information that is typically hidden in conventional ensemble experiments and addressing the previously "unanswerable" questions. Therefore, establishing a practical platform for achieving this goal is clearly of great importance to fundamental biology, diagnosis, and drug discovery. In this section, we review the recent progress of a system of single-molecule electrical biosensors, with a particular focus on those based on carbon electrode–molecule single-molecule junction platforms. It should be noted that there are a few other examples reported recently, where nanometer-scale materials (such as SWNTs and silicon nanowires) were used to build electrical circuits capable of reaching single-molecule sensitivity.[799,800,807−811] These studies are not within the topic of the current review and are

DOI: 10.1021/acs.chemrev.5b00680
Chem. Rev. 2016, 116, 4318−4440

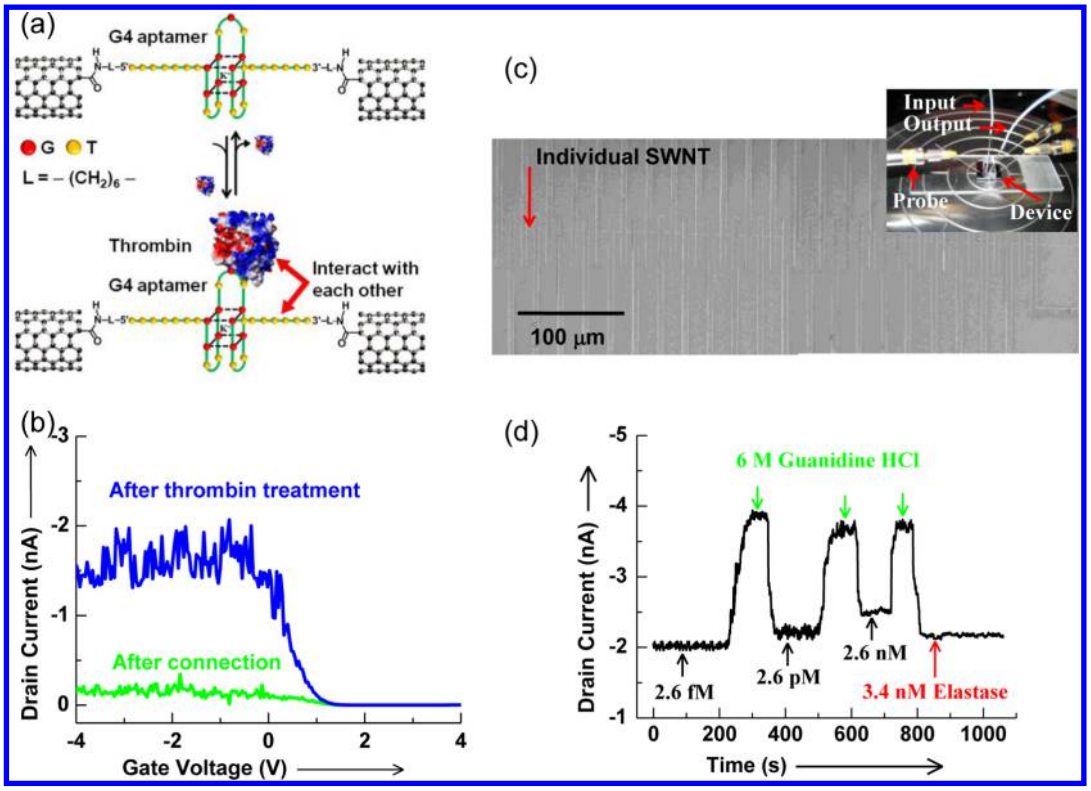

Figure 78. Real-time, label-free, reversible detection of DNA–protein interactions. (a) Schematic representation of the sensing mechanism, which indicates how single-molecule devices can detect proteins at the single-molecule level. (b) Device characteristics of a device rejoined by individual DNAs after DNA connection (green) and further treatment with thrombin (blue). (c) SEM images, which depict a highly integrated identical SWNT device array. The inset depicts an optical image of a single-molecule device during real-time measurements. (d) Current-versus-time data recorded for an aptamer-rejoined device upon alternate additions of the thrombin Tris-HCl buffer solution at different concentrations (from 2.6 fm to 2.6 pm and 2.6 nm), a 6 m guanidine HCl solution, and an elastase (3.4 nm) Tris-HCl buffer solution. Reprinted with permission from ref 668. Copyright 2004 Wiley-VCH.

thus not included in this section. Interested readers are recommended to read the literature listed above.

Among the different molecular junction platforms, as detailed in sections 2–4.2, single-molecule devices formed from the carbon electrode–molecule molecular junction platform are particularly appealing because they are synthesized through covalent amide bonds, thus significantly improving the device stability. Therefore, these devices are sufficiently robust to endure a wide range of chemistries and conditions, even in aqueous environments. Another unique feature of these devices is that they consist of one or two (at most) molecules as conductive elements. Because the current flow traverses a single molecule, the devices are sensitive to the local configuration and environment around the bridging molecule. In combination with their high stability, they have a great potential for further applications in building ultrasensitive functional optoelectronic devices and new classes of chemo-/biosensors with single-molecule sensitivity. In the first step toward biosensing, Guo et al.[812] developed a proof-of-principle strategy for realizing single-molecule biodetection based on carbon electrode–molecule single-molecule junctions by combining programmed chemical reactivity and directed biological self-assembly (Figure 77a). In this study, they used a molecular wire with a ketone side arm (diaminofluorenone) to bridge SWNT point contacts. They then demonstrated the capability of electrically sensing the oxime formation on the molecular bridge using a biochemical probe molecule and further monitoring the noncovalent binding between the probe and the protein (Figure 77b and c). Furthermore, the use of a biological assembly was demonstrated to localize individual nanoparticles at the molecular bridge, thus providing a method to sense the biological process at the single-event level.

Following this approach, one further primary effort is to integrate DNAs into electrical circuits[345,356,668] because DNA molecules bridging nanodevices could serve as powerful reporters to transduce biochemical events into electrical signals at the single-molecule level. Thus, a general method was described to incorporate DNA strands between the SWNT electrodes and measure their electrical properties. The statistical results demonstrated that the well-matched duplex DNA in the gap between the electrodes exhibited a resistance of approximately 1 MΩ, which is comparable to the bulk *c*-axis resistance of highly oriented pyrolytic graphite (HOPG) with similar dimensions, and a single GT or CA mismatch in a DNA 15-mer increased the resistance of the duplex ~300-fold relative to that of a well-matched one. More importantly, when certain DNA sequences, which are substrates for *Alu*I, that is, a blunt end restriction enzyme, were oriented within this gap, this enzyme sliced the DNA and eliminated the conductive path. This result is valuable because it supports the supposition that the DNA retains its native conformation and the corresponding biological activity when sandwiched between the SWNT point contacts, thus setting the foundation for developing future DNA-based molecular biosensors. This conclusion was further strengthened by the study performed by Wang et al.,[813] where they reported a molecular-scale electrical device that could

DOI: 10.1021/acs.chemrev.5b00680
Chem. Rev. 2016, 116, 4318–4440

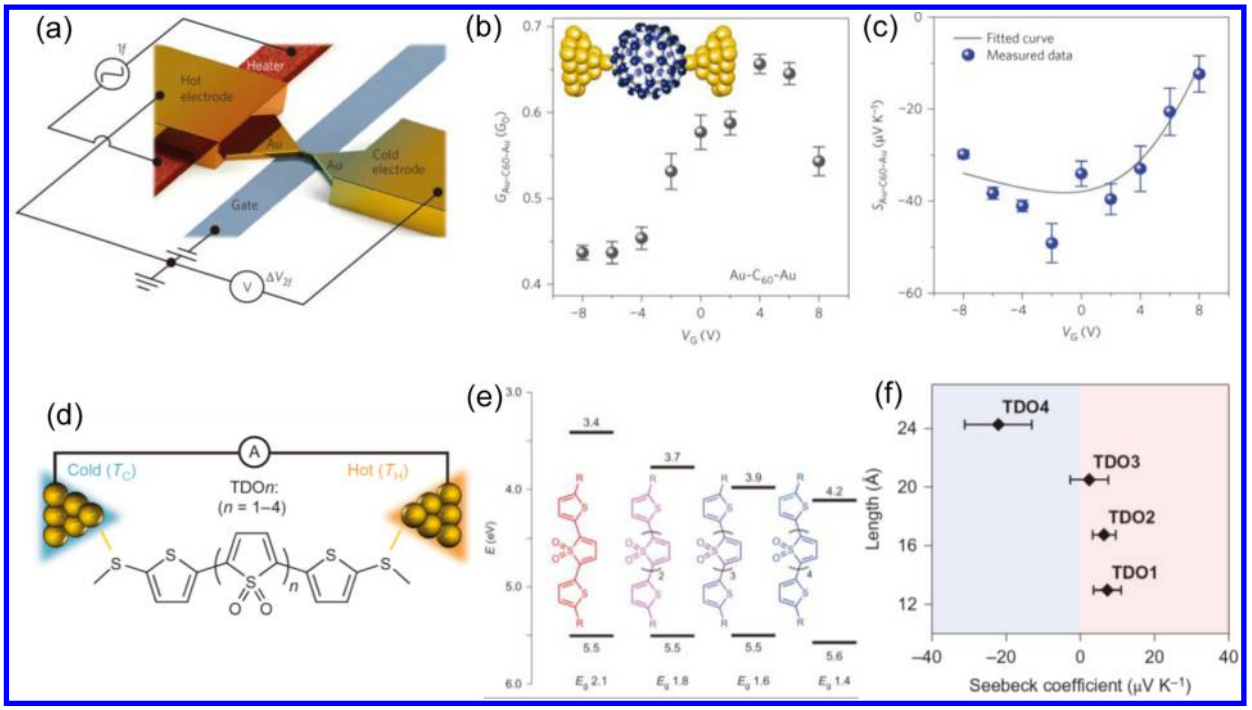

Figure 79. Tuning the thermoelectric properties of molecular junctions. (a) Schematic of the electromigrated break junctions with integrated heater (left). (b) Electrical conductance as a function of the gate voltage (V_G) for the C_{60} junction (see inset). (c) Seebeck coefficient of the molecular junction as a function of V_G. Reprinted with permission from ref 820. Copyright 2014 Nature Publishing Group. (d) Schematic representation of the STM junction. (e) CV-derived HOMO and LUMO levels (eV) and the HOMO–LUMO gap (E_g) for the TDOn family (R = SMe). (f) Plot of Seebeck coefficients as a function of the molecular length for the TDOn family. A shift from positive to negative Seebeck values with increasing length is observed, which indicates a change in the charge carriers from holes to electrons. Reprinted with permission from ref 822. Copyright 2015 Nature Publishing Group.

sense an individual reaction between a DNA duplex and a methyltransferase enzyme. The methyltransferase M.SssI can specifically and reversibly bind the sequence 5′-CG-3′ and, in the presence of the cofactor *S*-adenosyl methionine, catalyze the complete rotation of the cytosine base out of the π-stacked core of the DNA duplex (referred to as base flipping) followed by methylation, thus leading to an interruption of the charge transport.

Inspired by the above-mentioned studies, Liu et al. created an integrated system that could achieve rapid real-time measurements with single-molecule sensitivity.[668] In this study, individual metallo-DNA aptamers, which could selectively and reversibly interact with a target protein thrombin, were used to react with SWNT point contacts to form stable molecular devices (Figure 78a). After treatment with thrombin, these single-molecule devices depicted a consistent conductance increase (Figure 78b). This change results from enhanced DNA charge transfer because of the rigidification of the DNA conformation due to the DNA–thrombin interactions. To achieve a real-time measurement, an integrated SWNT transistor array was designed and fabricated (Figure 78c). Combining this pattern with microfluidics led to detecting protein and monitoring stochastic DNA–protein interactions in real time (Figure 78d). Reversible and consistent conductance changes at different thrombin concentrations without a concentration dependence (from 2.6 fM to 2.6 pM and 2.6 nM) were observed, therefore demonstrating the reproducibility and single-molecule sensitivity. These results distinguished this method as a unique platform to achieve real-time, label-free, reversible detection of DNA–protein interactions and enzymatic activity with high selectivity and actual single-molecule sensitivity. As compared to more conventional optical techniques, this nanocircuit-based architecture is complementary with clear advantages, such as no bleaching issues and no fluorescent labeling, which are of crucial importance for future single-molecule biodetection.

7.5.3. Sensing Based on Thermoelectrical Conversion.

In addition to the strong motivation for the development of molecular electrical biosensors, there is increasing interest in understanding the thermoelectric transport in single-molecule junctions.[370,814] If one side of a material is heated to a higher temperature ($T1$) and the other side is kept at a low temperature ($T2$), then free charges tend to accumulate at the cold end, resulting in a potential difference ΔV between the sides. This thermoelectricity enables the heat energy to be directly converted to electricity and vice versa, without using any mechanical components. Thus far, experimental studies on thermoelectricity for nanojunctions are limited. However, a few key results have already emerged. For example, Reddy et al. performed the first measurement of thermopower in molecular junctions, and the Seebeck coefficients ($\Delta V/\Delta T$) for several types of molecular junctions were determined.[27] A framework then was established for understanding heat dissipation for a range of mesoscopic systems, which demonstrated that the heat dissipation was asymmetric if the junctions had strong energy-dependent transmission characteristics.[109] Widawsky et al.[815] developed the STM-based break junction technique and simultaneously determined the conductance and thermopower of single-molecule junctions, revealing the dependence of the Seebeck coefficients on the conducting molecule orbitals. This dependence was also proven by the results obtained by Tao's group,[816] who determined that the thermopower correlated

DOI: 10.1021/acs.chemrev.5b00680
Chem. Rev. 2016, 116, 4318–4440

with the transition voltage, which was indicative of the molecular energy level alignment between the molecular energy levels and the electrodes' Fermi energy level.

These pioneering experimental studies combined with the recent systematic computational predictions[817−819] established the feasibility of achieving efficient thermoelectric energy conversion in molecular junctions. The key to obtaining deeper insights and optimizing the thermoelectric properties of molecular junctions is tuning their charge transmission characteristics at the Fermi level (E_F) of the electrodes. Thus, Evangeli et al.[820] utilized the imaging capability of the STM technique to simultaneously measure the thermopower and the conductance, thus demonstrating a potential approach of enhancing the thermoelectric performance by manipulating the intermolecular interactions. Kim et al.[821] used an electromigration approach to build three-terminal molecular junctions with large temperature gradients, which allowed for the simultaneous measurements of the Seebeck coefficient and the electrical conductance of the individual molecules (Figure 79a) to be obtained. Using this platform, the prototypical Au−biphenyl-4,4′-dithiol−Au and Au−fullerene−Au junctions were studied, indicating that both the Seebeck coefficient and the molecular conductance could be increased by electrostatic control (Figure 79b and c). Additionally, it was determined that the thermoelectric properties could be significantly enhanced when the dominant transport orbital was located close to the E_F of the electrodes (Figure 78b and c). Recently, Dell et al.[822] reported another interesting study, where the STM technique was used to demonstrate that the charge carriers in single-molecule junctions could be tuned by molecular engineering (Figures 78d and 79e). By performing thermopower measurements, it was proven that the dominant charge carriers changed from holes to electrons within a family of molecules that contained electron-deficient thiophene-1,1-dioxide (TDO) building blocks when the number of TDO units was increased (Figure 79f). This result provided a new method to tune the length-dependent p- and n-type transport in organic materials. Collectively, these rapid, impressive demonstrations suggest that molecular thermoelectricity is an area of research where new breakthroughs can occur in the future.

8. SUMMARY AND OUTLOOK

With the rapid development of molecular-scale electronics, using molecular devices as the future of next-generation electrical circuit units with lower power consumption, higher speed, and higher level of integration has received significant attention.[39,42,46,51,823] To conveniently and efficiently fabricate molecule-based devices, electrode fabrication is a key step. In this report, we presented the developments of different techniques for molecular junction fabrications using both metal and nonmetal materials as contacts. We summarized the characterization methods as well as the theoretical approaches for molecular electronics. Moreover, we highlighted the significant advancements in molecule-based functional devices toward practical applications. The history, challenges, and future of molecular electronics were also discussed.

Each type of material and technique has advantages as well as disadvantages. For example, metallic materials are the most widely used materials for the molecular junction fabrication due to their several advantages, such as few defects, low cost, and high conductance. However, from a device's standpoint, several serious concerns for metal nanoelectrodes exist. (1) Incompatibility: Several types of metals (e.g., commonly used gold) may form deep level traps in silicon, making it difficult to integrate gold tunnel junctions with complementary metal−oxide−semiconductor (CMOS) electronics.[824] (2) Unexpected mobility: The atom at the metal electrode surface may rearrange or move due to the electric field and local heating, especially under ambient conditions, which strongly influence the stability of single-molecule devices.[140] (3) Contact nature: Molecular electronics is often limited by the poorly defined nature of the contact between the molecules and the metal surface.[825] Even for the most well-studied system, such as thiolated molecules on Au contacts, there are no methods to control the types of metal−molecule bonds.[429] Carbon-based electrodes can overcome these problems, for example, incompatibility and unexpected mobility. Using SWNTs as point contacts, well-defined covalent bonds between the electrode and the molecule with a limited number of molecular bonding sites can be created.[825] However, single-molecule studies based on SWNTs also face considerable challenges before they can realize their full commercial application.[826] Because of a lack of precise diameter and chirality control for the SWNTs, the device-to-device properties varied. Developing a reliable fabrication technique for mass-producing identical SWNT arrays and integrating individual SWNTs into functional single-molecule devices with high yields are one of the future challenges.[827] Graphene does not have the inherent variability of the SWNTs and may therefore circumvent these problems. Graphene is currently considered a potential candidate for the post-CMOS era because its defect-free monolayer can be grown at the wafer scale, and the significant gate screening issues can be reduced as compared to that of metal electrodes, thus putting molecular electronics into a more favorable position due to the junction's dimensions being reduced to two dimensions. Nanometer-scale gaps in graphene have been obtained using different strategies, such as atomic force microscopy nanolithography,[120] anisotropic etching via thermally activated nanoparticles,[828] electron-beam sculpting,[829] "dash-line" lithography,[18,462] mechanical stress,[830] or electroburning.[464,465] Functional single-molecule devices based on graphene, such as optical switches with low-ohmic contacts,[490,766,831] transistors with low field screening,[366,373] and ultrasensitive biosensors,[806] have been reported. Carbon-based materials, such as SWNTs and graphene, may be better suited as electrode materials for molecular electronics. The realization of atomic-level precision in the cutting procedure, precise control of the molecular conformation on the substrate within the graphene gaps, and contact configuration are challenges for future studies to overcome.

Each electrode fabrication technique has its own unique advantages but is far from perfect.[249] For example, there are main three general techniques for forming top contacts for large-area electrical measurements on the SAMs. (1) Direct deposition of metals using an electron-beam or thermal evaporation ensures atomic-level contact; however, the device yield is low due to the damage of the evaporated hot metals and the formation of metal filaments that short the junctions. (2) The installation of a buffer-conducting polymer between the SAM and a metallic top contact exhibits a high device yield and efficiently avoids electrical shorts. However, the electrical properties of these molecular junctions may be influenced by the thermal treatment and the morphology of the interlayer conducting films. Also, the interface between the conducting polymer and molecular layer is not well understood. (3) The use of liquid metals allows the formation of the conformal

DOI: 10.1021/acs.chemrev.5b00680
Chem. Rev. 2016, 116, 4318−4440

contacts at low cost under room temperature conditions. However, liquid metal has difficulty forming small contacts at the individual molecular level. For single-molecule junctions, single molecules can be addressed using the electromigration method on the nanoconstrictions. However, the electrode separation is fixed, which indicates that the gap size cannot be further changed after electromigration, thus leading to a low yield of molecular junctions. The mechanically controllable junction technique with a precise adjustable gap size indicated a high yield of the junction. However, it is not facile to fabricate highly integrated molecular commercial devices because of the constraint of the out-of-plane push rod components and the difficulty of introducing a third electrode for gating.

Each characterization technique has drawbacks.[41] For example, STM continues to play an important role in understanding the electron transport in single molecules due to its capability for both microscopy and tunneling spectroscopy. However, STM requires well-defined surfaces, such as single crystals, and it is not available for several devices or samples. The surface spectroscopy techniques (e.g., photoemission spectroscopy) are powerful in determining the electronic properties of the molecule−electrode interfaces and the relative energy alignments.[543] X-ray spectroscopy has been demonstrated to provide angstrom-resolution structural information in silicon−molecule−mercury junctions.[832] However, most of the spectroscopic techniques are difficult to apply to molecules sandwiched between two electrodes due to the screen of electrodes. Inelastic electron tunneling spectroscopy can be easily used in sandwiched molecular junctions at the single-molecule level to provide information on molecular identity and conformation. However, it requires cryogenic temperatures to distinguish the vibration modes. Optical techniques, such as infrared and Raman spectroscopies, can be used to probe the chemical properties of molecules at room temperature, but it is still a considerable challenge at the single-molecule level.[833] Additionally, although several useful analytical techniques (e.g., transition voltage spectroscopy and thermoelectricity) have been developed for characterizing molecular junctions, those methods are indirect techniques to reveal the characterization of molecules. Developing new efficient techniques for directly extracting additional details from the molecular junctions is highly expected.

8.1. Main Challeges

8.1.1. In Situ Measurement. We had witnessed the in situ molecular synthesis of molecular wires to bridge OWL-fabricated nanogaps using the "click chemistry" method as demonstrated by Chen et al.[273] With this in situ approach, the molecule length can be increased to bridge two electrodes. In comparison with the in situ molecular synthesis, the in situ measurement is also essentially important but faces bigger challenges. For example, as a pioneer experiment, the IETS measurements were performed as molecules changed their conformations (cis−trans transition) when exposed to ultraviolet or visible light irradiation.[435] The IETS of cis and trans forms showed distinct vibrational fingerprints that can be used for identifying the isomers. However, due to the engineer technique limitation, this important experiment can only be performed ex situ; that is, the IETS measurement cannot be performed simultaneously with the cis−trans transition. To fully understand the switch mechanism for the cis−trans transition, the in situ IETS measurement is desired in the future. Also, due to the technique imitation, TEM images for nanogaps were captured ex situ after the electromigration process occurred. It will be wonderful if one can continuously take the TEM images with high frequency (behavior like video recorder) and simultaneously measure the conductance, and then the full mechanism for the quantized conductance change and the electron migration process will be cleared. Another challenge lies in obtaining a microscopic understanding of charge transport that involves reduction or oxidation of molecules in which the in situ measurements are especially important.

8.1.2. Device Yield. Over the past several decades, a variety of innovative approaches have been developed to experimentally conduct charge-transport studies at the few-molecule level, and functional devices based on individual molecules have been demonstrated. However, most of the studies were performed with only a limited number of molecular devices. The device yield was notoriously poor primarily because of the top electrode's penetration through the molecular layer in a vertically structured metal−molecule−metal device structure or an inaccurate electrodes' gap separation across the molecules in a horizontally structured metal−molecule−metal device structure. As mentioned previously, a few methods have been developed to improve the device yield significantly using a polymer interlayer, graphene film, or special metal layer (see section 2.2.8). However, these high-yield device structures possess both advantages and disadvantages, and there is still a great need to seek a better technique to fabricate molecular devices in a high yield with good reliability and stability.

8.1.3. Device-to-Device Variation and Instability. Once the number of active molecules in the junction was reduced to a single molecule, the devices became extremely sensitive to the microscopic detail of their atomistic configuration and local environment, resulting in an increase in the variability of the "devices". To our knowledge, only a few experiments have demonstrated the ability to control the crucial atoms in the devices.[768] Even for assembled molecular devices, there is little control over the atomic-level structure of the metal−molecule interface, thus leading to an increase in the "uniqueness" of each sample.[46] Although individual laboratories have achieved acceptable yield and reproducibility, an agreed-upon standard junction that can serve as the starting point for correlating the junction structure with the electronic properties is still absent.[51] It is a tremendous challenge to generate such a standard junction facilitating the changes in the contacts, molecular components, geometry, and integration.

It is essentially important to create molecular devices with high stability. However, as compared to the traditional semiconductor industry, there are additional factors resulting in the stability of molecular devices. First, to align the Fermi energy with the molecular orbital to enable resonant transport in certain cases, it was necessary to apply several volts over a few nanometer junctions. This high electric field gradient may lead to nonequilibrium dynamic changes in the molecular structure[475] and the diffusion of metal atoms at the electrode surface.[140] Both the atomic movements and the molecular structural changes, including the bond fluctuation, will result in a notable junction-to-junction variability and a limited stability. Second, molecular devices are generally sensitive to the local environment, for example, temperature, humidity, illumination, and the electromagnetic field. The changes in each element may result in instability. Third, laboratories typically use the SAM or L−B structures as the most common strategy to build the junctions. However, these structures involve several labile

DOI: 10.1021/acs.chemrev.5b00680
Chem. Rev. 2016, 116, 4318−4440

surface bonds so that they can evolve into a minimum-energy conformation. This process will also lead to instability and the stochastic behavior of the electronic properties.[51] Finally, the most critical issue hindering the development of the stable devices is the nature of the molecule−electrode interface. Because both the charge injection and the collection occur across the molecule−electrode interfaces, it is evident that the interfacial properties, such as the contact chemistry and the coupling strength between the molecules and the electrodes, play an important role in the electrical characteristics and stability of the molecular devices. Reliable approaches are greatly needed to develop robust molecular devices through a proper selection of electrode materials, anchoring groups, intramolecular connections, and external environments to precisely control the interfacial properties of the molecule−electrode interfaces.

8.1.4. Integration. The ultimate goal for molecular electronics is to fabricate commercial devices and apply them to daily life. Hence, it is inevitable for molecular electronic components to be integrated into modern microelectronics so that information can be easily read. Unfortunately, efficient integration strategies for bridging hard electronics with the vast store of the soft-molecular world are still lacking.[42,834] Thus far, most of the measurements were conducted in ideal media at the laboratory level. The actual devices are far more complex and can definitely introduce a range of interfering and ruining effects. The development of fabricating parallel integrated junction arrays with specific functionalities in selective areas remains challenging.[827] For an efficient integration, the molecular components and processing should be compatible with existing fabrication techniques and conventional semiconductor structures, such as CMOS. In addition to integration, there are further challenges that need to be addressed. (1) The SAM and L−B structures are extremely fragile for practical devices in packaging.[51] To package single-molecule devices, a clean environment and a gentle contact force are necessary to avoid contamination and damage. Taking this rigorous requirement into consideration, using an atomic layer deposition technology to bury the single molecule with dielectrics is one option for realization of a practical device in the future.[835] (2) Although a single molecule is relatively small, the electrodes for the outside connection and the read-out are relatively large, which strongly limits the device integration simultaneously on possibly hundreds of chips per wafer. (3) Today's silicon-based chips used for information processing are operated at gigahertz frequencies, and the typical times of charge transport processes in molecules are in the femtosecond range.[550] Although the charge transport process in molecules is quite fast, it is challenging to operate molecular devices at gigahertz frequencies considering the high resistance and correspondingly the small currents of single-molecule junctions. Therefore, the incompatibleness between silicon-based chips and molecular-based devices can be foreseen. (4) To make a reproducible device, the integration process should be reversible; that is, the devices should be able to be disassembled. Predictably, the next generation of electrical devices will be a network of interfaces where the molecules function as key elements to control the interface. Therefore, the challenge for integration remains significant.

8.1.5. Energy Consumption. For molecular devices to be widely used in the market, their energy consumption needs to be considered. It is expected that molecular devices can operate under low biases with minimum energy consumption. However, the contact resistance of the molecule−metal contacts (such as the Au−1,4-benzene dithiol−Au system) is in the range of 1−100 MΩ,[419] which indicates that the molecules behave more like insulators rather than conductors, thus leading to a heavy energy consumption. Fortunately, there are at least three strategies that can be used to achieve an efficient molecule−metal coupling. (1) A highly efficient coupling can be achieved via simple direct C−Au σ bonding, in which the junction conductance is 100 times larger than that of most other terminations.[54,836] This is a promising discovery for the efficient coupling of molecules to metals because it allows molecular devices to operate under significantly lower voltages. (2) Graphene can be used instead of metals to achieve high efficient coupling. Graphene is a remarkable material with extraordinary electronic properties, for example, high mobility, high conductance, and stable covalent bonding with molecules. Additionally, the geometry of the graphene electrodes can be designed as a triangle to reduce the resistance of the electrodes themselves.[30,373] (3) Last is seeking new molecules with a high conductance and a low transport decay constant β. For typical cases, the resistance across the molecular junctions obeys an approximately exponential decay of the measured conductance with an increasing molecular length. When the metal Fermi energies are resonant with the relevant bridging states, electrons (or holes) can be injected directly into the bridging molecule, resulting in a weak distance dependence of the conductance corresponding to a small value of β. As a case in point, Li et al. reported a quasi-ohmic single-molecule charge transport using highly conjugated molecule wires with the lowest β value (β = 0.034 Å^{-1}).[463]

8.1.6. Addressability. Despite the considerable developments in nanofabrication, significant challenges remain, such as how to manufacture electrodes with a nanogap in large numbers and how to precisely and unambiguously graft the desired molecules into the gap electrodes.[823] More importantly, when thousands of junctions are integrated into one wafer, each junction should be addressable, thus making them more competitive. However, to our knowledge, there are only a few methods thus far that possess the ability to address single-molecule junctions, as depicted in Table 1. One remaining challenge is to develop efficient methods to fabricate multiple single-molecule devices in a parallel way.[11] A way to achieve this goal would be to improve the resolution and decrease the feature sizes offered by the advanced nanofabrication techniques.[57,171] Another possible approach might be the development of a molecular network using chemical synthesis and design to materialize large-scale single-molecule electronics.

8.1.7. General Strategies To Meet Challenges. Here, we try to offer several constructive suggestions to address the challenges in different aspects. Regarding the challenges for devices fabrication, one should try as best as possible to consider all of the parameters as a holistic one. Because of a lack of precise control in the fabrication process, contact geometry, molecular conformation, exact number of molecules, and measurement condition, molecular electronics depicts heterogeneity and is still in its infancy despite significant developments achieved over the past decade. To fabricate reliable molecular devices, the electrode materials, molecular materials, contact interfaces, device fabrications, and experimental environments should be considered a whole because they are so closely interrelated and cannot be optimized independently. Consequently, developing a reliable and scalable fabrication methodology for mass producing identical molec-

DOI: 10.1021/acs.chemrev.5b00680
Chem. Rev. 2016, 116, 4318−4440

ular tunneling junction arrays in high yields by the holistic consideration of all of the parameters is a current research focus.

To promote a continuous development of molecular electronics, the combination of the newly development nanofabrication techniques, macro-techniques, various characterization techniques, and different techniques for data analysis will enable us to achieve new success. (1) Integrating different fabricated techniques: For example, a new technique was recently reported for molecular junction fabrication, known as the direct metal transfer method, which used the advantages of both the nanowell method and the nanotransfer printing method.[303] (2) Combining the newly developed fabrication techniques with the classical characterization techniques: For example, if a gated mechanically controllable break junction can be performed simultaneously using the TEM as a novel characterization technique, the gating mechanism can be clarified, and the new phenomenon may be observed. (3) Application of the well-studied technique to novel materials: For instance, several groups reported on fabricating a single-molecule junction using graphene electrodes by the lithographic and electrical breakdown methods.[373,837] In principle, if one applies the MCBJ technique to precisely stretch graphene ribbons, graphene nanogaps with a tunable gape size can be obtained in high yield. (4) Combining nanofabrication technique with a traditional controllable macro-technique: For example, from the merger of the traditional terahertz technique and the MCBJ technique, a new technique may be developed to control the nanogap size via terahertz modulation based on bimaterial microcantilever.[169]

To achieve a continuously rapid development of molecular electronics, the market motivation and its real application should be definitely taken into consideration. To obtain a strong support from enterprises in the market, we face two challenges: (1) a significantly enhanced function or cost advantage must be demonstrated before the traditional CMOS industry will consider a new technology and invest in it; and (2) the traditional electronics industry will be reluctant to suffer radical changes in the highly sophisticated and extensive fabrication infrastructure to incorporate molecular components.[51] For the former challenge, we had witnessed more novel functions in molecular devices, which are unavailable for traditional electronics. The small size of the molecules meets the needs of miniaturizing electronic devices, which is the principal driving force behind the semiconductor industry and has led to significant improvements in the computational power and energy efficiencies.[656] In view of the actual functional applications in the market, two-terminal devices, such as wires, rectifiers, and switches, and logic single-molecule devices can be regarded as the most feasible routes toward practical molecular devices. At the same time, three-terminal molecular devices not only offer an experimental platform to study electronics but also pave the road to realize fast market applications beyond the laboratory research. Hence, it is highly desirable to make a first breakthrough in market applications using a molecular transistor, for example, digital circuits based on molecular transistors. For the latter challenge, we should demonstrate the priority of the compatibility with the traditional industry when a molecular device is fabricated. Despite the rapid development of molecular electronics in past decades, it is still a long way to win the battle in the pure market.

8.2. Open Questions

Several open questions remain, which contend and contradict each other, even in the basic field of electron transport. For example, regarding the observation of the discrete conductance change during the separation of the two nanoscale electrodes, one opinion is that the rearrangement of metal atoms results in the discrete conductance, and G_0 corresponds to the single gold atom conductance.[838] However, another opinion claimed that the underneath quantum mechanism is responsible for the discrete conductance change, and G_0 corresponds to a small size of point contacts (few atomic diameter width comparable to the conduction electrons' Fermi wavelength) rather than a single gold atom.[839] Each of the opinions has solid evidence to support its claims, resulting in a remaining question. The relationship between the molecular structure and inner-molecule quantum interference has not yet achieved a standard answer also. Vazquez et al. demonstrated that the conductance of a double-backbone molecular junction can be more than twice that of a single-backbone junction, providing clear evidence for constructive interference.[25] At the same time, Guedon et al. demonstrated that the electron can transport through two different pathways via unaligned localized molecular orbitals, thus yielding a destructive partial wave interference and poor conductance of the molecules.[79] Thus far, there are only individual cases instead of systematical investigations and a general model to relate the molecular structure with the type of the interference. The similar awkward situation also exists for intermolecular interactions. A few groups reported that parallel molecular wires are not strongly coupled along their molecular backbone and thus can be thought as individual conductance channels.[308] However, certain groups pointed out that the intermolecular tunneling is quite important in the electron transport process and may lead to a considerable enhancement of the tunneling current.[840] To clarify this argument, it is important to realize junctions that provide a transition from single-molecule experiments to 2D multimolecule junctions, which would allow the influence of the intermolecular electron transport of the adjacent molecules and a dephasing of the coherent electron transport to be studied.[841]

We noted that several functional devices well-fabricated in the traditional semiconductor industry have no counterpart in molecular electronics, such as commercial resonant tunneling diodes, which are easily realized in the traditional semiconductor domain. Because of the coupling of the molecule–metal and the temperature effects, the discrete energy level of the molecules is broad, resulting in an inexact energy alignment during the voltage sweeping process. Hence, it is difficult to realize molecular resonant tunneling diodes (MRTD), especially at room temperature. There may be two strategies to address this untouched field. (1) The first is using Si–molecule–Si junctions to realize the MRTD because the silicon, unlike metal electrodes, has a forbidden energy gap between the conduction band and the valence band. When the molecular orbital level falls into the forbidden band of silicon during bias sweeping, a sharp decrease occurs in the tunneling current, thus facilitating the achievement of the MRTD. (2) The second is employing graphene as electrodes to realize the MRTD because the special Dirac-cone energy structure and a nonzero bandgap of graphene can be easily obtained via hybrid graphene or applying a gating voltage.[842]

In this Review, the topic mainly involves molecular-scale electronics, with a particular focus on single-molecule

DOI: 10.1021/acs.chemrev.5b00680
Chem. Rev. 2016, 116, 4318–4440

electronics. Numerous topics, which are related to molecular electronics, are not addressed in this report due to our limited knowledge. For example, bulk organic molecules are interesting materials because of their structures and their electronic, electrical, magnetic, optical, biological, and chemical properties. Functional conjugated organic molecules with structural features have been assembled into the nanostructures, and several organic molecules have been applied in the market.[843] Large-area devices containing thin films of molecular materials represent the ultimate scaling of flexible devices based on organic materials. Several significant results of flexible molecular-scale electronic devices for insulating molecules, rectifying molecules, and photoswitching molecules have been reported using polyimide as the flexible substrate.[326−328] The potential of molecule-based nanotechnology for energy related applications is enormous. For example, two-terminal molecular junctions have potential applications in THz rectification for energy harvesting, which has real-world frequency limitations for traditional devices.[844] Nanomaterials can address several unmet needs in energy applications: they can be used to improve energy densities, promote energy efficiencies, increase energy transfer rates, and increase stabilities. Within the field of nanotechnology, new material development will play an important role toward a sustainable energy future but also meet tremendous challenges. However, these interesting topics are mostly beyond the scope of this Review.

8.3. Outlook

The ultimate limit for electronic device minimization is controlling the building blocks with atomic accuracy. Only molecules can provide such precise control over subnanometer distances as well as the possibility to reproducibly fabricate identical building blocks. Therefore, molecular electronics may be the only option to overcome the bottleneck of semiconductor-based technologies. Although it appears that molecular-based electronics will not replace most of the silicon-based electronics, there are convincing reasons to believe that molecular electronic devices can complement silicon-based devices by providing small dimensions of the molecules and new functionalities beyond the scope of conventional solid-state devices.[845]

The first decade of experimental and theoretical research on molecular electronics exhibited both rapid growth and significant scientific achievement. Molecular electronics has become one of the fastest growing fields and has brought scientists and engineers from different disciplines together. However, in certain cases, the strong enthusiasm for rapid exploration of a new area works against the requirement for a careful and systematic science, which is essential in the microelectronics industry. Until now, we have not yet reached a consensus on a robust and reproducible junction fabrication, and it is a long way to reach very high yield fabrication, highly integrated, and wide market application.[51]

From the market's point of view, carbon-based architectures with multiple junctions may provide a more robust platform for laboratory research and help validate molecular electronic concepts for room-temperature operation, potentially providing a wider application in the future. According to the sophistication level of the technologies, we may first achieve the market breakthrough in molecule-based chemo-/biosensors, as previously demonstrated, and then move to realize molecule-based digital circuits for future information processing. For a wide application of general molecular electronics, it is expected that more chemical tools and building blocks provided by a huge molecular structural and functional variety are needed. It is desirable that using designed molecules, which can be either (a) linked together, where each molecule performs a different function, such as rectification/switching so that logical operations can be performed in a "single" molecule junction, or (b) conformational changes triggered by external stimuli (magnetic, optical, and chemical), leading to a tremendous change in the junction current. These conformational changes can be used to unlock a security junction, which requires a "chemical key".

As single-molecule research continues to grow, another aspect becoming increasingly important is the theoretical calculation. Side-by-side use of the molecular calculation theory and simulations is equally important for a better understanding of the molecular system, and therefore verifying and even guiding molecular experiments.[827] We expect that molecular-scale electronics will foster truly excellent collaboration in bringing chemistry, physics, materials, engineers, and biology together, in return promoting the rapid development of this field. We have enough reason to believe that molecular-scale electronics has a bright future for bridging hard electronics to the soft molecular world.

AUTHOR INFORMATION

Corresponding Authors

*E-mail: tlee@snu.ac.kr.
*E-mail: guoxf@pku.edu.cn.

Author Contributions

⊥D.X. and X.W. contributed equally to this work.

Notes

The authors declare no competing financial interest.

Biographies

Dr. Dong Xiang is a Professor in the College of Electronic Information and Optical Engineering, Nankai University. He received his M.S. degree in 2006 from Huazhong University of Science & Technology, China. He received his Ph.D. degree from RWTH Aachen University, Germany, in 2011. From 2012 to 2014, he was a postdoctoral research scientist at the Department of Physics and Astronomy, Seoul National University, Korea. His current research interests focus on single-molecule study and optoelectronic molecular devices.

Xiaolong Wang received his B.S. degree in 2012 from East China University of Science and Technology, China. He is currently working toward a Ph.D. degree in Chemistry at the College of Chemistry and Molecular Engineering, Peking University, Beijing, under the guidance of Prof. Xuefeng Guo. His current research interest is single-molecule biodetection.

Chuancheng Jia is currently a postdoctoral researcher in the College of Chemistry and Molecular Engineering, Peking University, and Institute of Chemistry, Chinese Academy of Sciences, with Xuefeng Guo and Daoben Zhu. He received his Ph.D. degree in 2014 from the College of Chemistry and Molecular Engineering, Peking University, with Xuefeng Guo. His research is focused on single-molecule devices and dynamics.

Dr. Takhee Lee is a Professor in the Department of Physics and Astronomy, Seoul National University, Korea. He graduated from Seoul National University, Korea, and received his Ph.D. from Purdue University, USA, in 2000. He was a postdoctoral researcher at Yale University, USA, until 2004. His current research interests are

DOI: 10.1021/acs.chemrev.5b00680
Chem. Rev. 2016, 116, 4318−4440

molecular electronics, polymer memory devices, and 2D atomic film nanoelectronic devices.

Dr. Xuefeng Guo received his Ph.D. in 2004 from the Institute of Chemistry, Chinese Academy of Sciences, Beijing. From 2004 to 2007, he was a postdoctoral research scientist at the Columbia University Nanocenter. He joined the faculty as a professor under "Peking 100-Talent" Program at Peking University in 2008. In 2012, he won the National Science Funds for Distinguished Young Scholars of China. His current research is focused on functional nanometer/molecular devices.

ACKNOWLEDGMENTS

We are grateful to Colin Nuckolls and Dirk Mayer for enlightening discussions. We appreciate the financial support received from the 973 Project (2012CB921404) and the National Natural Science Funds of China (21225311, 91333102, 21373014, and 61571242). T.L. is thankful for the financial support received from the National Creative Research Laboratory program (Grant no. 2012026372) through the National Research Foundation of Korea (NRF).

REFERENCES

(1) Lortscher, E. Wiring Molecules into Circuits. *Nat. Nanotechnol.* **2013**, *8*, 381−384.
(2) Wilson, L. *International Technology Roadmap for Semiconductors (ITRS)*; Semiconductor Industry Association, 2013.
(3) Haedler, A. T.; Kreger, K.; Issac, A.; Wittmann, B.; Kivala, M.; Hammer, N.; Kohler, J.; Schmidt, H. W.; Hildner, R. Long-Range Energy Transport in Single Supramolecular Nanofibres at Room Temperature. *Nature* **2015**, *523*, 196−199.
(4) Ratner, M. A Brief History of Molecular Electronics. *Nat. Nanotechnol.* **2013**, *8*, 378−381.
(5) Bryce, M. R.; Petty, M. C. Electrically Conductive Langmuir-Blodgett-Films of Charge-Transfer Materials. *Nature* **1995**, *374*, 771−776.
(6) Tour, J. M.; Reinerth, W. A.; Jones, L.; Burgin, T. P.; Zhou, C. W.; Muller, C. J.; Deshpande, M. R.; Reed, M. A. Recent Advances in Molecular Scale Electronics. *Ann. N. Y. Acad. Sci.* **1998**, *852*, 197−204.
(7) Petty, M. C.; Bryce, M. R.; Bloor, D. *An Introduction to Molecular Electronics*; Oxford University Press: New York, 1995.
(8) Cuevas, J. C.; Scheer, E. *Molecular Electronics: An Introduction to Theory and Experiment*; World Scientific: River Edge, NJ, 2010.
(9) Heath, J. R. Analytical Chemistry in Molecular Electronics. *Annu. Rev. Mater. Res.* **2009**, *39*, 1−23.
(10) Kagan, C. R.; Ratner, M. A. Molecular Transport Junctions: An Introduction. *MRS Bull.* **2004**, *29*, 376−384.
(11) Nitzan, A.; Ratner, M. A. Electron Transport in Molecular Wire Junctions. *Science* **2003**, *300*, 1384−1389.
(12) Metzger, R. M. Unimolecular Electronics. *Chem. Rev.* **2015**, *115*, 5056−5115.
(13) Mann, B.; Kuhn, H. Tunneling through Fatty Acid Salt Monolayers. *J. Appl. Phys.* **1971**, *42*, 4398−4405.
(14) Polymeropoulos, E. E.; Sagiv, J. Electrical-Conduction through Adsorbed Monolayers. *J. Chem. Phys.* **1978**, *69*, 1836−1847.
(15) Netzer, L.; Sagiv, J. A New Approach to Construction of Artificial Monolayer Assemblies. *J. Am. Chem. Soc.* **1983**, *105*, 674−676.
(16) Aviram, A.; Ratner, M. A. Molecular Rectifiers. *Chem. Phys. Lett.* **1974**, *29*, 277−283.
(17) Binning, G.; Rohrer, H.; Gerber, C.; Weibel, E. Surface Studies by Scanning Tunneling Microscopy. *Phys. Rev. Lett.* **1982**, *49*, 57−61.
(18) Zandvliet, H. J. W.; van Houselt, A. Scanning Tunneling Spectroscopy. *Annu. Rev. Anal. Chem.* **2009**, *2*, 37−55.
(19) Bumm, L. A.; Arnold, J. J.; Cygan, M. T.; Dunbar, T. D.; Burgin, T. P.; Jones, L.; Allara, D. L.; Tour, J. M.; Weiss, P. S. Are Single Molecular Wires Conducting? *Science* **1996**, *271*, 1705−1707.
(20) Reed, M. A.; Zhou, C.; Muller, C. J.; Burgin, T. P.; Tour, J. M. Conductance of a Molecular Junction. *Science* **1997**, *278*, 252−254.
(21) Park, J.; Pasupathy, A. N.; Goldsmith, J. I.; Chang, C.; Yaish, Y.; Petta, J. R.; Rinkoski, M.; Sethna, J. P.; Abruna, H. D.; McEuen, P. L.; et al. Coulomb Blockade and the Kondo Effect in Single-Atom Transistors. *Nature* **2002**, *417*, 722−725.
(22) Xiang, J.; Liu, B.; Wu, S. T.; Ren, B.; Yang, F. Z.; Mao, B. W.; Chow, Y. L.; Tian, Z. Q. A Controllable Electrochemical Fabrication of Metallic Electrodes with a Nanometer/Angstrom-Sized Gap Using an Electric Double Layer as Feedback. *Angew. Chem., Int. Ed.* **2005**, *44*, 1265−1268.
(23) Bonifas, A. P.; McCreery, R. L. 'Soft' Au, Pt and Cu Contacts for Molecular Junctions through Surface-Diffusion-Mediated Deposition. *Nat. Nanotechnol.* **2010**, *5*, 612−617.
(24) Pasupathy, A. N.; Bialczak, R. C.; Martinek, J.; Grose, J. E.; Donev, L. A. K.; McEuen, P. L.; Ralph, D. C. The Kondo Effect in the Presence of Ferromagnetism. *Science* **2004**, *306*, 86−89.
(25) Vazquez, H.; Skouta, R.; Schneebeli, S.; Kamenetska, M.; Breslow, R.; Venkataraman, L.; Hybertsen, M. S. Probing the Conductance Superposition Law in Single-Molecule Circuits with Parallel Paths. *Nat. Nanotechnol.* **2012**, *7*, 663−667.
(26) Diez-Perez, I.; Hihath, J.; Hines, T.; Wang, Z. S.; Zhou, G.; Mullen, K.; Tao, N. J. Controlling Single-Molecule Conductance through Lateral Coupling of π Orbitals. *Nat. Nanotechnol.* **2011**, *6*, 226−231.
(27) Reddy, P.; Jang, S. Y.; Segalman, R. A.; Majumdar, A. Thermoelectricity in Molecular Junctions. *Science* **2007**, *315*, 1568−1571.
(28) Akkerman, H. B.; Blom, P. W. M.; de Leeuw, D. M.; de Boer, B. Towards Molecular Electronics with Large-Area Molecular Junctions. *Nature* **2006**, *441*, 69−72.
(29) Sayed, S. Y.; Fereiro, J. A.; Yan, H. J.; McCreery, R. L.; Bergren, A. J. Charge Transport in Molecular Electronic Junctions: Compression of the Molecular Tunnel Barrier in the Strong Coupling Regime. *Proc. Natl. Acad. Sci. U. S. A.* **2012**, *109*, 11498−11503.
(30) Cao, Y.; Dong, S.; Liu, S.; He, L.; Gan, L.; Yu, X.; Steigerwald, M. L.; Wu, X.; Liu, Z.; Guo, X. Building High-Throughput Molecular Junctions Using Indented Graphene Point Contacts. *Angew. Chem., Int. Ed.* **2012**, *51*, 12228−12232.
(31) Guo, X.; Small, J. P.; Klare, J. E.; Wang, Y.; Purewal, M. S.; Tam, I. W.; Hong, B. H.; Caldwell, R.; Huang, L.; O'Brien, S. Covalently Bridging Gaps in Single-Walled Carbon Nanotubes with Conducting Molecules. *Science* **2006**, *311*, 356−359.
(32) Ratner, M. A.; Davis, B.; Kemp, M.; Mujica, V.; Roitberg, A.; Yaliraki, S. Molecular Wires: Charge Transport, Mechanisms, and Control. *Ann. N. Y. Acad. Sci.* **1998**, *852*, 22−37.
(33) Mujica, V.; Kemp, M.; Ratner, M. A. Electron Conduction in Molecular Wires.I. A Scattering Formalism. *J. Chem. Phys.* **1994**, *101*, 6849−6855.
(34) Lindsay, S. M.; Ratner, M. A. Molecular Transport Junctions: Clearing Mists. *Adv. Mater.* **2007**, *19*, 23−31.
(35) Zimbovskaya, N. A.; Pederson, M. R. Electron Transport through Molecular Junctions. *Phys. Rep.* **2011**, *509*, 1−87.
(36) Wang, W. Y.; Lee, T.; Reed, M. A. Electron Tunnelling in Self-Assembled Monolayers. *Rep. Prog. Phys.* **2005**, *68*, 523−544.
(37) Lambert, C. J. Basic Concepts of Quantum Interference and Electron Transport in Single-Molecule Electronics. *Chem. Soc. Rev.* **2015**, *44*, 875−888.
(38) Lin, L. L.; Jiang, J.; Luo, Y. Elastic and Inelastic Electron Transport in Metal-Molecule(S)-Metal Junctions. *Phys. E* **2013**, *47*, 167−187.
(39) Aradhya, S. V.; Venkataraman, L. Single-Molecule Junctions Beyond Electronic Transport. *Nat. Nanotechnol.* **2013**, *8*, 399−410.
(40) Sun, L.; Diaz-Fernandez, Y. A.; Gschneidtner, T. A.; Westerlund, F.; Lara-Avila, S.; Moth-Poulsen, K. Single-Molecule Electronics: From Chemical Design to Functional Devices. *Chem. Soc. Rev.* **2014**, *43*, 7378−7411.
(41) Tao, N. J. Electron Transport in Molecular Junctions. *Nat. Nanotechnol.* **2006**, *1*, 173−181.

DOI: 10.1021/acs.chemrev.5b00680
Chem. Rev. 2016, 116, 4318−4440

(42) Shen, Q.; Guo, X. F.; Steigerwald, M. L.; Nuckolls, C. Integrating Reaction Chemistry into Molecular Electronic Devices. *Chem. - Asian J.* **2010**, *5*, 1040−1057.
(43) Galperin, M.; Ratner, M. A.; Nitzan, A.; Troisi, A. Nuclear Coupling and Polarization in Molecular Transport Junctions: Beyond Tunneling to Function. *Science* **2008**, *319*, 1056−1060.
(44) van der Molen, S. J.; Liljeroth, P. Charge Transport through Molecular Switches. *J. Phys.: Condens. Matter* **2010**, *22*, 133001.
(45) Natelson, D.; Li, Y. J.; Herzog, J. B. Nanogap Structures: Combining Enhanced Raman Spectroscopy and Electronic Transport. *Phys. Chem. Chem. Phys.* **2013**, *15*, 5262−5275.
(46) Moth-Poulsen, K.; Bjornholm, T. Molecular Electronics with Single Molecules in Solid-State Devices. *Nat. Nanotechnol.* **2009**, *4*, 551−556.
(47) Carlson, A.; Bowen, A. M.; Huang, Y.; Nuzzo, R. G.; Rogers, J. A. Transfer Printing Techniques for Materials Assembly and Micro/Nanodevice Fabrication. *Adv. Mater.* **2012**, *24*, 5284−5318.
(48) Tyagi, P. Multilayer Edge Molecular Electronics Devices: A Review. *J. Mater. Chem.* **2011**, *21*, 4733−4742.
(49) Flood, A. H.; Stoddart, J. F.; Steuerman, D. W.; Heath, J. R. Whence Molecular Electronics? *Science* **2004**, *306*, 2055−2056.
(50) Li, T.; Hu, W. P.; Zhu, D. B. Nanogap Electrodes. *Adv. Mater.* **2010**, *22*, 286−300.
(51) McCreery, R. L.; Bergren, A. J. Progress with Molecular Electronic Junctions: Meeting Experimental Challenges in Design and Fabrication. *Adv. Mater.* **2009**, *21*, 4303−4322.
(52) Xu, B. Q.; Tao, N. J. J. Measurement of Single-Molecule Resistance by Repeated Formation of Molecular Junctions. *Science* **2003**, *301*, 1221−1223.
(53) Chen, F.; Hihath, J.; Huang, Z.; Li, X.; Tao, N. J. Measurement of Single-molecule Conductance. *Annu. Rev. Phys. Chem.* **2007**, *58*, 535−564.
(54) Cheng, Z. L.; Skouta, R.; Vazquez, H.; Widawsky, J. R.; Schneebeli, S.; Chen, W.; Hybertsen, M. S.; Breslow, R.; Venkataraman, L. In Situ Formation of Highly Conducting Covalent Au-C Contacts for Single-Molecule Junctions. *Nat. Nanotechnol.* **2011**, *6*, 353−357.
(55) Park, Y. S.; Whalley, A. C.; Kamenetska, M.; Steigerwald, M. L.; Hybertsen, M. S.; Nuckolls, C.; Venkataraman, L. Contact Chemistry and Single-Molecule Conductance: A Comparison of Phosphines, Methyl Sulfides, and Amines. *J. Am. Chem. Soc.* **2007**, *129*, 15768−15769.
(56) Kamenetska, M.; Quek, S. Y.; Whalley, A. C.; Steigerwald, M. L.; Choi, H. J.; Louie, S. G.; Nuckolls, C.; Hybertsen, M. S.; Neaton, J. B.; Venkataraman, L. Conductance and Geometry of Pyridine-Linked Single-Molecule Junctions. *J. Am. Chem. Soc.* **2010**, *132*, 6817−6821.
(57) Jia, C.; Guo, X. Molecule-Electrode Interfaces in Molecular Electronic Devices. *Chem. Soc. Rev.* **2013**, *42*, 5642−5660.
(58) Wold, D. J.; Frisbie, C. D. Fabrication and Characterization of Metal-Molecule-Metal Junctions by Conducting Probe Atomic Force Microscopy. *J. Am. Chem. Soc.* **2001**, *123*, 5549−5556.
(59) Wold, D. J.; Frisbie, C. D. Formation of Metal-Molecule-Metal Tunnel Junctions: Microcontacts to Alkanethiol Monolayers with a Conducting AFM Tip. *J. Am. Chem. Soc.* **2000**, *122*, 2970−2971.
(60) Li, W.; Sepunaru, L.; Amdursky, N.; Cohen, S. R.; Pecht, I.; Sheves, M.; Cahen, D. Temperature and Force Dependence of Nanoscale Electron Transport Via the Cu Protein Azurin. *ACS Nano* **2012**, *6*, 10816−10824.
(61) Aradhya, S. V.; Frei, M.; Hybertsen, M. S.; Venkataraman, L. Van Der Waals Interactions at Metal/Organic Interfaces at the Single-Molecule Level. *Nat. Mater.* **2012**, *11*, 872−876.
(62) Wagner, C.; Fournier, N.; Tautz, F. S.; Temirov, R. Measurement of the Binding Energies of the Organic-Metal Perylene-Teracarboxylic-Dianhydride/Au(111) Bonds by Molecular Manipulation Using an Atomic Force Microscope. *Phys. Rev. Lett.* **2012**, *109*, 076102.
(63) Pan, S.; Fu, Q.; Huang, T.; Zhao, A.; Wang, B.; Luo, Y.; Yang, J.; Hou, J. Design and Control of Electron Transport Properties of Single Molecules. *Proc. Natl. Acad. Sci. U. S. A.* **2009**, *106*, 15259−15263.
(64) Xie, Z. T.; Baldea, I.; Smith, C. E.; Wu, Y. F.; Frisbie, C. D. Experimental and Theoretical Analysis of Nanotransport in Oligophenylene Dithiol Junctions as a Function of Molecular Length and Contact Work Function. *ACS Nano* **2015**, *9*, 8022−8036.
(65) Schmaus, S.; Bagrets, A.; Nahas, Y.; Yamada, T. K.; Bork, A.; Bowen, M.; Beaurepaire, E.; Evers, F.; Wulfhekel, W. Giant Magnetoresistance through a Single Molecule. *Nat. Nanotechnol.* **2011**, *6*, 185−189.
(66) Fei, X. M.; Wu, G. F.; Lopez, V.; Lu, G.; Gao, H. J.; Gao, L. Spin-Dependent Conductance in Co/C_{60}/Co/Ni Single-Molecule Junctions in the Contact Regime. *J. Phys. Chem. C* **2015**, *119*, 11975−11981.
(67) Schwoebel, J.; Fu, Y.; Brede, J.; Dilullo, A.; Hoffmann, G.; Klyatskaya, S.; Ruben, M.; Wiesendanger, R. Real-Space Observation of Spin-Split Molecular Orbitals of Adsorbed Single-Molecule Magnets. *Nat. Commun.* **2012**, *3*, 953.
(68) Madhavan, V.; Chen, W.; Jamneala, T.; Crommie, M. F.; Wingreen, N. S. Tunneling into a Single Magnetic Atom: Spectroscopic Evidence of the Kondo Resonance. *Science* **1998**, *280*, 567−569.
(69) Andres, R. P.; Bein, T.; Dorogi, M.; Feng, S.; Henderson, J. I.; Kubiak, C. P.; Mahoney, W.; Osifchin, R. G.; Reifenberger, R. "Coulomb Staircase" at Room Temperature in a Self-Assembled Molecular Nanostructure. *Science* **1996**, *272*, 1323−1325.
(70) Wang, W.; Ji, Y.; Zhang, H.; Zhao, A.; Wang, B.; Yang, J.; Hou, J. G. Negative Differential Resistance in a Hybrid Silicon-Molecular System: Resonance between the Intrinsic Surface-States and the Molecular Orbital. *ACS Nano* **2012**, *6*, 7066−7076.
(71) Chen, L.; Hu, Z.; Zhao, A.; Wang, B.; Luo, Y.; Yang, J.; Hou, J. G. Mechanism for Negative Differential Resistance in Molecular Electronic Devices: Local Orbital Symmetry Matching. *Phys. Rev. Lett.* **2007**, *99*, 146803.
(72) Rascon-Ramos, H.; Artes, J. M.; Li, Y. H.; Hihath, J. Binding Configurations and Intramolecular Strain in Single-Molecule Devices. *Nat. Mater.* **2015**, *14*, 517−522.
(73) Li, Z. H.; Li, H.; Chen, S. J.; Froehlich, T.; Yi, C. Y.; Schonenberger, C.; Calame, M.; Decurtins, S.; Liu, S. X.; Borguet, E. Regulating a Benzodifuran Single Molecule Redox Switch Via Electrochemical Gating and Optimization of Molecule/Electrode Coupling. *J. Am. Chem. Soc.* **2014**, *136*, 8867−8870.
(74) Baghernejad, M.; Zhao, X. T.; Ornso, K. B.; Fueg, M.; Moreno-García, P.; Rudnev, A. V.; Kaliginedi, V.; Vesztergom, S.; Huang, C. C.; Hong, W. J.; et al. Electrochemical Control of Single-Molecule Conductance by Fermilevel Tuning and Conjugation Switching. *J. Am. Chem. Soc.* **2014**, *136*, 17922−17925.
(75) Li, Z.; Borguet, E. Determining Charge Transport Pathways through Single Porphyrin Molecules Using Scanning Tunneling Microscopy Break Junctions. *J. Am. Chem. Soc.* **2012**, *134*, 63−66.
(76) Wang, G.; Kim, T.-W.; Jo, G.; Lee, T. Enhancement of Field Emission Transport by Molecular Tilt Configuration in Metal-Molecule-Metal Junctions. *J. Am. Chem. Soc.* **2009**, *131*, 5980−5985.
(77) Loth, S.; Etzkorn, M.; Lutz, C. P.; Eigler, D. M.; Heinrich, A. J. Measurement of Fast Electron Spin Relaxation Times with Atomic Resolution. *Science* **2010**, *329*, 1628−1630.
(78) Kumagai, T.; Hanke, F.; Gawinkowski, S.; Sharp, J.; Kotsis, K.; Waluk, J.; Persson, M.; Grill, L. Controlling Intramolecular Hydrogen Transfer in a Porphycene Molecule with Single Atoms or Molecules Located Nearby. *Nat. Chem.* **2013**, *6*, 41−46.
(79) Guedon, C. M.; Valkenier, H.; Markussen, T.; Thygesen, K. S.; Hummelen, J. C.; van der Molen, S. J. Observation of Quantum Interference in Molecular Charge Transport. *Nat. Nanotechnol.* **2012**, *7*, 304−308.
(80) Manrique, D. Z.; Huang, C.; Baghernejad, M.; Zhao, X. T.; Al-Owaedi, O. A.; Sadeghi, H.; Kaliginedi, V.; Hong, W. J.; Gulcur, M.; Wandlowski, T.; et al. Quantum Circuit Rule for Interference Effects in Single-Molecule Electrical Junctions. *Nat. Commun.* **2015**, *6*, 6389.
(81) Markussen, T.; Stadler, R.; Thygesen, K. S. The Relation between Structure and Quantum Interference in Single Molecule Junctions. *Nano Lett.* **2010**, *10*, 4260−4265.

DOI: 10.1021/acs.chemrev.5b00680
Chem. Rev. 2016, 116, 4318−4440

(82) Ballmann, S.; Hartle, R.; Coto, P. B.; Elbing, M.; Mayor, M.; Bryce, M. R.; Thoss, M.; Weber, H. B. Experimental Evidence for Quantum Interference and Vibrationally Induced Decoherence in Single-Molecule Junctions. *Phys. Rev. Lett.* **2012**, *109*, 056801.
(83) Zhou, X.-Y.; Peng, Z.-L.; Sun, Y.-Y.; Wang, L.-N.; Niu, Z.-J.; Zhou, X.-S. Conductance Measurement of Pyridyl-Based Single Molecule Junctions with Cu and Au Contacts. *Nanotechnology* **2013**, *24*, 465204.
(84) Wilson, N. R.; Macpherson, J. V. Carbon Nanotube Tips for Atomic Force Microscopy. *Nat. Nanotechnol.* **2009**, *4*, 483−491.
(85) Leary, E.; Teresa González, M.; van der Pol, C.; Bryce, M. R.; Filippone, S.; Martin, N.; Rubio-Bollinger, G.; Agraït, N. Unambiguous One-Molecule Conductance Measurements under Ambient Conditions. *Nano Lett.* **2011**, *11*, 2236−2241.
(86) Smaali, K.; Clement, N.; Patriarche, G.; Vuillaume, D. Conductance Statistics from a Large Array of Sub-10 nm Molecular Junctions. *ACS Nano* **2012**, *6*, 4639−4647.
(87) Cui, X. D.; Primak, A.; Zarate, X.; Tomfohr, J.; Sankey, O. F.; Moore, A. L.; Moore, T. A.; Gust, D.; Harris, G.; Lindsay, S. M. Reproducible Measurement of Single-Molecule Conductivity. *Science* **2001**, *294*, 571−574.
(88) Li, J. J.; Bai, M. L.; Chen, Z. B.; Zhou, X. S.; Shi, Z.; Zhang, M.; Ding, S. Y.; Hou, S. M.; Schwarzacher, W.; Nichols, R. J.; Mao, B. W. Giant Single-Molecule Anisotropic Magnetoresistance at Room Temperature. *J. Am. Chem. Soc.* **2015**, *137*, 5923−5929.
(89) Zhou, X.-S.; Wei, Y.-M.; Liu, L.; Chen, Z.-B.; Tang, J.; Mao, B.-W. Extending the Capability of Stm Break Junction for Conductance Measurement of Atomic-Size Nanowires: An Electrochemical Strategy. *J. Am. Chem. Soc.* **2008**, *130*, 13228−13230.
(90) Dai, H. J.; Hafner, J. H.; Rinzler, A. G.; Colbert, D. T.; Smalley, R. E. Nanotubes as Nanoprobes in Scanning Probe Microscopy. *Nature* **1996**, *384*, 147−150.
(91) Nishijima, H.; Kamo, S.; Akita, S.; Nakayama, Y.; Hohmura, K. I.; Yoshimura, S. H.; Takeyasu, K. Carbon-Nanotube Tips for Scanning Probe Microscopy: Preparation by a Controlled Process and Observation of Deoxyribonucleic Acid. *Appl. Phys. Lett.* **1999**, *74*, 4061−4063.
(92) Hafner, J. H.; Cheung, C. L.; Oosterkamp, T. H.; Lieber, C. M. High-Yield Assembly of Individual Single-Walled Carbon Nanotube Tips for Scanning Probe Microscopies. *J. Phys. Chem. B* **2001**, *105*, 743−746.
(93) Wilson, N. R.; Macpherson, J. V. Single-Walled Carbon Nanotubes as Templates for Nanowire Conducting Probes. *Nano Lett.* **2003**, *3*, 1365−1369.
(94) Gross, L.; Mohn, F.; Moll, N.; Liljeroth, P.; Meyer, G. The Chemical Structure of a Molecule Resolved by Atomic Force Microscopy. *Science* **2009**, *325*, 1110−1114.
(95) Lee, H. J.; Ho, W. Single-Bond Formation and Characterization with a Scanning Tunneling Microscope. *Science* **1999**, *286*, 1719−1722.
(96) Moreno-García, P.; La Rosa, A.; Kolivoska, V.; Bermejo, D.; Hong, W. J.; Yoshida, K.; Baghernejad, M.; Filippone, S.; Broekmann, P.; Wandlowski, T.; et al. Charge Transport in C_{60}-Based Dumbbell-Type Molecules: Mechanically Induced Switching between Two Distinct Conductance States. *J. Am. Chem. Soc.* **2015**, *137*, 2318−2327.
(97) Clement, N.; Patriarche, G.; Smaali, K.; Vaurette, F.; Nishiguchi, K.; Troadec, D.; Fujiwara, A.; Vuillaume, D. Large Array of Sub-10-nm Single-Grain Au Nanodots for Use in Nanotechnology. *Small* **2011**, *7*, 2607−2613.
(98) Zhang, J.; Chen, P.; Yuan, B.; Ji, W.; Cheng, Z.; Qiu, X. Real-Space Identification of Intermolecular Bonding with Atomic Force Microscopy. *Science* **2013**, *342*, 611−614.
(99) Chiang, C.-l.; Xu, C.; Han, Z.; Ho, W. Real-Space Imaging of Molecular Structure and Chemical Bonding by Single-Molecule Inelastic Tunneling Probe. *Science* **2014**, *344*, 885−888.
(100) Mohn, F.; Gross, L.; Moll, N.; Meyer, G. Imaging the Charge Distribution within a Single Molecule. *Nat. Nanotechnol.* **2012**, *7*, 227−231.
(101) de Oteyza, D. G.; Gorman, P.; Chen, Y.-C.; Wickenburg, S.; Riss, A.; Mowbray, D. J.; Etkin, G.; Pedramrazi, Z.; Tsai, H.-Z.; Rubio, A.; et al. Direct Imaging of Covalent Bond Structure in Single-Molecule Chemical Reactions. *Science* **2013**, *340*, 1434−1437.
(102) Baró, A. M.; Miranda, R.; Alamán, J.; García, N.; Binnig, G.; Rohrer, H.; Gerber, C.; Carrascosa, J. L. Determination of Surface-Topography of Biological Specimens at High-Resolution by Scanning Tunnelling Microscopy. *Nature* **1985**, *315*, 253−254.
(103) Liu, Z.; Ding, S. Y.; Chen, Z. B.; Wang, X.; Tian, J. H.; Anema, J. R.; Zhou, X. S.; Wu, D. Y.; Mao, B. W.; Xu, X.; et al. Revealing the Molecular Structure of Single-Molecule Junctions in Different Conductance States by Fishing-Mode Tip-Enhanced Raman Spectroscopy. *Nat. Commun.* **2011**, *2*, 305.
(104) Qiu, X. H.; Nazin, G. V.; Ho, W. Vibrationally Resolved Fluorescence Excited with Submolecular Precision. *Science* **2003**, *299*, 542−546.
(105) Galperin, M.; Nitzan, A. Molecular Optoelectronics: The Interaction of Molecular Conduction Junctions with Light. *Phys. Chem. Chem. Phys.* **2012**, *14*, 9421−9438.
(106) Venkataraman, L.; Klare, J. E.; Nuckolls, C.; Hybertsen, M. S.; Steigerwald, M. L. Dependence of Single-Molecule Junction Conductance on Molecular Conformation. *Nature* **2006**, *442*, 904−907.
(107) Su, T. A.; Li, H.; Steigerwald, M. L.; Venkataraman, L.; Nuckolls, C. Stereoelectronic Switching in Single-Molecule Junctions. *Nat. Chem.* **2015**, *7*, 215−220.
(108) Huang, Z.; Xu, B.; Chen, Y.; Di Ventra, M.; Tao, N. Measurement of Current-Induced Local Heating in a Single Molecule Junction. *Nano Lett.* **2006**, *6*, 1240−1244.
(109) Lee, W.; Kim, K.; Jeong, W.; Angela Zotti, L.; Pauly, F.; Carlos Cuevas, J.; Reddy, P. Heat Dissipation in Atomic-Scale Junctions. *Nature* **2013**, *498*, 209−212.
(110) Zhou, J.; Chen, F.; Xu, B. Fabrication and Electronic Characterization of Single Molecular Junction Devices: A Comprehensive Approach. *J. Am. Chem. Soc.* **2009**, *131*, 10439−10446.
(111) Huang, Z.; Chen, F.; Bennett, P. A.; Tao, N. Single Molecule Junctions Formed Via Au-Thiol Contact: Stability and Breakdown Mechanism. *J. Am. Chem. Soc.* **2007**, *129*, 13225−13231.
(112) Bruot, C.; Hihath, J.; Tao, N. Mechanically Controlled Molecular Orbital Alignment in Single Molecule Junctions. *Nat. Nanotechnol.* **2011**, *7*, 35−40.
(113) Xu, B. Q.; Xiao, X. Y.; Tao, N. J. Measurements of Single-Molecule Electromechanical Properties. *J. Am. Chem. Soc.* **2003**, *125*, 16164−16165.
(114) Yu, M. F.; Lourie, O.; Dyer, M. J.; Moloni, K.; Kelly, T. F.; Ruoff, R. S. Strength and Breaking Mechanism of Multiwalled Carbon Nanotubes under Tensile Load. *Science* **2000**, *287*, 637−640.
(115) Eigler, D. M.; Schweizer, E. K. Positioning Single Atoms with a Scanning Tunneling Microscope. *Nature* **1990**, *344*, 524−526.
(116) Majumdar, A.; Oden, P. I.; Carrejo, J. P.; Nagahara, L. A.; Graham, J. J.; Alexander, J. Nanometer-Scale Lithography Using the Atomic Force Microscope. *Appl. Phys. Lett.* **1992**, *61*, 2293−2295.
(117) Mamin, H. J.; Guethner, P. H.; Rugar, D. Atomic Emission from a Gold Scanning-Tunneling-Microscope Tip. *Phys. Rev. Lett.* **1990**, *65*, 2418−2421.
(118) Min, S. Y.; Kim, T. S.; Kim, B. J.; Cho, H.; Noh, Y. Y.; Yang, H.; Cho, J. H.; Lee, T. W. Large-Scale Organic Nanowire Lithography and Electronics. *Nat. Commun.* **2013**, *4*, 1773.
(119) Pires, D.; Hedrick, J. L.; De Silva, A.; Frommer, J.; Gotsmann, B.; Wolf, H.; Despont, M.; Duerig, U.; Knoll, A. W. Nanoscale Three-Dimensional Patterning of Molecular Resists by Scanning Probes. *Science* **2010**, *328*, 732−735.
(120) He, Y.; Dong, H.; Li, T.; Wang, C.; Shao, W.; Zhang, Y.; Jiang, L.; Hu, W. Graphene and Graphene Oxide Nanogap Electrodes Fabricated by Atomic Force Microscopy Nanolithography. *Appl. Phys. Lett.* **2010**, *97*, 133301.
(121) Tseng, A. A.; Jou, S.; Notargiacomo, A.; Chen, T. P. Recent Developments in Tip-Based Nanofabrication and Its Roadmap. *J. Nanosci. Nanotechnol.* **2008**, *8*, 2167−2186.

DOI: 10.1021/acs.chemrev.5b00680
Chem. Rev. 2016, 116, 4318−4440

(122) Rosa, L. G.; Liang, J. Atomic Force Microscope Nanolithography: Dip-Pen, Nanoshaving, Nanografting, Tapping Mode, Electrochemical and Thermal Nanolithography. *J. Phys.: Condens. Matter* **2009**, *21*, 483001.
(123) Tseng, A. A.; Notargiacomo, A.; Chen, T. P. Nanofabrication by Scanning Probe Microscope Lithography: A Review. *J. Vac. Sci. Technol., B: Microelectron. Process. Phenom.* **2005**, *23*, 877−894.
(124) Moreland, J.; Ekin, J. W. Electron-Tunneling into Superconducting Filaments Using Mechanically Adjustable Barriers. *Appl. Phys. Lett.* **1985**, *47*, 175−177.
(125) Moreland, J.; Ekin, J. W. Electron-Tunneling Experiments Using Nb-Sn Break Junctions. *J. Appl. Phys.* **1985**, *58*, 3888−3895.
(126) Muller, C. J.; Vanruitenbeek, J. M.; Dejongh, L. J. Experiments on Mechanically Controllable Break Junctions of Niobium and Platinum. *Inst. Phys. Conf. Ser.* **1992**, 171−174.
(127) Muller, C. J.; Vanruitenbeek, J. M.; Dejongh, L. J. Conductance and Supercurrent Discontinuities in Atomic-Scale Metallic Constrictions of Variable Width. *Phys. Rev. Lett.* **1992**, *69*, 140−143.
(128) Scheer, E.; Agraït, N.; Cuevas, J. C.; Yeyati, A. L.; Ludoph, B.; Martin-Rodero, A.; Bollinger, G. R.; van Ruitenbeek, J. M.; Urbina, C. The Signature of Chemical Valence in the Electrical Conduction through a Single-Atom Contact. *Nature* **1998**, *394*, 154−157.
(129) Zhou, C.; Deshpande, M. R.; Reed, M. A.; Jones, L.; Tour, J. M. Nanoscale Metal Self-Assembled Monolayer Metal Heterostructures. *Appl. Phys. Lett.* **1997**, *71*, 611−613.
(130) Xiang, D.; Jeong, H.; Lee, T.; Mayer, D. Mechanically Controllable Break Junctions for Molecular Electronics. *Adv. Mater.* **2013**, *25*, 4845−4867.
(131) Vrouwe, S. A. G.; van der Giessen, E.; van der Molen, S. J.; Dulić, D.; Trouwborst, M. L.; van Wees, B. J. Mechanics of Lithographically Defined Break Junctions. *Phys. Rev. B: Condens. Matter Mater. Phys.* **2005**, *71*, 035313.
(132) Bohler, T.; Grebing, J.; Mayer-Gindner, A.; Lohneysen, H. V.; Scheer, E. Mechanically Controllable Break-Junctions for Use as Electrodes for Molecular Electronics. *Nanotechnology* **2004**, *15*, S465−S471.
(133) Grüter, L.; González, M. T.; Huber, R.; Calame, M.; Schonenberger, C. Electrical Conductance of Atomic Contacts in Liquid Environments. *Small* **2005**, *1*, 1067−1070.
(134) Xiang, D.; Zhang, Y.; Pyatkov, F.; Offenhäusser, A.; Mayer, D. Gap Size Dependent Transition from Direct Tunneling to Field Emission in Single Molecule Junctions. *Chem. Commun.* **2011**, *47*, 4760−4762.
(135) Moreno-García, P.; Gulcur, M.; Manrique, D. Z.; Pope, T.; Hong, W.; Kaliginedi, V.; Huang, C.; Batsanov, A. S.; Bryce, M. R.; Lambert, C.; et al. Single-Molecule Conductance of Functionalized Oligoynes: Length Dependence and Junction Evolution. *J. Am. Chem. Soc.* **2013**, *135*, 12228−12240.
(136) Gulcur, M.; Moreno-García, P.; Zhao, X. T.; Baghernejad, M.; Batsanov, A. S.; Hong, W. J.; Bryce, M. R.; Wandlowski, T. The Synthesis of Functionalised Diaryltetraynes and Their Transport Properties in Single-Molecule Junctions. *Chem. - Eur. J.* **2014**, *20*, 4653−4660.
(137) Martin, C. A.; Smit, R. H. M.; van Egmond, R.; van der Zant, H. S. J.; van Ruitenbeek, J. M. A Versatile Low-Temperature Setup for the Electrical Characterization of Single-Molecule Junctions. *Rev. Sci. Instrum.* **2011**, *82*, 82.
(138) Tian, J. H.; Liu, B.; Li, X. L.; Yang, Z. L.; Ren, B.; Wu, S. T.; Tao, N. J.; Tian, Z. Q. Study of Molecular Junctions with a Combined Surface-Enhanced Raman and Mechanically Controllable Break Junction Method. *J. Am. Chem. Soc.* **2006**, *128*, 14748−14749.
(139) Rodrigues, V.; Ugarte, D. Metal Nanowires: Atomic Arrangement and Electrical Transport Properties. *Nanotechnology* **2002**, *13*, 404−408.
(140) Xiang, D.; Lee, T.; Kim, Y.; Mei, T. T.; Wang, Q. L. Origin of Discrete Current Fluctuations in a Single Molecule Junction. *Nanoscale* **2014**, *6*, 13396−13401.
(141) Smit, R. H. M.; Noat, Y.; Untiedt, C.; Lang, N. D.; van Hemert, M. C.; van Ruitenbeek, J. M. Measurement of the Conductance of a Hydrogen Molecule. *Nature* **2002**, *419*, 906−909.
(142) Tian, J. H.; Yang, Y.; Liu, B.; Schöllhorn, B.; Wu, D. Y.; Maisonhaute, E.; Muns, A. S.; Chen, Y.; Amatore, C.; Tao, N. J.; Tian, Z. Q. The Fabrication and Characterization of Adjustable Nanogaps between Gold Electrodes on Chip for Electrical Measurement of Single Molecules. *Nanotechnology* **2010**, *21*, 274012.
(143) Arima, A.; Tsutsui, M.; Morikawa, T.; Yokota, K.; Taniguchi, M. Fabrications of Insulator-Protected Nanometer-Sized Electrode Gaps. *J. Appl. Phys.* **2014**, *115*, 114310.
(144) Lortscher, E.; Ciszek, J. W.; Tour, J.; Riel, H. Reversible and Controllable Switching of a Single-Molecule Junction. *Small* **2006**, *2*, 973−977.
(145) Parks, J. J.; Champagne, A. R.; Hutchison, G. R.; Flores-Torres, S.; Abruna, H. D.; Ralph, D. C. Tuning the Kondo Effect with a Mechanically Controllable Break Junction. *Phys. Rev. Lett.* **2007**, *99*, 026601.
(146) Yi, Z. W.; Trellenkamp, S.; Offenhäusser, A.; Mayer, D. Molecular Junctions Based on Intermolecular Electrostatic Coupling. *Chem. Commun.* **2010**, *46*, 8014−8016.
(147) Yi, Z. W.; Banzet, M.; Offenhäusser, A.; Mayer, D. Fabrication of Nanogaps with Modified Morphology by Potential-Controlled Gold Deposition. *Phys. Status Solidi RRL* **2010**, *4*, 73−75.
(148) Tian, J. H.; Yang, Y.; Zhou, X. S.; Schöllhorn, B.; Maisonhaute, E.; Chen, Z. B.; Yang, F. Z.; Chen, Y.; Amatore, C.; Mao, B. W.; Tian, Z. Q. Electrochemically Assisted Fabrication of Metal Atomic Wires and Molecular Junctions by MCBJ and STM-BJ Methods. *ChemPhysChem* **2010**, *11*, 2745−2755.
(149) Wen, H. M.; Yang, Y.; Zhou, X. S.; Liu, J. Y.; Zhang, D. B.; Chen, Z. B.; Wang, J. Y.; Chen, Z. N.; Tian, Z. Q. Electrical Conductance Study on 1,3-Butadiyne-Linked Dinuclear Ruthenium-(II) Complexes within Single Molecule Break Junctions. *Chem. Sci.* **2013**, *4*, 2471−2477.
(150) Xiang, D.; Jeong, H.; Kim, D.; Lee, T.; Cheng, Y.; Wang, Q.; Mayer, D. Three-Terminal Single-Molecule Junctions Formed by Mechanically Controllable Break Junctions with Side Gating. *Nano Lett.* **2013**, *13*, 2809−2813.
(151) Champagne, A. R.; Pasupathy, A. N.; Ralph, D. C. Mechanically Adjustable and Electrically Gated Single-Molecule Transistors. *Nano Lett.* **2005**, *5*, 305−308.
(152) Perrin, M. L.; Verzijl, C. J. O.; Martin, C. A.; Shaikh, A. J.; Eelkema, R.; van Esch, J. H.; van Ruitenbeek, J. M.; Thijssen, J. M.; van der Zant, H. S. J.; Dulić, D. Large Tunable Image-Charge Effects in Single-Molecule Junctions. *Nat. Nanotechnol.* **2013**, *8*, 282−287.
(153) Martin, C. A.; van Ruitenbeek, J. M.; van der Zant, H. S. J. Sandwich-Type Gated Mechanical Break Junctions. *Nanotechnology* **2010**, *21*, 265201.
(154) Parks, J. J.; Champagne, A. R.; Costi, T. A.; Shum, W. W.; Pasupathy, A. N.; Neuscamman, E.; Flores-Torres, S.; Cornaglia, P. S.; Aligia, A. A.; Balseiro, C. A.; et al. Mechanical Control of Spin States in Spin-1 Molecules and the Underscreened Kondo Effect. *Science* **2010**, *328*, 1370−1373.
(155) Li, Y.; Kaneko, S.; Fujii, S.; Kiguchi, M. Symmetry of Single Hydrogen Molecular Junction with Au, Ag, and Cu Electrodes. *J. Phys. Chem. C* **2015**, *119*, 19143−19148.
(156) Frisenda, R.; Gaudenzi, R.; Franco, C.; Mas-Torrent, M.; Rovira, C.; Veciana, J.; Alcon, I.; Bromley, S. T.; Burzuri, E.; van der Zant, H. S. J. Kondo Effect in a Neutral and Stable All Organic Radical Single Molecule Break Junction. *Nano Lett.* **2015**, *15*, 3109−3114.
(157) Konishi, T.; Kiguchi, M.; Takase, M.; Nagasawa, F.; Nabika, H.; Ikeda, K.; Uosaki, K.; Ueno, K.; Misawa, H.; Murakoshi, K. Single Molecule Dynamics at a Mechanically Controllable Break Junction in Solution at Room Temperature. *J. Am. Chem. Soc.* **2013**, *135*, 1009−1014.
(158) Yelin, T.; Vardimon, R.; Kuritz, N.; Korytar, R.; Bagrets, A.; Evers, F.; Kronik, L.; Tal, O. Atomically Wired Molecular Junctions: Connecting a Single Organic Molecule by Chains of Metal Atoms. *Nano Lett.* **2013**, *13*, 1956−1961.

DOI: 10.1021/acs.chemrev.5b00680
Chem. Rev. 2016, 116, 4318−4440

(159) Liu, C. Y.; Kaneko, S.; Komoto, Y.; Fujii, S.; Kiguchi, M. Highly Conductive Single Naphthalene and Anthracene Molecular Junction with Well-Defined Conductance. *Appl. Phys. Lett.* **2015**, *106*, 103103.
(160) Ponce, J.; Arroyo, C. R.; Tatay, S.; Frisenda, R.; Gavina, P.; Aravena, D.; Ruiz, E.; van der Zant, H. S. J.; Coronado, E. Effect of Metal Complexation on the Conductance of Single-Molecular Wires Measured at Room Temperature. *J. Am. Chem. Soc.* **2014**, *136*, 8314−8322.
(161) Xiang, D.; Pyatkov, F.; Schröper, F.; Offenhäusser, A.; Zhang, Y.; Mayer, D. Molecular Junctions Bridged by Metal Ion Complexes. *Chem. - Eur. J.* **2011**, *17*, 13166−13169.
(162) Sanvito, S. Molecular Spintronics. *Chem. Soc. Rev.* **2011**, *40*, 3336−3355.
(163) Wagner, S.; Kisslinger, F.; Ballmann, S.; Schramm, F.; Chandrasekar, R.; Bodenstein, T.; Fuhr, O.; Secker, D.; Fink, K.; Ruben, M.; Weber, H. B. Switching of a Coupled Spin Pair in a Single-Molecule Junction. *Nat. Nanotechnol.* **2013**, *8*, 575−579.
(164) Kim, Y.; Song, H.; Strigl, F.; Pernau, H. F.; Lee, T.; Scheer, E. Conductance and Vibrational States of Single-Molecule Junctions Controlled by Mechanical Stretching and Material Variation. *Phys. Rev. Lett.* **2011**, *106*, 196804.
(165) Secker, D.; Wagner, S.; Ballmann, S.; Hartle, R.; Thoss, M.; Weber, H. B. Resonant Vibrations, Peak Broadening, and Noise in Single Molecule Contacts: The Nature of the First Conductance Peak. *Phys. Rev. Lett.* **2011**, *106*, 136807.
(166) Tsutsui, M.; Taniguchi, M.; Kawai, T. Single-Molecule Identification Via Electric Current Noise. *Nat. Commun.* **2010**, *1*, 138.
(167) Sydoruk, V. A.; Xiang, D.; Vitusevich, S. A.; Petrychuk, M. V.; Vladyka, A.; Zhang, Y.; Offenhäusser, A.; Kochelap, V. A.; Belyaev, A. E.; Mayer, D. Noise and Transport Characterization of Single Molecular Break Junctions with Individual Molecule. *J. Appl. Phys.* **2012**, *112*, 014908.
(168) Meng, C.; Huang, P.; Zhou, J. W.; Duan, C. K.; Du, J. F. Thermally Controllable Break Junctions with High Bandwidths and High Integrabilities. *Chin. Phys. Lett.* **2015**, *32*, 076201.
(169) Gong, C.; Zhao, Y. J.; Dong, L. Q.; Hui, M.; Yu, X. M.; Liu, X. H. The Tolerable Target Temperature for Bimaterial Microcantilever Array Infrared Imaging. *Opt. Laser Technol.* **2013**, *45*, 545−550.
(170) Park, H.; Lim, A. K. L.; Alivisatos, A. P.; Park, J.; McEuen, P. L. Fabrication of Metallic Electrodes with Nanometer Separation by Electromigration. *Appl. Phys. Lett.* **1999**, *75*, 301−303.
(171) Song, H.; Kim, Y.; Jang, Y. H.; Jeong, H.; Reed, M. A.; Lee, T. Observation of Molecular Orbital Gating. *Nature* **2009**, *462*, 1039−1043.
(172) Van der Zant, H. S. J.; Osorio, E. A.; Poot, M.; O'Neill, K. Electromigrated Molecular Junctions. *Phys. Status Solidi B* **2006**, *243*, 3408−3412.
(173) Kim, T.-W.; Wang, G.; Lee, H.; Lee, T. Statistical Analysis of Electronic Properties of Alkanethiols in Metal-Molecule-Metal Junctions. *Nanotechnology* **2007**, *18*, 315204.
(174) Mangin, A.; Anthore, A.; Della Rocca, M. L.; Boulat, E.; Lafarge, P. Transport through Metallic Nanogaps in an in-Plane Three-Terminal Geometry. *J. Appl. Phys.* **2009**, *105*, 014313.
(175) van der Zant, H. S. J.; Kervennic, Y. V.; Poot, M.; O'Neill, K.; de Groot, Z.; Thijssen, J. M.; Heersche, H. B.; Stuhr-Hansen, N.; Bjornholm, T.; Vanmaekelbergh, D.; et al. Molecular Three-Terminal Devices: Fabrication and Measurements. *Faraday Discuss.* **2006**, *131*, 347−356.
(176) Ueno, S.; Tomoda, Y.; Kume, W.; Hanada, M.; Takiya, K.; Shirakashi, J. Field-Emission-Induced Electromigration Method for the Integration of Single-Electron Transistors. *Appl. Surf. Sci.* **2012**, *258*, 2153−2156.
(177) Houck, A. A.; Labaziewicz, J.; Chan, E. K.; Folk, J. A.; Chuang, I. L. Kondo Effect in Electromigrated Gold Break Junctions. *Nano Lett.* **2005**, *5*, 1685−1688.
(178) Kushmerick, J. G.; Lazorcik, J.; Patterson, C. H.; Shashidhar, R.; Seferos, D. S.; Bazan, G. C. Vibronic Contributions to Charge Transport across Molecular Junctions. *Nano Lett.* **2004**, *4*, 639−642.
(179) Henderson, J. J.; Ramsey, C. M.; del Barco, E.; Mishra, A.; Christou, G. Fabrication of Nanogapped Single-Electron Transistors for Transport Studies of Individual Single-Molecule Magnets. *J. Appl. Phys.* **2007**, *101*, 09E102.
(180) Trouwborst, M. L.; van der Molen, S. J.; van Wees, B. J. The Role of Joule Heating in the Formation of Nanogaps by Electromigration. *J. Appl. Phys.* **2006**, *99*, 114316.
(181) Lee, C. H.; Han, J. H.; Schneider, S. C.; Josse, F. Suspended and Localized Single Nanostructure Growth across a Nanogap by an Electric Field. *Nanotechnology* **2011**, *22*, 405301.
(182) Valladares, L.; Felix, L. L.; Dominguez, A. B.; Mitrelias, T.; Sfigakis, F.; Khondaker, S. I.; Barnes, C. H. W.; Majima, Y. Controlled Electroplating and Electromigration in Nickel Electrodes for Nanogap Formation. *Nanotechnology* **2010**, *21*, 445304.
(183) Baik, J. M.; Lee, S. J.; Moskovits, M. Polarized Surface-Enhanced Raman Spectroscopy from Molecules Adsorbed in Nano-Gaps Produced by Electromigration in Silver Nanowires. *Nano Lett.* **2009**, *9*, 672−676.
(184) Prins, F.; Hayashi, T.; van Steenwijk, B. J. A. D.; Gao, B.; Osorio, E. A.; Muraki, K.; van der Zant, H. S. J. Room-Temperature Stability of Pt Nanogaps Formed by Self-Breaking. *Appl. Phys. Lett.* **2009**, *94*, 123108.
(185) Arzubiaga, L.; Golmar, F.; Llopis, R.; Casanova, F.; Hueso, L. E. Tailoring Palladium Nanocontacts by Electromigration. *Appl. Phys. Lett.* **2013**, *102*, 193103.
(186) Asghar, W.; Ramachandran, P. P.; Adewumi, A.; Noor, M. R.; Iqbal, S. M. Rapid Nanomanufacturing of Metallic Break Junctions Using Focused Ion Beam Scratching and Electromigration. *J. Manuf. Sci. E-t. Asme* **2010**, *132*, 030911.
(187) Naitoh, Y.; Ohata, T.; Matsushita, R.; Okawa, E.; Horikawa, M.; Oyama, M.; Mukaida, M.; Wang, D. F.; Kiguchi, M.; Tsukagoshi, K.; et al. Self-Aligned Formation of Sub 1 nm Gaps Utilizing Electromigration During Metal Deposition. *ACS Appl. Mater. Interfaces* **2013**, *5*, 12869−12875.
(188) Lu, Y.; Goldsmith, B.; Strachan, D. R.; Lim, J. H.; Luo, Z. T.; Johnson, A. T. C. High-on/Off-Ratio Graphene Nanoconstriction Field-Effect Transistor. *Small* **2010**, *6*, 2748−2754.
(189) Zhang, H.; Bao, W. Z.; Zhao, Z.; Huang, J. W.; Standley, B.; Liu, G.; Wang, F. L.; Kratz, P.; Jing, L.; Bockrath, M.; et al. Visualizing Electrical Breakdown and on/Off States in Electrically Switchable Suspended Graphene Break Junctions. *Nano Lett.* **2012**, *12*, 1772−1775.
(190) Qi, P.; Javey, A.; Rolandi, M.; Wang, Q.; Yenilmez, E.; Dai, H. Miniature Organic Transistors with Carbon Nanotubes as Quasi-One-Dimensional Electrodes. *J. Am. Chem. Soc.* **2004**, *126*, 11774−11775.
(191) O'Neill, K.; Osorio, E. A.; van der Zant, H. S. J. Self-Breaking in Planar Few-Atom Au Constrictions for Nanometer-Spaced Electrodes. *Appl. Phys. Lett.* **2007**, *90*, 133109.
(192) Tsutsui, M.; Taniguchi, M.; Kawai, T. Fabrication of 0.5 nm Electrode Gaps Using Self-Breaking Technique. *Appl. Phys. Lett.* **2008**, *93*, 163115.
(193) Strachan, D. R.; Smith, D. E.; Johnston, D. E.; Park, T. H.; Therien, M. J.; Bonnell, D. A.; Johnson, A. T. Controlled Fabrication of Nanogaps in Ambient Environment for Molecular Electronics. *Appl. Phys. Lett.* **2005**, *86*, 043109.
(194) Xiang, C. X.; Kim, J. Y.; Penner, R. M. Reconnectable Sub-5 nm Nanogaps in Ultralong Gold Nanowires. *Nano Lett.* **2009**, *9*, 2133−2138.
(195) Strachan, D. R.; Johnston, D. E.; Guiton, B. S.; Datta, S. S.; Davies, P. K.; Bonnell, D. A.; Johnson, A. T. C. Real-Time Tem Imaging of the Formation of Crystalline Nanoscale Gaps. *Phys. Rev. Lett.* **2008**, *100*, 056805.
(196) Dong, J.; Parviz, B. A. Using Noise for Controlled Disassembly of Nanoscale Gold Wires. *Nanotechnology* **2006**, *17*, 5124−5130.
(197) Wu, Z. M.; Steinacher, M.; Huber, R.; Calame, M.; van der Molen, S. J.; Schonenberger, C. Feedback Controlled Electromigration in Four-Terminal Nanojunctions. *Appl. Phys. Lett.* **2007**, *91*, 053118.
(198) Johnston, D. E.; Strachan, D. R.; Johnson, A. T. C. Parallel Fabrication of Nanogap Electrodes. *Nano Lett.* **2007**, *7*, 2774−2777.

DOI: 10.1021/acs.chemrev.5b00680
Chem. Rev. 2016, 116, 4318−4440

(199) Heersche, H. B.; de Groot, Z.; Folk, J. A.; Kouwenhoven, L. P.; van der Zant, H. S. J.; Houck, A. A.; Labaziewicz, J.; Chuang, I. L. Kondo Effect in the Presence of Magnetic Impurities. *Phys. Rev. Lett.* **2006**, *96*, 017205.
(200) Sordan, R.; Balasubramanian, K.; Burghard, M.; Kern, K. Coulomb Blockade Phenomena in Electromigration Break Junctions. *Appl. Phys. Lett.* **2005**, *87*, 013106.
(201) Taychatanapat, T.; Bolotin, K. I.; Kuemmeth, F.; Ralph, D. C. Imaging Electromigration During the Formation of Break Junctions. *Nano Lett.* **2007**, *7*, 652−656.
(202) Strachan, D. R.; Smith, D. E.; Fischbein, M. D.; Johnston, D. E.; Guiton, B. S.; Drndic, M.; Bonnell, D. A.; Johnson, A. T. Clean Electromigrated Nanogaps Imaged by Transmission Electron Microscopy. *Nano Lett.* **2006**, *6*, 441−444.
(203) Rudneva, M.; Gao, B.; Prins, F.; Xu, Q.; van der Zant, H. S. J.; Zandbergen, H. W. In Situ Transmission Electron Microscopy Imaging of Electromigration in Platinum Nanowires. *Microsc. Microanal.* **2013**, *19*, 43−48.
(204) Fischbein, M. D.; Drndic, M. Sub-10 nm Device Fabrication in a Transmission Electron Microscope. *Nano Lett.* **2007**, *7*, 1329−1337.
(205) Gao, B.; Osorio, E. A.; Gaven, K. B.; van der Zant, H. S. J. Three-Terminal Electric Transport Measurements on Gold Nanoparticles Combined with Ex Situ TEM Inspection. *Nanotechnology* **2009**, *20*, 415207.
(206) Song, H.; Kim, Y.; Ku, J.; Jang, Y. H.; Jeong, H.; Lee, T. Vibrational Spectra of Metal-Molecule-Metal Junctions in Electromigrated Nanogap Electrodes by Inelastic Electron Tunneling. *Appl. Phys. Lett.* **2009**, *94*, 103110.
(207) Ward, D. R.; Halas, N. J.; Ciszek, J. W.; Tour, J. M.; Wu, Y.; Nordlander, P.; Natelson, D. Simultaneous Measurements of Electronic Conduction and Raman Response in Molecular Junctions. *Nano Lett.* **2008**, *8*, 919−924.
(208) Herzog, J. B.; Knight, M. W.; Li, Y. J.; Evans, K. M.; Halas, N. J.; Natelson, D. Dark Plasmons in Hot Spot Generation and Polarization in Interelectrode Nanoscale Junctions. *Nano Lett.* **2013**, *13*, 1359−1364.
(209) Ward, D. R.; Corley, D. A.; Tour, J. M.; Natelson, D. Vibrational and Electronic Heating in Nanoscale Junctions. *Nat. Nanotechnol.* **2011**, *6*, 33−38.
(210) Liang, W. J.; Shores, M. P.; Bockrath, M.; Long, J. R.; Park, H. Kondo Resonance in a Single-Molecule Transistor. *Nature* **2002**, *417*, 725−729.
(211) Yu, L. H.; Natelson, D. The Kondo Effect in C_{60} Single-Molecule Transistors. *Nano Lett.* **2004**, *4*, 79−83.
(212) Morpurgo, A. F.; Marcus, C. M.; Robinson, D. B. Controlled Fabrication of Metallic Electrodes with Atomic Separation. *Appl. Phys. Lett.* **1999**, *74*, 2084−2086.
(213) Li, C. Z.; He, H. X.; Tao, N. J. Quantized Tunneling Current in the Metallic Nanogaps Formed by Electrodeposition and Etching. *Appl. Phys. Lett.* **2000**, *77*, 3995−3997.
(214) Wu, Y. X.; Hong, W. J.; Akiyama, T.; Gautsch, S.; Kolivoska, V.; Wandlowski, T.; de Rooij, N. F. Batch Fabrication of Gold-Gold Nanogaps by E-Beam Lithography and Electrochemical Deposition. *Nanotechnology* **2013**, *24*, 235302.
(215) Li, X. L.; He, H. X.; Xu, B. Q.; Xiao, X. Y.; Nagahara, L. A.; Amlani, I.; Tsui, R.; Tao, N. J. Measurement of Electron Transport Properties of Molecular Junctions Fabricated by Electrochemical and Mechanical Methods. *Surf. Sci.* **2004**, *573*, 1−10.
(216) Liu, B.; Xiang, J.; Tian, J. H.; Zhong, C.; Mao, B. W.; Yang, F. Z.; Chen, Z. B.; Wu, S. T.; Tian, Z. Q. Controllable Nanogap Fabrication on Microchip by Chronopotentiometry. *Electrochim. Acta* **2005**, *50*, 3041−3047.
(217) Meszaros, G.; Kronholz, S.; Karthauser, S.; Mayer, D.; Wandlowski, T. Electrochemical Fabrication and Characterization of Nanocontacts and nm-Sized Gaps. *Appl. Phys. A: Mater. Sci. Process.* **2007**, *87*, 569−575.
(218) Kervennic, Y. V.; Van der Zant, H. S. J.; Morpurgo, A. F.; Gurevich, L.; Kouwenhoven, L. P. Nanometer-Spaced Electrodes with Calibrated Separation. *Appl. Phys. Lett.* **2002**, *80*, 321−323.
(219) He, H. X.; Boussaad, S.; Xu, B. Q.; Li, C. Z.; Tao, N. J. Electrochemical Fabrication of Atomically Thin Metallic Wires and Electrodes Separated with Molecular-Scale Gaps. *J. Electroanal. Chem.* **2002**, *522*, 167−172.
(220) Qing, Q.; Chen, F.; Li, P. G.; Tang, W. H.; Wu, Z. Y.; Liu, Z. F. Finely Tuning Metallic Nanogap Size with Electrodeposition by Utilizing High-Frequency Impedance in Feedback. *Angew. Chem., Int. Ed.* **2005**, *44*, 7771−7775.
(221) Chen, F.; Qing, Q.; Ren, L.; Wu, Z. Y.; Liu, Z. F. Electrochemical Approach for Fabricating Nanogap Electrodes with Well Controllable Separation. *Appl. Phys. Lett.* **2005**, *86*, 123105.
(222) Serdio, V. M.; Azuma, Y.; Takeshita, S.; Muraki, T.; Teranishi, T.; Majima, Y. Robust Nanogap Electrodes by Self-Terminating Electroless Gold Plating. *Nanoscale* **2012**, *4*, 7161−7167.
(223) Yasutake, Y.; Kono, K.; Kanehara, M.; Teranishi, T.; Buitelaar, M. R.; Smith, C. G.; Majima, Y. Simultaneous Fabrication of Nanogap Gold Electrodes by Electroless Gold Plating Using a Common Medical Liquid. *Appl. Phys. Lett.* **2007**, *91*, 203107.
(224) Lee, Y.; Ahn, S. K.; Roh, Y. Comparison of Nanometer-Scale Gold Structures Electrodeposited on Au and Pt Seed Electrode. *Surf. Coat. Technol.* **2005**, *193*, 137−141.
(225) Kiguchi, M.; Murakoshi, K. Fabrication of Stable Pd Nanowire Assisted by Hydrogen in Solution. *Appl. Phys. Lett.* **2006**, *88*, 253112.
(226) Zhou, X. S.; Liang, J. H.; Chen, Z. B.; Mao, B. W. An Electrochemical Jump-to-Contact Stm-Break Junction Approach to Construct Single Molecular Junctions with Different Metallic Electrodes. *Electrochem. Commun.* **2011**, *13*, 407−410.
(227) Bonifas, A. P.; McCreery, R. L. Assembling Molecular Electronic Junctions One Molecule at a Time. *Nano Lett.* **2011**, *11*, 4725−4729.
(228) Yablonovitch, E.; Hwang, D. M.; Gmitter, T. J.; Florez, L. T.; Harbison, J. P. Van der waals Bonding of Gaas Epitaxial Liftoff Films onto Arbitrary Substrates. *Appl. Phys. Lett.* **1990**, *56*, 2419−2421.
(229) Vilan, A.; Shanzer, A.; Cahen, D. Molecular Control over Au/GaAs Diodes. *Nature* **2000**, *404*, 166−168.
(230) Vilan, A.; Cahen, D. Soft Contact Deposition onto Molecularly Modified Gaas. Thin Metal Film Flotation: Principles and Electrical Effects. *Adv. Funct. Mater.* **2002**, *12*, 795−807.
(231) Shimizu, K. T.; Fabbri, J. D.; Jelincic, J. J.; Melosh, N. A. Soft Deposition of Large-Area Metal Contacts for Molecular Electronics. *Adv. Mater.* **2006**, *18*, 1499−1504.
(232) Haick, H.; Cahen, D. Contacting Organic Molecules by Soft Methods: Towards Molecule-Based Electronic Devices. *Acc. Chem. Res.* **2008**, *41*, 359−366.
(233) Selzer, Y.; Cahen, D. Fine Tuning of $Au/SiO_2/Si$ Diodes by Varying Interfacial Dipoles Using Molecular Monolayers. *Adv. Mater.* **2001**, *13*, 508−511.
(234) Salomon, A.; Berkovich, D.; Cahen, D. Molecular Modification of an Ionic Semiconductor-Metal Interface: ZnO/Molecule/Au Diodes. *Appl. Phys. Lett.* **2003**, *82*, 1051−1053.
(235) Haick, H.; Ambrico, M.; Ligonzo, T.; Tung, R. T.; Cahen, D. Controlling Semiconductor/Metal Junction Barriers by Incomplete, Nonideal Molecular Monolayers. *J. Am. Chem. Soc.* **2006**, *128*, 6854−6869.
(236) Ikram, I. M.; Rabinal, M. K.; Kalasad, M. N.; Mulimani, B. G. Formation of Electronic Junctions on Molecularly Modified Surfaces by Lift-and-Float Electrical Contacts. *Langmuir* **2009**, *25*, 3305−3309.
(237) Race, H. H.; Reynolds, S. I. Electrical Properties of Multimolecular Films. *J. Am. Chem. Soc.* **1939**, *61*, 1425−1432.
(238) Li, J.-C.; Wu, J.-Z.; Zhou, C.; Gong, X. Latest Studies on Metal-Molecule-Metal Junctions. *Acta Phys.-Chim. Sin.* **2013**, *29*, 1123−1144.
(239) Chabinyc, M. L.; Chen, X. X.; Holmlin, R. E.; Jacobs, H.; Skulason, H.; Frisbie, C. D.; Mujica, V.; Ratner, M. A.; Rampi, M. A.; Whitesides, G. M. Molecular Rectification in a Metal-Insulator-Metal Junction Based on Self-Assembled Monolayers. *J. Am. Chem. Soc.* **2002**, *124*, 11730−11736.
(240) Slowinski, K.; Fong, H. K. Y.; Majda, M. Mercury-Mercury Tunneling Junctions. 1. Electron Tunneling across Symmetric and

DOI: 10.1021/acs.chemrev.5b00680
Chem. Rev. 2016, 116, 4318−4440

Asymmetric Alkanethiolate Bilayers. *J. Am. Chem. Soc.* **1999**, *121*, 7257−7261.
(241) Rampi, M. A.; Whitesides, G. M. A Versatile Experimental Approach for Understanding Electron Transport through Organic Materials. *Chem. Phys.* **2002**, *281*, 373−391.
(242) Yaffe, O.; Scheres, L.; Puniredd, S. R.; Stein, N.; Biller, A.; Lavan, R. H.; Shpaisman, H.; Zuilhof, H.; Haick, H.; Cahen, D.; Vilan, A. Molecular Electronics at Metal/Semiconductor Junctions. Si Inversion by Sub-Nanometer Molecular Films. *Nano Lett.* **2009**, *9*, 2390−2394.
(243) von Wrochem, F.; Gao, D.; Scholz, F.; Nothofer, H.-G.; Nelles, G.; Wessels, J. M. Efficient Electronic Coupling and Improved Stability with Dithiocarbamate-Based Molecular Junctions. *Nat. Nanotechnol.* **2010**, *5*, 618−624.
(244) Holmlin, R. E.; Ismagilov, R. F.; Haag, R.; Mujica, V.; Ratner, M. A.; Rampi, M. A.; Whitesides, G. M. Correlating Electron Transport and Molecular Structure in Organic Thin Films. *Angew. Chem.* **2001**, *113*, 2378−2382.
(245) Thuo, M. M.; Reus, W. F.; Nijhuis, C. A.; Barber, J. R.; Kim, C.; Schulz, M. D.; Whitesides, G. M. Odd-Even Effects in Charge Transport across Self-Assembled Monolayers. *J. Am. Chem. Soc.* **2011**, *133*, 2962−2975.
(246) Reus, W. F.; Thuo, M. M.; Shapiro, N. D.; Nijhuis, C. A.; Whitesides, G. M. The Sam, Not the Electrodes, Dominates Charge Transport in Metal-Monolayer//Ga_2O_3/Gallium-Indium Eutectic Junctions. *ACS Nano* **2012**, *6*, 4806−4822.
(247) Cademartiri, L.; Thuo, M. M.; Nijhuis, C. A.; Reus, W. F.; Tricard, S.; Barber, J. R.; Sodhi, R. N. S.; Brodersen, P.; Kim, C.; Chiechi, R. C.; Whitesides, G. M. Electrical Resistance of Ag^{TS}-$S(CH_2)_{n-1}CH_3$//Ga_2O_3/EGaIn Tunneling Junctions. *J. Phys. Chem. C* **2012**, *116*, 10848−10860.
(248) Nijhuis, C. A.; Reus, W. F.; Barber, J. R.; Dickey, M. D.; Whitesides, G. M. Charge Transport and Rectification in Arrays of SAM-Based Tunneling Junctions. *Nano Lett.* **2010**, *10*, 3611−3619.
(249) Chiechi, R. C.; Weiss, E. A.; Dickey, M. D.; Whitesides, G. M. Eutectic Gallium-Indium (EGaIn): A Moldable Liquid Metal for Electrical Characterization of Self-Assembled Monolayers. *Angew. Chem., Int. Ed.* **2008**, *47*, 142−144.
(250) Wan, A.; Jiang, L.; Sangeeth, C. S. S.; Nijhuis, C. A. Reversible Soft Top-Contacts to Yield Molecular Junctions with Precise and Reproducible Electrical Characteristics. *Adv. Funct. Mater.* **2014**, *24*, 4442−4456.
(251) Jiang, L.; Yuan, L.; Cao, L.; Nijhuis, C. A. Controlling Leakage Currents: The Role of the Binding Group and Purity of the Precursors for Self-Assembled Monolayers in the Performance of Molecular Diodes. *J. Am. Chem. Soc.* **2014**, *136*, 1982−1991.
(252) Yuan, L.; Jiang, L.; Zhang, B.; Nijhuis, C. A. Dependency of the Tunneling Decay Coefficient in Molecular Tunneling Junctions on the Topography of the Bottom Electrodes. *Angew. Chem., Int. Ed.* **2014**, *53*, 3377−3381.
(253) Yoon, H. J.; Shapiro, N. D.; Park, K. M.; Thuo, M. M.; Soh, S.; Whitesides, G. M. The Rate of Charge Tunneling through Self-Assembled Monolayers Is Insensitive to Many Functional Group Substitutions. *Angew. Chem., Int. Ed.* **2012**, *51*, 4658−4661.
(254) Thuo, M. M.; Reus, W. F.; Simeone, F. C.; Kim, C.; Schulz, M. D.; Yoon, H. J.; Whitesides, G. M. Replacing -Ch2ch2- with -Conh- Does Not Significantly Change Rates of Charge Transport through Ag-Ts-Sam//Ga2o3/Egain Junctions. *J. Am. Chem. Soc.* **2012**, *134*, 10876−10884.
(255) Nerngchamnong, N.; Yuan, L.; Qi, D. C.; Li, J.; Thompson, D.; Nijhuis, C. A. The Role of Van Der Waals Forces in the Performance of Molecular Diodes. *Nat. Nanotechnol.* **2013**, *8*, 113−118.
(256) Fracasso, D.; Muglali, M. I.; Rohwerder, M.; Terfort, A.; Chiechi, R. C. Influence of an Atom in Egain/Ga_2O_3 Tunneling Junctions Comprising Self-Assembled Monolayers. *J. Phys. Chem. C* **2013**, *117*, 11367−11376.
(257) Fan, X. L.; Wang, C.; Yang, D. L.; Wan, L. J.; Bai, C. L. Molecule Rectifier Fabricated by Capillary Tunnel Junction. *Chem. Phys. Lett.* **2002**, *361*, 465−468.
(258) Liu, Y. H.; Fan, X. L.; Yang, D. L.; Wang, C.; Wan, L. J.; Bai, C. L. Tunneling Characteristics of Octadecyl Derivatives on Tin and Indium Electrodes. *Langmuir* **2004**, *20*, 855−861.
(259) Majumdar, N.; Gergel, N.; Routenberg, D.; Bean, J. C.; Harriott, L. R.; Li, B.; Pu, L.; Yao, Y.; Tour, J. M. Nanowell Device for the Electrical Characterization of Metal-Molecule-Metal Junctions. *J. Vac. Sci. Technol., B: Microelectron. Process. Phenom.* **2005**, *23*, 1417−1421.
(260) Chen, J.; Reed, M. A.; Rawlett, A. M.; Tour, J. M. Large on-Off Ratios and Negative Differential Resistance in a Molecular Electronic Device. *Science* **1999**, *286*, 1550−1552.
(261) Song, H.; Lee, T.; Choi, N.-J.; Lee, H. A Statistical Method for Determining Intrinsic Electronic Transport Properties of Self-Assembled Alkanethiol Monolayer Devices. *Appl. Phys. Lett.* **2007**, *91*, 253116.
(262) Krapf, D.; Wu, M. Y.; Smeets, R. M. M.; Zandbergen, H. W.; Dekker, C.; Lemay, S. G. Fabrication and Characterization of Nanopore-Based Electrodes with Radii Down to 2 nm. *Nano Lett.* **2006**, *6*, 105−109.
(263) Wang, G.; Kim, Y.; Choe, M.; Kim, T.-W.; Lee, T. A New Approach for Molecular Electronic Junctions with a Multilayer Graphene Electrode. *Adv. Mater.* **2011**, *23*, 755−760.
(264) He, J. L.; Chen, B.; Flatt, A. K.; Stephenson, J. J.; Doyle, C. D.; Tour, J. M. Metal-Free Silicon-Molecule-Nanotube Testbed and Memory Device. *Nat. Mater.* **2006**, *5*, 63−68.
(265) Mbindyo, J. K. N.; Mallouk, T. E.; Mattzela, J. B.; Kratochvilova, I.; Razavi, B.; Jackson, T. N.; Mayer, T. S. Template Synthesis of Metal Nanowires Containing Monolayer Molecular Junctions. *J. Am. Chem. Soc.* **2002**, *124*, 4020−4026.
(266) Qin, L. D.; Park, S.; Huang, L.; Mirkin, C. A. On-Wire Lithography. *Science* **2005**, *309*, 113−115.
(267) Banholzer, M. J.; Qin, L.; Millstone, J. E.; Osberg, K. D.; Mirkin, C. A. On-Wire Lithography: Synthesis, Encoding and Biological Applications. *Nat. Protoc.* **2009**, *4*, 838−848.
(268) Braunschweig, A. B.; Schmucker, A. L.; Wei, W. D.; Mirkin, C. A. Nanostructures Enabled by on-Wire Lithography (OWL). *Chem. Phys. Lett.* **2010**, *486*, 89−98.
(269) Chen, X.; Jeon, Y.-M.; Jang, J.-W.; Qin, L.; Huo, F.; Wei, W.; Mirkin, C. A. On-Wire Lithography-Generated Molecule-Based Transport Junctions: A New Testbed for Molecular Electronics. *J. Am. Chem. Soc.* **2008**, *130*, 8166−8168.
(270) Piner, R. D.; Zhu, J.; Xu, F.; Hong, S. H.; Mirkin, C. A. "Dip-Pen" Nanolithography. *Science* **1999**, *283*, 661−663.
(271) Chen, X.; Yeganeh, S.; Qin, L.; Li, S.; Xue, C.; Braunschweig, A. B.; Schatz, G. C.; Ratner, M. A.; Mirkin, C. A. Chemical Fabrication of Heterometallic Nanogaps for Molecular Transport Junctions. *Nano Lett.* **2009**, *9*, 3974−3979.
(272) Osberg, K. D.; Schmucker, A. L.; Senesi, A. J.; Mirkin, C. A. One-Dimensional Nanorod Arrays: Independent Control of Composition, Length, and Interparticle Spacing with Nanometer Precision. *Nano Lett.* **2011**, *11*, 820−824.
(273) Chen, X.; Braunschweig, A. B.; Wiester, M. J.; Yeganeh, S.; Ratner, M. A.; Mirkin, C. A. Spectroscopic Tracking of Molecular Transport Junctions Generated by Using Click Chemistry. *Angew. Chem., Int. Ed.* **2009**, *48*, 5178−5181.
(274) Kolb, H. C.; Finn, M. G.; Sharpless, K. B. Click Chemistry: Diverse Chemical Function from a Few Good Reactions. *Angew. Chem., Int. Ed.* **2001**, *40*, 2004−2021.
(275) Tang, J. Y.; Wang, Y. L.; Klare, J. E.; Tulevski, G. S.; Wind, S. J.; Nuckolls, C. Encoding Molecular-Wire Formation within Nanoscale Sockets. *Angew. Chem., Int. Ed.* **2007**, *46*, 3892−3895.
(276) Mayor, M. Watching the Gap Close. *Angew. Chem., Int. Ed.* **2009**, *48*, 5583−5585.
(277) Lee, B. Y.; Heo, K.; Schmucker, A. L.; Jin, H. J.; Lim, J. K.; Kim, T.; Lee, H.; Jeon, K.-S.; Suh, Y. D.; Mirkin, C. A.; Hong, S. Nanotube-Bridged Wires with Sub-10 nm Gaps. *Nano Lett.* **2012**, *12*, 1879−1884.
(278) Nam, G.-H.; Lee, J.-H.; Zahari, N. E. M.; Khalid, N. C.; Kang, W.-S.; Kim, J.-H. Single-Bundle Carbon-Nanotube-Bridged Nanorod

DOI: 10.1021/acs.chemrev.5b00680
Chem. Rev. 2016, 116, 4318−4440

Devices with Control of Gap Length. *J. Phys. Chem. C* **2014**, *118*, 10463−10471.
(279) Zhou, X.; Shade, C. M.; Schmucker, A. L.; Brown, K. A.; He, S.; Boey, F.; Ma, J.; Zhang, H.; Mirkin, C. A. Owl-Based Nanomasks for Preparing Graphene Ribbons with Sub-10 nm Gaps. *Nano Lett.* **2012**, *12*, 4734−4737.
(280) Liusman, C.; Li, S.; Chen, X.; Wei, W.; Zhang, H.; Schatz, G. C.; Boey, F.; Mirkin, C. A. Free-Standing Bimetallic Nanorings and Nanoring Arrays Made by on-Wire Lithography. *ACS Nano* **2010**, *4*, 7676−7682.
(281) Meng, F.; Hervault, Y.-M.; Shao, Q.; Hu, B.; Norel, L.; Rigaut, S.; Chen, X. Orthogonally Modulated Molecular Transport Junctions for Resettable Electronic Logic Gates. *Nat. Commun.* **2014**, *5*, 3023.
(282) Pedano, M. L.; Li, S.; Schatz, G. C.; Mirkin, C. A. Periodic Electric Field Enhancement Along Gold Rods with Nanogaps. *Angew. Chem., Int. Ed.* **2010**, *49*, 78−82.
(283) Osberg, K. D.; Rycenga, M.; Harris, N.; Schmucker, A. L.; Langille, M. R.; Schatz, G. C.; Mirkin, C. A. Dispersible Gold Nanorod Dimers with Sub-5 nm Gaps as Local Amplifiers for Surface-Enhanced Raman Scattering. *Nano Lett.* **2012**, *12*, 3828−3832.
(284) Schmucker, A. L.; Barin, G.; Brown, K. A.; Rycenga, M.; Coskun, A.; Buyukcakir, O.; Osberg, K. D.; Stoddart, J. F.; Mirkin, C. A. Electronic and Optical Vibrational Spectroscopy of Molecular Transport Junctions Created by on-Wire Lithography. *Small* **2013**, *9*, 1900−1903.
(285) Loo, Y. L.; Lang, D. V.; Rogers, J. A.; Hsu, J. W. P. Electrical Contacts to Molecular Layers by Nanotransfer Printing. *Nano Lett.* **2003**, *3*, 913−917.
(286) Coll, M.; Miller, L. H.; Richter, L. J.; Hines, D. R.; Jurchescu, O. D.; Gergel-Hackett, N.; Richter, C. A.; Hacker, C. A. Formation of Silicon-Based Molecular Electronic Structures Using Flip-Chip Lamination. *J. Am. Chem. Soc.* **2009**, *131*, 12451−12457.
(287) Williams, S. S.; Retterer, S.; Lopez, R.; Ruiz, R.; Samulski, E. T.; DeSimone, J. M. High-Resolution PFPE-Based Molding Techniques for Nanofabrication of High-Pattern Density, Sub-20 nm Features: A Fundamental Materials Approach. *Nano Lett.* **2010**, *10*, 1421−1428.
(288) Liang, X.; Jung, Y.-S.; Wu, S.; Ismach, A.; Olynick, D. L.; Cabrini, S.; Bokor, J. Formation of Bandgap and Subbands in Graphene Nanomeshes with Sub-10 nm Ribbon Width Fabricated Via Nanoimprint Lithography. *Nano Lett.* **2010**, *10*, 2454−2460.
(289) Jeong, J. W.; Park, W. I.; Do, L.-M.; Park, J.-H.; Kim, T.-H.; Chae, G.; Jung, Y. S. Nanotransfer Printing with Sub-10 nm Resolution Realized Using Directed Self-Assembly. *Adv. Mater.* **2012**, *24*, 3526−3531.
(290) Sanetra, N.; Karipidou, Z.; Wirtz, R.; Knorr, N.; Rosselli, S.; Nelles, G.; Offenhaeusser, A.; Mayer, D. Printing of Highly Integrated Crossbar Junctions. *Adv. Funct. Mater.* **2012**, *22*, 1129−1135.
(291) Lan, H. B.; Liu, H. Z. Uv-Nanoimprint Lithography: Structure, Materials and Fabrication of Flexible Molds. *J. Nanosci. Nanotechnol.* **2013**, *13*, 3145−3172.
(292) Kooy, N.; Mohamed, K.; Pin, L. T.; Guan, O. S. A Review of Roll-to-Roll Nanoimprint Lithography. *Nanoscale Res. Lett.* **2014**, *9*, 1−13.
(293) He, Z. B.; Zhang, W. J.; Tang, Y. B.; Wang, H. B.; Cao, Y. L.; Song, H. S.; Bello, I.; Lee, C. S.; Lee, S. T. Crossbar Heterojunction Field Effect Transistors of Cdse:In Nanowires and Si Nanoribbons. *Appl. Phys. Lett.* **2009**, *95*, 253107.
(294) Linn, E.; Rosezin, R.; Tappertzhofen, S.; Bottger, U.; Waser, R. Beyond Von Neumann-Logic Operations in Passive Crossbar Arrays Alongside Memory Operations. *Nanotechnology* **2012**, *23*, 305205.
(295) Kim, K. H.; Gaba, S.; Wheeler, D.; Cruz-Albrecht, J. M.; Hussain, T.; Srinivasa, N.; Lu, W. A Functional Hybrid Memristor Crossbar-Array/CMOS System for Data Storage and Neuromorphic Applications. *Nano Lett.* **2012**, *12*, 389−395.
(296) Martin, P.; Della Rocca, M. L.; Anthore, A.; Lafarge, P.; Lacroix, J. C. Organic Electrodes Based on Grafted Oligothiophene Units in Ultrathin, Large-Area Molecular Junctions. *J. Am. Chem. Soc.* **2012**, *134*, 154−157.
(297) Anariba, F.; Steach, J. K.; McCreery, R. L. Strong Effects of Molecular Structure on Electron Transport in Carbon/Molecule/Copper Electronic Junctions. *J. Phys. Chem. B* **2005**, *109*, 11163−11172.
(298) Xia, Q. F.; Yang, J. J. S.; Wu, W.; Li, X. M.; Williams, R. S. Self-Aligned Memristor Cross-Point Arrays Fabricated with One Nanoimprint Lithography Step. *Nano Lett.* **2010**, *10*, 2909−2914.
(299) Bang, G. S.; Chang, H.; Koo, J. R.; Lee, T.; Advincula, R. C.; Lee, H. High-Fidelity Formation of a Molecular-Junction Device Using a Thickness-Controlled Bilayer Architecture. *Small* **2008**, *4*, 1399−1405.
(300) Li, J. C. Optoelectronic Switching of Addressable Self-Assembled Monolayer Molecular Junctions. *Chem. Phys. Lett.* **2009**, *473*, 189−192.
(301) Li, J. C.; Wang, D.; Ba, D. C. Effects of Temperature and Light Illumination on the Current-Voltage Characteristics of Molecular Self-Assembled Monolayer Junctions. *J. Phys. Chem. C* **2012**, *116*, 10986−10994.
(302) Kim, J. J.; Cho, B.; Kim, K. S.; Lee, T.; Jung, G. Y. Electrical Characterization of Unipolar Organic Resistive Memory Devices Scaled Down by a Direct Metal-Transfer Method. *Adv. Mater.* **2011**, *23*, 2104−2107.
(303) Jeong, H.; Kim, D.; Kim, P.; Cho, M. R.; Hwang, W. T.; Jang, Y.; Cho, K.; Min, M.; Xiang, D.; Park, Y. D.; et al. A New Approach for High-Yield Metal-Molecule-Metal Junctions by Direct Metal Transfer Method. *Nanotechnology* **2015**, *26*, 025601.
(304) Jiao, L. Y.; Fan, B.; Xian, X. J.; Wu, Z. Y.; Zhang, J.; Liu, Z. F. Creation of Nanostructures with Poly(Methyl Methacrylate)-Mediated Nanotransfer Printing. *J. Am. Chem. Soc.* **2008**, *130*, 12612−12613.
(305) Duan, X. F.; Huang, Y.; Cui, Y.; Wang, J. F.; Lieber, C. M. Indium Phosphide Nanowires as Building Blocks for Nanoscale Electronic and Optoelectronic Devices. *Nature* **2001**, *409*, 66−69.
(306) Yoon, H. P.; Maitani, M. M.; Cabarcos, O. M.; Cai, L. T.; Mayer, T. S.; Allara, D. L. Crossed-Nanowire Molecular Junctions: A New Multispectroscopy Platform for Conduction-Structure Correlations. *Nano Lett.* **2010**, *10*, 2897−2902.
(307) Kushmerick, J. G.; Holt, D. B.; Yang, J. C.; Naciri, J.; Moore, M. H.; Shashidhar, R. Metal-Molecule Contacts and Charge Transport across Monomolecular Layers: Measurement and Theory. *Phys. Rev. Lett.* **2002**, *89*, 086802.
(308) Kushmerick, J. G.; Naciri, J.; Yang, J. C.; Shashidhar, R. Conductance Scaling of Molecular Wires in Parallel. *Nano Lett.* **2003**, *3*, 897−900.
(309) Beebe, J. M.; Moore, H. J.; Lee, T. R.; Kushmerick, J. G. Vibronic Coupling in Semifluorinated Alkanethiol Junctions: Implications for Selection Rules in Inelastic Electron Tunneling Spectroscopy. *Nano Lett.* **2007**, *7*, 1364−1368.
(310) Yu, L. H.; Gergel-Hackett, N.; Zangmeister, C. D.; Hacker, C. A.; Richter, C. A.; Kushmerick, J. G. Molecule-Induced Interface States Dominate Charge Transport in Si-Alkyl-Metal Junctions. *J. Phys.: Condens. Matter* **2008**, *20*, 374114.
(311) Song, H.; Reed, M. A.; Lee, T. Single Molecule Electronic Devices. *Adv. Mater.* **2011**, *23*, 1583−1608.
(312) Bufon, C. C. B.; Espinoza, J. D. A.; Thurmer, D. J.; Bauer, M.; Deneke, C.; Zschieschang, U.; Klauk, H.; Schmidt, O. G. Hybrid Organic/Inorganic Molecular Heterojunctions Based on Strained Nanomembranes. *Nano Lett.* **2011**, *11*, 3727−3733.
(313) Yu, H. Y.; Ah, C. S.; Baek, I. B.; Kim, A.; Yang, J. H.; Ahn, C. G.; Park, C. W.; Kim, B. H. Nanogap Array Fabrication Using Doubly Clamped Freestanding Silicon Nanowires and Angle Evaporations. *Etri J.* **2009**, *31*, 351−356.
(314) Wang, J. D.; Wang, Z. X.; Li, Q. C.; Gan, L.; Xu, X. J.; Li, L. D.; Guo, X. F. Revealing Interface-Assisted Charge-Transfer Mechanisms by Using Silicon Nanowires as Local Probes. *Angew. Chem., Int. Ed.* **2013**, *52*, 3369−3373.
(315) Preiner, M. J.; Melosh, N. A. Creating Large Area Molecular Electronic Junctions Using Atomic Layer Deposition. *Appl. Phys. Lett.* **2008**, *92*, 213301.

DOI: 10.1021/acs.chemrev.5b00680
Chem. Rev. 2016, 116, 4318−4440

(316) Milani, F.; Grave, C.; Ferri, V.; Samori, P.; Rampi, M. A. Ultrathin π-Conjugated Polymer Films for Simple Fabrication of Large-Area Molecular Junctions. *ChemPhysChem* **2007**, *8*, 515−518.
(317) Li, T.; Hauptmann, J. R.; Wei, Z.; Petersen, S.; Bovet, N.; Vosch, T.; Nygard, J.; Hu, W.; Liu, Y.; Bjornholm, T.; Norgaard, K.; Laursen, B. W. Solution-Processed Ultrathin Chemically Derived Graphene Films as Soft Top Contacts for Solid-State Molecular Electronic Junctions. *Adv. Mater.* **2012**, *24*, 1333−1339.
(318) Akkerman, H. B.; Naber, R. C. G.; Jongbloed, B.; van Hal, P. A.; Blom, P. W. M.; de Leeuw, D. M.; de Boer, B. Electron Tunneling through Alkanedithiol Self-Assembled Monolayers in Large-Area Molecular Junctions. *Proc. Natl. Acad. Sci. U. S. A.* **2007**, *104*, 11161−11166.
(319) Kronemeijer, A. J.; Katsouras, I.; Huisman, E. H.; van Hal, P. A.; Geuns, T. C. T.; Blom, P. W. M.; de Leeuw, D. M. Universal Scaling of the Charge Transport in Large-Area Molecular Junctions. *Small* **2011**, *7*, 1593−1598.
(320) Akkerman, H. B.; Kronemeijer, A. J.; van Hal, P. A.; de Leeuw, D. M.; Blom, P. W. M.; de Boer, B. Self-Assembled-Monolayer Formation of Long Alkanedithiols in Molecular Junctions. *Small* **2008**, *4*, 100−104.
(321) Van Hal, P. A.; Smits, E. C. P.; Geuns, T. C. T.; Akkerman, H. B.; De Brito, B. C.; Perissinotto, S.; Lanzani, G.; Kronemeijer, A. J.; Geskin, V.; Cornil, J.; et al. Upscaling, Integration and Electrical Characterization of Molecular Junctions. *Nat. Nanotechnol.* **2008**, *3*, 749−754.
(322) Katsouras, I.; Kronemeijer, A. J.; Smits, E. C. P.; van Hal, P. A.; Geuns, T. C. T.; Blom, P. W. M.; de Leeuw, D. M. Extending the Voltage Window in the Characterization of Electrical Transport of Large-Area Molecular Junctions. *Appl. Phys. Lett.* **2011**, *99*, 013303.
(323) Asadi, K.; Katsouras, I.; Harkema, J.; Gholamrezaie, F.; Smits, E. C. F.; Biscarini, F.; Blom, P. W. M.; de Leeuw, D. M. Organic Field-Effect Transistors as a Test-Bed for Molecular Electronics: A Combined Study with Large-Area Molecular Junctions. *Org. Electron.* **2012**, *13*, 2502−2507.
(324) Akkerman, H. B.; Kronemeijer, A. J.; Harkema, J.; van Hal, P. A.; Smits, E. C. P.; de Leeuw, D. M.; Blom, P. W. M. Stability of Large-Area Molecular Junctions. *Org. Electron.* **2010**, *11*, 146−149.
(325) Wang, G.; Na, S. I.; Kim, T. W.; Kim, Y.; Park, S.; Lee, T. Effect of Pedot:Pss-Molecule Interface on the Charge Transport Characteristics of the Large-Area Molecular Electronic Junctions. *Org. Electron.* **2012**, *13*, 771−777.
(326) Park, S.; Wang, G.; Cho, B.; Kim, Y.; Song, S.; Ji, Y.; Yoon, M. H.; Lee, T. Flexible Molecular-Scale Electronic Devices. *Nat. Nanotechnol.* **2012**, *7*, 438−442.
(327) Jeong, H.; Kim, D.; Wang, G.; Park, S.; Lee, H.; Cho, K.; Hwang, W. T.; Yoon, M. H.; Jang, Y. H.; Song, H.; et al. Redox-Induced Asymmetric Electrical Characteristics of Ferrocene- Alkanethiolate Molecular Devices on Rigid and Flexible Substrates. *Adv. Funct. Mater.* **2014**, *24*, 2472−2480.
(328) Kim, D.; Jeong, H.; Lee, H.; Hwang, W. T.; Wolf, J.; Scheer, E.; Huhn, T.; Jeong, H.; Lee, T. Flexible Molecular-Scale Electronic Devices Composed of Diarylethene Photoswitching Molecules. *Adv. Mater.* **2014**, *26*, 3968−3973.
(329) Neuhausen, A. B.; Hosseini, A.; Sulpizio, J. A.; Chidsey, C. E. D.; Goldhaber-Gordon, D. Molecular Junctions of Self-Assembled Monolayers with Conducting Polymer Contacts. *ACS Nano* **2012**, *6*, 9920−9931.
(330) Seo, S.; Min, M.; Lee, S. M.; Lee, H. Photo-Switchable Molecular Monolayer Anchored between Highly Transparent and Flexible Graphene Electrodes. *Nat. Commun.* **2013**, *4*, 1920.
(331) Li, T.; Jevric, M.; Hauptmann, J. R.; Hviid, R.; Wei, Z.; Wang, R.; Reeler, N. E. A.; Thyrhaug, E.; Petersen, S.; Meyer, J. A. S.; et al. Ultrathin Reduced Graphene Oxide Films as Transparent Top-Contacts for Light Switchable Solid-State Molecular Junctions. *Adv. Mater.* **2013**, *25*, 4164−4170.
(332) Ashwell, G. J.; Wierzchowiec, P.; Bartlett, C. J.; Buckle, P. D. Molecular Electronics: Connection across Nano-Sized Electrode Gaps. *Chem. Commun.* **2007**, 1254−1256.
(333) Chen, W.; Liu, X. Q.; Tan, Z. K.; Likharev, K. K.; Lukens, J. E.; Mayr, A. Fabrication and Characterization of Novel Cross Point Structures for Molecular Electronic Integrated Circuits. *J. Vac. Sci. Technol. B* **2006**, *24*, 3217−3220.
(334) Tyagi, P.; Li, D. F.; Holmes, S. M.; Hinds, B. J. Molecular Electrodes at the Exposed Edge of Metal/Insulator/Metal Trilayer Structures. *J. Am. Chem. Soc.* **2007**, *129*, 4929−4938.
(335) Howell, S. W.; Dirk, S. M.; Childs, K.; Pang, H.; Blain, M.; Simonson, R. J.; Tour, J. M.; Wheeler, D. R. Mass-Fabricated One-Dimensional Silicon Nanogaps for Hybrid Organic/Nanoparticle Arrays. *Nanotechnology* **2005**, *16*, 754−758.
(336) Luber, S. M.; Strobel, S.; Tranitz, H. P.; Wegscheider, W.; Schuh, D.; Tornow, M. Nanometre Spaced Electrodes on a Cleaved Algaas Surface. *Nanotechnology* **2005**, *16*, 1182−1185.
(337) Brinkman, W. F. Tunneling Conductance of Asymmetrical Barriers. *J. Appl. Phys.* **1970**, *41*, 1915.
(338) Tyagi, P. Multilayer Edge Molecular Electronics Devices: A Review. *J. Mater. Chem.* **2011**, *21*, 4733.
(339) Pang, P.; Ashcroft, B. A.; Song, W. S.; Zhang, P. M.; Biswas, S.; Qing, Q.; Yang, J. L.; Nemanich, R. J.; Bai, J. W.; Smith, J. T.; et al. Fixed-Gap Tunnel Junction for Reading DNA Nucleotides. *ACS Nano* **2014**, *8*, 11994−12003.
(340) Dai, H. Carbon Nanotubes: Synthesis, Integration, and Properties. *Acc. Chem. Res.* **2002**, *35*, 1035−1044.
(341) Novoselov, K. S.; Geim, A. K.; Morozov, S. V.; Jiang, D.; Zhang, Y.; Dubonos, S. V.; Grigorieva, I. V.; Firsov, A. A. Electric Field Effect in Atomically Thin Carbon Films. *Science* **2004**, *306*, 666−669.
(342) The Molecular Electronics Special Issue. *Nat. Nanotechnol.* **2013**, *8*, 377−467,10.1038/nnano.2013.116
(343) Iijima, S. Helical Microtubules of Graphitic Carbon. *Nature* **1991**, *354*, 56−58.
(344) Ajayan, P. M.; Ebbesen, T. W. Nanometre-Size Tubes of Carbon. *Rep. Prog. Phys.* **1997**, *60*, 1025−1062.
(345) Roy, S.; Vedala, H.; Roy, A. D.; Kim, D.-h.; Doud, M.; Mathee, K.; Shin, H.-k.; Shimamoto, N.; Prasad, V.; Choi, W. Direct Electrical Measurements on Single-Molecule Genomic DNA Using Single-Walled Carbon Nanotubes. *Nano Lett.* **2008**, *8*, 26−30.
(346) Collins, P. G.; Arnold, M. S.; Avouris, P. Engineering Carbon Nanotubes and Nanotube Circuits Using Electrical Breakdown. *Science* **2001**, *292*, 706−709.
(347) Collins, P. G.; Hersam, M.; Arnold, M.; Martel, R.; Avouris, P. Current Saturation and Electrical Breakdown in Multiwalled Carbon Nanotubes. *Phys. Rev. Lett.* **2001**, *86*, 3128.
(348) Tsukagoshi, K.; Yagi, I.; Aoyagi, Y. Pentacene Nanotransistor with Carbon Nanotube Electrodes. *Appl. Phys. Lett.* **2004**, *85*, 1021−1023.
(349) Yagi, I.; Tsukagoshi, K.; Watanabe, E.; Aoyagi, Y. Carbon Nanotubes with a Nanogap for Nanoscale Organic Devices. *Microelectron. Eng.* **2004**, *73*, 675−678.
(350) Feldman, A. K.; Steigerwald, M. L.; Guo, X.; Nuckolls, C. Molecular Electronic Devices Based on Single-Walled Carbon Nanotube Electrodes. *Acc. Chem. Res.* **2008**, *41*, 1731−1741.
(351) Cao, Y.; Steigerwald, M. L.; Nuckolls, C.; Guo, X. Current Trends in Shrinking the Channel Length of Organic Transistors Down to the Nanoscale. *Adv. Mater.* **2010**, *22*, 20−32.
(352) Guo, X.; Xiao, S.; Myers, M.; Miao, Q.; Steigerwald, M. L.; Nuckolls, C. Photoresponsive Nanoscale Columnar Transistors. *Proc. Natl. Acad. Sci. U. S. A.* **2009**, *106*, 691−696.
(353) Liu, S.; Wei, Z.; Cao, Y.; Gan, L.; Wang, Z.; Xu, W.; Guo, X.; Zhu, D. Ultrasensitive Water-Processed Monolayer Photodetectors. *Chem. Sci.* **2011**, *2*, 796−802.
(354) Marquardt, C. W.; Grunder, S.; Baszczyk, A.; Dehm, S.; Hennrich, F.; Löhneysen, H. v.; Mayor, M.; Krupke, R. Electroluminescence from a Single Nanotube-Molecule-Nanotube Junction. *Nat. Nanotechnol.* **2010**, *5*, 863−867.
(355) Wei, D.; Liu, Y.; Cao, L.; Wang, Y.; Zhang, H.; Yu, G. Real Time and in Situ Control of the Gap Size of Nanoelectrodes for Molecular Devices. *Nano Lett.* **2008**, *8*, 1625−1630.

DOI: 10.1021/acs.chemrev.5b00680
Chem. Rev. 2016, 116, 4318−4440

(356) Guo, X.; Gorodetsky, A. A.; Hone, J.; Barton, J. K.; Nuckolls, C. Conductivity of a Single DNA Duplex Bridging a Carbon Nanotube Gap. *Nat. Nanotechnol.* **2008**, *3*, 163−167.
(357) Liu, S.; Clever, G. H.; Takezawa, Y.; Kaneko, M.; Tanaka, K.; Guo, X.; Shionoya, M. Direct Conductance Measurement of Individual Metallo-DNA Duplexes within Single-Molecule Break Junctions. *Angew. Chem., Int. Ed.* **2011**, *50*, 8762−8762.
(358) Genereux, J. C.; Barton, J. K. Mechanisms for DNA Charge Transport. *Chem. Rev.* **2010**, *110*, 1642−1662.
(359) Xu, Zhang; Li, Tao Direct Conductance Measurement of Single DNA Molecules in Aqueous Solution. *Nano Lett.* **2004**, *4*, 1105−1108.
(360) Xiang, L.; Palma, J. L.; Bruot, C.; Mujica, V.; Ratner, M. A.; Tao, N. Intermediate Tunnelling−Hopping Regime in DNA Charge Transport. *Nat. Chem.* **2015**, *7*, 221−226.
(361) Liu, S. P.; Weisbrod, S. H.; Tang, Z.; Marx, A.; Scheer, E.; Erbe, A. Direct Measurement of Electrical Transport through G-Quadruplex DNA with Mechanically Controllable Break Junction Electrodes. *Angew. Chem., Int. Ed.* **2010**, *49*, 3313−3316.
(362) Wan, X.; Huang, Y.; Chen, Y. Focusing on Energy and Optoelectronic Applications: A Journey for Graphene and Graphene Oxide at Large Scale. *Acc. Chem. Res.* **2012**, *45*, 598−607.
(363) Yang, W.; Ratinac, K. R.; Ringer, S. P.; Thordarson, P.; Gooding, J. J.; Braet, F. Carbon Nanomaterials in Biosensors: Should You Use Nanotubes or Graphene? *Angew. Chem., Int. Ed.* **2010**, *49*, 2114−2138.
(364) Liu, S.; Guo, X. Carbon Nanomaterials Field-Effect-Transistor-Based Biosensors. *NPG Asia Mater.* **2012**, *4*, e23.
(365) Cao, Y.; Liu, S.; Shen, Q.; Yan, K.; Li, P.; Xu, J.; Yu, D.; Steigerwald, M. L.; Nuckolls, C.; Liu, Z.; Guo, X. High-Performance Photoresponsive Organic Nanotransistors with Single-Layer Graphenes as Two-Dimensional Electrodes. *Adv. Funct. Mater.* **2009**, *19*, 2743−2748.
(366) Cao, Y.; Wei, Z.; Liu, S.; Gan, L.; Guo, X.; Xu, W.; Steigerwald, M. L.; Liu, Z.; Zhu, D. High-Performance Langmuir−Blodgett Monolayer Transistors with High Responsivity. *Angew. Chem., Int. Ed.* **2010**, *49*, 6319−6323.
(367) Liu, W.; Jackson, B. L.; Zhu, J.; Miao, C.-Q.; Chung, C.-H.; Park, Y. J.; Sun, K.; Woo, J.; Xie, Y.-H. Large Scale Pattern Graphene Electrode for High Performance in Transparent Organic Single Crystal Field-Effect Transistors. *ACS Nano* **2010**, *4*, 3927−3932.
(368) Di, C.-a.; Wei, D.; Yu, G.; Liu, Y.; Guo, Y.; Zhu, D. Patterned Graphene as Source/Drain Electrodes for Bottom-Contact Organic Field-Effect Transistors. *Adv. Mater.* **2008**, *20*, 3289−3293.
(369) Lee, W. H.; Park, J.; Sim, S. H.; Lim, S.; Kim, K. S.; Hong, B. H.; Cho, K. Surface-Directed Molecular Assembly of Pentacene on Monolayer Graphene for High-Performance Organic Transistors. *J. Am. Chem. Soc.* **2011**, *133*, 4447−4454.
(370) Tsutsui, M.; Taniguchi, M. Single Molecule Electronics and Devices. *Sensors* **2012**, *12*, 7259−7298.
(371) Prins, F.; Barreiro, A.; Ruitenberg, J. W.; Seldenthuis, J. S.; Aliaga-Alcalde, N.; Vandersypen, L. M. K.; van der Zant, H. S. J. Room-Temperature Gating of Molecular Junctions Using Few-Layer Graphene Nanogap Electrodes. *Nano Lett.* **2011**, *11*, 4607−4611.
(372) Ullmann, K.; Coto, P. B.; Leitherer, S.; Molina-Ontoria, A.; Martin, N.; Thoss, M.; Weber, H. B. Single-Molecule Junctions with Epitaxial Graphene Nanoelectrodes. *Nano Lett.* **2015**, *15*, 3512−3518.
(373) Cao, Y.; Dong, S.; Liu, S.; Liu, Z.; Guo, X. Toward Functional Molecular Devices Based on Graphene−Molecule Junctions. *Angew. Chem.* **2013**, *125*, 3998−4002.
(374) Ahmed, T.; Kilina, S.; Das, T.; Haraldsen, J. T.; Rehr, J. J.; Balatsky, A. V. Electronic Fingerprints of DNA Bases on Graphene. *Nano Lett.* **2012**, *12*, 927−931.
(375) Kim, T.; Liu, Z.-F.; Lee, C.; Neaton, J. B.; Latha, V. Charge Transport and Rectification in Molecular Junctions Formed with Carbon-Based Electrodes. *Proc. Natl. Acad. Sci. U. S. A.* **2014**, *111*, 10928−10932.
(376) Buriak, J. M. Organometallic Chemistry on Silicon and Germanium Surfaces. *Chem. Rev.* **2002**, *102*, 1271−1308.
(377) Salomon, A.; Boecking, T.; Seitz, O.; Markus, T.; Amy, F.; Chan, C.; Zhao, W.; Cahen, D.; Kahn, A. What Is the Barrier for Tunneling through Alkyl Monolayers? Results from n- and p-Si−Alkyl/Hg Junctions. *Adv. Mater.* **2007**, *19*, 445−450.
(378) Cahen, D.; Kahn, A. Electron Energetics at Surfaces and Interfaces: Concepts and Experiments. *Adv. Mater.* **2003**, *15*, 271−277.
(379) Adam Johan, B.; Kenneth, D. H.; Fengjun, D.; Richard, L. M. Molecular Electronics Using Diazonium-Derived Adlayers on Carbon with Cu Top Contacts: Critical Analysis of Metal Oxides and Filaments. *J. Phys.: Condens. Matter* **2008**, *20*, 374117.
(380) Dirk, S. M.; Howell, S. W.; Zmuda, S.; Childs, K.; Blain, M.; Simonson, R. J.; Wheeler, D. R. Novel One-Dimensional Nanogap Created with Standard Optical Lithography and Evaporation Procedures. *Nanotechnology* **2005**, *16*, 1983−1985.
(381) Miramond, C.; Vuillaume, D. 1-Octadecene Monolayers on Si(111) Hydrogen-Terminated Surfaces: Effect of Substrate Doping. *J. Appl. Phys.* **2004**, *96*, 1529−1536.
(382) Sieval, A. B.; Demirel, A. L.; Nissink, J. W. M.; Linford, M. R.; van der Maas, J. H.; de Jeu, W. H.; Zuilhof, H.; Sudhölter, E. J. R. Highly Stable Si−C Linked Functionalized Monolayers on the Silicon (100) Surface. *Langmuir* **1998**, *14*, 1759−1768.
(383) Berg, J.; Che, F.; Lundgren, P.; Enoksson, P.; Bengtsson, S. Electrical Properties of Si-SiO_2-Si Nanogaps. *Nanotechnology* **2005**, *16*, 2197−2202.
(384) Ashwell, G. J.; Phillips, L. J.; Robinson, B. J.; Urasinska-Wojcik, B.; Lambert, C. J.; Grace, I. M.; Bryce, M. R.; Jitchati, R.; Tavasli, M.; Cox, T. I.; Sage, I. C.; et al. Molecular Bridging of Silicon Nanogaps. *ACS Nano* **2010**, *4*, 7401−7406.
(385) Ashwell, G. J.; Phillips, L. J.; Robinson, B. J.; Barnes, S. A.; Williams, A. T.; Urasinska-Wojcik, B.; Lambert, C. J.; Grace, I. M.; Cox, T. I.; Sage, I. C. Synthesis of Covalently Linked Molecular Bridges between Silicon Electrodes in CMOS-Based Arrays of Vertical Si/SiO_2/Si Nanogaps. *Angew. Chem., Int. Ed.* **2011**, *50*, 8722−8726.
(386) Okawa, Y.; Mandal, S. K.; Hu, C.; Tateyama, Y.; Goedecker, S.; Tsukamoto, S.; Hasegawa, T.; Gimzewski, J. K.; Aono, M. Chemical Wiring and Soldering toward All-Molecule Electronic Circuitry. *J. Am. Chem. Soc.* **2011**, *133*, 8227−8233.
(387) Garcia, R.; Knoll, A. W.; Riedo, E. Advanced Scanning Probe Lithography. *Nat. Nanotechnol.* **2014**, *9*, 577−587.
(388) Leary, R.; Midgley, P. A.; Thomas, J. M. Recent Advances in the Application of Electron Tomography to Materials Chemistry. *Acc. Chem. Res.* **2012**, *45*, 1782−1791.
(389) Tian, H. H.; Li, Y. C.; Shao, H. B.; Yu, H. Z. Thin-Film Voltammetry and Its Analytical Applications: A Review. *Anal. Chim. Acta* **2015**, *855*, 1−12.
(390) Kashyap, D.; Dwivedi, P. K.; Pandey, J. K.; Kim, Y. H.; Kim, G. M.; Sharma, A.; Goel, S. Application of Electrochemical Impedance Spectroscopy in Bio-Fuel Cell Characterization: A Review. *Int. J. Hydrogen Energy* **2014**, *39*, 20159−20170.
(391) Vivek, J. P.; Monsur, A.; Burgess, I. J. Differential Capacity and Chronocoulometry Studies of a Quaternary Ammonium Surfactant Adsorbed on Au(111). *Surf. Interface Anal.* **2013**, *45*, 1402−1409.
(392) Choi, S. H.; Kim, B.; Frisbie, C. D. Electrical Resistance of Long Conjugated Molecular Wires. *Science* **2008**, *320*, 1482−1486.
(393) Kim, Y.; Song, H.; Kim, D.; Lee, T.; Jeong, H. Noise Characteristics of Charge Tunneling Via Localized States in Metal-Molecule-Metal Junctions. *ACS Nano* **2010**, *4*, 4426−4430.
(394) Beebe, J. M.; Kim, B.; Gadzuk, J. W.; Frisbie, C. D.; Kushmerick, J. G. Transition from Direct Tunneling to Field Emission in Metal-Molecule-Metal Junctions. *Phys. Rev. Lett.* **2006**, *97*, 026801.
(395) Shamai, T.; Selzer, Y. Spectroscopy of Molecular Junctions. *Chem. Soc. Rev.* **2011**, *40*, 2293−2305.
(396) Mitsuishi, A. Progress in Far-Infrared Spectroscopy: Approximately 1890 to 1970. *J. Infrared, Millimeter, Terahertz Waves* **2014**, *35*, 243−281.
(397) Jentoft, F. C. Ultraviolet-Visible-near Infrared Spectroscopy in Catalysis: Theory, Experiment, Analysis, and Application under Reaction Conditions. *Adv. Catal.* **2009**, *52*, 129−211.

DOI: 10.1021/acs.chemrev.5b00680
Chem. Rev. 2016, 116, 4318−4440

(398) Surviliene, S.; Cesuniene, A.; Jasulaitiene, V.; Jureviciute, I. Investigation of the Surface Composition of Electrodeposited Black Chromium by X-Ray Photoelectron Spectroscopy. *Appl. Surf. Sci.* **2015**, *324*, 837−841.
(399) Yamamoto, S.; Matsuda, I. Time-Resolved Photoelectron Spectroscopies Using Synchrotron Radiation: Past, Present, and Future. *J. Phys. Soc. Jpn.* **2013**, *82*, 021003.
(400) Knuta, R.; Lindblad, R.; Gorgoi, M.; Rensmo, H.; Karis, O. High Energy Photoelectron Spectroscopy in Basic and Applied Science: Bulk and Interface Electronic Structure. *J. Electron Spectrosc. Relat. Phenom.* **2013**, *190*, 278−288.
(401) Hihath, J.; Tao, N. J. Electron-Phonon Interactions in Atomic and Molecular Devices. *Prog. Surf. Sci.* **2012**, *87*, 189−208.
(402) Okabayashi, N.; Paulsson, M.; Komeda, T. Inelastic Electron Tunneling Process for Alkanethiol Self-Assembled Monolayers. *Prog. Surf. Sci.* **2013**, *88*, 1−38.
(403) Hapala, P.; Temirov, R.; Tautz, F. S.; Jelinek, P. Origin of High-Resolution IETS-STM Images of Organic Molecules with Functionalized Tips. *Phys. Rev. Lett.* **2014**, *113*, 226101.
(404) Deng, M. S.; Ye, G.; Cai, S. H.; Sun, G. Y.; Jiang, J. Probing Flexible Conformations in Molecular Junctions by Inelastic Electron Tunneling Spectroscopy. *AIP Adv.* **2015**, *5*, 017144.
(405) Jaklevic, R. C.; Lambe, J. Molecular Vibration Spectra by Electron Tunneling. *Phys. Rev. Lett.* **1966**, *17*, 1139−1140.
(406) Stipe, B. C.; Rezaei, M. A.; Ho, W. Single-Molecule Vibrational Spectroscopy and Microscopy. *Science* **1998**, *280*, 1732−1735.
(407) Ho, W. Single-Molecule Chemistry. *J. Chem. Phys.* **2002**, *117*, 11033−11061.
(408) Tsutsui, M.; Taniguchi, M. Vibrational Spectroscopy of Single-Molecule Junctions by Direct Current Measurements. *J. Appl. Phys.* **2013**, *113*, 084301.
(409) Petit, C.; Salace, G. Inelastic Electron Tunneling Spectrometer to Characterize Metal-Oxide-Semiconductor Devices with Ultrathin Oxides. *Rev. Sci. Instrum.* **2003**, *74*, 4462−4467.
(410) Hipps, K. W.; Mazur, U. Inelastic Electron-Tunneling - an Alternative Molecular-Spectroscopy. *J. Phys. Chem.* **1993**, *97*, 7803−7814.
(411) Wang, W. Y.; Lee, T.; Kretzschmar, I.; Reed, M. A. Inelastic Electron Tunneling Spectroscopy of an Alkanedithiol Self-Assembled Monolayer. *Nano Lett.* **2004**, *4*, 643−646.
(412) Walmsley, D. G.; Tomlin, J. L. Compilation of Inelastic Electron Tunnelling Spectra of Molecules Chemisorbed on Metal-Oxides. *Prog. Surf. Sci.* **1985**, *18*, 247−447.
(413) Hansma, P. K. Tunneling Spectroscopy as a Probe of Adsorbate-Surface Interactions. *J. Electron Spectrosc. Relat. Phenom.* **1983**, *30*, 163−174.
(414) Jafri, S. H. M.; Löfås, H.; Fransson, J.; Blom, T.; Grigoriev, A.; Wallner, A.; Ahuja, R.; Ottosson, H.; Leifer, K. Identification of Vibrational Signatures from Short Chains of Interlinked Molecule-Nanoparticle Junctions Obtained by Inelastic Electron Tunnelling Spectroscopy. *Nanoscale* **2013**, *5*, 4673−4677.
(415) Gregory, S. Inelastic Tunneling Spectroscopy and Single-Electron Tunneling in an Adjustable Microscopic Tunnel Junction. *Phys. Rev. Lett.* **1990**, *64*, 689−692.
(416) Hihath, J.; Arroyo, C. R.; Rubio-Bollinger, G.; Tao, N. J.; Agraït, N. Study of Electron-Phonon Interactions in a Single Molecule Covalently Connected to Two Electrodes. *Nano Lett.* **2008**, *8*, 1673−1678.
(417) Okabayashi, N.; Paulsson, M.; Ueba, H.; Konda, Y.; Komeda, T. Site Selective Inelastic Electron Tunneling Spectroscopy Probed by Isotope Labeling. *Nano Lett.* **2010**, *10*, 2950−2955.
(418) Tal, O.; Krieger, M.; Leerink, B.; van Ruitenbeek, J. M. Electron-Vibration Interaction in Single-Molecule Junctions: From Contact to Tunneling Regimes. *Phys. Rev. Lett.* **2008**, *100*, 196804.
(419) Kim, Y.; Pietsch, T.; Erbe, A.; Belzig, W.; Scheer, E. Benzenedithiol: A Broad-Range Single-Channel Molecular Conductor. *Nano Lett.* **2011**, *11*, 3734−3738.
(420) Hihath, J.; Bruot, C.; Tao, N. J. Electron-Phonon Interactions in Single Octanedithiol Molecular Junctions. *ACS Nano* **2010**, *4*, 3823−3830.
(421) Tsutsui, M.; Taniguchi, M.; Shoji, K.; Yokota, K.; Kawai, T. Identifying Molecular Signatures in Metal-Molecule-Metal Junctions. *Nanoscale* **2009**, *1*, 164−170.
(422) Ren, H.; Yang, J. L.; Luo, Y. Identifying Configuration and Orientation of Adsorbed Molecules by Inelastic Electron Tunneling Spectra. *J. Chem. Phys.* **2010**, *133*, 064702.
(423) Leng, J.; Lin, L.; Song, X.; Li, Z.; Wang, C. Orientation of Decanethiol Molecules in Self-Assembled Monolayers Determined by Inelastic Electron Tunneling Spectroscopy. *J. Phys. Chem. C* **2009**, *113*, 18353−18357.
(424) Lin, L.; Wang, C.; Luo, Y. Inelastic Electron Tunneling Spectroscopy of Gold-Benzenedithiol-Gold Junctions: Accurate Determination of Molecular Conformation. *ACS Nano* **2011**, *5*, 2257−2263.
(425) Jiang, J.; Kula, M.; Lu, W.; Luo, Y. First-Principles Simulations of Inelastic Electron Tunneling Spectroscopy of Molecular Electronic Devices. *Nano Lett.* **2005**, *5*, 1551−1555.
(426) Seminario, J. M.; Zacarias, A. G.; Tour, J. M. Theoretical Study of a Molecular Resonant Tunneling Diode. *J. Am. Chem. Soc.* **2000**, *122*, 3015−3020.
(427) Di Ventra, M.; Kim, S. G.; Pantelides, S. T.; Lang, N. D. Temperature Effects on the Transport Properties of Molecules. *Phys. Rev. Lett.* **2001**, *86*, 288−291.
(428) Lang, N. D.; Avouris, P. Electrical Conductance of Parallel Atomic Wires. *Phys. Rev. B: Condens. Matter Mater. Phys.* **2000**, *62*, 7325−7329.
(429) Ramachandran, G. K.; Hopson, T. J.; Rawlett, A. M.; Nagahara, L. A.; Primak, A.; Lindsay, S. M. A Bond-Fluctuation Mechanism for Stochastic Switching in Wired Molecules. *Science* **2003**, *300*, 1413−1416.
(430) He, J.; Fu, Q.; Lindsay, S.; Ciszek, J. W.; Tour, J. M. Electrochemical Origin of Voltage-Controlled Molecular Conductance Switching. *J. Am. Chem. Soc.* **2006**, *128*, 14828−14835.
(431) Paulsson, M.; Frederiksen, T.; Brandbyge, M. Inelastic Transport through Molecules: Comparing First-Principles Calculations to Experiments. *Nano Lett.* **2006**, *6*, 258−262.
(432) Cai, L. T.; Cabassi, M. A.; Yoon, H.; Cabarcos, O. M.; McGuiness, C. L.; Flatt, A. K.; Allara, D. L.; Tour, J. M.; Mayer, T. S. Reversible Bistable Switching in Nanoscale Thiol-Substituted Oligoaniline Molecular Junctions. *Nano Lett.* **2005**, *5*, 2365−2372.
(433) Cao, H.; Jiang, J.; Ma, J.; Luo, Y. Identification of Switching Mechanism in Molecular Junctions by Inelastic Electron Tunneling Spectroscopy. *J. Phys. Chem. C* **2008**, *112*, 11018−11022.
(434) Long, D. P.; Lazorcik, J. L.; Mantooth, B. A.; Moore, M. H.; Ratner, M. A.; Troisi, A.; Yao, Y.; Ciszek, J. W.; Tour, J. M.; Shashidhar, R. Effects of Hydration on Molecular Junction Transport. *Nat. Mater.* **2006**, *5*, 901−908.
(435) Kim, Y.; Garcia-Lekue, A.; Sysoiev, D.; Frederiksen, T.; Groth, U.; Scheer, E. Charge Transport in Azobenzene-Based Single-Molecule Junctions. *Phys. Rev. Lett.* **2012**, *109*, 226801.
(436) Hihath, J.; Bruot, C.; Nakamura, H.; Asai, Y.; Díez-Pérez, I.; Lee, Y.; Yu, L.; Tao, N. Inelastic Transport and Low-Bias Rectification in a Single-Molecule Diode. *ACS Nano* **2011**, *5*, 8331−8339.
(437) Taniguchi, M.; Tsutsui, M.; Yokota, K.; Kawai, T. Mechanically-Controllable Single Molecule Switch Based on Configuration Specific Electrical Conductivity of Metal-Molecule-Metal Junctions. *Chem. Sci.* **2010**, *1*, 247−253.
(438) Kim, Y.; Hellmuth, T. J.; Burkle, M.; Pauly, F.; Scheer, E. Characteristics of Amine-Ended and Thiol-Ended Alkane Single-Molecule Junctions Revealed by Inelastic Electron Tunneling Spectroscopy. *ACS Nano* **2011**, *5*, 4104−4111.
(439) Kaneko, S.; Motta, C.; Brivio, G. P.; Kiguchi, M. Mechanically Controllable Bi-Stable States in a Highly Conductive Single Pyrazine Molecular Junction. *Nanotechnology* **2013**, *24*, 315201.
(440) Lykkebo, J.; Gagliardi, A.; Pecchia, A.; Solomon, G. C. Strong Overtones Modes in Inelastic Electron Tunneling Spectroscopy with

DOI: 10.1021/acs.chemrev.5b00680
Chem. Rev. 2016, 116, 4318−4440

Cross-Conjugated Molecules: A Prediction from Theory. *ACS Nano* **2013**, *7*, 9183−9194.
(441) Lorente, N.; Persson, M.; Lauhon, L. J.; Ho, W. Symmetry Selection Rules for Vibrationally Inelastic Tunneling. *Phys. Rev. Lett.* **2001**, *86*, 2593−2596.
(442) Fock, J.; Sørensen, J. K.; Lörtscher, E.; Vosch, T.; Martin, C. A.; Riel, H.; Kilså, K.; Bjornhølm, T.; van der Zant, H. A Statistical Approach to Inelastic Electron Tunneling Spectroscopy on Fullerene-Terminated Molecules. *Phys. Chem. Chem. Phys.* **2011**, *13*, 14325−14332.
(443) Hou, J. G.; Zhao, A. D. Detecting and Manipulating Single Molecules with STM. *Nano* **2006**, *1*, 15−33.
(444) Jeong, H.; Hwang, W. T.; Kim, P.; Kim, D.; Jang, Y.; Min, M.; Xiang, D.; Song, H.; Park, Y. D.; Jeong, H.; Lee, T. Investigation of Inelastic Electron Tunneling Spectra of Metal-Molecule-Metal Junctions Fabricated Using Direct Metal Transfer Method. *Appl. Phys. Lett.* **2015**, *106*, 063110.
(445) Luo, L.; Benameur, A.; Brignou, P.; Choi, S. H.; Rigaut, S.; Frisbie, C. D. Length and Temperature Dependent Conduction of Ruthenium-Containing Redox-Active Molecular Wires. *J. Phys. Chem. C* **2011**, *115*, 19955−19961.
(446) Wang, W. Y.; Lee, T.; Reed, M. A. Mechanism of Electron Conduction in Self-Assembled Alkanethiol Monolayer Devices. *Phys. Rev. B: Condens. Matter Mater. Phys.* **2003**, *68*, 035416.
(447) Luo, L. A.; Choi, S. H.; Frisbie, C. D. Probing Hopping Conduction in Conjugated Molecular Wires Connected to Metal Electrodes. *Chem. Mater.* **2011**, *23*, 631−645.
(448) Yamada, R.; Kumazawa, H.; Tanaka, S.; Tada, H. Electrical Resistance of Long Oligothiophene Molecules. *Appl. Phys. Express* **2009**, *2*, 025002.
(449) Hines, T.; Diez-Perez, I.; Hihath, J.; Liu, H. M.; Wang, Z. S.; Zhao, J. W.; Zhou, G.; Müllen, K.; Tao, N. J. Transition from Tunneling to Hopping in Single Molecular Junctions by Measuring Length and Temperature Dependence. *J. Am. Chem. Soc.* **2010**, *132*, 11658−11664.
(450) Choi, S. H.; Risko, C.; Delgado, M. C. R.; Kim, B.; Bredas, J. L.; Frisbie, C. D. Transition from Tunneling to Hopping Transport in Long, Conjugated Oligo-Imine Wires Connected to Metals. *J. Am. Chem. Soc.* **2010**, *132*, 4358−4368.
(451) Luo, L.; Frisbie, C. D. Length-Dependent Conductance of Conjugated Molecular Wires Synthesized by Stepwise "Click" Chemistry. *J. Am. Chem. Soc.* **2010**, *132*, 8854−8855.
(452) Choi, S. H.; Frisbie, C. D. Enhanced Hopping Conductivity in Low Band Gap Donor-Acceptor Molecular Wires up to 20 Nm in Length. *J. Am. Chem. Soc.* **2010**, *132*, 16191−16201.
(453) Hsu, L. Y.; Wu, N.; Rabitz, H. Gate Control of the Conduction Mechanism Transition from Tunneling to Thermally Activated Hopping. *J. Phys. Chem. Lett.* **2014**, *5*, 1831−1836.
(454) Zhao, X. T.; Huang, C. C.; Gulcur, M.; Batsanov, A. S.; Baghernejad, M.; Hong, W. J.; Bryce, M. R.; Wandlowski, T. Oligo(Aryleneethynylene)S with Terminal Pyridyl Groups: Synthesis and Length Dependence of the Tunneling-to-Hopping Transition of Single-Molecule Conductances. *Chem. Mater.* **2013**, *25*, 4340−4347.
(455) Lu, Q.; Yao, C.; Wang, X. H.; Wang, F. S. Enhancing Molecular Conductance of Oligo(P-Phenylene Ethynylene)S by Incorporating Ferrocene into Their Backbones. *J. Phys. Chem. C* **2012**, *116*, 17853−17861.
(456) Lu, Q.; Liu, K.; Zhang, H. M.; Du, Z. B.; Wang, X. H.; Wang, F. S. From Tunneling to Hopping: A Comprehensive Investigation of Charge Transport Mechanism in Molecular Junctions Based on Oligo(P-Phenylene Ethynylene)S. *ACS Nano* **2009**, *3*, 3861−3868.
(457) Ferreira, Q.; Braganca, A. M.; Alcacer, L.; Morgado, J. Conductance of Well-Defined Porphyrin Self-Assembled Molecular Wires up to 14 Nm in Length. *J. Phys. Chem. C* **2014**, *118*, 7229−7234.
(458) Poot, M.; Osorio, E.; O'Neill, K.; Thijssen, J. M.; Vanmaekelbergh, D.; van Walree, C. A.; Jenneskens, L. W.; van der Zant, H. S. J. Temperature Dependence of Three-Terminal Molecular Junctions with Sulfur End-Functionalized Tercyclohexylidenes. *Nano Lett.* **2006**, *6*, 1031−1035.
(459) Sedghi, G.; García-suárez, V. M.; Esdaile, L. J.; Anderson, H. L.; Lambert, C. J.; Martin, S.; Bethell, D.; Higgins, S. J.; Elliott, M.; Bennett, N.; Macdonald, J. E.; et al. Long-Range Electron Tunnelling in Oligo-Porphyrin Molecular Wires. *Nat. Nanotechnol.* **2011**, *6*, 517−523.
(460) Yan, H. J.; Bergren, A. J.; McCreery, R.; Della Rocca, M. L.; Martin, P.; Lafarge, P.; Lacroix, J. C. Activationless Charge Transport across 4.5 to 22 Nm in Molecular Electronic Junctions. *Proc. Natl. Acad. Sci. U. S. A.* **2013**, *110*, 5326−5330.
(461) Kolivoska, V.; Valasek, M.; Gal, M.; Sokolova, R.; Bulickova, J.; Pospisil, L.; Meszaros, G.; Hromadova, M. Single-Molecule Conductance in a Series of Extended Viologen Molecules. *J. Phys. Chem. Lett.* **2013**, *4*, 589−595.
(462) Sedghi, G.; Esdaile, L. J.; Anderson, H. L.; Martin, S.; Bethell, D.; Higgins, S. J.; Nichols, R. J. Comparison of the Conductance of Three Types of Porphyrin-Based Molecular Wires: B,Meso,B-Fused Tapes, Meso-Butadiyne-Linked and Twisted Meso-Meso Linked Oligomers. *Adv. Mater.* **2012**, *24*, 653−657.
(463) Li, Z. H.; Park, T. H.; Rawson, J.; Therien, M. J.; Borguet, E. Quasi-Ohmic Single Molecule Charge Transport through Highly Conjugated Meso-to-Meso Ethyne-Bridged Porphyrin Wires. *Nano Lett.* **2012**, *12*, 2722−2727.
(464) Kim, B.; Choi, S. H.; Zhu, X. Y.; Frisbie, C. D. Molecular Tunnel Junctions Based on Pi-Conjugated Oligoacene Thiols and Dithiols between Ag, Au, and Pt Contacts: Effect of Surface Linking Group and Metal Work Function. *J. Am. Chem. Soc.* **2011**, *133*, 19864−19877.
(465) Galperin, M.; Nitzan, A.; Ratner, M. A. Inelastic Tunneling Effects on Noise Properties of Molecular Junctions. *Phys. Rev. B: Condens. Matter Mater. Phys.* **2006**, *74*, 075326.
(466) Djukic, D.; van Ruitenbeek, J. M. Shot Noise Measurements on a Single Molecule. *Nano Lett.* **2006**, *6*, 789−793.
(467) Wheeler, P. J.; Russom, J. N.; Evans, K.; King, N. S.; Natelson, D. Shot Noise Suppression at Room Temperature in Atomic-Scale Au Junctions. *Nano Lett.* **2010**, *10*, 1287−1292.
(468) Wu, Z. M.; Wu, S. M.; Oberholzer, S.; Steinacher, M.; Calame, M.; Schönenberger, C. Scaling of 1/F Noise in Tunable Break Junctions. *Phys. Rev. B: Condens. Matter Mater. Phys.* **2008**, *78*, 235421.
(469) Adak, O.; Rosenthal, E.; Meisner, J.; Andrade, E. F.; Pasupathy, A. N.; Nuckolls, C.; Hybertsen, M. S.; Venkataraman, L. Flicker Noise as a Probe of Electronic Interaction at Metal-Single Molecule Interfaces. *Nano Lett.* **2015**, *15*, 4143−4149.
(470) Kumar, M.; Avriller, R.; Yeyati, A. L.; van Ruitenbeek, J. M. Detection of Vibration-Mode Scattering in Electronic Shot Noise. *Phys. Rev. Lett.* **2012**, *108*, 146602.
(471) Ochs, R.; Secker, D.; Elbing, M.; Mayor, M.; Weber, H. B. Fast Temporal Fluctuations in Single-Molecule Junctions. *Faraday Discuss.* **2006**, *131*, 281−289.
(472) Blanter, Y. M.; Buttiker, M. Shot Noise in Mesoscopic Conductors. *Phys. Rep.* **2000**, *336*, 1−166.
(473) Rogers, C. T.; Buhrman, R. A. Composition of 1/f Noise in Metal-Insulator-Metal Tunnel Junctions. *Phys. Rev. Lett.* **1984**, *53*, 1272−1275.
(474) van den Brom, H. E.; van Ruitenbeek, J. M. Quantum Suppression of Shot Noise in Atom-Size Metallic Contacts. *Phys. Rev. Lett.* **1999**, *82*, 1526−1529.
(475) Xiang, D.; Sydoruk, V.; Vitusevich, S.; Petrychuk, M. V.; Offenhäusser, A.; Kochelap, V. A.; Belyaev, A. E.; Mayer, D. Noise Characterization of Metal-Single Molecule Contacts. *Appl. Phys. Lett.* **2015**, *106*, 063702.
(476) Chen, R.; Matt, M.; Pauly, F.; Nielaba, P.; Cuevas, J. C.; Natelson, D. Shot Noise Variation within Ensembles of Gold Atomic Break Junctions at Room Temperature. *J. Phys.: Condens. Matter* **2014**, *26*, 474204.
(477) Djukic, D.; Thygesen, K. S.; Untiedt, C.; Smit, R. H. M.; Jacobsen, K. W.; van Ruitenbeek, J. M. Stretching Dependence of the Vibration Modes of a Single-Molecule Pt-H-2-Pt Bridge. *Phys. Rev. B: Condens. Matter Mater. Phys.* **2005**, *71*, 161402.

DOI: 10.1021/acs.chemrev.5b00680
Chem. Rev. 2016, 116, 4318−4440

(478) Paulsson, M.; Frederiksen, T.; Brandbyge, M. Modeling Inelastic Phonon Scattering in Atomic- and Molecular-Wire Junctions. *Phys. Rev. B: Condens. Matter Mater. Phys.* **2005**, *72*, 201101.
(479) Ben-Zvi, R.; Vardimon, R.; Yelin, T.; Tal, O. Electron-Vibration Interaction in Multichannel Single-Molecule Junctions. *ACS Nano* **2013**, *7*, 11147−11155.
(480) Galperin, M.; Ratner, M. A.; Nitzan, A. Inelastic Electron Tunneling Spectroscopy in Molecular Junctions: Peaks and Dips. *J. Chem. Phys.* **2004**, *121*, 1196−11979.
(481) Koch, J.; von Oppen, F. Franck-Condon Blockade and Giant Fano Factors in Transport through Single Molecules. *Phys. Rev. Lett.* **2005**, *94*, 206804.
(482) Schneider, N. L.; Lü, J. T.; Brandbyge, M.; Berndt, R. Light Emission Probing Quantum Shot Noise and Charge Fluctuations at a Biased Molecular Junction. *Phys. Rev. Lett.* **2012**, *109*, 186601.
(483) Haupt, F.; Novotný, T.; Belzig, W. Phonon-Assisted Current Noise in Molecular Junctions. *Phys. Rev. Lett.* **2009**, *103*, 136601.
(484) Brunner, J.; González, M. T.; Schönenberger, C.; Calame, M. Random Telegraph Signals in Molecular Junctions. *J. Phys.: Condens. Matter* **2014**, *26*, 474202.
(485) Donhauser, Z. J.; Mantooth, B. A.; Kelly, K. F.; Bumm, L. A.; Monnell, J. D.; Stapleton, J. J.; Price, D. W.; Rawlett, A. M.; Allara, D. L.; Tour, J. M.; Weiss, P. S. Conductance Switching in Single Molecules through Conformational Changes. *Science* **2001**, *292*, 2303−2307.
(486) Zandbergen, H. W.; Pao, C. W.; Srolovitz, D. J. Dislocation Injection, Reconstruction, and Atomic Transport on {001} Au Terraces. *Phys. Rev. Lett.* **2007**, *98*, 036103.
(487) Ohshiro, T.; Tsutsui, M.; Yokota, K.; Furuhashi, M.; Taniguchi, M.; Kawai, T. Detection of Post-Translational Modifications in Single Peptides Using Electron Tunnelling Currents. *Nat. Nanotechnol.* **2014**, *9*, 835−840.
(488) Chang, S. A.; He, J.; Lin, L. S.; Zhang, P. M.; Liang, F.; Young, M.; Huang, S.; Lindsay, S. Tunnel Conductance of Watson-Crick Nucleoside-Base Pairs from Telegraph Noise. *Nanotechnology* **2009**, *20*, 185102.
(489) Beebe, J. M.; Kim, B.; Frisbie, C. D.; Kushmerick, J. G. Measuring Relative Barrier Heights in Molecular Electronic Junctions with Transition Voltage Spectroscopy. *ACS Nano* **2008**, *2*, 827−832.
(490) Jia, C.; Wang, J.; Yao, C.; Cao, Y.; Zhong, Y.; Liu, Z.; Liu, Z.; Guo, X. Conductance Switching and Mechanisms in Single-Molecule Junctions. *Angew. Chem., Int. Ed.* **2013**, *52*, 8666−8670.
(491) Huisman, E. H.; Guedon, C. M.; van Wees, B. J.; van der Molen, S. J. Interpretation of Transition Voltage Spectroscopy. *Nano Lett.* **2009**, *9*, 3909−3913.
(492) Araidai, M.; Tsukada, M. Theoretical Calculations of Electron Transport in Molecular Junctions: Inflection Behavior in Fowler-Nordheim Plot and Its Origin. *Phys. Rev. B: Condens. Matter Mater. Phys.* **2010**, *81*, 235114.
(493) Vilan, A.; Cahen, D.; Kraisler, E. Rethinking Transition Voltage Spectroscopy within a Generic Taylor Expansion View. *ACS Nano* **2013**, *7*, 695−706.
(494) Bâldea, I. Ambipolar Transition Voltage Spectroscopy: Analytical Results and Experimental Agreement. *Phys. Rev. B: Condens. Matter Mater. Phys.* **2012**, *85*, 035442.
(495) Chen, J.; Markussen, T.; Thygesen, K. S. Quantifying Transition Voltage Spectroscopy of Molecular Junctions: Ab Initio Calculations. *Phys. Rev. B: Condens. Matter Mater. Phys.* **2010**, *82*, 121412.
(496) Wang, G.; Kim, Y.; Na, S.-I.; Kahng, Y. H.; Ku, J.; Park, S.; Jang, Y. H.; Kim, D.-Y.; Lee, T. Investigation of the Transition Voltage Spectra of Molecular Junctions Considering Frontier Molecular Orbitals and the Asymmetric Coupling Effect. *J. Phys. Chem. C* **2011**, *115*, 17979−17985.
(497) Tan, A.; Balachandran, J.; Dunietz, B. D.; Jang, S. Y.; Gavini, V.; Reddy, P. Length Dependence of Frontier Orbital Alignment in Aromatic Molecular Junctions. *Appl. Phys. Lett.* **2012**, *101*, 243107.
(498) Song, H.; Kim, Y.; Jeong, H.; Reed, M. A.; Lee, T. Coherent Tunneling Transport in Molecular Junctions. *J. Phys. Chem. C* **2010**, *114*, 20431−20435.
(499) Mirjani, F.; Thijssen, J. M.; van der Molen, S. J. Advantages and Limitations of Transition Voltage Spectroscopy: A Theoretical Analysis. *Phys. Rev. B: Condens. Matter Mater. Phys.* **2011**, *84*, 115402.
(500) Pakoulev, A. V.; Burtman, V. Temperature Dependent Barrier Crossover Regime in Tunneling Single Molecular Devices Based on the Matrix of Isolated Molecules. *J. Phys. Chem. C* **2009**, *113*, 21413−21421.
(501) Wu, K.; Bai, M.; Sanvito, S.; Hou, S. Transition Voltages of Vacuum-Spaced and Molecular Junctions with Ag and Pt Electrodes. *J. Chem. Phys.* **2014**, *141*, 014707.
(502) Brito Silva, C. A.; da Silva, S. J. S.; Leal, J. F. P.; Pinheiro, F. A.; Del Nero, J. Electronic Transport in Oligo-Para-Phenylene Junctions Attached to Carbon Nanotube Electrodes: Transition-Voltage Spectroscopy and Chirality. *Phys. Rev. B: Condens. Matter Mater. Phys.* **2011**, *83*, 245444.
(503) Bâldea, I. Effects of Stochastic Fluctuations at Molecule−Electrode Contacts in Transition Voltage Spectroscopy. *Chem. Phys.* **2012**, *400*, 65−71.
(504) Guo, S.; Hihath, J.; Diez-Perez, I.; Tao, N. Measurement and Statistical Analysis of Single-Molecule Current-Voltage Characteristics, Transition Voltage Spectroscopy, and Tunneling Barrier Height. *J. Am. Chem. Soc.* **2011**, *133*, 19189−19197.
(505) Bennett, N.; Xu, G.; Esdaile, L. J.; Anderson, H. L.; Macdonald, J. E.; Elliott, M. Transition Voltage Spectroscopy of Porphyrin Molecular Wires. *Small* **2010**, *6*, 2604−2611.
(506) Lennartz, M. C.; Atodiresei, N.; Caciuc, V.; Karthäuser, S. Identifying Molecular Orbital Energies by Distance-Dependent Transition Voltage Spectroscopy. *J. Phys. Chem. C* **2011**, *115*, 15025−15030.
(507) Ricœur, G.; Lenfant, S.; Guérin, D.; Vuillaume, D. Molecule/Electrode Interface Energetics in Molecular Junction: A "Transition Voltage Spectroscopy" Study. *J. Phys. Chem. C* **2012**, *116*, 20722−20730.
(508) Bâldea, I. Interpretation of Stochastic Events in Single-Molecule Measurements of Conductance and Transition Voltage Spectroscopy. *J. Am. Chem. Soc.* **2012**, *134*, 7958−7962.
(509) Xiang, A.; Li, H.; Chen, S.; Liu, S. X.; Decurtins, S.; Bai, M.; Hou, S.; Liao, J. Electronic Transport in Benzodifuran Single-Molecule Transistors. *Nanoscale* **2015**, *7*, 7665−7673.
(510) Lo, W. Y.; Bi, W.; Li, L.; Jung, I. H.; Yu, L. Edge-on Gating Effect in Molecular Wires. *Nano Lett.* **2015**, *15*, 958−962.
(511) Trouwborst, M. L.; Martin, C. A.; Smit, R. H. M.; Guédon, C. M.; Baart, T. A.; van der Molen, S. J.; van Ruitenbeek, J. M. Transition Voltage Spectroscopy and the Nature of Vacuum Tunneling. *Nano Lett.* **2011**, *11*, 614−617.
(512) Sotthewes, K.; Hellenthal, C.; Kumar, A.; Zandvliet, H. J. W. Transition Voltage Spectroscopy of Scanning Tunneling Microscopy Vacuum Junctions. *RSC Adv.* **2014**, *4*, 32438−32442.
(513) Bâldea, I. Transition Voltage Spectroscopy in Vacuum Break Junction: Possible Role of Surface States. *EPL (Europhys. Lett.)* **2012**, *98*, 17010.
(514) Wu, K.; Bai, M.; Sanvito, S.; Hou, S. Origin of the Transition Voltage in Gold-Vacuum-Gold Atomic Junctions. *Nanotechnology* **2013**, *24*, 025203.
(515) Bergren, A. J.; McCreery, R. L. Analytical Chemistry in Molecular Electronics. *Annu. Rev. Anal. Chem.* **2011**, *4*, 173−195.
(516) Elliott, A. B. S.; Horvath, R.; Gordon, K. C. Vibrational Spectroscopy as a Probe of Molecule-Based Devices. *Chem. Soc. Rev.* **2012**, *41*, 1929−1946.
(517) Campion, A.; Kambhampati, P. Surface-Enhanced Raman Scattering. *Chem. Soc. Rev.* **1998**, *27*, 241−250.
(518) Camp, C. H.; Cicerone, M. T. Chemically Sensitive Bioimaging with Coherent Raman Scattering. *Nat. Photonics* **2015**, *9*, 295−305.
(519) Hung, K. K.; Stege, U.; Hore, D. K. Ir Absorption, Raman Scattering, and Ir-Vis Sum-Frequency Generation Spectroscopy as

DOI: 10.1021/acs.chemrev.5b00680
Chem. Rev. 2016, 116, 4318−4440

Quantitative Probes of Surface Structure. *Appl. Spectrosc. Rev.* **2015**, *50*, 351−376.
(520) Bell, S. E. J.; Sirimuthu, N. M. S. Surface-Enhanced Raman Spectroscopy (Sers) for Sub-Micromolar Detection of DNA/Rna Mononucleotides. *J. Am. Chem. Soc.* **2006**, *128*, 15580−15581.
(521) Bantz, K. C.; Meyer, A. F.; Wittenberg, N. J.; Im, H.; Kurtulus, O.; Lee, S. H.; Lindquist, N. C.; Oh, S. H.; Haynes, C. L. Recent Progress in Sers Biosensing. *Phys. Chem. Chem. Phys.* **2011**, *13*, 11551−11567.
(522) Lee, H. M.; Jin, S. M.; Kim, H. M.; Suh, Y. D. Single-Molecule Surface-Enhanced Raman Spectroscopy: A Perspective on the Current Status. *Phys. Chem. Chem. Phys.* **2013**, *15*, 5276−5287.
(523) Schlucker, S. Surface-Enhanced Raman Spectroscopy: Concepts and Chemical Applications. *Angew. Chem., Int. Ed.* **2014**, *53*, 4756−4795.
(524) Yang, L. B.; Li, P.; Liu, H. L.; Tang, X. H.; Liu, J. H. A Dynamic Surface Enhanced Raman Spectroscopy Method for Ultra-Sensitive Detection: From the Wet State to the Dry State. *Chem. Soc. Rev.* **2015**, *44*, 2837−2848.
(525) Xu, W. G.; Mao, N. N.; Zhang, J. Graphene: A Platform for Surface-Enhanced Raman Spectroscopy. *Small* **2013**, *9*, 1206−1224.
(526) Jiang, N.; Foley, E. T.; Klingsporn, J. M.; Sonntag, M. D.; Valley, N. A.; Dieringer, J. A.; Seideman, T.; Schatz, G. C.; Hersam, M. C.; Van Duyne, R. P. Observation of Multiple Vibrational Modes in Ultrahigh Vacuum Tip-Enhanced Raman Spectroscopy Combined with Molecular-Resolution Scanning Tunneling Microscopy. *Nano Lett.* **2012**, *12*, 6506−6506.
(527) Cui, L.; Liu, B.; Vonlanthen, D.; Mayor, M.; Fu, Y. C.; Li, J. F.; Wandlowski, T. In Situ Gap-Mode Raman Spectroscopy on Single-Crystal Au(100) Electrodes: Tuning the Torsion Angle of 4,4 '-Biphenyldithiols by an Electrochemical Gate Field. *J. Am. Chem. Soc.* **2011**, *133*, 7332−7335.
(528) Ozaki, Y.; Morisawa, Y.; Ikehata, A.; Higashi, N. Far-Ultraviolet Spectroscopy in the Solid and Liquid States: A Review. *Appl. Spectrosc.* **2012**, *66*, 1−25.
(529) Li, Z.; Berger, H.; Okamoto, K.; Zhang, Q. F.; Luscombe, C. K.; Cao, G. Z.; Schlaf, R. Measurement of the Internal Orbital Alignment of Oligothiophene-Tio2 Nanoparticle Hybrids. *J. Phys. Chem. C* **2013**, *117*, 13961−13970.
(530) Kantchev, E. A. B.; Norsten, T. B.; Tan, M. L. Y.; Ng, J. J. Y.; Sullivan, M. B. Thiophene-Containing Pechmann Dyes and Related Compounds: Synthesis, and Experimental and Dft Characterisation. *Chem. - Eur. J.* **2012**, *18*, 695−708.
(531) Zhang, Y.; Jiang, Y. B.; Zhang, D. K.; Li, K. X.; Qian, Y. On-Line Concentration Measurement for Anti-Solvent Crystallization of Beta-Artemether Using Uv-Vis Fiber Spectroscopy. *J. Cryst. Growth* **2011**, *314*, 185−189.
(532) Doherty, M. D.; Grills, D. C.; Huang, K. W.; Muckerman, J. T.; Polyansky, D. E.; van Eldik, R.; Fujita, E. Kinetics and Thermodynamics of Small Molecule Binding to Pincer-Pcp Rhodium(I) Complexes. *Inorg. Chem.* **2013**, *52*, 4160−4172.
(533) Kobayashi, K. Hard X-Ray Photoemission Spectroscopy. *Nucl. Instrum. Methods Phys. Res., Sect. A* **2009**, *601*, 32−47.
(534) Cohen, H. Chemically Resolved Electrical Measurements in Organic Self-Assembled Molecular Layers. *J. Electron Spectrosc. Relat. Phenom.* **2010**, *176*, 24−34.
(535) Harada, Y.; Koitaya, T.; Mukai, K.; Yoshimoto, S.; Yoshinobu, J. Spectroscopic Characterization and Transport Properties of Aromatic Monolayers Covalently Attached to Si(111) Surfaces. *J. Phys. Chem. C* **2013**, *117*, 7497−7505.
(536) Ie, Y.; Hirose, T.; Nakamura, H.; Kiguchi, M.; Takagi, N.; Kawai, M.; Aso, Y. Nature of Electron Transport by Pyridine-Based Tripodal Anchors: Potential for Robust and Conductive Single-Molecule Junctions with Gold Electrodes. *J. Am. Chem. Soc.* **2011**, *133*, 3014−3022.
(537) Seitz, O.; Dai, M.; Aguirre-Tostado, F. S.; Wallace, R. M.; Chabal, Y. J. Copper-Metal Deposition on Self Assembled Monolayer for Making Top Contacts in Molecular Electronic Devices. *J. Am. Chem. Soc.* **2009**, *131*, 18159−18167.
(538) Zhu, Z. H.; Daniel, T. A.; Maitani, M.; Cabarcos, O. M.; Allara, D. L.; Winograd, N. Controlling Gold Atom Penetration through Alkanethiolate Self-Assembled Monolayers on Au {111} by Adjusting Terminal Group Intermolecular Interactions. *J. Am. Chem. Soc.* **2006**, *128*, 13710−13719.
(539) Kimberg, V.; Miron, C. Molecular Potentials and Wave Function Mapping by High-Resolution Electron Spectroscopy and Ab Initio Calculations. *J. Electron Spectrosc. Relat. Phenom.* **2014**, *195*, 301−306.
(540) Turner, D. W. Molecular Photoelectron Spectroscopy. *Philos. Trans. R. Soc., A* **1970**, *268*, 7−31.
(541) Svensson, S. Soft X-Ray Photoionization of Atoms and Molecules. *J. Phys. B: At., Mol. Opt. Phys.* **2005**, *38*, S821−S838.
(542) Nguyen, N. L.; Borghi, G.; Ferretti, A.; Dabo, I.; Marzari, N. First-Principles Photoemission Spectroscopy and Orbital Tomography in Molecules from Koopmans-Compliant Functionals. *Phys. Rev. Lett.* **2015**, *114*, 166405.
(543) Kim, B.; Beebe, J. M.; Jun, Y.; Zhu, X. Y.; Frisbie, C. D. Correlation between Homo Alignment and Contact Resistance in Molecular Junctions: Aromatic Thiols Versus Aromatic Isocyanides. *J. Am. Chem. Soc.* **2006**, *128*, 4970−4971.
(544) Yaffe, O.; Qi, Y. B.; Scheres, L.; Puniredd, S. R.; Segev, L.; Ely, T.; Haick, H.; Zuilhof, H.; Vilan, A.; Kronik, L.; Kahn, A.; Cahen, D. Charge Transport across Metal/Molecular (Alkyl) Monolayer-Si Junctions Is Dominated by the Lumo Level. *Phys. Rev. B: Condens. Matter Mater. Phys.* **2012**, *85*, 045433.
(545) Hill, I. G.; Rajagopal, A.; Kahn, A.; Hu, Y. Molecular Level Alignment at Organic Semiconductor-Metal Interfaces. *Appl. Phys. Lett.* **1998**, *73*, 662−664.
(546) Ferre, A.; Boguslavskiy, A. E.; Dagan, M.; Blanchet, V.; Bruner, B. D.; Burgy, F.; Camper, A.; Descamps, D.; Fabre, B.; Fedorov, N.; Gaudin, J.; Geoffroy, G.; et al. Multi-Channel Electronic and Vibrational Dynamics in Polyatomic Resonant High-Order Harmonic Generation. *Nat. Commun.* **2015**, *6*, 5952.
(547) Perry, D. L.; Ma, Z. X.; Olson, A.; Topp, E. Molecular Characterization of Gadolinium-Doped Zinc Telluride Films by X-Ray Photoelectron Spectroscopy. *Spectroscopy* **2015**, *30*, 38−43.
(548) Simmons, J. G. Generalized Formula for the Electric Tunnel Effect between Similar Electrodes Separated by a Thin Insulating Film. *J. Appl. Phys.* **1963**, *34*, 1793.
(549) Zhu, X. Electronic Structure and Electron Dynamics at Molecule?Metal Interfaces: Implications for Molecule-Based Electronics. *Surf. Sci. Rep.* **2004**, *56*, 1−83.
(550) Nitzan, A. Electron Transmission through Molecules and Molecular Interfaces. *Annu. Rev. Phys. Chem.* **2001**, *52*, 681−750.
(551) Xiang, D. *Fabrication and Utilization of Mechanically Controllable Break Junction for Bioelectronics*; Forschungszentrum Jülich, 2012.
(552) Holmlin, R. E.; Haag, R.; Chabinyc, M. L.; Ismagilov, R. F.; Cohen, A. E.; Terfort, A.; Rampi, M. A.; Whitesides, G. M. Electron Transport through Thin Organic Films in Metal-Insulator-Metal Junctions Based on Self-Assembled Monolayers. *J. Am. Chem. Soc.* **2001**, *123*, 5075−5085.
(553) Joachim, C.; Magoga, M. The Effective Mass of an Electron When Tunneling through a Molecular Wire. *Chem. Phys.* **2002**, *281*, 347−352.
(554) Tan, S. F.; Wu, L.; Yang, J. K. W.; Bai, P.; Bosman, M.; Nijhuis, C. A. Quantum Plasmon Resonances Controlled by Molecular Tunnel Junctions. *Science* **2014**, *343*, 1496−1499.
(555) Joachim, C.; Ratner, M. A. Molecular Electronics. *Proc. Natl. Acad. Sci. U. S. A.* **2005**, *102*, 8800−8800.
(556) Tersoff, J.; Hamann, D. R. Theory of the Scanning Tunneling Microscope. *Phys. Rev. B: Condens. Matter Mater. Phys.* **1985**, *31*, 805−813.
(557) He, J.; Sankey, O.; Lee, M.; Tao, N. J.; Li, X. L.; Lindsay, S. Measuring Single Molecule Conductance with Break Junctions. *Faraday Discuss.* **2006**, *131*, 145−154.
(558) Topinka, M. A.; LeRoy, B. J.; Shaw, S. E. J.; Heller, E. J.; Westervelt, R. M.; Maranowski, K. D.; Cossard, A. C. Imaging

DOI: 10.1021/acs.chemrev.5b00680
Chem. Rev. 2016, 116, 4318−4440

Coherent Electron Flow from a Quantum Point Contact. *Science* **2000**, *289*, 2323−2326.
(559) Hong, W. J.; Valkenier, H.; Meszaros, G.; Manrique, D. Z.; Mishchenko, A.; Putz, A.; Garcia, P. M.; Lambert, C. J.; Hummelen, J. C.; Wandlowski, T. An Mcbj Case Study: The Influence of Pi-Conjugation on the Single-Molecule Conductance at a Solid/Liquid Interface. *Beilstein J. Nanotechnol.* **2011**, *2*, 699−713.
(560) Kim, Y.; Hellmuth, T. J.; Sysoiev, D.; Pauly, F.; Pietsch, T.; Wolf, J.; Erbe, A.; Huhn, T.; Groth, U.; Steiner, U. E.; Scheer, E. Charge Transport Characteristics of Diarylethene Photoswitching Single-Molecule Junctions. *Nano Lett.* **2012**, *12*, 3736−3742.
(561) Osorio, E. A.; Bjornhølm, T.; Lehn, J. M.; Ruben, M.; van der Zant, H. S. J. Single-Molecule Transport in Three-Terminal Devices. *J. Phys.: Condens. Matter* **2008**, *20*, 374121.
(562) Wingreen, N. S.; Jacobsen, K. W.; Wilkins, J. W. Resonant Tunneling with Electron-Phonon Interaction - an Exactly Solvable Model. *Phys. Rev. Lett.* **1988**, *61*, 1396−1399.
(563) Buttiker, M.; Landauer, R. Traversal Time for Tunneling. *Phys. Scr.* **1985**, *32*, 429−434.
(564) Segal, D.; Nitzan, A. Steady-State Quantum Mechanics of Thermally Relaxing Systems. *Chem. Phys.* **2001**, *268*, 315−335.
(565) Landauer, R.; Martin, T. Barrier Interaction Time in Tunneling. *Rev. Mod. Phys.* **1994**, *66*, 217−228.
(566) Hauge, E. H.; Stovneng, J. A. Tunneling Times: a Critical Review. *Rev. Mod. Phys.* **1989**, *61*, 917−936.
(567) Marcus, R. A.; Sutin, N. Electron Transfers in Chemistry and Biology. *Biochim. Biophys. Acta, Rev. Bioenerg.* **1985**, *811*, 265−322.
(568) Gosavi, S.; Marcus, R. A. Nonadiabatic Electron-Transfer at Metal Surfaces. *J. Phys. Chem. B* **2000**, *104*, 2067−2072.
(569) Zhu, X. Y. Charge Transport at Metal-Molecule Interfaces: A Spectroscopic View. *J. Phys. Chem. B* **2004**, *108*, 8778−8793.
(570) Meir, Y.; Wingreen, N. Landauer Formula for the Current through an Interacting Electron Region. *Phys. Rev. Lett.* **1992**, *68*, 2512−2515.
(571) Troisi, A.; Ratner, M. A. Molecular Transport Junctions: Propensity Rules for Inelastic Electron Tunneling Spectra. *Nano Lett.* **2006**, *6*, 1784−1788.
(572) Papadopoulos, T. A.; Grace, I. M.; Lambert, C. J. Control of Electron Transport through Fano Resonances in Molecular Wires. *Phys. Rev. B: Condens. Matter Mater. Phys.* **2006**, *74*, 193306.
(573) Xu, Y. Q.; Fang, C. F.; Cui, B.; Ji, G. M.; Zhai, Y. X.; Liu, D. S. Gated Electronic Currents Modulation and Designs of Logic Gates with Single Molecular Field Effect Transistors. *Appl. Phys. Lett.* **2011**, *99*, 043304.
(574) Xue, Y. Q.; Ratner, M. A. Microscopic Study of Electrical Transport through Individual Molecules with Metallic Contacts. I. Band Lineup, Voltage Drop, and High-Field Transport. *Phys. Rev. B: Condens. Matter Mater. Phys.* **2003**, *68*, 115406.
(575) Kim, Y.-H.; Tahir-Kheli, J.; Schultz, P.; Goddard, W. First-Principles Approach to the Charge-Transport Characteristics of Monolayer Molecular-Electronics Devices: Application to Hexanedithiolate Devices. *Phys. Rev. B: Condens. Matter Mater. Phys.* **2006**, *73*, 235419.
(576) Yonehara, T.; Hanasaki, K.; Takatsuka, K. Fundamental Approaches to Nonadiabaticity: Toward a Chemical Theory Beyond the Born-Oppenheimer Paradigm. *Chem. Rev.* **2012**, *112*, 499−542.
(577) Segall, M. D.; Lindan, P. J. D.; Probert, M. J.; Pickard, C. J.; Hasnip, P. J.; Clark, S. J.; Payne, M. C. First-Principles Simulation: Ideas, Illustrations and the Castep Code. *J. Phys.: Condens. Matter* **2002**, *14*, 2717−2744.
(578) Jones, R. O. The Density Functional Formalism, Its Applications and Prospects. *Rev. Mod. Phys.* **1989**, *61*, 689−746.
(579) Becke, A. D. A New Mixing of Hartree-Fock and Local Density-Functional Theories. *J. Chem. Phys.* **1993**, *98*, 1372−1377.
(580) Perdew, J. P.; Burke, K.; Ernzerhof, M. Generalized Gradient Approximation Made Simple. *Phys. Rev. Lett.* **1996**, *77*, 3865−3868.
(581) Car, R.; Parrinello, M. Unified Approach for Molecular-Dynamics and Density-Functional Theory. *Phys. Rev. Lett.* **1985**, *55*, 2471−2474.
(582) Borshch, N. A.; Pereslavtseva, N. S.; Kurganskii, S. I. Electronic Structure and Spectral Characteristics of Zn-Substituted Clathrate Silicides. *Semiconductors* **2011**, *45*, 713−723.
(583) Khan, A. A.; Srivastava, V.; Rajagopalan, M.; Sanyal, S. P. Structural and Electronic Properties of Cd-Rich Lanthanide Intermetallics. *J. Phys. Conf. Ser.* **2012**, *377*, 012081.
(584) Muralidharan, B.; Ghosh, A. W.; Datta, S. Probing Electronic Excitations in Molecular Conduction. *Phys. Rev. B: Condens. Matter Mater. Phys.* **2006**, *73*, 155410.
(585) Perdew, J. P.; Levy, M. Extrema of the Density Functional for the Energy: Excited-States from the Ground-State Theory. *Phys. Rev. B: Condens. Matter Mater. Phys.* **1985**, *31*, 6264−6272.
(586) Baruah, T.; Pederson, M. R. Dft Calculations on Charge-Transfer States of a Carotenoid-Porphyrin-C60 Molecular Triad. *J. Chem. Theory Comput.* **2009**, *5*, 834−843.
(587) Stokbro, K. First-Principles Modeling of Electron Transport. *J. Phys.: Condens. Matter* **2008**, *20*, 064216.
(588) Li, Z. L.; Zou, B.; Wang, C. K.; Luo, Y. Electronic Transport Properties of Molecular Bipyridine Junctions: Effects of Isomer and Contact Structures. *Phys. Rev. B: Condens. Matter Mater. Phys.* **2006**, *73*, 075326.
(589) Weller, M. D.; Kariuki, B. M.; Cox, L. R. Beta-Halovinylsilanes in Oligoyne Synthesis: A Fluoride-Catalysed Unmasking of Alkynes from Beta-Fluorovinylsilanes. *Tetrahedron Lett.* **2008**, *49*, 4596−4600.
(590) Schrettl, S.; Contal, E.; Hoheisel, T. N.; Fritzsche, M.; Balog, S.; Szilluweit, R.; Frauenrath, H. Facile Synthesis of Oligoyne Amphiphiles and Their Rotaxanes. *Chem. Sci.* **2015**, *6*, 564−574.
(591) Zhou, N.; Zhao, Y. Conjugated Oligoyne-Bridged 60 Fullerene Molecular Dumbbells: Syntheses and Thermal and Morphological Properties. *J. Org. Chem.* **2010**, *75*, 1498−1516.
(592) Carroll, R. L.; Gorman, C. B. The Genesis of Molecular Electronics. *Angew. Chem., Int. Ed.* **2002**, *41*, 4378−4400.
(593) Robertson, N.; McGowan, C. A. A Comparison of Potential Molecular Wires as Components for Molecular Electronics. *Chem. Soc. Rev.* **2003**, *32*, 96−103.
(594) McCreery, R. L. 20-Molecular Electronic Junctions. *Chem. Mater.* **2004**, *16*, 4477−4496.
(595) Cotton, F. A.; Daniels, L. M.; Murillo, C. A.; Wang, X. P. Getting the Right Answer to a Key Question Concerning Molecular Wires. *Chem. Commun.* **1999**, 2461−2462.
(596) Wold, D. J.; Haag, R.; Rampi, M. A.; Frisbie, C. D. Distance Dependence of Electron Tunneling through Self-Assembled Monolayers Measured by Conducting Probe Atomic Force Microscopy: Unsaturated Versus Saturated Molecular Junctions. *J. Phys. Chem. B* **2002**, *106*, 2813−2816.
(597) Salomon, A.; Cahen, D.; Lindsay, S.; Tomfohr, J.; Engelkes, V. B.; Frisbie, C. D. Comparison of Electronic Transport Measurements on Organic Molecules. *Adv. Mater.* **2003**, *15*, 1881−1890.
(598) Wierzbinski, E.; Yin, X.; Werling, K.; Waldeck, D. H. The Effect of Oxygen Heteroatoms on the Single Molecule Conductance of Saturated Chains. *J. Phys. Chem. B* **2013**, *117*, 4431−4441.
(599) Sun, Y. Y.; Peng, Z. L.; Hou, R.; Liang, J. H.; Zheng, J. F.; Zhou, X. Y.; Zhou, X. S.; Jin, S.; Niu, Z. J.; Mao, B. W. Enhancing Electron Transport in Molecular Wires by Insertion of a Ferrocene Center. *Phys. Chem. Chem. Phys.* **2014**, *16*, 2260−2267.
(600) Wang, C.; Batsanov, A. S.; Bryce, M. R.; Martin, S.; Nichols, R. J.; Higgins, S. J.; García-suárez, V. M.; Lambert, C. J. Oligoyne Single Molecule Wires. *J. Am. Chem. Soc.* **2009**, *131*, 15647−15654.
(601) Weller, M. D.; Kariuki, B. M.; Cox, L. R. Synthesis of Hybrid Masked Triyne-Phenylene Axial Rods Containing (E)-Beta-Chlorovinylsilanes in the Pi-Conjugated Framework. *J. Org. Chem.* **2009**, *74*, 7898−7907.
(602) Champness, N. R.; Khlobystov, A. N.; Majuga, A. G.; Schroder, M.; Zyk, N. V. An Improved Preparation of 4-Ethynylpyridine and Its Application to the Synthesis of Linear Bipyridyl Ligands. *Tetrahedron Lett.* **1999**, *40*, 5413−5416.
(603) Lee, C. K. Y.; Groneman, J. L.; Turner, P.; Rendina, L. M.; Harding, M. M. Synthesis and X-Ray Crystallographic Analysis of

DOI: 10.1021/acs.chemrev.5b00680
Chem. Rev. 2016, 116, 4318−4440

Chiral Pyridyl Substituted Carbocyclic Molecular Clefts. *Tetrahedron* **2006**, *62*, 4870−4878.
(604) Taylor, J.; Brandbyge, M.; Stokbro, K. Conductance Switching in a Molecular Device: The Role of Side Groups and Intermolecular Interactions. *Phys. Rev. B: Condens. Matter Mater. Phys.* **2003**, *68*, 121101.
(605) James, P. V.; Sudeep, P. K.; Suresh, C. H.; Thomas, K. G.; Photophysical. and Theoretical Investigations of Oligo(P-Phenyleneethynylene)S: Effect of Alkoxy Substitution and Alkyne−Aryl Bond Rotations. *J. Phys. Chem. A* **2006**, *110*, 4329−4337.
(606) Fraysse, S.; Coudret, C.; Launay, J. P. Molecular Wires Built from Binuclear Cyclometalated Complexes. *J. Am. Chem. Soc.* **2003**, *125*, 5880−5888.
(607) Tour, J. M. Transition to Organic Materials Science. Passive, Active, and Hybrid Nanotechnologies. *J. Org. Chem.* **2007**, *72*, 7477−7496.
(608) Nishiyama, F.; Ogawa, K.; Tanaka, S.; Yokoyama, T. Direct Conformational Analysis of a 10 Nm Long Oligothiophene Wire. *J. Phys. Chem. B* **2008**, *112*, 5272−5275.
(609) Lee, S. K.; Yamada, R.; Tanaka, S.; Chang, G. S.; Asai, Y.; Tada, H. Universal Temperature Crossover Behavior of Electrical Conductance in a Single Oligothiophene Molecular Wire. *ACS Nano* **2012**, *6*, 5078−5082.
(610) Ie, Y.; Endou, M.; Lee, S. K.; Yamada, R.; Tada, H.; Aso, Y. Completely Encapsulated Oligothiophenes: Synthesis, Properties, and Single-Molecule Conductance. *Angew. Chem., Int. Ed.* **2011**, *50*, 11980−11984.
(611) Flatt, A. K.; Dirk, S. M.; Henderson, J. C.; Shen, D. E.; Su, J.; Reed, M. A.; Tour, J. M. Synthesis and Testing of New End-Functionalized Oligomers for Molecular Electronics. *Tetrahedron* **2003**, *59*, 8555−8570.
(612) Lipton-Duffin, J. A.; Ivasenko, O.; Perepichka, D. F.; Rosei, F. Synthesis of Polyphenylene Molecular Wires by Surface-Confined Polymerization. *Small* **2009**, *5*, 592−597.
(613) Lafferentz, L.; Ample, F.; Yu, H.; Hecht, S.; Joachim, C.; Grill, L. Conductance of a Single Conjugated Polymer as a Continuous Function of Its Length. *Science* **2009**, *323*, 1193−1197.
(614) Tour, J. M. Molecular Electronics. Synthesis and Testing of Components. *Acc. Chem. Res.* **2000**, *33*, 791−804.
(615) Blum, A. S.; Yang, J. C.; Shashidhar, R.; Ratna, B. Comparing the Conductivity of Molecular Wires with the Scanning Tunneling Microscope. *Appl. Phys. Lett.* **2003**, *82*, 3322−3324.
(616) Walzer, K.; Marx, E.; Greenham, N. C.; Less, R. J.; Raithby, P. R.; Stokbro, K. Scanning Tunneling Microscopy of Self-Assembled Phenylene Ethynylene Oligomers on Au(111) Substrates. *J. Am. Chem. Soc.* **2004**, *126*, 1229−1234.
(617) Wang, L. J.; Yong, A.; Zhou, K. G.; Tan, L.; Ye, J.; Wu, G. P.; Xu, Z. G.; Zhang, H. L. Conformation-Controlled Electron Transport in Single-Molecule Junctions Containing Oligo(Phenylene Ethynylene) Derivatives. *Chem. - Asian J.* **2013**, *8*, 1901−1909.
(618) Kaliginedi, V.; Moreno-García, P.; Valkenier, H.; Hong, W. J.; García-suárez, V. M.; Buiter, P.; Otten, J. L. H.; Hummelen, J. C.; Lambert, C. J.; Wandlowski, T. Correlations between Molecular Structure and Single-Junction Conductance: A Case Study with Oligo(Phenylene-Ethynylene)-Type Wires. *J. Am. Chem. Soc.* **2012**, *134*, 5262−5275.
(619) Teresa González, M.; Zhao, X.; Manrique, D. Z.; Miguel, D.; Leary, E.; Gulcur, M.; Batsanov, A. S.; Rubio-Bollinger, G.; Lambert, C. J.; Bryce, M. R.; et al. Structural Versus Electrical Functionalization of Oligo(Phenylene Ethynylene) Diamine Molecular Junctions. *J. Phys. Chem. C* **2014**, *118*, 21655−21662.
(620) Terao, J.; Tanaka, Y.; Tsuda, S.; Kambe, N.; Taniguchi, M.; Kawai, T.; Saeki, A.; Seki, S. Insulated Molecular Wire with Highly Conductive Pi-Conjugated Polymer Core. *J. Am. Chem. Soc.* **2009**, *131*, 18046−18047.
(621) Wang, H.; Tan, L.; Wang, L. J.; Yin, F. F.; Shi, Z. F.; Zhang, H. L.; Cao, X. P. Shell Dominated Molecular Packing in Dendrimer Encapsulated 'Core-Shell' Molecular Wires. *Chem. Phys. Lett.* **2008**, *461*, 271−275.
(622) Wang, L. J.; Zhou, K. G.; Tan, L.; Wang, H.; Shi, Z. F.; Wu, G. P.; Xu, Z. G.; Cao, X. P.; He, H. X.; Zhang, H. L. A Core-Shell Strategy for Constructing a Single-Molecule Junction. *Chem. - Eur. J.* **2011**, *17*, 8414−8423.
(623) Giacalone, F.; Herranz, M. A.; Grueter, L.; González, M. T.; Calame, M.; Schoenenberger, C.; Arroyo, C. R.; Rubio-Bollinger, G.; Velez, M.; Agraït, N.; Martin, N. Tetrathiafulvalene-Based Molecular Nanowires. *Chem. Commun.* **2007**, 4854−4856.
(624) Parker, C. R.; Leary, E.; Frisenda, R.; Wei, Z.; Jennum, K. S.; Glibstrup, E.; Abrahamsen, P. B.; Santella, M.; Christensen, M. A.; Della Pia, E. A.; et al. A Comprehensive Study of Extended Tetrathiafulvalene Cruciform Molecules for Molecular Electronics: Synthesis and Electrical Transport Measurements. *J. Am. Chem. Soc.* **2014**, *136*, 16497−16507.
(625) Seferos, D. S.; Szuchmacher Blum, A.; Kushmerick, J. G.; Bazan, G. C. Single-Molecule Charge-Transport Measurements That Reveal Technique-Dependent Perturbations. *J. Am. Chem. Soc.* **2006**, *128*, 11260−11267.
(626) Selzer, Y.; Cai, L.; Cabassi, M. A.; Yao, Y.; Tour, J. M.; Mayer, T. S.; Allara, D. L. Effect of Local Environment on Molecular Conduction: Isolated Molecule Versus Self-Assembled Monolayer. *Nano Lett.* **2005**, *5*, 61−65.
(627) Davis, W. B.; Svec, W. A.; Ratner, M. A.; Wasielewski, M. R. Molecular-Wire Behaviour in P-Phenylenevinylene Oligomers. *Nature* **1998**, *396*, 60−63.
(628) Prins, P.; Grozema, F. C.; Siebbeles, L. D. A. Efficient Charge Transport Along Phenylene-Vinylene Molecular Wires. *J. Phys. Chem. B* **2006**, *110*, 14659−14666.
(629) Martin, S.; Haiss, W.; Higgins, S. J.; Nichols, R. J. The Impact of E-Z Photo-Isomerization on Single Molecular Conductance. *Nano Lett.* **2010**, *10*, 2019−2023.
(630) Schull, T. L.; Kushmerick, J. G.; Patterson, C. H.; George, C.; Moore, M. H.; Pollack, S. K.; Shashidhar, R. Ligand Effects on Charge Transport in Platinum(Ii) Acetylides. *J. Am. Chem. Soc.* **2003**, *125*, 3202−3203.
(631) Ren, T. Diruthenium Sigma-Alkynyl Compounds: A New Class of Conjugated Organometallics. *Organometallics* **2005**, *24*, 4854−4870.
(632) Mas-Ballesté, R.; Castillo, O.; Sanz Miguel, P. J.; Olea, D.; Gómez-Herrero, J.; Zamora, F. Towards Molecular Wires Based on Metal-Organic Frameworks. *Eur. J. Inorg. Chem.* **2009**, *2009*, 2885−2896.
(633) Mayor, M.; von Hänisch, C.; Weber, H. B.; Reichert, J.; Beckmann, D. A Trans-Platinum(Ii) Complex as a Single-Molecule Insulator. *Angew. Chem., Int. Ed.* **2002**, *41*, 1183−1186.
(634) Mahapatro, A. K.; Ying, J. W.; Ren, T.; Janes, D. B. Electronic Transport through Ruthenium-Based Redox-Active Molecules in Metal-Molecule-Metal Nanogap Junctions. *Nano Lett.* **2008**, *8*, 2131−2136.
(635) Kim, B.; Beebe, J. M.; Olivier, C.; Rigaut, S.; Touchard, D.; Kushmerick, J. G.; Zhu, X. Y.; Frisbie, C. D. Temperature and Length Dependence of Charge Transport in Redox-Active Molecular Wires Incorporating Ruthenium(Ii) Bis(Sigma-Arylacetylide) Complexes. *J. Phys. Chem. C* **2007**, *111*, 7521−7526.
(636) Benameur, A.; Brignou, P.; Di Piazza, E.; Hervault, Y. M.; Norel, L.; Rigaut, S. Redox-Active Ruthenium(Ii) Sigma-Arylacetylide Wires for Molecular Electronics Incorporating Insulating Chains. *New J. Chem.* **2011**, *35*, 2105−2113.
(637) Albrecht, T.; Moth-Poulsen, K.; Christensen, J. B.; Guckian, A.; Bjornhølm, T.; Vos, J. G.; Ulstrup, J. In Situ Scanning Tunnelling Spectroscopy of Inorganic Transition Metal Complexes. *Faraday Discuss.* **2006**, *131*, 265−279.
(638) Chen, I. W. P.; Fu, M. D.; Tseng, W. H.; Yu, J. Y.; Wu, S. H.; Ku, C. J.; Chen, C. h.; Peng, S. M. Conductance and Stochastic Switching of Ligand-Supported Linear Chains of Metal Atoms. *Angew. Chem., Int. Ed.* **2006**, *45*, 5814−5818.
(639) Constable, E. C. Expanded Ligands—an Assembly Principle for Supramolecular Chemistry. *Coord. Chem. Rev.* **2008**, *252*, 842−855.

DOI: 10.1021/acs.chemrev.5b00680
Chem. Rev. 2016, 116, 4318−4440

(640) Tuccitto, N.; Ferri, V.; Cavazzini, M.; Quici, S.; Zhavnerko, G.; Licciardello, A.; Rampi, M. A. Highly Conductive Similar to 40-Nm-Long Molecular Wires Assembled by Stepwise Incorporation of Metal Centres. *Nat. Mater.* **2009**, *8*, 41−46.
(641) L. Anderson, H. Building Molecular Wires from the Colours of Life: Conjugated Porphyrin Oligomers. *Chem. Commun.* **1999**, 2323−2330.
(642) Tsuda, A.; Osuka, A. Fully Conjugated Porphyrin Tapes with Electronic Absorption Bands That Reach into Infrared. *Science* **2001**, *293*, 79−82.
(643) de la Torre, G.; Bottari, G.; Sekita, M.; Hausmann, A.; Guldi, D. M.; Torres, T. A Voyage into the Synthesis and Photophysics of Homo- and Heterobinuclear Ensembles of Phthalocyanines and Porphyrins. *Chem. Soc. Rev.* **2013**, *42*, 8049−8105.
(644) Katsunori, T.; Masaru, T. Theoretical Predictions of Electronic Transport Properties of Differently Conjugated Porphyrin Molecular Wires. *Jpn. J. Appl. Phys.* **2003**, *42*, 3606.
(645) Tanaka, T.; Osuka, A. Conjugated Porphyrin Arrays: Synthesis, Properties and Applications for Functional Materials. *Chem. Soc. Rev.* **2015**, *44*, 943−969.
(646) Anderson, S.; Anderson, H. L.; Sanders, J. K. M. Expanding Roles for Templates in Synthesis. *Acc. Chem. Res.* **1993**, *26*, 469−475.
(647) Nakamura, Y.; Aratani, N.; Osuka, A. Cyclic Porphyrin Arrays as Artificial Photosynthetic Antenna: Synthesis and Excitation Energy Transfer. *Chem. Soc. Rev.* **2007**, *36*, 831−845.
(648) Jurow, M.; Schuckman, A. E.; Batteas, J. D.; Drain, C. M. Porphyrins as Molecular Electronic Components of Functional Devices. *Coord. Chem. Rev.* **2010**, *254*, 2297−2310.
(649) Sedghi, G.; Sawada, K.; Esdaile, L. J.; Hoffmann, M.; Anderson, H. L.; Bethell, D.; Haiss, W.; Higgins, S. J.; Nichols, R. J. Single Molecule Conductance of Porphyrin Wires with Ultralow Attenuation. *J. Am. Chem. Soc.* **2008**, *130*, 8582−8583.
(650) Avouris, P. Molecular Electronics with Carbon Nanotubes. *Acc. Chem. Res.* **2002**, *35*, 1026−1034.
(651) Wong, H. S. P.; Akinwande, D. *Carbon Nanotube and Graphene Device Physics*; Cambridge University Press: UK, 2011.
(652) Derycke, V.; Martel, R.; Appenzeller, J.; Avouris, P. Carbon Nanotube Inter- and Intramolecular Logic Gates. *Nano Lett.* **2001**, *1*, 453−456.
(653) Javey, A.; Wang, Q.; Ural, A.; Li, Y.; Dai, H. Carbon Nanotube Transistor Arrays for Multistage Complementary Logic and Ring Oscillators. *Nano Lett.* **2002**, *2*, 929−932.
(654) Rueckes, T.; Kim, K.; Joselevich, E.; Tseng, G. Y.; Cheung, C.-L.; Lieber, C. M. Carbon Nanotube-Based Nonvolatile Random Access Memory for Molecular Computing. *Science* **2000**, *289*, 94−97.
(655) Chen, Z.; Appenzeller, J.; Lin, Y. M.; Sippel-Oakley, J.; Rinzler, A. G.; Tang, J.; Wind, S. J.; Solomon, P. M.; Avouris, P. An Integrated Logic Circuit Assembled on a Single Carbon Nanotube. *Science* **2006**, *311*, 1735.
(656) Shulaker, M. M.; Hills, G.; Patil, N.; Wei, H.; Chen, H. Y.; Wong, H. S. P.; Mitra, S. Carbon Nanotube Computer. *Nature* **2013**, *501*, 526−530.
(657) Yang, F.; Wang, X.; Zhang, D.; Yang, J.; LuoDa, Xu Z.; Wei, J.; Wang, J. Q.; Xu, Z.; Peng, F.; et al. Chirality-Specific Growth of Single-Walled Carbon Nanotubes on Solid Alloy Catalysts. *Nature* **2014**, *510*, 522−524.
(658) Chen, Y.; Zhang, J. Chemical Vapor Deposition Growth of Single-Walled Carbon Nanotubes with Controlled Structures for Nanodevice Applications. *Acc. Chem. Res.* **2014**, *47*, 2273−2281.
(659) Hu, Y.; Kang, L.; Zhao, Q.; Zhong, H.; Zhang, S.; Yang, L.; Wang, Z.; Lin, J.; Li, Q.; Zhang, Z.; et al. Growth of High-Density Horizontally Aligned SWNT Arrays Using Trojan Catalysts. *Nat. Commun.* **2015**, *6*, 6099.
(660) Taniguchi, M.; Kawai, T. DNA Electronics. *Phys. E* **2006**, *33*, 1−12.
(661) Porath, D.; Cuniberti, G.; Di Felice, R. Charge Transport in DNA-Based Devices. *Top. Curr. Chem.* **2004**, *237*, 183−277.
(662) Storm, A. J.; van Noort, J.; de Vries, S.; Dekker, C. Insulating Behavior for DNA Molecules between Nanoelectrodes at the 100 Nm Length Scale. *Appl. Phys. Lett.* **2001**, *79*, 3881−3883.
(663) Slinker, J. D.; Muren, N. B.; Renfrew, S. E.; Barton, J. K. DNA Charge Transport over 34 Nm. *Nat. Chem.* **2011**, *3*, 228−233.
(664) Giese, B.; Amaudrut, J.; Kohler, A.-K.; Spormann, M.; Wessely, S. Direct Observation of Hole Transfer through DNA by Hopping between Adenine Bases and by Tunnelling. *Nature* **2001**, *412*, 318−320.
(665) Artes, J. M.; Lopez-Martinez, M.; Giraudet, A.; Diez-Perez, I.; Sanz, F.; Gorostiza, P. Current-Voltage Characteristics and Transition Voltage Spectroscopy of Individual Redox Proteins. *J. Am. Chem. Soc.* **2012**, *134*, 20218−20221.
(666) Hihath, J.; Xu, B. Q.; Zhang, P. M.; Tao, N. J. Study of Single-Nucleotide Polymorphisms by Means of Electrical Conductance Measurements. *Proc. Natl. Acad. Sci. U. S. A.* **2005**, *102*, 16979−16983.
(667) van Zalinge, H.; Schiffrin, D. J.; Bates, A. D.; Starikov, E. B.; Wenzel, W.; Nichols, R. J. Variable-Temperature Measurements of the Single-Molecule Conductance of Double-Stranded DNA. *Angew. Chem., Int. Ed.* **2006**, *45*, 5499−5502.
(668) Liu, S.; Zhang, X.; Luo, W.; Wang, Z.; Guo, X.; Steigerwald, M. L.; Fang, X. Single-Molecule Detection of Proteins Using Aptamer-Functionalized Molecular Electronic Devices. *Angew. Chem.* **2011**, *123*, 2544−2550.
(669) Moore, T. A.; Gust, D.; Mathis, P.; Mialocq, J. C.; Chachaty, C.; Bensasson, R. V.; Land, E. J.; Doizi, D.; Liddell, P. A.; Lehman, W. R.; et al. Photodriven Charge Separation in a Carotenoporphyrin-Quinone Triad. *Nature* **1984**, *307*, 630−632.
(670) Leatherman, G.; Durantini, E. N.; Gust, D.; Moore, T. A.; Moore, A. L.; Stone, S.; Zhou, Z.; Rez, P.; Liu, Y. Z.; Lindsay, S. M. Carotene as a Molecular Wire: Conducting Atomic Force Microscopy. *J. Phys. Chem. B* **1999**, *103*, 4006−4010.
(671) Ramachandran, G. K.; Tomfohr, J. K.; Li, J.; Sankey, O. F.; Zarate, X.; Primak, A.; Terazono, Y.; Moore, T. A.; Moore, A. L.; Gust, D.; et al. Electron Transport Properties of a Carotene Molecule in a Metal−(Single Molecule)−Metal Junction. *J. Phys. Chem. B* **2003**, *107*, 6162−6169.
(672) He, J.; Chen, F.; Li, J.; Sankey, O. F.; Terazono, Y.; Herrero, C.; Gust, D.; Moore, T. A.; Moore, A. L.; Lindsay, S. M. Electronic Decay Constant of Carotenoid Polyenes from Single-Molecule Measurements. *J. Am. Chem. Soc.* **2005**, *127*, 1384−1385.
(673) Zhao, Y. A.; Lindsay, S.; Jeon, S.; Kim, H. J.; Su, L.; Lim, B.; Koo, S. Combined Effect of Polar Substituents on the Electronic Flows in the Carotenoid Molecular Wires. *Chem. - Eur. J.* **2013**, *19*, 10832−10835.
(674) Maeng, J.; Kim, S. B.; Lee, N. J.; Choi, E.; Jung, S.-Y.; Hong, I.; Bae, S.-H.; Oh, J. T.; Lim, B.; Kim, J. W.; Kang, C. J.; Koo, S. Conductance Control in Stabilized Carotenoid Wires. *Chem. - Eur. J.* **2010**, *16*, 7395−7399.
(675) Visoly-Fisher, I.; Daie, K.; Terazono, Y.; Herrero, C.; Fungo, F.; Otero, L.; Durantini, E.; Silber, J. J.; Sereno, L.; Gust, D.; et al. Conductance of a Biomolecular Wire. *Proc. Natl. Acad. Sci. U. S. A.* **2006**, *103*, 8686−8690.
(676) Karthaeuser, S. Control of Molecule-Based Transport for Future Molecular Devices. *J. Phys.: Condens. Matter* **2011**, *23*, 013001.
(677) Nitzan, A. A Relationship between Electron-Transfer Rates and Molecular Conduction. *J. Phys. Chem. A* **2001**, *105*, 2677−2679.
(678) Venkataraman, L.; Klare, J. E.; Tam, I. W.; Nuckolls, C.; Hybertsen, M. S.; Steigerwald, M. L. Single-Molecule Circuits with Well-Defined Molecular Conductance. *Nano Lett.* **2006**, *6*, 458−462.
(679) Rawlett, A. M.; Hopson, T. J.; Nagahara, L. A.; Tsui, R. K.; Ramachandran, G. K.; Lindsay, S. M. Electrical Measurements of a Dithiolated Electronic Molecule Via Conducting Atomic Force Microscopy. *Appl. Phys. Lett.* **2002**, *81*, 3043−3045.
(680) Ko, C. H.; Huang, M. J.; Fu, M. D.; Chen, C. H. Superior Contact for Single-Molecule Conductance: Electronic Coupling of Thiolate and Isothiocyanate on Pt, Pd, and Au. *J. Am. Chem. Soc.* **2010**, *132*, 756−764.

DOI: 10.1021/acs.chemrev.5b00680
Chem. Rev. 2016, 116, 4318−4440

(681) Joshua, H.; Nongjian, T. The Role of Molecule−Electrode Contact in Single-Molecule Electronics. *Semicond. Sci. Technol.* **2014**, *29*, 054007.
(682) Kim, C. M.; Bechhoefer, J. Conductive Probe Afm Study of Pt-Thiol and Au-Thiol Contacts in Metal-Molecule-Metal Systems. *J. Chem. Phys.* **2013**, *138*, 014707.
(683) Sen, A.; Kaun, C. C. Effect of Electrode Orientations on Charge Transport in Alkanedithiol Single-Molecule Junctions. *ACS Nano* **2010**, *4*, 6404−6408.
(684) Frei, M.; Aradhya, S. V.; Hybertsen, M. S.; Venkataraman, L. Linker Dependent Bond Rupture Force Measurements in Single-Molecule Junctions. *J. Am. Chem. Soc.* **2012**, *134*, 4003−4006.
(685) Li, H.; Su, T. A.; Zhang, V.; Steigerwald, M. L.; Nuckolls, C.; Venkataraman, L. Electric Field Breakdown in Single Molecule Junctions. *J. Am. Chem. Soc.* **2015**, *137*, 5028−5033.
(686) Davis, W. B.; Wasielewski, M. R.; Ratner, M. A.; Mujica, V.; Nitzan, A. Electron Transfer Rates in Bridged Molecular Systems: A Phenomenological Approach to Relaxation. *J. Phys. Chem. A* **1997**, *101*, 6158−6164.
(687) González, M. T.; Wu, S.; Huber, R.; van der Molen, S. J.; Schönenberger, C.; Calame, M. Electrical Conductance of Molecular Junctions by a Robust Statistical Analysis. *Nano Lett.* **2006**, *6*, 2238−2242.
(688) Jang, S. Y.; Reddy, P.; Majumdar, A.; Segalman, R. A. Interpretation of Stochastic Events in Single Molecule Conductance Measurements. *Nano Lett.* **2006**, *6*, 2362−2367.
(689) Fan, F. R. F.; Yang, J.; Cai, L.; Price, D. W.; Dirk, S. M.; Kosynkin, D. V.; Yao, Y.; Rawlett, A. M.; Tour, J. M.; Bard, A. J. Charge Transport through Self-Assembled Monolayers of Compounds of Interest in Molecular Electronics. *J. Am. Chem. Soc.* **2002**, *124*, 5550−5560.
(690) Kushmerick, J. G.; Holt, D. B.; Pollack, S. K.; Ratner, M. A.; Yang, J. C.; Schull, T. L.; Naciri, J.; Moore, M. H.; Shashidhar, R. Effect of Bond-Length Alternation in Molecular Wires. *J. Am. Chem. Soc.* **2002**, *124*, 10654−10655.
(691) Stewart, D. R.; Ohlberg, D. A. A.; Beck, P. A.; Chen, Y.; Williams, R. S.; Jeppesen, J. O.; Nielsen, K. A.; Stoddart, J. F. Molecule-Independent Electrical Switching in Pt/Organic Monolayer/Ti Devices. *Nano Lett.* **2004**, *4*, 133−136.
(692) Collier, C. P.; Mattersteig, G.; Wong, E. W.; Luo, Y.; Beverly, K.; Sampaio, J.; Raymo, F. M.; Stoddart, J. F.; Heath, J. R. A [2]Catenane-Based Solid State Electronically Reconfigurable Switch. *Science* **2000**, *289*, 1172−1175.
(693) Metzger, R. M. Electrical Rectification by a Molecule: The Advent of Unimolecular Electronic Devices. *Acc. Chem. Res.* **1999**, *32*, 950−957.
(694) Lörtscher, E.; Gotsmann, B.; Lee, Y.; Yu, L. P.; Rettner, C.; Riel, H. Transport Properties of a Single-Molecule Diode. *ACS Nano* **2012**, *6*, 4931−4939.
(695) Metzger, R. M. Unimolecular Electrical Rectifiers. *Chem. Rev.* **2003**, *103*, 3803−3834.
(696) Metzger, R. M. Unimolecular Electronics. *J. Mater. Chem.* **2008**, *18*, 4364−4396.
(697) Kornilovitch, P. E.; Bratkovsky, A. M.; Williams, R. S. Current Rectification by Molecules with Asymmetric Tunneling Barriers. *Phys. Rev. B: Condens. Matter Mater. Phys.* **2002**, *66*, 165436.
(698) Zahid, F.; Ghosh, A. W.; Paulsson, M.; Polizzi, E.; Datta, S. Charging-Induced Asymmetry in Molecular Conductors. *Phys. Rev. B: Condens. Matter Mater. Phys.* **2004**, *70*, 245317.
(699) Mahmoud, A.; Lugli, P. Designing the Rectification Behavior of Molecular Diodes. *J. Appl. Phys.* **2012**, *112*, 113720.
(700) Mujica, V.; Ratner, M. A.; Nitzan, A. Molecular Rectification: Why Is It So Rare? *Chem. Phys.* **2002**, *281*, 147−150.
(701) Ma, J.; Yang, C. L.; Wang, L. Z.; Wang, M. S.; Ma, X. G. Controllable Low-Bias Negative Differential Resistance, Switching, and Rectifying Behaviors of Dipyrimidinyl-Diphenyl Induced by Contact Mode. *Phys. B* **2014**, *434*, 32−37.
(702) Zhang, G.; Ratner, M. A.; Reuter, M. G. Is Molecular Rectification Caused by Asymmetric Electrode Couplings or by a Molecular Bias Drop? *J. Phys. Chem. C* **2015**, *119*, 6254−6260.
(703) Ng, M.-K.; Yu, L. Synthesis of Amphiphilic Conjugated Diblock Oligomers as Molecular Diodes. *Angew. Chem., Int. Ed.* **2002**, *41*, 3598−3601.
(704) Ashwell, G. J.; Sambles, J. R.; Martin, A. S.; Parker, W. G.; Szablewski, M. Rectifying Characteristics of Mg/(C16h33-Q3cnq Lb Film)/Pt Structures. *J. Chem. Soc., Chem. Commun.* **1990**, 1374−1376.
(705) Metzger, R. M.; Chen, B.; Höpfner, U.; Lakshmikantham, M. V.; Vuillaume, D.; Kawai, T.; Wu, X.; Tachibana, H.; Hughes, T. V.; Sakurai, H.; Baldwin, J. W.; et al. Unimolecular Electrical Rectification in Hexadecylquinolinium Tricyanoquinodimethanide. *J. Am. Chem. Soc.* **1997**, *119*, 10455−10466.
(706) Metzger, R. M.; Baldwin, J. W.; Shumate, W. J.; Peterson, I. R.; Mani, P.; Mankey, G. J.; Morris, T.; Szulczewski, G.; Bosi, S.; Prato, M.; et al. Electrical Rectification in a Langmuir−Blodgett Monolayer of Dimethyanilinoazafullerene Sandwiched between Gold Electrodes. *J. Phys. Chem. B* **2003**, *107*, 1021−1027.
(707) Honciuc, A.; Jaiswal, A.; Gong, A.; Ashworth, K.; Spangler, C. W.; Peterson, I. R.; Dalton, L. R.; Metzger, R. M. Current Rectification in a Langmuir−Schaefer Monolayer of Fullerene-Bis-[4-Diphenylamino-4″-(N-Ethyl-N-2‴-Ethyl)Amino-1,4-Diphenyl-1,3-Butadiene] Malonate between Au Electrodes. *J. Phys. Chem. B* **2005**, *109*, 857−871.
(708) Shumate, W. J.; Mattern, D. L.; Jaiswal, A.; Dixon, D. A.; White, T. R.; Burgess, J.; Honciuc, A.; Metzger, R. M. Spectroscopy and Rectification of Three Donor−Sigma−Acceptor Compounds, Consisting of a One-Electron Donor (Pyrene or Ferrocene), a One-Electron Acceptor (Perylenebisimide), and a C19 Swallowtail. *J. Phys. Chem. B* **2006**, *110*, 11146−11159.
(709) Honciuc, A.; Metzger, R. M.; Gong, A.; Spangler, C. W. Elastic and Inelastic Electron Tunneling Spectroscopy of a New Rectifying Monolayer. *J. Am. Chem. Soc.* **2007**, *129*, 8310−8319.
(710) Metzger, R. M.; Xu, T.; Peterson, I. R. Electrical Rectification by a Monolayer of Hexadecylquinolinium Tricyanoquinodimethanide Measured between Macroscopic Gold Electrodes. *J. Phys. Chem. B* **2001**, *105*, 7280−7290.
(711) Jaiswal, A.; Rajagopal, D.; Lakshmikantham, M. V.; Cava, M. P.; Metzger, R. M. Unimolecular Rectification of Monolayers of $CH_3C(O)S$-C14H28Q^+-3CNQ^- and $CH_3C(O)S$-$C_{16}H_{32}Q^+$-3CNQ^- Organized by Self-Assembly, Langmuir-Blodgett, and Langmuir-Schaefer Techniques. *Phys. Chem. Chem. Phys.* **2007**, *9*, 4007−4017.
(712) Honciuc, A.; Otsuka, A.; Wang, Y. H.; McElwee, S. K.; Woski, S. A.; Saito, G.; Metzger, R. M. Polarization of Charge-Transfer Bands and Rectification in Hexadecylquinolinium 7,7,8-Tricyanoquinodimethanide and Its Tetrafluoro Analog. *J. Phys. Chem. B* **2006**, *110*, 15085−15093.
(713) Ng, M. K.; Lee, D. C.; Yu, L. Molecular Diodes Based on Conjugated Diblock Co-Oligomers. *J. Am. Chem. Soc.* **2002**, *124*, 11862−11863.
(714) Jiang, P.; Morales, G. M.; You, W.; Yu, L. P. Synthesis of Diode Molecules and Their Sequential Assembly to Control Electron Transport. *Angew. Chem., Int. Ed.* **2004**, *43*, 4471−4475.
(715) Scheer, E. *Molecular Electronics: An Introduction to Theory and Experiment*; World Scientific: River Edge, NJ, 2010.
(716) Morales, G. M.; Jiang, P.; Yuan, S.; Lee, Y.; Sanchez, A.; You, W.; Yu, L. Inversion of the Rectifying Effect in Diblock Molecular Diodes by Protonation. *J. Am. Chem. Soc.* **2005**, *127*, 10456−10457.
(717) Díez-Pérez, I.; Hihath, J.; Lee, Y.; Yu, L.; Adamska, L.; Kozhushner, M. A.; Oleynik, I. I.; Tao, N. Rectification and Stability of a Single Molecular Diode with Controlled Orientation. *Nat. Chem.* **2009**, *1*, 635−641.
(718) Elbing, M.; Ochs, R.; Koentopp, M.; Fischer, M.; von Hanisch, C.; Weigend, F.; Evers, F.; Weber, H. B.; Mayor, M. A Single-Molecule Diode. *Proc. Natl. Acad. Sci. U. S. A.* **2005**, *102*, 8815−8820.
(719) Cui, B.; Zhao, W. K.; Wang, H.; Zhao, J. F.; Zhao, H.; Li, D. M.; Jiang, X. H.; Zhao, P.; Liu, D. S. Effect of Geometrical Torsion on the Rectification Properties of Diblock Conjugated Molecular Diodes. *J. Appl. Phys.* **2014**, *116*, 073301.

DOI: 10.1021/acs.chemrev.5b00680
Chem. Rev. 2016, 116, 4318−4440

(720) Luo, L.; Balhorn, L.; Vlaisavljevich, B.; Ma, D. X.; Gagliardi, L.; Frisbie, C. D. Hopping Transport and Rectifying Behavior in Long Donor-Acceptor Molecular Wires. *J. Phys. Chem. C* **2014**, *118*, 26485−26497.
(721) Hu, G. C.; Zhang, G. P.; Li, Y.; Ren, J. F.; Wang, C. K. Proportion Effect in Diblock Co-Oligomer Molecular Diodes. *Chem. Phys. Lett.* **2014**, *614*, 207−213.
(722) Zhang, G. P.; Hu, G. C.; Song, Y.; Li, Z. L.; Wang, C. K. Modulation of Rectification in Diblock Co-Oligomer Diodes by Adjusting Anchoring Groups for Both Symmetric and Asymmetric Electrodes. *J. Phys. Chem. C* **2012**, *116*, 22009−22014.
(723) Geddes, N. J.; Sambles, J. R.; Jarvis, D. J.; Parker, W. G.; Sandman, D. J. Fabrication and Investigation of Asymmetric Current-Voltage Characteristics of a Metal Langmuir-Blodgett Monolayer Metal Structure. *Appl. Phys. Lett.* **1990**, *56*, 1916−1918.
(724) Geddes, N. J.; Sambles, J. R.; Jarvis, D. J.; Parker, W. G.; Sandman, D. J. The Electrical-Properties of Metal-Sandwiched Langmuir-Blodgett Multilayers and Monolayers of a Redox-Active Organic Molecular-Compound. *J. Appl. Phys.* **1992**, *71*, 756−768.
(725) Martin, A. S.; Sambles, J. R.; Ashwell, G. J. Molecular Rectifier. *Phys. Rev. Lett.* **1993**, *70*, 218−221.
(726) Lenfant, S.; Krzeminski, C.; Delerue, C.; Allan, G.; Vuillaume, D. Molecular Rectifying Diodes from Self-Assembly on Silicon. *Nano Lett.* **2003**, *3*, 741−746.
(727) Kushmerick, J. G.; Whitaker, C. M.; Pollack, S. K.; Schull, T. L.; Shashidhar, R. Tuning Current Rectification across Molecular Junctions. *Nanotechnology* **2004**, *15*, S489−S493.
(728) Wang, K.; Zhou, J.; Hamill, J. M.; Xu, B. Measurement and Understanding of Single-Molecule Break Junction Rectification Caused by Asymmetric Contacts. *J. Chem. Phys.* **2014**, *141*, 054712.
(729) Batra, A.; Darancet, P.; Chen, Q.; Meisner, J. S.; Widawsky, J. R.; Neaton, J. B.; Nuckolls, C.; Venkataraman, L. Tuning Rectification in Single-Molecular Diodes. *Nano Lett.* **2013**, *13*, 6233−6237.
(730) Yu, H.; Luo, Y.; Beverly, K.; Stoddart, J. F.; Tseng, H.-R.; Heath, J. R. The Molecule−Electrode Interface in Single-Molecule Transistors. *Angew. Chem., Int. Ed.* **2003**, *42*, 5706−5711.
(731) Krzeminski, C.; Delerue, C.; Allan, G.; Vuillaume, D.; Metzger, R. M. Theory of Electrical Rectification in a Molecular Monolayer. *Phys. Rev. B: Condens. Matter Mater. Phys.* **2001**, *64*, 085405.
(732) Liu, R.; Ke, S. H.; Yang, W. T.; Baranger, H. U. Organometallic Molecular Rectification. *J. Chem. Phys.* **2006**, *124*, 024718.
(733) Taylor, J.; Brandbyge, M.; Stokbro, K. Theory of Rectification in Tour Wires: The Role of Electrode Coupling. *Phys. Rev. Lett.* **2002**, *89*, 138301.
(734) Guang-Ping, Z.; Gui-Chao, H.; Yang, S.; Zhen, X.; Chuan-Kui, W. Stretch or Contraction Induced Inversion of Rectification in Diblock Molecular Junctions. *J. Chem. Phys.* **2013**, *139*, 094702.
(735) Troisi, A.; Ratner, M. A. Molecular Rectification through Electric Field Induced Conformational Changes. *J. Am. Chem. Soc.* **2002**, *124*, 14528−14529.
(736) Troisi, A.; Ratner, M. A. Conformational Molecular Rectifiers. *Nano Lett.* **2004**, *4*, 591−595.
(737) Capozzi, B.; Xia, J.; Adak, O.; Dell, E. J.; Liu, Z. F.; Taylor, J. C.; Neaton, J. B.; Campos, L. M.; Venkataraman, L. Single-Molecule Diodes with High Rectification Ratios through Environmental Control. *Nat. Nanotechnol.* **2015**, *10*, 522−527.
(738) Zhang, Q. A Gate Controlled Conjugated Single Molecule Diode: Its Rectification Could Be Reversed. *Phys. B* **2014**, *450*, 90−93.
(739) Adak, O.; Korytar, R.; Joe, A. Y.; Evers, F.; Venkataraman, L. Impact of Electrode Density of States on Transport through Pyridine-Linked Single Molecule Junctions. *Nano Lett.* **2015**, *15*, 3716−3722.
(740) Perrin, M. L.; Burzurí, E.; van der Zant, H. S. J. Single-Molecule Transistors. *Chem. Soc. Rev.* **2015**, *44*, 902−919.
(741) Kubatkin, S.; Danilov, A.; Hjort, M.; Cornil, J.; Bredas, J. L.; Stuhr-Hansen, N.; Hedegard, P.; Bjornhølm, T. Single-Electron Transistor of a Single Organic Molecule with Access to Several Redox States. *Nature* **2003**, *425*, 698−701.
(742) Ghosh, A. W.; Rakshit, T.; Datta, S. Gating of a Molecular Transistor: Electrostatic and Conformational. *Nano Lett.* **2004**, *4*, 565−568.
(743) Martin, C. A.; Smit, R. H. M.; van der Zant, H. S. J.; van Ruitenbeek, J. M. Nanoelectromechanical Single-Atom Switch. *Nano Lett.* **2009**, *9*, 2940−2945.
(744) Lin, Y.; Guo, X. F. Chemical Modification of Graphene and Its Applications. *Huaxue Xuebao* **2014**, *72*, 277−288.
(745) Carrascal, D.; García-suárez, V. M.; Ferrer, J. Impact of Edge Shape on the Functionalities of Graphene-Based Single-Molecule Electronics Devices. *Phys. Rev. B: Condens. Matter Mater. Phys.* **2012**, *85*, 195434.
(746) Huang, C. C.; Rudnev, A. V.; Hong, W. J.; Wandlowski, T. Break Junction under Electrochemical Gating: Testbed for Single-Molecule Electronics. *Chem. Soc. Rev.* **2015**, *44*, 889−901.
(747) Xu, B. Q.; Xiao, X. Y.; Yang, X. M.; Zang, L.; Tao, N. J. Large Gate Modulation in the Current of a Room Temperature Single Molecule Transistor. *J. Am. Chem. Soc.* **2005**, *127*, 2386−2387.
(748) Chen, F.; He, J.; Nuckolls, C.; Roberts, T.; Klare, J. E.; Lindsay, S. Molecular Switch Based on Potential-Induced Changes of Oxidation State. *Nano Lett.* **2005**, *5*, 503−506.
(749) Pobelov, I. V.; Li, Z. H.; Wandlowski, T. Electrolyte Gating in Redox-Active Tunneling Junctions-an Electrochemical Stm Approach. *J. Am. Chem. Soc.* **2008**, *130*, 16045−16054.
(750) Guo, S. Y.; Artes, J. M.; Diez-Perez, I. Electrochemically-Gated Single-Molecule Electrical Devices. *Electrochim. Acta* **2013**, *110*, 741−753.
(751) Yang, Y.; Liu, J. Y.; Chen, Z. B.; Tian, J. H.; Jin, X.; Liu, B.; Li, X. L.; Luo, Z. Z.; Lu, M.; Yang, F. Z.; Tao, N. J.; Tian, Z. Q. Conductance Histogram Evolution of an EC-MCBJ Fabricated Au Atomic Point Contact. *Nanotechnology* **2011**, *22*, 275313.
(752) Baghernejad, M.; Manrique, D. Z.; Li, C.; Pope, T.; Zhumaev, U.; Pobelov, I.; Moreno-García, P.; Kaliginedi, V.; Huang, C.; Hong, W. J.; Lambert, C.; Wandlowski, T. Highly-Effective Gating of Single-Molecule Junctions: An Electrochemical Approach. *Chem. Commun.* **2014**, *50*, 15975−15978.
(753) Capozzi, B.; Chen, Q. S.; Darancet, P.; Kotiuga, M.; Buzzeo, M.; Neaton, J. B.; Nuckolls, C.; Venkataraman, L. Tunable Charge Transport in Single-Molecule Junctions Via Electrolytic Gating. *Nano Lett.* **2014**, *14*, 1400−1404.
(754) Katsonis, N.; Kudernac, T.; Walko, M.; van der Molen, S. J.; van Wees, B. J.; Feringa, B. L. Reversible Conductance Switching of Single Diarylethenes on a Gold Surface. *Adv. Mater.* **2006**, *18*, 1397−1400.
(755) Kronemeijer, A. J.; Akkerman, H. B.; Kudernac, T.; van Wees, B. J.; Feringa, B. L.; Blom, P. W. M.; de Boer, B. Reversible Conductance Switching in Molecular Devices. *Adv. Mater.* **2008**, *20*, 1467−1473.
(756) van der Molen, S. J.; Liao, J.; Kudernac, T.; Agustsson, J. S.; Bernard, L.; Calame, M.; van Wees, B. J.; Feringa, B. L.; Schönenberger, C. Light-Controlled Conductance Switching of Ordered Metal−Molecule−Metal Devices. *Nano Lett.* **2009**, *9*, 76−80.
(757) Meng, F.; Hervault, Y.-M.; Norel, L.; Costuas, K.; Van Dyck, C.; Geskin, V.; Cornil, J.; Hng, H. H.; Rigaut, S.; Chen, X. Photo-Modulable Molecular Transport Junctions Based on Organometallic Molecular Wires. *Chem. Sci.* **2012**, *3*, 3113−3118.
(758) Zhang, J. L.; Zhong, J. Q.; Lin, J. D.; Hu, W. P.; Wu, K.; Xu, G. Q.; Wee, A. T. S.; Chen, W. Towards Single Molecule Switches. *Chem. Soc. Rev.* **2015**, *44*, 2998−3022.
(759) Irie, M. Diarylethenes for Memories and Switches. *Chem. Rev.* **2000**, *100*, 1685−1716.
(760) Feringa, B. L. In Control of Motion: From Molecular Switches to Molecular Motors. *Acc. Chem. Res.* **2001**, *34*, 504−513.
(761) Glebov, E. M.; Pozdnyakov, I. P.; Plyusnin, V. F.; Khmelinskii, I. Primary Reactions in the Photochemistry of Hexahalide Complexes of Platinum Group Metals: A Minireview. *J. Photochem. Photobiol., C* **2015**, *24*, 1−15.
(762) Lara-Avila, S.; Danilov, A.; Geskin, V.; Bouzakraoui, S.; Kubatkin, S.; Cornil, J.; Bjørnholm, T. Bianthrone in a Single-Molecule

DOI: 10.1021/acs.chemrev.5b00680
Chem. Rev. 2016, 116, 4318−4440

Junction: Conductance Switching with a Bistable Molecule Facilitated by Image Charge Effects. *J. Phys. Chem. C* **2010**, *114*, 20686−20695.
(763) Lara-Avila, S.; Danilov, A. V.; Kubatkin, S. E.; Broman, S. L.; Parker, C. R.; Nielsen, M. B. Light-Triggered Conductance Switching in Single-Molecule Dihydroazulene/Vinylheptafulvene Junctions. *J. Phys. Chem. C* **2011**, *115*, 18372−18377.
(764) Broman, S. L.; Lara-Avila, S.; Thisted, C. L.; Bond, A. D.; Kubatkin, S.; Danilov, A.; Nielsen, M. B. Dihydroazulene Photoswitch Operating in Sequential Tunneling Regime: Synthesis and Single-Molecule Junction Studies. *Adv. Funct. Mater.* **2012**, *22*, 4249−4258.
(765) Dulić, D.; van der Molen, S. J.; Kudernac, T.; Jonkman, H. T.; de Jong, J. J. D.; Bowden, T. N.; van Esch, J.; Feringa, B. L.; van Wees, B. J. One-Way Optoelectronic Switching of Photochromic Molecules on Gold. *Phys. Rev. Lett.* **2003**, *91*, 207402.
(766) Whalley, A. C.; Steigerwald, M. L.; Guo, X.; Nuckolls, C. Reversible Switching in Molecular Electronic Devices. *J. Am. Chem. Soc.* **2007**, *129*, 12590−12591.
(767) Irie, M.; Eriguchi, T.; Takada, T.; Uchida, K. Photochromism of Diarylethenes Having Thiophene Oligomers as the Aryl Groups. *Tetrahedron* **1997**, *53*, 12263−12271.
(768) Schirm, C.; Matt, M.; Pauly, F.; Cuevas, J. C.; Nielaba, P.; Scheer, E. A Current-Driven Single-Atom Memory. *Nat. Nanotechnol.* **2013**, *8*, 645−648.
(769) Kay, N. J.; Higgins, S. J.; Jeppesen, J. O.; Leary, E.; Lycoops, J.; Ulstrup, J.; Nichols, R. J. Single-Molecule Electrochemical Gating in Ionic Liquids. *J. Am. Chem. Soc.* **2012**, *134*, 16817−16826.
(770) Zhang, J.; Kuznetsov, A. M.; Medvedev, I. G.; Chi, Q.; Albrecht, T.; Jensen, P. S.; Ulstrup, J. Single-Molecule Electron Transfer in Electrochemical Environments. *Chem. Rev.* **2008**, *108*, 2737−2791.
(771) Darwish, N.; Diez-Perez, I.; Da Silva, P.; Tao, N. J.; Gooding, J. J.; Paddon-Row, M. N. Observation of Electrochemically Controlled Quantum Interference in a Single Anthraquinone-Based Norbornylogous Bridge Molecule. *Angew. Chem., Int. Ed.* **2012**, *51*, 3203−3206.
(772) Sanvito, S.; Rocha, A. R. Molecular-Spintronics: The Art of Driving Spin through Molecules. *J.Comput. Theor. Nanosci.* **2006**, *3*, 624−642.
(773) Leuenberger, M. N.; Loss, D. Quantum Computing in Molecular Magnets. *Nature* **2001**, *410*, 789−793.
(774) Thomas, L.; Lionti, F.; Ballou, R.; Gatteschi, D.; Sessoli, R.; Barbara, B. Macroscopic Quantum Tunnelling of Magnetization in a Single Crystal of Nanomagnets. *Nature* **1996**, *383*, 145−147.
(775) Wernsdorfer, W.; Sessoli, R. Quantum Phase Interference and Parity Effects in Magnetic Molecular Clusters. *Science* **1999**, *284*, 133−135.
(776) Baadji, N.; Piacenza, M.; Tugsuz, T.; Sala, F. D.; Maruccio, G.; Sanvito, S. Electrostatic Spin Crossover Effect in Polar Magnetic Molecules. *Nat. Mater.* **2009**, *8*, 813−817.
(777) Sanvito, S. Injecting and Controlling Spins in Organic Materials. *J. Mater. Chem.* **2007**, *17*, 4455−4459.
(778) Bogani, L.; Wernsdorfer, W. Molecular Spintronics Using Single-Molecule Magnets. *Nat. Mater.* **2008**, *7*, 179−186.
(779) Affronte, M. Molecular Nanomagnets for Information Technologies. *J. Mater. Chem.* **2009**, *19*, 1731−1737.
(780) Camarero, J.; Coronado, E. Molecular Vs. Inorganic Spintronics: The Role of Molecular Materials and Single Molecules. *J. Mater. Chem.* **2009**, *19*, 1678−1684.
(781) Lehmann, J.; Gaita-Arino, A.; Coronado, E.; Loss, D. Quantum Computing with Molecular Spin Systems. *J. Mater. Chem.* **2009**, *19*, 1672−1677.
(782) Mas-Torrent, M.; Crivillers, N.; Mugnaini, V.; Ratera, I.; Rovira, C.; Veciana, J. Organic Radicals on Surfaces: Towards Molecular Spintronics. *J. Mater. Chem.* **2009**, *19*, 1691−1695.
(783) Stamp, P. C. E.; Gaita-Arino, A. Spin-Based Quantum Computers Made by Chemistry: Hows and Whys. *J. Mater. Chem.* **2009**, *19*, 1718−1730.
(784) Wiesendanger, R. Spin Mapping at the Nanoscale and Atomic Scale. *Rev. Mod. Phys.* **2009**, *81*, 1495−1550.
(785) Wahl, P.; Simon, P.; Diekhöner, L.; Stepanyuk, V. S.; Bruno, P.; Schneider, M. A.; Kern, K. Exchange Interaction between Single Magnetic Adatoms. *Phys. Rev. Lett.* **2007**, *98*, 056601.
(786) Hirjibehedin, C. F.; Lin, C.-Y.; Otte, A. F.; Ternes, M.; Lutz, C. P.; Jones, B. A.; Heinrich, A. J. Large Magnetic Anisotropy of a Single Atomic Spin Embedded in a Surface Molecular Network. *Science* **2007**, *317*, 1199−1203.
(787) Schwarz, F.; Kastlunger, G.; Lissel, F.; Egler-Lucas, C.; Semenov, S. N.; Venkatesan, K.; Berke, H.; Stadler, R.; Lörtscher, E. Field-induced Conductance Switching by Charge State Alternation in Organometallic Single-molecule Junctions. *Nat. Nanotechnol.* **2015**, *11*, 170−176.
(788) Gütlich, P.; Goodwin, H. A. *Spin Crossover in Transition Metal Compounds*; Springer Science & Business Media: New York, 2004.
(789) Rocha, A. R.; García-suárez, V. M.; Bailey, S. W.; Lambert, C. J.; Ferrer, J.; Sanvito, S. Towards Molecular Spintronics. *Nat. Mater.* **2005**, *4*, 335−339.
(790) Diefenbach, M.; Kim, K. S. Towards Molecular Magnetic Switching with an Electric Bias. *Angew. Chem.* **2007**, *119*, 7784−7787.
(791) Prins, F.; Monrabal-Capilla, M.; Osorio, E. A.; Coronado, E.; van der Zant, H. S. J. Room-Temperature Electrical Addressing of a Bistable Spin-Crossover Molecular System. *Adv. Mater.* **2011**, *23*, 1545−1549.
(792) Osorio, E. A.; Moth-Poulsen, K.; van der Zant, H. S. J.; Paaske, J.; Hedegård, P.; Flensberg, K.; Bendix, J.; Bjørnholm, T. Electrical Manipulation of Spin States in a Single Electrostatically Gated Transition-Metal Complex. *Nano Lett.* **2010**, *10*, 105−110.
(793) Liu, R.; Ke, S.-H.; Baranger, H. U.; Yang, W. Negative Differential Resistance and Hysteresis through an Organometallic Molecule from Molecular-Level Crossing. *J. Am. Chem. Soc.* **2006**, *128*, 6274−6275.
(794) Ouyang, M.; Awschalom, D. D. Coherent Spin Transfer between Molecularly Bridged Quantum Dots. *Science* **2003**, *301*, 1074−1078.
(795) Roy, S.; Gao, Z. Nanostructure-Based Electrical Biosensors. *Nano Today* **2009**, *4*, 318−334.
(796) Kauffman, D. R.; Star, A. Electronically Monitoring Biological Interactions with Carbon Nanotube Field-Effect Transistors. *Chem. Soc. Rev.* **2008**, *37*, 1197−1206.
(797) Patolsky, F.; Zheng, G. F.; Hayden, O.; Lakadamyali, M.; Zhuang, X. W.; Lieber, C. M. Electrical Detection of Single Viruses. *Proc. Natl. Acad. Sci. U. S. A.* **2004**, *101*, 14017−14022.
(798) Sorgenfrei, S.; Chiu, C. Y.; González, R. L.; Yu, Y. J.; Kim, P.; Nuckolls, C.; Shepard, K. L. Label-Free Single-Molecule Detection of DNA-Hybridization Kinetics with a Carbon Nanotube Field-Effect Transistor. *Nat. Nanotechnol.* **2011**, *6*, 125−131.
(799) Choi, Y.; Moody, I. S.; Sims, P. C.; Hunt, S. R.; Corso, B. L.; Perez, I.; Weiss, G. A.; Collins, P. G. Single-Molecule Lysozyme Dynamics Monitored by an Electronic Circuit. *Science* **2012**, *335*, 319−324.
(800) Liu, H.; He, J.; Tang, J.; Liu, H.; Pang, P.; Cao, D.; Krstic, P.; Joseph, S.; Lindsay, S.; Nuckolls, C. Translocation of Single-Stranded DNA through Single-Walled Carbon Nanotubes. *Science* **2010**, *327*, 64−67.
(801) Zhao, Y. A.; Ashcroft, B.; Zhang, P. M.; Liu, H.; Sen, S. M.; Song, W.; Im, J.; Gyarfas, B.; Manna, S.; Biswas, S.; Borges, C.; Lindsay, S. Single-Molecule Spectroscopy of Amino Acids and Peptides by Recognition Tunnelling. *Nat. Nanotechnol.* **2014**, *9*, 466−473.
(802) Huang, S.; He, J.; Chang, S. A.; Zhang, P. M.; Liang, F.; Li, S. Q.; Tuchband, M.; Fuhrmann, A.; Ros, R.; Lindsay, S. Identifying Single Bases in a DNA Oligomer with Electron Tunnelling. *Nat. Nanotechnol.* **2010**, *5*, 868−873.
(803) Chen, X.; Guo, Z.; Yang, G.-M.; Li, J.; Li, M.-Q.; Liu, J.-H.; Huang, X.-J. Electrical Nanogap Devices for Biosensing. *Mater. Today* **2010**, *13*, 28−41.
(804) Xiao, X. Y.; Xu, B. Q.; Tao, N. J. Changes in the Conductance of Single Peptide Molecules Upon Metal-Ion Binding. *Angew. Chem., Int. Ed.* **2004**, *43*, 6148−6152.

DOI: 10.1021/acs.chemrev.5b00680
Chem. Rev. 2016, 116, 4318−4440

(805) Gao, L.; Li, L.-L.; Wang, X.; Wu, P.; Cao, Y.; Liang, B.; Li, X.; Lin, Y.; Lu, Y.; Guo, X. Graphene-Dnazyme Junctions: A Platform for Direct Metal Ion Detection with Ultrahigh Sensitivity. *Chem. Sci.* **2015**, *6*, 2469−2473.
(806) Wang, X.; Gao, L.; Liang, B.; Li, X.; Guo, X. Revealing the Direct Effect of Individual Intercalations on DNA Conductance toward Single-Molecule Electrical Biodetection. *J. Mater. Chem. B* **2015**, *3*, 5150−5154.
(807) Choi, Y.; Moody, I. S.; Sims, P. C.; Hunt, S. R.; Corso, B. L.; Seitz, D. E.; Blaszczak, L. C.; Collins, P. G.; Weiss, G. A. Single-Molecule Dynamics of Lysozyme Processing Distinguishes Linear and Cross-Linked Peptidoglycan Substrates. *J. Am. Chem. Soc.* **2012**, *134*, 2032−2035.
(808) Lee, H. J.; Park, J.; Yoon, O. J.; Kim, H. W.; Lee, D. Y.; Kim, D. H.; Lee, W. B.; Lee, N.-E.; Bonventre, J. V.; Kim, S. S. Amine-Modified Single-Walled Carbon Nanotubes Protect Neurons from Injury in a Rat Stroke Model. *Nat. Nanotechnol.* **2011**, *6*, 121−125.
(809) Sorgenfrei, S.; Chiu, C. Y.; Johnston, M.; Nuckolls, C.; Shepard, K. L. Debye Screening in Single-Molecule Carbon Nanotube Field-Effect Sensors. *Nano Lett.* **2011**, *11*, 3739−3743.
(810) Patolsky, F.; Zheng, G.; Hayden, O.; Lakadamyali, M.; Zhuang, X.; Lieber, C. M. Electrical Detection of Single Viruses. *Proc. Natl. Acad. Sci. U. S. A.* **2004**, *101*, 14017−14022.
(811) Wang, J.; Shen, F.; Wang, Z.; He, G.; Qin, J.; Cheng, N.; Yao, M.; Li, L.; Guo, X. Point Decoration of Silicon Nanowires: An Approach toward Single- Molecule Electrical Detection. *Angew. Chem., Int. Ed.* **2014**, *53*, 5038−5043.
(812) Guo, X.; Whalley, A.; Klare, J. E.; Huang, L.; O'Brien, S.; Steigerwald, M.; Nuckolls, C. Single-Molecule Devices as Scaffolding for Multicomponent Nanostructure Assembly. *Nano Lett.* **2007**, *7*, 1119−1122.
(813) Wang, H.; Muren, N. B.; Ordinario, D.; Gorodetsky, A. A.; Barton, J. K.; Nuckolls, C. Transducing Methyltransferase Activity into Electrical Signals in a Carbon Nanotube-DNA Device. *Chem. Sci.* **2012**, *3*, 62−65.
(814) Dubi, Y.; Di Ventra, M. Heat Flow and Thermoelectricity in Atomic and Molecular Junctions. *Rev. Mod. Phys.* **2011**, *83*, 131−155.
(815) Widawsky, J. R.; Darancet, P.; Neaton, J. B.; Venkataraman, L. Simultaneous Determination of Conductance and Thermopower of Single Molecule Junctions. *Nano Lett.* **2012**, *12*, 354−358.
(816) Guo, S.; Zhou, G.; Tao, N. Single Molecule Conductance, Thermopower, and Transition Voltage. *Nano Lett.* **2013**, *13*, 4326−4332.
(817) Finch, C. M.; García-Suárez, V. M.; Lambert, C. J. Giant Thermopower and Figure of Merit in Single-Molecule Devices. *Phys. Rev. B: Condens. Matter Mater. Phys.* **2009**, *79*, 033405.
(818) Karlström, O.; Linke, H.; Karlström, G.; Wacker, A. Increasing Thermoelectric Performance Using Coherent Transport. *Phys. Rev. B: Condens. Matter Mater. Phys.* **2011**, *84*, 113415.
(819) Bergfield, J. P.; Solis, M. A.; Stafford, C. A. Giant Thermoelectric Effect from Transmission Supernodes. *ACS Nano* **2010**, *4*, 5314−5320.
(820) Evangeli, C.; Gillemot, K.; Leary, E.; González, M. T.; Rubio-Bollinger, G.; Lambert, C. J.; Agraït, N. Engineering the Thermopower of C60 Molecular Junctions. *Nano Lett.* **2013**, *13*, 2141−2145.
(821) Kim, Y.; Jeong, W.; Kim, K.; Lee, W.; Reddy, P. Electrostatic Control of Thermoelectricity in Molecular Junctions. *Nat. Nanotechnol.* **2014**, *9*, 881−885.
(822) Dell, E. J.; Capozzi, B.; Xia, J.; Venkataraman, L.; Campos, L. M. Molecular Length Dictates the Nature of Charge Carriers in Single-Molecule Junctions of Oxidized Oligothiophenes. *Nat. Chem.* **2015**, *7*, 209−214.
(823) Li, Z. Y.; Li, B.; Yang, J. L.; Hou, J. G. Single-Molecule Chemistry of Metal Phthalocyanine on Noble Metal Surfaces. *Acc. Chem. Res.* **2010**, *43*, 954−962.
(824) Chang, S.; Sen, S. M.; Zhang, P. M.; Gyarfas, B.; Ashcroft, B.; Lefkowitz, S.; Peng, H. B.; Lindsay, S. Palladium Electrodes for Molecular Tunnel Junctions. *Nanotechnology* **2012**, *23*, 425202.
(825) Liu, S.; Guo, X. F. Functional Single-Walled Carbon Nanotube-based Molecular Devices. *Huaxue Xuebao* **2013**, *71*, 478−484.
(826) Jia, C. C.; Ma, B. J.; Xin, N.; Guo, X. F. Carbon Electrode-Molecule Junctions: A Reliable Platform for Molecular Electronics. *Acc. Chem. Res.* **2015**, *48*, 2565−2575.
(827) Guo, X. F. Single-Molecule Electrical Biosensors Based on Single-Walled Carbon Nanotubes. *Adv. Mater.* **2013**, *25*, 3397−3408.
(828) Campos, L. C.; Manfrinato, V. R.; Sanchez-Yamagishi, J. D.; Kong, J.; Jarillo-Herrero, P. Anisotropic Etching and Nanoribbon Formation in Single-Layer Graphene. *Nano Lett.* **2009**, *9*, 2600−2604.
(829) Borrnert, F.; Fu, L.; Gorantla, S.; Knupfer, M.; Buchner, B.; Rummeli, M. H. Programmable Sub-Nanometer Sculpting of Graphene with Electron Beams. *ACS Nano* **2012**, *6*, 10327−10334.
(830) Wang, H. M.; Zheng, Z.; Wang, Y. Y.; Qiu, J. J.; Guo, Z. B.; Shen, Z. X.; Yu, T. Fabrication of Graphene Nanogap with Crystallographically Matching Edges and Its Electron Emission Properties. *Appl. Phys. Lett.* **2010**, *96*, 023106.
(831) Jia, C. C.; Li, H.; Jiang, J. L.; Wang, J. D.; Chen, H. L.; Cao, D.; Stoddart, J. F.; Guo, X. F. Interface-Engineered Bistable [2]Rotaxane-Graphene Hybrids with Logic Capabilities. *Adv. Mater.* **2013**, *25*, 6752−6259.
(832) Lefenfeldt, M.; Baumert, J.; Sloutskin, E.; Kuzmenko, I.; Pershan, P.; Deutsch, M.; Nuckolls, C.; Ocko, B. M. Direct Structural Observation of a Molecular Junction by High-Energy X-Ray Reflectometry. *Proc. Natl. Acad. Sci. U. S. A.* **2006**, *103*, 2541−2545.
(833) McCreery, R. L. Analytical Challenges in Molecular Electronics. *Anal. Chem.* **2006**, *78*, 3490−3497.
(834) Yu, X.; Lovrincic, R.; Kraynis, O.; Man, G.; Ely, T.; Zohar, A.; Toledano, T.; Cahen, D.; Vilan, A. Fabrication of Reproducible, Integration-Compatible Hybrid Molecular/Si Electronics. *Small* **2014**, *10*, 5151−5160.
(835) Javey, A.; Kim, H.; Brink, M.; Wang, Q.; Ural, A.; Guo, J.; McIntyre, P.; McEuen, P.; Lundstrom, M.; Dai, H. J. High-Kappa Dielectrics for Advanced Carbon-Nanotube Transistors and Logic Gates. *Nat. Mater.* **2002**, *1*, 241−246.
(836) Scholz, F.; Kaletova, E.; Stensrud, E. S.; Ford, W. E.; Kohutova, A.; Mucha, M.; Stibor, I.; Michl, J.; von Wrochem, F. Formation of N-Alkyl Mono Layers by Organomercury Deposition on Gold. *J. Phys. Chem. Lett.* **2013**, *4*, 2624−2629.
(837) Nef, C.; Posa, L.; Makk, P.; Fu, W. Y.; Halbritter, A.; Schönenberger, C.; Calame, M. High-Yield Fabrication of Nm-Size Gaps in Monolayer CVD Graphene. *Nanoscale* **2014**, *6*, 7249−7254.
(838) Yanson, A. I.; Bollinger, G. R.; van den Brom, H. E.; Agraït, N.; van Ruitenbeek, J. M. Formation and Manipulation of a Metallic Wire of Single Gold Atoms. *Nature* **1998**, *395*, 783−785.
(839) Ohnishi, H.; Kondo, Y.; Takayanagi, K. Quantized Conductance through Individual Rows of Suspended Gold Atoms. *Nature* **1998**, *395*, 780−783.
(840) Song, H.; Lee, H.; Lee, T. Intermolecular Chain-to-Chain Tunneling in Metal-Alkanethiol-Metal Junctions. *J. Am. Chem. Soc.* **2007**, *129*, 3806−3807.
(841) Dubi, Y. Transport Through Self-Assembled Monolayer Molecular Junctions: Role of In-Plane Dephasing. *J. Phys. Chem. C* **2014**, *118*, 21119−21127.
(842) Xu, H.; Chen, Y. B.; Xu, W. G.; Zhang, H. L.; Kong, J.; Dresselhaus, M. S.; Zhang, J. Modulating the Charge-Transfer Enhancement in Gers Using an Electrical Field under Vacuum and an N/P-Doping Atmosphere. *Small* **2011**, *7*, 2945−2952.
(843) Liu, H. B.; Xu, J. L.; Li, Y. J.; Li, Y. L. Aggregate Nanostructures of Organic Molecular Materials. *Acc. Chem. Res.* **2010**, *43*, 1496−1508.
(844) Celestin, M.; Krishnan, S.; Bhansali, S.; Stefanakos, E.; Goswami, D. Y. A Review of Self-Assembled Monolayers as Potential Terahertz Frequency Tunnel Diodes. *Nano Res.* **2014**, *7*, 589−625.
(845) Son, J. Y.; Song, H. Molecular Scale Electronic Devices Using Single Molecules and Molecular Monolayers. *Curr. Appl. Phys.* **2013**, *13*, 1157−1171.

DOI: 10.1021/acs.chemrev.5b00680
Chem. Rev. 2016, 116, 4318−4440